# Biophysikalische Untersuchung von Phloem-lokalisierten Carriern und Kaliumkanälen und deren Interaktion im Modellsystem der *Xenopus* Oozyte

Dissertation zur Erlangung des
naturwissenschaftlichen Doktorgrades
der Bayerischen Julius-Maximilians-Universität Würzburg

vorgelegt von

**Dietmar Geiger**

aus Coburg

Würzburg 2004

Eingereicht am: 13.10.2004

Mitglieder der Promotionskommission:

Vorsitzender: Prof. Dr. Ulrich Scheer
1. Gutachter: Prof. Dr. R. Hedrich
2. Gutachter: Prof. Dr. A. J. E. van Bel
3. Gutachter: Prof. Dr. E. Bamberg

Tag des Promotionskolloquiums:…….

Doktorurkunde ausgehändigt am:……

# Inhaltsverzeichnis

# 1. Einleitung

Erste Spuren pflanzlichen Lebens an Land konnten auf ein Alter von 475 Millionen Jahren datiert werden (Wellman *et al.*, 2003). Beim Übergang von der aquatischen Lebensweise zum Leben an Land mussten sich die Pflanzen einer Reihe neuer Anforderungen stellen. Es begann eine Coevolution von Organen, welche die Anpassung an das Landleben ermöglichten. Wurzeln und Rhizome stellten den Bedarf an Wasser und Nährstoffen aus dem Boden sicher, während sich oberirdische Organe zu Blättern ausbildeten, um Licht für die photosynthetische Reduktion von Kohlendioxid einzufangen. Mit zunehmender Komplexität und Größe der Landpflanzen reichte ein reiner Zell zu Zell Transport durch einfache Diffusion nicht mehr aus, um Photoassimilate effizient umzuverteilen und um die gesamte Pflanze mit Wasser und Mineralien ausreichend zu versorgen.

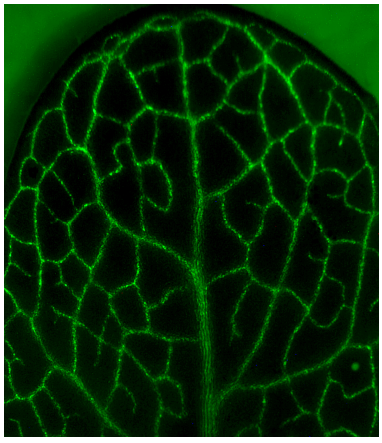

**Abb. 1.1: GFP-markierte Phloemgefäße in *Arabidopsis***
GFP-Fluoreszenz in den Phloemgefäßen eines *Arabidopsis* Rosettenblattes von AtSUC2-Promotor::GFP Pflanzen (von Prof. Sauer erhalten).

## 1.1 Das Phloem

Gefäßpflanzen entwickelten Ferntransportbahnen, um einen effektiven Austausch dieser Absorptions- und Assimilationsprodukte über große Distanzen zwischen Wurzel und Spross sicherzustellen (Abb. 1.1). Zwei Hauptleitsysteme sind dabei in Angiospermen zu unterscheiden, das Xylem und das Phloem, die zusammen die Leitbündel bilden. Angetrieben durch die Wasserpotentialdifferenz im Boden-Pflanze-Luft Kontinuum (Transpirationssog) ermöglichen Xylemgefäße einen Massenstrom von Wasser mit gelösten Mineralien in den Spross. Diese Gefäße weisen starke Verdickungen ihrer Sekundärwände auf und verlieren im ausgereiften, leitenden Zustand ihr Protoplasma. Sie sind also tot, wenn sie ihre

Ausdifferenzierung erreichen. Parenchymatische Zellen umgeben das Xylem und sorgen für die Be- und Entladung der Gefäße.

Im Gegensatz zum Xylem ist das zweite Transportsystem höherer Pflanzen, das Phloem, eine funktionelle Einheit zweier lebender Zelltypen, die ontogenetisch durch inäquale Teilung aus einer Mutterzelle entstehen. Zusammen bilden sie einen strukturellen und funktionellen Komplex mit hochspezialisierten, symplastischen Verbindungen (Poren-Plasmodesmen Einheiten, PPU) für den selektiven Austausch von Mikro- und Makromolekülen. Während die longitudinal gestreckten Siebelemente viele ihrer cytoplasmatischen Organellen sowie die Zentralvakuole und den Kern verloren haben, sind die dazugehörigen Geleitzellen überaus aktiv (Sjölund, 1997). Sie besitzen einen Kern und ein sehr dichtes Zytoplasma mit zahlreichen Mitochondrien zur Versorgung der Siebelemente mit Transkripten, Proteinen und Energie (ATP) über verzweigte Poren-Plasmodesmen Einheiten (Knoblauch und van Bel, 1998). Die Einheit aus Siebelementen und assoziierten Geleitzellen nennt man Siebelement-Geleitzell-Komplex (SE/CC Komplex, aus dem Englischen für sieve element/companion cell complex) (Abb. 1.2; van Bel, 2003 und Referenzen darin).

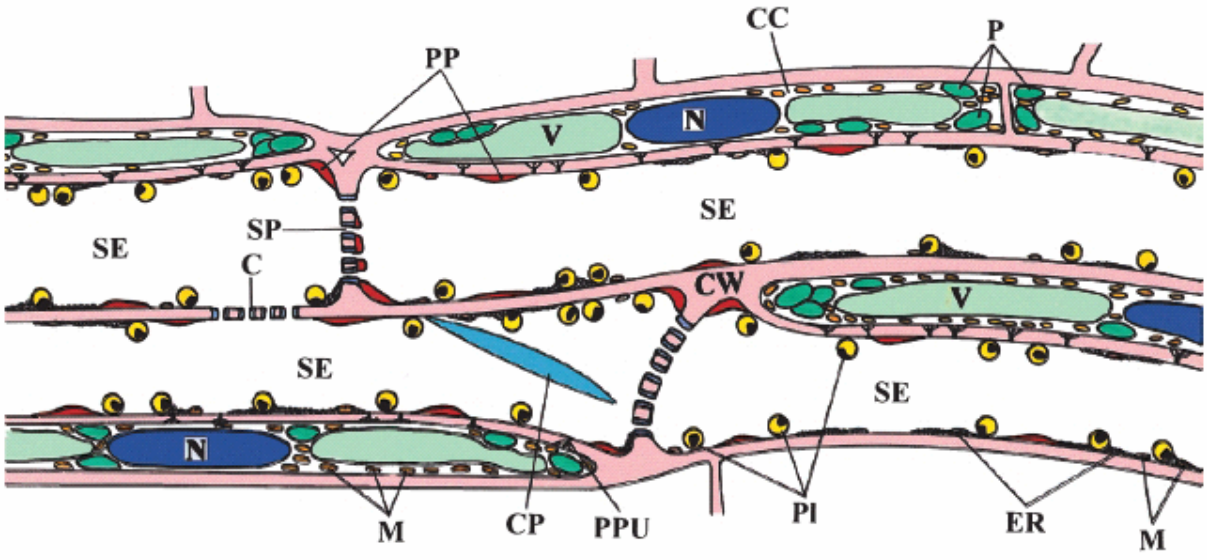


**Abb. 1.2: Aufbau eines Siebröhren/Geleitzellen Komplexes in *Vicia faba*, modifiziert nach van Bel, 2003.** SE (Siebröhren-Elemente) und CC (Geleitzellen) sind durch zahlreiche Poren/Plasmodesmen-Einheiten (PPUs) verbunden. Siebröhren-Plastiden (Pl), Mitochondrien (Mi) und endoplasmatisches Reticulum (ER) sind an der Plasmamembran des SE verteilt, dagegen sind die P-Proteine (PP) lokal begrenzt. PPs und ER befinden sich auch an den Siebplatten (SP), behindern aber nicht den Fluss durch die Siebporen. (C, Kallose; CW, Zellwand; N, Nucleus; P, Plastiden; V, Vakuole)

Durch Siebplatten, große Poren in den Endwänden der in vertikalen Reihen angeordneten Siebelemente, sind die einzelnen Röhrenglieder miteinander verbunden, so dass ein

Gefäßsystem entsteht, das den kompletten Pflanzenkörper durchzieht (Abb. 1.1). Aufbau und Funktion des SE/CC Komplexes sind jedoch nicht statisch. In den fein verzweigten Blattadern 4.-7. Ordnung (minor veins) photosynthetisch aktiver Blätter dominiert der Einstrom der Assimilate in die Siebelemente (Netto-Assimilatexport, van Bel, 1993). Dort stehen die, im Vergleich zu den Siebelementen, sehr großen Geleitzellen im direkten Kontakt mit den Mesophyllzellen, Phloemparenchymzellen oder Bündelscheidenzellen (Abb. 1.3; van Bel und Ehlers, 2000). Diesen Bereich des Phloems nennt man Sammel- bzw. Beladungsphloem. Blattadern 1.-3. Ordnung (major veins) transportieren dann die Assimilate zur Sprossachse und von dort aus in die Assimilat-verbrauchenden Zellen oder in Speichergewebe. Relativ große Siebelemente mit kleinen assoziierten Geleitzellen charakterisieren diesen Teilabschnitt des so genannten Transportphloems (Abb. 1.3). Es besitzt eine duale Funktion. Zum einen müssen aus dem SE/CC Komplex „heraussickernde“ Assimilate für den Weitertransport wieder aufgenommen werden und zum anderen muss eine bedarfsgerechte axiale Verteilung der Assimilate z.B. im Stängel, für die Versorgung der umliegenden Gewebe sichergestellt werden (van Bel und Ehlers, 2000). In den terminalen Sink-Geweben der Pflanze (Orte des Verbrauchs wie z.B. Wurzeln, Blüten und Samen) endet das Phloem und entlässt die Photoassimilate sowie Wasser. Diesen Bereich des Phloems nennt man Entladungsphloem. Im gesamten Verlauf des SE/CC Komplexes durch den Pflanzenkörper werden die Aufnahme als auch die Abgabe von Photoassimilaten von kompensatorischen Ionen- und Wasserflüssen zur Kontrolle des osmotischen aber auch des elektrischen Potentials begleitet.

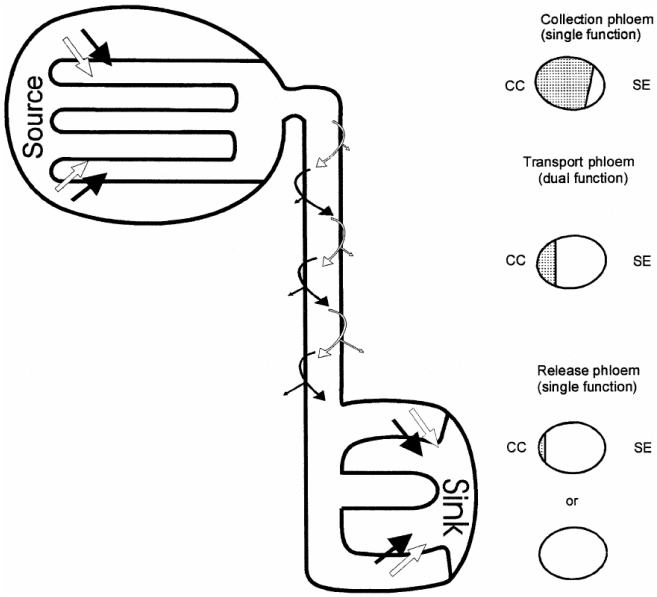


**Abb. 1.3: Größenverhältnis zwischen den Siebelementen und den Geleitzellen in den einzelnen Abschnitten des Phloems, modifiziert nach van Bel und Ehlers, 2000.**

Im Sammelphloem dominiert der Einstrom, während im Entladungsphloem der Ausstrom von Assimilaten vorherrschend ist. Das Transportphloem erfüllt eine zweifache Funktion: je nach Bedürfnissen der Pflanze muss eine Balance zwischen Einstrom und Ausstrom der Assimilate gefunden werden. Das Größenverhältnis zwischen SE und CC scheint dem Energiebedarf des SE/CC Komplexes zu folgen. Wo ein hoher Energiebedarf in Form des elektrochemischen Protonengradienten für die Aufnahme von Assimilaten besteht, nimmt die Größe der Geleitzellen im Verhältnis zu den Siebröhren zu.

Über den osmotisch generierten Druckunterschied zwischen Bereichen der Phloembeladung in photosynthetisch aktiven Blättern (Source; Netto-Assimilatexporter) und Bereichen der Phloementladung in heterotrophen Organen (Sink; Netto-Assimilatimporter) werden die Produkte der Photosynthese und anorganische Nährstoffe mittels eines Wasser-getriebenen Massenstroms durch das Phloem transloziert. Durch die Anatomie der Siebzellen wird sowohl ein Volumenstrom durch ihr Lumen ermöglicht als auch der Zellturgor aufrechterhalten (van Bel, 2003). Dabei können Transportgeschwindigkeiten von 40 bis 100 cm pro Stunde erreicht werden (Canny, 1975; Fisher, 1990). In Abhängigkeit von der Lage der Source- und Sinkgewebe innerhalb der Pflanze kann der Transport prinzipiell in jede Richtung stattfinden (Wright *et al.,* 2003). Bereits 1930 formulierte Münch diese Druck-Strom Hypothese (Münch, 1930), die bis heute im Wesentlichen ihre Gültigkeit behalten hat (van Bel, 1995).

## 1.2 Funktionen des Phloems

Quantitativ gesehen wird im Phloem vor allem Wasser transloziert, welches in einem Kreislauf, gebildet aus Xylem und Phloem, in der Pflanze zwischen Spross und Wurzel zirkuliert. Während des Transports durch den Pflanzenkörper ermöglichen spezialisierte Transferzellen den Austausch von Ionen und Wasser zwischen den Xylem- und den Phloemgefäßen (Taiz und Zeiger, 1998; de Boer und Volkov, 2003).

Den Hauptbestandteil gelöster Substanzen im Phloemsaft nehmen nicht-reduzierende Zucker (wie z.B. Disaccharide und Zuckeralkohole) ein. In vielen Pflanzenarten, wie z.B. der Ackerschmalwand (*Arabidopsis thaliana*), dem Mais (*Zea mays*), der Zuckerrübe (*Beta vulgaris*) und dem Tabak (*Nicotiana tabacum*), wird assimiliertes $CO_2$ ausschließlich in Form von Saccharose transportiert. Stachyose und Raffinose stellen dagegen bei Kürbissgewächsen (Cucurbitaceae) eine der wichtigsten Transportzucker dar (Kandler und Hopf, 1982; Keller und Pfarr, 1996), während Rosaceaen und Plantaginaceaen reduzierte Monosaccharide wie Sorbitol und Mannitol transportieren (Barker, 1955; Webb und Burley, 1962; Zimmermann und Ziegler, 1975). Der Vorteil dieser Transportzucker liegt in ihrer hohen Löslichkeit bei niedrigem Beitrag zur Viskosität des Phloemsafts. Außerdem sind sie chemisch inert und nicht Bestandteil des primären Stoffwechsels. Deshalb können sie in hohen Konzentrationen

transportiert und gespeichert werden, ohne die Zellen zu schädigen und ohne selbst modifiziert oder abgebaut zu werden.

Neben Zuckern werden Aminosäuren und anorganische Ionen, v. a. Kalium, in großen Mengen zur Versorgung der Pflanze umverteilt (Ohshima *et al.,* 1990; Riens *et al.,* 1991; Winter *et al.,* 1992; Lohaus *et al.,* 1994, 1998; Lohaus und Moellers, 2000). Aber auch Phytohormone und Makromoleküle, wie Nukleinsäuren und Proteine, werden im Phloemsaft gefunden (Ziegler, 1975; Golecki *et al.,* 1998, 1999; Jorgensen *et al.,* 1998; Imlau *et al.,* 1999; Ruiz-Medrano *et al.,* 1999; Thompson und Schulz, 1999; Xoconostle-Cazares *et al.,* 1999; Hayashi *et al.,* 2000). Anhand dieser Befunde wird vermutet, dass im Phloemstrom diese Signalmoleküle zwischen den Organen der Pflanze weitergegeben werden, um im Zielorgan entwicklungsspezifische und regulatorische Prozesse anzustoßen (Crawford and Zambryski, 1999; van Bel, 2003). Ebenso findet man sekundäre Pflanzenstoffe (z.B. Salizylsäure), kleine RNA-Spezies, Peptide (Systemin) und sogar Proteine, die nach einem Pathogenbefall produziert werden, um über die Sieberöhren eine systemische Resistenz (SAR, Systemic Aquired Resistance) in der gesamten Pflanze auszulösen (Murray und Christeller, 1995; Ryals *et al.,* 1996; Christeller *et al.,* 1998; Hartmann, 1999; Dannenhoffer *et al.,* 2001). Andere Pathogene wie z.B. Pflanzenviren haben sich soweit den strukturellen und funktionellen Gegebenheiten im Phloem angepasst, dass sie in der Lage sind, die Siebelemente als Vehikel zur Einnahme des gesamten Pflanzenkörpers zu benutzen (Nelson und van Bel, 1998; Oparka und Santa Cruz, 2000). Durch Verwundung und Insektenfraß breiten sich Aktionspotentiale entlang der Siebelemente aus, ähnlich wie in den Nervenbahnen von Tieren (Rhodes *et al.,* 1996). Durch die Arbeiten der letzten Jahre wird immer deutlicher, dass das Phloem weit mehr darstellt als nur ein Transportweg für Assimilate, sondern dass es ebenso wichtig für die Vermittlung von Langstreckensignalen in der Pflanze ist (Ruiz-Medrano *et al.,* 2001; van Bel, 2003).

## 1.3 Phloembeladung

Mesophyllzellen ausgewachsener Blätter stellen den Hauptsyntheseort von Zuckern dar. Der Überschuss an produzierten Assimilaten wird dem Phloem zugeleitet und in heterotrophe Gewebe wie Wurzel, Knollen, Blüten oder Samen befördert. Zunächst müssen diese

Assimilate jedoch von den Mesophyllzellen zum SE/CC Komplex gelangen, wo z.B. Saccharose in Konzentrationen von einigen hundert millimolar bis zu mehr als 1,5 molar akkumuliert werden kann (Lohaus *et al.,* 1994, 1995). Reichlich vorhandene Plasmodesmen ermöglichen den Transport auf symplastischen Weg bis zu den Bündelscheiden oder den Phloemparenchymzellen (van Bel, 1993; Turgeon, 2000). Diese Hypothese wird durch eine Export-defiziente Maismutante (sxd1) gestützt, die aufgrund ihrer strukturell deformierten Plasmodesmen zwischen den Bündelscheidenzellen und den Phloemparenchymzellen kaum noch Photoassimilate aus dem Blatt exportieren kann (Russin *et al.,* 1996; Botha *et al.,* 2000; Mezitt-Provencher *et al.,* 2001).

Die eigentliche Beladung des SE/CC-Komplexes ist unter den Gefäßpflanzen nicht universell, sondern kann prinzipiell auf zwei verschiedenen Wegen erfolgen: **1)** Apoplastische Beladung: Die Assimilate verlassen den Symplasten und werden mit Hilfe von sekundär aktiven Symportern (Cotransportern) im SE/CC Komplex, unter Ausnutzung des elektrochemischen Protonengradienten, im Phloem akkumuliert. **2)** Symplastische Beladung: Plasmodesmen geleiten die Assimilate durch symplastischen Transport direkt bis in die Siebelemente.

Anatomisch gesehen kann man einen offenen und einen geschlossenen Phloemtyp unterscheiden (Gamalei, 1989; van Bel, 1993). Beim geschlossenen Typ ist der SE/CC-Komplex von den Mesophyll- und Bündelscheidenzellen symplastisch isoliert, während beim offenen Typ zahlreiche Plasmodesmen auf dem Weg von den Mesophyllzellen bis in die Siebelemente eine symplastische Verbindung ermöglichen. Das Vorhandensein dieses symplastischen Kontinuums konnte durch die Injektion von membranimpermeablen Fluoreszenzfarbstoffen, die sich nur im Symplasten fortbewegten, nachgewiesen werden (Madore *et al.,* 1986; van Bel *et al.,* 1988). Dabei korreliert der offenen Phloemtyp mit einer symplastischen Phloembeladung und der geschlossene Phloemtyp mit einer apoplastischen Phloembeladung (van Bel, 1993; Stitt, 1996; Turgeon, 1996; Sauer, 1997; Oparka und Turgeon, 1999). Diese Klassifizierung wurde aufgrund der Häufigkeit von Plasmodesmen zwischen dem SE/CC-Komplex und den umgebenen Zellen getroffen. Experimentell konnte diese Einteilung bisher noch nicht verifiziert werden, zumal auch innerhalb einer Pflanze mehrere verschiedene Typen von SE/CC-Komplexen vorkommen können (van Bel *et al.,* 1988, 1992). Eine Koexistenz dieser beiden Beladungsstrategien ist wahrscheinlich und kann anhand bisheriger Studien nicht ausgeschlossen werden (Lalonde *et al.,* 2003).

### 1.3.1 Symplastische Phloembeladung

Der Mechanismus der symplastischen Phloembeladung ist weitgehend unbekannt. Eine Reihe von Modellen versuchen die Assimilatakkumulation und –selektivität bei dem entscheidenden symplastischen Transportschritt in den SE/CC-Komplex zu erklären. Das einfachste Modell beschreibt den Transport von Saccharose (und anderen Assimilaten) als symplastische interzelluläre Diffusion über Plasmodesmata entlang eines Zuckerkonzentrationsgradienten (Altus und Canny, 1985; Turgeon und Medville, 1998). In Pflanzen, wo dieser symplastische Weg angenommen wird, sind die Geleitzellen über relativ wenig Plasmodesmata mit den umgebenden Bündelscheiden- und Mesophyllzellen verbunden. In diesem Fall werden die Geleitzellen als „gewöhnliche“ Geleitzellen bezeichnet und sie treten vor allem in Farnen und Gymnospermen sowie in primitiven Angiospermen auf (van Bel, 1999).

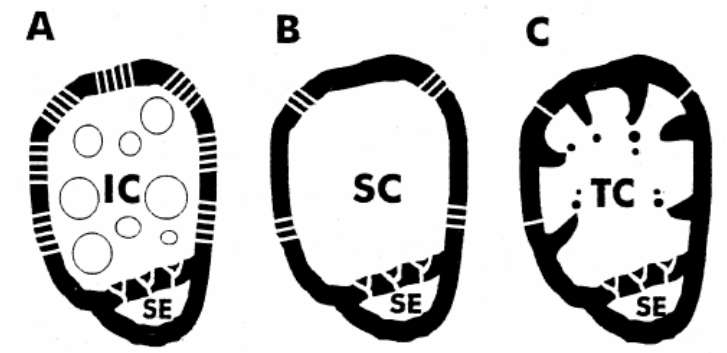


| Number of plasmodesmata | Large >10 per µm² | Intermediate 10–0.1 per µm² | Small <0.1 per µm² |
|---|---|---|---|
| Uphill sugar gradient | Gentle | No | Steep |
| Predominant transport sugars | Sucrose; galactosyl-oligosaccharides | Mainly sucrose, possibly sugar alcohols | Mainly sucrose |

**Abb. 1.4: SE/CC Komplexe in den Feinadern von Angiospermenblättern, modifiziert nach van Bel, 1999.**
Unterscheidung zwischen drei Geleitzellentypen anhand von subzellulären Strukturen und der Plasmodesmen-Häufigkeit:

A) Intermediärzellen (IC) mit fragmentierten Vakuolen und unbekannten Vesikeln (Typ 1 laut der Klassifizierung von Gamalei, 1989).
B) Gewöhnliche Geleitzellen (SC) mit normalem Aufbau (Typ 1-2a, 2a nach Gamalei, 1989).
C) Transferzelle (TC) mit starken Zellwand Einstülpungen und wenigen Plasmodesmen (Typ 2b nach Gamalei, 1989).

Höher entwickelte Pflanzen mit offener Phloemanatomie transportieren in ihren Siebzellen oft neben Saccharose noch andere Zucker, wie Raffinose-Oligosaccharide. Sie weisen einen spezialisierten Geleitzellentyp auf, den man Intermediär- oder Übergangszelle nennt (Turgeon

*et al.*, 1993). Diese Zellen sind durch zahlreiche Plasmodesmen mit den sie umgebenden Bündelscheiden- und Phloemparenchymzellen verbunden. Für Pflanzen, die vor allem Raffinose und Stachyose neben Saccharose transportieren und diese Intermediärzellen besitzen, entwickelte Turgeon (1991, 1996, 2000) das Polymer-Fallen Modell (Abb. 1.5). Hierbei dienen die Intermediärzellen als „Molekülfallen". Saccharose, die in diese Zellen diffundiert, wird mit dem dort synthetisierten Galactinol zu Raffinose oder Stachyose umgewandelt. Turgeons Konzept basiert darauf, dass Raffinose und Stachyose zu groß seien (ca. 500 Dalton), um über die Plasmodesmen zurück zu diffundieren. Dies soll zu der notwendigen Akkumulation dieser Raffinose-Oligosaccharide im SE/CC Komplex führen und so die Vorraussetzungen für die Druck-Strom Hypothese von Münch (1930) erfüllen. Gestützt wird das Polymer-Fallen Modell durch die PCMBS (Para-Chloromercuribenzenesulphonic-acid) Unempfindlichkeit dieses Transportwegs. Dieser unspezifische membranimpermeable Sulfhydrylgruppenblocker für Plasmamembran Transporter wird als Routinetest auf eine apoplastische Beladung verwendet.

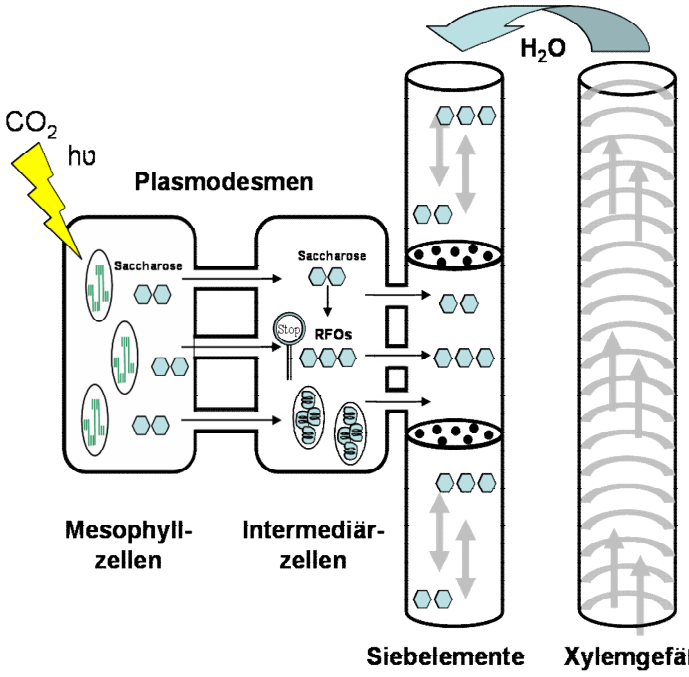


**Abb. 1.5: Schema der symplastischen Phloem-beladung (Polymer-Fallen Modell)**
Die im Mesophyll synthetisierte Saccharose gelangt über zahlreich vorhandene Plasmodesmen auf symplastischem Weg bis in die Intermediärzellen. Nach dem Polymer-Fallen Modell (Turgeon, 1991, 1996) reagiert die Saccharose dort mit Galactinol zu Raffinose-Oligosacchariden (RFOs). Diese Tri- (Raffinose) und Tetra-saccharide (Stachyose) sind zu groß, um über die Plasmodesmen zurückzu-diffundieren. Diese Anreicherung im SE/CC Komplex soll damit die Translokation der Zucker über das Phloem ermöglichen.

Bisher konnte allerdings noch nicht gezeigt werden, dass Plasmodesmata zwischen Saccharose und Raffinose unterscheiden können. Außerdem liegen die Ausschlussgrößen von Intermediärzellen-Plasmodesmata im Bereich von 1 K Dalton und nicht bei 500 Dalton, was für die selektive Aufnahme von Raffinose gegenüber Saccharose notwendig wäre (Robards und Lucas, 1990). Andererseits konnte jedoch gezeigt werden, dass Plasmodesmen eine

komplexe Struktur aufweisen und eine dynamische Kontrollstation für interzelluläre Diffusion von kleinen Molekülen darstellen können (Lucas *et al.*, 1993, 2004).

Ein alternatives Modell von Gamalei und van Bel nimmt Bezug auf den Hauptsynthese Ort von Stachyose, das Mesophyll. Hierbei wird die Stachyose bereits in den Mesophyllzellen in das endoplasmatische Retikulum aufgenommen, das sich vom Mesophyll bis in die Übergangszellen erstreckt.

Der Mechanismus der symplastischen Phloembeladung ist nicht endgültig geklärt, zumal in den letzten Jahren auch in potentiell symplastischen Beladern cDNAs von $H^+$/Saccharose-Symportern kloniert und im Phloem lokalisiert wurden (Knop *et al.*, 2001).

### 1.3.2 Apoplastische Phloembeladung

Im Gegensatz zur symplastischen Phloembeladung ist die apoplastische Phloembeladung ein Energie verbrauchender Prozess. Bereits vor etwa 30 Jahren wurde diese Beladungsvariante postuliert (Sovonick *et al.*, 1974; Giaquinta, 1976, 1977; Fondy und Geiger, 1977; Komor *et al.*, 1977). Pflanzen, die diesen Phloembeladungstyp nutzen, translozieren ausschließlich Saccharose und/oder Polyole als Transportzucker (Moing *et al.*, 1997; Noiraud *et al.*, 2000, 2001; Ramsperger-Gleixner *et al.*, 2003). Ihre Geleitzellen sind oft, aber nicht notwendiger Weise, zu Transferzellen ausgebildet. Fingerartige Einstülpungen der Zellwand und meist eine geringen Anzahl an Plasmodesmen zu den umgebenden Zellen charakterisieren diesen Geleitzelltyp (Abb. 1.4; van Bel, 2003 und Referenzen darin). Durch diese Einstülpungen wird die Oberfläche der Plasmamembran stark vergrößert und damit ihre Transportkapazität aus dem Apoplasten erhöht. Kommt zu diesen morphologischen Gegebenheiten noch eine PCMBS Sensitivität des Zuckerexports aus dem Blatt, dann geht man von einer apoplastischen Beladung des SE/CC Komplexes aus.

Vor der Phloembeladung müssen die Assimilate jedoch erst in den Apoplasten gelangen. Über die Natur dieses Exportprozesses und die beteiligten Zellen ist bis jetzt nur wenig bekannt. Auch hier gibt lediglich die Export defiziente Maismutante sxd1 einen Hinweis auf den Entladungsort. Da die Plasmodesmen dieser Mutante zwischen den Bündelscheidenzellen und den Phloemparenchymzellen unterbrochen sind und damit der Export gestört ist, wird

vermutet, dass die Entladung der Assimilate in den Phloemparenchymzellen statt findet (Russin *et al.,* 1996). Prinzipiell kommen dabei eine einfache oder erleichterte Diffusion sowie ein energieabhängiger Transportmechanismus in Frage.

Schätzungen der Saccharose Konzentration im gesamten Blattapoplasten liegen bei 1 bis 5 mM (Delrot *et al.,* 1983; Tetlow und Farrar, 1993; Lohaus *et al.,* 1995, 2001; Voitsekhovskaja *et al.,* 2000). Lalonde *et al.* (2003) gehen aber in der Nähe des feinadrigen Beladungsphloems von einer apoplastische Konzentration von 27 bis 133 mM aus. Der pH-Wert des Apoplasten liegt zwischen 5 und 6 (Grignon und Sentenac, 1991; Tetlow und Farrar, 1993; Mühling *et al.*, 1995; Savchenko *et al.*, 2000), während die Phloemzellen selbst einen stabilen pH-Wert von ca. 7,5 besitzen. Dieser Protonengradient wird von Plasmamembran $H^+$-ATPasen in den Geleitzellen unter Verbrauch von ATP aufgebaut (DeWitt *et al.,* 1991; Bouche´-Pillon *et al.,* 1994; DeWitt und Sussman, 1995; Zhao *et al.,* 2000). Saccharose-, Polyol- und Aminosäuretransporter in der Plasmamembran des SE/CC Komplexes nutzen diesen elektrochemischen Protonengradienten, um im Symport mit Protonen die entsprechenden Assimilate ins Phloem zu laden.

### 1.3.3 Sekundär aktive Transporter des Phloems

Jahrzehnte lang konnte der Zuckertransport in verschiedensten Pflanzenarten meist nur biochemisch studiert werden. Mit dem PCMBS-Test konnten viele Pflanzenarten ausgemacht werden, die ihre Metabolite mit Hilfe von Membranproteinen in das Phloem transportieren. Unter ihnen befinden sich sowohl Monokotyledonen (z.B. Thompson und Dale, 1981; van Bel *et al.,* 1992, 1994; Ng und Hew, 1996) als auch Dikotyledonen (z.B. Giaquinta, 1976; Turgeon und Wimmers, 1988; Bourquin, Bonnemain und Delrot, 1990; van Bel *et al.,* 1992, 1994; Flora und Madore, 1996; Moing, Escobar-Gutierrez und Gaudillere, 1997; Goggin, Medville und Turgeon, 2001). Die Identifizierung des ersten Saccharosetransporter Gens (*SoSUT1*, *Spinacia oleracea* sucrose transporter) durch die Komplementation von Hefemutanten mit einer cDNA-Expressionsbibliothek aus dem Spinat, erlaubte es zum ersten Mal die biochemisch gewonnenen Beobachtungen mit den genetischen Informationen und heterologen Aufnahmestudien zu vergleichen (Riesmeier *et al.,* 1992, 1993). Mittlerweile sind fast 50 Saccharosetransporter aus unterschiedlichsten Pflanzenarten bekannt (Abb. 1.5; vgl.:

Kühn *et al.*, 2003). Sie werden entweder SUT (sucrose transporter) oder SUC (sucrose carrier) genannt. Phylogenetisch unterscheidet man drei Unterfamilien an Saccharosetransportern benannt nach den bereits charakterisierten Saccharosetransportern aus Solanaceaen: SUT1, SUT2 und SUT4 (Abb. 1.6). SUT3 wurde nur in Tabakpflanzen gefunden und später aufgrund seiner Sequenzhomologien und seiner funktionellen Eigenschaften der SUT1-Familie zugeordnet.

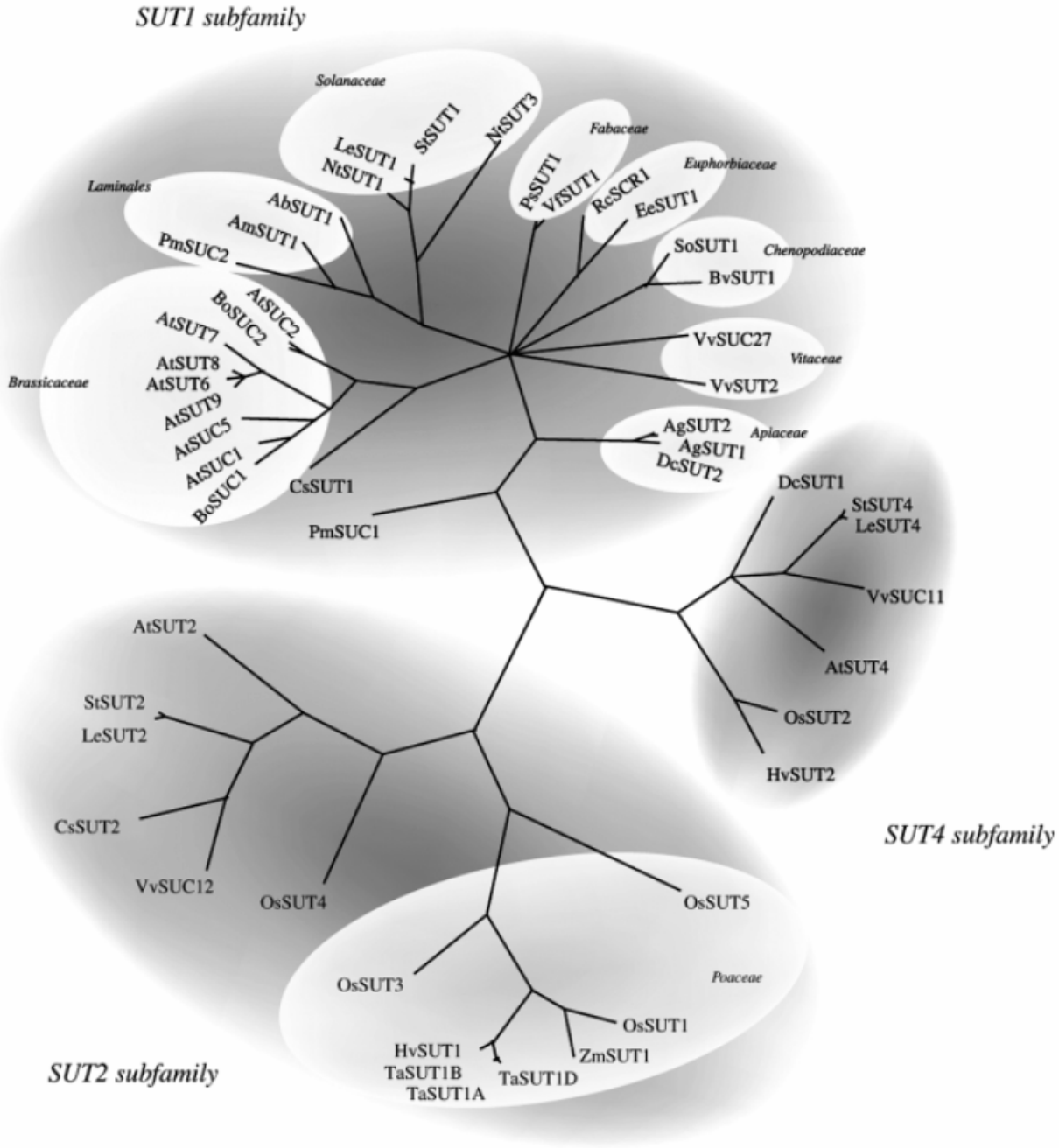


**Abb. 1.6: Phylogenetischer Baum der pflanzlichen Saccharosetransporter-Familie, modifiziert nach Kühn *et al.*, 2003.**

Der Baum wurde basierend auf einen Aminosäuresequenzenvergleich zwischen Saccharosetransportern aus verschiedenen Pflanzen erstellt (Swoford, 1998).

Diese Einteilung spiegelt nicht nur die Sequenzhomologien wieder, sondern reflektiert auch die Substrataffinität sowie die Funktion in der Pflanze wieder. So sind z.B. alle Mitglieder der SUT1-Familie hoch affine Saccharosetransporter mit $K_m$-Werten zwischen 139 µM und 1,5 mM, während die meisten Mitglieder der SUT4-Familie niedrig affine Transporter mit $K_m$-Werten zwischen 5 und 6 mM repräsentieren (Kühn *et al.*, 2003). Die SUT2-Familie kann in zwei Unterfamilien unterteilt werden. Auf der einen Seite alle Transporter, die aus Monokotyledonen stammen und auf der anderen Seite Saccharosetransporter oder Saccharosetransporter-ähnliche Proteine aus Dikotyledonen mit niedriger Substratspezifität und geringer Transportkapazität oder gar keiner Saccharosetransportfunktion (Kühn *et al.*, 2003).

Viele der Transporter sind funktionell durch heterologe Expression in Hefe oder *Xenopus* Oozyten charakterisiert worden (z.B. Riesmeier, 1992, 1993; Gahrtz *et al.*, 1994; Sauer und Stolz, 1994; Boorer *et al.*, 1996; Zhou *et al.*, 1997; Ludwig *et al.*, 2000; Noiraud *et al.*, 2000; Lemoine, 2000; Schulze *et al.*, 2000). Neben den oben genannten Saccharoseaffinitäten der Transporter konnte dabei auch eine gewisse Transportkapazität für Maltose und andere Glucoside gezeigt werden (Chandran *et al.*, 2003). Für den Symport von Saccharose und Protonen wurde eine Stöchiometrie von 1 zu 1 ermittelt (Zhou *et al.*, 1997). Die funktionellen Analysen bestätigten auch die Sensitivität gegenüber dem Sulfhydrylgruppenblocker PCMBS und dem Protonophor CCCP.

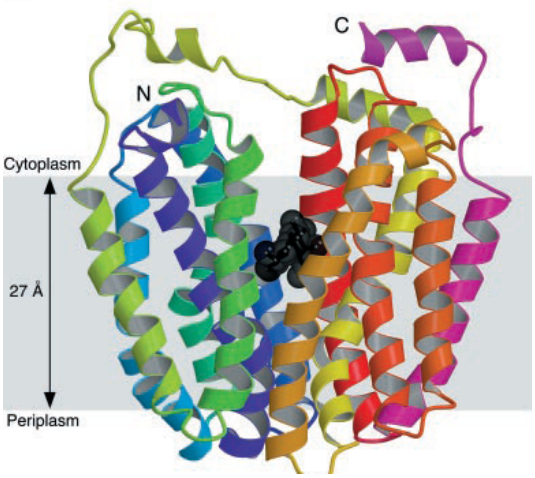


**Abb. 1.7: Überblick Struktur von LacY mit gebundenem Substrat aus E. coli, nach Abramson *et al.*, 2003.**
Die Struktur der Lactosepermease aus E. coli wird wie auch die pflanzlichen Saccharosetransporter in die „major facilitator superfamily“ eingruppiert. Gut sind die zwölf transmembranen Helices zu erkennen, die in zwei sechser Gruppen aufgeteilt sind. Die N-terminale und die C-terminale Hälfte sind durch eine zentrale Schleife miteinander verbunden und bilden zusammen das funktionelle Enzym mit einer zentralen Tasche für die Substratbindung und den Transport.

Alle Saccharosetransporter, die bisher in Pflanzen gefunden wurden, zeigen eine typische Struktur mit zwölf membrandurchspannenden α-Helices und gehören somit der „major facilitator superfamily“ an (Marger und Saier, 1993; Saier, 2000). Erst kürzlich konnte die Struktur einer Lactosepermease aus *E. coli* , die strukturell auch zu dieser Transporterfamilie

gehört und einen Lactose/Protonen-Symport betreibt, mit einer Auflösung von 3,5 Angström bestimmt werden (Abb. 1.7; Abramson *et al.*, 2003). Diese Röntgenstrukturanalyse hat ergeben, dass diese Transporter aus einer N-terminalen und einer C-terminalen Hälfte bestehen, die jeweils sechs transmembrane α-Helices umfassen und durch eine zentrale Schleife verbunden sind. Beide Hälften bilden zusammen das funktionelle Protein mit einer zentralen hydrophilen Tasche für Substratbindung und Transport.

Immunolokalisationsstudien in verschiedenen Pflanzenarten haben die Expressionsorte, der für die Phloembeladung verantwortlichen Saccharosetransporter, in Source-Blättern aufgedeckt. Dabei konnten sowohl in Geleitzellen als auch in Siebelementen Lokalisationssignale detektiert werden. Die wichtigsten Saccharosetransporter im Source-Blatt von *Arabidopsis* scheinen AtSUC2 und AtSUT4 (Truernit and Sauer, 1995; Stadler and Sauer, 1996; Weise *et al.*, 2000), in *Plantago major* PmSUC2 (Stadler *et al.*, 1995), in der Tomate LeSUT1 (Kühn *et al.*, 1997), in der Kartoffel StSUT1 und StSUT4 (Kühn *et al.*, 1997; Weise *et al.*, 2000) sowie im Tabak NtSUT1 (Bürkle *et al.*, 1998) zu sein. Die bisher bekannten Saccharosetransporter unterliegen einem hohen „Turnover“ und exprimieren teilweise in einem diurnalen Rhythmus (Kühn *et al.*, 1997; Delrot *et al.*, 2000). Ihre Aktivität ist außerdem reguliert durch ihr Substrat Saccharose sowie durch Phosphorylierung und Dephosphorylierung (Chiou und Bush, 1998; Roblin *et al.*, 1998).

Der genetischer Beweis für die essentielle Bedeutung dieser $H^+$/Saccharose-Symporter bei der Phloembeladung und dem Langstreckentransport konnte durch antisense-Repression (Riesmeier *et al.*, 1994; Kühn *et al.*, 1996; Lemoine *et al.*, 1996; Bürkle *et al.*, 1998) und Knockout-Pflanzen (Gottwald *et al.*, 2000) erbracht werden. Diese genetischen Veränderungen der Pflanzen resultierten in verlangsamtem Wachstum, schwächerem Knollenertrag bis hin zu Zwergwuchs und Sterilität.

Ein Vergleich der Modelle für die apoplastischen Phloembeladung bei *Arabidopsis* und den Solanaceaen zeigt, dass auch unter den apoplastisch-ladenden Pflanzen Unterschiede auftreten (Abb. 1.8; Kühn *et al.*, 2003). Bei den Solanaceaen geht man davon aus, dass Saccharose die Mesophyllzellen über einen unbekannten Transporter verlässt und über $H^+$/Saccharose-Symporter aus dem Apoplasten in die Siebelemente wieder aufgenommen wird. Bei Arabidopsis hingegen nimmt man zwei apoplastische Schritte an. Saccharose wird aus den Mesophyllzellen in den extrazellulären Raum entlassen und von den Bündelscheidenzellen

wieder in den Symplasten mit Hilfe von Cotransportern aufgenommen. Nach einem symplastischen Transport bis zu den Phloemparenchymzellen verlässt der Zucker wieder den Symplasten und wird in die Geleitzellen über Zuckertransporter aufgenommen.

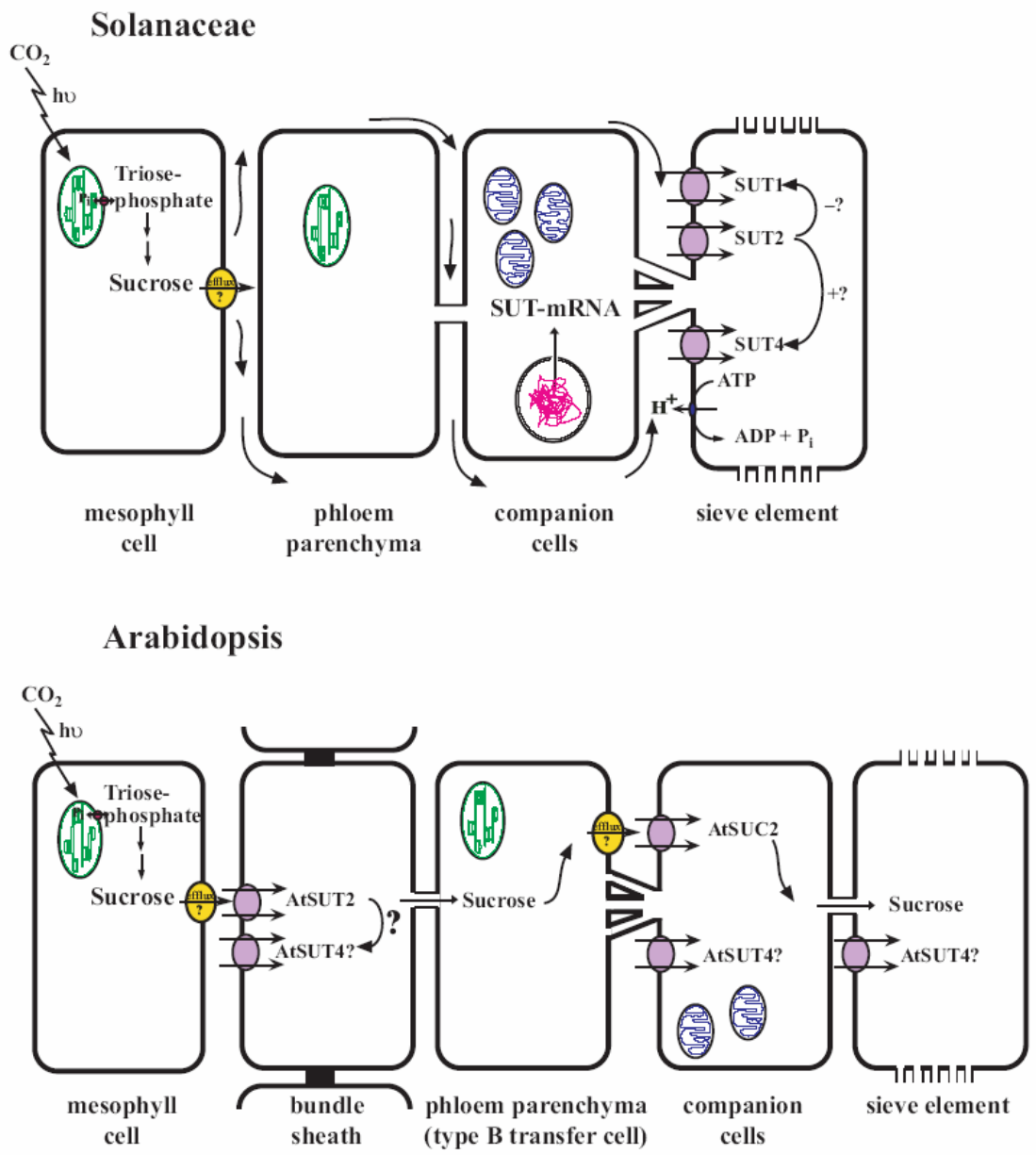


**Abb. 1.8: Vergleich der unterschiedlichen Beladungsmechanismen von Solanaceaen und Arabidopsis, modifiziert nach Kühn *et al.*, 2003.**

In den Solanaceaen sind alle Saccharosetransporter in der Siebzellmembran lokalisiert. Die Saccharose verlässt die Mesophyllzellen und gelangt apoplastisch bis zu den Siebelementen.

Bei *Arabidopsis* werden dagegen zwei apoplastische Schritte vermutet, zum einem an den Bündelscheidenzellen und zum anderen bei der Aufnahme in die Geleitzellen. Wie die Saccharose in den Apoplasten gelangt, ist bisher noch nicht geklärt.

### 1.3.4 Apoplastische Phloementladung

Interessanterweise konnten auch in Sink-Geweben sowohl die Transkripte als auch die Proteine von Saccharosetransportern lokalisiert werden, was auf eine Rolle dieser Transporter bei der Phloementladung hinweisen könnte (Riesmeier *et al.,* 1994; Truernit and Sauer, 1995; Kühn *et al.,* 1997; Weber *et al.,* 1997; Bick *et al.,* 1998; Shakya and Sturm, 1998; Stadler *et al.,* 1999; Lemoine *et al.,* 1999). StSUT1 z.B. wurde in den Siebelementen photosynthetisch aktiver Source-Blätter genauso gefunden wie in sich entwickelnden Sink-Blättern, in der Wurzel sowie in den Wurzelknollen (Kühn *et al.,* 1997; Kühn *et al.,* 2003; Viola *et al.,* 2001). Mit einem antisense Repressionskonstrukt gegen StSUT1 unter der Kontrolle eines knollen-spezifischen Promotors konnten Kühn *et al.* (2003) demonstrieren, dass dieser Saccharosetransporter in der frühen Knollenentwicklung eine wichtige Rolle spielt und damit wahrscheinlich auch bei der Phloementladung. Ähnliche Ergebnisse erbrachte die knollenspezifische Expression einer extrazellulären Hefeinvertase, was darauf hinweist, dass Saccharose auf dem Weg vom SE/CC Komplex zu den Speicherparenchymzellen den Symplasten verlässt und aus dem Apoplasten wieder aufgenommen wird. Weitere Hinweise auf eine apoplastische Phloementladung konnte durch die Lokalisation von $H^+$/Saccharose-Transportern in symplastisch isolierten Geweben gewonnen werden. So exprimieren z.B. VfSUT1 oder PsSUT1 in Samen von Fabaceaen, die vom maternalen Gewebe isoliert vorliegen (Weber *et al.,* 1997; Tegeder *et al.,* 1999). Auch symplastisch isolierte Einzelzellen, wie die wachsenden Pollenschläuche im Tabak, exprimieren einen Saccharosetransporter, NtSUT3 (Lemoine *et al.,* 1999). In allen Fällen muss vor der Wiederaufnahme der Saccharose in die Zelle ein Entladungsschritt in den Apoplasten erfolgen. Zur Erklärung dieses Entladungsschrittes wurden Saccharoseantiporter oder Facilitatorsysteme postuliert, die aber bis heute nicht auf molekularer Ebene beschrieben werden konnten (Patrick, 1994; Patrick and Offler, 1995; Wang *et al.,* 1995; Patrick, 1997; Walker *et al.,* 2000; Lalonde *et al.,* 2003). Um diese Frage zu beantworten, wurde eine weitere Möglichkeit in Betracht gezogen. Basierend auf Lokalisationsstudien von AtSUC2 und AtSUC3 in Source- und Sink-Geweben wurde diesen Transportern eine duale Funktion zugedacht und zwar sowohl bei der Saccharoseakkumulation in Source-Geweben als auch bei der Saccharoseentladung in Sink-Geweben (Truernit and Sauer, 1995; Meyer *et al.,* 2000). Diese Hypothese setzt die Reversibilität dieser Transporter unter Sink-spezifischen Bedingungen voraus, so dass sie dort zu Saccharoseexportern werden. Eine solche Bedingung könnte durch die Expression Zellwand-gebundener Invertasen geschaffen werden. Die Spaltung der Saccharose in Glucose

und Fructose durch Invertasen gewährleistet, dass die apoplastische Saccharosekonzentration permanent auf einem niedrigen Niveau bleibt und somit das Konzentrationsgefälle zwischen dem SE/CC Komplex und dem Apoplasten aufrechterhalten wird (Strum und Tang, 1999; Roitsch *et al.,* 2000, 2003). Die freigesetzten Monosaccharide werden dann über Hexosetransporter in die Speichergewebe aufgenommen (Büttner und Sauer, 2000).

Eine solche Reversibilität wurde bereits 1974 für einen $H^+$/Hexose-Symporter aus *Chlorella* von Komor und Tanner indirekt gezeigt. Die Substrataffinität und die Translokations-konstante dieses Transporters hängen stark vom elektrochemischen Protonengradienten über der Plasmamembran ab, was sowohl einen Import als auch einen Export von Hexosen ermöglicht. Dieser Grünalgen $H^+$/Hexose-Symporter wie auch der $Na^+$/Glucose-Transporter SGLT1 des Menschen und des Hasen verhalten sich bezüglich der Reversibilität des Transports wie eine thermodynamische Maschine (Sauer *et al.,* 2000; Quick *et al.,* 2003).

### 1.3.5 Phloembeladung durch Polyoltransporter

Die Translokation von Polyolen wie Sorbitol oder Mannitol anstatt oder in Kombination mit Saccharose kann ein physiologischer Vorteil für die Pflanze sein. So ist der Transport von stark reduzierten Zuckern in die Wurzel vorteilhaft bei $NADPH^+$-abhängigen Reaktionen, wie z.B. die Reduktion von $NO_3^-$ (Hansch *et al.,* 2001). Für Mannitol wurde auch gezeigt, dass es als Antioxidanz wirken kann oder eine wichtige Funktion bei der Pathogeninteraktion einnimmt (Shen *et al.,* 1997; Jennings *et al.,* 1998). Darüber hinaus ist bei Sellerie die Rolle von Mannitol als Osmoprotektor gut dokumentiert. Der Anstieg der Mannitolkonzentration unter Stressbedingungen ist dabei nicht auf eine höhere Syntheserate zurückzuführen, sondern primär auf die verminderte Degradation von Mannitol und dem ständigen Nachschub aus dem Phloem (Tarczynski *et al.,* 1993; Everard *et al.,* 1994; Stoop und Pharr, 1994a, 1994b). Auch die Phloemmobilität von Bor wird positiv von Polyolen beeinflusst. Sowohl Mannitol als auch Sorbitol können mit Bor lösliche Komplexe bilden, die zu einer höheren Effizienz des Bortransports führen (Penn *et al.,* 1997; Hu *et al.,* 1997).

Trotz dieser wichtigen Funktionen und der offensichtlichen Vorteile für die Physiologie polyoltransportierender Pflanzen ist bisher nur wenig über die Proteine bekannt, die für die Beladung des Phloems mit Polyolen verantwortlich sind. Lediglich zwei cDNAs für

Sorbitoltransporter aus der Sauerkirsche (PcSOT1 und PcSOT2; Gao *et al.*, 2003) und eine cDNA aus Sellerie (*Apium graveolens*), die für einen Mannitoltransporter kodiert, (AgMAT1; Noiraud *et al.,* 2001) wurden bisher kloniert. Eine direkte Beteiligung an der Phloembeladung wird allerdings nur bei AgMAT1 vermutet, wobei man auch hier noch keine eindeutige Lokalisation der AgMAT1 exprimierenden Zellen gezeigt werden konnte (Noiraud *et al.,* 2001). Strukturell gehören Polyoltransporter zur Superfamilie der Monosaccharidtransporter-ähnlichen Transporter (MST), wie z.B. auch die gut untersuchte Unterfamilie der *Arabidopsis* Monosaccharidtransporter (AtSTPs)

Der breitblättrige Wegerich (*Plantago major*) transloziert neben Saccharose (800mM) auch erhebliche Mengen Sorbitol (300mM) in seinen Siebelementen (Lohaus und Fischer, 2002). Er ist sehr resistent gegenüber Umwelteinflüssen wie z.B. Trockenheit und mechanischem Stress. Seine Leitgefäße lassen sich leicht vom umliegenden Gewebe trennen und so Phloem-spezifische mRNA isolieren und quantifizieren oder cDNAs klonieren. Die verantwortlichen Saccharosetransporter PmSUC2 und PmSUC3 wurden bereits auf diese Weise kloniert und charakterisiert (Gahrtz *et al.,* 1994; Stadler *et al.,* 1995a; Barth *et al.,* 2003). In Kapitel VI wird nun zum ersten Mal die Identifikation, zelluläre Lokalisation und biophysikalische Analyse von zwei Phloem-lokalisierten Polyoltransportern (PmPLT1 und PmPLT2) aus *Plantago* beschrieben (Ramsperger-Gleixner *et al.,* 2003).

Obwohl im Phloem von *Arabidopsis* nur Saccharose und kleine Mengen an Raffinose, aber keine Polyole, transloziert werden (Haritatos *et al.,* 2000), wurden im Genom dieser Pflanze ebenfalls sechs Gene MST-ähnlicher Transporter gefunden, die eine signifikante Homologie zu den Polyoltransportern aus Sellerie, Sauerkirsche und Wegerich zeigen. Bisher konnte aber keiner dieser putativen Polyoltransporter funktionell exprimiert werden, was für eine Aussage über die physiologische Rolle dieser Transporter unabdingbar ist. In Kapitel VII konnte nun zum ersten Mal mit AtPLT5 ein Vertreter der MST-ähnlichen Polyoltransporter aus *Arabidopsis thaliana* charakterisiert werden. Mit Hilfe der heterologen Expression von AtPLT5 in Hefe (AG Sauer) und in *Xenopus* Oozyten war es möglich die Spezifität und die Transportkinetik dieses Transporters zu bestimmen. Die Organ-spezifische Expression und die zelluläre sowie die subzelluläre Lokalisation wurden mit RT-PCR Analysen, mit AtPLT5 Promoter::GUS oder Promoter::GFP Pflanzen und mit Anti-AtPLT5 Antiseren von der AG Sauer untersucht.

## 1.4 Phloem-lokalisierte Kaliumkanäle

Mit Hilfe der Aphiden-Technik kann das Membranpotential der Siebröhren abgeleitet werden (Wright and Fischer, 1981; Fromm and Eschrich, 1988). Diese Untersuchungen zeigen, dass die elektrischen Eigenschaften des SE/CC-Komplexes, neben der Beteiligung von $H^+$-ATPasen am elektrochemischen Gradienten, vor allem von einer Kaliumleitfähigkeit bestimmt werden, die durch im Phloem exprimierte Kaliumkanäle aufrechterhalten wird (Riesmeier *et al.,* 1994; Ache *et al.,* 2001, Ivashikina *et al.,* 2003). Durch apoplastische Veränderungen der Protonen-, Kalium- und Kalziumkonzentrationen können diese Kaliumkanäle reguliert werden (siehe unten). Außerdem konnten Ache *et al.* (2001) und Deeken *et al.* (2000 und 2002) zeigen, dass Kaliumkanäle eine wesentliche Rolle bei der Be- und Entladung des Phloems mit Zucker und bei der Remobilisierung des Kaliums aus dem Phloem spielen. Auch der Saccharoseefflux aus den Mesophyllzellen und somit die apoplastische Beladung wird durch eine hohe Kaliumkonzentration im Apoplasten stimuliert, was eine Beteiligung von Kaliumtransportsystemen nahe legt (Schobert *et al.,* 1998).

### 1.4.1 Struktur pflanzlicher Kaliumkanäle

In der Modellpflanze *Arabidopsis thaliana* sind durch die Sequenzierung des Genoms (2000) alle molekular-genetischen Informationen hinsichtlich der primären Struktur pflanzlicher Kaliumkanäle zugänglich. Strukturvorhersagen, basierend auf vergleichenden Sequenzanalysen, haben drei unterschiedliche Strukturklassen von Kaliumkanälen ergeben (Abb. 1.9). Die einfachste Strukturklasse repräsentiert ein einziges Kanalgen in *Arabidopsis*, *KCO3*. Dieser Kanaltyp besitzt zwei transmembrane Domänen, die eine Porenregion flankieren (2TM/1P). Alle bisher untersuchten Organismen, vom Bakterium bis zum Menschen, besitzen diesen Minimalkanal. Selbst im Genom von Pflanzenviren konnte man diesen Kaliumkanaltyp finden (Plugge *et al.,* 2000). Durch eine Verdopplung des KCO3-Motifs ist die zweite Strukturklasse gekennzeichnet (4TM/2P). Aufgrund ihrer zwei Porenregionen werden sie Tandem-Kanäle genannt (TPK, Becker *et al.,* 2004). Im Genom von *Arabidopsis* konnten fünf Vertreter ausgemacht werden, wovon nur TPK1 lokalisiert werden konnte, und zwar im Tonoplasten (Schönknecht *et al.,* 2002; Czempinski *et al.,* 1997).

Die bislang am intensivsten untersuchten Kanalproteine gehören zur Familie der pflanzlichen *Shaker*-Kanäle. Sie bilden die dritte Strukturklasse mit sechs transmembranen Domänen (S1 bis S6) und einer hoch konservierten, amphiphilen Porenregion (P) zwischen der Transmembrane fünf und sechs (Uozumi *et al.*, 1995, 1998). Diese Porenregion taucht in die Membran ein und formt eine hydrophile Pore für den selektiven Transport von Kalium. Die Kalium-Selektivität aller bisher bekannten Kanäle wird durch die Aminosäureabfolge –TTXGY/FG- in der aufsteigenden Seite der Porenschleife maßgeblich bestimmt (Becker *et al.*, 1996).

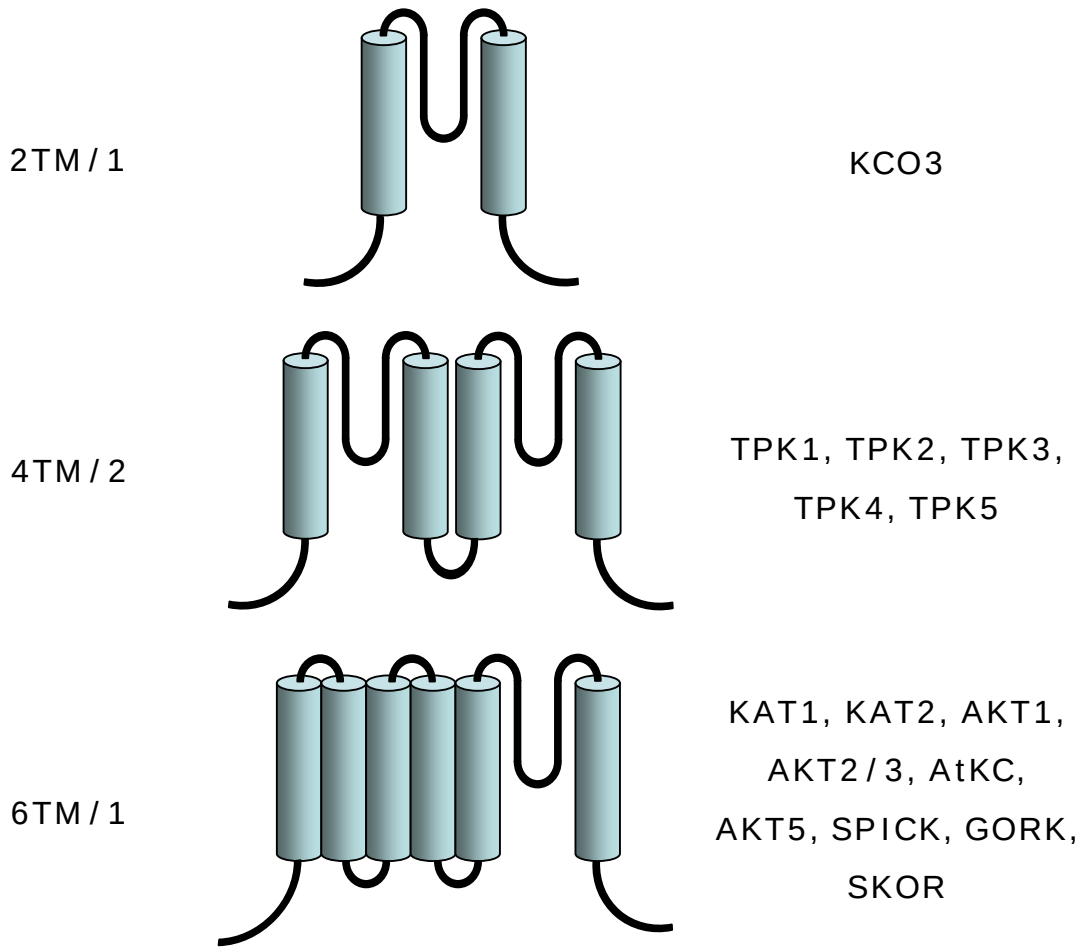


**Abb. 1.9: Strukturmodelle pflanzlicher Kaliumkanäle in *Arabidopsis thaliana***
TM = transmembrane Domäne, P = Porenregion, Der N- und C-Terminus ragen jeweils in das Zytosol

Die transmembrane Domäne S4 ist durch eine Anhäufung positiv geladener Aminosäuren charakterisiert, was in Struktur- Funktionsstudien bei tierischen als auch bei pflanzlichen Kaliumkanälen zur Identifizierung dieser Domäne als Spannungssensor führte (Marten und Hoshi, 1998; Zei und Aldrich, 1998; Bezanilla, 2000; Latorre *et al.*, 2003). Sowohl der N-Terminus als auch der C-Terminus der Proteine ragen in das Cytosol der Zelle. Während der

N-Terminus bei tierischen auswärtsgleichrichtenden Kaliumkanälen für das Inaktivierungsverhalten und die Multimerisierung der Kanaluntereinheiten verantwortlich gemacht wird (Hoshi *et al.*, 1990, 1991; MacKinnon *et al.*, 1993; Kreusch *et al.*, 1998; Papazian, 1999; Bixby *et al.*, 1999; Zerangue *et al.*, 2000), scheint der N-Terminus pflanzlicher Kanäle eine regulatorische Funktion beim spannungsabhängigen Schaltverhalten zu erfüllen (Cao *et al.*, 1995; Marten und Hoshi, 1998). In pflanzlichen *Shaker*-Kanälen, hingegen, besitzt der C-Terminus ein Oligomerisierungsmotiv (Daram *et al.*, 1997; Erhardt *et al.*, 1997). Des Weiteren ist der C-Terminus durch eine Reihe weiterer Domänen charakterisiert. So konnten neben Sequenzmotiven für die Bindung zyklischer Nukleotide (CNB, Hoshi, 1995) noch mögliche Bindestellen für 14-3-3 Proteine (de Boer, 2002) oder für Häm (Tang *et al.*, 2003) sowie Ankyrin-ähnliche Strukturbereiche identifiziert werden.

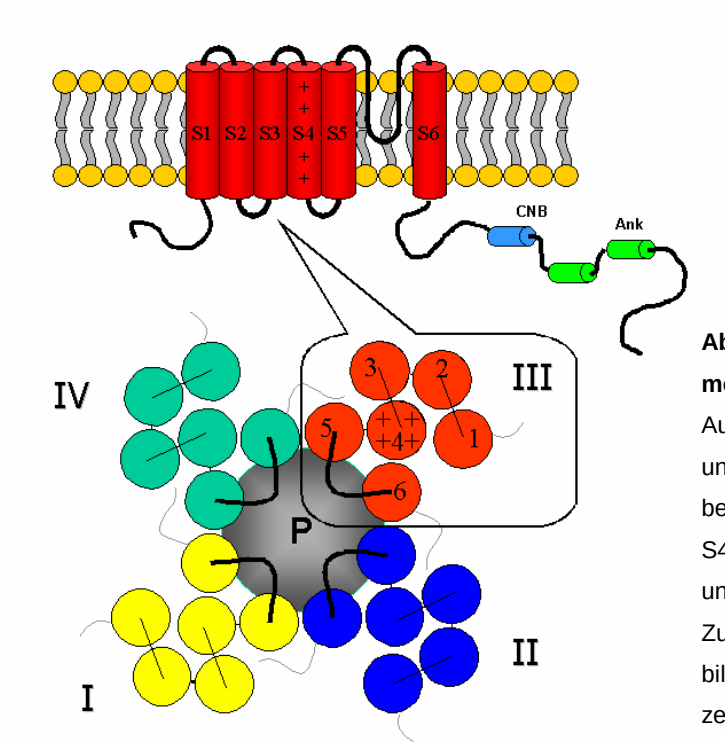


**Abb. 1.10: Topologie- und Tetramerisierungsmodell der *Shaker*-Kaliumkanäle**
Aus sechs transmembranen Helices S1 bis S6 und einer Porenregion zwischen S5 und S6 besteht eine α-Untereinheit eines *Shaker*-Kanals. S4 ist reich an positiv geladenen Aminosäuren und dient als Spannungssensor. Durch die Zusammenlagerung von vier α-Untereinheiten bildet sich ein funktioneller $K^+$-Kanal mit einer zentralen Pore.

Ein kompletter funktionstüchtiger *Shaker*-Kaliumkanal entsteht durch die Aggregation von vier α-Untereinheiten, wobei sich die Porenregionen der einzelnen Untereinheiten zu einer hydrophilen Pore zusammenlagern (Abb. 1.10). Röntgenstrukturanalysen des bakteriellen Kaliumkanals KcsA (*Streptomyces lividans*) und des MthK sowie des KvAP bestätigen den tetrameren Charakter eines funktionellen Kanals (Doyle *et al.*, 1998; Zhorov und Tikhonov, 2004). Coexpressionsstudien in Oozyten von *Xenopus laevis* haben darüber hinaus gezeigt, dass α-Untereinheiten unterschiedlicher, pflanzlicher *Shaker*-Kaliumkänale funktionelle

Heterotetramere bilden können (Dreyer *et al.*, 1997; Baizabal-Aguirre *et al.*, 1999; Paganetto *et al.*, 2001; Pilot *et al.*, 2001; Reintanz *et al.*, 2002). Die biophysikalischen Eigenschaften dieser Heterotetramere sind abhängig von der Zusammensetzung der aggregierten α-Untereinheiten und können somit zur funktionellen Diversität dieser Kanalklasse beitragen.

Die *Shaker*-Superfamilie in *Arabidopsis* umfasst neun Vertreter, die wiederum basierend auf Sequenzhomologien in fünf Unterfamilien aufgeteilt werden kann (Abb. 1.11; Mäser *et al.*, 2001; Very und Sentenac, 2002). Hinsichtlich der Phloemphysiologie sind dabei die Phloem-lokalisierten Vertreter aus zwei Unterfamilien interessant und wurden deshalb im Rahmen dieser Arbeit untersucht:

- Aus der KAT1-Familie sind dies KAT1 selbst, KAT2 ($K^+$-Transporter *Arabidopsis thaliana* 1 bzw. 2) und KZM1 ($K^+$-Transporter *Zea maize* 1).
- Aus der AKT2/3 Unterfamilie wurden AKT2/3 selbst (*Arabidopsis thaliana* $K^+$-Transporter 2/3) und PTK2 (*Populus tremuloides* $K^+$-Transporter 2) sowie ZMK2 (*Zea maize* $K^+$-Transporter 2) im Phloem lokalisiert.

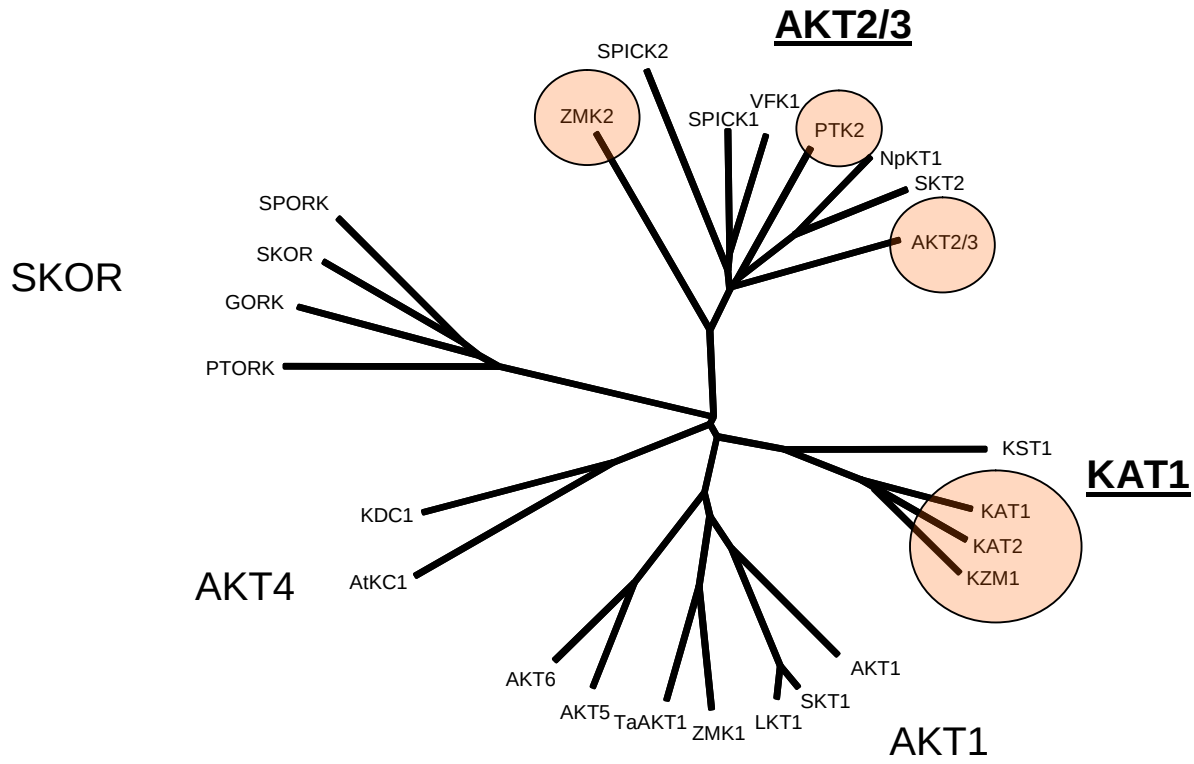


**Abb. 1.11: Phylogenetischer Baum pflanzlicher Kaliumkanäle der *Shaker*-Familie**

Fünf Unterfamilien umfasst die pflanzliche *Shaker*-Familie. Mitglieder aus zwei Familien, der KAT1- und der AKT2/3-Unterfamilie, wurden im Phloem lokalisiert. Die in dieser Arbeit relevanten Kanäle wurden farblich hervorgehoben.

### 1.4.1 Kaliumkanäle der KAT1-Unterfamilie

KAT1 wurde von Anderson *et al.* (1992) durch die Komplementation einer Kaliumtransport defizienten Hefemutante identifiziert und kloniert. Elektrophysiologische Messungen in Hefe und *Xenopus* Oozyten charakterisierten KAT1 als spannungsabhängigen, einwärtsgleichrichtenden, kaliumselektiven Kanal (Schachtmann *et al.*, 1992; Bertl *et al.*, 1995; Hedrich *et al.*, 1995). Diese Analysen zeigten weiterhin, dass elektrophysiologische Eigenschaften, wie die Spannungsabhängigkeit und die Gleichrichtung, vom Protein selbst (intrinsisch) vermittelt werden (Hedrich *et al.*, 1995). Ausgiebige Struktur-Funktionsanalysen mit mutierten KAT1-Kanalproteinen in Oozyten deckten Schlüsselaminosäuren innerhalb der Pore (Aminosäuren L251, T256, T259 und T260) und am Rand der Pore auf (Aminosäure H267), die die elektrophysiologischen Eigenschaften dramatisch veränderten (Becker *et al.*, 1996; Dreyer *et al.*, 1998). Abhängig vom jeweiligen Aminosäureaustausch werden die Permeabilität, die Sensitivität gegenüber Kanalblockern und/oder das spannungsabhängige Schaltverhalten von KAT1 manipuliert. Der Permeationsweg sowie das Selektivitätsfilter pflanzlicher Einwärtsgleichrichter des *Shaker*-Typs besitzen also die gleiche strukturelle und funktionelle Domäne wie die verwandten tierischen Kaliumkanäle (Ichida und Schröder, 1996; Uozumi *et al.*, 1998; Baizabal-Aguirre *et al.*, 1999). Insbesondere die Verschiebung der halbmaximalen Aktivierungsspannung ($U_{1/2}$) ohne eine Veränderung der Einzelkanalleitfähigkeit, deutet auf eine Interaktion der ionenleitenden Pore mit dem Spannungssensor (S4) hin (siehe auch Latorre *et al.*, 2003).

Eine Erhöhung der externen Protonenkonzentration führt in KAT1 zu einer Verschiebung von $U_{1/2}$ zu positiveren Spannungen. Diese Säureaktivierung resultiert bei gleicher Membranspannung in einer höheren Offenwahrscheinlichkeit ($P_o$) des Kanals und somit in einem stärkeren Kaliumeinstrom. In Mutagenesestudien an KST1, einem ebenfalls säureaktivierten Einwärtsgleichrichters der KAT1-Unterfamilie aus der Kartoffel, konnten Hoth *et al.* (1997a) zwei extrazellulär exponierte Histidine identifizieren, die gemeinsam die molekulare Basis für die pH-Sensitivität von KST1 bilden. Entsprechende Mutationen in KAT1 führten jedoch nicht zu einer Veränderung oder zu einem Verlust seiner pH-Abhängigkeit (Hoth und Hedrich, 1999).

Veränderungen der externen Kaliumkonzentration bis in den sub-millimolaren Bereich haben dagegen keinen Einfluss auf das spannungsabhängige Öffnen von KAT1 (Brüggemann *et al.*,

1999). Diese Charakteristik unterscheidet die Kanäle der KAT1-Unterfamilie von Kanälen der AKT2/3- und der SKOR-Unterfamilie (Auswärtsgleichrichter), die ein Kalium-abhängiges Aktivierungsverhalten besitzen (Ache *et al.*, 2000; Gaymard *et al.*, 1998; Geiger *et al.*, 2002). Durch diese Eigenschaft von KAT1 wird ein „hochaffiner" Kaliumeinstrom ermöglicht, sobald das Membranpotential der Zelle negativer als das Umkehrpotential für Kalium ($E_K$) ist. So wurde z.B. gezeigt, dass Kaliumtransport-defiziente Hefemutanten, die mit der cDNA von KAT1 komplementiert wurden, noch bei einer externen Kaliumkonzentration von 10 µM wachsen können. Auch Messungen von Strom-Spannungscharakteristiken an $K^+$-Aufnahmekanälen in Schließzellprotoplasten von *Arabidopsis* haben ergeben, dass auch bei sub-optimaler Kaliumversorgung eine $K^+$-Aufnahme gewährleistet ist, und somit eine Stomaöffnung ermöglicht wird (Brüggemann *et al.*, 1999). Eine ebenso wichtige physiologische Bedeutung bei der Kaliumaufnahme sollten die Vertreter dieser KAT1-Unterfamilie im Phloem spielen (Ivashikina *et al.*, 2003).

Nakamura *et al.* (1995) konnte mit Promotor::GUS transformierten *Arabidopsis* Keimlingen zeigen, dass KAT1 vornehmlich in den Schließzellen exprimiert ist. Weitere Untersuchungen des Expressionsmuster von KAT1 und KAT2 deckten auf, dass die Expression zwischen den *Arabidopsis* Ecotypen stark variiert (Ivashikina *et al.*, 2003). Dies hat zur Folge, dass z.B. im Ecotyp Col-0, KAT2 der dominante Einwärtsgleichrichter im Phloem ist (Pilot *et al.*, 2001), während im Ecotyp C24 KAT1 diese Rolle übernimmt (Ivashikina *et al.*, 2003). Die Tatsache, dass beide Kanäle 72% identische Aminosäuren und daneben identische elektrophysiologische Eigenschaften aufweisen, erklärt die Redundanz im Expressionsmuster zwischen den *Arabidopsis* Ecotypen und weist auf eine Genduplikation im Laufe der Evolution von *Arabidopsis* hin.

KZM1 der orthologe Kaliumkanal in *Zea maize* besitzt ein sehr ähnliches Expressionsmuster wie die beiden *Arabidopsis* Einwärtsgleichrichter. Philippar *et al.* (2003) konnten *kzm1*-Transkripte sowohl im Phloem als auch in den Schließzellen finden (Kapitel IV).

Die elektrophysiologische Charakterisierung von KZM1 und KAT2 in *Xenopus* Oozyten wird später in den Kapiteln IV und IX beschrieben.

## 1.4.2 Die AKT2/3-Unterfamilie

Der einzige Vertreter dieser Unterfamilie in *Arabidopsis* ist AKT2/3 selbst. Bereits 1995 konnten Cao *et al.* die Klonierung von AKT2 durch die Rekonstruktion der cDNA des $K^+$-Kanals aus genomischer DNA beschreiben. Dieser Klon vermochte es, einen $K^+$-Aufnahme defizienten *E.coli* Stamm zu komplementieren (Uozumi *et al.*, 1998), allerdings konnte keine funktionelle Analyse nach heterologer Expression in Oozyten durchgeführt werden. Die Verkürzung am 5´-Ende bis zu einem zweiten Startcodon dieser AKT2-cDNA im gleichen Leseraster, führte zu einem funktionell exprimierenden Kanal, AKT3 (Ketchum *et al.*, 1996). Ob nun der verkürzte AKT3 oder der um 14 Aminosäuren längere AKT2 *in vivo* exprimiert wird, bleibt zu klären.

Marten *et al.* (1999) konnten in einer detaillierten Analyse in *Xenopus* Oozyten AKT3 als Phloem-lokalisierten, schwach spannungsabhängigen und Protonen- sowie $Ca^{2+}$ -sensitiven $K^+$-Kanal beschreiben. Mit diesen einzigartigen elektrophysiologischen Eigenschaften repräsentiert AKT2/3 einen der interessantesten *Shaker*-Kaliumkanäle in *Arabidopsis*, vor allem auch in Hinblick auf die Phloemphysiologie. Durch seine schwache Spannungsabhängigkeit erscheint er bei allen Membranspannungen als „offener" Kanal und ist damit in der Lage sowohl einen Kaliumausstrom als auch einen Kaliumeinstrom zu vermitteln. Außerdem klemmt AKT2/3 aufgrund dieser Charakteristik das Membranpotential der Zellen, in denen er exprimiert ist, zur Kaliumumkehrspannung ($E_K$) und verhält sich somit wie eine Kaliumselektive Elektrode. Auch die Inhibierung der Ströme durch extrazelluläre Protonen wird nicht wie bei Vertretern der KAT1-Unterfamilie über die Verschiebung der spannungsabhängigen Offenwahrscheinlichkeit reguliert, sondern über eine Verringerung der Einzelkanalleitfähigkeit mit steigender Protonenkonzentration. Später wurden dann von Lacombe *et al.* (2000) durch die Injektion der kompletten AKT2-cDNA in *Xenopus* Oozyten diese Beobachtungen auch mit dem längeren Klon bestätigt. Darüber hinaus konnte in dieser Arbeit eine Expression von AKT2/3 sowohl im Phloem von Sink-Geweben als auch im Phloem von Source-Geweben detektiert werden. Das Expressionslevel der Transkripte konnte durch die Gabe des Stressphytohormons Abscisinsäure (ABA) noch gesteigert werden. Außerdem förderte das Screening einer Yeast-Two-Hybrid cDNA-Bibliothek mit der Proteinphosphatase 2C (AtPP2CA) einen möglichen Interaktionspartner von AKT2 ans Tageslicht (Cherel *et al.*, 2002). Diese im ABA-Signalweg involvierte Phosphatase reduzierte in Coexpressionsversuchen AKT2-vermittelte Kaliumströme und verschob die Spannungs-

abhängigkeit in Richtung eines Einwärtsgleichrichters wie z.B. KAT1. Somit scheint AtPP2CA den AKT2-Kanal ABA/Stress-abhängig zu regulieren.

ZMK2 aus Mais wie auch PTK2 aus der Pappel und VFK1 aus der Saubohne stellen die orthologen Vertreter der AKT2/3-Unterfamilie der jeweiligen Pflanzenarten dar (Philippar *et al.,* 1999; Langer *et al.,* 2002; Ache *et al.,* 2001). Der Hauptexpressionsort dieser Kanalproteine liegt wie bei AKT2/3 in den Zellen des SE/CC Komplexes. Bis auf VFK1, der alleine in *Xenopus laevis* Oozyten keinen funktionellen Kanal bildet, sind diese Kaliumkanal α-Untereinheiten heterolog exprimiert und charakterisiert worden. Während VFK1 nur durch Coexpression mit einer KAT1-Selektivitätsmutante (KAT1 T256G) in *Xenopus* Oozyten im Heterotetramer als $K^+$-selektiver Kanal charakterisiert werden konnte, zeigten PTK2 und ZMK2 nach Expression in Oozyten die gleiche schwache Spannungsabhängigkeit wie AKT2/3. Alle drei orthologen Kaliumkanäle der AKT2/3-Unterfamilie teilen ihre weiteren elektrophysiologischen Eigenschaften mit AKT2/3: Sie sind $K^+$-selektive Kanäle, inhibierbar durch extrazelluläre Ansäuerung und spannungsabhängig durch $Ca^{2+}$ geblockt. Bauer *et al.* (2000) haben mit ZMK2 in Patch-Clamp-Untersuchungen an Mais Phloemprotoplasten zum ersten Mal nachweisen können, dass Kanäle mit diesen außergewöhnlichen biophysikalischen Eigenschaften auch *in vivo* in dieser Form zu finden sind.

Erste Hinweise auf die Beteiligung dieser Kaliumkanal-Unterfamilie an der Be- und Entladung des Phloems lieferten Arbeiten von Deeken *et al.* (2000) an AKT2/3 und von Ache *et al.* (2001) an VFK1. Betrachtungen der transkriptionellen Regulation von AKT2/3 erbrachten, dass die Kanalgenaktivierung durch Licht und Photoassimilate gesteuert wird. Eine enge Kopplung zwischen der Kanalaktivität und der Photosynthese belegt auch die Tatsache, dass die Fütterung von Fructose über die Petiole von *Vicia faba* Blättern bereits nach einer Stunde zu einer erhöhten VFK1-Genaktivität und zu einer signifikanten Erhöhung der Kaliumleitfähigkeit in der Phloemmembran führte. Unter diesen VFK1-induktiven Bedingungen dominiert VFK1 die Leitfähigkeit der Siebelemente, so dass bei einer 10-fachen Änderung der $K^+$-Konzentration eine Potentialverschiebung um 53 mV zu beobachten ist. Im Gegensatz zu AKT2/3, der sowohl im Phloem von Source-Blättern als auch in Sink-Geweben zu finden ist (Lacombe *et al.,* 2000), beschränkt sich die Expression von VFK1 auf heterotrophe Gewebe wie z.B. junge Blätter, Blüten und Stängel. Aus diesem Grund wird eine Beteiligung von VFK1 an der Phloementladung angenommen.

All diese, zum größten Teil intrinsischen, Eigenschaften dieser *Shaker*-Kaliumkanalproteine ermöglichen eine Feinregulierung des Kaliumstroms an der Phloemmembran über den extrazellulären und zytosolischen pH-Wert, die $Ca^{2+}$-Konzentration, das Membranpotential sowie der $K^+$-Konzentration. Da ein Teil dieser Kanäle die Fähigkeit besitzen, Heteromere untereinander zu bilden, entscheidet schließlich das Verhältnis der Expressionsraten individueller Untereinheiten im funktionellen $K^+$-Kanal über die physiologischen Eigenschaften des Kaliumtransports über die Phloemmembran.

In den Kapiteln I und II wird detailliert auf Struktur-Funktionsanalysen in *Xenopus* Oozyten und die drei gefundenen Charakteristiken von AKT2/3 eingegangen. Mittels einer AKT2/3 Knockout Pflanze wird die Bedeutung dieses Kaliumkanals in der Phloemphysiologie unterstrichen und seine Funktion durch Coexpressionsexperimente mit AtSUC2 bei der Saccharosebeladung in Oozyten nachgestellt (Kapitel III). Eine Charakterisierung des AKT2/3 orthologen Kanals (PTK2) aus den kambialen Zellen der Pappel wird in Kapitel V gezeigt.

## 1.5 $H^+$-ATPasen energetisieren den Transport über die Phloemmembran

Die meisten Transportproteine in pflanzlichen Zellen ziehen die für den Transport benötigte Energie aus dem elektrochemischen Protonengradienten über der Plasmamembran. Für die Bildung dieses Gradienten ist die Aktivität von ATP-getriebenen Plasmamembran Protonenpumpen ($H^+$-ATPasen) verantwortlich (DeWitt *et al.,* 1991; Bouche´-Pillon *et al.,* 1994; DeWitt und Sussman, 1995; Zhao *et al.,* 2000). Lediglich in der Plasmamembran von Pflanzen und Pilzen sind diese $H^+$-ATPasen zu finden. Sie sind primär aktive Protonentransporter, die mit Hilfe der Hydrolyse von ATP eine Energiequelle für sekundär aktive Transportproteine, wie z.B. für Symporter und Antiporter bereitstellen. Durch das aktive Pumpen von Protonen sorgen $H^+$-ATPasen nicht nur für eine Ansäuerung des Apoplasten zu pH-Werten zwischen 5 und 6, sondern auch für die Verschiebung von positiven Ladungen ($H^+$) vom Zytosol in den extrazellulären Raum. Protonen-ATPasen sind also elektrogene Enzyme, die durch ihre auswärtsgerichtete Pumpaktivität von positiven Ladungen ein negatives Membranpotential (-120 bis -240 mV) aufbauen. Diese gleichzeitige Verschiebung von Ladungen und Masse über die Plasmamembran errichtet einen elektrochemischen Gradienten, der als treibende Kraft zur Aufnahme oder zur Abgabe von Ionen oder Metaboliten durch Transportproteine dient (Serrano, 1989; Sussman, 1994; Michelet and Boutry, 1995; Palmgren, 1998, 2001).

Plasmamembran oder P-Typ $H^+$-ATPasen unterscheiden sich deutlich, hinsichtlich ihrer Biochemie, ihrer Struktur, ihrem Transportmechanismus und ihrer evolutionären Herkunft, von den vakuolären V-Typ und den mitochondrialen F-Typ $H^+$-ATPasen. P-ATPasen sind aus einer einzelnen Polypeptidkette von ungefähr 100 kDa aufgebaut (Vara und Serrano, 1982). Sie wurden mit einem „P“ benannt, um zu unterstreichen, dass dieser Typ von ATPasen eine kovalente Phosphorylierung an einer Aspartatseitenkette während des Transportübergangszustandes (E-P Form) im Reaktionszyklus trägt (Briskin und Poole, 1983; Serrano, 1989). Plasmamembran $H^+$-ATPasen teilen ihre Membrantopologie und ihren Transportmechanismus mit anderen Kationen-ATPasen des P-Typs, aber sie unterscheiden sich deutlich in ihren regulatorischen Eigenschaften. Zu diesen Kationen-ATPasen gehören unter anderem auch die tierischen $Na^+/K^+$-ATPasen, die $Ca^{2+}$-ATPasen aus dem sarkoplasmatischen Retikulum und die $H^+/K^+$-ATPase aus der Magenschleimhaut. All diese

Ionen-Pumpen besitzen eine konservierte Aminosäuresequenz, die das phosphorylierte Aspartat umgibt: DKTGT[L/I/V/M][T/I].

AHA1 und AHA3 waren die ersten beiden Plasmamembran $H^+$-ATPasen und auch gleichzeitig die ersten beiden Transporter überhaupt, die aus *Arabidopsis* kloniert wurden (Pardo und Serrano, 1989; Harper *et al.*, 1989). Weitere Isoformen wurden bald darauf isoliert (Harper *et al.*, 1990, 1994; Houlne und Boutry, 1994) bis schließlich nach dem Abschluss des *Arabidopsis* Genom Sequenzierungsprojekts (2000) fest stand, dass es sich in diesem Organismus um eine $H^+$-ATPasen-Genfamilie mit 12 Vertretern handelt (Palmgren, 2001). Eines dieser Gene (AHA12) repräsentiert allerdings aufgrund von zwei großen Deletionen wahrscheinlich eher ein Pseudogen als eine funktionelle $H^+$-ATPase. Auch im Genom anderer Pflanzenarten wie z.B. *Nicotiana plumbaginifolia* wurden viele Isoformen (9) von $H^+$-ATPasen gefunden (Boutry *et al.*, 1989; Oufattole *et al.*, 2000).

Die einzelnen Isoformen werden abhängig vom Zelltyp, vom Entwicklungsstatus, und von Umwelteinflüssen differentiell exprimiert (Ewing und Bennett, 1994; Harper *et al.*, 1994; Michelet *et al.*, 1994; Moriau *et al.*, 1999; Qufattole *et al.*, 2000). Ein weiterer Unterschied konnte nach heterologer Expression von verschiedenen $H^+$-ATPasen in Hefe gezeigt werden. Zwischen den Isoformen, selbst aus der gleichen Unterfamilie, wurden unterschiedliche Transportkinetiken gefunden (Palmgren and Christensen, 1994; Luo *et al.*, 1999). Der Isoform-spezifische Expressionsort und -zeitpunkt sowie die Isoform-spezifische $H^+$-Transportkinetiken ermöglichen der Pflanze durch diese Vielfalt der $H^+$-ATPasen-Gene eine optimale Anpassung des elektrochemischen Gradienten an veränderliche Umwelt-bedingungen zu finden.

In allen bisher untersuchten Zelltypen sind $H^+$-ATPasen zu finden. Zellen, die auf die Akkumulation von Substanzen aus ihrer Umgebung spezialisiert sind (z.B. Schließzellen und das Phloem), besitzen im Allgemeinen jedoch wesentlich höhere Konzentrationen an Protonenpumpen als andere (Becker *et al.*, 1993). Jede einzelne Protonpumpe macht in einer aufgereinigten Plasmamembranfraktion 1 - 5% vom gesamten Proteingehalt aus (review Sze *et al.*, 1999). Diese große Menge an $H^+$-ATPasen in der Membran kompensiert die niedrigen Transportraten von nur ~100 Ionen pro Sekunde. Cotransporter (300 bis 1000 Ionen pro Sekunde) und Kanäle ($10^6$ bis $10^8$ Ionen pro Sekunde) erreichen wesentlich höhere Transportraten und kommen dem entsprechend weniger häufig vor.

### 1.5.1 Transportmechanismus und Regulation von $H^+$-ATPasen

Es wird angenommen, dass P-ATPasen zwischen zwei Hauptkonformationen, $E_1$ und $E_2$, alternieren (Abb. 1.12; Palmgren, 2001). Die $E_1$ Form besitzt eine hohe Affinität sowohl für das aus dem Zytosol zu transportierende Ion als auch für ATP. Die $E_2$ Form hingegen hat nur eine geringe Affinität für den Liganden und für ATP, jedoch eine hohe Sensitivität gegenüber Vanadat, einem P-Typ spezifischen Blocker (Buch-Pedersen, 2000). Während des Transports eines gebundenen Kations findet eine Konformationsänderung von $E_1$ zu $E_2$ statt. Nach dem Post-Albers Schema (Albers, 1967; Post *et al.*, 1972) wird das Kation auf der zytosolischen Seite an das Protein in der $E_1$ Konformation gebunden. Die Phosphorylierung eines konservierten Aspartatrestes resultiert in der $E_1P$ Form und führt zu einer Konformationsänderung in die $E_2P$ Form, bei der das Kation an der gleichen Bindestelle mit geringerer Affinität gebunden ist. Durch die Konformationsänderung von $E_1P$ zu $E_2P$ steht das Kation zudem in Kontakt mit der anderen Seite der Membran und wird aufgrund der geringeren Affinität in das extrazelluläre Medium entlassen. Danach wird der Phosphatrest am Aspartat hydrolisiert und das Enzym kehrt wieder in die $E_1$ Form zurück.

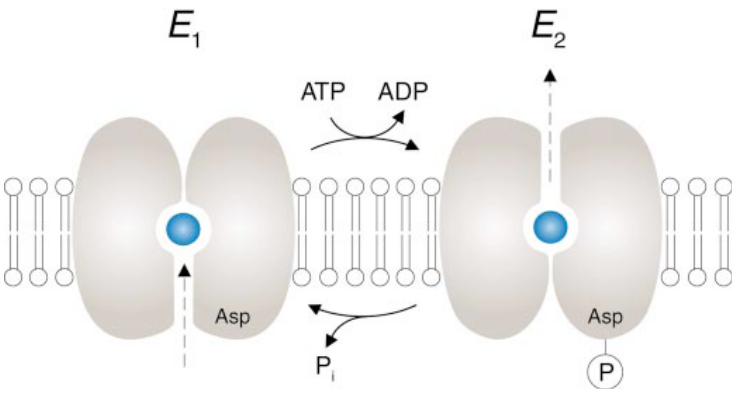


**Abb. 1.12: Schematische Darstellung der beiden Hauptkonformationen $E_1$ und $E_2$ im Reaktionszyklus von P-Typ ATPasen, nach Palmgren, 2001.**
Eine detaillierte Beschreibung des Reaktionszyklus befindet sich im Text.

Im Fall von $H^+$-ATPasen stellen Protonen den Liganden dar, der über die Membran gepumpt werden muss. Kinetische Analysen haben bestätigt, dass die Transportaktivität stark vom internen pH-Wert abhängig ist, was zur Identifizierung eines protonierbaren Aminosäurerestes in der $H^+$-ATPase AHA2 führte (Regenberg *et al.*, 1995). Dieser pH-Sensor verfügt über einen pK-Wert von 6,7 und ermöglicht eine Stabilisierung des Enzyms in der hoch-affinen $E_1$ Konformation. Experimente unter verschiedenen Bedingungen haben außerdem ergeben, dass pro hydrolysiertem ATP ein Proton transportiert wird (Stöchiometrieverhältnis von 1 zu 1) (Birskin *et al.*, 1995; Birskin und Reynolds-Niesman, 1991; Slayman und Sanders, 1985).

Neben diesen intrinsischen Eigenschaften spielt vor allem der C-Terminus (R-Domäne, regulatorische Domäne) von pflanzlichen $H^+$-ATPasen eine wichtige regulatorischen Rolle (Abb. 1.13). Initiale Studien, in denen ein Teil vom C-Terminus durch Proteasen entfernt wurde, konnten zeigen, dass diese Deletion zu einer gesteigerten $H^+$-ATPase Aktivität führte (Palmgren *et al.*, 1990, 1991). Spätere Analysen ergaben, dass die Phosphorylierung eines Threonins oder Serins, der vorletzten Aminosäure am C-Terminus, die Bindung eines 14-3-3 Proteins ermöglicht, wodurch die $H^+$-ATPase aktiviert wird (Fuglsang *et al.*, 1999; Svennelid *et al.*, 1999; Maudoux *et al.*, 2000; Jaspert und Oecking, 2002). Jelich-Ottmann *et al.* (2001) konnten schließlich die Beteiligung eines zweiten amphipatischen helikalen Motivs im C-Terminus an der Bindestelle für das 14-3-3 Protein zeigen. Die Zugabe des Phytotoxins Fusicoccin führt zur irreversiblen Aktivierung der $H^+$-ATPase durch die Stabilisierung dieses Komplexes zwischen dem 14-3-3 Protein und der Bindestelle in der R-Domäne (Baunsgard *et al.*, 1998; Piotrowski *et al.*, 1998; Oecking und Hagemann, 1999; Jaspert und Oecking, 2002). Eine Interaktion zwischen der R-Domäne und der katalytischen Region wird für die Inhibierung der Pumpaktivität verantwortlich gemacht (Sze *et al.*, 1999; Jaspert und Oecking, 2002). Der C-Terminus stellt also eine autoinhibitorische Domäne dar, reguliert über Phosphatasen und Kinasen, die wiederum durch Stimuli wie z.B. Blaulicht, Hormone und Umwelteinflüsse moduliert werden (Kinoshita und Shimazaki, 1999; Kinoshita *et al.*, 2003; Camoni *et al.*, 2000).

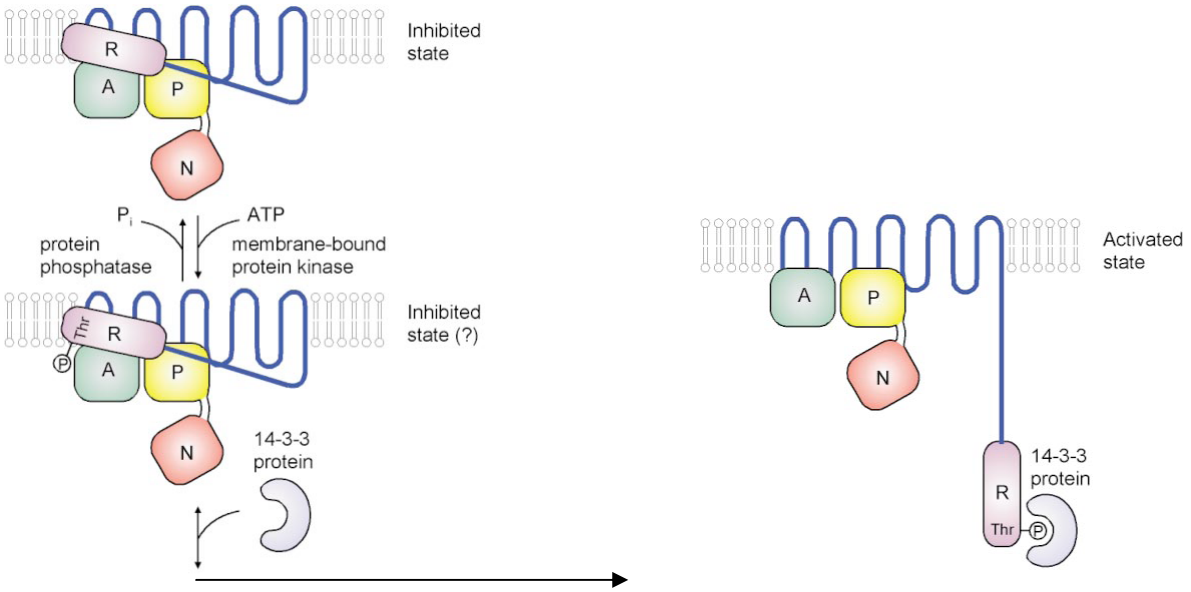


**Abb. 1.13: Modell der posttranslationalen Regulation von $H^+$-ATPasen über die autoinhibitorische Domäne im C-Terminus, nach Palmgren, 2001**

Proteinkinasen und Proteinphosphatasen bestimmen den Phosphorylierungszustand der R-Domäne. Liegt das Threonin in der R-Domäne phosphoryliert vor, so erkennt ein regulatorisches 14-3-3 Protein diese Bindestelle und aktiviert das Enzym.

## 1.5.2 Physiologische Bedeutung der $H^+$-ATPasen beim Phloemtransport

Die Beteiligung pflanzlicher $H^+$-ATPasen an physiologischen Prozessen der Pflanze ist vielfältig. Sie stellen die Ausgangskomponente für den sekundär aktiven Transport über die Plasmamembran dar. Die Beteiligung reicht von der Salz- und Osmotoleranz über die Blatt- und Stomatabewegung, die cytosolische pH-Regulation, das Säure-induzierte Streckenwachstum, das Pollen- und Wurzelhaarwachstum bis hin zum Phloemtransport (Palmgren, 2001 und Referenzen darin).

In ersten Immunolokalisationsstudien haben Parets-Soler *et al.* (1990) und Villalba *et al.* (1991) mit Anti-$H^+$-ATPase Antikörpern zeigen können, dass Protonenpumpen auch im Phloem stark vertreten sind. Später konnten die Expressionsmuster von Promotor::GUS-Reportergenen die Lokalisation der $H^+$-ATPase Isoformen AHA3 aus *Arabidopsis* und PMA4 aus *N. plumbaginifolia* im Phloem nachweisen (Desbrosses *et al.*, 1998; Moriau *et al.*, 1999). Eine zelluläre Lokalisation gelang schließlich durch die Expression von AHA3 in transgenen Pflanzen nach Fusion mit einem viralen Epitop (DeWitt und Sussman, 1995). In diesen Lokalisationsstudien wurde AHA3 in den Geleitzellen der Phloemgefäße detektiert. Diese sind reich an Mitochondrien, die in der Lage sind große Mengen an ATP für die Pumpaktivität der ATPasen bereitzustellen. In *Arabidopsis* (Stadler und Sauer, 1996; Truernit und Sauer, 1995) sowie in *Plantago major* (Stadler *et al.*, 1995) werden auch die $H^+$/ Saccharose-Symporter in der Plasmamembran der Geleitzellen gefunden, die energetisiert durch den elektrochemischen Protonengradienten Zucker akkumulieren können. Durch Diffusion über PPUs gelangen die Zucker schließlich von den Geleitzellen in die Siebelemente.

Bei den Solanaceaen findet man eine andere Konstellation. Hier sind die Saccharose-transporter ausschließlich in den Siebzellen lokalisiert (Kühn *et al.*, 1997). $H^+$-ATPasen konnten jedoch in Siebelementen bisher nicht nachgewiesen werden. Außerdem durchlaufen diese Zellen eine partielle Autolyse während ihrer Differenzierung zu Siebelementen, bei der sie unter anderem auch eine Großzahl ihrer Mitochondrien verlieren. Durch die zahlreichen Plasmodesmen sollte allerdings eine elektrische Kopplung des SE/CC Komplexes sowie eine ausreichende Diffusion für Protonen sichergestellt sein, so dass der Saccharose/Protonen-Symport energetisiert werden kann.

Ein direkter genetischer Beweis für die essentielle Beteiligung von Plasmamembran $H^+$-ATPasen bei der Phloembeladung gelang durch die Generierung von transgenen *N. plumbaginifolia* Pflanzen (Zhao *et al.,* 2000). Die Cosuppression der $H^+$-ATPase Isoform PMA4 bewirkte ein reduziertes Pflanzenwachstum, gestörte Stomaöffnung und die Akkumulation von Zuckern im Blatt. Das defiziente Zuckertranslokationsvermögen wurde auch bei Pflanzen beobachtet, die durch antisense-Repression einen Saccharosetransporter verloren haben (Riesmeier *et al.,* 1994; Kühn *et al.,* 1996; Lemoine *et al.,* 1996; Bürkle *et al.,* 1998) oder in $H^+$/Saccharose-Symporter Verlustmutanten (Gottwald *et al.,* 2000). Die Ähnlichkeit beider Phänotypen scheint die enge Kopplung zwischen dem primär aktiven Protonentransport durch $H^+$-ATPasen und der Energetisierung von Saccharosetransportern über diesen Protonengradienten zu belegen.

## 1.6 Zielsetzung

Das Phloem ist tief in den Leitbündeln der Pflanze eingebettet und von anderen Geweben, wie z.B. dem Phloemparenchym und den Bündelscheidenzellen, umgeben. Diese schwere Zugänglichkeit, die weite Ausdehnung und der komplexe Aufbau des Phloems gestalten die Untersuchungen der Prozesse an der Phloemmembran sehr schwierig. Der Einsatz von Mikroelektroden sowie der Aphidentechnik können aufgrund der elektrischen Kopplung der Phloemzellen über Plasmodesmen nur Veränderungen des Membranpotentials aufnehmen. Hierbei sind die experimentellen Bedingungen im Apoplasten und im Phloem selbst nicht genau definierbar. Des Weiteren sind Siebelemente mit P-Proteinen (Phloem-spezifische Proteine) oder sogar mit Fabaceaen-spezifischen Forisomen ausgestattet, die bei einer Verletzung innerhalb von Sekunden zu einem Verschluss der Siebplatten führen (z.B. Knoblauch und van Bel, 1998, 2001). Um dennoch die elektrophysiologischen Vorgänge in der Phloemmembran verstehen zu können, wurde im Rahmen dieser Arbeit auf das heterologe Expressionssystem der *Xenopus* Oozyten zurückgegriffen. Da von vielen Transportern und Kanälen bereits die cDNA identifiziert und kloniert werden konnte, ist es möglich diese Transportproteine in Oozyten zu exprimieren und biophysikalisch unter definierten Bedingungen mit der DEVC-Technik zu charakterisieren. Mit dem Wissen um die elektrophysiologischen Eigenschaften der Einzelkomponenten dieser Beladungsmaschinerie des Phloems, war es dann möglich in Coexpressionsstudien die Interaktion zwischen den einzelnen Transportern und Kanälen zu studieren. Mittels Coexpression von $K^+$-Kanälen und sekundär aktiven $H^+$-Symportern in *Xenopus* Oozyten wurde das Phloem rekonstruiert und auf die Prozesse *in planta* rückgeschlossen.

Im Einzelnen wurde dabei wie folgt vorgegangen:

- Elektrophysiologische Charakterisierung von Phloem-lokalisierten *Shaker*-Kaliumkanälen der KAT1-Unterfamilie (KZM1 und KAT2) und der AKT2/3-Unterfamilie (AKT3 und PTK2);
- Struktur-Funktionsuntersuchungen an AKT3 durch Mutagenesestudien und einem Porenaustausch mit einem Vertreter der KAT1-Unterfamilie (KST1); Lokalisierung von Domänen und einzelnen Aminosäuren, die die besonderen elektrophysiologischen Eigenschaften von AKT3 bestimmen;

- Charakterisierung des $H^+$/Saccharose-Symporters ZmSUT1 aus *Zea maize* in Hinblick auf die Spannungsabhängigkeit der Transportkinetik und der Reversibilität des Zuckertransports;
- Untersuchung der Transportkinetiken und der Substratspezifität des Phloem-lokalisierten Polyoltransporters PmPLT1 aus *Plantago major* und des Polyoltransporters AtPLT5 aus *Arabidopsis thaliana;*
- Coexpressionsexperimente der einzelnen Saccharoseransporter und Kaliumkanäle zur Simulation der Prozesse an der Phloemmembran in Oozyten von *Xenopus laevis*;

# 2. Ergebnisse

## Kapitel I: The Pore of Plant $K^+$-Channels is Involved in Voltage and pH Sensing: Domain-Swapping between Different $K^+$ Channel α-Subunits

**Stefan Hoth, Dietmar Geiger, Dirk Becker und Rainer Hedrich**

**Publiziert in The Plant Cell, Vol. 13, 943–952, April 2001**

**Eigene Beteiligung an der Arbeit:**

- Generierung der $K^+$-Kanal Chimäre KST1/(p)AKT3.
- Elektrophysiologische Charakterisierung von AKT3 und KST1/(p)AKT3 in *Xenopus* Oozyten in Bezug auf Spannungsabhängigkeit, Gleichrichtung, $Ca^{2+}$- und pH-Empfindlichkeit mit Hilfe der DEVC Technik.
- Auswertung der Daten.

The Plant Cell, Vol. 13, 943–952, April 2001, www.plantcell.org © 2001 American Society of Plant Physiologists

# The Pore of Plant $K^+$ Channels Is Involved in Voltage and pH Sensing: Domain-Swapping between Different $K^+$ Channel $\alpha$-Subunits

**Stefan Hoth,[1,2] Dietmar Geiger,[1] Dirk Becker, and Rainer Hedrich[3]**

Molekulare Pflanzenphysiologie und Biophysik, Julius-von-Sachs-Institut für Biowissenschaften, Universität Würzburg, Julius-von-Sachs-Platz 2, D-97082 Würzburg, Germany

**Plant $K^+$ uptake channel types differ with respect to their voltage, $Ca^{2+}$, and pH dependence. Here, we constructed recombinant chimeric channels between KST1, a member of the inward-rectifying, acid-activated KAT1 family, and AKT3, a member of the weakly voltage-dependent, proton-blocked AKT2/3 family. The homologous pore regions of AKT3 (amino acids 216 to 287) and KST1 (amino acids 217 to 289) have been exchanged to generate the two chimeric channels AKT3/(p)KST1 and KST1/(p)AKT3. In contrast to AKT3 wild-type channels, AKT3/(p)KST1 revealed a strong inward rectification reminiscent of that of KST1. Correspondingly, the substitution of the KST1 by the AKT3 pore led to less pronounced rectification properties of KST1/(p)AKT3 compared with wild-type KST1. Besides the voltage dependence, the interaction between the chimera and extracellular $H^+$ and $Ca^{2+}$ resembled the properties of the inserted rather than the respective wild-type pore. Whereas AKT3/(p)KST1 was acid activated and $Ca^{2+}$ insensitive, extracellular protons and $Ca^{2+}$ inhibited KST1/(p)AKT3. The regulation of the chimeric channels by cytoplasmic protons followed the respective wild-type backbone of the chimeric channels, indicating that the intracellular pH sensor is located outside the P domain. We thus conclude that essential elements for external pH and $Ca^{2+}$ regulation and for the rectification of voltage-dependent $K^+$ uptake channels are located within the channel pore.**

## INTRODUCTION

The function of the majority of $K^+$-transporting plant channel proteins depends on the membrane voltage. Among the isolated, functionally expressed, and electrophysiologically characterized $K^+$ channels, three different channel types can be distinguished with respect to their voltage-dependent gating: (1) outward-rectifying (KCO1, SKOR, and GORK) (Czempinski et al., 1997; Gaymard et al., 1998; Ache et al., 2000), (2) inward-rectifying (e.g., KAT1, AKT1, and KST1) (Anderson et al., 1992; Sentenac et al., 1992; Schachtman et al., 1994; Müller-Röber et al., 1995), and (3) weakly voltage-dependent $K^+$ channels (AKT2/3 and ZMK2) (Marten et al., 1999; Philippar et al., 1999; Lacombe et al., 2000). With the exception of KCO1 exhibiting four transmembrane helices and two pore regions, the voltage-dependent $K^+$ channels contain six putative transmembrane segments (S1 to S6) including an ion-conducting pore region P and a highly charged S4 segment (Doyle et al., 1998; Durell et al., 1998; Uozumi et al., 1998). The S4 domain of these plant $K^+$ channels is important for sensing changes in the membrane electric field (Dreyer et al., 1997; Hoth et al., 1997a; Marten and Hoshi, 1998). It does not, however, exclusively represent the voltage-sensing structure. Both the N and C termini affect the voltage-dependent gating behavior, too (Marten and Hoshi, 1997, 1998). Furthermore, single mutations in the P region of the guard cell inward rectifiers KAT1 and KST1 modulated the voltage dependence of the channel proteins, suggesting a role for the pore in the gating process (Becker et al., 1996; Hoth et al., 1997b). Regarding the distinct rectification properties, however, it is unclear why the six-transmembrane $K^+$ channels share not only the same overall structure but even the highly charged S4 segment.

Apart from the differences in the voltage-dependent gating, members of the KAT1 (KAT1 and KST1) and AKT2/3 (AKT3 and ZMK2) plant $K^+$ channel families differ in their regulation by extracellular protons and sensitivity toward extracellular calcium ions. Whereas KAT1 and KST1 are activated by external acidification due to a positive shift of the half-maximal activation voltage (Hedrich et al., 1995; Müller-Röber et al., 1995; Hoth et al., 1997b; Hoth and Hedrich, 1999a), AKT3 and ZMK2 are inhibited by an increased proton concentration (Marten et al., 1999; Philippar et al., 1999). This inhibition of AKT3 resulted from a decrease of the single-channel conductance, indicating an $H^+$ block of the $K^+$

[1] Both authors contributed equally to this study.
[2] Current address: Laboratory of Plant Molecular Biology, The Rockefeller University, 1230 York Avenue, New York, NY 10021-6399.
[3] To whom correspondence should be addressed. E-mail hedrich@botanik.uni-wuerzburg.de; fax 49-931-8886157.

channel pore (Marten et al., 1999; Lacombe et al., 2000). In KST1, essential molecular elements of the pH sensor could be identified using site-directed mutagenesis and electrophysiological analysis of the channel mutants (Hoth et al., 1997b; Hoth and Hedrich, 1999a). Whereas the simultaneous substitution of the only two extracellular histidine residues in KST1, located in the S3–S4 linker (H160) and in the channel pore (H271), generated a pH-insensitive mutant, the mutation of the pore histidine at position 271 into an arginine resulted in a channel mutant with an inverted pH regulation compared with the wild type (Hoth et al., 1997b). In contrast to KST1, the molecular structure of the pH sensor in AKT3 has not been characterized.

Patch-clamp studies on isolated protoplasts from different plant cells and species showed that extracellular $Ca^{2+}$ ions block $K^+$ uptake channels in a voltage-dependent manner (Wegner et al., 1994; Roberts and Tester, 1995; Thiel et al., 1996; Dietrich et al., 1998). Whereas the susceptibility toward $Ca^{2+}$ of the cloned guard cell $\alpha$-subunits KAT1 and KST1 was very low (Brüggemann et al., 1998; Dreyer et al., 1998), AKT3 was significantly blocked by physiological concentrations of external $Ca^{2+}$ (Marten et al., 1999). Although the voltage-dependent properties suggested that the $Ca^{2+}$ ions partially enter the channel pore, the $Ca^{2+}$ binding site remained unknown.

In this study, we generated chimeric channels between KST1 and AKT3 by exchanging the pore region of AKT3 (amino acids 216 to 287) and the homologous region of KST1 (amino acids 217 to 289). The electrophysiological characterization of these chimeric channels in Xenopus oocytes revealed that the channel pore plays a crucial role in the voltage-dependent gating of $K^+$ channels and harbors all basic molecular structures required for extracellular pH regulation and $Ca^{2+}$ block.

## RESULTS

To investigate the role of the pore region of plant $K^+$ uptake channels in rectification, $Ca^{2+}$ inhibition, and pH regulation, we generated chimeric channels between KST1 and AKT3.

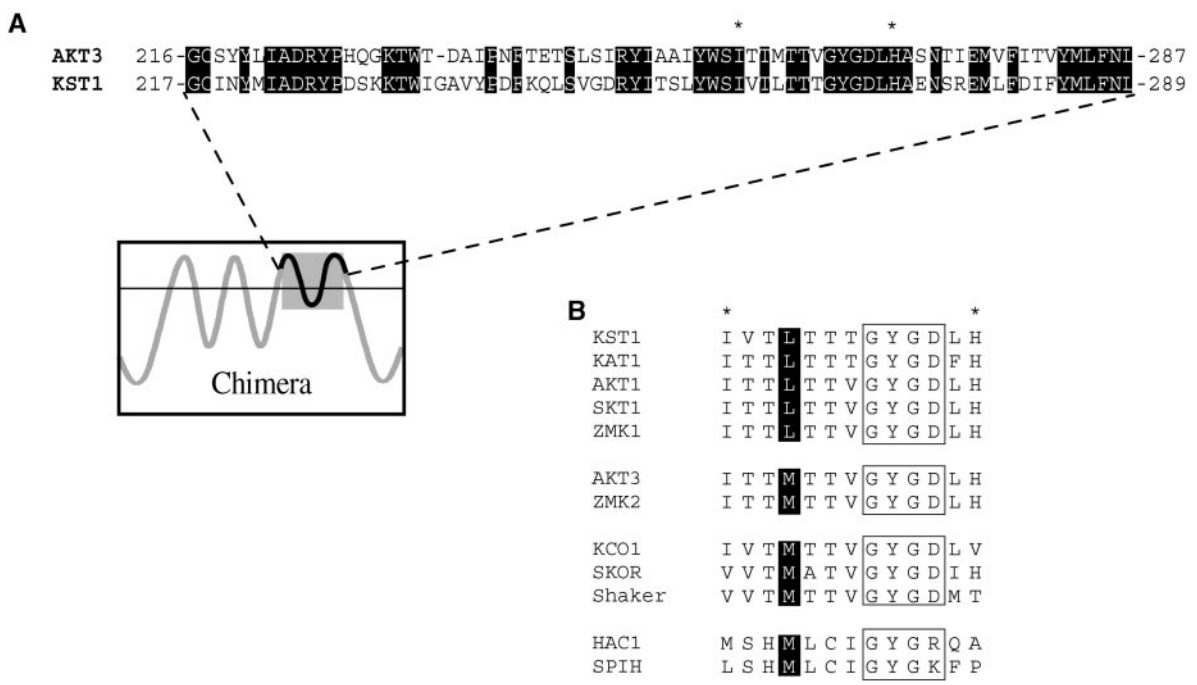


**Figure 1.** Alignments of Amino Acids within the Pore Region of $K^+$ Channels.

**(A)** Alignment of the pore region with parts of S5 and S6 of the voltage-dependent $K^+$ channels AKT3 and KST1. Amino acids 216 to 287 of AKT3 and amino acids 217 to 289 of KST1 are shown. The identical residues in both channel proteins are highlighted by black boxes. A schematic model of the membrane topology of the chimeric channels indicates the exchanged fragment.

**(B)** Alignment of plant and animal $K^+$ channel amino acid sequences in the pore region. Ten amino acids (c.f. sequence marked by asterisks in **[A]**) including the selectivity filter GYGD motif (boxed) are shown for the indicated $K^+$ channels. Four amino acids upstream, the GYG sequence conserved leucine and methionine residues are marked by black boxes. The GenBank accession numbers of the aligned channels sequences are as follows: KST1, X79779; KAT1, M86990; AKT1, X62907; SKT1, X86021; ZMK1; Y07632; AKT3, U44745; ZMK2, AJ132686; KCO1, X97323; SKOR, AJ223358; *Shaker*, M17211; HAC1, AJ225122; SPIH1, Y16880.

The channel pore of AKT3 with parts of S5 and S6 (amino acids 216 to 287) was substituted by the homologous region of KST1 (amino acids 217 to 289) and vice versa, as shown in Figure 1. In this particular region, both channels share ~58% identity on the amino acid level. The electrophysiological properties of the resulting chimeric channels AKT3/(p)KST1 and KST1/(p)AKT3 were studied in double-electrode voltage-clamp experiments after heterologous expression in Xenopus oocytes.

### Voltage Dependence

Typical current recordings of AKT3 wild-type channels in the voltage range of +40 to −150 mV are shown in Figure 2A (left side). Both the instantaneous and the time-dependent current components were mediated by the AKT3 gene product (c.f. Marten et al., 1999). At voltages more positive than the $K^+$ equilibrium potential ($V_{rev} \approx 0$ mV), outward currents through AKT3 were elicited. The steady state currents ($I_{ss}$) plotted against the membrane voltage clearly visualize the weak voltage dependence and rectification of AKT3 (Figure 2B, left side). KST1, however, revealed a strong inward rectification conducting $K^+$ ions only upon hyperpolarization to voltages less than −90 mV (Figures 2A and 2B, second right). In contrast to AKT3 but in line with KST1, the chimera AKT3/(p)KST1 containing the KST1 pore exhibited the voltage-dependent properties of an inward rectifier lacking an AKT3-like instantaneous current component (Figures 2A and 2B, second left). Outward currents of oocytes expressing AKT3/(p)KST1 did not differ from background outward currents of KST1 (Figures 2A and 2B, second left) or noninjected oocytes (not shown; $n > 100$). KST1 lost its strong rectification after substitution of its native pore by the AKT3 pore (Figures 2A and 2B, right side). The chimera KST1/(p)AKT3 mediated $K^+$ efflux at membrane potentials positive of the $K^+$ equilibrium potential and resembled the two current components that are characteristic for AKT3. Instantaneous currents could be observed at positive and negative voltages, whereas the time-dependent current was restricted to voltages more negative than −90 mV (Figure 2A, right side). In >100 control experiments, outward currents of this magnitude and instantaneous current components have not been observed in either noninjected or KST-expressing oocytes.

A detailed analysis of the voltage dependence of the chimeric channels compared with the wild-type channels has been performed using Boltzman statistics. Figure 2C shows the open probabilities $p_o$ plotted against the membrane voltage. The chimera AKT3/(p)KST1 ($V_{1/2} = -147 \pm 0.9$ mV, apparent gating charge $z = 1.65 \pm 0.03$) revealed voltage-dependent gating characteristics identical to KST1 ($V_{1/2} = -143 \pm 0.8$ mV, $z = 1.63 \pm 0.04$) but completely different from wild-type AKT3 ($V_{1/2} = -112 \pm 4.5$ mV, $z = 0.66 \pm 0.07$). This indicated that the KST1 pore was sufficient to confer a strong inward rectification on the channel. The substitution of the KST1 pore by the AKT3 pore in KST1/(p)AKT3 resulted in a decreased steepness of the $p_o$/V-curve ($V_{1/2} = -130 \pm 2.9$ mV, $z = 0.90 \pm 0.09$). This chimeric channel also resembled the AKT3-like minimal open probability different from zero at membrane voltages positive to −40 mV (c.f. Marten et al., 1999). However, its voltage-dependent gating parameters $V_{1/2}$ and z as well as the minimal open probability were slightly different from AKT3, indicating that other components of the AKT3 backbone might be needed for a complete conversion.

To identify residues in the P region that could account for the differences in rectification among members of the KAT1, AKT1, and AKT2/3 channel family, respectively, we compared the channels with respect to their amino acid sequences in the pore (Figure 1B). Whereas all members of the inward-rectifying KAT1 and AKT1 families contain a leucine residue four amino acids upstream of the GYGD sequence of the selectivity filter, a methionine is highly conserved at the identical position in the AKT2/3 family. This methionine residue is also present in outward-rectifying $K^+$ channels of the *Shaker* family as well as in the plant outward rectifiers SKOR and KCO1 (Figure 1B). To study the possible role of this residue for the rectification properties of $K^+$ channels, we generated the channel mutants AKT3-M260L and KST1-L262M. Like AKT3, the single mutant AKT3-M260L mediated $K^+$ influx and efflux, resembling the weak voltage dependence and the proton inhibition of the wild type (Figure 3, upper traces). The strong inward rectification and the acid activation of wild-type KST1 were unaffected in the mutant KST1-L262M (Figure 3B, lower traces). Thus, our analyses regarding the site-directed channel mutants KST1-L262M and AKT3-M260L identified that this position was not fundamental for the rectification of voltage-regulated $K^+$ channels. This finding is supported by Gauss et al. (1998) and Ludwig et al. (1998), showing that the animal six-transmembrane $K^+$ channels HAC1 and SPIH containing a methionine residue at the respective position represent, in fact, inward rectifiers (Figure 1B). Future experiments based on scanning mutagenesis are therefore required to identify structural determinants for rectification in the pore region of voltage-dependent $K^+$ channels.

### Interaction with External Cations

Structural domains responsible for proton block and $Ca^{2+}$ inhibition of AKT3 are most likely located in the pore of the channel protein. To obtain further information about the respective binding sites, we investigated the $Ca^{2+}$ sensitivity and pH dependence of AKT3/(p)KST1 and KST1/(p)AKT3.

#### *Calcium*

Figure 4A shows the susceptibility of AKT3/(p)KST1 to extracellular $Ca^{2+}$ in comparison to AKT3 wild-type channels.

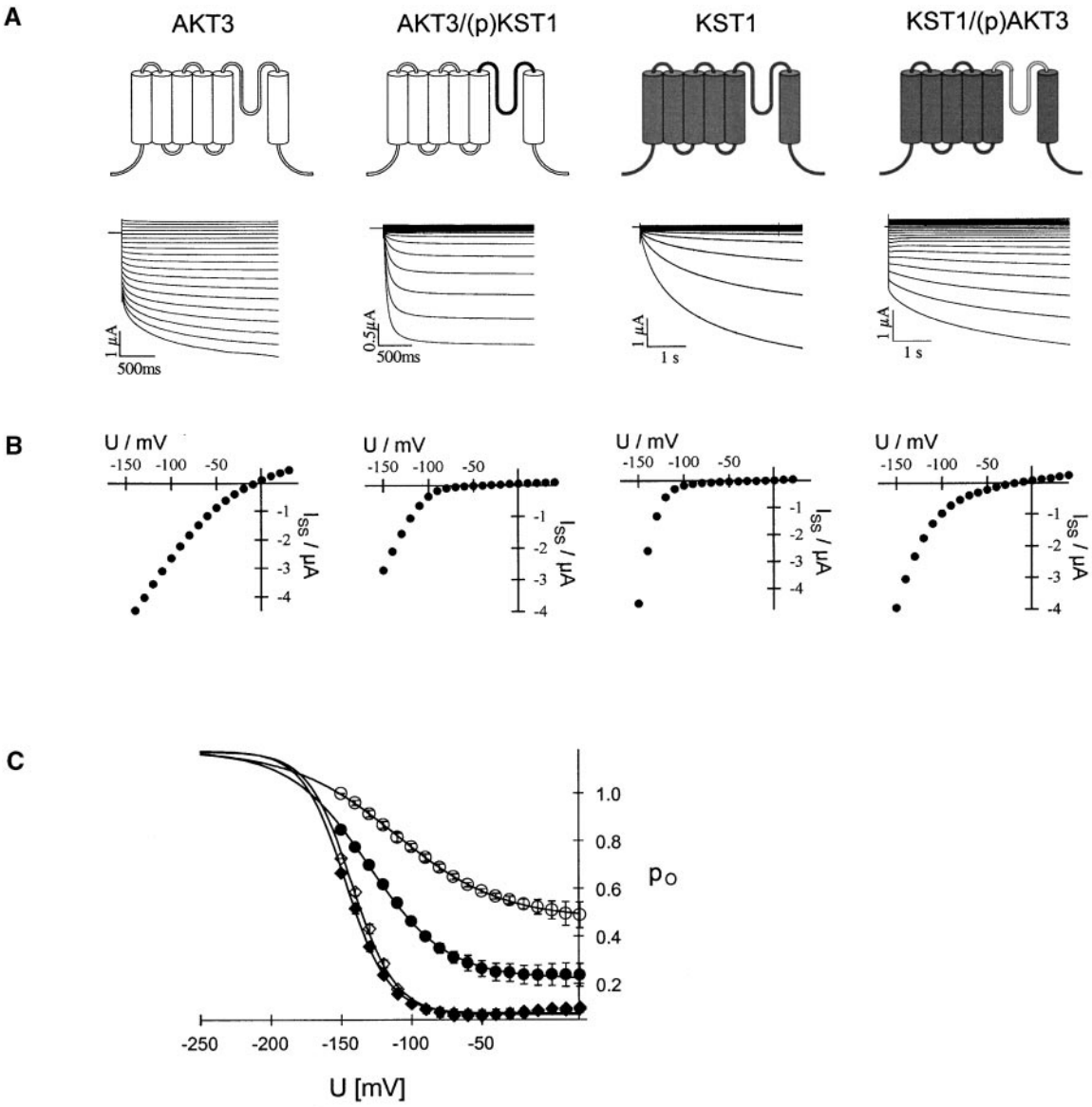


**Figure 2.** Voltage-Dependent Properties of AKT3, AKT3/(p)KST1, KST1, and KST1/(p)AKT3.

**(A)** Representative current traces in response to voltage pulses from +40 to −150 mV of AKT3 (left traces), KST1 (second right traces), and the chimeric channels AKT3/(p)KST1 (second left traces) as well as KST1/(p)AKT3 (right traces). Voltage pulses were applied in 10-mV decrements from a holding voltage of −10 mV for AKT3 and KST1/(p)AKT3 and −20 mV for KST1 and AKT3/(p)KST1, respectively. Oocytes with similar expression levels have been selected. AKT3 as well as KST1/(p)AKT currents were recorded at $pH_{ext.}$ 7.4, whereas KST1 and the chimera AKT3/(p)KST1 were recorded at $pH_{ext.}$ 5.6.

**(B)** The steady state currents $I_{ss}$ were derived from the data shown in **(A)** and plotted against the membrane voltage. Note pronounced outward currents in AKT3 and KST1/(p)AKT3 but not in KST1 and AKT3/(p)KST1 in **(A)** and **(B)**.

**(C)** The open probabilities $p_o$ in 30 mM $K^+$ and pH 7.4 for KST1 (◇), AKT3 (○), KST1/(p)AKT3 (●), and AKT3/(p)KST1 (◆) were plotted against the membrane voltage. Solid lines represent best Boltzman fits to the data. Error bars indicate standard deviation ($n = 3$).

In the presence of 20 mM $K^+$ and 30 mM $Ca^{2+}$, tail-current recordings in the range of +20 to −170 mV were performed after preactivating the channels at a membrane voltage of −150 mV. Whereas AKT3 resembled the characteristics of a voltage-dependent $Ca^{2+}$ block (c.f. Marten et al., 1999), the chimera AKT3/(p)KST1 was $Ca^{2+}$ insensitive even in the presence of 30 mM $Ca^{2+}$. The lack of a divalent cation block therefore corresponds with the $Ca^{2+}$ phenotype observed for KST1 (Figure 4B; Brüggemann et al., 1998). Equipped with the AKT3 pore, however, KST1 became more sensitive to extracellular $Ca^{2+}$. Under identical experimental conditions, the chimera KST1/(p)AKT3 was blocked by $Ca^{2+}$ at membrane voltages less than −110 mV in a voltage-dependent manner (Figure 4B).

### *Protons*

The hyperpolarization-induced inward $K^+$ currents through AKT3/(p)KST1 reversibly increased upon a drop in the extracellular solution from pH 7.4 to 5.6 (Figure 4C). As shown for KST1 (Hoth et al., 1997b), the acid activation in this chimera was accompanied by a positive shift of the half-maximal activation voltage $V_{1/2}$ ($\Delta V_{1/2}$ = 13.1 ± 1.5 mV, $n$ = 4). Thus, the replacement of the AKT3 by the KST1 pore in AKT3/(p)KST1 transformed the proton-blocked AKT3 into an acid-activated inward rectifier. Accordingly, the acid activation of KST1 was converted into an inhibition of $K^+$ influx by external protons in the chimera KST1/(p)AKT3, as demonstrated by a decrease in steady state currents of −77.9 ± 5.9% at −150 mV (Figure 4D).

### Separation of the Intra- and Extracellular pH Sensor

Recently, Tang et al. (2000) showed that the intracellular pH sensor of the *Arabidopsis thaliana* guard cell $K^+$ uptake channel KAT1 is located in the cytosolic linker between the transmembrane helices S2 and S3. A histidine residue in this linker (H118) was fundamental for pH-sensitive changes in activation kinetics but not for the proton-induced shift in the half-maximal activation voltage. Because this domain was not substituted in the two chimeric channels, the dependence on internal protons should remain unaffected compared with AKT3 and KST1 wild-type channels, respectively. To confirm this prediction, 10 mM Na-acetate at pH 5.6 was applied to the extracellular solution. The nondissociated acid is able to permeate across the membrane and to release protons into the cell (c.f. Lacombe et al., 2000). Whereas KST1, like KAT1 (Tang et al., 2000), was activated by increasing the intracellular proton concentration (29.4 ± 2.9% at −130 mV; Figure 5C), AKT3 was inhibited by cytosolic acidification (−66.5 ± 6.3% at −130 mV; Figure 5A). Like AKT3 in the presence of 10 mM acetate, the currents through AKT3/(p)KST1 were almost completely suppressed (−59.2 ± 7.0% at −130 mV; Figure 5B). Although KST1/(p)AKT3-mediated currents are largely inhibited at pH 5.6 in the bath (c.f. Figure 4D), the equipment of KST1 with the AKT3 pore did not affect the cytosolic pH regulation of KST1. As for the wild type (Figure 5C), the acidification of the cytoplasm resulted in an increased inward current (62.4 ± 2.7% at −130 mV; Figure 5D). These results therefore provide strong evidence that the pore region of $K^+$ uptake channels does not interact with intracellular protons. As a

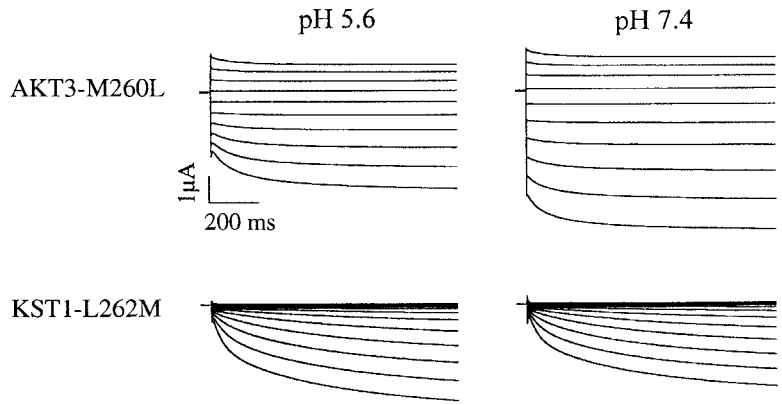


**Figure 3.** Voltage and pH Regulation of AKT3-M260L and KST1-L262M.

$K^+$ currents in 30 mM $K^+$ of the channel mutants AKT3-M260L (upper traces) and KST1-L262M (lower traces) were recorded at membrane voltages in the range from +30 to −150 mV. From the holding voltage of −33 mV and −20 mV for AKT3-M260L and KST1-L262M, respectively, the membrane voltage was changed in steps of −20 mV. Upon a change in the extracellular pH from 5.6 to 7.4, $K^+$ currents through AKT3-M260L increased (42.8 ± 1.2% at −130 mV), whereas those through KST1-L262M decreased (−27.6 ± 6.4% at −130 mV). For both channel mutants, representative current recordings out of three to four experiments are shown. The observed changes in steady state currents during the pH shift experiments were significantly different in the voltage range from −80 to −150 mV ($P < 0.01$).

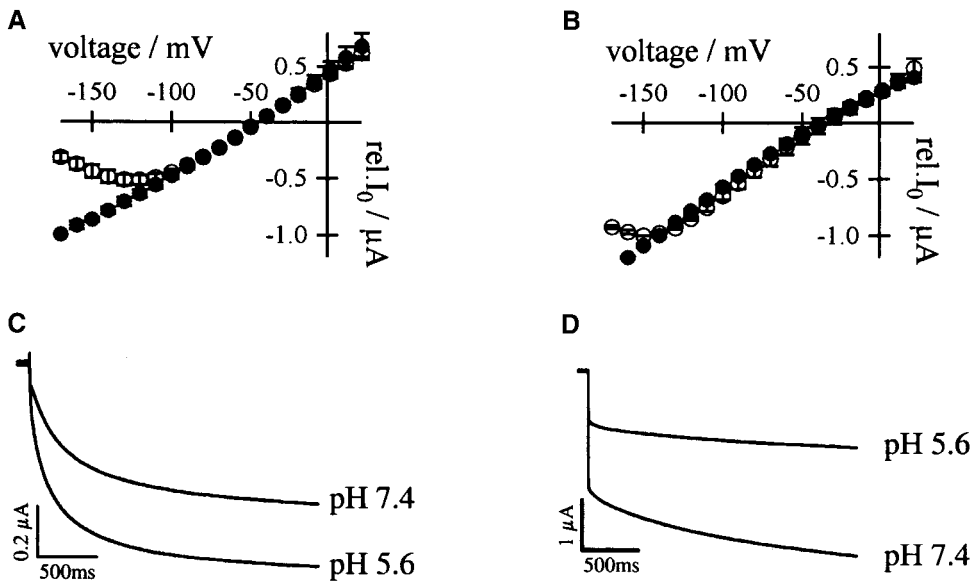


**Figure 4.** Dependence of AKT3/(p)KST1 and KST1/(p)AKT3 on Extracellular $Ca^{2+}$ and $H^+$.

**(A)** Relative (rel.) instantaneous tail-current amplitudes $I_0$ plotted against the membrane voltage revealed a voltage-dependent $Ca^{2+}$ block for AKT3 (○, $n = 3$) but not for the chimeric channels AKT3/(p)KST1 (●, $n = 3$). The $Ca^{2+}$ solution contained 20 mM KCl, 10 mM Tris/Mes, pH 7.2, and 30 mM $CaCl_2$. In the control solution, $CaCl_2$ was replaced with 30 mM $MgCl_2$. Error bars were smaller than symbols and represent the standard deviation ($n \geq 3$). $I_0$ currents in the presence of calcium were significantly different in the voltage range of −130 to −170 mV for the chimera AKT3/(p)KST1 compared with AKT3 wild type ($P < 0.01$).

**(B)** Superimposed $I_0$/V-plot of KST1 and KST1/(p)AKT3 . Under the same experimental conditions as described in **(A)**, the chimera KST1/(p)AKT3 was blocked by extracellular $Ca^{2+}$ (○, $n = 4$) in contrast to KST1 wild type (●, $n = 3$). Error bars were smaller than symbols and represent the standard deviation ($n \geq 3$). $I_0$ currents in the presence of calcium were significantly different in the voltage range of −150 to −170 mV for the chimera KST1/(p)AKT3 compared with KST1 wild type ($P < 0.01$).

**(C)** Acid-activated inward $K^+$ currents of AKT3/(p)KST1 in response to 2.5-sec voltage pulses to −150 mV from the holding voltage of −20 mV. Currents were recorded in the presence of standard external media buffered to pH values as indicated.

**(D)** Voltage pulses to −150 mV from the holding voltage of −20 mV elucidated that $K^+$ currents of KST1/(p)AKT3 decreased upon a change from pH 7.4 to 5.6.

**(C)** and **(D)** show representative current traces out of four independent experiments. Steady state currents in **(C)** and **(D)** at pH 5.6 were significantly different from currents at pH 7.4 at −150 mV ($P < 0.01$).

consequence, it is very unlikely that extracellular protons reach the internal pH sensor via the pore.

## DISCUSSION

The generation of point mutations and chimeric channels led to the identification of the S4 segment as well as the N and C termini as important elements of the voltage-sensing structure of *Shaker*-like $K^+$ channels (Papazian et al., 1991; Perozo et al., 1994; Tytgat et al., 1994; Yusaf et al., 1996; Dreyer et al., 1997; Hoth et al., 1997a; Marten and Hoshi, 1997; Terlau et al., 1997; Chanda et al., 1999; Chiara et al., 1999). Here, we show that the pore region contributes to the rectification of voltage-dependent plant $K^+$ channels. On one hand, the substitution of the pore region including parts of S5 and S6 in the chimeric channel AKT3/(p)KST1 was sufficient to transform the weak voltage-dependent AKT3 into an inward rectifier (Figures 2A and 2B, left). On the other hand, KST1 equipped with the AKT3 pore lost its strong inward rectification (Figures 2A and 2B, right). In KAT1 and KST1, several point mutations in the P region resulted in a modulation of the voltage-dependent gating (Becker et al., 1996; Hoth et al., 1997b). A molecular link between the pore and the putative voltage sensor S4 was therefore anticipated (Hoth and Hedrich, 1999a). The pore histidine (H271) and the histidine in the S3–S4 linker (H160), which represent key amino acids of the pH sensor of KST1, as well as the arginine at position 181 in the S4 segment have been proposed as putative elements within this molecular link. Furthermore, $Zn^{2+}$ binding studies on KST1 wild type and histidine mutants suggested that the S3–S4 linker is involved in the formation of the outer mouth of the pore (Hoth and Hedrich, 1999b). Together with specific pore amino acids, this S3–S4 loop could link the movement of S4 to chan-

nel opening. This model would also explain the data obtained with chimeric channels between KAT1 and Xsha2 that located components for inward rectification in the first third of the KAT1 channel including S1 to S4 and the S4–S5 linker (Cao et al., 1995). Local protein arrangements in the pore underlying the slow inactivation of the *Shaker* channel have also been postulated from voltage clamp fluorometry experiments (Loots and Isacoff, 1998).

The difference in the $Ca^{2+}$ sensitivity of voltage-dependent $K^+$ channels results from distinct amino acids in the channel pore. Upon replacement of the AKT3 pore by the KST1 pore, which is almost $Ca^{2+}$ insensitive (Brüggemann et al., 1998), AKT3/(p)KST1 lost its $Ca^{2+}$ susceptibility (Figure 4A). The AKT3 pore, however, transformed the $Ca^{2+}$ phenotype of KST1 from weakly sensitive to $Ca^{2+}$ blocked (Figure 4B). Our experiments concerning the dependence of the chimeric channels on extracellular protons show that the pore of KST1 is sufficient to confer the acid activation of AKT3/(p)KST1 (Figure 4C). As deduced from a proton-induced decrease of the single-channel conductance (Marten et al., 1999), the binding site for protons seems to be located in the AKT3 pore. This was confirmed by the proton inhibition of KST1/(p)AKT3 (Figure 4D). Because the mutant AKT3-M262L is still inhibited by protons (Figure 3), this residue reminiscent of members of the AKT2/3 channel family does not account for the proton block of AKT3. The comparison of residues within the exchanged 60–amino acid pore peptide between AKT3 and KST1, however, limits the putative candidates for the binding site to 29 amino acids. Future analysis of the conserved exchanges between both channels and site-directed mutations should therefore identify the key amino acids of the $Ca^{2+}$ binding site as well as the pH sensor of AKT3.

On the basis of studies with the chimera, we were able to

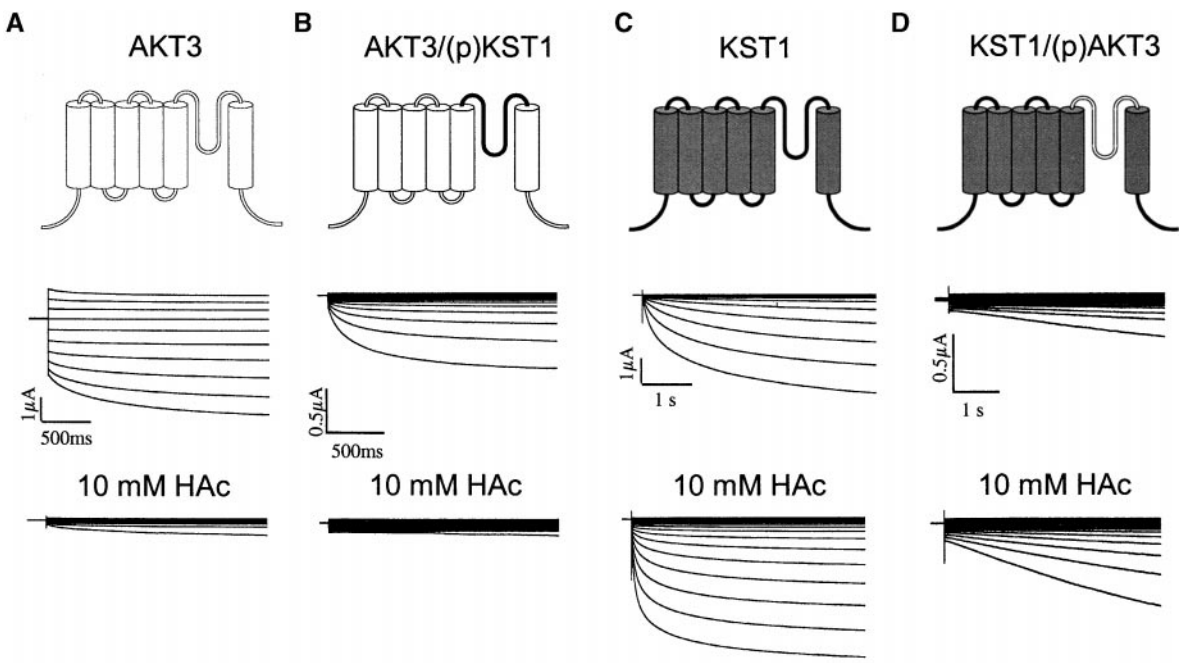


**Figure 5.** Regulation of AKT3, AKT3/(p)KST1, KST1, and KST1/(p)AKT3 by Intracellular Protons.

**(A)** In the voltage range of +30 to −150 mV, voltage pulses from a holding voltage of −30 mV in steps of 20 mV for a duration of 2.5 sec demonstrate the inhibition of $K^+$ fluxes through AKT3 in the presence of 10 mM acetate compared with control conditions ($n = 4$). Note the decrease of outward as well as inward $K^+$ currents.

**(B)** $K^+$ currents mediated by AKT3/(p)KST1 before and after addition of 10 mM acetate to the extracellular solution ($n = 3$). From the holding voltage of −20 mV, the membrane voltage was changed to −120 mV in 10-mV decrements.

**(C)** $K^+$ currents through KST1 were elicited by 5-sec voltage pulses in the range of +20 to −150 mV (10-mV decrements) in the absence and in the presence of 10 mM acetate ($n = 6$).

**(D)** Activation of $K^+$ inward currents through KST1/(p)AKT3 upon addition of 10 mM HAc. Current traces in response to voltages in the range from +30 to −130 mV (10-mV decrements) are shown ($n = 3$).

The solutions used for results shown in **(A)** to **(D)** were composed of 30 mM KCl, 1 mM $CaCl_2$, 2 mM $MgCl_2$, and 10 mM Mes/Tris, pH 5.6, as well as 10 mM NaCl or 10 mM Na-acetate, respectively. Steady state currents in the presence of sodium acetate were significantly different from those in sodium chloride in the voltage range from −80 to −130 mV ($P < 0.05$).

show that the intracellular pH sensor of voltage-dependent $K^+$ channels is distinct from the extracellular pH-sensing structure. This observation is supported by the following results. (1) AKT3 is inhibited by both external and internal protons, whereas the substitution of the pore provides the chimera AKT3/(p)KST1 with an activation upon extracellular acidification (Figure 4), leaving its intracellular pH dependence unaffected (Figure 5). (2) KST1 containing the AKT3 pore maintained its activation by intracellular protons (Figure 5). (3) The KST1 double mutant H160A/H271A, which is insensitive to external protons, still activated upon a pH drop in the cytoplasm (S. Hoth and R. Hedrich, unpublished results). In this context, it should be mentioned that the participation of the cytosolic S2–S3 linker in KAT1 in sensing intracellular pH changes has recently been shown (Tang et al., 2000).

In conclusion, the pore region of voltage-gated $K^+$ channels contains essential sites for $H^+$ and $Ca^{2+}$ binding as well as for rectification. Future experiments on additional channel mutants and chimeric channels will help to identify the individual molecular entities of these fundamental processes.

## METHODS

### Generation of Chimeric Channels

For the generation of the chimeric channels, two site-directed silent mutations (QuikChange site-directed mutagenesis kit; Stratagene, Heidelberg, Germany) in AKT3 and KST1, respectively, were performed, introducing a BstXI and an AatI restriction site in both plasmids (pKST1#8 in the pGEMHE vector and pAKT3 in the pGEMA vector) at identical sites. In pAKT3, the BstXI site at position 644 was generated by primers 5′-TTGTTTCTAGTCCACTGTGCTGGATGCAG-3′ and 5′-CTGCATCCAGCACAGTGGACTAGAAACAA-3′ and the AatI site at position 864 was generated by primers 5′-GTTATTCAATCTAGGCCTCACTGCTTACC-3′ and 5′-GGTAAGCAGTGAGGCCTAGATTGAATAAC-3′. The primers 5′-TGTTTGCAGTCCACTGTGCTGGATGCATTAAC-3′ and 5′-GTTAATGCATCCAGCACAGTGGACTGCAAACA-3′ as well as primers 5′-TGTTATTCAACTTAGGCCTGACATCTTAC-3′ and 5′-GTAAGATGTCAGGCCTAAGTTGAATAACA-3′ were used to introduce the BstXI site at position 647 and the AatI site at position 870 in pKST1#8, respectively. Chimeric channels AKT3/(p)KST1 and KST1/(p)AKT3 were derived by exchanging the corresponding DNA fragments of pAKT3 and pKST1#8 between the generated BstXI and AatI sites. The cDNA sequences were verified by DNA sequence analysis (Thermo sequenase fluorescent labeled primer cycle sequencing kit with 7-deaza-dGTP; Amersham Pharmacia, Braunschweig, Germany). The single mutants AKT3-M260L and KST1-L262M were generated as described by Hoth and Hedrich (1999a).

### Electrophysiology

The cRNAs of wild-type channels KST1 and AKT3 as well as the chimera were generated by in vitro transcription (T7-Megascript kit; Ambion Inc., Austin, TX) and injected into oocytes of *Xenopus laevis* (Nasco, Fort Atkinson, WI) using a Picospritzer II microinjector (General Valve, Fairfield, NJ). Two to 6 days after injection, double-electrode voltage-clamp recordings were performed with a Turbotec-01C amplifier (npi Instruments, Tamm, Germany). The electrodes were filled with 3 M KCl and had typical input resistances of 2 to 6 MΩ. Solutions were composed of 100 mM KCl, 2 mM $MgCl_2$, 1 mM $CaCl_2$, and 10 mM Tris/Mes or Mes/Tris, pH 7.4 and 5.6, respectively. For measurements with respect to changes in external $Ca^{2+}$ and in the intracellular pH, the composition of solutions is listed in the legends to Figures 4 and 5. All media were adjusted to a final osmolality of 215 to 235 mosmol $kg^{-1}$ with D-sorbitol. Analyses of voltage dependence, pH dependence, and $Ca^{2+}$ block were performed as described previously (Hoth et al., 1997b; Marten et al., 1999). Data points with error bars represent the mean ±SD, and statistical significance was verified by a paired Student's *t* test.

## ACKNOWLEDGMENTS

We are grateful to Petra Dietrich and Natalya Ivashikina for helpful comments on the manuscript. This work was supported by grants to R.H. from the Deutsche Forschungsgemeinschaft.

Received October 12, 2000; accepted January 29, 2001.

## REFERENCES

**Ache, P., Becker, D., Ivashikina, N., Dietrich, P., Roelfsema, R.M.G., and Hedrich, R.** (2000). GORK, a delayed outward rectifier expressed in guard cells of *Arabidopsis thaliana*, is a $K^+$-selective, $K^+$-sensing ion channel. FEBS Lett. **486,** 93–98.

**Anderson, J.A., Huprikar, S.S., Kochian, L.V., Lucas, W.J., and Gaber, R.F.** (1992). Functional expression of a probable *Arabidopsis thaliana* potassium channel in *Saccharomyces cerevisiae*. Proc. Natl. Acad. Sci. USA **89,** 3736–3740.

**Becker, D., Dreyer, I., Hoth, S., Reid, J.D., Busch, H., Lehnen, M., Palme, K., and Hedrich, R.** (1996). Changes in the voltage activation, $Cs^+$ sensitivity, and ion permeability in H5 mutants of the plant $K^+$ channel KAT1. Proc. Natl. Acad. Sci. USA **93,** 8123–8128.

**Brüggemann, L., Dietrich, P., Dreyer, I., and Hedrich, R.** (1998). Pronounced differences between guard cell $K^+$ channels in vivo and their respective α-subunit homomers in *Xenopus* oocytes. Planta **207,** 370–376.

**Cao, Y., Crawford, N.M., and Schroeder, J.I.** (1995). Amino terminus and the first four membrane-spanning segments of the Arabidopsis $K^+$ channel KAT1 confer inward-rectification property of plant–animal chimeric channels. J. Biol. Chem. **270,** 17697–17701.

**Chanda, B., Tiwari, J.K., Varshney, A., and Mathew, M.K.** (1999). Transplanting the N-terminus from Kv1.4 to Kv1.1 generates an inwardly rectifying $K^+$ channel. Neuroreport **10,** 237–241.

**Chiara, M.D., Monje, F., Castellano, A., and Lopez-Barneo, J.** (1999). A small domain in the N terminus of the regulatory alpha-

subunit kv2.3 modulates kv2.1 potassium channel gating. J. Neurosci. **19,** 6865–6873.

**Czempinski, K., Zimmermann, S., Erhardt, T., and Müller-Röber, B.** (1997). New structure and function in plant $K^+$ channels: KCO1, an outward rectifier with a steep $Ca^{2+}$ dependency. EMBO J. **16,** 3455–3463.

**Dietrich, P., Dreyer, I., Wiesner, P., and Hedrich, R.** (1998). Cation sensitivity and kinetics of guard-cell potassium channels differ among species. Planta **205,** 277–287.

**Doyle, D.A., Cabral, J.M., Pfuetzner, R.A., Kuo, A., Gulbis, J.M., Cohen, S.L., Chait, B.T., and MacKinnon, R.** (1998). The structure of the potassium channel: Molecular basis of $K^+$ conduction and selectivity. Science **280,** 69–77.

**Dreyer, I., Antunes, S., Hoshi, T., Müller-Röber, B., Palme, K., Pongs, O., Reintanz, B., and Hedrich, R.** (1997). Plant $K^+$ channel $\alpha$-subunits assemble indiscriminately. Biophys. J. **72,** 2143–2150.

**Dreyer, I., Becker, D., Bregante, M., Gambale, F., Lehnen, M., Palme, K., and Hedrich, R.** (1998). Single mutations strongly alter the $K^+$-selective pore of the $K_{in}$ channel KAT1. FEBS Lett. **430,** 370–376.

**Durell, S.R., Hao, Y.H., and Guy, H.R.** (1998). Structural models of the transmembrane region of voltage-gated and other $K^+$ channels in open, closed, and inactivated conformations. J. Struct. Biol. **121,** 263–284.

**Gauss, R., Seifert, R., and Kaupp, B.** (1998). Molecular identification of a hyperpolarization-activated channel in sea urchin sperm. Nature **393,** 583–587.

**Gaymard, F., Pilot, G., Lacombe, B., Bouchez, D., Bruneau, D., Boucherez, J., Michaux-Ferriere, N., Thibaud, J.B., and Sentenac, H.** (1998). Identification and disruption of a plant *Shaker*-like outward channel involved in $K^+$ release into the xylem sap. Cell **94,** 647–655.

**Hedrich, R., Moran, O., Conti, F., Busch, H., Becker, D., Gambale, F., Dreyer, I., Küch, A., Neuwinger, K., and Palme, K.** (1995). Inward rectifier potassium channels in plants differ from their animal counterparts in response to voltage and channel modulators. Eur. Biophys. J. **66,** 1061–1067.

**Hoth, S., and Hedrich, R.** (1999a). Distinct molecular bases for pH sensitivity of the guard cell $K^+$ channels KST1 and KAT1. J. Biol. Chem. **274,** 11599–11603.

**Hoth, S., and Hedrich, R.** (1999b). Susceptibility of the guard cell $K^+$ uptake channel KST1 towards $Zn^{2+}$ requires histidine residues in the S3–S4 linker and in the channel pore. Planta **209,** 543–546.

**Hoth, S., Dreyer, I., and Hedrich, R.** (1997a). Mutational analysis of functional domains within plant $K^+$ uptake channels. J. Exp. Bot. **48,** 415–420.

**Hoth, S., Dreyer, I., Dietrich, P., Becker, D., Müller-Röber, B., and Hedrich, R.** (1997b). Molecular basis of plant-specific acid activation of $K^+$ uptake channels. Proc. Natl. Acad. Sci. USA **94,** 4806–4810.

**Lacombe, B., Pilot, G., Michard, E., Gaymard, F., Sentenac, H., and Thibaud, J.-B.** (2000). A *Shaker*-like $K^+$ channel with weak rectification is expressed in both source and sink phloem tissues of *Arabidopsis*. Plant Cell **12,** 837–851.

**Loots, E., and Isacoff, E.Y.** (1998). Protein rearrangements underlying slow inactivation of the *Shaker* $K^+$ channel. J. Gen. Physiol. **112,** 377–389.

**Ludwig, A., Zong, X., Jeglitsch, M., Hofmann, F., and Biel, M.** (1998). A family of hyperpolarization-activated mammalian cation channels. Nature **393,** 587–591.

**Marten, I., and Hoshi, T.** (1997). Voltage-dependent gating characteristics of the $K^+$ channel KAT1 depend on the N and C termini. Proc. Natl. Acad. Sci. USA **94,** 3448–3453.

**Marten, I., and Hoshi, T.** (1998). The N-terminus of the K channel KAT1 controls its voltage-dependent gating by altering the membrane electric field. Biophys. J. **74,** 2953–2962.

**Marten, I., Hoth, S., Deeken, R., Ache, P., Ketchum, K.A., Hoshi, T., and Hedrich, R.** (1999). AKT3, a phloem-localized $K^+$ channel, is blocked by protons. Proc. Natl. Acad. Sci. USA **96,** 7581–7586.

**Müller-Röber, B., Busch, H., Ellenberg, J., Becker, D., Provart, N., Dietrich, P., Willmitzer, L., Hoth, S., and Hedrich, R.** (1995). Cloning and electrophysiological analysis of KST1, an inward-rectifying $K^+$ channel expressed in potato guard cells. EMBO J. **14,** 2409–2416.

**Papazian, D.M., Timpe, L.C., Jan, Y.N., and Jan, L.Y.** (1991). Alteration of voltage-dependence of Shaker potassium channel by mutations in the S4 sequence. Nature **349,** 305–310.

**Perozo, E., Santa-Cruz-Toloza, L., Stefani, E., Bezanilla, F., and Papazian, D.M.** (1994). S4 mutations alter gating currents of *Shaker* K channels. Biophys. J. **66,** 345–354.

**Philippar, K., Fuchs, I., Lüthen, H., Hoth, S., Bauer, C., Haga, K., Thiel, G., Ljung, K., Sandberg, G., Böttger, M., Becker, D., and Hedrich, R.** (1999). Auxin-induced $K^+$ channel expression represents an essential step in coleoptile growth and gravitropism. Proc. Natl. Acad. Sci. USA **96,** 12186–12191.

**Roberts, S.K., and Tester, M.** (1995). Inward and outward $K^+$-selective currents in the plasma membrane of protoplasts from maize root cortex and stele. Plant J. **8,** 811–825.

**Schachtman, D.P., Schroeder, J.I., Lucas, W.J., Anderson, J.A., and Gaber, R.F.** (1994). Expression of an inward-rectifying potassium channel by the Arabidopsis KAT1 cDNA. Science **258,** 1654–1658.

**Sentenac, H., Bonneaud, N., Minet, M., Lacroute, F., Salmon, J.M., Gaymard, F., and Grignon, C.** (1992). Cloning and expression in yeast of a plant potassium ion transport system. Science **256,** 663–665.

**Tang, X.D., Marten, I., Dietrich, P., Ivashikina, N., Hedrich, R., and Hoshi, T.** (2000). Histidine$^{118}$ in the S2–S3 linker specifically controls activation of the KAT1 channel expressed in *Xenopus* oocytes. Biophys. J. **78,** 1255–1269.

**Terlau, H., Heinemann, S.H., Stühmer, W., Pongs, O., and Ludwig, J.** (1997). Amino terminal–dependent gating of the potassium channel rat eag is compensated by a mutation in the S4 segment. J. Physiol. Lond. **502,** 537–543.

**Thiel, G., Brüdern, A., and Gradmann, D.** (1996). Small inward rectifying $K^+$ channels in coleoptiles: Inhibition by external $Ca^{2+}$ and function in cell elongation. J. Membr. Biol. **149,** 9–26.

**Tytgat, J., Vereecke, J., and Carmeliet, E.** (1994). Reversal of rectification and alteration of selectivity and pharmacology in a mammalian Kv1.1 potassium channel by deletion of domains S1 to S4. J. Physiol. **481.1,** 7–13.

**Uozumi, N., Nakamura, T., Schroeder, J.I., and Muto, S.** (1998). Determination of transmembrane topology of an inward-rectifying potassium channel from *Arabidopsis thaliana* based on functional expression in *Escherichia coli*. Proc. Natl. Acad. Sci. USA **95,** 9773–9778.

**Wegner, L.H., De Boer, A.H., and Raschke, K.** (1994). Properties of the $K^+$ inward rectifier in the plasma membrane of xylem parenchyma cells from barley roots: Effects of $TEA^+$, $Ca^{2+}$, $Ba^{2+}$ and $La^{3+}$. J. Membr. Biol. **142,** 363–379.

**Yusaf, S.P., Wray, D., and Sivaprasadarao, A.** (1996). Measurement of the movement of the S4-segment during the activation of a voltage-gated potassium channel. Pflügers Arch. **433,** 91–97.

# Kapitel II: Outer Pore Residues Control the $H^+$ and $K^+$ Sensitivity of the *Arabidopsis* Potassium Channel AKT3

**Dietmar Geiger, Dirk Becker, Benoit Lacombe und Rainer Hedrich**

**Publiziert in The Plant Cell, Vol. 14, 1859-1868, August 2002**

**Eigene Beteiligung an der Arbeit:**

- Molekularbiologische Arbeiten zur Generierung sämtlicher AKT3 Porenmutanten.
- Biophysikalische Charakterisierung des AKT3-WT Kanals und der Porenmutanten in *Xenopus* Oozyten mit Hilfe der DEVC-Technik in Bezug auf pH- und $Ca^{2+}$-Empfindlichkeit sowie der Sensitivität gegenüber Kaliumionen.
- Auswertung der Daten.

The Plant Cell, Vol. 14, 1859–1868, August 2002, www.plantcell.org © 2002 American Society of Plant Biologists

# Outer Pore Residues Control the $H^+$ and $K^+$ Sensitivity of the Arabidopsis Potassium Channel AKT3

**Dietmar Geiger,[1] Dirk Becker,[1] Benoit Lacombe, and Rainer Hedrich[2]**

Julius-von-Sachs-Institute, Molecular Plant Physiology and Biophysics, Julius-von-Sachs-Platz 2, D-97082 Würzburg, Germany

**The Arabidopsis phloem channel AKT3 is the founder of a subfamily of *shaker*-like plant potassium channels characterized by weak rectification, $Ca^{2+}$ block, proton inhibition, and, as shown in this study, $K^+$ sensitivity. In contrast to inward-rectifying, acid-activated $K^+$ channels of the KAT1 family, extracellular acidification decreases AKT3 currents at the macroscopic and single-channel levels. Here, we show that two distinct sites within the outer mouth of the $K^+$-conducting pore provide the molecular basis for the pH sensitivity of this phloem channel. After generation of mutant channels and functional expression in *Xenopus* oocytes, we identified the His residue His-228, which is proximal to the $K^+$ selectivity filter (GYGD) and the distal Ser residue Ser-271, to be involved in proton susceptibility. Mutations of these sites, H228D and S271E, drastically reduced the $H^+$ and $K^+$ sensitivity of AKT3. Although in $K^+$-free bath solutions outward $K^+$ currents were abolished completely in wild-type AKT3, S271E as well as the AKT3-HDSE double mutant still mediated $K^+$ efflux. We conclude that the pH- and $K^+$-dependent properties of the AKT3 channel involve residues in the outer mouth of the pore. Both properties, $H^+$ and $K^+$ sensitivity, allow the fine-tuning of the phloem channel and thus seem to represent important elements in the control of membrane potential and sugar loading.**

## INTRODUCTION

The Arabidopsis genome encodes nine *shaker*-like potassium channels that share a common structure composed of six transmembrane domains (S1 to S6) and a pore region (P) located between S5 and S6 (Roelfsema and Hedrich, 1999; Zimmermann and Sentenac, 1999). Based on sequence similarity, these channels group into five subfamilies exhibiting different molecular and biophysical properties (Mäser et al., 2001). These five branches were named according to the first channel identified within each subfamily: KAT1, AKT1, AKT2/3, ATKC1, and SKOR.

Members of the KAT1 subfamily are voltage-dependent, acid-activated inward rectifiers, providing a molecular pathway for potassium uptake into guard cells (Schachtman et al., 1992; Hedrich et al., 1995; Müller-Röber et al., 1995; Nakamura et al., 1995; Pilot et al., 2001; Szyroki et al., 2001). The voltage-dependent gating of the Arabidopsis guard cell inward rectifier as well as the KAT1 $\alpha$-subunit is potassium insensitive and thus independent of the reversal potential for potassium ($E_K$) (Very et al., 1995; Brüggemann et al., 1999). Thus, in the membrane potential range positive to $E_K$ and negative to the activation potential, the inward rectifier will even mediate $K^+$ release (Brüggemann et al., 1999).

The acid activation of this channel, as well as that of the potato guard cell channel KST1, has been shown to result from a positive shift of the half-maximal activation voltage upon extracellular acidification, which in turn increases the open probability of this channel type at a given membrane potential (Hoth and Hedrich, 1999a). Although structure–function studies identified two His residues in the S3-S4 linker and in the pore region to control the pH regulation in KST1 (Hoth et al., 1997), distinct molecular elements seem to regulate the proton-induced activation of KAT1 (Hoth and Hedrich, 1999a).

AKT2/3-like channels represent phloem-localized transporters, the pH sensitivity of which determines the redistribution of potassium, control of the membrane potential, sugar loading, and thus long-distance solute transport within the phloem network (Philippar et al., 1999; Deeken et al., 2000; Ache et al., 2001; Dennison et al., 2001). AKT2 and AKT3 are two proteins encoded by the same gene (At4 g22200); AKT3 (Ketchum and Slayman, 1996; Marten et al., 1999; Hoth et al., 2001) represents a truncated version of AKT2 (Cao et al., 1995; Lacombe et al., 2000b) characterized by a 15–amino acid shorter cytoplasmic N terminus. The presence of one or both of these proteins in planta has not yet been determined. Nevertheless, AKT2 and AKT3 have the same functional properties in *Xenopus* oocytes (Marten et al., 1999; Lacombe et al., 2000b).

[1] These authors contributed equally to this work

[2] To whom correspondence should be addressed. E-mail hedrich@botanik.uni-wuerzburg.de; fax 49-931-888-6157.

Article, publication date, and citation information can be found at www.plantcell.org/cgi/doi/10.1105/tpc.003244.

Members of the AKT2/3 subfamily (Cao et al., 1995), such as AKT2/3 and ZMK2, exhibit weak rectification properties only, allowing the uptake of potassium ions at membrane potentials negative and potassium release positive to $E_K$ (Marten et al., 1999; Philippar et al., 1999; Bauer et al., 2000; Lacombe et al., 2000b; Dreyer et al., 2001). Furthermore, AKT2/3-like channels are inhibited by extracellular protons. The proton-mediated decrease in macroscopic currents of AKT2/3 channels results from a reduction in single-channel conductance (Marten et al., 1999) rather than a decrease in the number of active channels (Lacombe et al., 2000a).

In a previous study, in which we characterized a chimera between members of the KAT1 and AKT2/3 families, we were able to demonstrate that the pore region contains all of the structural elements for rectification, susceptibility toward extracellular $Ca^{2+}$, and regulation by extracellular protons (Hoth et al., 2001). The interaction of AKT2/3 with $H^+$ represents a feature that distinguishes this channel type from the $K^+$ uptake channels but that is shared with the Arabidopsis outward rectifiers SKOR and GORK (Lacombe et al., 2000a).

Gating of the latter has been shown to be sensitive to extracellular potassium. Decreasing extracellular potassium concentrations shift the half-maximal activation potential of SKOR and GORK towards negative membrane potentials, whereas complete removal of potassium renders these channels nonactive (Gaymard et al., 1998; Ache et al., 2000). This behavior and modulation of $K^+$ susceptibility by $H^+$ is well known for animal potassium channels of the *shaker* family (Schönherr and Heinemann, 1996; Jäger et al., 1998; Jäger and Grissmer, 2001).

In this report, we have investigated the molecular determinants of extracellular proton and potassium sensitivity in AKT3. Using site-directed mutagenesis in combination with heterologous expression in *Xenopus* oocytes, we provide evidence that the pH and potassium sensitivity of AKT3 depends on two distinct positions, His-228 and Ser-271,

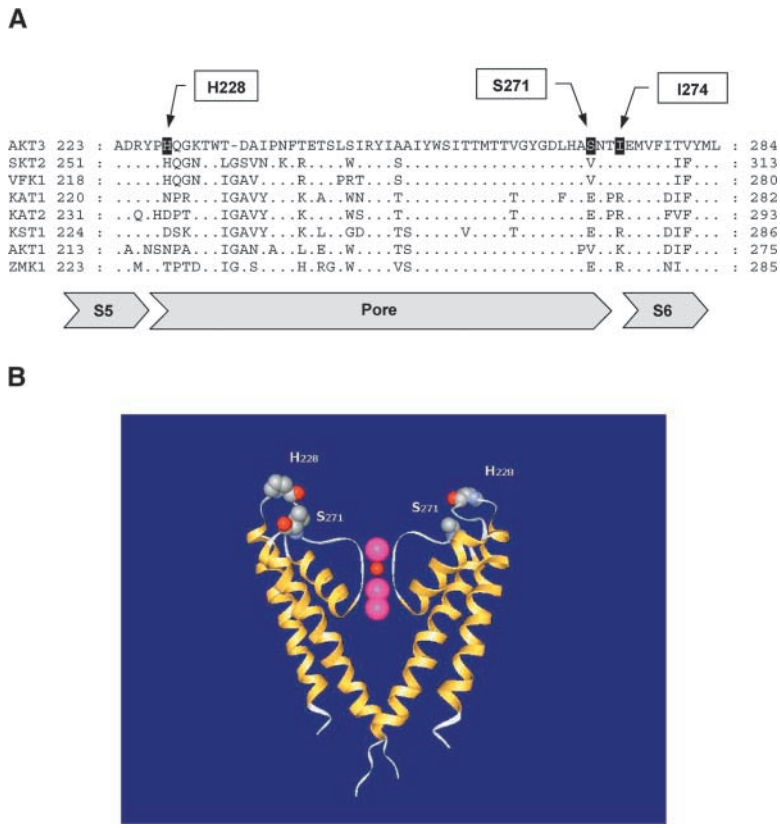


**Figure 1.** Alignment of the Pore Region of Plant *shaker*-Like $K^+$ Channels.

**(A)** Fifty-one amino acids from the end of the transmembrane region of S5 to the beginning of S6 are shown. The amino acids mutated in this study are indicated with arrows. Regions of interest are emphasized by boxes. Gray boxes indicate the predicted S5, pore, and S6 regions.
**(B)** Structural model of the KcsA channel depicting the equivalent positions of His-228 and Ser-271 in AKT3. An alignment of AKT3 with KcsA revealed that His-228 would reside in the descending loop and Ser-271 would reside in the ascending loop of the AKT3 channel.

within the outer mouth of the pore region. Although the single mutants S271E and H228D exhibit a pronounced decrease in pH sensitivity, any mutant exhibiting changes at Ser-271, including the double mutant HDSE, lacks susceptibility to extracellular potassium. This finding indicates that $H^+$ and $K^+$ seem to compete for binding sites at the extracellular face of the channel pore.

## RESULTS

Based on the analysis of chimeric channels between the proton-activated KST1 and the proton-blocked AKT3, we recently showed that the pore region harbors the AKT2/3-specific $H^+$ sensor (Hoth et al., 2001). This finding is in agreement with a pore block of AKT3 channels by extracellular protons. Mutation of a Met (Met-260) highly conserved in the narrow pore of members of the AKT2/3 family, however, did not affect pH sensitivity. To explore the molecular basis for the peculiar pH sensitivity of this phloem $K^+$ channel, we focused on residues in the outer mouth of the AKT3 pore. As a result of their pKa in the physiological range, His residues as well as charged amino acids have been implicated in mediating pH sensitivity in a number of potassium channels (Guy and Durell, 1995; Jäger and Grissmer, 2001).

Comparing the extended pore region of different *shaker*-like plant potassium channels (Figure 1A) shows that the AKT3-like channels differ at three conspicuous positions with respect to members of the KAT1 and AKT1 subfamily. A conserved HQG motif in the S5-P linker is characteristic of AKT2/3 family members (Ehrhardt et al., 1997; Ache et al., 2001). In addition, the uncharged residues Ser-271 and Ile-274 in the ascending loop of the AKT3 pore are represented by charged amino acids at the corresponding positions in the inward rectifiers (Figure 1A).

### His-228 Is a Key Element of the Proton Sensor

Marten et al. (1999) have shown that the macroscopic current in wild-type AKT3 (AKT3-WT) is decreased by external acidification. Although a 1.5-unit pH decrease from 7.5 to 6.0 resulted in a 32% ± 7.7% reduction of macroscopic current at −160 mV, the current was blocked almost completely at pH 4.5 (Figures 2A, 2B, and 3). To investigate the role of His-228 in pH sensing, we mutated this residue in AKT3 to Ala (H228A), Asn (H228N), Arg (H228R), and Asp (H228D). The macroscopic currents of AKT3 wild-type and mutant channels expressed in *Xenopus* oocytes were monitored in response to stepwise changes in extracellular pH (7.5, 6.0, and 4.5).

Instantaneous and time-dependent activation, like AKT3-WT gating (Figure 2A), was conserved in all mutant channels studied (Figure 2A). This finding demonstrates that these residues are very unlikely to play a role in voltage-dependent

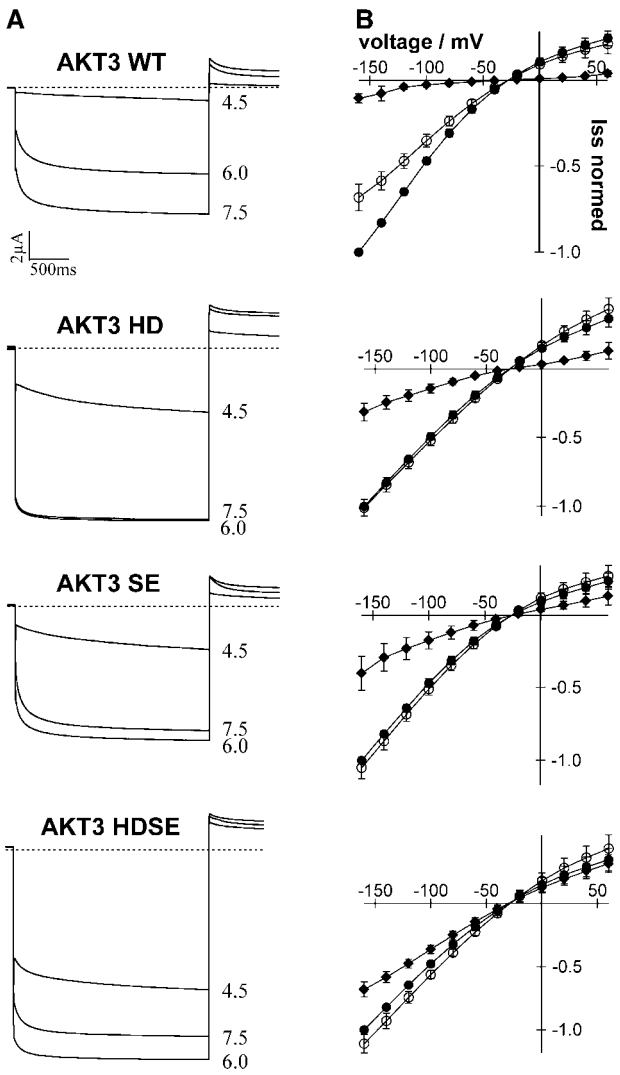


**Figure 2.** pH Effect on Macroscopic Currents for AKT3-WT and Mutants.

**(A)** Whole-oocyte currents in 30 mM $K^+$ of AKT3-WT and mutants in response to three different external pH values (7.5, 6.0, and 4.5) were studied. Currents were elicited by a test pulse to −160 mV from a holding potential of −30 mV. Tail currents were recorded at 0 mV. Traces depict representative cells from at least three independent experiments.

**(B)** Current-voltage relationships of AKT3-WT and mutants of steady state currents ($I_{ss}$). Currents were normalized to the current recorded at −160 mV at pH 7.5 and plotted as a function of applied voltage at pH 7.5 (closed circles), pH 6.0 (open circles), and pH 4.5 (closed diamonds). Results shown are means ± SD of three or more experiments.

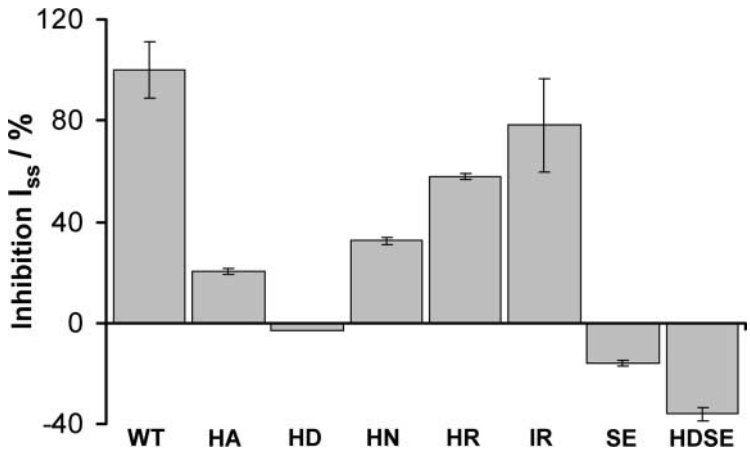


**Figure 3.** Proton Sensitivity of AKT3-WT and Mutant Channels.

$H^+$-dependent block of steady state currents at −160 mV in response to a stepwise change of the extracellular proton concentration from pH 7.5 to 6.0. The $H^+$ sensitivity of the AKT3 mutants is given as relative inhibition compared with AKT3-WT. Data shown are means ± SD of three or more experiments. HA, H228A; HD, H228D; HN, H228N; HR, H228R; IR, I274R; SE, S271E.

gating of the AKT3 channel. In contrast to AKT3-WT, however, channel mutants at position His-228 were characterized by a pronounced reduction in pH sensitivity, indicating that this residue is involved in $H^+$ sensing. When comparing macroscopic currents of wild-type and mutant channels in response to a pH shift from 7.5 to 6.0, the relative block by protons was still 57.86% ± 1.4% for AKT3-H228R, whereas the mutants AKT3-H228N and AKT3-H228A were inhibited by 32.47% ± 1.6% and 20.38% ± 1.09%, respectively (Figure 3).

The strongest effect, however, was obtained when His-228 was replaced with the negatively charged amino acid Asp. The AKT3-H228D mutant was completely insensitive to changes in external proton concentration in the pH range of 7.5 to 6.0. At more acidic pH (pH 4.5), almost no currents were recorded in oocytes injected with AKT3-WT, whereas AKT3-H228D still provoked inward as well outward potassium currents. The proton block at pH 4.5 compared with pH 7.5 was only 69% ± 6.3% (Figures 2A and 2B, second panel, and Figure 3).

### His-228 and Ser-271 Work Together

To determine whether additional residues besides His-271 contribute to the $H^+$ susceptibility of AKT3, we extended our studies to Ser-271 and Ile-274, which are distal to the selectivity filter GYGD (Figure 1, positions +4 and +7). Although these positions are occupied by charged amino acids in most of the inward-rectifying channels, noncharged or hydrophobic amino acids are present in members of the AKT3 subfamily. Therefore, these two positions in AKT3 were mutated by replacing Ser-271 with Glu (S271E) and Ile-274 with Arg (I274R) in the positions of acid-activated inward rectifiers.

The AKT3 channels carrying mutations at Ser-271 and Ile-274 distal to the pore region responded differentially to changes in extracellular pH. Although the AKT3-I274R mutant displayed pH sensitivity similar to that of the AKT3-WT channel (Figure 3), the mutant AKT3-S271E behaved like the AKT3-H228D mutant (Figures 2A and 2B, third panel). Again, a pH shift from 7.5 to 6.0 was ineffective at modulating macroscopic currents through AKT3-S271E, whereas at pH 4.5, steady state currents were reduced by 60% ± 1.5% (Figure 2, third panel).

To test the hypothesis that both residues, His-228 and Ser-289, contribute to the extracellular pH sensor of AKT3, we exposed the double mutant H228D-S289E (AKT3-HDSE) to pH changes (Figures 2A and 2B, bottom panel). In contrast to the single-mutant responses to a pH change from 7.5 to 6.0, $K^+$ currents mediated by the double-mutant channel increased. Inhibition of steady state currents upon a shift from pH 7.5 to 4.5 was only 32% ± 5.9%. Thus, AKT3-HDSE displayed the strongest reduction in proton susceptibility among the mutants analyzed.

### Single-Mutant Channels Are pH Insensitive

To analyze the altered pH dependence of the AKT3 mutants H228D, S289E, and HDSE in more detail, the single-channel conductance of the mutants in response to a pH change from 7.5 to 5.6 were compared with that of AKT3-WT (Figure 4). At neutral pH, the single-channel currents of all mu-

tants were wild type like (Figure 3). In contrast to the AKT3-WT channel, however, a decrease in external pH from 7.5 to 5.6 did not change the single-channel conductance in any of the three mutants (Figures 4C to 4F). This behavior provides evidence that both residues, His-228 and Ser-271, seem to control the pH-dependent $K^+$ permeation through AKT3.

**AKT3 Is $K^+$ Sensitive**

When studying the pH dependence of AKT3 at different $K^+$ concentrations, we recognized a peculiar $K^+$ dependence in the AKT3-WT channel. Therefore, we analyzed the macroscopic currents of AKT3-WT and mutants in response to

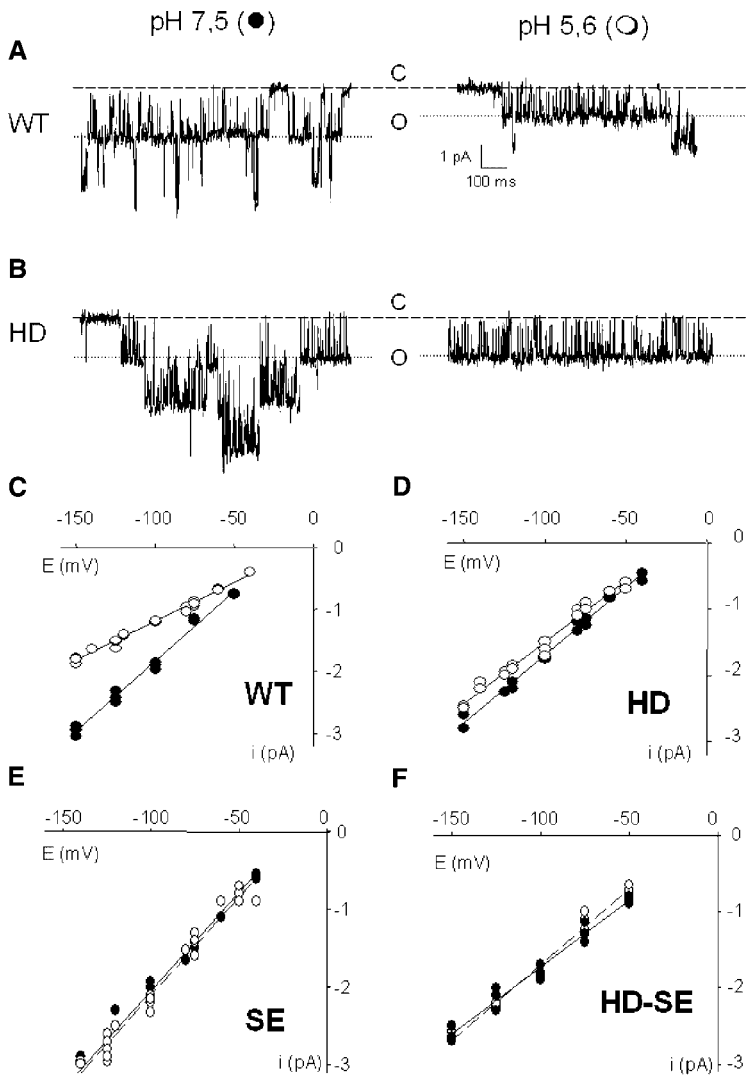


**Figure 4.** Effect of Extracellular pH on the Single-Channel Conductance of AKT3-WT and Mutants.

**(A)** and **(B)** Single-channel fluctuations at pH 7.5 (left) and pH 5.6 (right) for wild-type (WT) and H228D channels recorded in the cell-attached patch-clamp configuration at −100 mV. The closed state is marked with ticked lines (C), and the first open channel line is marked with a dotted line (O).

**(C)** to **(F)** Single-channel current-voltage relationship at pH 7.5 (closed circles) and pH 5.6 (open circles) for wild-type **(C)**, H228D **(D)**, S271E **(E)**, and HDSE **(F)** channels. Linear regressions on three to six different patches in each condition revealed the following single-channel conductance values: wild-type (pH 7.5), 22.5 ± 0.3 pS; wild-type (pH 5.6), 12.3 ± 0.3 pS; H228D (pH 7.5), 21.1 ± 0.8 pS; H228D (pH 5.6), 18.3 ± 0.2 pS; S271E (pH 7.5), 25.4 ± 1.1 pS; S271E (pH 5.6), 25.4 ± 0.5 pS; HDSE (pH 7.5), 17.5 ± 0.8 pS; and HDSE (pH 5.6), 20.2 ± 0.8 pS. Data represent means ± SE of three or more experiments.

varying external potassium concentrations. We found both $K^+$ uptake and $K^+$ release through AKT3 to depend strongly on the presence of external $K^+$ ions (Figure 5A). A decrease of the $K^+$ concentration from 100 to 30 mM and finally to 10 mM in the bath solution gradually decreased steady state inward currents but left outward currents at +40 mV unaffected. Omitting $K^+$ from the perfusion solution and thereby maximizing the driving force for $K^+$ release resulted in the complete loss of outward $K^+$ currents through AKT3 (Figure 5A). In this context, it should be mentioned that the voltage-dependent gating of inward-rectifying *shaker*-like plant potassium channels is insensitive to changes in the external $K^+$ concentration (Very et al., 1995; Blatt and Gradmann, 1997; Brüggemann et al., 1999).

When we compared the different mutants with respect to $K^+$ dependence, we recognized that the mutant AKT3-S271E, although reduced, even at nominally zero $K^+$, carried outward currents (Figure 5B). The double mutant AKT3-HDSE, however, was completely insensitive to changes in external $K^+$ concentrations. After the replacement of $K^+$ with $Rb^+$ or $Cs^+$, we found that these monovalent cations were able to activate the AKT3 channel as well (Figure 6). In these experiments, outward currents through AKT3-WT and AKT3-H228D at +40 mV were of the same order of magnitude (Figure 6). In contrast, $Na^+$ and $Li^+$ were not able to restore outward currents.

The distal pore mutant AKT3-S271E as well as the double mutant AKT3-HDSE, which is characterized by outward currents even at nominally zero external $K^+$, mediated $K^+$ efflux irrespective of the nature of the external cations present. These experiments suggest that the $K^+$-dependent modulation of outward currents in AKT3 relies on potassium binding in the outer pore region rather than in the ion permeation pathway. However, when probing potassium sensitivity after a shift to pH 5.6, we found that the AKT3-S271E mutant regained its $K^+$ sensitivity (Figure 7). Like AKT3-WT and the AKT3-H228D mutant, at pH 5.6, the outward $K^+$ currents through channels harboring mutations at position Ser-271 declined significantly.

## DISCUSSION

### pH Sensitivity

The performance of ion channels in response to both internal and external pH changes is of crucial physiological importance for plants (Dietrich et al., 2001; Felle, 2001). Here, we have studied the molecular basis of the proton block and $K^+$ sensitivity of the Arabidopsis phloem channel AKT3 (Marten et al., 1999; Deeken et al., 2000; Lacombe et al., 2000b). Using site-directed mutagenesis followed by heterologous characterization in *Xenopus* oocytes, we showed that two titratable sites located in the outer mouth of the $K^+$ channel pore are essential for the peculiar pH dependence of AKT3. A His residue at position 228 in the S5-P linker of AKT3, when replaced with Asp (H228D), was characterized by a loss of proton susceptibility (Figure 3). In addition, we determined that a second site on the ascending loop of the AKT3 pore (Figure 2B) was involved in proton sensing.

Mutations at the second site, S271E, like H228D, significantly shifted the pKa of the proton-mediated block toward more acidic pH values. Thus, our findings are in agreement with previous studies that have shown that the molecular basis of the proton sensitivity of ion channels can be attributed to the protonation of titratable amino acids such as His, Cys, and Lys (Guy and Durell, 1995; Jäger and Grissmer, 2001). However, different molecular mechanisms have been proposed to account for the proton sensitivity of ion channels such as the inward-rectifying plant potassium channel KST1 or animal $K^+$ channels such as hKir3.4, hKv1.3, and

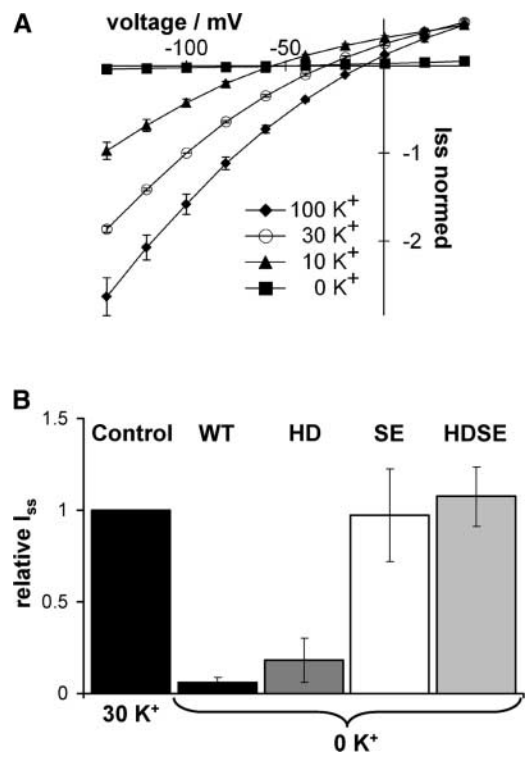


**Figure 5.** Potassium Sensitivity of AKT3-WT and Mutant Channels.

**(A)** Steady state current-voltage relationship of AKT3-WT channels at 100 mM (closed diamonds), 30 mM (open circles), 10 mM (closed triangles), and 0 mM (closed squares) external $K^+$ concentrations. Currents were normalized to −100 mV in 30 mM at pH 7.5. Note that the reversal potential of AKT3 current is close to the $K^+$ equilibrium potential in 100, 30, and 10 mM.

**(B)** Relative steady state outward $K^+$ currents ($I_{ss}$) at +40 mV in response to a shift from 30 to nominal 0 mM external $K^+$ concentration. Currents were normalized to $I_{ss}$ of AKT3-WT recorded in 30 mM external $K^+$ concentration. Results represent means ± SD of three or more experiments.

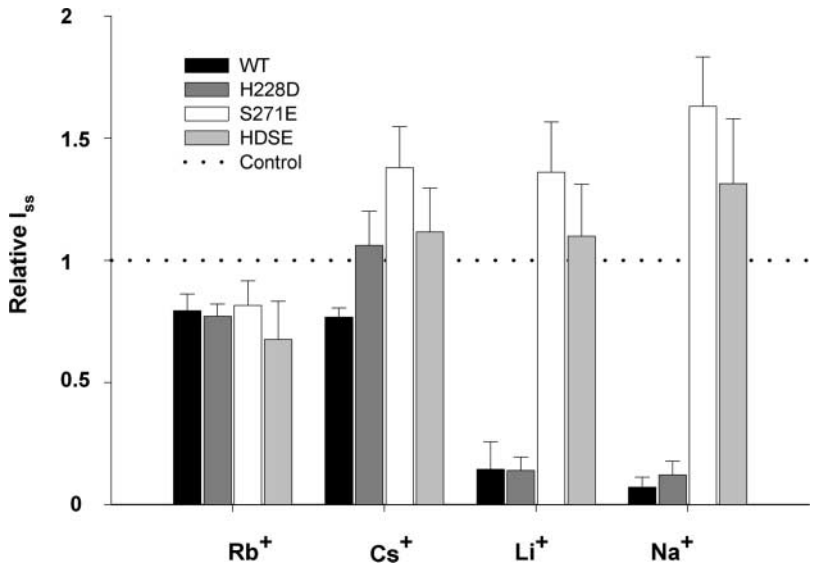


**Figure 6.** Sensitivity of AKT3-WT and Mutant Channels towards Monovalent Cations.

Relative steady state outward $K^+$ currents ($I_{ss}$) at +40 mV in response to a replacement of 100 mM external $K^+$ by $Rb^+$, $Cs^+$, $Li^+$, or $Na^+$. Currents were normalized to $I_{ss}$ in 100 mM external $K^+$ concentration (dotted line). Results represent means ± SD of three or more experiments. Note that in AKT3-WT and H228D, neither $Li^+$ nor $Na^+$ can substitute for $K^+$, whereas mutants carrying a mutation at Ser-271 mediate outward currents irrespective of the nature of the cation present in the bath.

rKv1.5 (Coulter et al., 1995; Hoth et al., 1997; Jäger et al., 1998; Steidl and Yool, 1999).

KST1 activation by acidic pH involves the protonation of two extracellular His residues. Although one His is located within the KST1 pore, the second resides in the S3-S4 linker, which very likely contributes to the formation of the outer pore (Hoth and Hedrich, 1999b). Protonation of these His residues leads to a shift in the voltage-dependent open probability of KST1 toward less negative membrane potentials and thereby increases $K^+$ uptake (Hoth et al., 1997). In contrast, hKir3.4, like AKT3, undergoes proton-induced reductions in single-channel conductance. Structure–function analyses revealed that in hKir3.4, upon protonation of a His near the pore, a titratable Cys residue influences ion conductance (Coulter et al., 1995). In line with the molecular mechanism proposed for the proton-induced block of hKir3.4, the pH-mediated decrease in single-channel conductance observed in AKT3-WT is lost in the AKT3 mutants H228D and S271E and in the double mutant AKT3-HDSE.

### Potassium Sensitivity

The current amplitude and magnitude of inactivation of hKv1.3 and rKv1.5 are reduced by acidic extracellular pH, an effect hypothesized to be induced by the protonation of a His residue located near the channel pore (Busch et al., 1991; Jäger et al., 1998; Steidl and Yool, 1999). These studies have shown that pH sensitivity interferes with $K^+$-dependent gating of these voltage-dependent outward-rectifier channels. Although this phenomenon is well known for vertebrate *shaker*-like $K^+$ channels (Yellen, 1997), this behavior was demonstrated only recently for plant outward rectifiers (Gaymard et al., 1998; Ache et al., 2000; Lacombe et al., 2000a).

The Arabidopsis delayed rectifiers SKOR and GORK are affected by external $K^+$ in a dual fashion: (1) the activation potential is sensitive to $E_K$; and (2) $K^+$ release through these channels requires external potassium (Gaymard et al., 1998; Ache et al., 2000; Ivashikina et al., 2001). In this context, it should be noted that the gating of TOK1, the yeast outward rectifier, is sensitive to external changes in $K^+$ ions as well. TOK1 comprises four transmembrane domains (S1 to S4) followed by two pore motifs (S5-P1-S6 and S7-P2-S8) in tandem, and Vergani and colleagues (Vergani et al., 1998; Vergani and Blatt, 1999) have shown that mutations on either site of the selectivity filter affect the $K^+$-dependent gating of this channel.

Here, we have shown that $K^+$ efflux mediated by the weak inward rectifier AKT3 is sensitive to extracellular potassium. As in GORK, SKOR, and the animal *shaker*-like potassium channels, removal of potassium from the bath solution abolished outward currents through AKT3. S271E and the HDSE double mutant, however, which have been shown to be involved in proton sensing, have counterparts in the potassium-insensitive *shaker*-like plant inward rectifiers (Brüggemann et

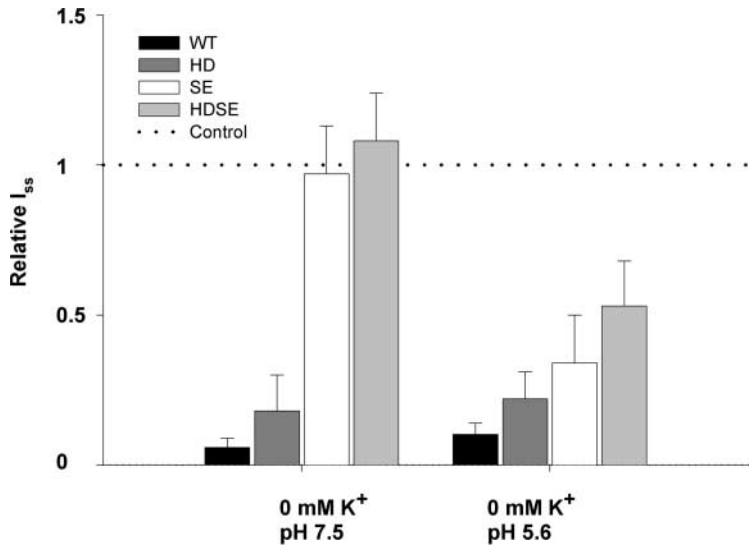


**Figure 7.** AKT3 Mutants Regain $K^+$ Sensitivity at Acidic pH.

Relative steady state outward $K^+$ currents ($I_{ss}$) at +40 mV in response to a shift from 30 to nominal 0 mM external $K^+$ concentration at pH 7.5 compared with pH 5.6. Currents were normalized to $I_{ss}$ recorded in 30 mM external $K^+$ concentration at the corresponding pH values (dotted line). Results represent means ± SD of three or more experiments.

al., 1999). In contrast to the AKT3-WT channel and the H228D mutant, these mutants still conduct outward potassium currents in the absence of external potassium.

Future experiments replacing Ser-271 with other amino acids and the test of the role of neighboring positions will allow us to determine if the elimination of potassium dependence is caused by the absence of Ser or just by the presence of any negatively charged residue at position 271. In agreement with the behavior of rKv1.4, outward $K^+$ currents could be restored by replacing external potassium with rubidium or cesium but not with sodium or lithium (Pardo et al., 1992). The fact that the well-known voltage-dependent $K^+$ channel blocker $Cs^+$ is able to maintain the outward current suggests the existence of an external $K^+$ lock-in site in the outer mouth of the AKT3 channel (Vergara et al., 1999; Jäger and Grissmer, 2001). However, this site is not abolished in the AKT3-S271E mutant, because this mutant, like its animal counterparts, regains its potassium sensitivity at acidic extracellular pH (Jäger and Grissmer, 2001).

In recent work on the KcsA potassium channel, it has been shown that a $K^+$ ion is present at the outer month of the pore (Morais-Cabral et al., 2001; Zhou et al., 2001). Thus, the amino acids His-228 and Ser-271 could play a major role in the maintenance of the electrostatic field that stabilized this $K^+$ ion at this position (Figure 1B).

Based on our observations that (1) two peripheral residues modulate the pH sensitivity of the AKT3 channel and (2) one of these residues confers potassium sensitivity to AKT3, we conclude that protonation of these amino acids in the outer pore controls $K^+$-dependent $K^+$ currents through the phloem $K^+$ channel. The role of $H^+$ and $K^+$ sensitivity of the AKT2/3 channels will now be addressed in planta by expressing the mutant channels under the control of the AKT2/3 promoter in the *akt2/3-1* background.

## METHODS

AKT3 mutants were generated using the Quick-Change site-directed mutagenesis kit (Stratagene, Amsterdam, The Netherlands) as described in Hoth and Hedrich (1999a). The complementary RNAs of AKT3 wild-type and mutant channels were generated by in vitro transcription (T7-Megascript kit; Ambion, Austin, TX) and injected into oocytes of *Xenopus laevis* (Centre de Recherche en Biochimie Macromoléculaire, Centre National de la Recherche Scientifique, Montpellier, France) using a PicospritzerII microinjector (General Valve, Fairfield, NJ). Two to 6 days after injection, double-electrode voltage-clamp recordings were made with a Turbotec-01C amplifier (NPI Instruments, Tamm, Germany). The electrodes were filled with 3 M KCl and had typical input resistances of ~2 MΩ.

Solutions for pH measurements were composed of 30 mM KCl, 2 mM $MgCl_2$, 1 mM $CaCl_2$, and 10 mM Tris/Mes, pH 7.5, Mes/Tris, pH 6.0, or citrate/Tris, pH 4.5. The solution used to determine the sensitivity toward extracellular cations contained 100 mM XCl (where X = K, Na, Li, Rb, or Cs), 2 mM $MgCl_2$, 1 mM $CaCl_2$, and 10 mM Tris/Mes, pH 7.5. Solutions for Figures 5 and 7 were composed of 100, 30, and 10 mM KCl, 2 mM $MgCl_2$, 1 mM $CaCl_2$, and 10 mM Tris/Mes, pH 7.5, or Mes/Tris pH 5.6. The ionic strength was kept constant by replacing $K^+$ with *N*-methyl-D-glucamine. All media were adjusted to a final osmolality of 215 to 235 mosmol/kg with D-sorbitol.

For patch-clamp experiments, devitellinized oocytes were placed

in a bath solution containing 100 mM KCl, 2 mM $MgCl_2$, 1 mM $CaCl_2$, and 10 mM Tris/Mes, pH 7.5. Pipettes were filled with solution containing 100 mM KCl, 2 mM $MgCl_2$, 1 mM $CaCl_2$, and 10 mM Tris/Mes, pH 7.5, or Mes/Tris, pH 5.6. Currents were recorded in the cell-attached configuration using an EPC-9 amplifier (HEKA, Lambrecht, Germany) as described previously (Marten et al., 1999).

Upon request, all novel material described in this article will be made available in a timely manner for noncommercial research purposes. No restrictions or conditions will be placed on the use of any materials described in this article that would limit their use for noncommercial purposes.

### Accession Numbers

The GenBank accession numbers for the sequences shown in Figure 1 are as follows: KST1, X79779; KAT1, M86990; KAT2, NP_193563; AKT1, X62907; AKT3, U44745; VFK1, CAC29435; ZMK1, CAA68912; and SKT2, CAA70870.

### ACKNOWLEDGMENTS

We are grateful to Kerstin Neuwinger for technical assistance. This work was founded by a European Molecular Biology Organization long-term fellowship to B.L. and Deutsche Forschungsgemeinschaft grants to R.H.

Received March 20, 2002; accepted May 6, 2002.

### REFERENCES

**Ache, P., Becker, D., Deeken, R., Dreyer, I., Weber, H., Fromm, J., and Hedrich, R.** (2001). VFK1, a *Vicia faba* $K^+$ channel involved in phloem unloading. Plant J. **27,** 571–580.

**Ache, P., Becker, D., Ivashikina, N., Dietrich, P., Roelfsema, M.R., and Hedrich, R.** (2000). GORK, a delayed outward rectifier expressed in guard cells of *Arabidopsis thaliana*, is a $K^+$-selective, $K^+$-sensing ion channel. FEBS Lett. **486,** 93–98.

**Bauer, C.S., Hoth, S., Haga, K., Philippar, K., Aoki, N., and Hedrich, R.** (2000). Differential expression and regulation of $K^+$ channels in the maize coleoptile: Molecular and biophysical analysis of cells isolated from cortex and vasculature. Plant J. **24,** 139–145.

**Blatt, M.R., and Gradmann, D.** (1997). $K^+$-sensitive gating of the $K^+$ outward rectifier in *Vicia* guard cells. J. Membr. Biol. **158,** 241–256.

**Brüggemann, L., Dietrich, P., Becker, D., Dreyer, I., Palme, K., and Hedrich, R.** (1999). Channel-mediated high-affinity $K^+$ uptake into guard cells from *Arabidopsis*. Proc. Natl. Acad. Sci. USA **96,** 3298–3302.

**Busch, A.E., Hurst, R.S., North, R.A., Adelman, J.P., and Kavanaugh, M.P.** (1991). Current inactivation involves a histidine residue in the pore of the rat lymphocyte potassium channel RGK5. Biochem. Biophys. Res. Commun. **179,** 1384–1390.

**Cao, Y., Ward, J.M., Kelly, W.B., Ichida, A.M., Gaber, R.F., Anderson, J.A., Uozumi, N., Schroeder, J.I., and Crawford, N.M.** (1995). Multiple genes, tissue specificity, and expression-dependent modulation contribute to the functional diversity of potassium channels in *Arabidopsis thaliana*. Plant Physiol. **109,** 1093–1106.

**Coulter, K.L., Perier, F., Radeke, C.M., and Vandenberg, C.A.** (1995). Identification and molecular localization of a pH-sensing domain for the inward rectifier potassium channel HIR. Neuron **15,** 1157–1168.

**Deeken, R., Sanders, C., Ache, P., and Hedrich, R.** (2000). Developmental and light-dependent regulation of a phloem-localised $K^+$ channel of *Arabidopsis thaliana*. Plant J. **23,** 285–290.

**Dennison, K.L., Robertson, W.R., Lewis, B.D., Hirsch, R.E., Sussman, M.R., and Spalding, E.P.** (2001). Functions of AKT1 and AKT2 potassium channels determined by studies of single and double mutants of *Arabidopsis*. Plant Physiol. **127,** 1012–1019.

**Dietrich, P., Sanders, D., and Hedrich, R.** (2001). The role of ion channels in light-dependent stomatal opening. J. Exp. Bot. **52,** 1959–1967.

**Dreyer, I., Michard, E., Lacombe, B., and Thibaud, J.B.** (2001). A plant Shaker-like $K^+$ channel switches between two distinct gating modes resulting in either inward-rectifying or "leak" current. FEBS Lett. **505,** 233–239.

**Ehrhardt, T., Zimmermann, S., and Müller-Röber, B.** (1997). Association of plant $K^+_{in}$ channels is mediated by conserved C-termini and does not affect subunit assembly. FEBS Lett. **409,** 166–170.

**Felle, H.H.** (2001). pH: Signal and messenger in plant cells. Plant Biol. **3,** 577–591.

**Gaymard, F., Pilot, G., Lacombe, B., Bouchez, D., Bruneau, D., Boucherez, J., Michaux-Ferriere, N., Thibaud, J.B., and Sentenac, H.** (1998). Identification and disruption of a plant shaker-like outward channel involved in $K^+$ release into the xylem sap. Cell **94,** 647–655.

**Guy, H.R., and Durell, S.R.** (1995). Structural models of $Na^+$, $Ca^{2+}$, and $K^+$ channels. Soc. Gen. Physiol. Ser. **50,** 1–16.

**Hedrich, R., Moran, O., Conti, F., Busch, H., Becker, D., Gambale, F., Dreyer, I., Küch, A., Neuwinger, K., and Palme, K.** (1995). Inward rectifier potassium channels in plants differ from their animal counterparts in response to voltage and channel modulators. Eur. Biophys. J. **24,** 107–115.

**Hoth, S., Dreyer, I., Dietrich, P., Becker, D., Müller-Röber, B., and Hedrich, R.** (1997). Molecular basis of plant-specific acid activation of $K^+$ uptake channels. Proc. Natl. Acad. Sci. USA **94,** 4806–4810.

**Hoth, S., Geiger, D., Becker, D., and Hedrich, R.** (2001). The pore of plant $K^+$ channels is involved in voltage and pH sensing: Domain-swapping between different $K^+$ channel $\alpha$-subunits. Plant Cell **13,** 943–952.

**Hoth, S., and Hedrich, R.** (1999a). Distinct molecular bases for pH sensitivity of the guard cell $K^+$ channels KST1 and KAT1. J. Biol. Chem. **274,** 11599–11603.

**Hoth, S., and Hedrich, R.** (1999b). Susceptibility of the guard-cell $K^+$-uptake channel KST1 to $Zn^{2+}$ requires histidine residues in the S3-S4 linker and in the channel pore. Planta **209,** 543–546.

**Ivashikina, N., Becker, D., Ache, P., Meyerhoff, O., Felle, H.H., and Hedrich, R.** (2001). $K^+$ channel profile and electrical properties of *Arabidopsis* root hairs. FEBS Lett. **508,** 463–469.

**Jäger, H., and Grissmer, S.** (2001). Regulation of a mammalian Shaker-related potassium channel, hKv1.5, by extracellular potassium and pH. FEBS Lett. **488,** 45–50.

**Jäger, H., Rauer, H., Nguyen, A.N., Aiyar, J., Chandy, K.G., and Grissmer, S.** (1998). Regulation of mammalian Shaker-related $K^+$ channels: Evidence for non-conducting closed and non-conducting inactivated states. J. Physiol. **506,** 291–301.

**Ketchum, K.A., and Slayman, C.W.** (1996). Isolation of an ion channel gene from *Arabidopsis thaliana* using the H5 signature sequence from voltage-dependent $K^+$ channels. FEBS Lett. **378,** 19–26.

**Lacombe, B., Pilot, G., Gaymard, F., Sentenac, H., and Thibaud, J.B.** (2000a). pH control of the plant outwardly-rectifying potassium channel SKOR. FEBS Lett. **466,** 351–354.

**Lacombe, B., Pilot, G., Michard, E., Gaymard, F., Sentenac, H., and Thibaud, J.B.** (2000b). A shaker-like $K^+$ channel with weak rectification is expressed in both source and sink phloem tissues of *Arabidopsis*. Plant Cell **12,** 837–851.

**Marten, I., Hoth, S., Deeken, R., Ache, P., Ketchum, K.A., Hoshi, T., and Hedrich, R.** (1999). AKT3, a phloem-localized $K^+$ channel, is blocked by protons. Proc. Natl. Acad. Sci. USA **96,** 7581–7586.

**Mäser, P., et al.** (2001). Phylogenetic relationships within cation transporter families of *Arabidopsis*. Plant Physiol. **126,** 1646–1667.

**Morais-Cabral, J.H., Zhou, Y., and MacKinnon, R.** (2001). Energetic optimization of ion conduction rate by the $K^+$ selectivity filter. Nature **414,** 37–42.

**Müller-Röber, B., Ellenberg, J., Provart, N., Willmitzer, L., Busch, H., Becker, D., Dietrich, P., Hoth, S., and Hedrich, R.** (1995). Cloning and electrophysiological analysis of KST1, an inward rectifying $K^+$ channel expressed in potato guard cells. EMBO J. **14,** 2409–2416.

**Nakamura, R.L., McKendree, W.L., Jr., Hirsch, R.E., Sedbrook, J.C., Gaber, R.F., and Sussman, M.R.** (1995). Expression of an *Arabidopsis* potassium channel gene in guard cells. Plant Physiol. **109,** 371–374.

**Pardo, L.A., Heinemann, S.H., Terlau, H., Ludewig, U., Lorra, C., Pongs, O., and Stühmer, W.** (1992). Extracellular $K^+$ specifically modulates a rat brain $K^+$ channel. Proc. Natl. Acad. Sci. USA **89,** 2466–2470.

**Philippar, K., Fuchs, I., Luthen, H., Hoth, S., Bauer, C.S., Haga, K., Thiel, G., Ljung, K., Sandberg, G., Bottger, M., Becker, D., and Hedrich, R.** (1999). Auxin-induced $K^+$ channel expression represents an essential step in coleoptile growth and gravitropism. Proc. Natl. Acad. Sci. USA **96,** 12186–12191.

**Pilot, G., Lacombe, B., Gaymard, F., Cherel, I., Boucherez, J., Thibaud, J.B., and Sentenac, H.** (2001). Guard cell inward $K^+$ channel activity in *Arabidopsis* involves expression of the twin channel subunits KAT1 and KAT2. J. Biol. Chem. **276,** 3215–3221.

**Roelfsema, M.R.G., and Hedrich, R.** (1999). Plant ion transport. In Encyclopedia of Life Sciences (Macmillan Reference Ltd., www.els.net).

**Schachtman, D.P., Schroeder, J.I., Lucas, W.J., Anderson, J.A., and Gaber, R.F.** (1992). Expression of an inward-rectifying potassium channel by the *Arabidopsis* KAT1 cDNA. Science **258,** 1654–1658.

**Schönherr, R., and Heinemann, S.H.** (1996). Molecular determinants for activation and inactivation of HERG, a human inward rectifier potassium channel. J. Physiol. **493,** 635–642.

**Steidl, J.V., and Yool, A.J.** (1999). Differential sensitivity of voltage-gated potassium channels Kv1.5 and Kv1.2 to acidic pH and molecular identification of pH sensor. Mol. Pharmacol. **55,** 812–820.

**Szyroki, A., Ivashikina, N., Dietrich, P., Roelfsema, M.R., Ache, P., Reintanz, B., Deeken, R., Godde, M., Felle, H., Steinmeyer, R., Palme, K., and Hedrich, R.** (2001). KAT1 is not essential for stomatal opening. Proc. Natl. Acad. Sci. USA **98,** 2917–2921.

**Vergani, P., and Blatt, M.R.** (1999). Mutations in the yeast two pore $K^+$ channel YKC1 identify functional differences between the pore domains. FEBS Lett. **458,** 285–291.

**Vergani, P., Hamilton, D., Jarvis, S., and Blatt, M.R.** (1998). Mutations in the pore regions of the yeast $K^+$ channel YKC1 affect gating by extracellular $K^+$. EMBO J. **17,** 7190–7198.

**Vergara, C., Alvarez, O., and Latorre, R.** (1999). Localization of the $K^+$ lock-in and the $Ba^{2+}$ binding sites in a voltage-gated calcium-modulated channel: Implications for survival of $K^+$ permeability. J. Gen. Physiol. **114,** 365–376.

**Very, A.A., Gaymard, F., Bosseux, C., Sentenac, H., and Thibaud, J.B.** (1995). Expression of a cloned plant $K^+$ channel in *Xenopus* oocytes: Analysis of macroscopic currents. Plant J. **7,** 321–332.

**Yellen, G.** (1997). Single channel seeks permeant ion for brief but intimate relationship. J. Gen. Physiol. **110,** 83–85.

**Zhou, Y., Morais-Cabral, J.H., Kaufman, A., and MacKinnon, R.** (2001). Chemistry of ion coordination and hydration revealed by a $K^+$ channel-Fab complex at 2.0 A resolution. Nature **414,** 43–48.

**Zimmermann, S., and Sentenac, H.** (1999). Plant ion channels: From molecular structures to physiological functions. Curr. Opin. Plant Biol. **2,** 477–482.

# <u>Kapitel III</u>: Loss of the AKT2/3 potassium channel affects sugar loading into the phloem of *Arabidopsis*

**Rosalia Deeken, Dietmar Geiger, Jörg Fromm, Olga Koroleva, Peter Ache, Rosemarie Langenfeld-Heyser, Norbert Sauer, Sean T. May und Rainer Hedrich**

**Publiziert in Planta, Vol. 216, 334-344, September 2002**

**Eigene Beteiligung an der Arbeit:**

- Saccharose induzierte Membranpotentialmessungen von AtSUC2 exprimierenden *Xenopus* Oozyten mit Hilfe der Zwei-Elektroden Spannungsklemmen Technik.
- Bestimmung der Kalium-Empfindlichkeit des Saccharosetransports von AtSUC2.
- Strom- und Membranpotentialmessungen in Coexpressionsexperimenten zwischen dem Saccharosetransporter AtSUC2 und den Kaliumkanälen AKT2/3 und KAT2. Untersuchung des Einflusses von Phloem-lokalisierten $K^+$-Kanälen auf die Saccharose-induzierte Depolarisation der Oozytenmembran.
- Auswertung der Daten.

Planta (2002) 216: 334–344
DOI 10.1007/s00425-002-0895-1

ORIGINAL ARTICLE

**Rosalia Deeken · Dietmar Geiger · Jörg Fromm
Olga Koroleva · Peter Ache
Rosemarie Langenfeld-Heyser · Norbert Sauer
Sean T. May · Rainer Hedrich**

# Loss of the AKT2/3 potassium channel affects sugar loading into the phloem of *Arabidopsis*

Received: 25 May 2002 / Accepted: 7 August 2002 / Published online: 21 September 2002


**Abstract** Members of the AKT2/3 family have been identified as photosynthate-induced phloem $K^+$ channels. Here we describe the isolation and characterisation of an AKT2/3 loss-of-function mutant (*akt2/3-1*) from *Arabidopsis thaliana* (L.) Heynh. Microautoradiography following $^{14}CO_2$ incubation in the light revealed that a major fraction of $^{14}CO_2$-derived photosynthates leaking out of sieve tubes appears not to be effectively reloaded (retrieval) into the phloem of the mutant. Using the aphid stylectomy technique we showed that the phloem sap of the mutant, lacking the phloem channels of the AKT2/3 type, contained only half the sucrose content of the wild type. Furthermore, the *akt2/3-1* mutant exhibited a reduced $K^+$ dependence of the phloem potential. *Xenopus* oocytes expressing the phloem sucrose/proton symporter depolarise upon sucrose application. When, however, the phloem channel was co-expressed – mimicking the situation in the sieve tube/companion cell complex – depolarisation was prevented. From our studies we thus conclude that AKT2/3 regulates the sucrose/$H^+$ symporters via the phloem potential.

**Keywords** *Arabidopsis* · Development (*akt2/3-1* mutant) · Phloem · Potassium channel · Sugar loading

**Abbreviations** SE/CC: sieve element/companion cell · TEA: tetraethylammonium · WT: wild type

R. Deeken · D. Geiger · P. Ache · R. Hedrich (✉)
Julius-von-Sachs-Institute for Biosciences,
Molecular Plant Physiology and Biophysics,
Julius-von-Sachs-Platz 2, 97082 Würzburg, Germany
E-mail: hedrich@botanik.uni-wuerzburg.de
Fax: +49-931-8886158

J. Fromm
Fachgebiet Angewandte Holzbiologie,
Wissenschaftszentrum Weihenstephan der TU München,
Winzerer Str. 4, 80797 München, Germany

O. Koroleva
School of Biological Sciences, University of Wales,
Bangor, LL57 2UW, UK

R. Langenfeld-Heyser
Forstbotanisches Institut/Baumphysiologie,
Büsgenweg 2, 37077 Göttingen, Germany

N. Sauer
Lehrstuhl für Botanik II,
Universität Erlangen, Staudstr. 5, 91058 Erlangen, Germany

S.T. May
Plant Science Division, School of Biosciences,
University of Nottingham, University Park,
Nottingham, NG7 2RD, UK

## Introduction

The phloem presents a network for assimilate allocation and retrieval of minerals (Pate and Jeschke 1995; Marschner et al. 1996; Marcelis 1996), as well as chemical and electrical communication within the plant (Fromm and Bauer 1994). Potassium is the major cation in the phloem and stimulates sugar loading into the phloem sap (Giaquinta 1980; Peel and Rogers 1982) through an as yet unidentified mechanism. Recently, however, it has been shown that a sink–source-regulated and sugar-inducible $K^+$ channel dominates the electrical properties of the sieve-tube plasma membrane (Ache et al. 2001). In the search for a $K^+$ channel involved in the control of sugar loading into the sieve element/companion cell (SE/CC) complex, we previously identified members of the AKT2/3 family expressed in the vascular system of *Arabidopsis*, maize, broad bean and poplar (Marten et al. 1999; Philippar et al. 1999; Ache et al. 2001). In situ hybridisation analyses and promoter–*GUS* studies localised the sites of gene expression predominately in phloem cells (Marten et al. 1999; Deeken et al. 2000; Lacombe et al. 2000). When cortex-free vascular strands were excised from the mesocotyl of maize seedlings and enzymatically digested, a phloem-derived protoplast fraction enriched in ZMK2 was obtained (Bauer et al. 2000). ZMK2 represents the maize homologue of AKT2/3 in *Arabidopsis*. In line with the predicted regulatory role of this $K^+$ channel type in phloem loading, Northern blots co-localised the mRNA

of the maize sucrose/$H^+$ symporter ZmSUT1 to the same protoplast population. In patch-clamp studies the electrical properties of the plasma membrane of these protoplasts were dominated by a new type of $K^+$ channel. This channel type shared its basic features with ZMK2 heterologously expressed in *Xenopus* oocytes (Bauer et al. 2000; cf. Philippar et al. 1999). In contrast to members of the KAT1 and AKT1 family of inward-rectifying $K^+$ channels, ZMK2 and AKT2/3 encode a largely voltage-independent, proton-blocked $K^+$ channel type (Hedrich et al. 1995; Hoth et al. 1997; Philippar et al. 1999; Downey et al. 2000; Marten et al. 1999; Bauer et al. 2000).

Since *AKT2/3* transcripts were found predominantly in the phloem of the green parts of the shoot, including sepals of the flower, a source-specific function was proposed for this phloem channel (Deeken et al. 2000). During the light period, following a delay of 30 min after illumination onset, transcript levels gradually increased, peaked around noon, and dropped again in the afternoon and night to the background level. This light-induction was dependent on $CO_2$, indicating that photosynthates regulate *AKT2/3* transcription. Experiments with half of the rosette leaves illuminated and the other half shaded or rosette leaves illuminated and the inflorescence stalk shaded showed elevated expression in the light-treated tissues only (Deeken et al. 2000). The fact that *AKT2/3* transcription is not activated in shaded parts of the plant provides evidence that the *AKT2/3*-inducing signal is not phloem-mobile.

In order to address the regulatory role of AKT2/3 in phloem loading and long-distance transport of photoassimilates, this study reports the isolation of an *Arabidopsis* mutant lacking the functional AKT2/3 channel. We describe how the phenotype was analysed and provide evidence for AKT2/3 controlling sucrose loading via the phloem electrical potential.

## Materials and methods

### Plant material

*Arabidopsis thaliana* (L.) Heynh. (cv. Wassilewskija; Lehle Seeds, Round Rock, USA) plants were either grown on soil (Type P; Gebr. Hagera, Sinntal-Jossa, Germany) or on 0.8% agar medium (Sigma), containing 1× MS salts (Murashige and Skoog; Sigma), supplemented with either 2% D-glucose, D-fructose or D-sucrose (Roth, Karlsruhe, Germany) at pH 5.7. Before growth on agar medium seeds were surface-sterilized with 5% hypochlorite. All plants were illuminated for 8 h at a photon flux density of 160 μmol $m^{-2}$ $s^{-1}$ and kept in growth chambers at 22 °C during the light, and 16 °C during the 16-h dark period. Plants incubated in continuous light were illuminated with 300 μmol photons $m^{-2}$ $s^{-1}$.

### Isolation of the *akt2/3-1* mutant

The *Agrobacterium*-mediated transferred DNA (T-DNA) tagging procedure described by Feldmann (1991) for *Arabidopsis* was used to isolate the *akt2/3-1* mutant. The T-DNA-tagged lines were screened by applying the reverse genetic technique (Schulz et al. 1995; Krysan et al. 1999). Genomic DNA pools prepared from the original 7000 lines generated by K. Feldmann (Tuscon, Arizona, USA) were screened by polymerase chain reaction (PCR) using the gene-specific primer *AKT2/3as* in antisense orientation (5′-TTCAATCTTGGCCTCACTGCTT-3′) and the T-DNA-specific left border (LB) primer (5′-GATGCACTCGAAATCAGCCA ATTTTAGAC-3′). The LB and *AKT2/3as* primer generated a 698-bp DNA fragment. To identify homozygous *akt2/3-1* plants with T-DNA insertions in both alleles of the *AKT2/3* gene, the gene-specific *AKT2/3s* primer in sense orientation (5′-TGTGTTAGTT-CTTGCTTAATGC-3′) together with the *AKT2/3as* primer were used for PCR. DNA from homozygous *akt2/3-1* plants gave no amplification product, because a T-DNA of ca. 17 kb inserted into the *AKT2/3* gene between the two primer positions cannot be amplified.

### RNA extraction, Northern blot analysis, and quantitative reverse transcription (RT)–PCR

Total-RNA was isolated from *Arabidopsis* using the RNeasy plant mini kit (Qiagen, Hilden, Germany) according to the manufacturer's protocol. RNA was separated by electrophoreses through a formaldehyde-containing 1% agarose gel and transferred onto a nylon membrane (Hybond N; Amersham) using standard protocols (Sambrook et al. 1989). The hybridisation probe was the $^{32}$P-labelled *AKT2/3* gene fragment, described by Deeken et al. (2000). Quantitative RT–PCR was performed as described earlier (Szyroki et al. 2001).

### Gas-exchange measurements

Transpiration and $CO_2$ exchange were determined as previously described (Hedrich et al. 2001; Szyroki et al. 2001) using an infrared gas analyser in the differential mode (Binos, Leypold-Heraeus, Hanau, Germany). Modulated chlorophyll fluorescence was measured using a PAM 101 fluorometer as described by Schreiber et al. (1986).

### Microautoradiography

Microautoradiographs were prepared according to Fromm and Eschrich (1988). Small sections of the stem of 1–2 mm in diameter from $^{14}CO_2$-exposed plants were quickly frozen in isopentane, which was pre-cooled in liquid nitrogen. After freeze-drying and embedding in Spurr's resin medium (Spurr 1969), sections of 1 μm were cut with a Reichert Ultracut E microtome and treated with 0.1 N NaOH and 5% periodic acid, which improved the subsequent staining with 0.05% toluidine blue (pH 7.0). The sections were coated with liquid photoemulsion (Ilford K2), exposed for 3 weeks (Salpeter and Bachmann 1964) and after gold-latensification they were developed in D-19 A/S developer (Sanderson 1981). Dark spots, representing silver grains, were quantified with the software program Scion Image (Scion Corporation, Frederick, Md., USA).

### Phloem sap sampling

To obtain samples of phloem sap the stylet of an aphid was cut under a microscope (microcautery) with a needle heated by radiofrequency (aphid stylectomy technique; Pritchard 1996). Aphids (*Mysus persicae*) were placed on *Arabidopsis* plants and allowed to feed on the tested plants several days before the start of the experiment. The stylets of aphids feeding on the main inflorescence stalk were cut while observing under the microscope. A ring of lanolin paste was put around exuding stylets and the resulting circle was flooded with water-saturated paraffin oil, in order to avoid evaporation of the droplet of exudate. Phloem exudate from cut stylets covered by paraffin oil was collected with an oil-filled glass microcapillary as sequential portions, each time attempting to remove the whole droplet from the end of the stylet. From each stylet 2–8 microcapillaries were filled with ca. 10–300 pl of exudate. All samples were immediately frozen and kept at –20 °C until analysis.

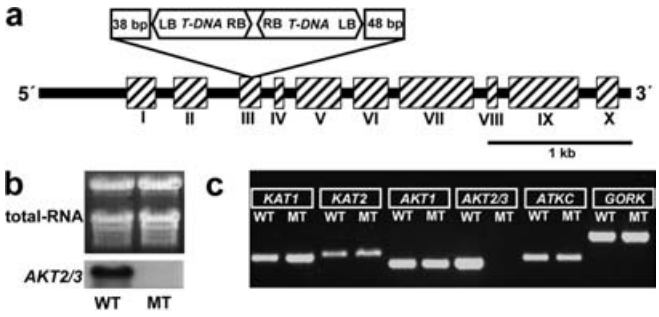


**Fig. 1a–c** T-DNA-insertion within the *AKT2/3* gene of *Arabidopsis thaliana* disrupts transcription. **a** *AKT2/3* gene structure, comprising ten exons (*hatched boxes*, *I–X*), and position of T-DNA-insertion within the third exon. *LB* T-DNA left border, *RB* T-DNA right border. **b** Ethidium bromide-stained agarose gel with total RNA (10 µg per lane) from rosette leaves of 5-week-old wild-type (*WT*) and *akt2/3-1* (*MT*) plants, and Northern blot experiment, hybridised with $^{32}$P-labelled *AKT2/3* gene as probe. **c** Gel electrophoresis of RT–PCR products quantified with real-time RT–PCR (LightCycler). Fragment lengths are: *KAT1* = 379 bp, *KAT2* = 392 bp, *AKT1* = 347 bp, *AKT2/3* = 353 bp, *ATKC1* = 373 bp, *AtGORK* = 496 bp. One representative of three experiments with either WT or MT inflorescence stalks is shown. Note that *AKT2/3* transcripts are not detectable in the *akt2/3-1* mutant

## Sugar determination in leaf extracts and phloem sap

*Arabidopsis* leaf samples (0.2 g FW) were ground in liquid nitrogen, suspended in 2 ml deionised water and centrifuged (17,000 *g*) immediately after thawing at 4 °C for 5 min. The supernatant was boiled at 100 °C for 3 min in order to inactivate proteins. Insoluble material was removed by centrifugation (17,000 *g*, 5 min) and the concentration of sugars was determined in the supernatant using isocratic ion chromatography with pulsed amperometric detection (4500 I; Dionex, Idstein, Germany).

Concentrations of sugars in the sap from phloem exudates were measured using a micro-fluorometric assay (Tomos et al. 1994; Koroleva et al. 1998). The assay involves enzymatic dehydrogenation of glucose-6-phosphate derived sequentially from glucose, fructose, and sucrose, with corresponding reduction of NADP to NADPH. A Leitz MPV Compact 2 Fluorovert microscope photometer fitted with filter block A and Leitz software (Leitz, Wetzlar, Germany) was used to measure fluorescence of 4- to 5-nl droplets of reaction mixture, placed on a microscope slide inside a 4-mm-deep aluminium ring, under 3 mm of water-saturated paraffin oil. The standards and samples (volume ca. 10 pl) were added with a constriction pipette.

## Measurement of electrical potential differences in the phloem

The phloem electrical potential was measured, using the aphid stylectomy technique (Wright and Fisher 1981). Before the measurements started an aphid cage with 10–15 aphids was applied to the main inflorescence stalk. The aphids were allowed to settle overnight. On the following day an aphid that produced honeydew was severed from its stylet by using a laser beam generator (Beck, Neu-Isenburg, Germany) connected to a Zeiss microscope. When the stylet stump exuded sieve-tube sap, all other aphids were brushed away and the stem was kept at about 90% relative humidity. The cut stem tip was immersed in a vial containing 200 mM sorbitol, 1 mM NaCl, 0.1 mM KCl, 0.1 mM $CaCl_2$, 1 mM Mes (pH 6.0). Into this vial, a window was cut through which the reference electrode (Ag/AgCl) was inserted, and through which the

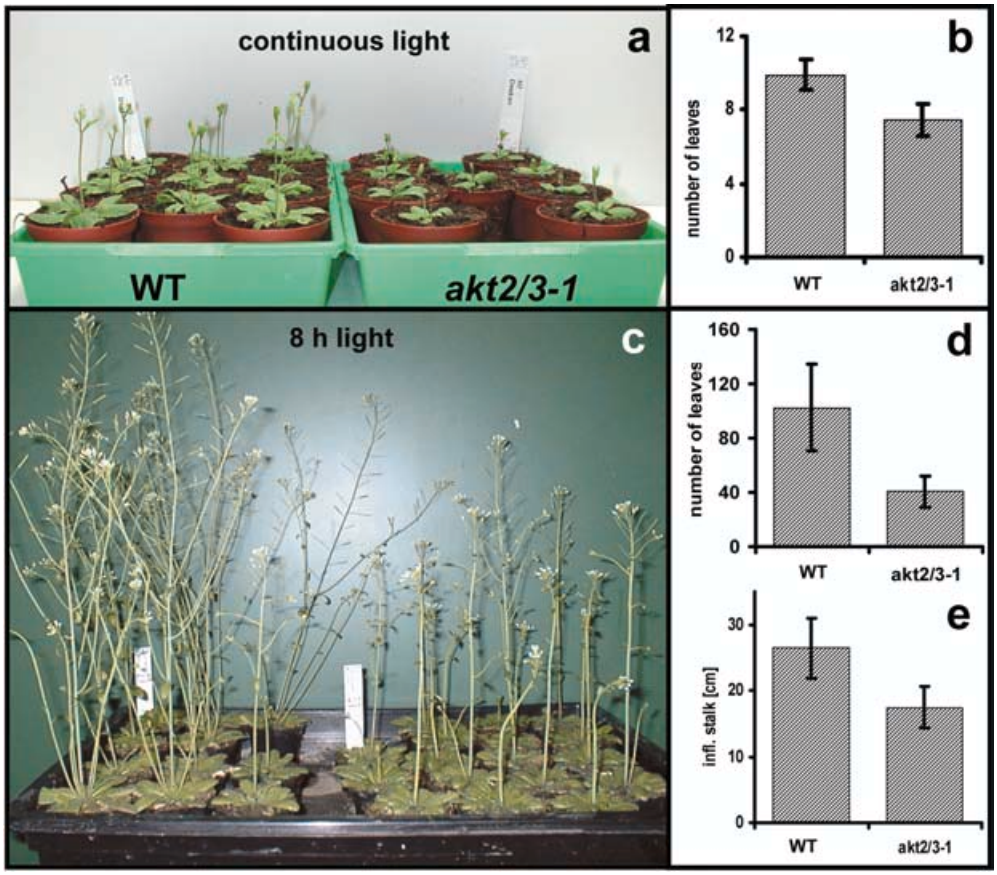


**Fig. 2a–e** Flower induction and rosette development of the *Arabidopsis akt2/3-1* mutant is delayed. **a** Flowering WT and *akt2/3-1* mutant plants grown on soil under continuous light for 10 days. **b** Number of rosette leaves of the plants in **a**; $n = 11$ for WT, $n = 9$ for *akt2/3-1*. **c** WT and *akt2/3-1* mutant plants after 10 weeks under short-day conditions (8 h light). **d** Number of rosette leaves from plants like those in **c**; $n = 16$ for WT, $n = 21$ for *akt2/3-1*. **e** Length of the main inflorescence stalk as calculated from plants like those in **c**; $n = 38$ for WT, $n = 40$ for *akt2/3-1*. **b, d, e** Data are means ± SD

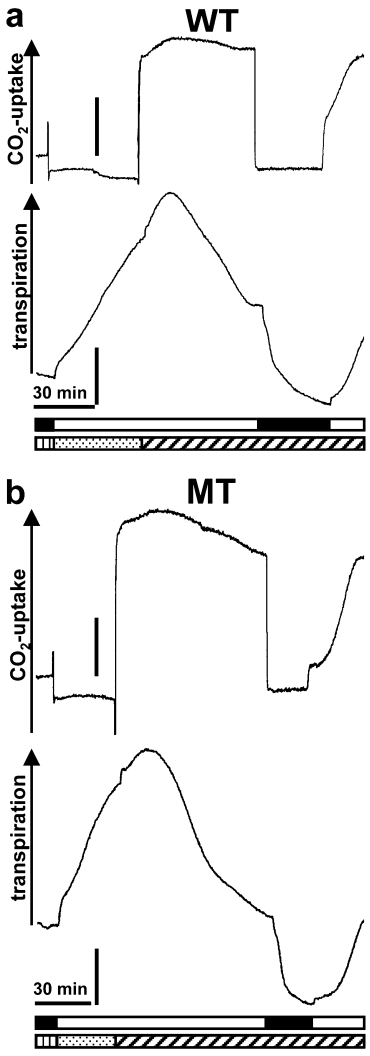


**Fig. 3a, b** $CO_2$ uptake and transpiration of 8-week-old rosette leaves from *Arabidopsis* plants grown under short-day conditions (8 h). Leaves from predarkened plants of the WT (**a**) and *akt2/3-1* mutant (*MT*; **b**) were incubated in $CO_2$-free air and illuminated for stomatal opening. Application of 1,000 µl $l^{-1}$ $CO_2$ and darkness induced stomatal closure. *Black box* darkness, *white box* 700 µmol photons $m^{-2}$ $s^{-1}$ light, *vertical stripes* 500 µl $l^{-1}$ $CO_2$, *dots* $CO_2$-free air, *hatched* 1,000 µl $l^{-1}$ $CO_2$. *Vertical bars* represent 5 µmol $CO_2$ $m^{-2}$ $s^{-1}$ and 0.5 mmol $H_2O$ $m^{-2}$ $s^{-1}$ ($n \geq 3$)

electrolyte solution could be replaced by other solutions. The tip of a microelectrode was placed into the exudate droplet of the stylet by using a Leitz micromanipulator. The glass microelectrode, fabricated from microcapillaries on a vertical electrode puller (PP-83; Narishige) had a tip diameter of ca. 1 µm. The microelectrodes were back-filled with 100 mM KCl and connected via an Ag/AgCl half-cell to a microelectrode headstage (input impedance $10^{12}$ ohms) of a WPI-amplifier (Model 750; WPI, Sarasota, Fla., USA). The resistance for an electrical current inside the stylet is relatively low (around $10^9$ ohms according to Wright and Fisher 1981) compared to the high input impedance of the electric equipment used.

### Oocyte experiments

Current-clamp and voltage-clamp experiments on $K^+$ channel- and sucrose/proton symporter-expressing *Xenopus laevis* oocytes were performed as described before (Marten et al. 1999). The glass microelectrodes were fabricated on a horizontal laser puller (Model P2000; Sutter Instruments, Novato, Calif., USA). Solutions used for membrane depolarisation studies were composed of 30 mM KCl, 70 mM NaCl, 5 mM sucrose, 2 mM $MgCl_2$, 1 mM $CaCl_2$ and 10 mM Mes–Tris (pH 5.6). In the $K^+$-channel-blocking solutions, NaCl was replaced by 20 mM $BaCl_2$ and 40 mM tetraethylammonium (TEA) chloride. In Fig. 8b the solutions contained 10, 30 and 100 mM KCl, 5 mM sucrose, 2 mM $MgCl_2$, 1 mM $CaCl_2$, and 10 mM Mes–Tris (pH 5.6). The ionic strength was kept constant by replacing $K^+$ with $Na^+$. All media were adjusted to a final osmolality of 215–235 mosmol $kg^{-1}$ with D-sorbitol.

## Results

### Isolation of an *akt2/3-1* knockout mutant

In order to find mutants with disruptions in genes encoding ion channels a collection of T-DNA-tagged *A. thaliana* (ecotype WS) was screened using PCR with a combination of T-DNA and gene-specific primers (Schulz et al. 1995; Krysan et al. 1999). A T-DNA insertion was found in the *AKT2/3* gene of plants from a collection of 7,000 transformants of the T2-generation (Feldmann 1991). Unique PCR products were generated in combination with gene-specific primers from the 3′ and 5′ ends of the *AKT2/3* gene and the T-DNA left border primer. The T-DNA right border primer together with *AKT2/3* primers failed to give any product. This result indicates that the T-DNA was inserted as an inverted repeat. Sequence analysis confirmed this concatemer arrangement and showed that the T-DNA had inserted into the third exon of the *AKT2/3* gene such that at the 3′ end 38 nucleotides and at the 5′ end 48 nucleotides of unknown origin were inserted next to the borders of the T-DNA sequence (Fig. 1a). Homozygous T-DNA transformants were identified by kanamycin resistance and PCR. To determine whether in the knockout mutant just the *AKT2/3* gene is tagged with a T-DNA, genomic Southern hybridisation experiments were performed. Genomic DNA of mutant and wild-type (WT) plants was digested with four different restriction enzymes each. Samples that hybridised with the T-DNA also bound the AKT2/3 probe (data not shown). Moreover, the morphological phenotype (see below) always segregated with kanamycin resistance and the T-DNA insertion.

Insertion of two copies of a ca. 17-kb T-DNA sequence into the middle of the *AKT2/3* gene would be expected to completely disrupt expression. To prove this, RNA was extracted from leaves of the WT and *akt2/3-1* mutant plants, and analysed by Northern blot hybridisation. *AKT2/3* mRNA was clearly detected in WT plants, but not in the *akt2/3-1* mutant (Fig. 1b). Using real-time RT–PCR (LightCycler, Roche) with RNA samples from inflorescence stalks, no *akt2/3* cDNA fragment was detected in the *akt2/3-1* mutant (Fig. 1c). Moreover, mRNA steady-state levels of potassium channels, detectable in the inflorescence stalk (*KAT1*, *KAT2*, *AKT1*, *ATKC*, *GORK*), remained unchanged compared with WT plants.

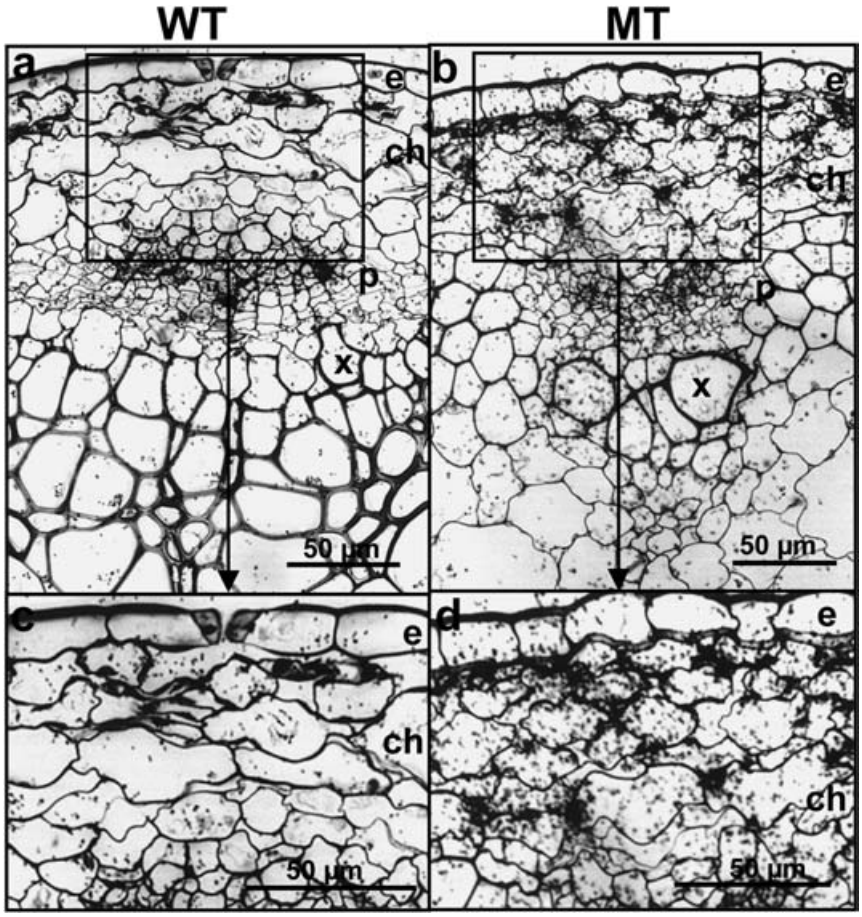


**Fig. 4a–d** Distribution of $^{14}C$-labelled assimilates in the main inflorescence stalk of *Arabidopsis* WT and *akt2/3-1* mutant (*MT*) plants with rosette leaves incubated in $^{14}CO_2$ only. **a, b** Microautoradiographs from cross-sections (1 µm) of an area around vascular bundles after 3.5 h of illumination. **c, d** Enlargements of the boxed chlorenchyma areas in **a** and **b**. *e* Epidermis, *ch* chlorenchyma, *p* phloem, *x* xylem. Density of black dots represents amount of $^{14}C$-labelled assimilates. One representative out of three plants analysed is shown

## Sink growth is impaired in the mutant

In order to analyse the consequences of the loss of *AKT2/3* $K^+$ channel gene function, mutant development was studied under several growth conditions. Neither WT nor mutant plants showed pronounced differences during seedling growth. Rosette development and flower initiation of mutant plants were, however, delayed (Fig. 2). Following a 3-week incubation in continuous light, WT plants grew 10 leaves while the mutant grew only 7 (Fig. 2a, b). A reduced number of rosette leaves was also observed with 10-week-old *akt2/3-1* plants grown under short-day conditions (Fig. 2c, d). Upon flowering, WT plants initiated four to six inflorescence stalks whereas the mutant formed only one or two shorter stalks of increased diameter [$1.9 \pm 0.15$ mm (mean ± SD) compared to $1.5 \pm 0.24$ mm, Fig. 2c–e]. This phenotype is consistent with gene induction by $CO_2$ assimilates and the phloem of the inflorescence stalk being the major site of *AKT2/3* expression (10–15% of actin, data not shown; Deeken et al. 2000).

Recently, AKT2/3 was identified in guard cells, too (Szyroki et al. 2001).To exclude the possibility that the delayed development of the mutant was caused by a change in guard cell performance, we followed stomatal movement and photosynthesis by measuring water loss and $CO_2$ assimilation with infrared gas analysers (cf. Hedrich et al. 2001). In both WT and *akt2/3-1* mutant plants, transpiration and $CO_2$-uptake were, however, similar (Fig. 3a, b, $n \geq 3$). Predarkened leaves opened their stomata in response to light and $CO_2$-free air, while they closed them with 1,000 µl $l^{-1}$ $CO_2$ and darkness. $CO_2$-uptake rates were comparable for mutant and WT plants. Furthermore, in PAM chlorophyll fluorescence measurements, no difference between the photosynthetic capacity of the *akt2/3-1* mutant and the WT could be detected. A ratio of $1 \pm 0.1$ (mean ± SD, $n = 10$) was determined for the relative electron transport rate of *akt2/3-1* compared to WT (data not shown). Thus the mutant phenotype seems not to result from altered stomatal properties or reduced $CO_2$ fixation in mesophyll cells.

## Altered distribution of $^{14}C$-labeled assimilates

To substantiate our hypothesis that the phloem AKT2/3 $K^+$ channel promotes assimilate loading and retrieval we traced the fate of photosynthetically fixed $^{14}C$. Rosette leaves of WT and mutant plants were incubated with $^{14}CO_2$. After illumination for 3.5 h the inflorescence

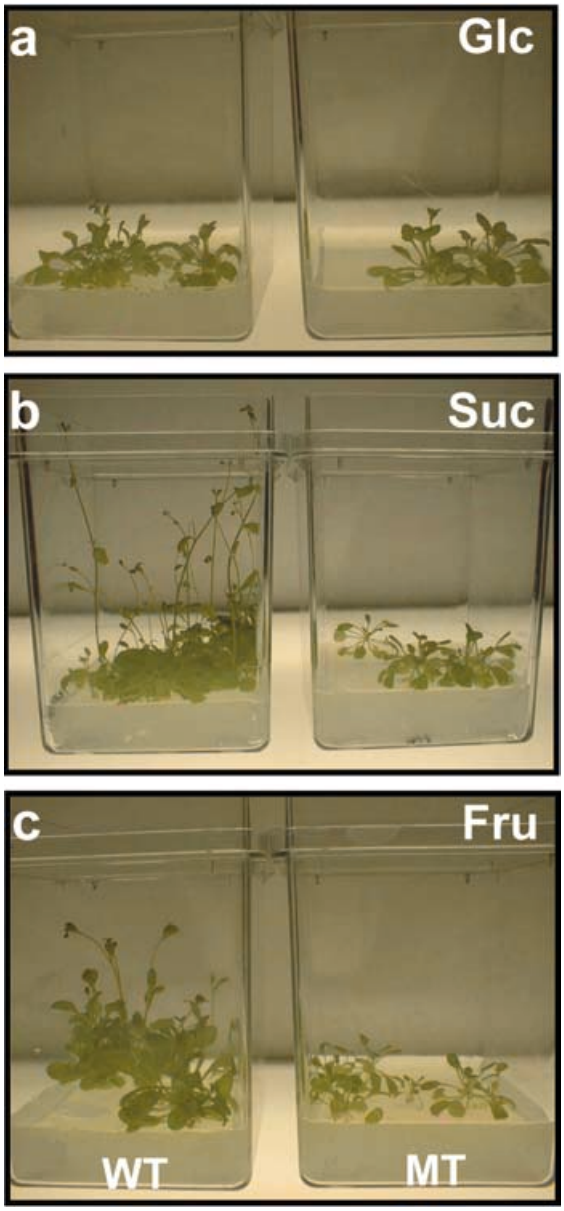


**Fig. 5a–c** Growth and development of WT and *akt2/3-1* (*MT*) *Arabidopsis* plants in response to different sugars. Plants were continuously grown under short-day conditions (8 h light) on agar supplemented with 2% sucrose (**a**), glucose (**b**) or fructose (**c**) until flowering

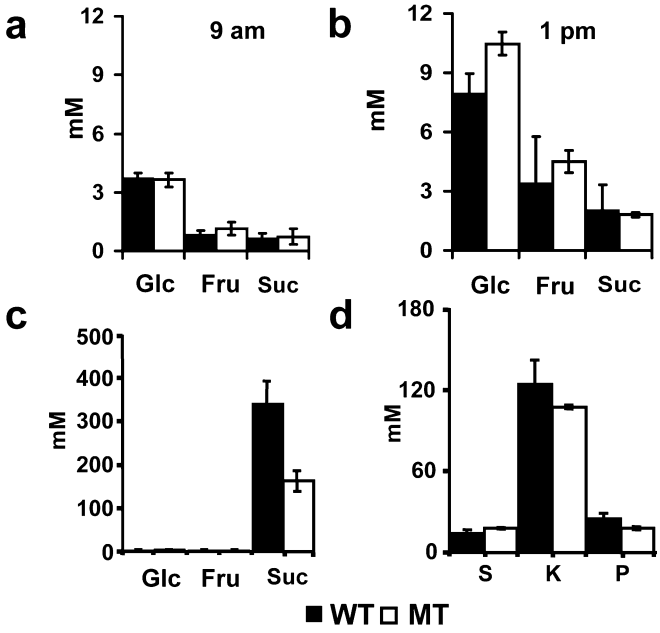


**Fig. 6a–d** Sugar and potassium contents of WT and *akt2/3-1* mutant (*MT*) plants of *Arabidopsis*. **a, b** Concentrations of glucose (*Glc*), fructose (*Fru*) and sucrose (*Suc*) in total leaf extracts determined in the morning (9 a.m.) and afternoon (1 p.m.). Means ± SD of three independent measurements. **c** Concentrations of glucose (*Glc*), fructose (*Fru*) and sucrose (*Suc*) in the phloem sap of WT ($n = 10$) and MT ($n = 11$) plants. Means ± SE. **d** Sulphur (*S*), potassium (*K*) and phosphorus (*P*) concentrations in phloem sap of WT ($n = 11$) and MT ($n = 13$) plants. Means ± SE. All plants were grown on soil under long-day conditions (16 h)

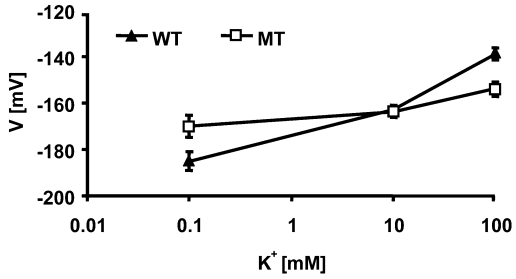


**Fig. 7** Potassium-dependent changes in the phloem electrical potential of WT and *akt2/3-1* mutant (*MT*) *Arabidopsis* plants. Phloem potentials of sieve tube elements from the main inflorescence stalk after increasing the $K^+$ concentration in the standard solution from 0.1 to 10 and 100 mM. Means ± SD

stalks were harvested and prepared for microautoradiography. Ultrathin cross-sections through inflorescence stalks (1 μm) were coated with liquid photoemulsion, and exposed for 3 weeks. The distribution of $^{14}C$-fixation products was visualised on the basis of the deposition of dark silver grains. When cross-sections covered by silver particles were quantified in WT plants the corresponding radioactivity was detected predominately in the phloem (37%, Fig. 4a). In contrast, the phloem-localised signal was reduced in the mutant (22%, Fig. 4b). Instead, 54% of silver grains covered the chlorenchyma, two to three layers of photosynthetically active cells between the epidermis and sclerenchyma, of the mutant compared to 26% for WT chlorenchyma (Fig. 4c, d). Thus in WT and mutant plants, $^{14}C$-labelled products are allocated by the phloem of the inflorescence stalk to satisfy the high assimilate demand of flowers and seeds. However, in the inflorescence stalk of the mutant, assimilates leaking away from the sieve tube appear not to be efficiently reloaded into the main phloem stream and thus accumulate in the chlorenchyma (Fig. 4d). To quantify the sugar content in the sieve tube the aphid stylectomy technique was applied (see below).

Reduced sucrose content in the phloem

It is well known that growth of *A. thaliana* is strongly dependent on supply of external sugars. Furthermore, *A. thaliana* roots have been shown to express monosaccharide (AtSTP4) and sucrose (AtSUC2, AtSUC3) transporters (Truernit and Sauer 1995; Truernit et al. 1996; Meyer et al. 2000; and own data not shown). Carbohydrate transporters in the root are capable of taking up sugars from the medium (Jones and Darrah 1996). Moreover, the expression of *AKT2/3*-type channels is triggered by sugars (Ache et al. 2001). Thus an overload of externally applied sugars would be expected to generate an even more pronounced phenotypic difference between the WT and the *akt2/3-1* mutant than in soil. To test this hypothesis, WT and mutant plants were grown on agar media enriched with D-sucrose, D-glucose or D-fructose. On glucose medium, growth and flowering were similar in WT and mutant plants (Fig. 5a). In the presence of D-sucrose and D-fructose, however, growth and flower induction of the *akt2/3-1* knockout plants were largely delayed (Fig. 5b, c). This indicates that in the case of sucrose, *akt2/3-1* plants lacking the phloem $K^+$ channel cannot allocate this sugar as effectively as the WT.

To address the question of whether the impaired carbon allocation of the *akt2/3-1* mutant is due to reduced uptake of sucrose into the phloem, we directly determined the sugar and mineral contents of the phloem sap, using the aphid stylectomy technique (Wright and Fischer 1981; Fischer and Frame 1984; Pritchard 1996), and compared them with the soluble sugar contents (glucose, fructose, sucrose) of leaves. At 9 a.m. in the morning the glucose contents of WT and *akt2/3-1* mutant leaves were the same (3.73 mM versus 3.63 mM, Fig. 6a). In the afternoon (1 p.m.) the glucose content in the mutant leaves (10.47 mM) was significantly higher than in the WT (7.95 mM, student's *t*-test, $P = 0.003$; Fig. 6b). The fructose (0.83 and 3.43 mM WT versus 1.13 and 4.50 mM mutant, at 9 a.m. and 1 p.m., respectively) and sucrose (0.68 and 2.08 mM WT versus 0.73 and 1.82 mM mutant) contents were much lower but similar in both plants (Fig. 6a, b). In contrast the sucrose content found in the phloem sap of the $K^+$-channel mutant ($163 \pm 23$ mM, mean ± SE) was only half that of WT plants ($341 \pm 52$ mM, Fig. 6c). Glucose and fructose contents of these samples were very low and did not differ between WT and mutant plants. With respect to the elements sulphur, potassium, and phosphorus, no statistically significant differences were observed either (student's *t*-test: potassium, $P = 0.345$; sulphur, $P = 0.355$; phosphorus, $P = 0.170$; Fig. 6d). Thus the phenotype of the mutant very likely reflects a defect in sucrose (re)loading into the phloem.

$K^+$-dependence of phloem electrical potential is altered in *akt2/3-1*

To analyse the effects of the *AKT2/3* mutation on the membrane potential of the SE/CC complex and thereby the voltage-dependent activity of the $H^+$/sucrose carrier (Boorer et al. 1996; Zhou et al. 1997), we applied the aphid stylectomy technique (Wright and Fischer 1981; Pritchard 1996). When microelectrodes were brought into contact with the phloem sap at the cut end of the aphid's stylet the phloem potential could be monitored. Following feeding a solution containing 0.1 mM $K^+$ into the xylem sap of excised main inflorescence stalks, a resting potential of $-185 \pm 4.0$ mV (mean ± SD) was recorded for the phloem of WT plants and $-170 \pm 4.7$ mV for the *akt2/3-1* knockout (Fig. 7). Upon an increase from 10 to 100 mM in $K^+$ concentration in the bathing solution the phloem potential dropped by 25 mV in the WT (from $-165 \pm 2.1$ to $-139 \pm 2.6$ mV) and by only 10 mV in the mutant (from $-163 \pm 2$ to $-154 \pm 3.1$ mV). These results indicate that the membrane potential and $K^+$ conductance of the SE/CC complex in the mutant is reduced with respect to the WT. Interestingly the $K^+$-dependence of the phloem potential in broad bean correlates with the expression of *VFK1*, the *Vicia faba* homologue of *AKT2/3* (Ache et al. 2001). In this context it should also be mentioned that apical root cells of the *akt1-1* mutant exhibited a similar reduced response to extracellular $K^+$ concentration changes (Hirsch et al. 1998).

**Fig. 8a–f** $K^+$-channel-dependent sucrose uptake in *Xenopus* oocytes. **a** AtSUC2-mediated depolarisation of the membrane potential in response to 5 mM sucrose (pH 5.6). *Open circles* Means ± SD (5 oocytes) normalised to the steady-state level after 45 s. *Solid line* A representative normalised recorded trace. **b** Sucrose-induced depolarisation of AtSUC2 is unaffected in the presence of 10, 30 and 100 mM $K^+$. Means + SD (4 oocytes) normalised to the steady-state level after 45 s in 30 mM KCl. Timescale is like that in **a**. *Open circles* 10 mM $K^+$, *filled circles* 30 mM $K^+$, *filled triangles* 100 mM external $K^+$. *Inset* Original membrane potential measurements of AtSUC2 and AKT2/3 co-expressing oocytes at $K^+$ concentrations indicated. Note that AKT2/3 clamps the membrane to the Nernst potential for $K^+$. **c** $K^+$ currents in 30 mM KCl of *AtSUC2/AKT2/3* co-injected oocytes were recorded at membrane voltages between 40 and –120 mV in 20 mV decrements from a holding potential as indicated. Typical instantaneous- and time-dependent current components were mediated by AKT2/3 (*upper traces*). At voltages more positive than the $K^+$ equilibrium potential, AKT2/3 elicited outward $K^+$ currents. After addition of 40 mM $TEA^+$ and 20 mM $Ba^{2+}$, outward as well as inward currents were inhibited (*lower traces*). **d** KAT2 currents in response to voltage pulses from 40 to –140 mV (20 mV decrements) in external solutions as described in **c** (*upper traces*). Currents of *AtSUC2/KAT2* co-injected oocytes decreased after application of the $K^+$ channel blockers (*lower traces*). Note that in contrast to AKT2/3, KAT2 is strictly inward rectifying. **e** Membrane potential ($V_m$) measurements of *AtSUC2/AKT2/3* co-injected oocytes during perfusion with 5 mM sucrose in 30 mM KCl (pH 5.6). Sucrose induced depolarisation of the membrane in the presence and absence of $Ba^{2+}$ plus $TEA^+$. With the blockers present in the bath solution AKT2/3 is no longer able to clamp the membrane potential. **f** Depolarisation of the membrane through AtSUC2 is not prevented in the presence of KAT2. In **a**, **b**, **e** and **f** external solutions containing 5 mM sucrose were perfused at a rate of 2 ml/min. *Arrows* indicate the beginning of sucrose application

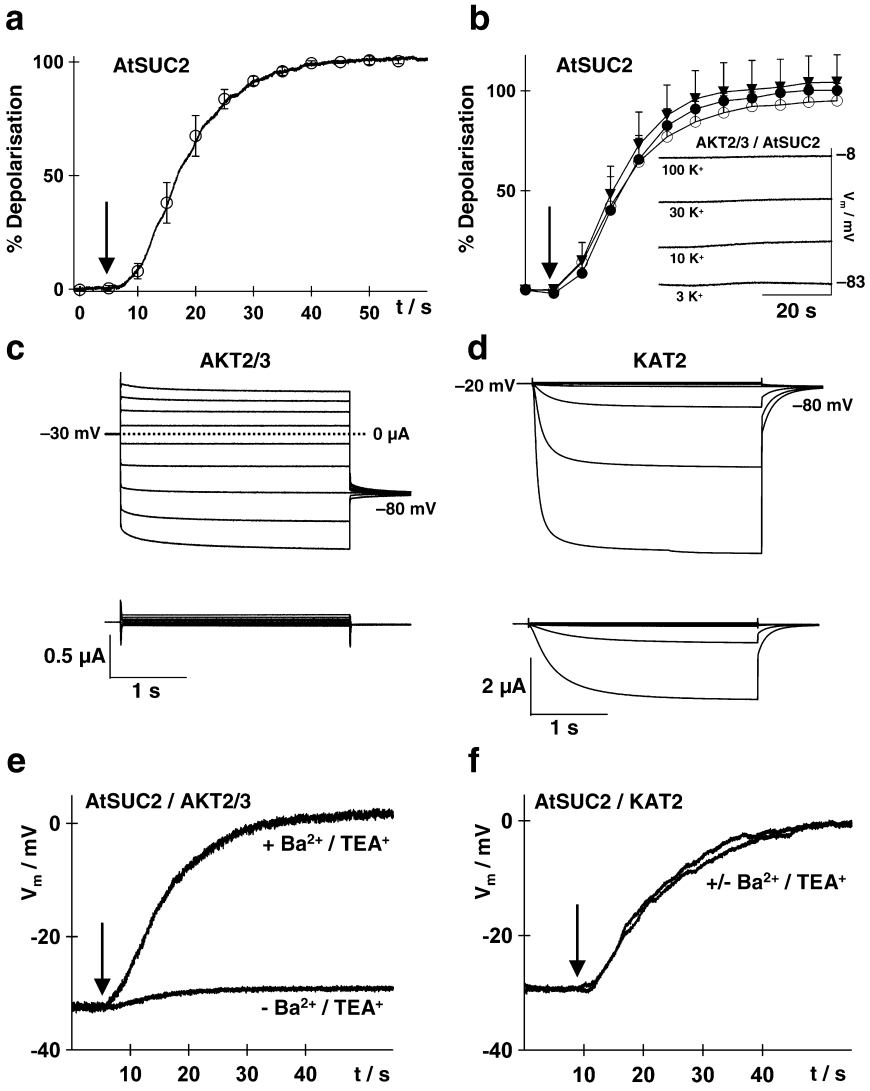


AKT2/3 prevents sucrose-induced membrane depolarisation

The reduced $K^+$-dependence of the membrane potential and reduced sucrose content of the phloem sap found for *akt2/3-1* plants indicates that AKT2/3 seems to control sugar loading via a voltage-dependent process.

When the phloem-specific sucrose/$H^+$ co-transporter, AtSUC2 was expressed in *Xenopus leavis* oocytes, a sucrose-induced depolarisation of the membrane was monitored (Fig. 8a). Application of 5 mM sucrose in the presence of 10, 30 and 100 mM $K^+$ did not alter the degree of depolarisation imposed by the sucrose transporter (Fig. 8b). Properties like the sucrose specificity of AtSUC2, as well as its concentration and pH dependence, were well in agreement with studies on the phloem sucrose/$H^+$ symporter homologues from potato, carrot, and maize (Boorer et al. 1996; Shakya and Sturm 1998; and own data not shown). In contrast to AKT2/3, KAT2, which is also expressed in the phloem (Pilot et al. 2001), was not able to clamp the membrane to the Nernst potential for $K^+$ (data not shown). While KAT2 is activated at hyperpolarizing potentials only (Fig. 8d, upper traces), AKT2/3-injected oocytes behaved almost like $K^+$ electrodes (Fig. 8b, inset). When, however, oocytes expressing both the phloem $K^+$ channel AKT2/3 and the sucrose/proton symporter AtSUC2 were challenged with sucrose the drop in membrane potential was prevented (Fig. 8e). Blocking AKT2/3 with $Ba^{2+}$ and $TEA^+$, however, diminished the $K^+$ conductance (Fig. 8c, lower traces). When blocked, this phloem channel no longer prevented the sucrose-induced depolarisation (Fig. 8e). Co-expression of the sucrose symporter with the inward rectifier KAT2 in the absence or in the presence of $Ba^{2+}$ and $TEA^+$ (Fig. 8d lower traces) did not prevent the sucrose-dependent depolarisation either (Fig. 8f). This indicates that AKT2/3 – due to its peculiar kinetics and voltage-dependence – stabilises the membrane potential in the presence of the sucrose-fuelled sugar/proton symporter.

In vivo this phloem $K^+$ channel thus very likely repolarises the membrane rather than catalysing the bulk flow of potassium. The latter function could be provided by KAT2 and thereby the phloem $K^+$ concentration in the mutants was maintained at a similar level as in the WT (Fig. 6d). In this context it should be mentioned that the number of KAT2 transcripts was not affected by the loss of AKT2/3 (Fig. 1).

## Discussion

### $K^+$ transporters required for $K^+$ uptake, $K^+$ homoeostasis and phloem function

In pioneering studies by Hirsch et al. (1998) and Gaymard et al. (1998) the first $K^+$-channel knockout plants lacking either AKT1 or SKOR were isolated and characterised. AKT1 represents the inward rectifier in the root. The growth phenotype of loss-of-AKT1-function plants exhibited a severe defect in $K^+$ uptake from the soil when exposed to micromolar $K^+$ and millimolar $NH_4^+$ concentrations. In contrast to WT plants, the mutant root membrane potential was less sensitive to changes in $K^+$ concentration. A similar reduction in $K^+$ sensitivity of the phloem potential was observed with *akt2/3-1* knockout plants (Fig. 7). Moreover, in root cells of the *akt1-1* mutant and sieve tubes of the *akt2/3-1* mutant the $H^+$-ATPase kept the membrane potential rather hyperpolarized. SKOR, which encodes an outward-rectifying $K^+$ channel, is expressed in the stele (xylem parenchyma cells) of *Arabidopsis* roots only. Plants lacking this channel contain only half the normal $K^+$ concentration in the xylem exudate (Gaymard et al. 1998). The phenotypes of mutants lacking AKT1 (Hirsch et al. 1998), SKOR or AKT2/3 show that growth and long-distance solute allocation is reduced, but vital functions are not affected. Since none of the shaker-like $K^+$ channels encoded by the *Arabidopsis* genome is upregulated in the mutant (Fig. 1c), other channel types and transporters seem to compensate for the AKT2/3 defects at least in part. In this context it should be mentioned that the loss of TRK1 and TRK2 $K^+$ carrier function in yeast could be complemented by plant $K^+$ channels and thereby led to the cloning of the first plant $K^+$-channel genes (Anderson et al. 1992; Sentenac et al. 1992). We thus cannot exclude the possibility that $K^+$ uptake by the root, and $K^+$ loading into the xylem sap and phloem are backed up by other ion channels or $K^+$ carriers of the plant TRK-type, ATKUP or HKT1 and TRH1 (Rigas et al. 2001 and papers cited therein).

### How does loss of AKT2/3 affect the sucrose level in the phloem?

Here we have provided evidence that the phloem $K^+$ channel AKT2/3 affects sugar loading (Figs. 4, 6) and long-distance transport, most likely through the modulation of the phloem electrical potential (Figs. 7, 8). The phloem electrical potential measured through an aphid stylet results from a voltage drop across the SE/CC membranes (Fig. 7) and maybe other membranes in series as well. Using the same technique Ache et al. (2001) could correlate $K^+$ conductance changes with the rate of expression of the *Vicia faba AKT2/3* homologue. Thus the sieve-tube plasma membrane potential reflects a dominant fraction of the phloem potential.

The sucrose/$H^+$ symporter mediates electrogenic, proton-coupled transport of sucrose into the SE/CC complex (Giaquinta 1980; Mengel 1980) and is itself voltage-dependent as shown by Zhou et al. (1997) and Boorer et al. (1996). The proton gradient and voltage drop across the membrane is generated by $H^+$ pumps (De Witt and Sussman 1995; Langhans et al. 2001), which coexist with sucrose carriers (Stadler and Sauer 1996) and $K^+$ channels (Marten et al. 1999; Bauer et al. 2000; Lacombe et al. 2000; Deeken et al. 2000; Pilot et al. 2001) in the plasma membrane of phloem cells. The inward rectifier in the voltage range between $E_K$ and the activation threshold of the inward rectifier (e.g. –180 and –100 mV; Brüggemann et al. 1999) together with AKT2/3 can stabilize sucrose-induced depolarisation. At potentials positive to the activation threshold of the inward rectifier (possibly KAT2) and under conditions where "KAT2" is inactive, AKT2/3 is maintaining the $K^+$-dependent membrane potential when challenged with sucrose. In the *akt2/3-1* knockout the phloem potential is maintained at –170 mV (–185 mV in the WT). This indicates that AKT2/3 is not predominantly contributing to the steady-state potential (Fig. 7) rather than its $K^+$-dependent repolarization (Fig. 8).

Earlier work has demonstrated that photosynthates tend to leak away from the sieve tubes along the translocation path (Patrick and Turvey 1981; Minchin and Thorpe 1984, 1987; Minchin et al. 1984; Hayes et al. 1985, 1987). Steady retrieval is therefore required to maintain the photosynthate concentrations at levels sufficient to drive the pressure flow and to nourish sink tissues. Due to the lack of AKT2/3 the long-distance sugar transport pathway is less efficient, with impaired retrieval of sugars because of diffusive leaks along the long-distance path (loss = 6% $cm^{-1}$; Minchin and Thorpe 1987). As a consequence the mutant generates only one or two shoot inflorescences (Fig. 2), a morphology that might develop to compensate for the inefficient sugar loading into the sieve tubes. These findings imply that the loss of AKT2/3 function very likely impairs phloem loading and thus retrieval and allocation of sugars.

**Acknowledgements** The authors gratefully acknowledge Dr. Jeremy Pritchard for providing the opportunity to use aphid stylectomy equipment to gain phloem sap samples. We thank J. Arnold for excellent technical assistance and S. Neimanis for gas-exchange measurements. This project was funded by DFG grants to Rainer Hedrich.

## References

Ache P, Becker D, Deeken R, Dreyer I, Weber H, Fromm J Hedrich R (2001) VFK1, a *Vicia faba* $K^+$ channel involved in phloem unloading. Plant J 27:571–580

Anderson, JA, Huprikar SS, Kochian LV, Lucas WJ, Gaber RF (1992) Functional expression of a probable *Arabidopsis thaliana* potassium channel in *Saccharomyces cerevisiae*. Proc Natl Acad Sci USA 89:3736–40

Bauer CS, Hoth S, Haga K, Philippar K, Aoki N, Hedrich R (2000) Differential expression and regulation of $K^+$ channels in the maize coleoptile: molecular and biophysical analysis of cells isolated from cortex and vasculature. Plant J 24:139–145

Boorer KJ, Loo DDF, Frommer WB, Wright EM (1996) Transport mechanism of the cloned potato $H^+$/sucrose cotransporter StSUT1. J Biol Chem 41:25139–25144

Brüggemann L, Dietrich P, Becker D, Dreyer I, Palme K, Hedrich R (1999) Channel-mediated high-affinity $K^+$ uptake into guard cells from *Arabidopsis*. Proc Natl Acad Sci 96:3298–3302

Deeken R, Sanders C, Ache P, Hedrich R (2000) Developmental and light-dependent regulation of a phloem-localised $K^+$ channel of *Arabidopsis thaliana*. Plant J 23:285–290

De Witt ND, Sussman MR (1995) Immunocytological localization of an epitope-tagged plasma membrane proton pump (H(+)-ATPase) in phloem companion cells. Plant Cell 7:2053–2067

Downey P, Szabò I, Ivashikina N, Negro A, Guzzo, F, Ache P, Hedrich R, Terzi M, Schiavo FL (2000) *KDC1*, a novel carrot root hair $K^+$ channel. J Biol Chem 275:39420–39426

Feldmann KA (1991) T-DNA insertion mutagenesis in *Arabidopsis* mutational spectrum. Plant J 1:71–82

Fisher DB, Frame JM (1984) A guide to the use of the exuding-stylet technique in phloem physiology. Planta 161:385–393

Fromm J, Bauer T (1994) Action potentials in maize sieve tubes change phloem translocation. J Exp Bot 45:463–469

Fromm J, Eschrich W (1988) Transport processes in stimulated and non-stimulated leaves of *Mimosa pudica*. I. The movement of $^{14}C$-labelled photoassimilates. Trees 2:7–17

Gaymard F, Pilot G, Lacombe B, Bouchez D, Bruneau D, Boucherez J, Michaux-Ferrière N, Thibaud J-B, Sentenac H (1998) Identification and disruption of a plant shaker-like outward channel involved in $K^+$ release into the xylem sap. Cell 94:647–655

Giaquinta R (1980) Mechanism and control of phloem loading of sucrose. Ber Dtsch Bot Ges 93:187–201

Hayes PM, Offler CE, Patrick JW (1985) Cellular structures, plasma membrane surface areas and plasmodesmatal frequencies of the stem of *Phaseolus vulgaris* L. in relation to radial photosynthate transfer. Ann Bot 56:125–138

Hayes PM, Patrick JW, Offler CE (1987) The cellular pathway of radial transfer of photosynthates in stems of *Phaseolus vulgaris* L.: effects of cellular pathway plasmolysis and *p*-chloromercuribenzene sulphonic acid. Ann Bot 59:635–642

Hedrich R, Moran O, Conti F, Busch H, Becker D, Gambale F, Dreyer I, Küch A, Neuwinger K, Palme K (1995) Inward rectifier potassium channels in plants differ from their animal counterparts in response to voltage and channel modulators. Eur Biophys J 24:107–115

Hedrich R, Neimanis S, Savchenko G, Felle H, Kaiser W, Heber U (2001) Changes in apoplastic pH and membrane potential in leaves in relation to stomatal responses to $CO_2$, malate, abscisic acid or interruption of water supply. Planta 213:594–601

Hirsch RE, Lewis BD, Spalding EP, Sussman MR (1998) A role for AKT1 potassium channel in plant nutrition. Science 280:918–921

Hoth S, Dreyer I, Dietrich P, Becker D, Müller-Röber B (1997) Molecular basis of plant-specific acid activation of $K^+$ uptake channels. Proc Natl Acad Sci USA 94:4806–4810

Jones DL, Darrah PR (1996) Re-sorption of compounds by roots of *Zea mays* L. and its consequences in the rhizophere. III. Characteristics of sugar influx and efflux. Plant Soil 178:153–160

Koroleva OA, Farrar JF, Tomos AD, Pollock CJ (1998) Carbohydrates in individual cells of epidermis, mesophyll and bundle sheath in barley leaves with changed export or photosynthetic rate. Plant Phys 118:1525–1532

Krysan PJ, Young JC, Tax F, Sussman MR (1999) T-DNA as an insertional mutagen in *Arabidopsis*. Plant Cell 11:2283–2290

Lacombe B, Pilot G, Michard E, Gaymard F, Sentenac H, Thibaud J-B (2000) A shaker-like $K^+$ channel with weak rectification is expressed in both source and sink phloem tissues of *Arabidopsis*. Plant Cell 12:837–851

Langhans M, Ratajczak R, Lützelschwab M, Michalke W, Wächter R, Fischer-Schliebs E, Ullrich CI (2001) Immunolocalization of plasma-membrane $H^+$-ATPase and tonoplast-type pyrophosphatase in the plasma membrane of the sieve tube element–companion cell complex in the stem of *Ricinus communis* L. Planta 213:11–19

Marcelis LFM (1996) Sink strength as a determinant of dry matter partitioning in the whole plant. J Exp Bot 47:1281–1291

Marschner H, Kirkby EA, Cakmak I (1996) Effect of mineral nutritional status on root–shoot partitioning of photoassimilates and cycling of mineral nutrients. J Exp Bot 47:1255–1263

Marten I, Hoth S, Deeken R, Ache P, Ketchum KA, Hoshi T, Hedrich R (1999) *AKT3*, a phloem-localised $K^+$ channel, is blocked by protons. Proc Natl Acad Sci USA 96:7581–7586

Mengel K (1980) Effect of potassium on the assimilate conduction to storage tissue. Ber Dtsch Bot Ges 93:353–362

Meyer S, Melzer M, Truernit E, Hümmer C, Bessenbeck R, Stadler R, Sauer N (2000) AtSUC3, a gene encoding a new *Arabidopsis* sucrose transporter, is expressed in cells adjacent to the vascular tissue and in a carpel cell layer. Plant J 24:869–882

Minchin PEH, Thorpe MR (1984) Apoplastic phloem unloading in the stem of bean. J Exp Bot 35:538–550

Minchin PEH, Thorpe MR (1987) Measurement of unloading and reloading of photoassimilate within the stem of bean. J Exp Bot 38:211–220

Minchin PEH, Ryan KG, Thorpe MR (1984) Further evidence of apoplastic unloading into the stem of bean: identification of the phloem buffering pool. J Exp Bot 35:1744–1753

Pate JS, Jeschke WD (1995) Role of stems in transport, storage, and circulation of ions and metabolites by the whole plant. In: Gartner B (ed) Plant stems physiology and functional morphology. Academic Press, New York, pp 177–204

Patrick JW, Turvey PM (1981) The pathway of radial transfer of photosynthate in decapitated stems of *Phaseolus vulgaris* L. Ann Bot 47:611–621

Peel AJ, Rogers S (1982) Stimulation of sugar loading into sieve elements of willow by potassium and sodium salts. Planta 154:94–96

Philippar K, Fuchs I, Lüthen H, Hoth S, Bauer CS, Haga K, Thiel G, Ljung K, Sandberg G, Böttger M, Becker D, Hedrich R (1999) Auxin-induced $K^+$ channel expression represents an essential step in coleoptile growth and gravitropism. Proc Natl Acad Sci USA 96:12186–12191

Pilot G, Lacombe B, Gaymard F, Chérel I, Boucherez J, Thibaud J-B, Sentenac H (2001) Guard cell inward $K^+$ channel activity in *Arabidopsis* involves expression of the twin channel subunits KAT1 and KAT2. J Biol Chem 276:3215–3221

Pritchard J (1996) Aphid stylectomy reveals an osmotic step between sieve tube and cortical cells in barley roots. J Exp Bot 47:1519–1524

Rigas S, Debrosses G, Haralampidis K, Vicente-Agullo F, Feldmann KA, Grabov A, Dolan L, Hatzopoulos P (2001) TRH1 encodes a potassium transporter required for tip growth in *Arabidopsis* root hairs. Plant Cell 13:139–151

Salpeter MM, Bachmann L (1964) Autoradiography with the electron microscope. A procedure for improving resolution sensitivity and contrast. J Cell Biol 22:469–477

Sambrook J, Maniatis T, Fritsch EF (1989) Molecular cloning. Cold Spring Harbor Laboratory Press, New York

Sanderson J (1981) Modified development to improve the performance of AR-10 stripping emulsions for use with the more energetic isotopes. J Microsc 12:177–182

Schreiber U, Schliwa U, Bilger W (1986) Continuous recording of photochemical and non-photochemical chlorophyll fluorescence quenching with a new type of modulation fluorometer. Photosynth Res 10:51–62

Schulz B, Bennett MJ, Dilkes BP, Feldmann KA (1995) T-DNA tagging in *Arabidopsis thaliana*: cloning by gene disruption. In: Plant molecular biology manual K3. Kluwer, Dordrecht, pp 1–17

Sentenac H, Bonneaud N, Minet M, Lacroute F, Salmon J M, Gaymard F, Grignon C (1992) Cloning and expression in yeast of a plant potassium ion transport system. Science 256:663–5

Shakya R, Sturm A (1998) Characterization of source- and sink-specific sucrose/$H^+$ symporters from carrot. Plant Physiol 118:1473–1480

Spurr AR (1969) A low-viscosity epoxy resin embedding medium for electron microscopy. J Ultrastruct Res 26:31–43

Stadler R, Sauer N (1996) The *Arabidopsis thaliana AtSUC2* gene is specifically expressed in companion cells. Bot Acta 109:299–306

Szyroki A, Ivashikina N, Dietrich P, Roelfsema MRG, Ache P, Reintanz B, Deeken R, Godde M, Felle H, Steinmeyer R, Palme K, Hedrich R (2001) KAT1 is not essential for stomatal opening. Proc Natl Acad Sci USA 98:2917–2921

Tomos AD, Hinde P, Richardson P, Pritchard J, Fricke W (1994) Microsampling and measurement of solutes in single cells. In: Harris, N, Oparka, KJ (eds) Plant cell biology – a practical approach. IRL Press, Oxford, pp 297–314

Truernit R, Sauer N (1995) The promoter of the *Arabidopsis thaliana SUC2* sucrose-$H^+$ symporter gene directs expression of $\beta$-glucuronidase to the phloem: evidence for phloem loading and unloading by SUC2. Planta 196:564–570

Truernit E, Schmid J, Epple P, Illig J, Sauer N (1996) The sink-specific and stress-regulated *Arabidopsis STP4* gene: enhanced expression of a gene encoding a monosaccharide transporter by wounding, elicitors, and pathogen challenge. Plant Cell 8:2169–2182

Wright JP, Fisher DB (1981) Measurement of the sieve tube membrane potential. Plant Phys 67:845–848

Zhou J-J, Theodoulou F, Sauer N, Sanders D, Miller AJ (1997) A kinetic model with ordered cytoplasmic dissociation for SUC1, an *Arabidopsis* $H^+$/Sucrose cotransporter expressed in *Xenopus* oocytes. J Membr Biol 159:113–125

# Kapitel IV: The $K^+$ Channel KZM1 Mediates Potassium Uptake into the Phloem and Guard Cells of the $C_4$ Grass *Zea mays*

**Katrin Philippar, Kai Büchsenschütz, Maike Abshagen, Ines Fuchs, Dietmar Geiger, Benoit Lacombe und Rainer Hedrich**

**Publiziert in The Journal of Biological Chemistry, Vol. 278, 16973-16981, Mai 2003**

**Eigene Beteiligung an der Arbeit:**

- Biophysikalische Charakterisierung von KZM1 in *Xenopus* Oozyten mit Hilfe der DEVC-Technik in Bezug auf Spannungsabhängigkeit, externe und interne pH-Empfindlichkeit, Selektivität und Inhibierung durch $K^+$-Kanal spezifische Blocker
- Auswertung der Daten

THE JOURNAL OF BIOLOGICAL CHEMISTRY Vol. 278, No. 19, Issue of May 9, pp. 16973–16981, 2003

*Printed in U.S.A.*

# The $K^+$ Channel KZM1 Mediates Potassium Uptake into the Phloem and Guard Cells of the $C_4$ Grass *Zea mays**

Received for publication, December 13, 2002, and in revised form, February 27, 2003
Published, JBC Papers in Press, February 27, 2003, DOI 10.1074/jbc.M212720200

**Katrin Philippar‡, Kai Büchsenschütz‡, Maike Abshagen§, Ines Fuchs‡, Dietmar Geiger‡, Benoit Lacombe‡¶, and Rainer Hedrich‡‖**

*From the ‡Julius-von-Sachs-Institut, Lehrstuhl Molekulare Pflanzenphysiologie und Biophysik, Universität Würzburg, Julius-von-Sachs-Platz 2, D-97082 Würzburg and §Zentrum für Biochemie und Molekularbiologie, Christian-Albrechts-Universität zu Kiel, Leibnizstrasse 11, D-24098 Kiel, Germany*

**In search of $K^+$ channel genes expressed in the leaf of the $C_4$ plant *Zea mays*, we isolated the cDNA of *KZM1* (for $K^+$ channel *Zea mays 1*). KZM1 showed highest similarity to the *Arabidopsis* $K^+$ channels KAT1 and KAT2, which are localized in guard cells and phloem. When expressed in *Xenopus* oocytes, KZM1 exhibited the characteristic features of an inward-rectifying, potassium-selective channel. In contrast to KAT1- and KAT2-type $K^+$ channels, however, KZM1 currents were insensitive to external pH changes. Northern blot analyses identified the leaf, nodes, and silks as sites of *KZM1* expression. Following the separation of maize leaves into epidermal, mesophyll, and vascular fractions, quantitative real-time reverse transcriptase-PCR allowed us to localize *KZM1* transcripts predominantly in vascular strands and the epidermis. Cell tissue separation and *KZM1* localization were followed with marker genes such as the bundle sheath-specific ribulose-1,5-bisphosphate carboxylase, the phloem $K^+$ channel *ZMK2*, and the putative sucrose transporter *ZmSUT1*. When expressed in *Xenopus* oocytes, ZmSUT1 mediated proton-coupled sucrose symport. Coexpression of ZmSUT1 with the phloem $K^+$ channels KZM1 and ZMK2 revealed that ZMK2 is able to stabilize the membrane potential during phloem loading/unloading processes and KZM1 to mediate $K^+$ uptake. During leaf development, sink-source transitions, and diurnal changes, *KZM1* is constitutively expressed, pointing to a housekeeping function of this channel in $K^+$ homeostasis of the maize leaf. Therefore, the voltage-dependent $K^+$-uptake channel KZM1 seems to mediate $K^+$ retrieval and $K^+$ loading into the phloem as well as $K^+$-dependent stomatal opening.**

Since the first isolation of a plant $K^+$ channel gene 10 years ago, plant science has focused on their cell-specific localization and structure-function relationship. Therefore, new insights into the physiological role of the different $K^+$ channel genes have been gained. The *Arabidopsis thaliana* genome contains at least 15 $K^+$ channel genes (1). Among them, the *Shaker* family of *Arabidopsis* $K^+$ channels consists of nine members (for review see Ref. 2). According to their localization, structure, and function, these genes can be assigned to different subfamilies. In 1992, the first plant $K^+$ channel genes isolated were *AKT1* and *KAT1* (3, 4). Both proteins represent $K^+$-uptake channels (5, 6). AKT1-like channels are involved in $K^+$ uptake into growing roots (AKT1) (7, 8) and pollen tubes (SPIK) (9), and KAT1 plays a role in *Arabidopsis* guard cells (10–12). Recently, the inward rectifier KAT2 could be characterized as the closest relative to KAT1 (13). *KAT2* is expressed in guard cells, too, but in contrast to *KAT1*, *KAT2* transcripts were identified in the phloem parenchyma of the leaf. A coding sequence of the channel gene *AKT5* (AKT1 subfamily) could be isolated from hypocotyl tissue,[1] but its function still remains unknown. The *AtKC1* gene splits into another subfamily and together with AKT1 subunits seems to generate the functional properties of the root hair $K^+$-influx channel (14, 15). In contrast to the mentioned inward rectifiers within the AKT1 and KAT1 family, members of the AKT2/3 subfamily are characterized by weak voltage dependence, a $Ca^{2+}$ and $H^+$ block, and seem to control phloem function (16–19). The $K^+$ channel genes *SKOR*, localized in xylem vessels of the root (20), and *GORK,* in guard cells, vasculature, and roots (14, 21), build the subfamily of outward-rectifying $K^+$ channels in *Arabidopsis*.

Because the *Arabidopsis* genome reveals the complete set of *Shaker*-like $K^+$ channel genes in plants, we can assign the orthologs from different plant species to the respective subfamilies. So far $K^+$ channel genes have been isolated from 12 different plants (compare with Ref. 22) including the $C_4$ plant *Zea mays*. In maize, the two $K^+$ channel genes *ZMK1* and *ZMK2*, isolated from the coleoptile, belong to the AKT1- and AKT2/3-type subfamilies, respectively (23). ZMK1 is involved in auxin-induced $K^+$ uptake, coleoptile growth, and tropisms. ZMK2 displays the voltage-independent features of the AKT2/3-type $K^+$ channels and thus seems to serve phloem-associated functions (24). Besides rice, the maize plant is not only a model system for monocotyledonous crops but $C_4$ photosynthesis as well. This involves a special anatomic feature called Kranz anatomy: mesophyll cells, involved in the prefixation of $CO_2$, transport $C_4$ compounds to the bundle sheath cells, which surround the vascular strands and finally fix $CO_2$ in the Calvin cycle (reviewed in Ref. 25). Due to this cell and chloroplast dimorphism, $C_4$ plants are characterized by a better water-use efficiency than $C_3$ plants. The carbohydrate transport between mesophyll, bundle sheath, and vascular parenchyma cells of the maize leaf is accomplished by numerous

* This work was supported in part by grants from the Deutsche Forschungsgemeinschaft (to R. H.). The costs of publication of this article were defrayed in part by the payment of page charges. This article must therefore be hereby marked "*advertisement*" in accordance with 18 U.S.C. Section 1734 solely to indicate this fact.

¶ Supported by an EMBO long term fellowship. Present address: Biochimie et Physiologie Moléculaire des Plantes, UMR 5004 Agro-M/CNRS/INRA/UMII, Place Viala, 34060 Montpellier Cedex 1, France.

‖ To whom correspondence should be addressed. Tel.: 49-931-888-6101; Fax: 49-931-888-6158; E-mail: hedrich@botanik.uni-wuerzburg.de.

[1] S. Scheuermann, unpublished results.

plasmodesmata (26–28). The loading of sucrose from the vascular parenchyma to the thin-walled sieve tubes, representing the site of assimilate export, however, is thought to involve an apoplastic step (reviewed in Refs. 29 and 30). To characterize the sugar import machinery, Aoki *et al.* (31) isolated ZmSUT1, a putative sucrose transporter from source leaves of maize. By heterologous expression in *Xenopus* oocytes, we showed that ZmSUT1 indeed represents a sucrose/$H^+$ symporter under the voltage control of the AKT2/3 ortholog ZMK2.

Because the AKT2/3-type channels such as AKT2/3 from *Arabidopsis*, VFK1 from *Vicia faba*, and ZMK2 from *Z. mays* seem to play an important role in the control of phloem sucrose loading and unloading (16, 17, 24, 32), we here studied $K^+$ channels expressed in the dimorphic structure of the maize leaf. In addition to ZMK2 (23), we isolated the cDNA of *KZM1*. *KZM1* represents the maize ortholog to *KAT2* from *Arabidopsis*. Like *KAT2* we found this new maize $K^+$ channel gene expressed in vascular/bundle sheath strands as well as guard cell- and subsidiary cell-enriched epidermal fractions of the maize leaf. However, KZM1 is characterized by unique functional properties that enabled us to discriminate between the function of KAT2 in the dicotyledonous plant *Arabidopsis* and KZM1 in the monocotyledonous $C_4$ plant maize. The $K^+$-uptake channel KZM1 is able to mediate phloem $K^+$ loading and retrieval as well as $K^+$-dependent stomatal movement. The function of the inward-rectifier KZM1 in combination with ZMK2 and the sucrose/$H^+$ symporter ZmSUT1 as well as its expression pattern point to a housekeeping function of KZM1 for $K^+$ homeostasis in the phloem of the maize leaf.

## MATERIALS AND METHODS

*Plant Material*—Cloning, Northern blot procedures, and quantitative real-time RT[2]-PCR analysis were performed on tissues isolated from maize plants (*Z. mays* L., hybrid corn cv. "Oural FA0230," Deutsche Saatveredelung, Lippstadt, Germany). Seeds were sown in soil and grown in a greenhouse with a 16-h light (25 °C) and 8-h dark (18 °C) cycle. The white light used had a photon-flux density of 210 $\mu mol \cdot m^{-2} \cdot s^{-1}$ (LiCOR Quantum Sensor LI-250, Walz GmbH, Effeltrich, Germany). After harvesting, all maize tissues were stored in liquid nitrogen prior to RNA extraction. The age of plants or organs is denoted in days after sowing.

*Cloning of KZM1 cDNA*—Degenerated oligonucleotide primers, directed toward homologous regions of known plant inward-rectifying $K^+$ channels, were used to amplify a corresponding region of potassium channels from reverse-transcribed maize leaf RNA (RT-PCR). By using the SMART RACE cDNA Amplification kit (Clontech, Heidelberg, Germany) in combination with gene-specific primers, we amplified overlapping N- and C-terminal $K^+$ channel fragments according to the RACE technique. The corresponding full-length cDNA was generated in a single PCR step using primers flanking the 5′- and 3′-ends of the coding sequence of *KZM1* and ligated into pCRII-TOPO TA vector (Invitrogen). Besides the N- and C-terminal clones of *KZM1*, three identical full-length clones of the channel cDNA were sequenced using the LiCOR 4200 sequencer (LiCOR, Bad Homburg, Germany).

*Northern Blot Analysis*—Total RNA was isolated from the respective maize organs using the Plant RNeasy Extraction kit (Qiagen, Hilden, Germany). Poly(A)$^+$ RNA was purified from total RNA using Dynabeads (Dynal, Hamburg, Germany) and subjected to Northern blot analysis as described (33). The blotted poly(A)$^+$ RNA was hybridized against $^{32}$P-radiolabeled full-length cDNA probes of the $K^+$ channel genes *KZM1* and *ZMK2* as described in Philippar *et al.* (23). For the sucrose transporter *ZmSUT1*, a 339-bp-long 3′-terminal cDNA fragment, amplified between the primers ZmSUT LCfw (5′-cccacaaaggcaaac-3′) and ZmSUT LCrev (5′-tggtgtgggtgacg-3′), served as a probe. Each probe exhibited specific signals at 2.5 kb for *KZM1*, 2.8 kb for *ZMK2*, and 2.0 kb for *ZmSUT1*. To standardize transcript abundance, 15 ng of dotted poly(A)$^+$ was hybridized against a [$\gamma$-$^{32}$P]dATP end-labeled oligo(dT) probe as described (23).

*Separation of Leaf Tissues*—Tissue from the last fully developed leaf of 5-week-old maize plants was separated into epidermis, mesophyll cells, and vascular strands by a procedure modified according to Keunecke and Hansen (34). The central vascular strand was excised, and the lower epidermis was collected in 1 mM $CaCl_2$, 5 mM Mes/KOH, pH 6.5, adjusted with mannitol to 530 mosmol $kg^{-1}$, and frozen in liquid nitrogen for mRNA extraction. To test the vitality of epidermal cells before freezing, an aliquot of the epidermal fraction was stained with neutral red (see Fig. 4). To isolate mesophyll protoplasts, the remaining leaf sections were incubated for 90 min at 30 °C in enzyme solution containing 1.5% cellulase (Cellulase R-10, Yakult Honsha Co., Tokyo, Japan), 2% pektinase (Sigma), 10 mM KCl, 10 mM Mes/KOH, pH 6.2, adjusted with D-sorbitol to 480 mosmol $kg^{-1}$. The digestion was stopped before the bundle sheath cells were released from the vascular strands. Isolated vascular/bundle sheath strands were pooled and frozen in liquid nitrogen. Mesophyll protoplasts were sedimented at 60 × *g* for 5 min at 4 °C and frozen in liquid nitrogen.

*Quantitative Real-time RT-PCR*—For real-time RT-PCR experiments, total RNA from the fractionated maize leaves was isolated using the Plant RNeasy Extraction kit (Qiagen, Hilden, Germany). To minimize DNA contaminations, mRNA was purified twice with the Dynabeads mRNA Direct kit (Dynal, Hamburg, Germany), or total RNA was subjected to digestion with RNase-free DNase and purified by phenol/chloroform extraction (33). Mesophyll protoplast mRNA was directly purified with the Dynabeads mRNA Direct kit (Dynal). First-strand cDNA synthesis and quantitative real-time RT-PCR were performed as described before (12) using a LightCycler (Roche Molecular Biochemicals). The following $K^+$ channel-specific primers were used: KZM1 LCfw (5′-aagaagcatggttgttac-3′), KZM1 LCrev (5′-tgaaaccaaagaagtctc-3′), ZMK2 LCfw (5′-gacggctcaggttcag-3′), and ZMK2 LCrev (5′-gagaaggcgttgatcg-3′). For detection of the coding sequence of the small subunit of the ribulose-1,5-bisphosphate carboxylase (ZmRuBPCsu, GenBank™ accession number X06535) and the 3′-untranslated region of the $C_4$ form phosphoenolpyruvate carboxylase (Zm$C_4$-PEPC, GenBank™ accession number X15238), we used the primer pairs RuBPCssu LCfw (5′-caacaagaagttcgagacg-3′), RuBPCssu LCrev (5′-cgggtaggatttgatggc-3′), and $C_4$-PEPC LCfw (5′-ggcttctcttcactcacc-3′), $C_4$-PEPC LCrev (5′-tccaatgggctgggata-3′), respectively. All quantifications were normalized to the signal of actin cDNA fragments generated by the primers ZmAct 81/83fw (5′-acacagtgccaatct-3′) and ZmAct 81/83rev (5′-actgagcacaatgttac-3′), which amplified cDNA from the maize actins ZmAct 81 (GenBank™ accession number AAB40106) and ZmAct 83 (GenBank™ accession number AAB40105). The relative amount of channel cDNA was calculated from the correlation $2^{(n\ \text{actin} - n\ \text{channel})}$ with $n$ = threshold cycle of the respective PCR product. To identify contaminating genomic DNA, the primers for ZMK2 were selected to flank an intron.

*Two-electrode Voltage Clamp Experiments*—For heterologous expression in *Xenopus laevis* oocytes, the cDNAs of *KZM1* in pCRII and *ZmSUT1* in pBS SK(−) were subcloned as *Xho*I/*Spe*I and *Bam*HI/*Xho*I fragments, respectively, into the pGEMHE vector (35). Expression of *ZMK2* in oocytes was performed as described (23). The respective cRNA was generated by *in vitro* transcription (T7-Megascript kit, Ambion Inc., Austin, TX) and injected into *Xenopus* oocytes (CRBM, CNRS, Montpellier, France) using a PicospritzerII microinjector (General Valve, Fairfield, NJ). Two to 6 days following injection, double-electrode voltage clamp recordings were performed with a Turbotec-01C amplifier (NPI Instruments, Tamm, Germany). The electrodes were filled with 3 M KCl and had typical input resistance of about 2–4 megaohm. Solutions were composed of 30 mM KCl, 2 mM $MgCl_2$, 1 mM $CaCl_2$, and 10 mM Tris/Mes, pH 7.5, 10 mM Mes/Tris, pH 5.6, and 10 mM citrate/Tris, pH 4.5, respectively. Acidification of the cytosolic pH was accomplished by perfusion with 30 mM KCl, 2 mM $MgCl_2$, 1 mM $CaCl_2$ and 10 mM Mes/Tris, pH 5.6, as well as 10 mM NaAc. The control solution contained 10 mM NaCl instead of NaAc. When recording KZM1-mediated currents at 100, 30, 10, and 3 mM external $K^+$ concentrations, the ionic strength was adjusted with $Na^+$. In $K^+$-free solutions, $K^+$ was substituted with $Na^+$ or $Li^+$ as indicated. All media were adjusted to a final osmolality of 215–235 mosmol $kg^{-1}$ with D-sorbitol. Analyses of voltage and pH dependence were performed as described previously (19, 36). Membrane potential measurements with ZmSUT1-expressing oocytes and coexpression of ZmSUT1 with KZM1 and ZMK2 were performed as described for AtSUC2, KAT2, and AKT2/3 in Deeken *et al.* (17).

*Patch Clamp Experiments*—For patch clamp experiments, devitellinized oocytes were placed in a bath solution containing 100 mM KCl, 2

[2] The abbreviations used are: RT, reverse transcriptase; RACE, rapid amplification of cDNA ends; Mes, 2-morpholinoethanesulfonic acid; NaAc, sodium acetate; RuBPCssu, ribulose-1,5-bisphosphate carboxylase small subunit; PEPC, phosphoenolpyruvate carboxylase.

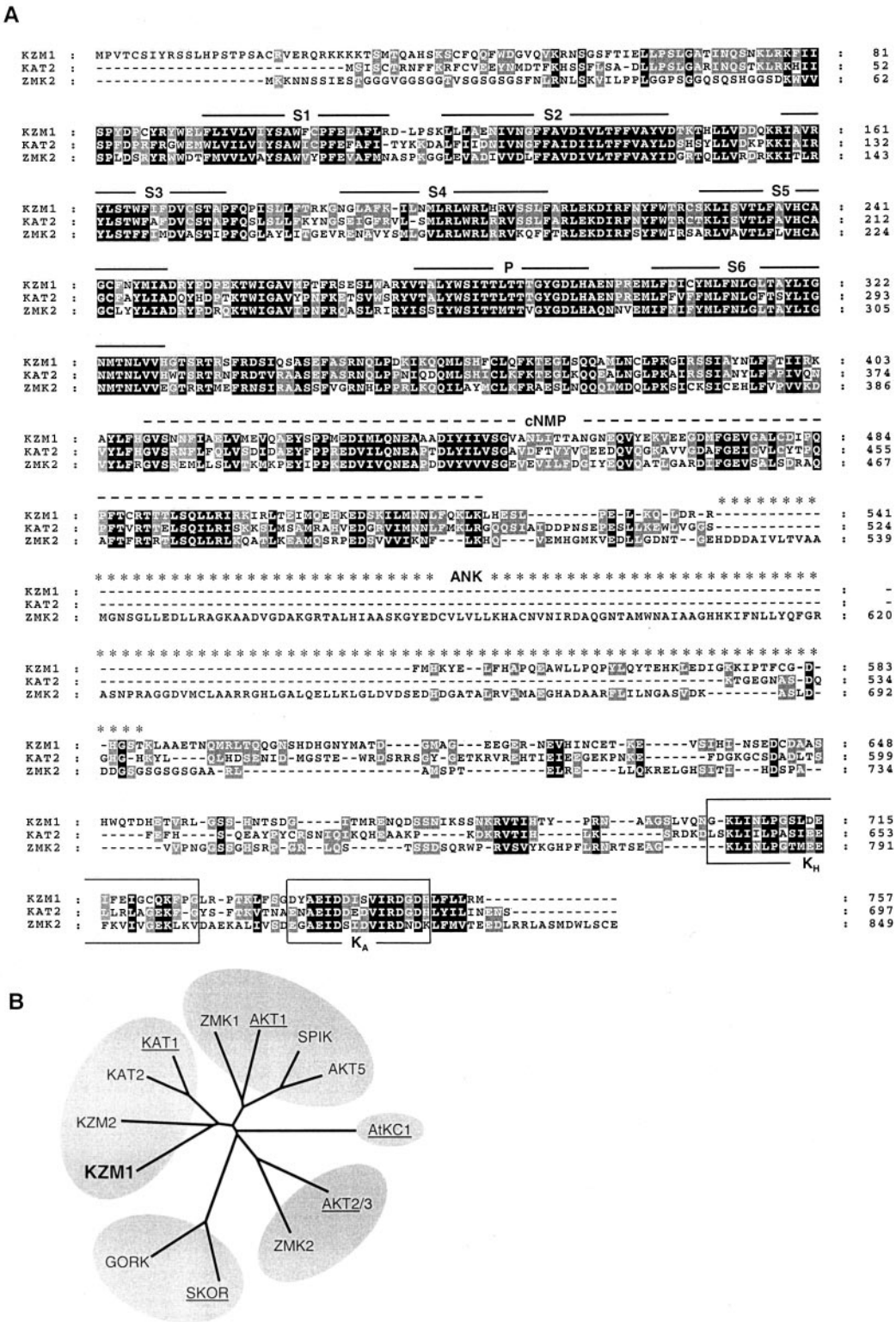


FIG. 1. **KZM1 belongs to the KAT1 subfamily of plant *Shaker* potassium channels.** *A*, sequence comparison of *Shaker* $K^+$ channels from maize and *Arabidopis*. Alignment of the deduced amino acid sequences of *KZM1* cDNA (GenBank™ accession number AJ421640) with the $K^+$ channels KAT2 from *Arabidopis* and ZMK2 from maize is shown. The start and stop codons of KZM1 were used as end positions of the alignment. Amino acids identical in all 3 channel proteins are shown as *black-boxed letters*, and residues conserved in 2 sequences are shown as *gray-boxed letters*. The predicted transmembrane regions (S1 to S6) and the pore region (*P*) are marked with *solid lines*. The C-terminal region of all 3 channels contains a conserved cyclic nucleotide binding motive (*cNMP, dashed line*), whereas only ZMK2 exhibits a putative ankyrin binding domain (*ANK, asterisks*). Blocks denote hydrophobic ($K_H$) and acidic ($K_A$) core sequences according to Ref. 40. The alignment was generated using ClustalX (41) and GeneDoc 2.0 (42), and protein domains were identified with InterPro (43). *B*, phylogenetic tree, demonstrating that KZM1 is a member of the KAT1-type plant $K^+$ channel subfamily. The 9 *Shaker*-type $K^+$ channels from *A. thaliana* KAT1 (M86990), KAT2 (AJ288900), AKT1 (X62907), SPIK (AJ309323), AKT5 (AJ249479), AtKC1 (Z83202), AKT2/3 (AJ243703, U44745), SKOR (AJ223357), and GORK (AJ279009) group into 5 subfamilies (highlighted by *gray backgrounds*). *A. thaliana* members, which named the subfamilies, are *underlined*. Whereas ZMK1 (Y07632) from maize is similar to AKT1 and ZMK2 (AJ132686) is the ortholog to AKT2/3, KZM1 and KZM2[3] belong to the KAT1-type subfamily. GenBank™ accession numbers of the respective channels are shown in *parentheses*. The alignment was generated using ClustalX (41); the tree was drawn with TreeView (44).

mM $MgCl_2$, 1 mM $CaCl_2$, and 10 mM Tris/Mes, pH 7.5. Pipettes were filled with solution containing 100 mM KCl, 2 mM $MgCl_2$, 1 mM $CaCl_2$, and 10 mM Tris/Mes, pH 7.5. Currents were recorded in the cell-attached configuration using an EPC-9 amplifier (HEKA, Lambrecht, Germany) as described previously (37).

## RESULTS

*KZM1 Represents a KAT1-type Shaker $K^+$ Channel Gene*—To study the role of $K^+$ channels in $C_4$ leaves, characterized by Kranz anatomy, we isolated *KZM1* from maize leaf cDNA via RT-PCR and RACE techniques. The cloning strategy took advantage of highly conserved regions in the *Shaker* gene family of plant $K^+$ channels (for review see Ref. 2). Sequence analysis of the open reading frame of the *KZM1* cDNA (2274 bp) revealed the basic features of the KAT1 subfamily (Fig. 1*A*) as follows: six putative transmembrane domains (S1–S6) with a proposed voltage sensor in segment 4 and a $K^+$-selective pore (P), formed by the amphiphilic linker between S5 and S6 (for structure-function analysis of plant $K^+$ channels see Refs. 38 and 39). The deduced KZM1 protein spans 758 amino acids with a predicted molecular mass of 86.7 kDa. When compared on the amino acid level to the *Arabidopsis* $K^+$ channels of the *Shaker* family, KZM1 showed highest similarity to KAT2 (48% identity, Ref. 13) and KAT1 (47% identity, Ref. 3), whereas the identity to the previously identified maize $K^+$ channels ZMK1 and ZMK2 (23) was only 36 and 34%, respectively. Thus, KZM1 represents a member of the KAT1 subfamily of plant $K^+$ channels (Fig. 1*B*). The proposed cytoplasmic C terminus of KZM1 contains a region, which shares structural homologies to cyclic nucleotide binding domains (Fig. 1*A*). In contrast to ZMK2 (five ankyrin repeats), the sequence of KZM1 did not contain an ankyrin binding domain (Fig. 1*A*), a feature that is conserved among $K^+$ channels of the KAT1 subfamily (1), beside the SIRK protein from *Vitis vinifera* (22) and KPT1 from *Populus tremula* (GenBank™ accession number AJ344623, for details see "Discussion"). In the 5′-region of the open reading frame of *KZM1*, we could identify two possible translational start positions ("ATG"), a structural element also found with the *Arabidopsis* ortholog *KAT2* (Fig. 1*A*). In addition, plant-specific hydrophobic and acidic C-terminal domains, involved in plant $K^+$ channel clustering (40, 45), could be identified. Based on Southern blot analysis with maize DNA, we characterized *KZM1* as a single copy gene within the maize genome (not shown). Besides *KZM1* we could also identify *KZM2*,[3] the second maize member of the KAT1 subfamily (Fig. 1*B*), most likely representing the ortholog to *KAT1* from *Arabidopsis*.

*KZM1 Is a Voltage-dependent $K^+$-uptake Channel*—When expressed in *Xenopus* oocytes, the gene product of *KZM1* showed the characteristic properties of a voltage-dependent, inward-rectifying plant $K^+$ channel (Fig. 2). In two-electrode voltage clamp experiments, KZM1 activated upon hyperpolarization to membrane potentials negative to −60 mV (Fig. 2*A*). The steady-state current-voltage curve of the data shown in Fig. 2*A* underlines the strong inward rectification of KZM1 (Fig. 2*B*). From activation curve analyses, a half-maximal activation voltage $U_{½}$ of −105.4 ± 6.9 mV ($n$ = 5) was calculated. Recordings in the cell-attached patch clamp configuration allowed us to resolve single KZM1 channel-fluctuations (Fig. 2*C*). The channel amplitude and time-dependent activity increased with increasing negative voltages. From the current-voltage relationship of the single channels (Fig. 2*D*), a unitary conductance of 20 ± 0.7 pS ($n$ = 3, mean ± S.E. with 100 mM $K^+$ in the pipette) was deduced. Thus, KZM1 exhibits a 2–4-fold higher conductance than the previously characterized $K^+$ channels of the KAT1 subfamily (6.7 pS for KAT2 (13), 5 pS for KAT1 (37), 7 pS for KST1 (46), and 13 pS for SIRK (22)).

[3] K. Büchsenschütz, unpublished results.

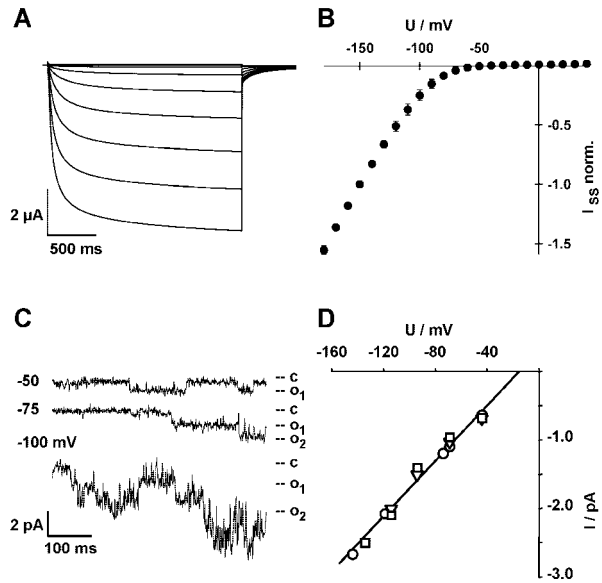


FIG. 2. **KZM1 is an inward-rectifying $K^+$ channel.** *A* and *B*, two-electrode voltage clamp recordings. *A*, representative macroscopic recordings of inward currents recorded from *KZM1*-injected *Xenopus* oocytes. Inward currents of KZM1 were elicited in response to 2-s voltage pulses from +40 to −180 mV (−20-mV steps) from a holding potential of −50 mV. The bath solution was composed of 30 mM KCl, 1 mM $CaCl_2$, 2 mM $MgCl_2$, and 10 mM Tris/Mes, pH 7.5. *B*, steady-state currents ($I_{SS}$) at the end of the voltage pulses were normalized to $I_{SS}$ (−150 mV) and plotted against the membrane voltage ($U$) as mean ± S.D. ($n$ = 6). *C* and *D*, patch clamp recordings. *C*, single channel fluctuations recorded at −50, −75, and −100 mV in the cell-attached patch clamp configuration. Closed ($c$) and open channel states ($o_1$ and $o_2$) are indicated. *D*, single channel current-voltage relationship. Linear regression on 3 different patches (*circles*, *squares*, and *triangles*) reveal the single channel conductance of 20 ± 0.7 pS (mean ± S.E., $n$ = 3).

In agreement with a $K^+$-selective channel, $K^+$ currents through KZM1 increased as a function of the external $K^+$ concentration (not shown) with the current reversal potential following the Nernst potential for potassium (60.8 ± 4.7 mV per 10-fold change in external $K^+$ concentration, Fig. 3*A*). Replacing $K^+$ by $Rb^+$ (100 mM) caused a drop in the inward current (at −150 mV, $I_{Rb^+}/I_{K^+}$ = 0.190 ± 0.041, $n$ = 4). Comparison of the reversal potential in either $K^+$ or $Rb^+$ solutions allowed us to determine the permeability ratio $P_{Rb}/P_K$ = 0.437 ± 0.085, $n$ = 4. In contrast to other KAT1-like channels, the permeability ratios for $Na^+$ and $Li^+$ ions could not be determined, because KZM1 did not even conduct outward currents in $Na^+$- or $Li^+$-based media (Fig. 3, *B* and *C*). Similar results were obtained with *N*-methyl-D-glucamine solution, pointing to gating properties shared with the AKT3 channel (compare with Ref. 39).

KAT1-like channels are stimulated by external acidification (13, 22, 47). When we analyzed the sensitivity of KZM1 to extracellular pH changes in *Xenopus* oocytes, however, the relative open probabilities ($P_o$), obtained at different external proton concentrations, rendered KZM1 pH-insensitive (Fig. 3*D*). Thus, KZM1 seems to represent the first KAT1-type $K^+$ channel not affected by external pH changes (for details see "Discussion"). In contrast, $K^+$ currents through KZM1 increased upon cytoplasmic acidification of the oocyte in response to 10 mM sodium acetate, pH 5.6 in the bath solution (Fig. 3*E*, compare with Refs. 18 and 38). As shown in Fig. 3*F*, the cytosolic acid activation of KZM1 results from a shift of the half-maximal activation voltage $U_{½}$ ($\Delta U_{½}$ = 36.9 ± 10.3 mV, $n$ = 3) toward more positive values.

*KZM1 Is Expressed in Vascular Strands and Epidermis of the Maize Leaf*—To identify *KZM1*-expressing tissues, mRNA from different organs of the maize plant was isolated. In North-

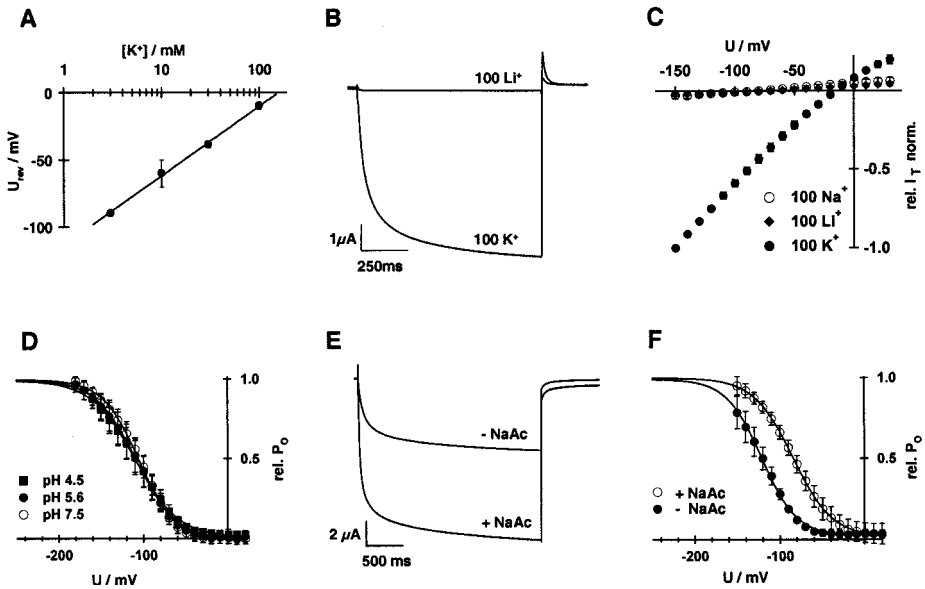


FIG. 3. **KZM1 is $K^+$-selective and independent on external pH.** *A*, shift in reversal potential ($U_{rev}$) in response to changes in extracellular $K^+$ concentration. In tail-current experiments, *KZM1*-expressing oocytes were challenged with an activating prepulse to −150 mV. In subsequent voltage jumps to potentials ranging from +40 to −180 mV, tail currents were elicited that reversed direction ($U_{rev}$) around the predicted Nernst potential for $K^+$. Changing the $K^+$ concentration 10-fold caused a shift in $U_{rev}$ of 60.8 ± 4.7 mV. *Error bars* indicate S.D. ($n \geq 4$). *B*, tail-current recordings of KZM1-injected oocytes at 20 mV after a 1-s preactivating pulse to −130 mV in 100 mM $K^+$ or $Li^+$, respectively. The bath solution was composed of 100 mM KCl/LiCl, 1 mM $CaCl_2$, 2 mM $MgCl_2$, and 10 mM Tris/Mes, pH 7.5. Note that the outward currents in $Li^+$ decay, although the driving force for $K^+$ release increases. *C*, relative instantaneous tail-current amplitudes (*rel.* $I_T$) plotted against the membrane voltage (*U*) revealed outward currents positive from the reversal potential in 100 mM $K^+$ (*closed circles*), but not in 100 mM $Li^+$ or $Na^+$ (*closed diamonds* and *open circles*, respectively). KZM1-expressing oocytes were challenged with an activating prepulse to −130 mV. In subsequent voltage jumps to potentials from +30 to −150 mV in 10-mV decrements, relative instantaneous tail-current amplitudes were measured at $t = 0$. $I_T$ was normalized to the values in 100 mM $K^+$ at −140 mV. Results represent mean ± S.D., $n = 6$. *D*, Boltzmann analysis of voltage-dependent gating at various external pH values (pH 7.5, 5.6, and 4.5, *open* and *closed circles* and *squares*, respectively) normalized to the maximal conductance of 1.0 obtained by Boltzmann fittings. The relative open probabilities (*rel.* $P_o$) were plotted against the membrane voltage (*U*). *Solid lines* represent best Boltzmann fits to the data (gating parameters: half-maximal activation voltage $U_{½}$, gating charge Z: pH 7.5: $U_{½} = -105.4 \pm 6.9$ mV, Z = 1.17 ± 0.12; pH 5.6: $U_{½} = -108.8 \pm 11.4$ mV, Z = 1.05 ± 0.13; pH 4.5: $U_{½} = -110.1 \pm 10.1$ mV, Z = 0.97 ± 0.07). *Error bars* indicate S.D. ($n \geq 5$). pH changes had no effect on the gating of KZM1 channels. *E*, lowering the internal proton concentration by perfusion with 10 mM NaAc at pH 5.6 (+*NaAc*) the inward currents, elicited by 2-s voltage pulses to −160 mV, increased with respect to those in the absence of acetate (−*NaAc*). *F*, the voltage-dependent gating in response to internal acidification was analyzed with a Boltzmann function as described in *B* (gating parameters: half-maximal activation voltage $U_{½}$, gating charge Z: +NaAc (*open circles*): $U_{½} = -84.8 \pm 3.5$ mV, Z = 1.08 ± 0.17; −*NaAc* (*closed circles*): $U_{½} = -121.6 \pm 7.1$ mV, Z = 1.22 ± 0.22). *Error bars* indicate S.D. ($n = 3$). KZM1 is activated by internal acidification due to a positive-going shift of the half-maximal activation voltage (36.9 ± 10.3 mV).

ern analyses *KZM1* transcripts were found in developing (1-week-old) and mature (5-week-old) leaves (not shown). High transcript levels were also detected in nodes, husks, and silks, whereas *KZM1* mRNA was rare in internodes and not detectable in young cobs and developing tassels (not shown). To study *KZM1* expression within the $C_4$ leaf in more detail, we fractionated the last fully developed leaf of 5-week-old maize plants into epidermal tissue, mesophyll protoplasts, and vascular strands (Fig. 4*A*). During enzymatic digestion, the bundle sheath cells remained attached to the vascular strands (compare with Ref. 34). In the following, the latter fraction will be addressed as "vascular/bundle sheath strands." To estimate contaminations of this fraction, the small subunit of the ribulose-1,5-bisphosphate carboxylase (ZmRuBPCssu), specifically expressed in maize bundle sheath cells, was used as marker for vascular/bundle sheath strands. In addition the $C_4$ form of the phosphoenolpyruvate carboxylase ($ZmC_4$-PEPC) served as marker for mesophyll cells (compare with Refs. 25 and 48). By using quantitative real-time RT-PCR to determine the transcript density of those two marker genes, we could show that the epidermis and mesophyll protoplast fractions were contaminated by less than 1% of the vascular/bundle sheath RuBPCsu transcripts (Fig. 4*B*). In contrast, 35 and 40% of the mesophyll-specific $C_4$-PEPC were detected in epidermis and vascular/bundle sheath strands, showing that these tissue preparations contained residual mesophyll fractions, probably from protoplasts still attached to the epidermal strips or vascular strands (for separation of mesophyll and bundle sheath cells compare Refs. 49 and 50). We cannot, however, exclude that the $C_4$ form of PEPC is expressed in guard cells and/or subsidiary cells as well (for discussion see Refs. 51 and 52).

Quantitative real-time RT-PCR on mRNA from the three different samples demonstrated that *KZM1* expression in the maize leaf is restricted to vascular/bundle sheath strands and the epidermis (Fig. 4*B*). The transcripts were about 13 times more abundant in the vascular/bundle sheath strands than in the epidermis. In mesophyll protoplasts the *KZM1* mRNA level was at the detection limit of the real-time RT-PCR method. Upon peeling of the epidermis, common epidermal cells rupture, whereas viable guard and subsidiary cells, visualized by neutral red staining (Fig. 4*A*, *inset*, compare with Ref. 53), survive this mechanical treatment. Thus, *KZM1* expression in the maize leaf is restricted to guard/subsidiary cells and the phloem-enriched vascular/bundle sheath strands. As a phloem marker we used the $K^+$ channel gene *ZMK2* (23, 24), which was detected in vascular bundles only (not shown, compare for phloem localization of AKT2/3 (16, 18, 19)). These results suggest that *KZM1* displays an expression pattern similar to its *Arabidopsis* ortholog *KAT2* (phloem tissue and guard cells (13), for differences see "Discussion").

*Expression of KZM1 during Development, Sink-Source Transitions, and Diurnal Changes*—To explore the role of *KZM1* in phloem physiology, we followed the expression of this $K^+$ channel gene along different developmental stages of the primary

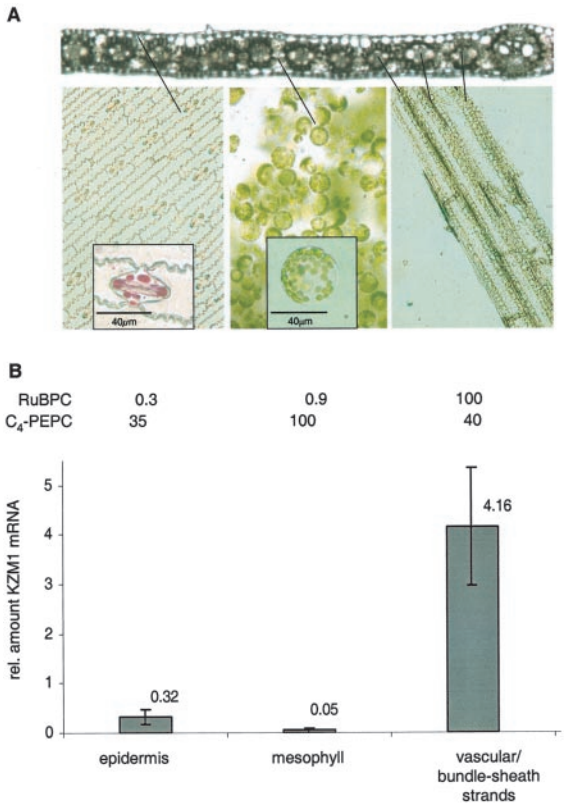


FIG. 4. **KZM1 transcripts in the leaf originate from vascular strands and epidermis.** *A*, photographs of fractionated maize leaf tissues and cells. *Top*, cross-section through a 5-week-old leaf. Epidermal, mesophyll, and vascular/bundle sheath sections are indicated by *solid lines. Left*, epidermal strips, excised from maize leaves. *Inset*, neutral red viability stain of guard and subsidiary cells. *Middle*, mesophyll protoplast suspension. *Inset*, single mesophyll protoplast at higher magnification. *Right*, vascular strands with bundle sheath cells attached. *B*, quantitative real-time RT-PCR analysis on mRNA from tissues of the last fully developed leaf from 5-week-old maize plants. *Top*, quantification of ZmRuBPCssu and $ZmC_4$-PEPC transcripts relative to actin ($n = 3$) in the tissue fractions shown in *A*. The transcript content of ZmRuBPCssu and $ZmC_4$-PEPC was set to 100% in vascular/bundle sheath strands and mesophyll protoplasts, respectively. *Bottom*, quantification of *KZM1* transcripts relative to actin ($n = 6$, mean ± S.E.) in epidermis, mesophyll protoplasts, and vascular/bundle sheath strands as shown in *A*. The transcript content measured in a total leaf fraction was set to 1.0 (arbitrary units).

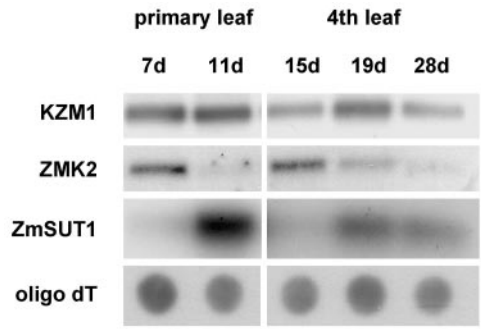


FIG. 5. **KZM1 is constitutively expressed during leaf development.** Northern blot with 0.7 µg mRNA, isolated from young (7 days (*7d*)) and mature (11 days (*11d*)) maize primary leaves (*left*) and from the 4th leaf of the maize plant (*right*) at juvenile (15 days (*15d*)), intermediate (19 days (*19d*)), and mature stage (28 days (*28d*)). Young leaves were just emerging from the plant (sink tissue), and the mature leaves were characterized by a visible leaf collar (source tissue). The RNA was blotted against radiolabeled cDNA probes of *KZM1*, *ZMK2,* and *ZmSUT1* (GenBank™ accession number AB008464). To standardize mRNA levels, 15 ng of dotted mRNA were hybridized against a radiolabeled oligo(dT) probe (*lower panel*).

leaf and the 4th leaf of the maize plant (Fig. 5). Here the juvenile, just emerging organs of the leaves represent carbohydrate sinks (54), whereas the mature leaves serve as source tissue. In contrast to the broad pattern of *KZM1* expression, transcripts of the phloem $K^+$ channel gene *ZMK2* were restricted to sink tissues such as young leaves (Fig. 5) and coleoptiles (23, 24). The sucrose transporter gene *ZmSUT1* (31), however, was prominent in the RNA fraction isolated from mature source leaves (Fig. 5). Because *ZmSUT1* expressed in oocytes mediates proton-coupled sucrose uptake (compare Fig. 8), this may indicate a source-specific function of ZmSUT1 for sucrose loading into the phloem.

The tip region of the maize leaf contains the oldest cells and mostly minor veins, in which thin-walled sieve tubes in combination with companion cells serve as the source site of apoplastic phloem loading (25, 29). In contrast, the leaf base is dominated by young cells and thick vascular bundles. In young leaves the latter are involved in phloem unloading (sink) to support growth in this expanding leaf zone, and in mature leaves they mediate long distance transport of carbohydrates in the thin-walled sieve tubes (compare with Refs. 28 and 54). In contrast to the leaf blade, characterized by sucrose production and phloem loading in a $C_4$-specific manner, the sheath of the maize leaf does not show the $C_4$ intrinsic Kranz anatomy (55). Here the sheath contains mostly large vascular bundles with thin-walled sieve tubes, considered to mediate transport of photosynthates out of the leaf. Moreover, veins of the leaf blade contain thick-walled sieve tubes, not present in the leaf sheath (55). Thick-walled sieve tubes in combination with vascular parenchyma cells are thought to mediate retrieval of solutes leaking out of the xylem vessels (56, 57). Northern blot analyses with mRNA extracted from 6 different zones of a 20-day-old maize leaf blade showed *KZM1* to be evenly expressed from tip to base. With leaf sheath mRNA, however, no signal was obtained (Fig. 6), pointing to a role for KZM1 in $K^+$ retrieval from xylem vessels of the leaf blade via phloem parenchyma and thick-walled sieve tubes. As noticed for leaf development before (Fig. 5), *ZMK2* was predominantly expressed in the sink and transport regions of the leaf, represented by the leaf base and sheath (Fig. 6). In addition *ZMK2* mRNA was seen in the very tip. As was shown by Aoki *et al.* (31), transcripts of the source-specific sucrose transporter *ZmSUT1* in expanding leaf blades increase from the unexpanded base (sink) toward the expanded tip region (source).

During the day, *ZmSUT1* transcript levels in the leaf increase, reach a maximum at the end of the light period, and decrease during the night (31). Thus, the expression pattern of this sugar transporter correlates with carbohydrate synthesis and phloem loading. In line with a constitutively active gene, *KZM1* expression in the leaf blade was not affected by diurnal changes (Fig. 7). In contrast, *ZMK2* transcripts accumulated during the dark period, again pointing to an important function of this phloem $K^+$ channel in sink control.

These studies show that *KZM1* expression in contrast to the source- (*ZmSUT1*) and sink-specific (*ZMK2*) genes is not affected by leaf development, sink-source transitions, or diurnal changes. However, expression of *KZM1* is clearly associated with $K^+$ retrieval by phloem parenchyma cells of the leaf blade and not with long distance transport of photosynthates in the leaf sheath or internodes. Based on this expression pattern, one would conclude that KZM1 has a housekeeping function in the vascular bundles of the maize leaf, controlling $K^+$ retrieval into the phloem and $K^+$ homeostasis.

*Cooperation of Phloem $K^+$ Channels and Sucrose Transporters*—To gain insight into the feedback control between $K^+$ channels and sucrose transporters in the phloem of the maize

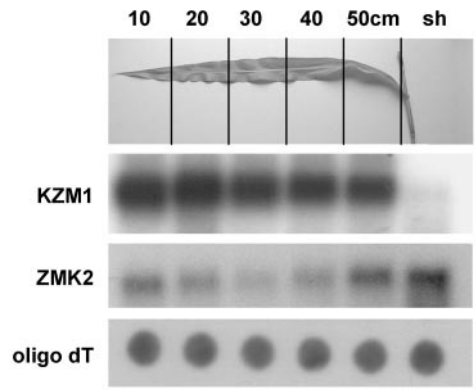


FIG. 6. **KZM1 is evenly expressed in the leaf blade.** Northern blot with 0.7 $\mu$g mRNA from the 4th leaf of the maize plant (20 days), dissected into 5 zones (10 cm each) from tip to base, and the leaf sheath (*sh, upper panel*). The RNA was blotted against radiolabeled cDNA probes of *KZM1* and *ZMK2,* and 15 ng of dotted mRNA were standardized with a radiolabeled oligo(dT) probe (*lower panel*).

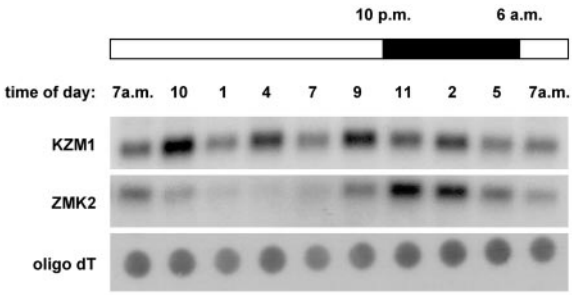


FIG. 7. **KZM1 is constitutively expressed throughout the day-night cycle.** Northern blot with 0.7 $\mu$g mRNA from the 4th leaf of the maize plant (33 days) at different times of a 16-h day (25 °C, *white bar*) and 8-h night (18 °C, *dark bar*) cycle. The light period lasted from 6 a.m. to 10 p.m. Leaf samples were collected at 9 time points as indicated. The RNA was hybridized against radiolabeled cDNA probes of *KZM1* and *ZMK2,* and 15 ng of dotted mRNA were standardized with a radiolabeled oligo(dT) probe (*lower panel*).

leaf, we studied the functional properties of the sucrose transporter ZmSUT1 alone and in the presence of either KZM1 or ZMK2 in *Xenopus* oocytes (Fig. 8). When the phloem-specific sucrose/$H^+$ co-transporter ZmSUT1 (31) was expressed in *Xenopus* oocytes, a sucrose-induced depolarization of the membrane was monitored. Properties like the sucrose specificity of ZmSUT1, as well as its concentration and pH dependence (not shown), were well in agreement with studies on the phloem sucrose/$H^+$ symporter ortholog AtSUC2 from *Arabidopsis* (17). However, when oocytes expressing both the voltage-independent phloem $K^+$ channel ZMK2 (23) and ZmSUT1 were challenged with sucrose, the drop in membrane potential was prevented (Fig. 8). This indicates that ZMK2, because of its peculiar kinetics and voltage dependence (compare Refs. 23 and 24), stabilizes the membrane potential in the presence of the sucrose-fueled sugar/$H^+$ symporter. *In vivo* this phloem $K^+$ channel thus very likely repolarizes the membrane rather than catalyzing the bulk flow of potassium, a function of which KZM1 is capable (see below). In contrast to ZMK2, KZM1 is activated at hyperpolarizing potentials only (compare Fig. 2). Coexpression of the sucrose/$H^+$ symporter with the inward rectifier KZM1 therefore did not prevent the sucrose-dependent depolarization of the membrane potential. Thus, voltage-independent, proton-blocked $K^+$ channels like ZMK2, which clamp the membrane to the Nernst potential for $K^+$, during phloem loading and unloading processes interact with the sucrose transporter ZmSUT1 via the membrane potential and extracellular pH. The voltage-dependent but pH-insensitive inward

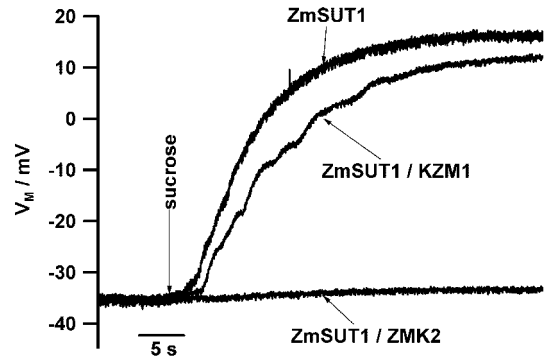


FIG. 8. **Coexpression of ZmSUT1 with KZM1 and ZMK2 in *Xenopus* oocytes.** Membrane potential ($V_M$) measurements with *ZmSUT1* injected and *ZmSUT1/KZM1*, *ZmSUT1/ZMK2* coinjected oocytes, respectively. The external solution was composed of 30 mM KCl, 1 mM $CaCl_2$, 1.5 mM $MgCl_2$, and 10 mM Mes/Tris, pH 5.6. The *arrow* indicates the start of perfusion with 10 mM sucrose. ZmSUT1 mediates a sucrose-dependent depolarization of the membrane potential (*upper trace*), whereas ZmSUT1 in the presence of ZMK2 is not able to collapse the membrane potential (*lower trace*). ZMK2 stabilizes the membrane potential by balancing the $H^+$ influx by $K^+$ efflux. Under these conditions, the depolarization of the membrane potential through ZmSUT1 is not prevented by coinjection of *ZmSUT1* with the inward rectifier *KZM1*.

rectifier KZM1 is able to maintain the $K^+$ homeostasis of the leaf phloem. Under physiological conditions the phloem $H^+$-ATPase at the source site often hyperpolarizes the membrane negative to −80 mV. Membrane polarization in the long run is accompanied by a drop in external pH. The latter effect will inhibit ZMK2, but not KZM1 which is activated negative to −60 mV (compare Fig. 2*A*). Thus, the inward rectifier provides for $K^+$ uptake as well as for a membrane control unit at more hyperpolarized potentials. With the voltage-independent, $H^+$-blocked ZMK2 and the voltage-dependent, $H^+$-insensitive KZM1 working hand in hand, membrane potential and $K^+$ homeostasis can be controlled over a broad voltage and pH range.

## DISCUSSION

In this study we have focused on *KZM1*, a new $K^+$ channel gene from *Z. mays*, belonging to the *Shaker* family of plant $K^+$ channels. *KZM1* displays structural, functional, and expression patterns reminiscent of the KAT2 $K^+$ channel from *Arabidopsis*. Thus, KZM1 represents the first KAT-type $K^+$ channel isolated from a $C_4$ species. In *Arabidopsis* the KAT1 subfamily consists of two members, KAT1 and KAT2 (compare with Fig. 1). With the isolation of *KZM2,*[3] another KAT-type $K^+$ channel gene from maize, most likely representing the orthologous gene to *KAT1*, the genome of *Z. mays* also seems to harbor two KAT1 subfamily members.

The KZM1 protein is characterized by the absence of an ankyrin repeat domain, a feature that was assigned to be specific for the KAT1-type *Shaker* $K^+$ channels (1). Only very recently it was reported that SIRK, a KAT-like $K^+$ channel from grapevine (*V. vinifera*), contains an ankyrin repeat (22). Because this ankyrin repeat is truncated (one repeat and two half-motifs) compared with complete ankyrin binding domains of the AKT1-, AKT2/3-, and SKOR-like channels (five to six repeats), it was concluded that this atypical feature of SIRK gives insight into the evolution of the plant *Shaker* $K^+$ channel family. The KAT-type channel KPT1 from poplar trees (*P. tremula*) contains such a truncated ankyrin domain as well,[4] indicating that the KAT1 subfamily of woody species may be identified by this motif. KZM1 from the monocot *Z.*

[4] K. Langer, unpublished results.

*mays*, however, is more closely related to KAT1, KAT2 from *Arabidopsis,* and KST1 from *Solanum tuberosum*, all characterized by the absence of ankyrin repeat motifs. Like *KAT2* (13) and *AKT2* (18), *KZM1* contains two possible translational start positions within the 5′-region of the open reading frame. The cRNA including both methionines was functional in *Xenopus* oocytes. Future experiments similar to those performed with *AKT2* will address the role of the second possible translational start position (compare with Ref. 18).

When expressed in *Xenopus* oocytes, KZM1 showed the characteristic properties of a voltage-dependent, inward-rectifying plant $K^+$ channel. Differences between the monocotyledonous KZM1 and the dicotyledonous KAT-type $K^+$ channels KAT1, KAT2, KST1, and SIRK could be assigned to the higher single channel conductance of KZM1 (20 pS) and the fact that the gating of KZM1 required potassium. The latter property could recently be recognized for AKT3, another phloem $K^+$ channel (for discussion see Ref. 39). These channels, sensing the $K^+$ concentration in the sink and source and along the transport phloem, are able to control $K^+$ release into growing tissue and resorption from mature or even senescing leaves.

Another unique feature of KZM1 is displayed by its insensitivity to external pH changes. All previously characterized KAT1-like $K^+$ channels are activated by an increase in the extracellular proton concentration (13, 22, 38), whereas channels from the AKT2/3 and SKOR subfamilies are proton blocked (19, 21, 58). Thus, structural elements of KZM1 might provide a new molecular tool for future structure-function experiments to access the external pH sensor of plant $K^+$ channels. This proton sensor of the potato guard cell $K^+$ channel KST1 could be assigned to two extracellular histidine residues in the outer pore (His-271) and between the linker of the transmembrane helices S3 and S4 (His-160) of the protein (36). The histidine of the outer pore is unique to all plant $K^+$ channels. However, KZM1 lacks the histidine residue in the linker between S3 and S4 but possesses a more positive charged arginine at this site. When the adequate mutation H160R was introduced into KST1, the protein lost its pH sensitivity almost completely (36). Therefore, it is tempting to speculate that the absence of histidine residue 160 might contribute to the insensitivity of KZM1 to external pH changes. In contrast, we found the histidine of the internal pH sensor, originally identified for the *Arabidopsis* KAT1 (59), located in the intracellular loop between the transmembrane helices S2 and S3 of KZM1, very likely responsible for the sensitivity of KZM1 to internal protons. The insensitivity of KZM1 toward changes in the extracellular proton concentration clearly distinguishes this channel from its *Arabidopsis* ortholog KAT2 and therefore might reflect a feature required to operate a monocotyledonous plant like maize, characterized by Kranz anatomy and $C_4$-acid metabolism (see below).

By quantitative real-time RT-PCR analysis, we could identify guard cells, subsidiary cells, and vascular/bundle sheath strands as sites of *KZM1* expression. By using the patch clamp technique, KZM1-like, inward-rectifying $K^+$ channels have been identified in maize guard cells (60, 61) and subsidiary cells (53). Thus KZM1, together with KZM2,[3] seems to carry a major part of the inward $K^+$ current in *Z. mays* guard cells and subsidiary cells during stomatal movement (compare Refs. 12 and 13). Likewise in bundle sheath cells, KZM1 might contribute to the inward $K^+$ currents recorded by Keunecke and Hansen (34) and Keunecke *et al.* (62).

Because KZM1 expression was most pronounced in vascular/bundle sheath strands, we investigated the role of this channel protein for carbohydrate export and import during leaf development, sink-source transitions, and diurnal changes. Sugar transport from the bundle sheath cells of the $C_4$ plant *Z. mays* to the phloem parenchyma cells occurs symplastically (26–28), whereas the subsequent loading to the thin-walled sieve element-companion cell complex is believed to involve an apoplastic step (29, 30, 56, 57). Aoki *et al.* (31) provided evidence for a role of the sucrose transporter ZmSUT1 during phloem loading of carbohydrates exported from source leaf blades. This hypothesis is supported by our finding that *ZmSUT1* encodes a $H^+$/sucrose cotransporter, and its expression is restricted to source tissues (*e.g.* mature leaves). In contrast, the $K^+$ channel gene *ZMK2* displayed an inverse expression pattern pointing to a more sink-specific function. The phloem $K^+$ channel ZMK2 belongs to the AKT2/3-type subfamily of *Shaker* $K^+$ channels (compare Fig. 1*B*). In *Arabidopsis, AKT2/3* is expressed predominantly in source organs and plays a role in sugar loading of the phloem (16, 17). In contrast to *AKT2/3* but in line with *ZMK2*, their ortholog *VFK1* from *V. faba* is found in sink tissues and during transition from source to sink and therefore related to phloem unloading (32). However, we localized *ZMK2* expression also in the tip of the leaf (source), indicating that ZMK2 can be involved in phloem loading as well, as discussed for AKT2/3-like channels (18, 32).

The expression of *KZM1* in the maize leave was highest in the vascular/bundle sheath. In contrast to *ZmSUT1* or *ZMK2* this gene was constitutively expressed during leaf development, sink-source transitions, and diurnal changes. The tip of the maize leaf, responsible for loading of sucrose to the phloem, alkalinizes the apoplast, whereas the expansion growth of young cells in the leaf base results in an acidification of the extracellular medium (63). Moreover during phloem unloading in sink tissues, the apoplastic pH increases, activating $K^+$ channels like ZMK2 to control the membrane potential (for discussion see Ref. 32). In such an environment, the $K^+$-uptake channel KZM1 is insensitive to external pH changes, providing a mechanism that is robust to sink-source changes, day-night cycles, and even development and thus maintains phloem $K^+$ uptake and homeostasis. Testing the potential feedback loops between the maize phloem $K^+$ channels and the sucrose/$H^+$ symporter ZmSUT1 in *Xenopus* oocytes, we could show that the voltage-independent ZMK2 prevents a collapse of membrane potential during $H^+$/sucrose transport via ZmSUT1. In contrast, KZM1 in the presence of ZmSUT1 is able to mediate the bulk flow of potassium into the maize phloem. At hyperpolarized potentials and acidic apoplast following enhanced $H^+$-ATPase activity, KZM1 is able to substitute ZMK2 in control of phloem potential. In addition, *KZM1* gene expression is linked to $K^+$ retrieval from xylem vessels in the leaf blade and not to long distance transport in the leaf sheath or stem internodes. The orthologous $K^+$ channel gene *KAT2* in *Arabidopsis* shows a similar expression pattern as *KZM1* but is characterized by distinct functional properties such as activation by external protons, $K^+$-independent gating, and a smaller single channel conductance (13). Up to now data on the regulation and phloem function of the *KAT2* gene are lacking. Here we could show that KZM1 in contrast is equipped with unique functional characteristics ($K^+$-dependent gating, insensitivity to external pH, and high single channel conductance) and a specific expression pattern in the leaf phloem, all pointing to a housekeeping function of KZM1 for $K^+$ homeostasis in the phloem of a $C_4$ leaf and $K^+$ transport required for the related organic acid-based metabolism.

REFERENCES

1. Mäser, P., Thomine, S., Schroeder, J. I., Ward, J. M., Hirschi, K., Sze, H., Talke, I. N., Amtmann, A., Maathuis, F. J. M., Sanders, D., Harper, J. F., Tchieu, J., Gribskov, M., Persans, M. W., Salt, D. E., Kim, S. A., and Guerinot, M. L. (2001) *Plant Physiol.* **126,** 1646–1667
2. Very, A. A., and Sentenac, H. (2002) *Trends Pharmacol. Sci.* **7,** 168–175
3. Anderson, J. A., Huprikar, S. S., Kochian, L. V., Lucas, W. J., and Gaber, R. F.

(1992) *Proc. Natl. Acad. Sci. U. S. A.* **89,** 3736–3740
4. Sentenac, H., Bonneaud, N., Minet, M., Lacroute, F., Salmon, J. M., Gaymard, F., and Grignon, C. (1992) *Science* **256,** 663–665
5. Gaymard, F., Cerutti, M., Horeau, C., Lemaillet, G., Urbach, S., Ravallec, M., Devauchelle, G., Sentenac, H., and Thibaud, J. B. (1996) *J. Biol. Chem.* **271,** 22863–22870
6. Schachtman, D. P., Schroeder, J. I., Lucas, W. J., Anderson, J. A., and Gaber, R. F. (1994) *Science* **258,** 1654–1658
7. Dennison, K. L., Robertson, W. R., Lewis, B. D., Hirsch, R. E., Sussman, M. R., and Spalding, E. P. (2001) *Plant Physiol.* **127,** 1012–1019
8. Hirsch, R. E., Lewis, B. D., Spalding, E. P., and Sussman, M. R. (1998) *Science* **280,** 918–921
9. Mouline, K., Very, A. A., Gaymard, F., Boucherez, J., Pilot, G., Devic, M., Bouchez, D., Thibaud, J. B., and Sentenac, H. (2002) *Genes Dev.* **16,** 339–350
10. Kwak, J. M., Murata, Y., Baizabal-Aguirre, V. M., Merrill, J., Wang, M., Kemper, A., Hawke, S. D., Tallman, G., and Schroeder, J. I. (2001) *Plant Physiol.* **127,** 473–485
11. Nakamura, R. L., McKendree, W. L. J., Hirsch, R. E., Sedbrook, J. C., Gaber, R. F., and Sussman, M. R. (1995) *Plant Physiol.* **109,** 371–374
12. Szyroki, A., Ivashikina, N., Dietrich, P., Roelfsema, M. R. G., Ache, P., Reintanz, B., Deeken, R., Godde, M., Felle, H., Steinmeyer, R., Palme, K., and Hedrich, R. (2001) *Proc. Natl. Acad. Sci. U. S. A.* **98,** 2917–2921
13. Pilot, G., Lacombe, B., Gaymard, F., Cherel, I., Boucherez, J., Thibaud, J. B., and Sentenac, H. (2001) *J. Biol. Chem.* **276,** 3215–3221
14. Ivashikina, N., Becker, D., Ache, P., Meyerhoff, O., Felle, H. H., and Hedrich, R. (2001) *FEBS Lett.* **508,** 463–469
15. Reintanz, B., Szyroki, A., Ivashikina, N., Ache, P., Godde, M., Becker, D., Palme, K., and Hedrich, R. (2002) *Proc. Natl. Acad. Sci. U. S. A.* **99,** 4079–4084
16. Deeken, R., Sanders, C., Ache, P., and Hedrich, R. (2000) *Plant J.* **23,** 285–290
17. Deeken, R., Geiger, D., Fromm, J., Koroleva, O., Ache, P., Langenfeld-Heyser, R., Sauer, N., Bennett, M., and Hedrich, R. (2002) *Planta* **216,** 334–344
18. Lacombe, B., Pilot, G., Michard, E., Gaymard, F., Sentenac, H., and Thibaud, J. B. (2000) *Plant Cell* **12,** 837–851
19. Marten, I., Hoth, S., Deeken, R., Ache, P., Ketchum, K. A., Hoshi, T., and Hedrich, R. (1999) *Proc. Natl. Acad. Sci. U. S. A.* **96,** 7581–7586
20. Gaymard, F., Pilot, G., Lacombe, B., Bouchez, D., Bruneau, D., Boucherez, J., Michaux-Ferriere, N., Thibaud, J. B., and Sentenac, H. (1998) *Cell* **94,** 647–655
21. Ache, P., Becker, D., Ivashikina, N., Dietrich, P., Roelfsema, M. R. G., and Hedrich, R. (2000) *FEBS Lett.* **486,** 93–98
22. Pratelli, R., Lacombe, B., Torregrosa, L., Gaymard, F., Romieu, C., Thibaud, J. B., and Sentenac, H. (2002) *Plant Physiol.* **128,** 564–577
23. Philippar, K., Fuchs, I., Lüthen, H., Hoth, S., Bauer, C., Haga, K., Thiel, G., Ljung, K., Sandberg, G., Böttger, M., Becker, D., and Hedrich, R. (1999) *Proc. Natl. Acad. Sci. U. S. A.* **96,** 12186–12191
24. Bauer, C. S., Hoth, S., Haga, K., Philippar, K., Aoki, N., and Hedrich, R. (2000) *Plant J.* **24,** 139–145
25. Nelson, T., and Langdale, J. A. (1992) *Annu. Rev. Plant Physiol. Plant. Mol. Biol.* **43,** 25–47
26. Botha, C. E. J., Cross, R. H. M., Van Bel, A. J. E., and Peter, C. I. (2000) *Protoplasma* **214,** 65–72
27. Russin, W. A., Evert, R. F., Vanderveer, P. J., Sharkey, T. D., and Briggs, S. P. (1996) *Plant Cell* **8,** 645–658
28. Stitt, M. (1996) *Plant Cell* **8,** 565–571
29. Prioul, J. L. (1996) in *Photoassimilate Distribution in Plants and Crops, Source-Sink Relationships* (Zamski, E., and Schaffer, A. A., eds) pp. 549–594, Marcel Dekker, Inc., New York
30. Van Bel, A. J. E. (1993) *Annu. Rev. Plant Physiol. Plant. Mol. Biol.* **44,** 253–281
31. Aoki, N., Hirose, T., Takahashi, S., Ono, K., Ishimaru, K., and Ohsugi, R. (1999) *Plant Cell Physiol.* **40,** 1072–1078
32. Ache, P., Becker, D., Deeken, R., Dreyer, I., Weber, H., Fromm, J., and Hedrich, R. (2001) *Plant J.* **27,** 571–580
33. Sambrook, J., Fritsch, E. F., and Maniatis, T. (1989) *Molecular Cloning: A Laboratory Manual*, 2nd Ed., Cold Spring Harbor Laboratory Press, Cold Spring Harbor, NY
34. Keunecke, M., and Hansen, U. P. (2000) *Planta* **210,** 792–800
35. Liman, E. R., Tytgat, J., and Hess, P. (1992) *Neuron* **9,** 861–871
36. Hoth, S., Dreyer, I., Dietrich, P., Becker, D., Müller-Röber, B., and Hedrich, R. (1997) *Proc. Natl. Acad. Sci. U. S. A.* **94,** 4806–4810
37. Hedrich, R., Moran, O., Conti, F., Busch, H., Becker, D., Gambale, F., Dreyer, I., Kuech, A., Neuwinger, K., and Palme, K. (1995) *Eur. Biophys. J.* **24,** 107–115
38. Hoth, S., Geiger, D., Becker, D., and Hedrich, R. (2001) *Plant Cell* **13,** 943–952
39. Geiger, D., Becker, D., Lacombe, B., and Hedrich, R. (2002) *Plant Cell* **14,** 1859–1868
40. Ehrhardt, T., Zimmermann, S., and Müller-Röber, B. (1997) *FEBS Lett.* **409,** 166–170
41. Thompson, J. D., Higgins, D. G., and Gibson, T. J. (1994) *Nucleic Acids Res.* **22,** 4673–4680
42. Nicholas, K. B., Nicholas, H. B., Jr., and Deerfield, D. W. (1997) *EMBNEW News* **4,** 14
43. Apweiler, R., Attwood, K., Bairoch, A., Bateman, A., Birney, E., Biswas, M., Bucher, P., Cerutti, L., Corpet, F., Croning, M. D. R., Durbin, R., Falquet, L., Fleischmann, W., Gouzy, J., Hermjakob, H., Hulo, N., Jonnassen, I., Kahn, D., Kanapin, A., Karavidopoulou, Y., Lopez, R., Marx, B., Mulder, N. J., Oinn, T. M., Pagni, M., Servant, F., Sigrist, and Zdobnov, E. M. (2001) *Nucleic Acids Res.* **29,** 37–40
44. Page, R. D. M. (1996) *Comput. Appl. Biosci.* **12,** 357–358
45. Daram, P., Urbach, S., Gaymard, F., Sentenac, H., and Cherel, I. (1997) *EMBO J.* **16,** 3455–3463
46. Müller-Röber, B., Ellenberg, J., Provart, N., Willmitzer, L., Busch, H., Becker, D., Dietrich, P., Hoth, S., and Hedrich, R. (1995) *EMBO J.* **14,** 2409–2416
47. Hoth, S., and Hedrich, R. (1999) *J. Biol. Chem.* **274,** 11599–11603
48. Matsuoka, M., Kyozuka, J., Shimamoto, K., and Kano-Murakami, Y. (1994) *Plant J.* **6,** 311–319
49. Kanai, R., and Edwards, G. E. (1973) *Plant Physiol.* **51,** 1133–1137
50. Furbank, R., Stitt, M., and Foyer, C. H. (1985) *Planta* **164,** 172–178
51. Müller-Röber, B., Ehrhardt, T., and Plesch, G. (1998) *J. Exp. Bot.* **49,** 293–304
52. Outlaw, J., Du, Z., Xia Meng, F., Aghoram, K., Riddle, K. A., and Chollet, R. (2002) *Arch. Biochem. Biophys.* **407,** 63–71
53. Majore, I., Wilhelm, B., and Marten, I. (2002) *Plant Cell Physiol.* **43,** 844–852
54. Evert, R. E., Russin, W. A., and Bosabalidis, A. M. (1996) *Int. J. Plant. Sci.* **157,** 247–261
55. Russell, S. H., and Evert, R. E. (1985) *Planta* **164,** 448–458
56. Evert, R. E., Eschrich, W., and Heyser, W. (1978) *Planta* **138,** 279–294
57. Fritz, E., Evert, R. E., and Heyser, W. (1983) *Planta* **159,** 193–206
58. Lacombe, B., Pilot, G., Gaymard, F., Sentenac, H., and Thibaud, J. B. (2000) *FEBS Lett.* **466,** 351–354
59. Tang, X. D., Marten, I., Dietrich, P., Ivashikina, N., Hedrich, R., and Hoshi, T. (2000) *Biophys. J.* **78,** 1255–1269
60. Fairley-Grenot, K. A., and Assmann, S. M. (1992) *Planta* **186,** 282–293
61. Fairley-Grenot, K. A., and Assmann, S. M. (1993) *Planta* **189,** 410–419
62. Keunecke, M., Sutter, J. U., Sattelmacher, B., and Hansen, U. P. (1997) *Plant Soil* **196,** 239–244
63. Neves-Piestun, B. G., and Bernstein, N. (2001) *Plant Physiol.* **125,** 1419–1428

# Kapitel V: Poplar Potassium Transporters Capable of Controlling $K^+$ Homeostasis and $K^+$-Dependent Xylogenesis

**Katharina Langer, Peter Ache, Dietmar Geiger, Andrea Stinzing, Matthias Arend, Christa Wind, Sharon Regan, Jörg Fromm und Rainer Hedrich**

**Publiziert in The Plant Journal, Vol. 32, 997-1009, September 2002**

**Eigene Beteiligung an der Arbeit:**

- Biophysikalische Charakterisierung von PTK2 und PTORK in *Xenopus* Oozyten mit Hilfe der DEVC-Technik in Bezug auf Spannungsabhängigkeit, Gleichrichtung, externe pH-Empfindlichkeit, Selektivität und Inhibierung durch $K^+$-Kanal spezifische Blocker
- Auswertung der Daten

*The Plant Journal* (2002) **32**, 997–1009

# Poplar potassium transporters capable of controlling $K^+$ homeostasis and $K^+$-dependent xylogenesis

**Katharina Langer[1,†], Peter Ache[1,†], Dietmar Geiger[1], Andrea Stinzing[1], Matthias Arend[2], Christa Wind[2], Sharon Regan[3], Jörg Fromm[2] and Rainer Hedrich[1,*]**

[1]*Julius-von-Sachs-Institut, Molekulare Pflanzenphysiologie und Biophysik, Universität Würzburg, Julius-von-Sachs-Platz 2, 97082 Würzburg, Germany,*

[2]*Institut für Holzforschung der TU München, Winzererstr. 45, 80797 München, Germany, and*

[3]*Carleton University, 1125 Colonel By Drive, Ottawa, Ont., Canada ON K1S 5B6*

Received 16 July 2002; revised 5 September 2002; accepted 16 September 2002.

[*]For correspondence (fax +49 931 888 6157; e-mail hedrich@botanik.uni-wuerzburg.de).

[†]These authors contributed equally to this work.

**Summary**

**The cambial $K^+$ content of poplar increases during the growth period in a $K^+$ supply dependent manner. Upon $K^+$ starvation or application of tetraethylammoniumchloride ($TEA^+$), a $K^+$ channel blocker, the average vessel lumen and expansion zone area were significantly reduced. In search for the molecular basis of potassium-dependent xylogenesis in poplar, $K^+$ transporters homologous to those of known function in *Arabidopis* phloem- and xylem-physiology were isolated from a poplar wood EST library. The expression profile of three distinct $K^+$ channel types and one $K^+$ transporter, *Populus tremula* $K^+$ uptake transporter 1 (PtKUP1), was analysed by quantitative RT-PCR. Thereby, we found *P. tremula* outward rectifying $K^+$ channel (PTORK) and *P. tremula* $K^+$ channel 2 (PTK2) correlated with the seasonal wood production. $K^+$ transporter *P. tremula* 1 (KPT1) was predominantly found in guard cells. Following the heterologous expression in *Xenopus* oocytes the biophysical properties of the different channels were determined. PTORK, upon membrane de-polarization mediates potassium release. PTK2 is almost voltage independent, carrying inward $K^+$ flux at hyperpolarized potential and $K^+$ release upon de-polarization. PtKUP1 was expressed in a $K^+$ uptake-deficient *Escherichia coli* strain, where this $K^+$ transporter rescued $K^+$-dependent growth. In order to link the different $K^+$ transporters to the cambial activity and wood production, we compared the expression profiles to seasonal changes in the $K^+$ content of the bark as well as xylem vessel diameter. Thereby, we found PTORK and PTK2 transcripts to follow the annual $K^+$ variations in poplar branches. PtKUP1 was expressed at a low level throughout the year, suggesting a housekeeping function. From these data, we conclude that $K^+$ channels are involved in the regulation of $K^+$-dependent wood production.**

**Keywords: $K^+$ channel, poplar, wood formation, quantitative RT-PCR, DEVC, patch-clamp technique.**

## Introduction

The most abundant cation in plants is potassium, playing a central role in many aspects of plant physiology. Potassium is transported within cells, tissues and organs, and its uptake and transport mechanisms have been studied extensively in different cell types of the root, shoot and leaf (Hedrich and Roelfsema, 1999). Potassium taken up by the root is transported to the shoot via the xylem. A high percentage of the $K^+$ content received by mature leaves is further transported to young leaves, flowers, seeds, fruits or growing roots via the phloem (Ache *et al.*, 2001; Deeken *et al.*, 2000; Fromm and Bauer, 1994).

Potassium is taken up from the soil via potassium uptake channels of the AKT1- and AtKC1-type (*Arabidopsis thaliana* $K^+$ channel) and carriers of the high-affinity $K^+$ transporter (HKT1) and $K^+$ uptake (KUP) family (Brüggemann *et al.*, 1999; Gassman *et al.*, 1996; Hirsch *et al.*, 1998; Ivashikina *et al.*, 2001; Kim *et al.*, 1998; Reintanz *et al.*, 2002; Rodriguez-Navarro, 2000; Schroeder and Fang, 1991; Spalding *et al.*, 1999). The requirement of three-root Shaker-like $K^+$ channels for $K^+$ uptake into and transport within roots was shown by the use of loss-of-channel function mutants (Gaymard *et al.*, 1998; Hirsch *et al.*,

1998; Reintanz *et al*., 2002). In the *Arabidopsis* genome there are two potassium efflux channels of the Shaker-type, stelar K outward rectifier (SKOR, Gaymard *et al*., 1998) and guard cell outward rectifying $K^+$ channel (GORK, Ache *et al*., 2000). SKOR plays an important role in the loading of potassium into the xylem. The expression of this channel is induced by potassium and re-pressed by the dormancy hormone ABA and conditions of $K^+$ depletion (Gaymard *et al*., 1998). In contrast to SKOR, the high-affinity potassium carrier *A. thaliana* $K^+$ uptake transporter (AtKUP1) is enhanced by $K^+$ depletion (Fu and Luan, 1998; Kim *et al*., 1998). The membrane potential of the phloem, as measured with the aphid technique, has been shown to be dominated by $K^+$ conductance (Ache *et al*., 2001). This led to the identification of corresponding specifically light-regulated AKT2/3-like $K^+$ channels ($K^+$ transporter *A. thaliana*), involved in phloem transport. These channels have been identified in several species such as *Arabidopsis*, maize and broad bean (Ache *et al*., 2001; Bauer *et al*., 2000; Deeken *et al*., 2000, 2002; Marten *et al*., 1999).

Annual rings in wood are caused by periodic growth activity of the trees. Their width can fluctuate strongly from year to year depending on various environmental factors. The amount of wood produced by a tree depends on its cambial activity. Fusiform initial cells differentiate to form axial elements such as tracheides, vessels, fibres, parenchyma cells and sieve elements, whereas ray initials produce radial transporting rays (e.g. Aloni, 1987; Hampp *et al*., 1990; Krabel *et al*., 1994; Larson, 1994; Roberts *et al*., 1988; Savidge, 1996, 2000). Potassium homeostasis in higher plants in general, and trees in particular, depends on nutrient availability, degree of mycorrhizal association, and physiological state of the plant. Potassium ions are involved in various aspects of tree growth and wood formation. In the cambial region and xylem differentiation zone, a strong potassium demand has been shown (Dünisch and Bauch, 1994a,b; Kuhn *et al*., 1997), especially during cell enlargement when the symplastic potassium content increases (Dünisch *et al*., 1998). This behaviour suggests that differentiating xylem cells involved in earlywood formation represent a strong sink for potassium and that the accumulation of this osmolyte provides the driving force for cell expansion during primary wall formation. Similarly, fertilized spruce stands, develop 30% more biomass and enlarged annual rings compared to unfertilized controls (Dünisch and Bauch, 1994a,b). The cambium showed prolonged cambial activity characterized by an elevated periclinal division rate and radially enlarged early tracheids. Kuhn *et al*. (1995, 1997) analysed the distribution of potassium in xylem, cambium and phloem of spruce wood and found the highest levels in the cambium. Moreover, a detailed X-ray microprobe analysis revealed a radial interchange of mineral nutrients between xylem, cambium and phloem (Kuhn *et al*., 1997). The high levels of potassium in the rays were suggested to indicate that rays are the major re-loading point in wood tissue of trees. During leaf senescence in the fall, evidence for a rapid potassium export out of the leaf blade into the sieve tubes of the subtending stem was shown in beech (Eschrich *et al*., 1988). Upon onset of vegetative dormancy $K^+$ accumulates in the rays from where it can be re-mobilized in the spring and used for wood production.

Energy dispersive X-ray analysis (EDXA) of seasonal changes in the cambial potassium and calcium content of the balsam poplar (*Populus trichocarpa*) revealed that the re-activation of the cambium in spring is accompanied by high concentrations of potassium and calcium (Arend and Fromm, 2000). In summer, when the cambium starts to develop latewood, the $K^+$ concentration remained high, whereas calcium decreased after cambial re-activation.

While some information on seasonal changes in the $K^+$ content within trees is available, the molecular mechanism of $K^+$ transport in these perennial plants remains unknown. To characterize the fundamental processes involved in potassium supply during xylogenesis, molecular and biophysical techniques have been used to analyse $K^+$ transporters of poplar. We have isolated one $K^+$ uptake channel (KPT1), one $K^+$ release channel (PTORK) and one weak voltage-independent channel (PTK2) as well as a broadly expressed KUP-type of $K^+$ transporter from a poplar wood EST library (Sterky *et al*., 1998). Transporter functions were verified by heterologous expression in *Xenopus* oocytes or *Escherichia coli* and their properties and expression patterns are discussed in the context of potassium-dependent wood formation.

## Results

### *Distribution and seasonal changes in potassium content*

The $K^+$ content of different poplar tissues was analysed by EDXA (Eschrich *et al*., 1988; Fromm *et al*., 1987). In spring, the increase in metabolic activity is accompanied by the initiation of $K^+$ uptake (Fromm and Eschrich, 1986) and by changes in the membrane potential of cortex and phloem cells (Fromm and Spanswick, 1993). Similarly, we found a seasonal variation in potassium levels in the poplar cambium, where a strong reduction of $K^+$ content was found in winter and high levels were found in summer (Figure 1a). Experimental changes in potassium nutrition showed that the $K^+$ content of cambial and differentiating xylem cells depends on the $K^+$ supply (Figure 1b). Plants grown under limiting $K^+$ concentrations (0.05 mM) showed low and equally distributed $K^+$ contents in different cell types. Elevating the $K^+$ supply to 5 or 10 mM led to higher potassium contents in general (Figure 1b). In 10 mM $K^+$, however, the distribution was altered towards maximal $K^+$ content

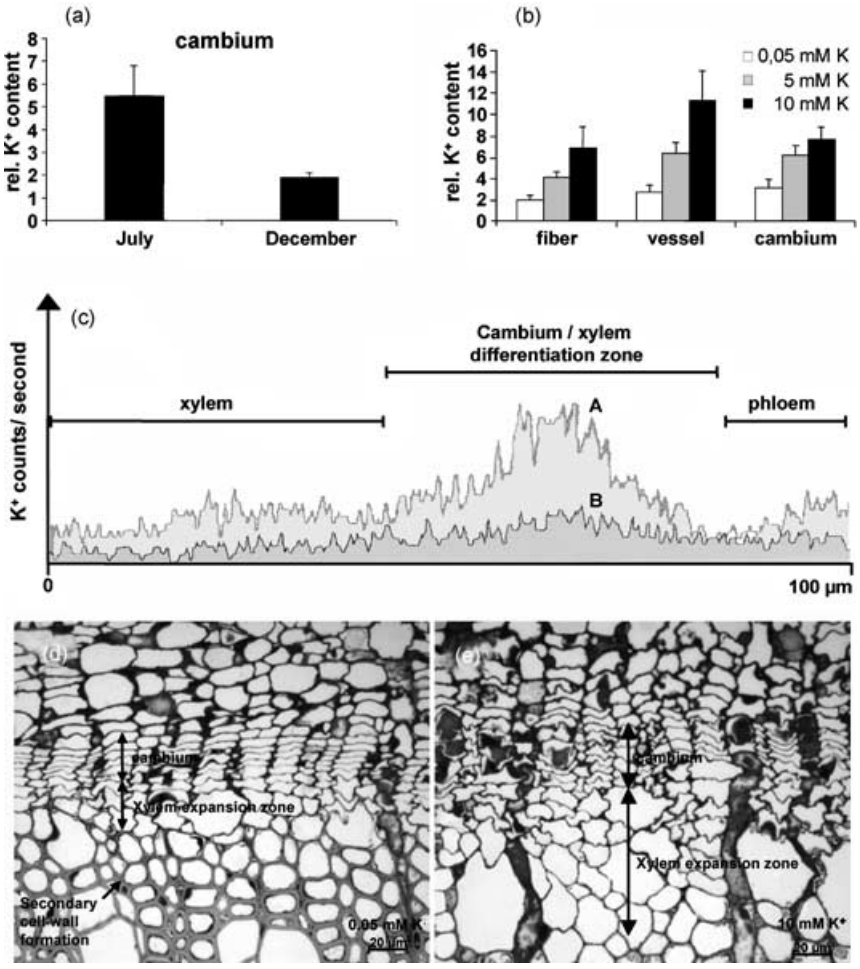


**Figure 1.** Effect of $K^+$ supply on wood production of *P. tremula* × *P. tremuloides*.
(a) Seasonal changes in relative cambium $K^+$ content, EDXA peak:background ratios ($n = 10$, mean ± SD).
(b) Relative $K^+$ content of cambial cells, differentiating fibres and vessels grown in different potassium concentrations, EDXA peak:background ratios ($n = 10$, mean ± SD).
(c) EDXA-linescan of relative $K^+$ distribution in active twig tissue (sequential EDXA from 100 overlaid single scans). A = 10 mM $K^+$ supply, B = 0.05 mM $K^+$ supply.
(d and e) The extension of the vessel cell-expansion zone is affected by the potassium supply (arrows). Transverse sections of poplar stems of the same age grown with 0.05 mM $K^+$ (d) or 10 mM $K^+$ (e). Note: under $K^+$ limiting conditions cambial and cell-expansion zones lack 2–3 cell layers each. Secondary cell wall formation under potassium depletion starts early.

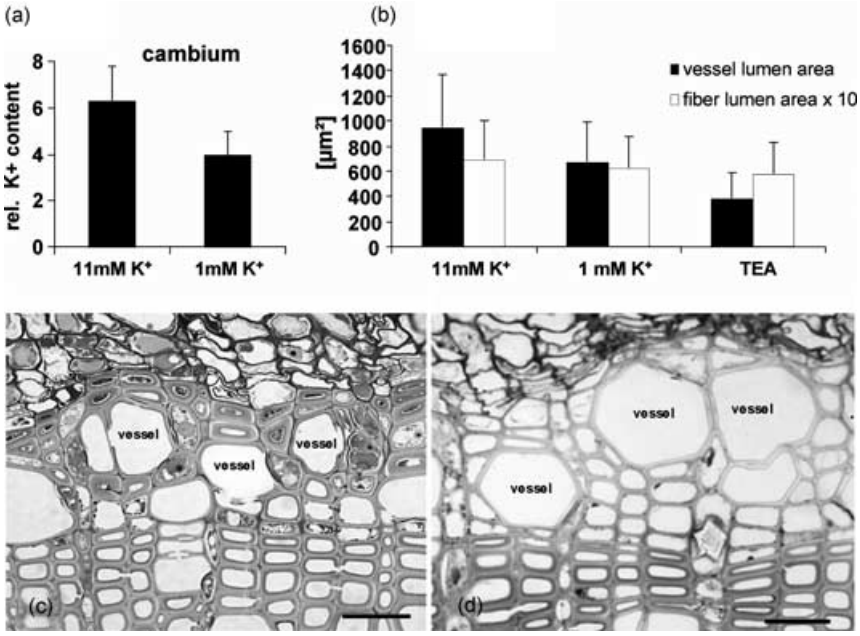


**Figure 2.** Relative cambium $K^+$ content and potassium-dependent vessel lumen.
(a) EDXA: Relative potassium concentrations of the cambium. Peak:background ratios increase with root potassium supply from 1 to 11 mM.
(b) Effect of 2 weeks root $K^+$ supply and $TEA^+$ (5 mM) on vessel size. Vessel lumen area (black bars) depends on $K^+$ supply. $TEA^+$ reduces vessel size. Note: the fibre lumen (white bars) does not significantly alter with different $K^+$ levels or $TEA^+$ treatment.
(c and d) $K^+$ channel blocker $TEA^+$ reduces vessel size. Cross-section of the active cambial zone after treatment of twigs with 5 mM $TEA^+$ (c). The vessel size is significantly reduced when compared with the untreated control (d), taken from the same twig below the $TEA^+$-treated zone. Bar, 20 µm.

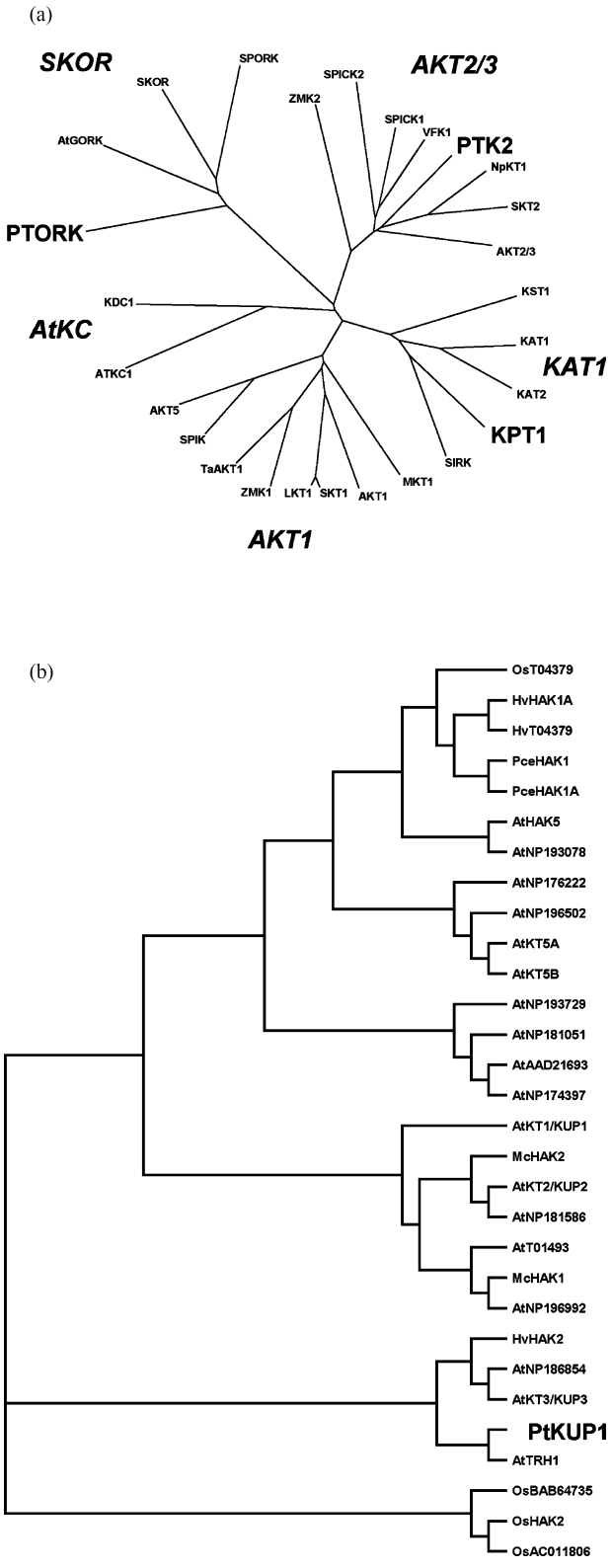


**Figure 3.** Phylogenetic trees of plant potassium transporters.
(a) Phylogenetic tree of plant *Shaker* channels. Accession numbers: PTORK, AJ271446; AtGORK, AJ279009; SKOR, NM_123109; SPORK, AJ299019; ZMK2, AJ132686; SPICK2, AF145272; SPICK1, AF099095; VFK1, Y10579; PTK2, AJ271447; NpKt1, AB032074; SKT2, Y09699; AKT2/3, NM_118342; KST1, X79779; KAT1, NM_123993; KAT2, NM_117939; KPT1, AJ344623; SIRK, AF359521; MKT1, AF267753; AKT1, NM_128222; SKT1, AF237951; LKT1, X96390; ZMK1, Y07632; TaAKT1, AF207745; SPIK, AC006053; AKT5, AJ249479; AtKC1, U81239; KDC1, AJ249962.
(b) Phylogenetic tree of plant KT/KUP/HAK transporters. Accession numbers: HvHAK1A, AF025292; HvHAK2, AF129479; AtKT1/KUP1, AF012656; AtKT2/KUP2, AF012657; AtHAK5, AF129478; PtKUP1, AJ299422; AtTrh1, AJ296155; McHAK1, AF367864; McHAK2, AF367865; OsHAK2, C011806; AtNP_181586; AtNP_196992; AtT01493; OsAC011806; AtNP_186854; AtKT3/KUP3, AF207621; AtNP_181051; OsBAB64735; AtAAD21693; AtNP_174397; AtNP_176222; AtNP_193729; PceHAK1, BAB32443/AB055630; PceHAK1A, BAB32444/AB055631; HvT04379; OsT04379/AP003272; AtKT5A, T04970; AtKT5B, NP_195079/Nc 003075; AtNP_196502; AtNP_193078. Phylogenetic trees were constructed using Clustal X and TreeView programs with translated sequences of the transporters.

in differentiating vessels. When we analysed the distribution of potassium in actively growing twigs, we found the highest $K^+$ concentrations in the cambium and the xylem differentiation zone (Figure 1c). In line with the potassium distribution shown in Figure 1(b), this pattern was most pronounced in plants grown in nutrient solution with 10 mM potassium (scan A) rather than with those supplied with 0.05 mM potassium (scan B). In addition, the zone of expanding xylem cells was three-fold larger when trees were grown in 10 mM $K^+$ versus 0.05 mM $K^+$ (Figure 1d,e). Coinciding with the narrow expanding xylem cell zone in the $K^+$ starved trees was an earlier initiation of secondary cell walls (Figure 1d).

### *Influence of potassium supply on cell enlargement of cambial cell derivatives*

Rooted cuttings of *P. trichocarpa* were cultivated either on 1 or 11 mM $K^+$ during the time of active cambial growth. The amount of potassium supplied via the nutrient solution determined the potassium levels in the cambial region as measured by X-ray analysis (Figure 2a). The effect of potassium on the enlargement of xylem cells derived from the cambium was investigated by measurements of the lumen area of newly formed vessel and fibre cells. Vessel cells showed a distinct tendency to have an increased lumen area with increasing potassium levels in the nutrient solution (Figure 2b, black bars). After treatment of the stem with 5 mM tetraethylammoniumchloride ($TEA^+$), a $K^+$ channel blocker, in the presence of 6 mM $K^+$, the vessel lumen area did not expand as much as untreated stems (Figure 2b–d). In contrast to vessel cells, the lumen area of newly formed fibre cells was not affected by potassium nutrition or $TEA^+$ treatments (Figure 2b, white bars).

### *Molecular analysis of poplar $K^+$ transporters*

The content of free and bound potassium and the respective buffering/exchange capacity of the cell walls were analysed throughout the year using percolation analysis (Sauter, personal communication). With the onset of

growth in late winter/early spring, the potassium concentration rose dramatically, whereas it dropped in the fall and winter. Potassium channel blockers, such as $Cs^+$ and $TEA^+$ led to a 20% reduced potassium uptake (Sauter, personal communication), pointing to the involvement of $K^+$ channels in these processes.

To examine the molecular basis of $K^+$ transport in poplar, we searched the EST database from the cambial region of *P. tremula* × *P. tremuloides* (Sterky *et al.*, 1998) for sequence homologies to known $K^+$ transporters (Figure 3). We identified DNA fragments with relevant homologies to *Arabidopsis* potassium channels and carriers. Following complete sequencing of these fragments we identified distinct homologues to *SKOR*, the gene for the outward rectifier expressed in endodermis and xylem parenchyma cells (Gaymard *et al.*, 1998), the phloem channels of the AKT2/3 type (Ache *et al.*, 2001; Deeken *et al.*, 2000; Lacombe *et al.*, 2000; Marten *et al.*, 1999), the guard cell channel of the KAT1 type ($K^+$ channel *A. thaliana*, Anderson *et al.*, 1992), and to AtTrh1 which mediates $K^+$ transport (Rigas *et al.*, 2001). We cloned the corresponding full-length cDNAs and named the *SKOR* homologue *PTORK* (*P. tremula* outward rectifying $K^+$ channel), the *AKT2/3* homologue *PTK2* (*P. tremula* $K^+$ channel 2), the *KAT1* homologue *KPT1* (Figure 3a), and the Trh1 homologue *PtKUP1* (*P. tremula* $K^+$ uptake transporter) (Figure 3b). The deduced proteins PTORK, PTK2 and KPT1 (GenBank accession numbers AJ271446, AJ271447 and AJ344623) exhibited all structural features of members of the 'green' Shaker channel family (Hedrich and Becker, 1994).

### *Functional expression of PTORK and PTK2 in oocytes*

KPT1 is most similar to the KAT1-like guard cell $K^+$ channel and was only found in the leaf epidermis (data not shown). The *Arabidopsis* homologues of PTORK and PTK2 are involved in xylem and phloem $K^+$ transport. To better understand the functional properties of the putative $K^+$ channels in xylogenesis, we thus focused on PTORK and PTK2 rather than KPT1. *PTORK* and *PTK2* cRNA's were injected into *Xenopus* oocytes and gene products were analysed 3–5 days post-injection using the double-electrode voltage-clamp technique (cf. Ache *et al.*, 2000; Geiger *et al.*, 2002).

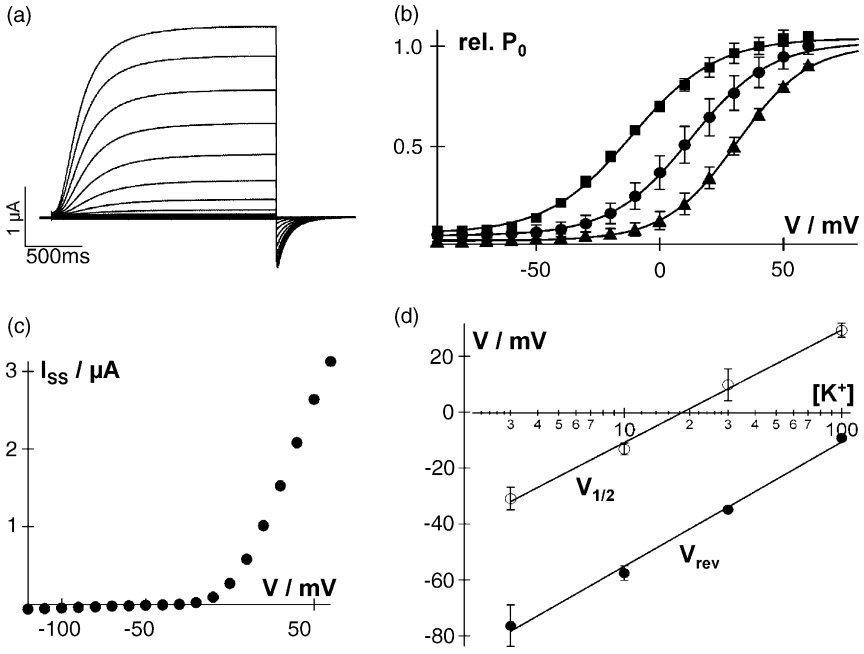


**Figure 4.** PTORK mediates outward currents in *PTORK* cRNA-injected oocytes.

(a) Using the double-electrode voltage-clamp technique, time-dependent, outwardly rectifying currents were elicited upon de-polarizing voltage steps between −120 and 60 mV in 10 mV increments, starting from a holding potential of −100 mV. The bath solution contained 30 mM K gluconate, 1.5 mM $MgCl_2$, 1 mM $CaCl_2$ and 10 mM Tris–MES pH 7.4.

(b) Steady-state current–voltage curve of PTORK-mediated currents shown in (a).

(c) $K^+$-dependent activation curves. Relative open probabilities $P_o$ in 10, 30 and 100 mM $K^+$, pH 7.4 plotted against the applied membrane voltage. $P_o$ was measured at the onset ($t = 0$) of the tail pulse at −100 mV and normalized to the maximal open probability ($P_o = 1$). Solid lines represent the best Boltzmann fits (gating parameters: 10 mM $K^+$: $V_{1/2} = -11.44 \pm 2.12$, apparent gating charge $z_g = 1.46 \pm 0.15$; 30 mM $K^+$: $V_{1/2} = 12.33 \pm 5.69$, $z_g = 1.56 \pm 0.08$; 100 mM $K^+$: $V_{1/2} = 31.10 \pm 2.58$, $z_g = 1.73 \pm 0.19$). Error bars indicate standard deviation ($n = 3$). LiCl was added to the external solutions to adjust the ionic strength to 100 mM in each solution.

(d) Shift in reversal potentials ($V_{rev}$) and half-activation potential ($V_{1/2}$) in response to changes in extracellular $K^+$ concentrations. Upon increase in $K^+$ concentration the activation potential ($V_{1/2}$) shifts positive. A 10-fold increase in $K^+$ concentration resulted in a 40-mV shift of the half-maximal activation potential ($V_{1/2}$) (c). The reversal potential ($V_{rev}$) shifted 45 mV upon a 10-fold increase in $K^+$ concentration.

 

Membrane de-polarization elicited an outward rectifying current with a slow sigmoidal activation kinetic in PTORK-expressing oocytes (Figure 4a,b). The steady-state value was reached within 1.5 sec and $K^+$ channels did not inactivate during prolonged de-polarization (10 sec at +50 mV, data not shown). Increasing the external $K^+$ concentration from 10 to 100 mM resulted in a positive shift of the activation threshold ($V_{1/2}$) following the $K^+$ equilibrium potential ($E_K$) (Figure 4c,d). The reversal potential ($V_{rev}$) shifted in a $K^+$ dependent manner too (Figure 4d), which, together with the susceptibility of PTORK towards $K^+$ channel blockers (data not shown but cf. Ache *et al.*, 2000; Gaymard *et al.*, 1998), classifies PTORK as a $K^+$ selective channel. Both external and internal acidification led to a decrease in the steady-state currents as observed with SKOR and GORK (data not shown; but cf. Ache *et al.*, 2000; Lacombe *et al.*, 2000). Thus, PTORK represents an outward rectifying $K^+$ channel the activity of which is under control of the membrane potential and external $K^+$ concentration.

In contrast to PTORK but similar to its *Arabidopsis* homologue AKT2/3, PTK2 was active at positive and negative membrane potentials. Figure 5(a) depicts the typical instantaneous and time-dependent current components mediated by PTK2 in response to stepwise changes in membrane potential. At voltages more positive than the $K^+$ equilibrium potential, outward $K^+$ currents were elicited. The steady-state currents ($I_{ss}$) plotted against the membrane voltage revealed the weak voltage dependence and rectification of PTK2 (Figure 5b). In contrast to AKT2/3 but similar to ZMK2, PTK2 exhibits almost no rectification (Figure 5a,b). The Nernstian behaviour of the reversal potential to $K^+$ concentration changes, lack of inward current in $Na^+$- and $Li^+$-based external media and susceptibility to $K^+$ channel blockers $Cs^+$ and $TEA^+$, classifies PTK2 as a $K^+$-selective channel (data not shown; but cf. Geiger *et al.*, 2002; Lacombe *et al.*, 2000; Marten *et al.*, 1999). Another characteristic of the AKT2/3 family is their susceptibility towards voltage-dependent blocking by $Ca^{2+}$ (Marten *et al.*, 1999). In order to prove whether PTK2 is blocked by extracellular $Ca^{2+}$ tail current recordings were performed. After pre-activating the channels at a membrane voltage of −150 mV followed by tail pulses ($t = 0$) in the range of 20 to −170 mV revealed a voltage-dependent $Ca^{2+}$ block (Figure 5c). Similar results were obtained with 10-fold lower $K^+$ and $Ca^{2+}$ concentrations (not shown). When the extracellular proton concentration was increased from pH 7.4 to 5.6, currents through PTK2 were reduced (Figure 5d) a behaviour characteristic for members of the AKT2/3 family

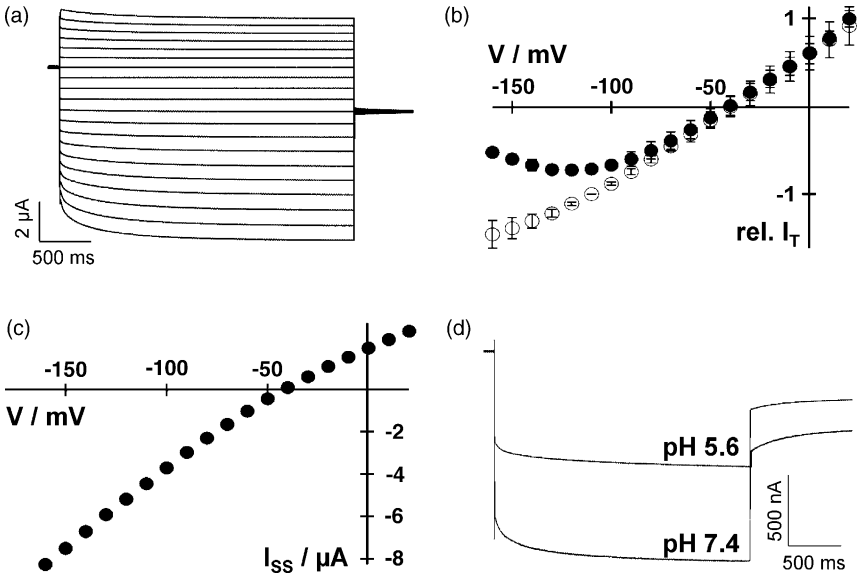


**Figure 5.** Calcium and protons block $K^+$ currents mediated by PTK2.
(a) Representative macroscopic recordings of inward and outward currents obtained from PTK2-RNA-injected *Xenopus* oocytes. Typical instantaneous and time-dependent current components were mediated by PTK2. From a holding potential of $V_H = -30$ mV, the membrane voltage was successively changed during 2.5 sec pulses from + 30 mV to −160 mV in 10 mV decrements. The bath solution was composed of 30 mM K gluconate, 1 mM $CaCl_2$, 1.5 mM $MgCl_2$ and 10 mM Tris–MES (pH 7.4).
(b) Corresponding current–voltage curve: Steady-state currents $I_{ss}$ determined in (a) plotted against the membrane voltage. Note: the weak voltage dependence and rectification of PTK2.
(c) Relative (rel.) instantaneous tail-current amplitudes $I_T$ plotted against the membrane voltage in the presence of 30 mM $CaCl_2$ (●) or 30 mM $MgCl_2$ (○). $I_T$ currents were normalized to the currents at −110 mV in the control solution. The $Ca^{2+}$ solution contained 20 mM KCl, 10 mM Tris–MES, pH 7.2 and 30 mM $CaCl_2$. In the control solution, $CaCl_2$ was replaced by $MgCl_2$. Error bars indicate standard deviation ($n = 3$).
(d) $K^+$ currents through PTK2 in responses to single voltage pulses of −150 mV ($V_H = -30$ mV) with the bath solution buffered to pH 5.6 and 7.4. Note: protons block both, instantaneous and time-dependent PTK2 currents. The pH solutions were composed of 30 mM K gluconate, 1 mM $CaCl_2$, 1.5 mM $MgCl_2$ buffered with 10 mM MES–Tris to pH 5.6 or pH 7.4, respectively.

(Bauer *et al.*, 2000; Marten *et al.*, 1999; Philippar *et al.*, 1999). Taken together, PTK2 represents an ion channel capable of mediating $K^+$ uptake and efflux under the control of membrane potential, calcium and pH.

### *PtKUP1 functionally complements a $K^+$ uptake-deficient E. coli mutant*

*E. coli* LB2003, lacking the $K^+$ uptake systems, Trk, Kup, and Kdp, does not grow on $K^+$-limited media (Uozumi *et al.*, 1998). This triple $K^+$ transport deficient strain requires 25 mM $K^+$ for half-maximal cell growth (Epstein and Kim, 1971). Therefore, cells transformed with the empty vector pCRII TOPO did not grow in media supplemented with 3 mM $K^+$, while *E. coli* expressing the Trh1 homologue PtKUP1 formed colonies (Figure 6a). To further characterize the transport properties of PtKUP1, the effects of calcium and $K^+$ channel blockers on growth were tested by placing an impregnated paper disk on a nascent lawn of *E. coli* cells suspended in growth agar. After incubation for 36–48 h, growth inhibition was reflected by a decreased cell density (halo) around the disk (Figure 6b). $Ca^{2+}$ and $Cs^+$, but not $TEA^+$ and $Ba^{2+}$, strongly inhibited growth of the PtKUP1 strain. These results demonstrate that PtKUP1 represents a functional $K^+$ uptake transporter sensitive to $Ca^{2+}$ and $Cs^+$ ions.

### *Localization and seasonal changes in $K^+$ transporters expression*

To localise the site of PTORK, PTK2 and PtKUP1 expression, we isolated mRNA from leaves, epidermal fragments, petioles, xylem and phloem of young branches, and roots for quantitative RT-PCR analyses (Figure 7a). The highest levels of all three transcripts were detected in the vascular-rich petioles and in the phloem. Following the separation of the bark from annual branches into cambium/phloem/bast and cambium/xylem/wood, *PTORK* and *PTK2* were found in both fractions, but *PTK2*, was predominantly found in the bast and only at background levels in the root. PtKUP1 in contrast seems to be expressed ubiquitous but at low levels.

In order to determine whether the seasonal changes in cambial activity, xylogenesis and thus wood formation are accompanied with changes in the $K^+$ transporter expression, branch segments were collected throughout the year and mRNA was isolated from each sample. The expression profile depicted in Figure 7(b) shows quantitative RT-PCR of poplar stem RNA collected in February and June. *PTORK* and *PTK2* were highly expressed when temperatures increased above 10–15°C and wood production was initiated, while *PtKUP1* expression remained at low levels throughout the seasons.

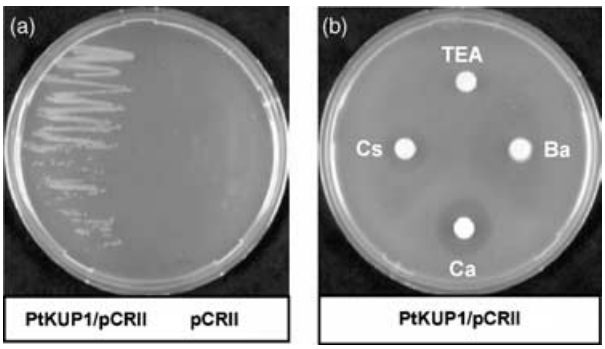


**Figure 6.** Functional expression of PtKUP1.
(a) PtKUP1 complements the *E. coli* strain LB2003, which lacks the bacterial $K^+$ uptake systems Kdp, TrkA and Kup. Growth of LB2003 transformed with PtKUP1 (left) or the empty plasmid pCRII TOPO as control (right) on KML plates containing 3 mM $K^+$.
(b) Effect of $TEA^+$, $Cs^+$, $Ba^{2+}$and $Ca^{2+}$ on growth of PTKUP1-expressing bacteria. A lawn of $10^5$ PtKUP1 expressing cells was plated in 0.7% agarose on KML plates with 3 mM of $K^+$. A paper disk containing 10 µl of the 1 M test cation solution was placed on the agar surface and the plates were incubated at 28°C for 36–48 h. Note: inhibition by $Cs^+$ and $Ca^{2+}$ in the growth zone around the disk creates a dark halo.

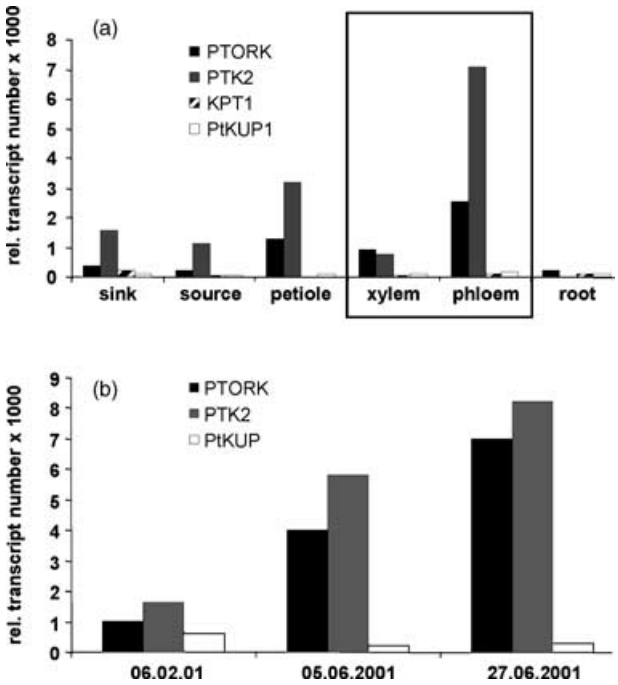


**Figure 7.** Expression pattern of *PTORK, PTK2, KPT1* and *PtKUP1* analysed by quantitative RT-PCR, $K^+$ transporter transcript numbers were normalized to 10 000 molecules of actin transcripts.
(a) Highest amounts of *PTORK* and *PTK2* transcripts were detected in the vascular-rich petioles and in the phloem. *PtKUP1*, in contrast, seems to be expressed ubiquitous at low levels. Total RNA isolated from sink and source leaves, petiole, xylem, phloem and root was analysed with specific primers for all cloned poplar potassium transporters.
(b) Seasonal changes in $K^+$ transporter transcripts of poplar stem (phloem + xylem) RNA. All transcript levels were low during winter (average February temperature = 7.4°C). In contrast to *PtKUP1*, *PTORK* and *PTK2* expression was induced at temperatures above 10°C which initiate wood production (average June temperature = 19.8°C).

From this behaviour, we may thus conclude that PTORK and PTK2 initiate and/or accompany xylogenesis. The fact that *PtKUP1* transcript levels were low but constant throughout the year might point to a housekeeping function of this transporter in $K^+$ homeostasis.

### *$K^+$ currents in callus cells*

Studies on the physiology, molecular biology and biophysics of poplar ion channels *in vivo* require proper access to the individual cell types. Best suited for this purpose are patch-clamp studies on isolated protoplasts. Therefore, we isolated protoplasts from suspension cultures expressing PTORK and PTK2. Poplar branches were induced to build callus and the resulting meristematic tissues to generate suspension cultures. When analysing mRNA isolated from this cell culture, the $K^+$ channel *PTORK* and the $K^+$ transporter *PtKUP1* were highly expressed, the *PTK2* gene was weakly expressed and *KPT1*, the KAT/guard cell homologue was not detected (data not shown). Since this culture represents a model system for poplar cells expressing PTORK and PTK2, protoplasts were isolated and the plasma membrane potassium conductance's were compared to the electrical properties of *Xenopus* oocytes expressing PTORK and PTK2 individually. The whole cell configuration of the patch-clamp technique was established with 150 mM $K^+$ in the cytoplasm (pipette solution) and 30 mM in the extracellular medium, and both inward and outward $K^+$ currents were observed (Figures 8 and 9). With the membrane potential clamped to −45 mV, hyperpolarizing 1.5 sec voltage pulses activated inward rectifying currents (Figure 8a). To further characterize this channel type, we challenged the suspension cells with 5 mM $Cs^+$ in the bathing solution. Under these conditions inward currents were completely blocked (Figure 8b), while a reduction from 30 mM potassium to 3 mM in the bathing solution of protoplasts resulted in a decrease of the inward current (Figure 8c). The Nernstian behaviour of the reversal potential to $K^+$ changes (not shown) and $K^+$-dependent current amplitude together with the susceptibility to $K^+$ channel blocker $Cs^+$ classified the inward rectifier as a $K^+$-selective channel.

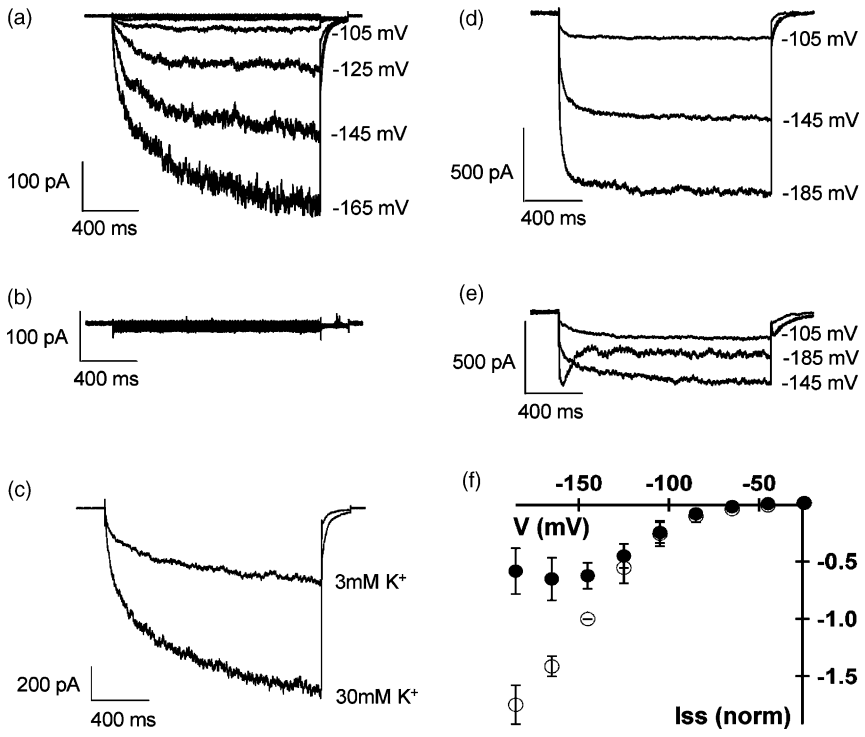


**Figure 8.** Patch-clamp analyses on cultured poplar cells show PTK2-like features.
(a) Whole cell recordings of representative $K^+$ currents on protoplasts isolated from suspension culture in standard bathing medium containing 30 mM K gluconate. Voltage- and time-dependent inward $K^+$ currents could be observed at voltages less than −100 mV using the standard pulse protocol.
(b) After the addition of 5 mM CsCl to the standard solution inward currents were completely abolished. The corresponding inward currents without $Cs^+$ are shown in (a). (c) Upon lowering the external $K^+$ concentration from 30 to 3 mM $K^+$ inward currents decreased at hyperpolarized voltages. Currents were recorded in response to a pulse of −185 mV.
(d and e) A rise in external calcium from 1 mM (d) to 20 mM (e) caused a voltage-dependent current inhibition. Compared to the time-dependent activation in the presence of 1 mM $Ca^{2+}$, a pulse to −185 mV in the presence of 20 mM $Ca^{2+}$ induced current activation followed by voltage-dependent block.
(f) Quantification of the $Ca^{2+}$ block shown in (d and e). Steady-state currents $I_{SS}$ of three independent experiments were plotted against the membrane potential. In the presence of 20 mM $Ca^{2+}$ (●) a voltage-dependent block of the inward currents could be observed, whereas in 1 mM $Ca^{2+}$ (○) no reduction was visible. The steady-state currents were normalized to the currents at −145 mV in 1 mM $CaCl_2$. Error bars indicate standard errors.

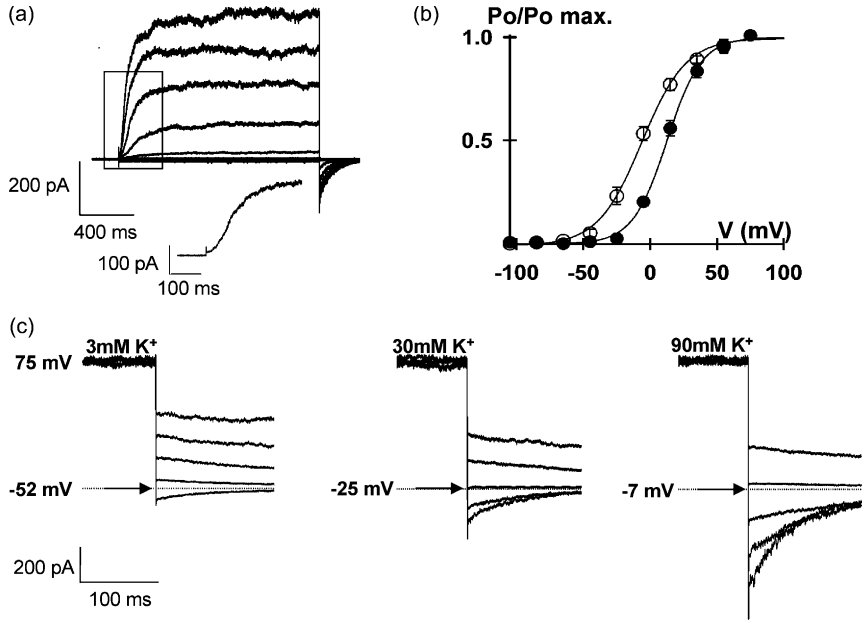


**Figure 9.** Outward currents of cell culture protoplasts are PTORK-like.
(a) Typical time dependent, outwardly rectifying currents from poplar cell culture protoplasts recorded in the whole-cell configuration of the patch-clamp techniques. Voltage pulses from 75 to 185 mV were applied in 20 mV decrements. The holding potential was clamped to −85 mV. The lower single trace visualizes the sigmoidal activation kinetics of the observed outward currents, which show high similarity to PTORK currents in oocytes (cf. Figure 4a).
(b) Open probabilities $P_o$ in 3 (○) and 30 mM (●) $K^+$ of outward rectifying channels were plotted against the membrane potential. Data were retrieved from tail currents ($t=0$) at −85 mV of three independent experiments. Alike PTORK this outward rectifier shows a positive shift of the activation potential ($V_{1/2}$) with increasing $K^+$ concentrations. Solid lines represent best Boltzmann fits to the data. The Boltzmann parameters for 3 mM $K^+$ were $V_{1/2}=-6.1\,\text{mV}\pm3.0\,\text{mV}$, apparent gating charge $z_g=1.6\pm0.2$ and for 30 mM $K^+$ $V_{1/2}=12.9\,\text{mV}\pm1.7$, $z_g=2.0\pm0.2$ ($n=3$). Error bars indicate standard deviation.
(c) Tail currents were obtained in 3, 30 and 90 mM K gluconate. Zero currents reflecting the reversal potential ($V_{rev}$) are indicated by arrows. Reversal potentials shifted in a $K^+$ dependent manner. The theoretical Nernst potentials for the given potassium concentration in the pipette (150 mM $K^+$) and the bathing solutions are for 3 mM $K^+=100$ mV, for 30 mM $K^+=41$ mV and for 90 mM $K^+=13$ mV. Voltage pulses from 15 to −65 mV in 20 mV steps were applied, following a pre-activating pulse to 75 mV.

Following the rise in external calcium from 1 to 20 mM, inward currents progressively declined with more negative membrane potentials (Figure 8d–f). This type of voltage-dependent calcium block has so far only been observed with AKT2/3-type channels and not with other members of the plant Shaker family (Hoth *et al.*, 2001; Marten *et al.*, 1999). In contrast to AKT2/3 channels, the $K^+$ currents in cultured cells were time-dependent and strongly inward rectifying (Figure 8).

When the membrane potential was clamped at −85 mV and 1.5 sec pulses stepped to de-polarizing potentials were applied, outward $K^+$ currents could be observed (Figure 9a). These currents were strongly outward rectifying and characterized by a sigmoidal activation kinetic, a feature reminiscent of PTORK and other members of the SKOR family when expressed in oocytes (Figure 4a; Ache *et al.*, 2000; Gaymard *et al.*, 1998). A reduction from 30 mM potassium to 3 mM in the bathing solution of protoplasts resulted in a negative shift of the voltage dependence of the outward rectifier (Figure 9b) which was also found in the PTORK-expressing oocytes (Figure 4c,d). The positive shift of the reversal potential was induced by an elevation of external potassium from 3 to 30 and 90 mM (Figure 9d). Both the shift of the half maximal activation potential and the Nernstian behaviour of the reversal potential classified this outward rectifier as $K^+$ permeable channel.

## Discussion

Cell division and expansion are potassium dependent (Philippar *et al.*, 1999) and the $K^+$ nutrition status was shown to strongly affect the development of wood producing cells. The expansion of vessel initials under potassium depletion ceased early followed by untimely secondary cell wall formation. The lack of 1–2 cell divisions in the vessel development region and limited cell expansion resulted in reduced wood formation. The application of the potassium channel blocker $TEA^+$ led to the same effect and, therefore, pointed to a link between potassium channels and wood production.

The data presented here and in previous experiments by others reveal a strong $K^+$ dependency of wood formation. To determine which $K^+$ transporters might control potassium-dependent xylogenesis, we screened a poplar cambium EST database and identified two $K^+$ channel-like sequences that we called PTORK, PTK2 and one potential $K^+$ carrier, PtKUP1. PTORK shared closest structural and functional similarities with its *Arabidopsis* counterpart

SKOR, a stelar $K^+$ outward rectifier, expressed in the root xylem parenchyma. Thus, PTORK enables potassium release in a voltage- and potassium-dependent manner. PTK2 was classified as a member of the AKT2/3 phloem $K^+$ channel family with similar structures and functions. Like AKT2/3, PTK2 is able to mediate both uptake and release of potassium in response to changes in membrane potential in a calcium- and pH-dependent fashion.

When we compared the properties of outward rectifying $K^+$ channels in PTORK-expressing poplar suspension cells and PTORK-injected *Xenopus* oocytes they were shown to share basic features and furthermore were similar to other plant de-polarization-activated $K^+$ release channels (Ache *et al.*, 2000; Gaymard *et al.*, 1998). The inward $K^+$ channel from poplar suspension culture showed a voltage-dependent calcium block and was highly sensitive to $Cs^+$. Although these features were characteristic for PTK2 and AKT2/3, its voltage dependency differed from that recorded in PTK2 expressing oocytes. Inward rectification was weak in PTK2-injected oocytes but strong in PTK2-expressing poplar cells. This feature could reflect the finding that functional Shaker $K^+$ channels are formed by four alpha subunits (MacKinnon, 1991), and that members of different subfamilies are able to form hetero-tetramers (Daram *et al.*, 1997; Dreyer *et al.*, 1997; Ehrhardt *et al.*, 1997). In this context, it should be mentioned that when KAT1 (KPT1 homologue expressed in guard cells) was co-expressed with AKT3 (PTK2 homologue expressed in the phloem and guard cells) in *Xenopus* oocytes, the voltage dependence was dominated by the strong inward rectifier KAT1 (Baizabal-Aguirre *et al.*, 1999 and own unpublished data). In guard cells that express several different Shaker channel types including AKT2/3, a calcium-sensitive and highly caesium-sensitive inward rectifier represents the dominant inward $K^+$ conductance (Szyroki *et al.*, 2001). *Arabidopsis* plants, however, lacking the AKT2/3 subunit were no longer blocked by external calcium ions (Ivashikina *et al.*, 2001). Furthermore, a protein phosphatase interacting with the AKT3 has been identified (Vranova *et al.*, 2001). When co-expressed with AKT2/3 this phosphatase turns the weak voltage-dependence of this channel type into an inward rectifier (Chérel *et al.*, 2002). We, thus, propose that poplar suspension cells express an additional $K^+$ channel alpha subunit or a channel modulator which transforms PTK2 into an inward rectifier.

Both $K^+$ channel genes are expressed in young poplar twigs, while *PTK2* was predominantly found in the phloem fraction *PTORK* was detected in both phloem and xylem fractions. The seasonal changes in expression levels of both channels coincided with cambial activity and xylogenesis and the functions of their *Arabidopsis* homologues in xylem and phloem transport, point to a role of PTORK in $K^+$ release from xylem parenchyma and of PTK2 in $K^+$ uptake of cambium and phloem cells.

## Experimental procedures

### *Plant growth conditions*

*Populus tremula* × *P. tremuloides* plants were grown in soil under natural conditions. Suspension cell cultures from shoots were grown in liquid MS medium (≈20 mM K), containing 5 μM 2,4 dichlorophenoxyacetic acid (2,4 D) or in modified Hoagland nutritional solution (1 mM K) with 5 μM 2,4-D. Cell cultures were shaken at 133 ***g*** in darkness at 26°C.

Rooted cuttings from mature poplar trees (*P. trichocarpa*) were cultivated hydroponically at different $K^+$ concentrations (modified Hoagland nutritional solution) in a controlled environment chamber at 20°C with a photon flux density of 300 $\mu E\ m^{-2}\ s^{-1}$ and were used for anatomical analysis of fibre and vessel lumen areas. Additionally, a few cuttings grown in Hoagland nutritional solution with 6 mM $K^+$ were treated with 5 mM $TEA^+$ for 2 weeks. To avoid systemic responses $TEA^+$ was applied on the scraped twig surface and not within the nutrition solution. Controls were treated with water (not shown).

### *Light microscopy and image analysis*

Twig tissue was sampled and fixed with 3% formaldehyde in phosphate-buffered solution (PBS) for 2 h, washed in buffer and dehydrated in a graded series of ethanol. After embedding in LR White acryl resin, semithin sections were cut with a diamond knife and stained with Toluidine Blue for light microscopy. The lumen areas of fibres and vessels of newly formed wood tissue were measured by digital image analysis using a Zeiss Axio Vision system.

### *X-ray microanalysis*

Small sections of twig tissue were cut with a razor blade and immediately shock frozen in liquid isopentane at its melting point. After freeze drying, the samples were coated with chromium and examined in a Leitz AMR 1200 scanning electron microscope fitted with a Kevex 4000 X-ray analyser. Element specific X-ray spectra were obtained from a reduced scan raster area at 1000× magnification. Relative potassium concentrations were expressed as peak to background ratio from 10 recorded spectra. For visualizing the distribution of potassium in the twig tissue, potassium specific X-ray signals were recorded using the element specific scan modus of the microscope.

### *Cloning*

*Populus tremula* × *P. tremuloides* cDNA fragments homologous to potassium channels and transporters were identified from the expressed sequence tag (EST) database using BLAST (Altschul *et al.*, 1990). The poplar data base entries of the selected *Populus* ESTs are as follows: A020P20, B007P19 μ, A043P54 μ.

Amplification of 5′cDNA ends were performed by RACE technique (Marathon™ cDNA Amplification Kit, SMART™ RACE cDNA Amplification Kit, Clontech) using the following gene-specific primers: PTORK Mrev position 195 (5′-AAG AAA CTT CCC CAA ATG AGC-3′), PTK2 Mrev position 172 (5′-GTG CAT TCT TGT TCC CCT TCA C-3′) and PtKUP1 Mrev position 39 (5′-CAC GGG AAT CCT TGT ATG TTG-3′).

Full-length cDNAs were amplified from reverse transcribed RNA derived from xylem, cambium and phloem tissues of *P. tremula* ×

*P. tremuloides* (RT-PCR) with the following primers: PTORKfwd (5′-TTGCAGATTATGATGATGATC C-3′) and PTORKrev (5′-TGATATACCCCATAAATCAGAACA-3′), PTK2fwd (5′-GGGCACGTAACGAAGTT-3′) and PTK2rev (5′-TGCCTGATGAGTATTGATTG-3′) and PtKUP1fwd (5′-ACCGCAAAACACTCTAAAAA-3′), PtKUP1rev (5′-CGG CCC TCT AAG CAA T-3′). The xylem, cambium and phloem tissues were obtained as previously described (Tuominen *et al.*, 2000).

### *Cloning of* KPT1

Within the increasing number of plant $K^+$ uptake channels cloned so far, amino acid sequences within the second (S2) and sixth (S6) putative transmembrane domain and the amphiphilic linker between S5 and S6 (H5) are highly conserved (Hedrich and Roelfsema, 1999). Using degenerative oligonucleotides (Ache *et al.*, 2001), we cloned a 200-bp (H5 ± S6) fragment of the *KPT1* cDNA from a leaf cDNA library. Amplification of 5′- and 3′-cDNA ends were performed by RACE technique (SMART™ RACE cDNA Amplification Kit, Clontech) using the following gene-specific primers:

3′-KPT1GSP1 (5′-ATA CCC TGA TCC GAA GAG AAC C-3′), Nested 3′-KPT1 GSP2 (5′-TAC CAC ATT AAC CAC AAC AGG G-3′), 5′-KPT1 GSP1 (5′-CCC ATA CCC TGT TGT GGT T-3′), Nested 5′-KPT1 GSP2 (5′-TGC AGT CAC GTA TCT ATT CCA TAG T-3′).

The full length cDNA was amplified with KPT VL fw (5′-TGA GAA TTC AAG CAA CCA GTG-3′) and KPT VL rev (5′-CAC TTG GCC ATG ATG TAT TGC-3′) Primers.

### *Heterologous expression in Xenopus oocytes*

The cRNAs of *PTORK* and *PTK2* were generated by *in vitro* transcription (T7-Megascript kit; Ambion Inc., Austin, TX) and injected into oocytes of *Xenopus laevis* (Nasco, Fort Atkinson, WI) using a Picospritzer II microinjector (General Valve, Fairfield, NJ). Oocyte preparation and cRNA injection have been described elsewhere (Becker *et al.*, 1996). In two-electrode voltage-clamp studies oocytes were perfused with potassium gluconate containing Tris–MES buffers. Further used solutions are described in the figure legends. All media were adjusted to a final osmolality of 215–235 mosmol $kg^{-1}$ with D sorbitol. Analyses of voltage dependence, pH dependence, selectivity and $Ca^{2+}$ block were performed as described previously (Hoth *et al.*, 1997; Marten *et al.*, 1999).

### *Expression analysis by quantitative RT-PCR*

RNA of stem fragments (see below) was isolated using the Plant RNeasy Extraction kit (Qiagen, Hilden, Germany) DNA was digested on-column during RNA purification (RNase-Free DNase kit, Qiagen, Hilden, Germany).

First-strand cDNA was prepared using the Superscript RT kit (Gibco_BRL) and diluted for RT-PCR 20-fold in water. PCR was performed in a LightCycler (Roche Molecular Biochemicals) with the LightCycler-FastStart DNA Master SYBR Green I Kit (Roche Molecular Biochemicals). Primers used: PtACT2fwd (5′-CCC AGA AGT CCT CTT-3′) and PtACT2rev (5′-ACT GAG CAC AAT GTT AC-3′), PTORKLCfw (5′-CAG GGG CAT CAC TGG CA-3′) and PTORKLCrev (5′-GGT AAC CAC CTG AAG AT-3′), PTKLCfw (5′-ATG CGA TAT ACA CCT G-3′) and PTKLCrev (5′-TGC TCA CCC TAA TAC A-3′) and KPTLCfw (5′-GAT GTC CCC ATG ATA GG-3′), KPTLCrev (5′-CAT GAT GTA TTG CGC T-3′).

All quantifications were normalized to actin cDNA fragments amplified by PtACT2fwd and PtACT2rev. These fragments are homologous to the constitutively expressed *Arabidopsis* actins 2 and 8 (for details see Szyroki *et al.*, 2001 and references therein). Each transcript was quantified using individual standards. To enable detection of contaminating genomic DNA, PCR was performed with the same RNA as template, which was used for cDNA synthesis. All kits were used according to the manufacturer's protocols.

### *Complementation tests of PtKUP1 in* E. coli.

The *PtKUP1* cDNA was inserted into the expression vector pCRII TOPO (Invitrogen), the resultant plasmid containing the entire PtKUP1 coding region was designated PtKUP1.

The plasmid was expressed in *E. coli* LB2003, which lacks the three $K^+$ uptake systems, Trk (TrkG and TrkH), Kup (Tr kDa), and Kdp (a kind gift from K. Altendorf, University of Osnabrück, Germany). The *E. coli* strain was grown at 28°C on solid KML-medium (10 g tryptone, 5 g yeast extract, and 10 g KCl $l^{-1}$) (Epstein and Kim, 1971). As a control *E. coli* LB2003 strain was transformed with the empty pCRII TOPO vector. Transformants were tested for their ability to grow in medium containing low (3 mM) potassium (10 g of tryptone, 2 g of yeast extract, and 100 mmol of mannitol per litre), pH 7.0, for 2 days. $K^+$ concentrations were determined by ICP–OES–Elemtaranalysis.

The effect of monovalent and divalent cations on growth was detected by the halo assay (Becker *et al.*, 1996). A lawn of $10^5$ cells of LB2003 expressing PtKUP1 was plated in 0.7% agarose on KML plates with 3 mM of $K^+$. A paper disk containing 10 µl of the test cation solution ($TEA^+$ (1 M), upper disk; $Cs^+$ (1 M), left disk; $Ba^{2+}$ (1 M), right disk; $Ca^{2+}$ (1 M), lower disk) was placed on the agar surface and the plates were incubated at 28°C for 36–48 h. In the growth zone around the disk, inhibition creates a dark halo.

### *Cell culture and protoplasts isolation*

Cell culture protoplasts were enzymatically isolated from young and white tissue at the border of callus pieces. Two to five days after exchange of the nutrient solution, the young tissue was separated from the old, brown coloured tissue using a razorblade.

The enzyme solution contained 0.8% (w/v) Cellulase (Onozuka R10), 0.1% (w/v) Pectolyase (Sigma), 0.5% (w/v) BSA (Serva), 0.5% (w/v) PVP (Sigma), 1 mM $CaCl_2$, 8 mM MES/KOH pH 5.5, π 280 mosmol $kg^{-1}$ (D-sorbitol). The protoplasts were filtered through a 50-µm nylon-net, washed 2 times with a solution containing 1 mM $CaCl_2$ (π 280 mosmol $kg^{-1}$ (D-sorbitol)) and finally they were centrifuged at 600 *g* for 10 min at 4°C.

### *Patch-clamp*

Ion fluxes were studied in the whole-cell configuration of the patch-clamp technique. Current measurements were performed using an EPC-7 patch-clamp amplifier (HEKA, Lambrecht, Germany). The patch pipettes were prepared from Kimax-51 glass (Kimble products, Vineland, NY, USA) and coated with silicone (Sylgard 184 silicone elastomer kit; Dow Corning, USA).

Whole cell measurements were performed by stepwise voltage pulses starting from 75 to 185 mV in 20 mV decrements. After a preactivating voltage pulse of 75 mV, tail currents were observed by changing the membrane voltage successively from 75 to 185 mV in 20 mV steps. Voltage values were corrected for liquid junction potential 5 mV (Neher, 1992). The difference between the liquid junction potential correction of voltage values and $R_s$ compensation corrected voltage values was smaller than 5 mV, so this difference was not taken into consideration.

Solutions: The standard pipette solution (cytoplasm) contained 150 mM K gluconate, 2 mM $MgCl_2$, 2 mM MgATP, 10 mM HEPES/Tris pH 7.4. Cytosolic $Ca^{2+}$ was buffered with 10 mM EGTA. The standard bathing medium contained 30 mM K gluconate, 1 mM $CaCl_2$ and 10 mM MES–Tris pH 5.6. In order to test the calcium dependence of the inward rectifiers we increased the $CaCl_2$ concentration from 1 to 20 mM. By changing the external potassium concentration from 3 to 30 and 90 mM the $K^+$ selectivity of inward and outward rectifiers was studied. 5 mM of the specific $K^+$ channel blocker CsCl was added to the standard bathing medium to test the susceptibility towards $Cs^+$. All solutions were adjusted to a final osmolality of 280 mosmol $kg^{-1}$ with D-sorbitol.

## Acknowledgements

We thank Dr K. Altendorf for providing the *E. coli* LB2003 strain. We are grateful to Petra Dietrich for critical reading of the manuscript. This work was supported by grants of the Deutsche Forschungsgemeinschaft and Körber award to RH.

## References

**Ache, P., Becker, D., Deeken, R., Dreyer, I., Weber, H., Fromm, J. and Hedrich, R.** (2001) VFK1, a *Vicia faba* $K^+$ channel involved in phloem unloading. *Plant J.* **27**, 571–580.

**Ache, P., Becker, D., Ivashikina, N., Dietrich, P., Roelfsema, M.R.G. and Hedrich, R.** (2000) GORK, a delayed outward rectifier expressed in guard cells of *Arabidopsis thaliana*, is a $K^+$-selective, $K^+$-sensing ion channel. *FEBS Lett.* **486**, 93–98.

**Aloni, R.** (1987) Differentiation of vascular tissues. *Ann. Rev. Plant Physiol.* **38**, 179–204.

**Altschul, S.F., Gish, W., Miller, W., Myers, E.W. and Lipman, D.J.** (1990) Basic local alignment search tool. *J. Mol. Biol.* **215**, 403–410.

**Anderson, J.A., Huprikar, S.S., Kochian, L.V., Lucas, W.J. and Gaber, R.F.** (1992) Functional expression of a probable *Arabidopsis thaliana* potassium channel in *Saccharomyces cerevisiae*. *Proc. Natl. Acad. Sci. USA*, **89**, 3736–3740.

**Arend, M. and Fromm, J.** (2000) Seasonal variation in the K, Ca and P content and distribution of plasma membrane $H^+$-ATPase in the cambium of *Populus trichocarpa*. In *Cell and Molecular Biology of Wood Formation* (Savidge, R.A., Barnet, J.R. and Napier, R. eds). Oxford: BIOS Scientific Publishers Ltd, pp. 67–70.

**Baizabal-Aguirre, V.M., Clemens, S., Uozumi, N. and Schroeder, J.I.** (1999) Suppression of inward-rectifying $K^+$ channels KAT1 and AKT2 by dominant negative point mutations in the KAT1 alpha-subunit. *J. Membr. Biol.* **167**, 119–125.

**Bauer, C.S., Hoth, S., Haga, K., Philippar, K., Aoki, N. and Hedrich, R.** (2000) Differential expression and regulation of $K^+$ channels in the maize coleoptile: molecular and biophysical analysis of cells isolated from cortex and vasculature. *Plant J.* **24**, 139–145.

**Becker, D., Dreyer, I., Hoth, S., Reid, J.D., Busch, H., Lehnen, M., Palme, K. and Hedrich, R.** (1996) Changes in voltage activation, $Cs^+$ sensitivity, and ion permeability in H5. *Proc. Natl. Acad. Sci. USA*, **93**, 8123–8128.

**Brüggemann, L., Dietrich, P., Becker, D., Dreyer, I., Palme, K. and Hedrich, R.** (1999) Channel-mediated high-affinity $K^+$ uptake into guard cells from *Arabidopsis*. *Proc. Natl. Acad. Sci. USA*, **96**, 3298–3302.

**Chérel, I., Michard, E., Platet, N., Mouline, K., Alcon, C., Sentenac, H. and Thibaud, J.-B.** (2002) Physical and functional interaction of the *Arabidopsis* $K^+$ channel AKT2 and Phosphatase AtPP2CA. *Plant Cell*, **14**, 1–14.

**Daram, P., Urbach, S., Gaymard, F., Sentenac, H. and Cherel, I.** (1997) Tetramerization of the AKT1 plant potassium channel involves its C-terminal cytoplasmic domain. *EMBO J.* **16**, 3455–3463.

**Deeken, R., Fromm, J., Koroleva, O., Ache, P., Langenfeld-Heyser, R., Geiger, D., Sauer, N., May, S.T. and Hedrich, R.** (2002) Loss of the AKT2/3 potassium channel affects sugar loading into the phloem of *Arabidopsis*. *Planta*, in press.

**Deeken, R., Sanders, C., Ache, P. and Hedrich, R.** (2000) Developmental and light-dependent regulation of a phloem-localised $K^+$ channel of *Arabidopsis thaliana*. *Plant J.* **23**, 285–290.

**Dreyer, I., Antunes, S., Hoshi, T., Müller-Röber, B., Palme, K., Pongs, O., Reintanz, B. and Hedrich, R.** (1997) Plant $K^+$ channel $\alpha$-subunits assemble indiscriminately. *Biophys. J.* **72**, 2143–2150.

**Dünisch, O. and Bauch, J.** (1994a) Influence of mineral elements on wood formation of old growth spruce (*Picea abies* L. Karst.). *Holzforschung*, **48**, 5–14.

**Dünisch, O. and Bauch, J.** (1994b) Influence of soil substrate and drought on wood formation of spruce (*Picea abies* L. Karst.) under controlled conditions. *Holzforschung*, **48**, 447–457.

**Dünisch, O., Bauch, J., Müller, M. and Greis, O.** (1998) Subcellular quantitative determination of K and Ca in phloem, cambium, and xylem cells of spruce (*Picea abies* L. Karst.) during early-wood and latewood formation. *Holzforschung*, **52**, 582–588.

**Ehrhardt, T., Zimmermann, S. and Müller-Röber, B.** (1997) Association of plant $K^+_{in}$ channels is mediated by conserved C-termini and does not affect subunit assembly. *FEBS Lett.* **409**, 166–170.

**Epstein, W. and Kim, A.S.** (1971) Potassium transport loci in *Escherichia coli* K-12. *J. Bacteriol.* **108**, 639–644.

**Eschrich, W., Fromm, J. and Essiamah, S.** (1988) Mineral partitioning in the phloem during autumn senescence of beech leaves. *Trees*, **2**, 73–83.

**Fromm, J. and Bauer, T.** (1994) Action potentials in maize sieve tubes change phloem translocation. *J. Exp. Bot.* **45**, 463–469.

**Fromm, J. and Eschrich, W.** (1986) Changes of adenine nucleotide and orthophosphate concentrations in buds of deciduous trees during spring activation. *Trees*, **1**, 42–46.

**Fromm, J., Essiamah, S. and Eschrich, W.** (1987) Displacement of frequently occurring heavy metals in autumn leaves of beech (*Fagus sylvatica*). *Trees*, **1**, 164–171.

**Fromm, J. and Spanswick, R.** (1993) Characteristics of action potentials in willow (*Salix viminalis*). *J. Exp. Bot.* **44**, 1119–1125.

**Fu, H.H. and Luan, S.** (1998) AtKUP1: a dual-affinity $K^+$ transporter from *Arabidopsis*. *Plant Cell*, **10**, 63–73.

**Gassman, W., Rubio, F. and Schroeder, J.I.** (1996) Alkali cation seletivity of the root high-affinity potassium transporter HKT1. *Plant J.* **10**, 852–869.

**Gaymard, F., Pilot, G., Lacombe, B., Bouchez, D., Bruneau, D., Boucherez, J., Michaux-Ferriere, N., Thibaud, J.-B. and Sentenac, H.** (1998) Identification and disruption of a plant Shaker-like outward channel involved in $K^+$ release into the xylem sap. *Cell.* **94**, 647–655.

**Geiger, D., Becker, D., Lacombe, B. and Hedrich, R.** (2002) Outer pore residues control $H^+$- and $K^+$-sensitivity of the *Arabidopsis* potassium channel AKT3. *Plant Cell.* **14**, 1859–1868.

**Hampp, R., Rieger, A. and Outlaw, W.H., Jr** (1990) Microdissection and biochemical analysis of plant tissues. In *Physical Methods in Plant Sciences* (Linskens, H.F., and Jackson, J.F. eds). Berlin: Springer-Verlag, pp. 124–147.

**Hedrich, R. and Becker, D.** (1994) Green circuits – the potential of plant specific ion channels. *Plant Mol. Biol.* **26**, 1637–1650.

**Hedrich, R. and Roelfsema, M.-R.G.** (1999) Plant ion transport. In *Encyclopedia of Life Sciences.* Available: http://www.els.net: Macmillan Reference Ltd.

**Hirsch, R., Lewis, B.D., Spalding, E.P. and Sussmann, M.R.** (1998) A role for the AKT1 potassium channel in plant nutrition. *Science*, **280**, 918–921.

**Hoth, S., Dreyer, I., Dietrich, P., Becker, D., Müller-Röber, B. and Hedrich, R.** (1997) Molecular basis of plant-specific acid activation of $K^+$ uptake channels. *Proc. Natl. Acad. Sci. USA*, **94**, 4806–4810.

**Hoth, S., Geiger, D., Becker, D. and Hedrich, R.** (2001) The pore of plant $K^+$ channels is involved in voltage and pH sensing. Domain-swapping between different $K^+$ channel alpha-subunits. *Plant Cell*, **13**, 943–952.

**Ivashikina, N., Becker, D., Ache, P., Meyerhoff, O., Felle, H.H. and Hedrich, R.** (2001) $K^+$ channel profile and electrical properties of *Arabidopsis* root hairs. *FEBS Lett.* **25503**, 1–7.

**Kim, E.J., Kwak, J.M., Uozumi, N. and Schroeder, J.I.** (1998) AtKUP1: an *Arabidopsis* gene encoding high-affinity potassium transport activity. *Plant Cell*, **10**, 51–62.

**Krabel, D., Bodson, M. and Eschrich, W.** (1994) Seasonal changes in the cambium of trees. I. Sucrose content in *Thuja occidentalis*. *Bot. Acta*, **107**, 54–59.

**Kuhn, A.J., Bauch, J. and Schröder, W.H.** (1995) Monitoring uptake and contents of Mg, Ca and K in Norway spruce as influenced by pH and Al, using microprobe analysis and stable isotope labelling. *Plant Soil*, **168–169**, 135–150.

**Kuhn, A.J., Schröder, W.H. and Bauch, J.** (1997) On the distribution and transport of mineral elements in xylem, cambium and phloem of spruce (*Picea abies* L. Karst.). *Holzforschung*, **51**, 487–496.

**Lacombe, B., Pilot, G., Michard, E., Gaymard, F., Sentenac, H. and Thibaud, J.B.** (2000) A shaker-like $K^+$ channel with weak rectification is expressed in both source and sink phloem tissues of *Arabidopsis*. *Plant Cell*, **12**, 837–851.

**Larson, P.R.** (1994) *The Vascular Cambium: Development and Structure*. Berlin: Springer-Verlag (Series in Wood Science).

**MacKinnon, R.** (1991) Determination of the subunit stoichiometry of a voltage-activated potassium channel. *Nature*, **350**, 232–235.

**Marten, I., Hoth, S., Deeken, R., Ache, P., Ketchum, K.A., Hoshi, T. and Hedrich, R.** (1999) AKT3, a phloem-localized $K^+$ channel, is blocked by protons. *Proc. Natl. Acad. Sci. USA*, **96**, 7581–7586.

**Neher, E.** (1992) Corrections for liquid junction potentials in patch-clamp experiments. *Meth. Enzymol.* **207**, 123–131.

**Philippar, K., Fuchs, I., Lüthen, H. *et al.*** (1999) Auxin-induced $K^+$ channel expression represents an essential step in coleoptile growth and gravitropism. *Proc. Natl. Acad. Sci. USA*, **96**, 12186–12191.

**Reintanz, B., Szyroki, A., Ivashikina, N., Ache, P., Godde, M., Becker, D., Palme, K. and Hedrich, R.** (2002) AtKC1, a silent *Arabidopsis* potassium channel $\alpha$-subunit modulates root hair $K^+$ influx. *Proceedings of the Natl. Acad. Sci. USA*, **99**, 4079–4084.

**Rigas, S., Debrosses, G., Haralampidis, K., Vicente-Agullo, F., Feldmann, K., Grabov, A., Dolan, L. and Hatzopoulos, P.** (2001) Trh1 encodes a potassium transporter required for tip growth in *Arabidopsis* root hairs. *Plant Cell*, **13** (1), 139–151.

**Roberts, L.W., Gahan, P.B. and Aloni, R.** (1988) Vascular differentiation and plant growth regulators. *Springer Series in Wood Science*. Berlin: Springer-Verlag.

**Rodriguez-Navarro, A.** (2000) Potassium transport in fungi and plants. *Biochim. Biophys. Acta*, **1469**, 1–30.

**Savidge, R.A.** (1996) Xylogenesis, genetic and environmental regulation. *IAWA J.* **17**, 269–310.

**Savidge, R.A.** (2000) Biochemistry of seasonal cambial growth and wood formation – an overview of the challenges. In *Cell and Molecular Biology of Wood Formation* (Savidge, R.A. Barnett, J.R. and Napier, R. eds). Oxford.: BIOS Scientific Publishers Ltd, pp. 1–30.

**Schroeder, J.I. and Fang, H.H.** (1991) Inward rectifying $K^+$ channels in guard cells provide a mechanism for low-affinity $K^+$ uptake. *Proc. Natl. Acad. Sci. USA*, **88**, 11583–11587.

**Spalding, E.P., Hirsch, R.E., Lewis, D.R., Qi, Z., Sussman, M.R. and Lewis, B.D.** (1999) Potassium uptake supporting plant growth in the absence of AKT1 channel activity. *J. Gen. Physiol.* **113**, 909–918.

**Sterky, F., Regan, S., Karlsson, J. *et al.*** (1998) Gene discovery in the wood-forming tissues of poplar: analysis of 5692 expressed sequence tags. *Proc. Natl. Acad. Sci. USA*, **95**, 13330–13335.

**Szyroki, A., Ivashikina, N., Dietrich, P. *et al.*** (2001) KAT1 is not essential for stomatal opening. *Proc. Natl. Acad. Sci. USA*, **98**, 2917–2921.

**Tuominen, H., Puech, L., Regan, S., Fink, S., Olsson, O. and Sundberg, B.** (2000) Cambial-region-specific expression of the *Agrobacterium iaa* genes in transgenic aspen visualized by a linked *uidA* reporter gene. *Plant Physiol.* **123**, 531–542.

**Uozumi, N., Nakamura, T., Schroeder, J.I. and Muto, S.** (1998) Determination of transmembrane topology of an inward-rectifying potassium channel from *Arabidopsis thaliana* based on functional expression in *Escherichia coli*. *Proc. Natl. Acad. Sci. USA*, **95**, 9773–9778.

**Vranova, V., Tähtiharju, S., Sriprang, R., Willekens, H., Heino, P., Palva, E.T., Inze, D. and van Camp, W.** (2001) The AKT3 potassium channel protein interacts with the AtPP2CA protein phosphtase 2C. *J. Exp. Bot.* **52**, 181–182.

# Kapitel VI: Differential Expression of Sucrose Transporter and Polyol Transporter Genes during Maturation of *Common Plantain* Companion Cells

**Martina Ramsperger-Gleixner, Dietmar Geiger, Rainer Hedrich und Norbert Sauer**

**Publiziert in Plant Physiology, Vol. 134, 147-160, Januar 2004**

**Eigene Beteiligung an der Arbeit:**

- Biophysikalische Charakterisierung von PmPLT1 in *Xenopus* Oozyten mit Hilfe der DEVC-Technik in Bezug auf die pH- und Polyol-abhängigen Transportkinetiken.
- Ermittlung der Spannungsabhängigkeit des $K_m$-Wertes und von $I_{max}$.
- Bestimmung der Substratspezifität von PmPLT1.
- Auswertung der Daten.

# Differential Expression of Sucrose Transporter and Polyol Transporter Genes during Maturation of Common Plantain Companion Cells

**Martina Ramsperger-Gleixner, Dietmar Geiger, Rainer Hedrich, and Norbert Sauer***

Molekulare Pflanzenphysiologie, Universität Erlangen-Nürnberg, Staudtstrasse 5, D–91058 Erlangen, Germany (M.R.-G., N.S.); and Julius-von-Sachs-Institut für Biowissenschaften, Lehrstuhl Botanik I, Molekulare Pflanzenphysiologie und Biophysik, Julius-von-Sachs-Platz 2, D–97082 Würzburg, Germany (D.G., R.H.)

The cDNAs of two sorbitol transporters, common plantain (*Plantago major*) polyol transporter (PLT) 1 and 2 (PmPLT1 and PmPLT2), were isolated from a vascular bundle-specific cDNA library from common plantain, a dicot plant transporting Suc plus sorbitol in its phloem. Here, we describe the kinetic characterization of these sorbitol transporters by functional expression in Brewer's yeast (*Saccharomyces cerevisiae*) and in *Xenopus* sp. oocytes and for the first time the localization of plant PLTs in specific cell types of the vascular tissue. In the yeast system, both proteins were shown to be uncoupler sensitive and could be characterized as low-affinity and low-specificity polyol symporters. The $K_m$ value for the physiological substrate sorbitol is 12 mM for PmPLT1 and even higher for PmPLT2, which showed an almost linear increase in sorbitol transport rates up to 20 mM. These data were confirmed in the *Xenopus* sp. system, where PmPLT1 was analyzed in detail and characterized as a $H^+$ symporter. Using peptide-specific polyclonal antisera against PmPLT1 or PmPLT2 and simultaneous labeling with the monoclonal antiserum 1A2 raised against the companion cell-specific PmSUC2 Suc transporter, both PLTs were localized to companion cells of the phloem in common plantain source leaves. These analyses revealed two different types of companion cells in the common plantain phloem: younger cells expressing PmSUC2 at higher levels and older cells expressing lower levels of PmSUC2 plus both PLT genes. The putative role of these low-affinity transporters in phloem loading is discussed.

The export of photoassimilates from higher plant source leaves occurs via the sieve element/companion cell complex (SE/CCC) of the phloem. In many plant species, such as in Arabidopsis, maize (*Zea mays*), sugar beet (*Beta vulgaris*), or tobacco (*Nicotiana tabacum*), assimilated $CO_2$ is exported exclusively in the form of Suc. In numerous other plants, however, additional carbohydrates are used for this long distance transport. Examples are raffinose or stachyose in Cucurbitaceae (Kandler and Hopf, 1982; Keller and Pharr, 1996) or reduced monosaccharides, such as mannitol or sorbitol in Rosaceae, Plantaginaceae, or several other families (Barker, 1955; Webb and Burley, 1962; Zimmermann and Ziegler, 1975). The common properties of Suc and these additional compounds are that they are highly soluble, chemically inert, and not readily accessible for primary cellular metabolism. They can thus be stored and transported in high concentrations with no damage to the cells and without being degraded or modified.

cDNAs encoding Suc transporters involved in phloem loading have been cloned from several plants (Riesmeier et al., 1992; Riesmeier et al., 1993; Gahrtz et al., 1994; Sauer and Stolz, 1994; Bürkle et al., 1998; Aoki et al., 1999; Noiraud et al., 2000; Williams et al., 2000). In contrast, only a single cDNA of a mannitol transporter, *AgMAT1* from celery (*Apium graveolens*; Noiraud et al., 2001) and two cDNAs for sorbitol transporters, *PcSOT1* and *PcSOT2* from sour cherry (Gao et al., 2003), has been cloned. So far, no transporters for raffinose or stachyose have been identified. This does not at all reflect the relative importance of Suc versus these other substances in phloem transport, because in many plants, phloem concentrations of oligosaccharides from the raffinose family or of polyols are comparable with or even higher than the concentrations of Suc. For example, Suc, raffinose, and stachyose concentrations in pumpkin (*Cucurbita maxima*) were found to be 180, 120, and 180 mM, and in peach (*Prunus persica*), the concentrations of Suc and sorbitol were shown to be 140 and 550 mM in the phloem sap. In common plantain, Suc and sorbitol concentrations are 800 and 300 mM, respectively (Lohaus and Fischer, 2002; G. Lohaus, unpublished data).

It is not really understood, why different plants use different compounds for long distance carbon allocation. For raffinose-transporting symplastic phloem loaders, such as cucurbits, it has been postulated that the difference in the Stoke's radii between Suc and raffinose (or stachyose) represents the actual "driv-

* Corresponding author; e-mail nsauer@biologie.uni-erlangen.de; fax 49–9131–85–28751.

Article, publication date, and citation information can be found at www.plantphysiol.org/cgi/doi/10.1104/pp.103.027136.

ing force" for long distance transport (Turgeon, 1996). The so-called "polymer trap model" is based on the assumption that Suc, the first precursor in raffinose biosynthesis, can traffic symplastically from mesophyll cells into the SE/CCC. The model is also based on the observation that galactinol, the second precursor in raffinose formation, is synthesized inside the companion cells (also called intermediary cells) of these plants (Bebee and Turgeon, 1992; Haritatos et al., 2000). The unproven conclusion is that Suc and monosaccharides can traffic into the companion cells, but raffinose cannot traffic back due to its higher Stoke's radius (trapping mechanism). According to this model, phloem transport of oligosaccharides from the raffinose family might be essential to drive phloem transport in symplastic loaders. The major drawback of this model is, however, that it has never been possible to show that plasmodesmata can discriminate between molecules, such as Suc or raffinose.

In contrast, there are several physiological reasons that might explain the long distance transport of polyols. Obviously, phloem transport of more reduced sugar alcohols may be advantageous for $NADPH^+$-dependent reactions in sinks, such as the reduction of $NO_3^-$, which in many plants is performed in roots (Hansch et al., 2001). Mannitol has also been shown to act as antioxidant (Shen et al., 1997) and may have important functions in plant-pathogen interactions (Jennings et al., 1998). Moreover, it is known that polyols can serve as compatible solutes and the role of mannitol as an osmoprotectant in celery is well documented (Tarczynski et al., 1993; Everard et al., 1994; Stoop and Pharr, 1994a). Interestingly, mannitol synthesis is not up-regulated under stress (Everard et al., 1994), and increased mannitol concentrations in roots of stressed plants result primarily from reduced degradation of mannitol (Stoop and Pharr, 1994a, 1994b), which is constantly supplied by the phloem. Finally, phloem polyols were also shown to influence the phloem mobility of boron (B) by the formation of soluble mannitol-B-mannitol complexes in celery or of sorbitol-B-sorbitol complexes in peach (Penn et al., 1997). These complexes were identified in the phloem sap of these plants and are assumed to be the basis for the increased B efficiency of these plants (Hu et al., 1997). Genetically modified tobacco plants with enhanced sorbitol synthesis were shown to transport B in their phloem, whereas control plants did not (Bellaloui et al., 1999; Brown et al., 1999).

Despite these important functions of mannitol or sorbitol in higher plant physiology, little is known about the proteins involved in phloem loading of polyols—only the mannitol transporter AgMAT1 is thought to be involve in phloem loading (Noiraud et al., 2001)—and nothing is known about the identity of the cells catalyzing this step. Common plantain, a sorbitol-translocating plant (Wallart, 1981; Lohaus and Fischer, 2002), is highly resistant to drought, trampling, and other environmental stresses. Moreover, vascular tissue is easily purified from common plantain leaves and has been used to clone and characterize the Suc transporters PmSUC2 (Gahrtz et al., 1994; Stadler et al., 1995a) and PmSUC3 (Barth et al., 2003). Here, we describe the identification, characterization, and cellular localization of two phloem-localized sorbitol transporters from plantain, an important step toward the understanding of potential physiological roles of sorbitol in higher plants.

## RESULTS

### Cloning of Two Polyol Transporter (PLT) cDNAs

The only characterized plant PLT putatively involved in phloem loading is the product of the *AgMAT1* cDNA from celery (Noiraud et al., 2001), a Suc and mannitol translocating plant. Homologous cDNAs encoding sorbitol transporters were identified in fruits of sour cherry (Gao et al., 2003), and related genes have also been found in plants that neither transport polyols inside their phloem nor store polyols, such as in Arabidopsis (Munich Information Center for Protein Sequences nos. At2g16120, At2g20780, At2g16130, At3g18830, At2g18480, and At4g36670) and sugar beet (accession nos. U64902 and U64903). None of the encoded gene products has been characterized so far, but the presence of these genes suggests that they may have functions different from phloem loading and that mannitol or similar substrates may be transported in these plants under specific physiological conditions.

AgMAT1, PcSOT1, PcSOT2, and the uncharacterized proteins from Arabidopsis and sugar beet share a high degree of similarity (about 70% similarity on the protein level). Therefore, we hoped that a low-stringency screening (Sauer et al., 1990) of a vascular tissue-specific cDNA library (Gahrtz et al., 1994) from sorbitol-translocating common plantain (Wallart, 1981; Lohaus and Fischer, 2002) with an *AgMAT1*-derived probe might identify cDNAs potentially encoding transporters involved in the phloem loading of sorbitol.

After the first screening, 10 to 15 positive signals were obtained per filter (7,000 plaque forming units), suggesting that between 0.05% and 0.1% of the clones in this library may encode PLT-like sequences. This was confirmed by sequencing the inserts of numerous randomly chosen positive λ-clones. All sequences could be assigned to two different, highly homologous cDNAs. The genes were named *P. major* PLT 1 and 2 (*PmPLT1* and *PmPLT2*). The encoded proteins (Fig. 1A) are 529 amino acids (PmPLT1) and 530 amino acids (PmPLT2) long and share 83.0% identical amino acids. Moreover, they share 67.5% (PmPLT1) and 65.8% (PmPLT2) identity with AgMAT1. The number of identical amino acids shared with the cherry sorbitol transporters are similar.

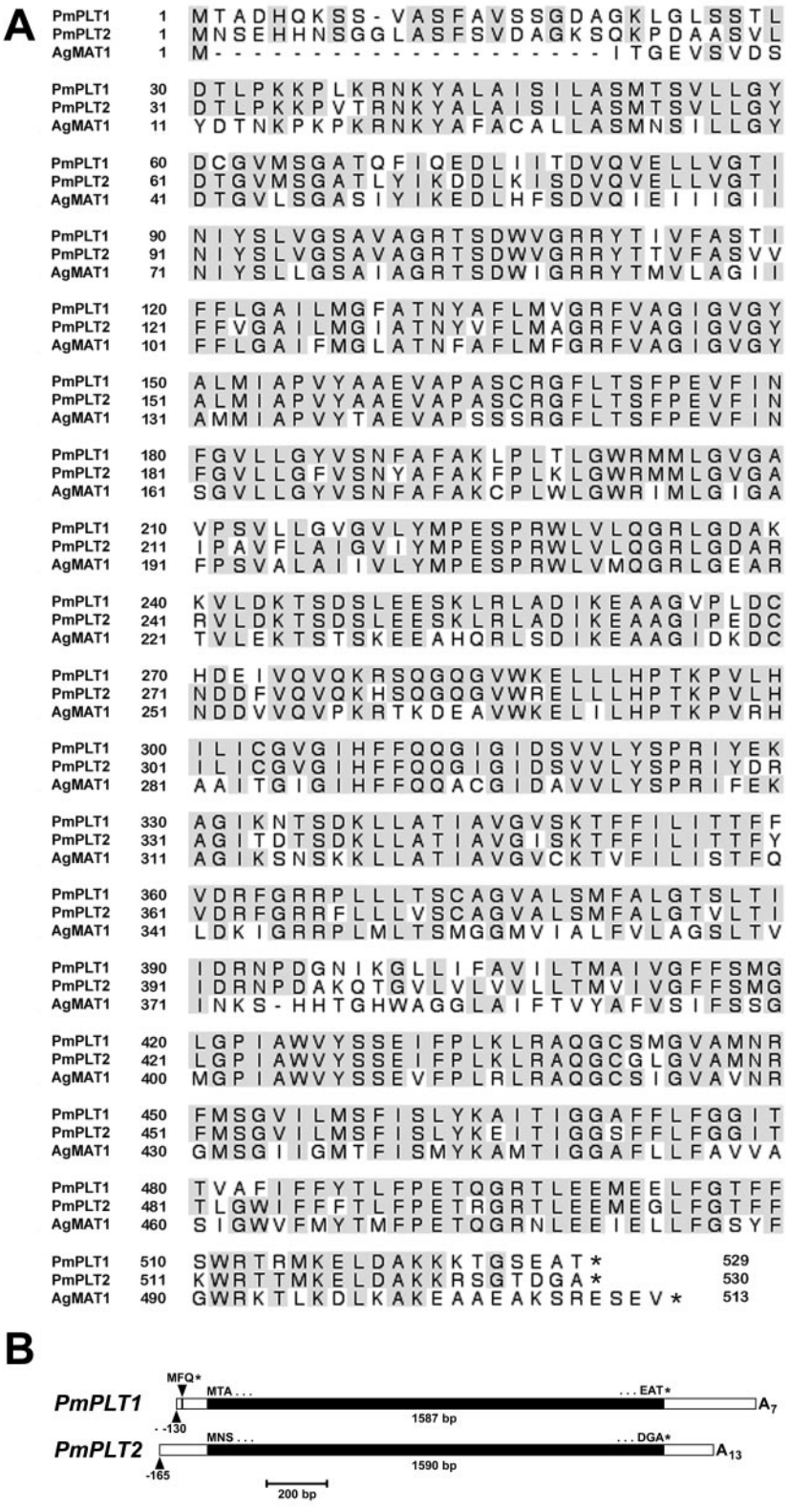


**Figure 1.** Comparison of PmPLT1, PmPLT2 (sorbitol transporters), and AgMAT1 (mannitol transporter) protein sequences and of the cDNA structures of *PmPLT1* and *PmPLT2*. A, Amino acid sequences of PmPLT1, PmPLT2, and AgMAT1 were aligned with the program SeqVu (James Gardner, Garvan Institute of Medical Research, Sydney), and residues identical in all three sequences were highlighted. B, The structure of the longest *PmPLT1* and *PmPLT2* cDNAs are presented including the information from the 5′-RACE reactions. Arrowheads indicate the transcriptional start sites and the start (−111 bp) of the short ORF in the 5′-untranslated region of PmPLT1. The complete cDNA sequences were deposited in the EMBL data library. Accession numbers are AJ532589 (*PmPLT1*) and AJ532590 (*PmPLT2*).

Interestingly, the longest cDNA of *PmPLT1* (1,987 bp) with 115-bp 5′-flanking sequence and 285-bp 3′-flanking sequence contained a short open reading frame (ORF) for the tripeptide Met-Phe-Gln starting 111 bp upstream from the predicted start-ATG of the cDNA. Such a 5′-ORF was absent from the 5′-flanking sequence of the longest *PmPLT2* cDNA (1,891 bp with 145-bp 5′-flanking sequence and

156-bp 3′-flanking sequence). To test, whether this short 5′-ORF in *PmPLT1* corresponds to the C terminus of an even longer ORF and whether a similar 5′-ORF is present in the complete 5′-untranslated sequence of *PmPLT2*, 5′-RACEs were performed with total RNA from common plantain vascular tissue. The *PmPLT1*-specific RACE-reactions showed that translation of the *PmPLT1* gene starts at position −130 bp and that the 5′-ORF encodes only the tripeptide Met-Phe-Gln (Fig. 1B). The *PmPLT2*-specific 5′-RACE reactions showed that translation in the *PmPLT2* gene starts at −165 and that the corresponding mRNA does not have a 5′-ORF (Fig. 1B).

### Functional Expression in Yeast Depends on the 5′-Flanking Sequences

It had been claimed that acyclic polyols cannot be metabolized by Brewer's yeast (*Saccharomyces cerevisiae*; Canh et al., 1975). This was disproven later by the observation that bakers' yeast can induce expression of the sorbitol dehydrogenase gene, SDH1, when grown on sorbitol as the sole carbon source for at least 2 weeks (Sarthy et al., 1994). Such a delayed induction of sorbitol catabolism does not interfere with sorbitol transport tests performed with Glc-grown yeast cells, where endogenous genes for polyol uptake and metabolism stay repressed. Therefore, transport properties of PmPLT1 and PmPLT2 were analyzed by expressing of the longest cDNAs in the bakers' yeast strain SEY2102 (Emr et al., 1983) in sense and antisense orientation in the unique *Eco*RI-site of the NEV-E expression vector (Sauer and Stolz, 1994).

However, uptake analyses with $^{14}$C-sorbitol showed no detectable transport activity for any of the sense transformants (data not shown). For PmPLT1, this might be explained by the presence of the 5′-ORF described above. Therefore, truncated clones were generated by PCR lacking this 5′-ORF. But again, no transport activities could be observed after NEV-E-based expression of these cDNAs in yeast (data not shown). In a final attempt, cDNA constructs were generated for *PmPLT1* and *PmPLT2* with modified 5′-flanking sequences. This approach had been applied successfully before (Stadler et al., 1995b) and replaces the 5′-flanking sequence of a given cDNA by the sequence AAGCTTGTAAAAGAA*ATG*. This sequence was taken from the 5′-flanking region of *AtSTP1*, the first higher plant transporter successfully expressed in yeast (Sauer et al., 1990). This sequence seems to be ideal for the bakers' yeast translation machinery and fits well to the consensus sequence (A/Y) A(A/Y) A(A/Y) A*ATG* published for bakers' yeast (Hinnebusch and Liebman, 1991). With the modified *PmPLT1* and *PmPLT2* cDNAs, a third set of sense and antisense yeast lines was generated for and transport of $^{14}$C-sorbitol was analyzed.

Obviously, the native 5′-flanking sequences of both cDNAs were the reason for the observed lack in expression with the first two sets of constructs. Sense yeast strains harboring *PmPLT1* (strain MRYs1) or *PmPLT2* (strain MRYs2) cDNA constructs with modified 5′-flanking sequences expressed the cDNAs and were able to incorporate $^{14}$C-sorbitol (Fig. 2). No transport activity was observed in control strains harboring the cDNAs in antisense direction (strains MRYas1 and MRYas2).

### Transport Properties and Kinetic Parameters

All previously analyzed plant sugar transporters as well as the celery mannitol transporter were described as energy-dependent $H^+$ symporters driven by the proton motive force (*pmf*) across the plasma membrane (Boorer et al., 1994, 1996; Williams et al., 2000; Noiraud et al., 2001). It was, therefore, expected that sorbitol transport by PmPLT1 and PmPLT2 might also be energy dependent. A first clue came from the observation that $^{14}$C-sorbitol transport in transgenic yeast was enhanced in the presence of Glc (Fig. 2). This has also been described for Suc transporters expressed in yeast cells (Riesmeier et al., 1992; Gahrtz et al., 1994; Sauer and Stolz, 1994), and the idea is that Glc metabolism provides energy for active transport of non-metabolizable substrates or activates the plasma membrane $H^+$-ATPase.

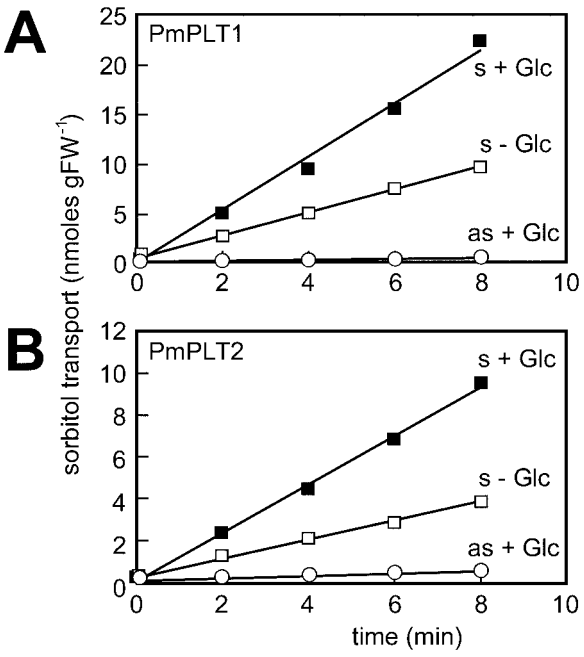


**Figure 2.** *PmPLT1* and *PmPLT2* can be expressed in yeast cells and catalyze the uptake of $^{14}$C-sorbitol. Transport rates for $^{14}$C-sorbitol were determined with the transgenic yeast cells MRYs1 and MRYas1 (expressing *PmPLT1* in sense or antisense orientation) or with MRYs2 and MRYas2 (expressing *PmPLT2* in sense or antisense orientation). The concentration of $^{14}$C-labeled sorbitol was 0.1 mM in all experiments. Where indicated, D-Glc was added to a final concentration of 10 mM.

In addition, active sorbitol transport by PmPLT1 was shown more directly by comparing intracellular and extracellular sorbitol concentrations in MRYs1 cells after a 60-min incubation in 0.1 mM $^{14}$C-sorbitol. During this time, the extracellular concentration of $^{14}$C-sorbitol was reduced to 0.075 mM, and from the incorporated amount of label, it was calculated that the cells should have an intracellular sorbitol concentration of 1.6 mM sorbitol, if sorbitol is not metabolized. This was confirmed by thin-layer chromatography of cellular extracts showing that the entire incorporated label was still $^{14}$C-sorbitol (Fig. 3). Thus, accumulation of sorbitol inside the yeast cells was more than 20-fold, which strongly supports an active transport mechanism by PmPLT1.

Finally, analyses of the sensitivities of PmPLT1 and PmPLT2 to uncouplers of proton gradients, such as carbonyl cyanide-*m*-chlorophenylhydrazone and dinitrophenol, confirmed that this active transport is driven by the proton motive force (Fig. 4).

PmPLT1 is also sensitive to the SH-group inhibitor *p*-(chloromercuri) benzene sulfonic acid (PCMBS; Fig. 4A), whereas PmPLT2 is not (Fig. 4B). So far, PCMBS was known to inhibit the activity of plant Suc transporters with high specificity (Riesmeier et al., 1992; Sauer and Stolz, 1994) but not the activity of plant monosaccharide transporters (Ludwig et al., 2000). For mannitol transport in celery, it has been reported that the transporter is not (Salmon et al., 1995) or is only slightly (Noiraud et al., 2001) inhibited by PCMBS; the sorbitol transporters from cherry

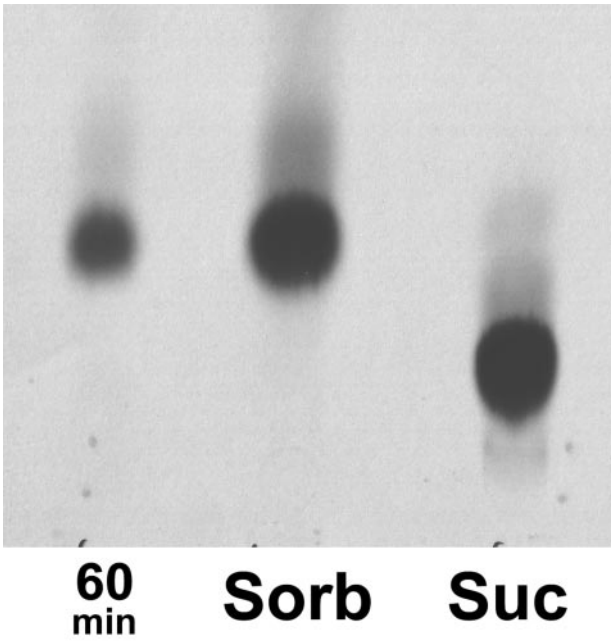


**Figure 3.** Thin-layer chromatography of $^{14}$C-sorbitol accumulated in *PmPLT1*-expressing yeast cells. Cell extracts prepared with 80% (v/v) ethanol from yeast strain MRYs1 after a 60-min incubation in $^{14}$C-labeled sorbitol (60 min). $^{14}$C-Sorbitol (Sorb) and $^{14}$C-Suc (Suc) were used as standards.

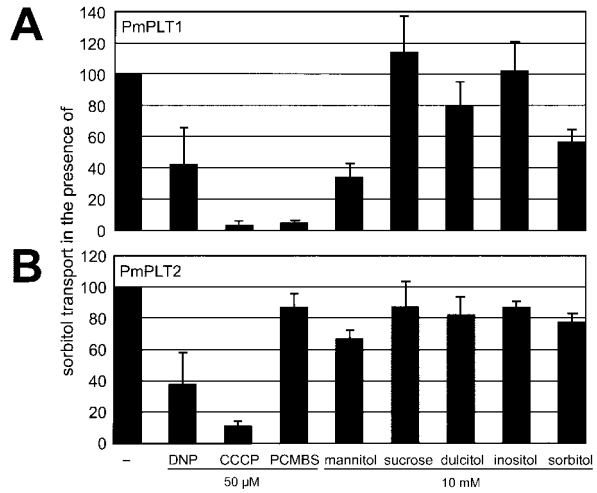


**Figure 4.** Transport properties of PmPLT1 and PmPLT2 in yeast cells. Transport of $^{14}$C-sorbitol (0.1 mM initial outside concentration) was analyzed in the presence of uncouplers (dinitrophenol or carbonyl cyanide-*m*-chlorophenylhydrazone) or in the presence of the SH-group inhibitor PCMBS. Inhibitors were added to a final concentration of 50 $\mu$M. Transport of 0.1 mM $^{14}$C-sorbitol was also analyzed in the presence of potential substrates added at a 100-fold excess (final concentrations 10 mM). Each bar results from at least three independent analyses (mean ± SD).

were not sensitive to PCMBS (Gao et al., 2003). The observed PCMBS sensitivity of PmPLT1 can be explained by comparing the Cys residues in PmPLT1 (six Cys residues) and PmPLT2 (five Cys residues). All five Cys residues found in PmPLT2 are conserved in PmPLT1. The sixth Cys is specific for PmPLT1 ($Cys_{61}$ in Fig. 1) and is located in the predicted first extracellular loop between transmembrane helices 1 and 2. At this position, it seems to be accessible for the SH-group inhibitor. This Cys is not conserved in AgMAT1 (six Cys residues), PcSOT1 (five Cys residues), or PcSOT2 (six Cys residues) explaining the poor inhibition of these transporters by PCMBS (Noiraud et al., 2001).

Competition of $^{14}$C-sorbitol uptake with other compounds, such as unlabeled sorbitol, mannitol, dulcitol, inositol, or Suc (Fig. 4) revealed little effect of any of these compounds on $^{14}$C-sorbitol transport by PmPLT2, whereas a significant inhibition was observed for mannitol and unlabeled sorbitol on PmPLT1-driven $^{14}$C-sorbitol transport. On one hand, the observed lack of inhibition with PmPLT2 was in agreement with the high specificity described for the sorbitol transporters in cherry (Gao et al., 2003) and with earlier results from Salmon et al. (1995). These latter authors analyzed mannitol transport in plasma membrane vesicles prepared from celery phloem tissue and showed that a 20-fold excess of sorbitol had no inhibitory effect on $^{3}$H-mannitol transport. On the other hand, more recent analyses of recombinant AgMAT1 protein showed strong inhibition of mannitol transport by other sugar alcohols, such as sorbitol, xylitol, or dulcitol (Noiraud et al., 2001). Therefore,

the mannitol transport capacity of *PmPLT1*- and *PmPLT2*-expressing yeast cells was tested directly using radiolabeled $^{14}$C-mannitol. Interestingly, both common plantain transporters catalyzed the transport of $^{14}$C-mannitol despite a poor inhibition of $^{14}$C-sorbitol transport by unlabeled mannitol in MRYs1. But again, the transport of $^{14}$C-mannitol (initial concentration 0.1 mM) was hardly inhibited by a 10-fold excess of unlabeled sorbitol (data not shown).

This result can only be explained with $K_m$ values that are significantly higher than the $K_m$ values published for AgMAT1 ($K_m$ = 0.3 mM) or PcSOT1 ($K_m$ = 0.6 mM) and PcSOT2 ($K_m$ = 0.3 mM). In this case, unlabeled polyol could be transported in addition to but not in competition with a second $^{14}$C-labeled polyol.

Analysis of the $K_m$ values confirmed this interpretation of the competition data. Figure 5 shows that the $K_m$ value for sorbitol of PmPLT1 is 12.3 $\pm$ 0.9 mM and even higher for PmPLT2 (the $K_m$ values for mannitol are about 5 and 30 mM for PmPLT1 and PmPLT2 in the yeast system; average of two analyses; data not shown). Thus, the $K_m$ values for both tested substrates are 1 to 2 orders of magnitude higher than the $K_m$ values of AgMAT1 (Noiraud et al., 2001) or the PcSOTs (Gao et al., 2003). These results characterize both common plantain PLTs as low-specificity and low-affinity sorbitol transporters.

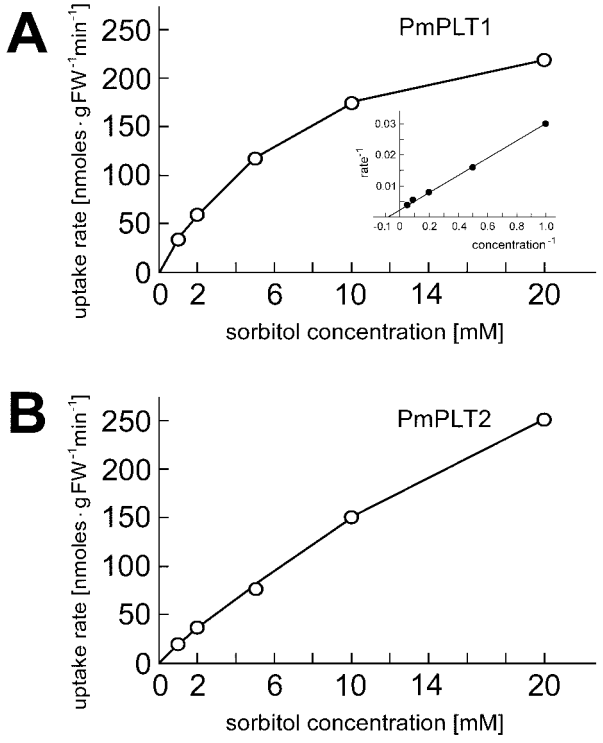


**Figure 5.** Analysis of substrate affinities of PmPLT1 and PmPLT2 for sorbitol in transgenic yeast cells. A, Michaelis-Menten plot for the sorbitol uptake by PmPLT1. Inset, Lineweaver-Burk plot of the same data set. B, Michaelis-Menten plot for the sorbitol uptake by PmPLT2. Uptake rates could not be saturated under the conditions analyzed. Each curve represents one out of three independent transport tests. From these analyses, the $K_m$ value for sorbitol of PmPLT1 was calculated to be 12.3 $\pm$ 0.9 mM. No $K_m$ value could be calculated for PmPLT2.

### Functional Expression in *Xenopus* sp. Oocytes

The accumulation of sorbiol in *PmPLT*-expressing yeast cells, the sensitivity of polyol transport to uncouplers, and the increased transport rates in the presence of D-Glc provide indirect evidence for $H^+$ polyol transport. For a direct analysis of the potential driving force, PmPLT1 transport was also analyzed in *Xenopus* sp. oocytes expressing injected *PmPLT1* cRNA.

Inward currents were obtained in the presence of 30 mM sorbitol or mannitol, but little or no currents were observed with myoinositol (Fig. 6A) or Suc (data not shown) confirming the specificity of PmPLT1 for linear polyols. Due to the higher currents obtained with mannitol, this polyol was used for all further analyses. The mannitol-derived currents increased over a wide range of concentrations (Fig. 6B). $K_m$ values for mannitol (18.03 $\pm$ 2.38 mM at 0 mV, 16.94 $\pm$ 2.03 mM at $-60$ mV, and 15.15 $\pm$ 1.97 mM at $-120$ mV; mean $\pm$ SD; Fig. 6C) as well as analyses at different membrane potentials (Fig. 6D) revealed the dependence of this low-affinity transporter of the membrane potential. The slightly lower $K_m$ value (5 mM) that was determined for mannitol in the yeast system may reflect a higher membrane potential and other differences between the two expression systems.

Figure 6, D and E, show that mannitol import by PmPLT1 is also proton dependent, and that PmPLT1 has a pH optimum at about pH 6.5. Addition of 10 mM $Na^+$ did not alter the polyol-induced currents (data not shown).

### Immunolocalization of the Sorbitol Transporters in Planta

The large number of *PmPLT1* and *PmPLT2* cDNAs identified within the vascular tissue-specific library (0.05%–0.1% of all clones) suggests that both encoded proteins are strongly expressed in the phloem and involved in phloem loading of sorbitol. However, for a detailed understanding of their physiological function it is necessary to identify the precise cell type(s) where each of these genes is expressed. Therefore, antibodies were raised against peptides corresponding to the very N termini and the very C termini of the two transporters (amino acids 1–11 and 522–529 of PmPLT1 and amino acids 1–12 and 523–530 of PmPLT2). The specificity of the obtained antisera was tested on cross sections of the yeast strains MRYs1 (expresses *PmPLT1*) and MRYs2 (expresses *PmPLT2*). Figure 7 shows that the anti-PmPLT1 antiserum binds only to sections of yeast strain MRYs1 but not

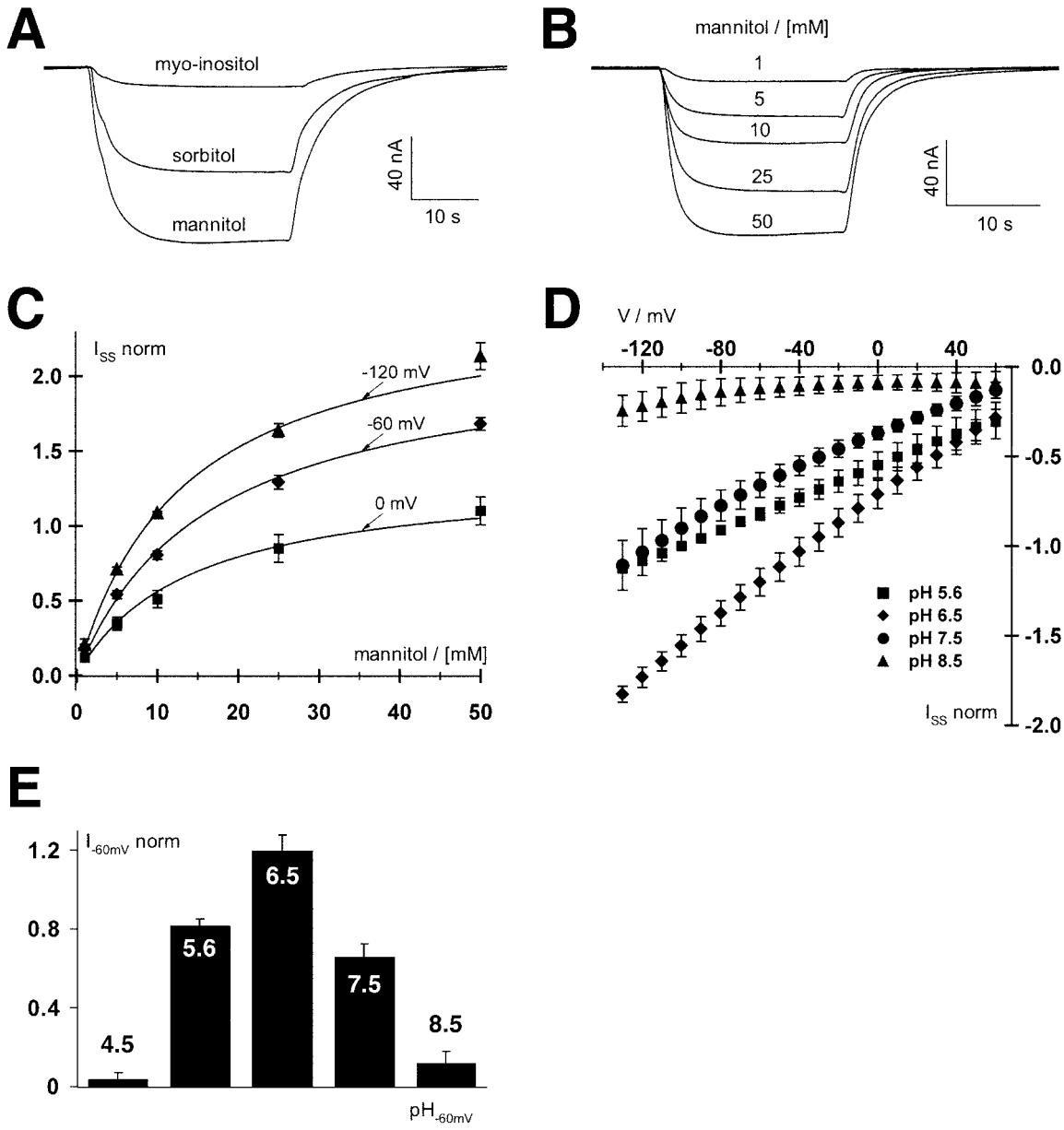


**Figure 6.** Biophysical analyses of PmPLT1 expressed in *Xenopus* sp. oocytes with the double-electrode voltage clamp technique. A, Polyol-induced inward $H^+$ currents mediated by *PmPLT1*-injected oocytes. Increase in $H^+$ currents in response to 30-s pulses of 30 mM mannitol, sorbitol, or myoinositol at pH 5.6 at a holding potential of −60 mV. Only mannitol and sorbitol but not myoinositol are substrates of PmPLT1. Relative currents were: $I_{mannitol} = 1$, $I_{sorbitol} = 0.66 \pm 0.11$, and $I_{myoinositol} = 0.12 \pm 0.05$ (data points were normalized to the currents at −60 mV in 30 mM mannitol; mean ± SD, $n = 4$). B, Whole-cell currents through PmPLT1 in response to a stepwise increase of mannitol concentration at pH 5.6 and a holding potential of −60 mV. C, Michaelis-Menten kinetics of PmPLT1 for mannitol at membrane potentials of 0, −60, and −120 mV. Data points represent the mean ± SD of five independent experiments normalized to the currents at −100 mV in 10 mM mannitol. Currents in the absence of mannitol were subtracted for leak correction. Continuous lines show the best nonlinear regression fits of the data points to the Michaelis-Menten equation. D and E, Mannitol-induced currents of oocytes injected with *PmPLT1* cDNA are voltage and pH dependent. D, Whole-cell steady-state currents ($I_{SS}$) in response to 10-mV voltage steps from 60 to −130 mV were recorded upon perfusion with 10 mM mannitol solutions at varying pH values from 4.5 to 8.5, as indicated. E, The pH optimum of PmPLT1 (determined at −120 mV) is 6.5. Data points represent mean ± SD, $n = 4$. Normalization to the currents at −100 mV in pH 5.6 and leak subtraction were performed as in C.

to sections of MRYs2 cells. Vice versa, anti-PmPLT2 antiserum binds only to sections of yeast strain MRYs2 but not to sections of MRYs1 cells. This shows the specificity of both antisera that were now used for immunolocalization of PmPLT1 and PmPLT2 in sections of common plantain source leaves.

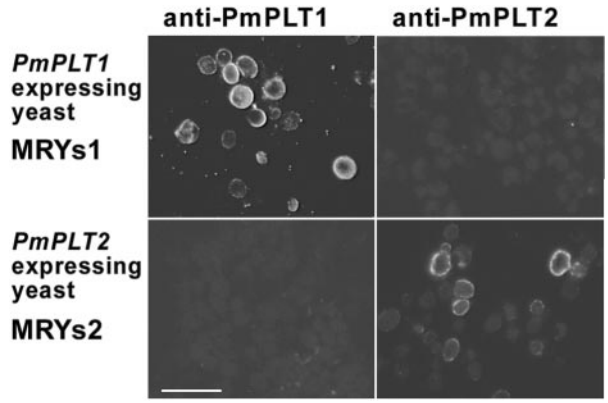


**Figure 7.** Specificity of anti-PmPLT1 and anti-PmPLT2 antisera. Sections of the *PmPLT1*-expressing yeast strain MRYs1 and the *PmPLT2*-expressing strain MRYs2 were fixed and embedded under the same conditions that were used for common plantain leaf material (Fig. 7). Sections were treated with anti-PmPLT1 or anti-PmPLT2 antiserum. Binding of antibody was detected under a fluorescence microscope by decoration with a fluorescent goat anti-rabbit IgG antiserum. Scale bar = 10 $\mu$m.

Figure 8A shows a cross section through a common plantain leaf treated with anti-PmPLT1 antiserum and decorated with Alexa Fluor 488-conjugated goat anti-rabbit IgG. Green fluorescence is clearly visible in individual cells of the phloem, suggesting that the labeled cells are part of the SE/CCC. Similar results were obtained with anti-PmPLT2 antiserum (data not shown). For a further characterization of the precise cell type, sections were double-stained with anti-PmPLT1 antiserum and with the monoclonal anti-PmSUC2 1A2 (Stolz et al., 1999). For detection of antibody binding, sections were decorated with Alexa Fluor 488-conjugated goat anti-rabbit IgG (green fluorescence, localization of PmPLT1 or PmPLT2) and with Alexa Fluor 546-conjugated goat anti-mouse IgG (red fluorescence, localization of PmSUC2). PmSUC2 has previously been documented as a companion cell-specific Suc transporter by immunodetection (Stadler et al., 1995a) and can thus be used as an internal standard for the common plantain vascular system.

Figure 8, B and C, clearly shows that PmSUC2 and PmPLT1 are localized within the very same cell type of the common plantain phloem. In contrast to the vascular bundle shown in Figure 8A, this section is from a larger bundle, where phloem is already seen on both sides of the xylem. The green fluorescence in Figure 8B results from the immunodetection of PmPLT1 and is identical to the PmSUC2-specific red fluorescence in Figure 8C. The identical result was obtained in double labeling-analyses with anti-PmPLT2 and anti-PmSUC2 antisera (Fig. 8, D and E). The green fluorescence in Figure 8D results from the immunodetection of PmPLT2 and is identical to the PmSUC2-specific red fluorescence in Figure 8E. These data show that the PLT genes *PmPLT1* and *PmPLT2* are expressed in the companion cells of the common plantain phloem.

In our immunohistochemical analyses, we found that sometimes, especially in smaller and medium-sized common plantain vascular bundles, not all companion cells that were labeled with the anti-PmSUC2 antiserum were also labeled with the antisera raised against PmPLT1 or PmPLT2 (Fig. 9). Typically, companion cells that were labeled only by the monoclonal anti-PmSUC2 antibody seem to have higher levels of PmSUC2 protein than the other companion cells (i.e. stronger red fluorescence). Moreover, these "PmSUC2-only companion cells" are more frequently seen in the vicinity of the xylem, whereas the "PmSUC2-plus-PmPLT companion cells" are concentrated on the side of the phloem adjacent to the mesophyll (Fig. 9, B and D). One example for such a "PmSUC2-only" companion cell is also seen in the medium-sized vascular bundle shown in Figure 8D, where part of the strong PmSUC2-specific fluorescence is seen even with the filter for the green PmPLT2 signal.

## DISCUSSION

This paper describes the molecular cloning and functional characterization of two higher plant sorbitol transporters and for the first time, to our knowledge, the immunohistochemical localization of the corresponding proteins. Moreover, the presented immunohistochemical data provide the first direct evidence for the existence of different types of companion cells in smaller veins during phloem development.

The model plant used for these analyses was common plantain, a dicot plant that allows simple isolation of pure vascular tissue (Gahrtz et al., 1994) and that is known to transport Suc and sorbitol in its phloem (Wallart, 1981; Lohaus and Fischer, 2002). The common plantain Suc transporters PmSUC1, PmSUC2, and PmSUC3 have been characterized (Gahrtz et al., 1994, 1996; Barth et al., 2003), and PmSUC2 was the first plant Suc transporter that has been localized on the cellular level (Stadler et al., 1995a). In the present paper, the analysis of the common plantain phloem is extended by the detailed characterization of two sorbitol transporters, PmPLT1 and PmPLT2. These two transporters differ in several functional properties, such as their $K_m$, their sensitivity to PCMBS, their substrate specificity, or their response to Glc, from the previously described PLTs PcSOT1 and PcSOT2 from cherry (Gao et al., 2003).

### PmPLT1 and PmPLT2 Are Low-Affinity $H^+$ Symporters

Functional analyses of PmPLT1 and PmPLT2 in the yeast expression system clearly demonstrate that both transporters catalyze the transport of sorbitol, the polyol transported in the common plantain phloem (Fig. 2). Both transporters can also mediate

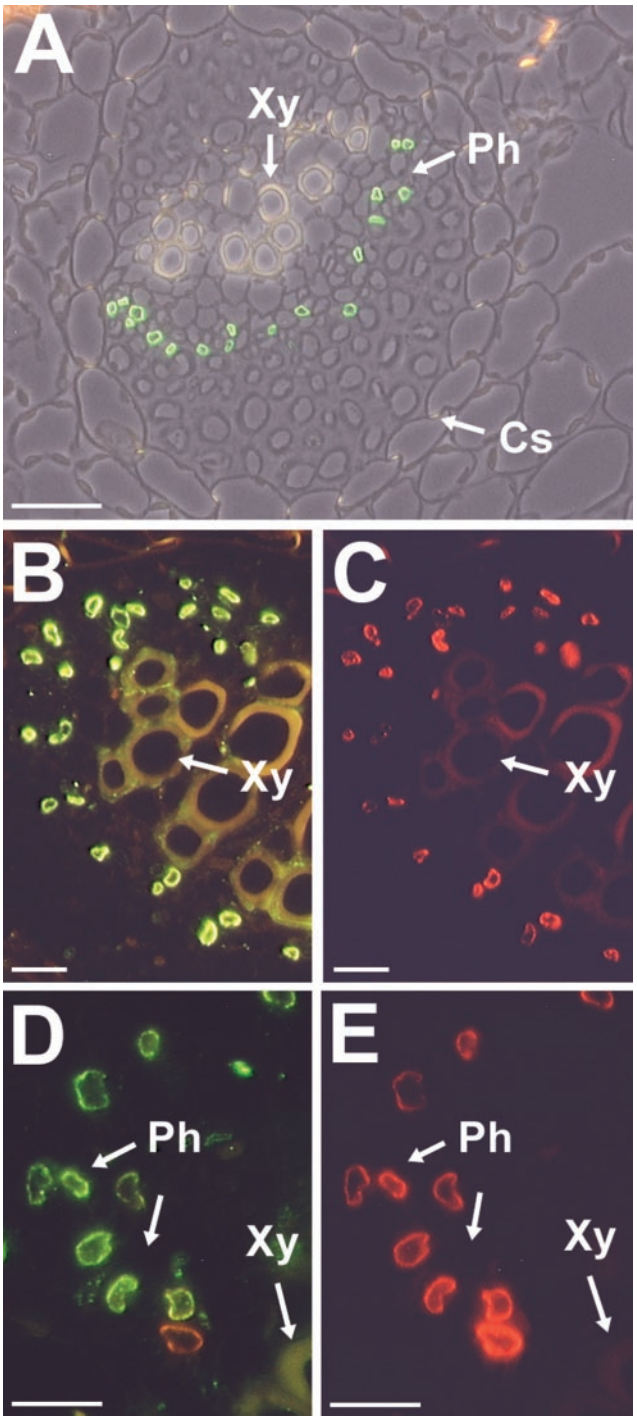


**Figure 8.** Immunodetection of PmPLT1 and PmPLT2 proteins in sections from common plantain source leaves. A, The section was labeled with anti-PmPLT1 antiserum and with fluorescent goat anti-rabbit IgG antiserum. The resulting green fluorescence is found only in cells of the common plantain phloem. For this figure, a fluorescence image was superposed on a photo taken under white light. Similar results were obtained with sections treated with anti-PmPLT2 antiserum and with fluorescent goat anti-rabbit IgG antiserum (data not shown). B and C, The presented section was double labeled with anti-PmPLT1 antiserum (B) and with the monoclonal anti-PmSUC2 antiserum 1A2 (C). Binding of antibodies was visualized under a fluorescent microscope after simultaneous incubation with fluorescent goat anti-rabbit IgG antiserum (B; green fluorescence, PmPLT1 localization) and fluorescent goat anti-mouse IgG antiserum (C; red fluorescence, PmSUC2 localization in companion cells). D and E, The presented section was double labeled with anti-PmPLT2 antiserum in D and with the monoclonal anti-PmSUC2 antiserum 1A2 in E. Binding of antibodies was visualized under a fluorescent microscope after simultaneous incubation with fluorescent goat anti-rabbit IgG antiserum (D; green fluorescence, PmPLT2 localization) and fluorescent goat anti-mouse IgG antiserum (E; red fluorescence, PmSUC2 localization in companion cells). The weak orange signal in one of the companion cells in D results from the extremely strong PmSUC2 signal of this cell, which is seen in E. Xy, Xylem; Ph, phloem; Cs, Casparian stripes. Scale bars = 25 $\mu$m in A, 10 $\mu$m in B and C, and 10 $\mu$m in D and E.

the uptake of mannitol (data not shown; Fig. 3) and, therefore, it seems sensible to name these genes PLT1 and PLT2, although their physiological function is the transport of sorbitol. A low specificity for polyols was also described for the AgMAT1 mannitol transporter from celery (Noiraud et al., 2001), whereas a high specificity was found for the sour cherry sorbitol transporters (Gao et al., 2003).

In contrast to all previously described PLTs with $K_m$ values below 1 mM, PmPLT1 has a $K_m$ value for its physiological substrate sorbitol of 12 mM (Fig. 5), and the $K_m$ value for PmPLT2 seems to be even higher, because no saturation was observed over the concentration range analyzed (Fig. 5). Similar results were obtained for mannitol (yeast data not shown; Fig. 6). These substrate affinities are in the same order of magnitude as the $K_m$ values described for sorbitol transport in apple (*Malus domestica*) tissue (35–55 mM; Berüter, 1997) and in the same range like the $K_m$ value for phloem loading with sorbitol calculated from modeled carbon fluxes in a mature peach leaf (Moing et al., 1994). This not only shows that the common plantain sorbitol transporters have a more than 40- to 100-fold lower affinity than the proteins encoded by the previously cloned PLT cDNAs, but it also suggests different mechanism for the regulation of phloem loading with mannitol in celery and with sorbitol in common plantain. In celery, mannitol synthesis stays constant under stress, and the increase in root mannitol concentrations of stressed celery plants results from reduced mannitol catabolism (Everard et al., 1994; Stoop and Pharr, 1994a, 1994b). If AgMAT1 is responsible for phloem loading, maximal transport rates are reached already at 1 mM mannitol in the apoplast (Noiraud et al., 2001), which is ideal for a system where polyol synthesis is constant under stressed and unstressed conditions. In common plantain, however, a set of two transporters could respond with increased phloem loading rates to increasing apoplastic sorbitol concentrations between 0 and 100 mM. Therefore, it will be interesting to investigate whether in common plantain leaves the synthesis of sorbitol and its supply to the apoplastic space is increased under stress conditions.

Both common plantain transporters are highly sensitive to uncouplers of proton gradients (Fig. 4), both

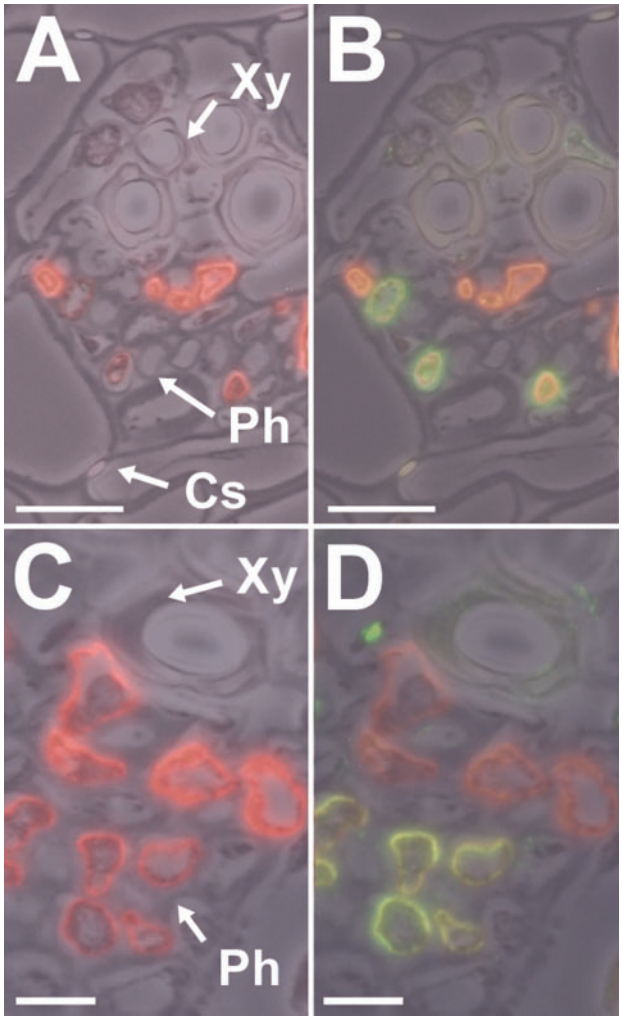


**Figure 9.** Immunodetection of PmPLT1 and PmPLT2 proteins in medium-sized veins of common plantain source leaves. A, Immunolocalization of PmSUC2 Suc transporter protein (red fluorescence) by immunodetection with the anti-PmSUC2 monoclonal antibody 1A2 in a small vein from a common plantain leaf. B, Additional labeling of the section shown in A with anti-PmPLT1 antiserum (green fluorescence). C, Immunolocalization of PmSUC2 Suc transporter protein (red fluorescence) by immunodetection with the anti-PmSUC2 monoclonal antibody 1A2 in a small vein from a common plantain leaf. D, Additional labeling of the section shown in C with anti-PmPLT2 antiserum (green fluorescence). Xy, Xylem; Ph, phloem; Cs, Casparian stripes. For the presented figures one (A and C) or two (B and D) fluorescence images were superposed on a photo taken under white light. Scale bars = 10 $\mu$m in A and B, and 5 $\mu$m in C and D.

show increased transport rates, when Glc is added to activate the yeast plasma membrane ATPase in the recombinant yeast cells MRYs1 and MRYs2 (Fig. 2), and PmPLT1 was shown to accumulate sorbitol more than 20-fold inside the yeast strain MRYs1 (Fig. 3). A similar accumulation of sorbitol inside MRYs2 cells could be shown for PmPLT2 (data not shown). Taken together, these data suggest that both common plantain sorbitol transporters mediate an energy-dependent $H^+$ sorbitol symport.

Direct proof for a $H^+$ symport mechanism was obtained by expressing *PmPLT1* in *Xenopus* sp. oocytes (Fig. 6). The observed inward currents were only obtained with mannitol and sorbitol, increased at higher substrate concentrations and with increasing membrane potentials, and did not respond to variations in the $Na^+$ concentration. This demonstrates that the uptake of polyols depends on the electrical potential ($\Delta\psi$) and on the protongradient ($\Delta$pH) across the plasma membrane.

Noiraud et al. (2001) and Gao et al. (2003) found a strong inhibition of polyol transport by D-Glc and D-Fru. This unexpected observation could not really be explained, and the authors speculated that the inhibition of AgMAT1 or of PcSOTs by D-Glc does not result from Glc uptake via the mannitol transporter and may thus rather be an artifact of the yeast system (Noiraud et al., 2001; Gao et al., 2003). The effect of D-Glc is totally different for the common plantain sorbitol transporters PmPLT1 and PmPLT2. Sorbitol transport (Fig. 2) and mannitol transport (data not shown) are significantly enhanced in the presence of D-Glc. This is identical to previous analyses of plant Suc transporters in the yeast system (e.g. Gahrtz et al., 1994; Barth et al., 2003).

PmPLT1 has a consensus sequences for *N*-glycosylation at $Asn_{334}$ (Fig. 1). This sequence is located in the predicted extracellular loop between the transmembrane helices 7 and 8 and is not conserved in PmPLT2 or in any of the other cloned PLTs. During secretion, it might be exposed to the lumen of the endoplasmic reticulum and be glycosylated. However, western-blot analyses with plasma membrane extracts from the recombinant yeast strains MRYs1 and MRYs2 showed no difference between the apparent $M_r$ of PmPLT1 and PmPLT2, suggesting that this site in PmPLT1 is not used for *N*-glycosylation (data not shown).

### PmPLT1 Is Sensitive to PCMBS

An interesting observation is the inhibition of PmPLT1-driven but not of PmPLT2-driven sorbitol transport by PCMBS (Fig. 4). A comparison of the deduced protein sequences shows that there is one extra Cys residue in PmPLT1 that is exposed to the predicted extracellular side of the protein. The observed inhibition can only be explained by PCMBS binding to the unique $Cys_{61}$ in the PmPLT1 protein. This finding is not only a confirmation for the predicted topology of these proteins but may also be used for future structure/function analyses.

Most importantly, however, this difference in PCMBS sensitivity shows that inhibition of phloem loading of sorbitol (and possibly also of other substrates) by PCMBS does not allow a prediction on the mechanism of loading. The PCMBS sensitivity or insensitivity of substrate import (including sorbitol) into leaf discs of several plant species has previously been used to predict an apoplastic or symplastic

loading mechanism for the different plant species (Flora and Madore, 1996). However, our data clearly show that the PCMBS sensitivity of sorbitol transport can vary between different transporters of the very same species and the very same cell type.

### PmPLT1 and PmPLT2 Are Phloem-Specific Transporters

Although both sorbitol transporters from common plantain are highly similar (83% sequence identity on the amino acid level), it was possible to raise antisera against N- and C-terminal peptides that specifically recognize only one of the two proteins (Fig. 7). These antisera were used for immunohistochemical analyses of common plantain leaf sections. Both transporters reacted exclusively with cells located in the phloem of the vascular tissue (Fig. 8A). Double labeling of leaf sections with anti-PmPLT1 antiserum and with the monoclonal anti-PmSUC2 antibody 1A2 (Stolz et al., 1999) revealed that these cells are the companion cells of the common plantain phloem (Fig. 8, B and C). Moreover, double labeling of leaf sections with anti-PmPLT2 antiserum and with the monoclonal anti-PmSUC2 antiserum 1A2 (Stolz et al., 1999) revealed an identical localization (Fig. 8, D and E). These analyses were possible because the PmSUC2 Suc transporter had previously been located in the companion cells of the common plantain vascular tissue (Stadler et al., 1995a).

The localization of both common plantain PLTs in the companion cells demonstrates that phloem loading of both compounds transported in common plantain, sorbitol and Suc, occurs primarily in the phloem companion cells of this plant (this paper; Stadler et al., 1995a). This is supported by the observation that expression of the PLT genes is source specific. In vascular bundles of sink leaves, neither PmSUC2 nor PmPLT proteins could be identified (data not shown). Also in Arabidopsis, phloem loading is catalyzed by a companion cell-specific transporter (AtSUC2; Truernit and Sauer, 1995; Stadler and Sauer, 1996). This is what one would expect according to the anatomical facts in minor veins, where the relatively large companion cells surround the small sieve elements in the center and mediate the contact to the leaf mesophyll. Moreover, the importance of companion cell-specific phloem loading is supported by the observation that a knock out-mutant in the Arabidopsis *AtSUC2* gene (Gottwald et al., 2000) shows a severe phenotype and can hardly survive under normal growth conditions. Nevertheless, solanaceous plants, which represent the only group of plants that has been analyzed besides common plantain and Arabidopsis, seem to behave differently. All phloem Suc transporters that have been studied in different members of this family (potato, tomato, and tobacco) so far were found in the phloem sieve elements (Kühn et al., 1997; Barker et al., 2000; Weise et al., 2000). It will, therefore, be important to study the cellular localization e.g. of the celery mannitol and Suc transporters (Noiraud et al., 2000, 2001) for a better understanding of the physiological basis for these differences in the cell-specific expression of phloem loaders in different plant species.

Only recently, Barth et al. (2003) showed that common plantain has also a transport protein in its sieve elements. The Suc transporter PmSUC3 could be localized in common plantain sieve elements. Interestingly, this sieve element-specific transporter has a lower affinity to its substrate Suc than its companion cell-specific partner PmSUC2, and expression of *PmSUC3* is also seen in the sink phloem (Barth et al., 2003). It was discussed that this might be a mechanism to regulate release and retrieval of Suc along the transport phloem and in apoplastically unloading sinks.

### Smaller Veins Possess Different Types of Companion Cells

Most interestingly, not all companion cells seem to have the identical physiological function. As shown in Figure 9, certain companion cells seem to be specialized on the phloem loading of Suc, whereas others, with lower levels of PmSUC2 protein, seem to catalyze the simultaneous loading of Suc plus sorbitol. These different types of companion cells are only seen in smaller vascular bundles. Larger veins, as shown in Figure 8, or mature veins with bicollateral phloem (not shown) possess only or almost exclusively (Fig. 8, B–D) companion cells with both types of transporters. These data are likely to reflect different steps during phloem development. Obviously, the youngest SE/CCCs (next to the xylem) start with the expression of *PmSUC2*, and expression of both *PmPLT* genes is initiated only at later developmental stages. Moreover, this might be a mechanism to modulate the supply of Suc and/or sorbitol to different sink organs.

Differences between individual companion cells of the same vascular bundle have previously been described by Haritatos et al. (2000). In this paper, tobacco plants were analyzed expressing the *GUS* reporter gene under the control of the galactinol synthase promoter from melon (*Cucumis melo*). GUS histochemical staining was observed only in some of the companion cells and was absent from others, suggesting differences in the transcriptional activity for this transgene. Our data support this interpretation and represent the first direct proof for differences in the physiological functions of individual companion cells.

### Similar Transporters Are Found in Other Plant Species That Do Not Translocate Polyols in Their Phloem

Database searches revealed a group of six sequences highly homologous to PmPLT1 and PmPLT2 also in the Arabidopsis genome (Munich Information

Center for Protein Sequences nos. AtPLT1, At2g16120; AtPLT2, At2g16130; AtPLT3, At2g18480; AtPLT4, At2g20780; AtPLT5, At3g18830; and AtPLT6, At4g36670). Due to sequence identities of 50% to 66% (on the amino acid level) between these transporters and the so-far characterized PLTs (Noiraud et al., 2001; this paper), these genes are likely to encode PLTs. It will be interesting to study the physiological roles and the physiological substrates of these proteins in Arabidopsis, a plant that does not transport polyols in the phloem. Similarly, two homologous transporter genes (GenBank accession nos. U64902 and U64903) were found in sugar beet. The function of these transporters might be necessary during local polyol synthesis in specific cell types or under certain environmental conditions. The identification of the physiological roles of these genes but also the detailed physiological roles of phloem localized sorbitol transporters, such as PmPLT1 and PmPLT2, will have to be analyzed further in the future. This will include analyses in plants that do normally not translocate polyols, such as Arabidopsis, but also mutants of polyol transporting plant species.

## MATERIALS AND METHODS

### Strains

Common plantain (*Plantago major*) wild-type plants were grown in potting soil in the greenhouse under ambient conditions. For cloning in *Escherichia coli*, we used strain DH5a (Hanahan, 1983). Yeast (*Saccharomyces cerevisiae*) expression was performed with strain SEY2102 (Emr et al., 1983). For the preparation of genomic DNA, leaves of celery (*Apium graveolens*) were purchased on a local market.

### Cloning of PmPLT1 and PmPLT2 cDNAs

A common plantain cDNA library in λ-gt10 that had previously been used for the cloning of the Suc transporter cDNAs *PmSUC1* and *PmSUC2* (Gahrtz et al., 1996) was screened with a radiolabeled probe derived from the *AgMAT1* mannitol transporter gene of celery. To this end, genomic DNA was isolated from celery leaves, and a 1,700-bp *AgMAT1* genomic fragment was isolated by PCR (AgMAT1–5′ primer, 5′-AAG TAT GCT TTT GCT TGT GCT C-3′; AgMAT1–3′primer, 5′-AGC CTG TTG GAA GAA ATG AAT AC-3′). The radiolabeled probe was used to screen 120,000 pfu of the λ-gt10 library at a density of 7,000 pfu plate$^{-1}$. Phage-DNA was transferred to nitrocellulose filters, prehybridized, hybridized, and washed as described (Sauer et al., 1990). From more than 200 positive signals obtained after exposure of the filters to x-ray films (Kodak X-Omat AR, Eastman Kodak, Rochester, NY), 25 plaques were isolated and rescreened, and their *Eco*RI inserts were cloned into pGEM-T-easy (Promega, Mannheim, Germany) and sequenced. The obtained sequences turned out to result from two different common plantain mRNAs. For further analyses, the longest cDNAs for each mRNA were cloned into the *Eco*RI site of pUC19, yielding the plasmids pMR7 (*PmPLT1*) and pMR8 (*PmPLT2*). The corresponding genes were named *PmPLT1* (insert from λ-phage 5B) and *PmPLT2* (insert from λ-phage 9B).

### Analysis of 5′-Flanking Sequences by 5′-RACE

The complete 5′-flanking regions of the *PmPLT1* and *PmPLT2* cDNAs were determined using the 5′/3′-RACE kit of Roche Diagnostics (Mannheim, Germany). The nested primers PmSBT1-SP1 (5′-GAG CTT TCC GGC ATC ACC GGA G-3′), PmSBT1-SP2 (5′-CTG GTG ATC AGC AGT CAT AGT TG-3′), PmPSBT1-SP3 (5′-GGT TTA ATT GAC TAG CTA GC-3′), PmSBT2-SP1 (5′-CGT CTG GCT TTT GAG ACT TAC-3′), PmSBT2-SP2 (5′-GCC ACC GGA GTT ATG GTG TTC AC-3′), and PmSBT2-SP3 (5′-GTG TGA GCC TAC TTG TGT GTT TGG C-3′) were used to generate full-length 5′ sequences from both cDNA clones after in vitro polyadenylation of their very 5′ ends. All treatments were performed according to the manufacturer's protocol.

### Functional Expression of the cDNAs in Bakers' Yeast

For the functional expression in bakers' yeast, the *Eco*RI inserts from pMR7 and pMR8 were cloned into the unique *Eco*RI site of the yeast/*E. coli* shuttle vector NEV-E (Sauer and Stolz, 1994) in sense and antisense orientation. The four resulting plasmids were used to transform into yeast. In a second approach, the primers SBT1-5 (5′-AGT CTG CTT GAA TTC AAC TAT GAC TGC TGA TCA CCA GA-3′), SBT1-3 (5′-TCA GCA CAT AAG AAT TCT TAG GTA GCT TCA GAA CCA GT-3′), SBT2-5 (5′-ACA CTT GTT GAA TTC CCT AAC CAT CAT GAA TAG TGA AC-3′), and SBT2-3 (5′-CTC ACT ACT GAA TTC TTA GGC ACC ATC AGT ACC ACT CC-3′) were used to generate cDNAs lacking their 5′- and 3′-flanking sequences. Again, the four plasmids resulting from cloning of these cDNAs into NEV-E were used to transform yeast. In a third approach, cDNA clones were generated with a modified 5′-flanking sequence using the primers SBT1–5Eco (5′-CTC CGG AAT TCA AGC TTG TAA AAG AAA TGA CTG CTG ATC ACC AGA AGT CAA G-3′), SBT1–3, SBT2–5Eco (5′-CTC CGG AAT TCA AGC TTG TAA AAG AAA TGA ATA GTG AAC ACC ATA ACT CC-3′), and SBT2–3. Ligation into NEV-E gave the plasmids NEV::PLT1s (*PmPLT1* in sense orientation), NEV::PLT1as (*PmPLT1* in antisense orientation), NEV::PLT2s (*PmPLT2* in sense orientation), and NEV::PLT2as (*PmPLT2* in antisense orientation). These plasmids were used to transform the yeast strain SEY2102. The resulting strains were named MRYs1 (expressing *PmPLT1* in sense orientation), MRYas1 (expressing *PmPLT1* in antisense orientation), MRYs2 (expressing *PmPLT2* in sense orientation), and MRYas2 (expressing *PmPLT2* in antisense orientation).

### Transport Measurements in Transgenic Yeast Cells

Uptake of radiolabeled substrates and analyses of inhibitor sensitivities and $K_m$ values were performed in 50 mM Na-$PO_4$ buffer, pH 5.5, as described (Sauer et al., 1990).

### Thin-Layer Chromatography

Yeast cells ($A_{600}$ was 20) were incubated in 50 mM Na-$PO_4$ buffer, pH 5.5, in the presence of 0.1 mM $^{14}$C-sorbitol for 60 min. At this point, 1 mL of yeast cells was harvested, washed extracted with 80% (v/v) ethanol, and subjected to thin-layer chromatography as described (Gahrtz et al., 1994). Radioactivity was determined by exposure to x-ray films (Kodak X-Omat AR, Eastman Kodak).

### Immunohistochemical Techniques

The anti-PmPLT1 and anti-PmPLT2 antisera used in this paper were raised against mixtures of two protein-specific oligopeptides (PmPLT1, MTADHQKSSVA and KKTGSEAT; PmPLT2, MNSEHHNSGGLA and KRSGTDGA) that were used to immunize two rabbits and one guinea pig after coupling to a protein carrier (Pineda, Antikörper-Service, Berlin).

Common plantain tissue and yeast cells were prepared, fixed in methacrylate, sectioned, and transferred to adhesion microscope slides (Linaris, Wertheim-Bettingen, Germany) as previously described (Stadler and Sauer, 1996). Methacrylate was removed by incubation of the slides for 3 min in acetone. Sections were rehydrated by sequential incubation in ethanol of decreasing concentrations (100%, 95%, 80%, 60%, and 30% [v/v]) and blocked for 1 h (50 mM Tris-HCl, pH 7.5, 150 mM NaCl, and 1% [w/v] skim milk powder). After overnight incubation with affinity-purified anti-PmSUC3 antiserum (diluted 1:10 in blocking buffer) and/or monoclonal anti-PmSUC2 antiserum (Stolz et al., 1999; diluted 1:2), sections were washed five times with blocking buffer. For detection of bound anti-PmPLT1 or anti-PmPLT2 antisera, sections were incubated for 1 h with a 1:300 dilution of Alexa Fluor 488 goat anti-rabbit IgG (Molecular Probes, Leiden, Netherlands). For double stainings of sections with polyclonal anti-PmPLT1 or anti-PmPLT2 antisera and with monoclonal anti-PmSUC2 antiserum, Alexa Fluor 546 goat anti-mouse IgG (Molecular Probes) was used in addition (diluted 1:100). After five final washes with blocking

buffer, the slides were rinsed with water and mounted in ProLong Antifade kit (Molecular Probes). Photographs were taken on a fluorescence microscope (Zeiss, Göttingen, Germany) with appropriate excitation light.

For antibody-peptide competition experiments, a conjugate of the specific peptide with ovalbumin was used. Before immunolocalization, the affinity-purified antiserum was incubated for 2 to 3 h at room temperature with 200 $\mu$g mL$^{-1}$ conjugate or pure ovalbumin, respectively.

### Heterologous Expression in *Xenopus* sp. Oocytes

For functional analysis, *PmPLT1* cRNA was prepared using the mMESSAGE mMACHINE RNA Transcription Kit (Ambion, Austin, TX). Oocyte preparation and cRNA injection have been described elsewhere (Becker et al., 1996). In two-electrode voltage-clamp studies, oocytes were perfused with 30 mM $K^+$ gluconate-containing solutions, based on Tris/MES buffers for pH values from 5.6 to 8.5 or citrate/Tris buffers for pH 4.5. The standard solution contained 10 mM MES/Tris, pH 5.6, 30 mM $K^+$ gluconate, 1 mM $CaCl_2$, and 1 mM $MgCl_2$. In addition, 20 mM $BaCl_2$ and 30 mM TEA-Cl were used to reduce cationic background conductances. Osmolarity was adjusted to 220 mOsmol using Suc. The content of polyols and the pH values are indicated in the figure legends. Steady-state currents ($I_{SS}$) were recorded with single-pulse protocols to 500-ms test voltages from 60 to −130 mV from a holding potential ($V_H$) of 0 mV.

## ACKNOWLEDGMENTS

We thank Anja Schillinger for excellent technical assistance and Angelika Wolf for growing the common plantain plants.

Received May 21, 2003; returned for revision July 7, 2003; accepted September 16, 2003.

## LITERATURE CITED

**Aoki N, Hirose T, Takahashi S, Ono K, Ishimaru K, Ohsugi R** (1999) Molecular cloning and expression analysis of a gene for a sucrose transporter in maize (*Zea mays* L.). Plant Cell Physiol **40:** 1072–1078

**Barker L, Kühn C, Weise A, Schulz A, Gebhardt C, Hirner B, Hellmann H, Schulze W, Ward JM, Frommer WB** (2000) SUT2, a putative sucrose sensor in sieve elements. Plant Cell **12:** 1153–1164

**Barker SA** (1955) Acyclic sugar alcohols. *In* K Peach, MV Tracey, eds, Modern Methods of Plant Analysis. Springer Verlag, Berlin, pp 158–192

**Barth I, Meyer S, Sauer N** (2003) PmSUC3: kinetic characterization and cellular localization of a SUC3-type sucrose transporter from *Plantago major*. Plant Cell **15:** 1375–1385

**Bebee DU, Turgeon R** (1992) Localization of galactinol and raffinose, and stachyose synthesis in *Cucurbita pepo* leaves. Planta **188:** 354–361

**Becker D, Dreyer I, Hoth S, Reid JD, Busch H, Lehnen M, Palme K, Hedrich R** (1996) Changes in voltage activation, $Cs^+$ sensitivity, and ion permeability in H5 mutants of the plant $K^+$ channel KAT1. Proc Natl Acad Sci USA **93:** 8123–8128

**Bellaloui N, Brown PH, Dandekar AM** (1999) Manipulation of in vivo sorbitol production alters boron uptake and transport in tobacco. Plant Physiol **119:** 735–742

**Berüter J** (1997) Characterization of the permeability of excised apple tissue for sorbitol. J Exp Bot **44:** 519–528

**Boorer KJ, Loo DDF, Frommer WB, Wright EM** (1996) Transport mechanism of the cloned potato $H^+$/sucrose cotransporter StSUT1. J Biol Chem **271:** 25139–25144

**Boorer KJ, Loo DDF, Wright EM** (1994) Steady-state and pre-steady-state kinetics of the $H^+$/hexose cotransporter (STP1) from *Arabidopsis thaliana* expressed in *Xenopus* oocytes. J Biol Chem **269:** 20417–20424

**Brown PH, Bellaloui N, Hu H, Dandekar A** (1999) Transgenically enhanced sorbitol synthesis facilitates phloem boron transport and increases tolerance of tobacco to boron deficiency. Plant Physiol **119:** 17–20

**Bürkle L, Hibberd JM, Quick WP, Kühn C, Hirner B, Frommer WB** (1998) The $H^+$-sucrose cotransporter NtSUT1 is essential for sugar export from tobacco leaves. Plant Physiol **118:** 59–68

**Canh DS, Horak J, Kotyk A, Rihova L** (1975) Transport of acyclic polyols in *Saccharomyces cerevisiae*. Folia Microbiol (Praha) **20:** 320–325

**Emr SD, Scheckman R, Flessel MC, Thorner J** (1983) An MF$\alpha$1-SUC2 ($\sigma$-factor-invertase) gene fusion for study of protein localisation and gene expression in yeast. Proc Natl Acad Sci USA **80:** 7080–7084

**Flora LL, Madore MA** (1996) Significance of minor-vein anatomy to carbohydrate transport. Planta **198:** 171–178

**Everard JD, Gucci R, Kann SC, Flore JA, Loescher WH** (1994) Gas exchange and carbon partitioning in the leaves of celery (*Apium graveolens* L.) at various levels of root zone salinity. Plant Physiol **106:** 281–292

**Gahrtz M, Schmelzer E, Stolz J, Sauer N** (1996) Expression of the *PmSUC1* sucrose carrier gene from *Plantago major* L. is induced during seed development. Plant J **9:** 93–100

**Gahrtz M, Stolz J, Sauer N** (1994) A phloem specific sucrose-$H^+$ symporter from *Plantago major* L. supports the model of apoplastic phloem loading. Plant J **6:** 697–706

**Gao Z, Maurousset L, Lemoine R, Yoo SD, Van Nocker S, Loescher W** (2003) Cloning, expression, and characterization of sorbitol transporters from developing sour cherry fruit and leaf sink tissues. Plant Physiol **131:** 1566–1575

**Gottwald JR, Krysan PJ, Young JC, Evert RF, Sussman MR** (2000) Genetic evidence for the in planta role of phloem-specific plasma membrane sucrose transporters. Proc Natl Acad Sci USA **97:** 13979–13984

**Hanahan D** (1983) Studies on transformation of *E. coli* with plasmids. J Mol Biol **166:** 557–580

**Hansch R, Fessel DG, Witt C, Hesberg C, Hoffmann G, Walch-Liu P, Engels C, Kruse J, Rennenberg H, Kaiser WM et al.** (2001) Tobacco plants that lack expression of functional nitrate reductase in roots show changes in growth rates and metabolite accumulation. J Exp Bot **52:** 1251–1258

**Haritatos E, Ayre BG, Turgeon R** (2000) Identification of phloem involved in assimilate loading in leaves by the activity of the galactinol synthase promoter. Plant Physiol **123:** 929–937

**Hinnebusch AG, Liebman SW** (1991) Protein synthesis and translational control in *Saccharomyces cerevisiae*. *In* JR Broach, JR Pringle, EW Jones, The Molecular and Cellular Biology of the Yeast *Saccharomyces*. Volume I, Genome Dynamics, Protein Synthesis, and Energetics. Cold Spring Harbor Laboratory Press, Cold Spring Harbor, NY, pp 627–735

**Hu H, Penn SG, Lebrilla CB, Brown PH** (1997) Isolation and characterization of soluble boron complexes in higher plants: the mechanism of phloem mobility of boron. Plant Physiol **113:** 649–655

**Jennings DB, Ehrenshaft M, Pharr DM, Williamson JD** (1998) Roles for mannitol and mannitol dehydrogenase in active oxygen-mediated plant defense. Proc Natl Acad Sci USA **95:** 15129–15133

**Kandler O, Hopf H** (1982) Oligosaccharides based on sucrose (sucrosyl oligosaccharides). *In* FA Loewus, W Tanner, eds, Encyclopedia of Plant Physiology: Plant Carbohydrates I, Intracellular Carbohydrates New Series. Vol. 13a. Springer-Verlag, Berlin, pp 348–383

**Keller F, Pharr DM** (1996) Metabolism of carbohydrates in sinks and sources: galactosyl-sucrose oligosaccharides. *In* E Zamski, AA Schaffer, eds, Photoassimilate Distribution in Plants and Crops: Source-Sink Relationships. Marcel Dekker, New York, pp 157–183

**Kühn C, Franceschi VR, Schulz A, Lemoine R, Frommer WB** (1997) Macromolecular trafficking indicated by localization and turnover of sucrose transporters in enucleate sieve elements. Science **275:** 1298–1300

**Lohaus G, Fischer K** (2002) Intracellular and intercellular transport of nitrogen and carbon. *In* C Foyer, G Noctor, eds, Advances in Photosynthesis. Kluwer Academic Publishers (in press)

**Ludwig A, Stolz J, Sauer N** (2000) Plant sucrose-$H^+$ symporters mediate the transport of vitamin H. Plant J **24:** 503–509

**Moing A, Escobar-Gutiérrez A, Gaudillère JP** (1994) Modeling carbon export out of mature peach leaves. Pant Physiol **106:** 591–600

**Noiraud N, Delrot S, Lemoine R** (2000) The sucrose transporter of celery: identification and expression during salt stress. Plant Physiol **122:** 1447–1455

**Noiraud N, Maurousset L, Lemoine R** (2001) Identification of a mannitol transporter, AgMaT1, in celery phloem. Plant Cell **13:** 695–705

**Penn SG, Hu H, Brown PH, Lebrilla CB** (1997) Direct analysis of sugar alcohol borate complexes in plant extracts by matrix-assisted laser desorption/ionization Fourier transform mass spectrometry. Anal Chem **69:** 2471–2477

**Riesmeier JW, Hirner B, Frommer WB** (1993) Potato sucrose transporter expression in minor veins indicates a role in phloem loading. Plant Cell **5:** 1591–1598

**Riesmeier JW, Willmitzer L, Frommer WB** (1992) Isolation and characterization of a sucrose carrier cDNA from spinach by functional expression in yeast. EMBO J **11:** 4705–4713

**Salmon S, Lemoine R, Jamai A, Bouché-Pillon S, Fromont C** (1995) Study of sucrose and mannitol transport in plasma-membrane vesicles from phloem and non-phloem tissues of celery (*Apium graveolens* L.) petioles. Planta **197:** 76–83

**Sarthy AV, Schopp C, Idler KB** (1994) Cloning and sequence determination of the gene encoding sorbitol dehydrogenase from *Saccharomyces cerevisiae*. Gene **140:** 121–126

**Sauer N, Friedländer K, Gräml-Wicke U** (1990) Primary structure, genomic organization and heterologous expression of a glucose transporter from *Arabidopsis thaliana*. EMBO J **9:** 3045–3050

**Sauer N, Stolz J** (1994) SUC1 and SUC2: two sucrose transporters from *Arabidopsis thaliana*. Expression and characterization in baker's yeast and identification of the histidine tagged protein. Plant J **6:** 67–77

**Shen B, Jensen RG, Bohnert HJ** (1997) Mannitol protects against oxidation by hydroxyl radicals. Plant Physiol **115:** 527–532

**Stadler R, Brandner J, Schulz A, Gahrtz M, Sauer N** (1995a) Phloem loading by the PmSUC2 sucrose carrier from *Plantago major* occurs into companion cells. Plant Cell **7:** 1545–1554

**Stadler R, Sauer N** (1996) The *Arabidopsis thaliana AtSUC2* gene is specifically expressed in companion cells. Bot Acta **109:** 299–306

**Stadler R, Wolf K, Hilgarth C, Tanner W, Sauer N** (1995b) Subcellular localization of the inducible *Chlorella* HUP1 monosaccharide-$H^+$ symporter and cloning of a co-induced galactose-$H^+$ symporter. Plant Physiol **107:** 33–41

**Stolz J, Ludwig A, Stadler R, Biesgen C, Hagemann K, Sauer N** (1999) Structural analysis of a plant sucrose carrier using monoclonal antibodies and bacteriophage lambda surface display. FEBS Lett **453:** 375–379

**Stoop JMH, Pharr DM** (1994a) Mannitol metabolism in celery stressed by excess macronutrients. Plant Physiol **106:** 503–511

**Stoop JMH, Pharr DM** (1994b) Growth substrate and nutrient salt environment alter mannitol to hexose partitioning in celery petioles. J Am Soc Hortic Sci **119:** 237–242

**Tarczynski MC, Jensen RG, Bohnert HJ** (1993) Stress protection of transgenic tobacco by production of the osmolyte mannitol. Science **259:** 508–510

**Truernit E, Sauer N** (1995) The promoter of the *Arabidopsis thaliana* SUC2 sucrose-$H^+$ symporter gene directs expression of $\beta$-glucuronidase to the phloem: evidence for phloem loading and unloading by SUC2. Planta **196:** 564–570

**Turgeon R** (1996) Phloem loading and plasmodesmata. Trends Plant Sci **1:** 418–423

**Wallart RAM** (1981) Acyclic polyols as taxonomic characters. Proc K Ned Akad Wet Ser C **84:** 77–87

**Webb KL, Burley JWA** (1962) Sorbitol translocation in apple. Science **137:** 766

**Weise A, Barker L, Kühn C, Lalonde S, Buschmann H, Frommer WB, Ward JM** (2000) A new subfamily of sucrose transporters, SUT4, with low affinity/high capacity is localized in enucleate sieve elements of plants. Plant Cell **12:** 1345–1355

**Williams LE, Lemoine R, Sauer N** (2000) Sugar transporters in higher plants: a diversity of roles and complex regulation. Trends Plant Sci **5:** 283–290

**Zimmermann MH, Ziegler H** (1975) List of sugars and sugar alcohols in sieve-tube exudates. *In* MH Zimmermann, JA Milburn, eds, Encyclopedia of Plant Physiology. Springer Verlag, Berlin, pp 480–503

# Kapitel VII: The new *Arabidopsis* transporter AtPLT5 mediates $H^+$-symport of numerous substrates including *myo*-inositol, glycerol and ribose

**Yvonne-Simone Klepek, Dietmar Geiger, Franz Klebl, Rémi Lemoine, Rainer Hedrich and Norbert Sauer**

**Angenommen bei Plant Cell, September 2004**

**Eigene Beteiligung an der Arbeit:**

- Biophysikalische Charakterisierung von AtPLT5 in *Xenopus* Oozyten mit Hilfe der DEVC-Technik in Bezug auf pH-, Spannungs- und Substrat-abhängige Transportkinetiken.
- Bestimmung der Substratspezifität.
- Auswertung der Daten.

**ABSTRACT**

Six genes of the *Arabidopsis* monosaccharide transporter-like (*MST-like*) superfamily share significant homology with polyol transporter genes previously identified in plants translocating polyols (mannitol or sorbitol) in their phloem [celery (*Apium graveolens*), common plantain (*Plantago major*) or sour cherry (*Prunus cerasus*)]. The physiological role and the functional properties of this group of proteins were unclear in *Arabidopsis*, which translocates sucrose and small amounts of raffinose rather than polyols. Here we describe AtPLT5, the first member of this subgroup of *Arabidopsis MST*-like transporters. Functional analyses of this protein in yeast and *Xenopus* oocytes suggest that AtPLT5 is located in the plasma membrane and characterize this protein as a broad-spectrum H+-symporter for linear polyols, such as sorbitol, xylitol, erythritol or glycerol, but unexpectedly also for the cyclic polyol *myo*-inositol and for different hexoses and pentoses. RT-PCR analyses and *AtPLT5* promoter-reporter gene plants revealed that *AtPLT5* is most strongly expressed in *Arabidopsis* roots, but also in the vascular tissue of leaves and in specific floral organs. Our data represent the first report on an energydependent, plasma membrane-localized plant transporter for substrates like inositol, glycerol or ribose. The potential physiological role of AtPLT5 is discussed.

**INTRODUCTION**

Linear polyols, such as sorbitol or mannitol, are found in high concentrations in the phloem sap of plants from certain families, such as Rosaceae, Apiaceae or Plantaginaceae (Zimmermann and Ziegler, 1975). After their synthesis in leaves by sugar phosphate reductases and polyol phosphate phosphatases, linear polyols are loaded into the phloem by polyol-H+ symporters, which accumulate their substrates to concentrations of several hundred millimolar (Zimmermann and Ziegler, 1975; Lohaus and Fischer, 2002; unpublished data from Gertrud Lohaus, Göttingen, Germany). cDNAs encoding these transporters have been cloned recently from celery (*Apium graveolens*, Apiaceae; Noriaud *et al.*, 2001), from sour cherry (*Prunus cerasus*, Rosaceae; Gao *et al.*, 2003) and from common plantain (*Plantago major*, Plantaginaceae; Ramsperger-Gleixner *et al.*, 2004). In celery, the AgMAT1 transporter

is discussed to be responsible for the loading of mannitol into the phloem (Noriaud *et al.*, 2001). The same function was also suggested for the sorbitol transporters PmPLT1 and PmPLT2 from common plantain, and in fact these proteins were immunolocalized to phloem companion cells (Ramsperger- Gleixner *et al.*, 2004). In contrast, both sorbitol transporters identified in sour cherry (PcSOT1 and PcSOT2) seem to be responsible for sorbitol import into cherries during the later stages of fruit development. Functional analyses of the encoded proteins from all three species in yeast (Noriaud *et al.*, 2001; Gao *et al*., 2003; Ramsperger-Gleixner *et al*., 2004) and of the *Plantago* transporter in *Xenopus* oocytes (Ramsperger-Gleixner *et al.*, 2004) showed that irrespective of their physiological substrate, these proteins do catalyze the transport of both, mannitol and sorbitol with similar rates.

*Arabidopsis*, a member of the Brassicaceae, translocates sucrose in its phloem together with small amounts of raffinose (Haritatos *et al*., 2000) but no polyols. Nevertheless, *Arabidopsis* has 6 genes (At2g16120, At2g16130, At2g18480, At2g20780, At3g18830 and At4g36670) sharing significant homology with the polyol transporter genes mentioned above. The physiological role of these potential sorbitol and/or mannitol transporters was unclear in *Arabidopsis*, and a physiological role or a substrate specificity different from that in celery, sour cherry or common plantain seemed reasonable.

Here we report the isolation of cDNAs for five of these six *Arabidopsis* polyol transporter-like genes and the detailed characterization of one of the encoded proteins by functional expression of its cDNA in yeast and in *Xenopus laevis* oocytes. Our data show that in contrast to the previously described polyol transporters from polyol translocating plants, the *Arabidopsis* homolog AtPLT5 (At3g18830) has a strong preference for sorbitol. Competition analyses revealed that sorbitol transport into *AtPLT5*-expressing *Saccharomyces cerevisiae* cells was inhibited by a wide range of different compounds, including polyols with shorter chain-lengths, such as xylitol, erythritol or glycerol, the cyclic polyol *myo*-inositol or hexoses and pentoses forming or pyranose (e.g. glucose and xylose) or furanose (e.g. fructose or ribose) rings. Uptake analyses with several of these compounds in *AtPLT5*-expressing yeast cells and electrophysiological analyses in *AtPLT5* cRNAinjected *Xenopus* oocytes revealed that all tested competitors are also substrates of AtPLT5. The $K_m$-values of AtPLT5 were determined for several substrates and were found to be in the millimolar range characterizing AtPLT5 as low affinity $H^+$-symporter. The organ-specific expression and the cellular and subcellular localization were determined by RT-PCR analyses, in *AtPLT5* promoter::*GUS* or *AtPLT5* promoter::*GFP* plants and with anti-AtPLT5 antisera.

## RESULTS

### Cloning of the *AtPLT* cDNAs

The open reading frames of the six putative polyol transporter genes from *Arabidopsis* had been predicted from in silico analyses of the *Arabidopsis* genome. To prove or disprove these predictions, cDNAs covering the entire open reading frames and flanked by a 15-bp fragment from the 5´-untranslated region of the high affinity monosaccharide-$H^+$ symporter gene *AtSTP1* were generated by RT-PCR from whole plant mRNA and sequenced. The 15-bp *AtSTP1* fragment (AAG CTT GTA AAA GAA) has been used repeatedly to optimize the 5´-flanking regions of other cDNAs for expression in yeast and turned out to enhance expression levels in all cases (Stadler *et al.*, 1995; Ramsperger-Gleixner *et al.*, 2004). Due to their homology to the previously described *PmPLT* genes from *Plantago* (Ramsperger- Gleixner *et al.*, 2003) the *Arabidopsis* genes were named *AtPLTs* (At2g16120 = *AtPLT1*; At2g16130 = *AtPLT2*; At2g18480 = *AtPLT3*; At2g20780 = *AtPLT4*; At3g18830 = *AtPLT5*; At4g36670 = *AtPLT6*).

The obtained cDNA sequences confirmed the predicted and deduced protein sequences of AtPLT1 (511 amino acids), AtPLT2 (511 amino acids), AtPLT3 (508 amino acids) and AtPLT5 (539 amino acids). For AtPLT4 two different open reading frames had been predicted, one with 526 amino acids (e.g. NM 127643) and one with 547 amino acids (e.g. AC006234). Our analyses clearly confirmed the shorter open reading frame encoding the 526-amino acid AtPLT4 protein. We were not able to isolate a cDNA for *AtPLT6*. The corresponding gene is predicted to encode the shortest AtPLT protein with only 493 amino acids (e.g. NM 119831). The predicted *AtPLT6* intron after 100 bp of the *AtPLT6* open reading frame was confirmed by the sequence of a full length cDNA obtained during the large scale cDNA sequencing of clones isolated from hormone-treated callus (http://www.genoscope.cns.fr; BX827774). However, this clone differes strongly from the genomic *AtPLT6* sequence in a downstream region of about 150 nucleotides and yields the quite likely incorrect protein size of 497 amino acids.

Fig. 1 presents a phylogenetic tree based on the experimentally confirmed protein sequences of AtPLT1 to AtPLT5 and on the predicted sequence of AtPLT6 (NM119831). Clearly, AtPLT1 and AtPLT2, which are encoded by adjacent genes on chromosome 2 show the

highest degree of sequence conservation (93.5% identity) suggesting that one of these genes formed during a recent duplication event. AtPLT4, the most distant member of the family, shares only about 60% identical amino acids with all other AtPLTs. AtPLT3, AtPLT5 and AtPLT6 share about 70 to 80% identity.

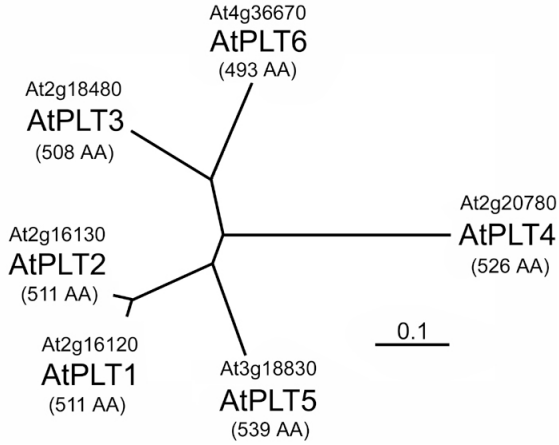


**Figure 1. Phylogenetic tree of the AtPLT family from *Arabidopsis*.**
The deduced sequences of the 6 *Arabidopsis* AtPLTs were aligned with the program ClustalX (Thompson *et al*., 1997) and an unrooted tree was calculated using the TreeViewX software (Page, 1996). The protein names and the MIPS numbers of the corresponding genes are given. The lengths of the proteins (AA = amino acids) were confirmed by sequencing the corresponding cDNAs for AtPLT1 to AtPLT5. The length of the AtPLT6 protein was deduced from the genomic sequence (accessions are given in the text).

Hydropathy analyses of the protein sequences predicted 12 transmembrane helices for all AtPLT proteins (not shown) and characterized them as a separate group within the *Arabidopsis* monosaccharide transporter-like (MST-like) superfamily (http://www.arabidopsis.org/info/genefamily/genefamily.html/). The different lengths of the AtPLT proteins result mainly from differences in the N- and Ctermini, with AtPLT5 (539 amino acids) having the longest C-terminus, AtPLT4 (526 amino acids) having the longest N-terminus and AtPLT6 (493 amino acids) having both, the shortest N-terminus and the shortest C-terminus.
The identity values determined for AtPLTs and polyol transporters from other species (AgMAT1, PmPLT1 or PcSOT1) are quite similar (60 to 75%) indicating the high degree of sequence conservation between these proteins from different plant species.

**Expression of the *AtPLT5* cDNA in *Saccharomyces cerevisiae***

To determine the functional properties of this new family of *Arabidopsis* transporters we cloned the cDNA of *AtPLT5*, the first full length clone obtained, into the unique EcoRI site of the yeast expression vector NEV-E (Sauer and Stolz, 1994) and used the resulting plasmids harboring cDNA inserts in sense (pYK23) or antisense orientation (pYK24) to transform the yeast strain SEY2102 (Emr *et al.*, 1983). The resulting yeast strains YKY1 (sense *AtPLT5*)

and YKY4 (antisense *AtPLT5*) were used to study the possible sorbitol and mannitol transport capacity of there combinant AtPLT5 protein.

Fig. 2 shows that YKY1 cells imported 14C-labelled sorbitol at a high rate, whereas no uptake of sorbitol was seen in YKY4 antisense cells. However, in contrast to all previously described polyol transporters, the AtPLT5 protein did not seem to transports 14C-labelled mannitol (Fig. 2). As for other H+-symporters (Sauer *et al.*, 1990; Barth *et al.*, 2003; Ramsperger-Gleixner *et al.*, 2004), we analyzed the uptake of sorbitol in the presence and absence of glucose, a metabolizable carbon source for yeast cells that is expected to enhance proton motive force-dependent transport rates by providing additional energy for the plasma membrane H+-ATPase. In contrast to what has been shown for the polyol transporters PmPLT1 and PmPLT2 from common plantain (Ramsperger-Gleixner *et al.*, 2004), sorbitol transport by AtPLT5 was inhibited by glucose (Fig. 2).

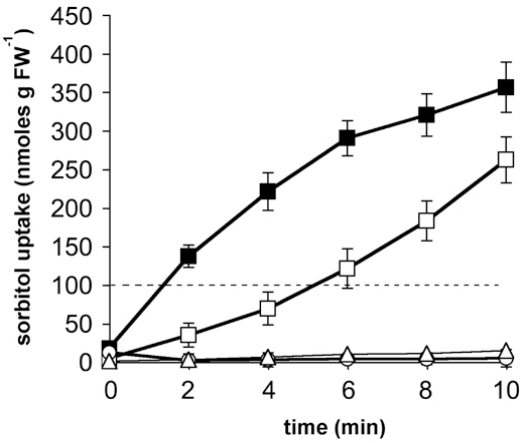


**Figure 2. Transport of sorbitol and mannitol in YKY1 and YKY4 cells.**
The transport capacity for sorbitol of yeast cells expressing the *AtPLT5* cDNA in sense orientation (strain YKY1) was analysed in the presence (open squares) or absence (closed squares) of 10 mM D-glucose. Open circles show the uptake rates for sorbitol in yeast cells expressing *AtPLT5* in antisense orientation (strain YKY4). Mannitol uptake rates in YKY1 cells are shown by open triangles. Values represent the mean of at least 3 independent transport analyses (± standard deviation). The broken line indicates the value, where the intracellular sorbitol concentration exeeds the extracellular concentration of sorbitol.

The obvious interpretation for this observed inhibition was that glucose may also be a substrate of AtPLT5. To test this hypothesis we transformed the yeast strain EBY.VW-4000 with the plasmids pYK23 and pYK24, yielding strains YKY5 (sense *AtPLT5*) and YKY8 (antisense *AtPLT5*). Due to multiple gene disruptions, EBY.VW- 4000 has no endogenous plasma membrane transporters for D-glucose (Wieczorke *et al.*, 1999) and can, therefore, be used to analyze the glucose transport capacity of recombinant transporters. Fig. 3 shows that AtPLT5 catalyzes the uptake of 14C-labelled glucose in YKY5, whereas no transport of 14C-glucose is seen in the antisense strain YKY8, confirming that both, sorbitol and glucose are substrates of AtPLT5. This capacity to transport sugars has not been described for any of the previously published plant polyol transporters.

For further analyses of the substrate specificity, we studied the uptake of $^{14}$C-sorbitol in YKY5 cells in the presence (100-fold excess) or absence of other potential substrates. We tested the inhibitory effect of the disaccharide sucrose, of hexoses and pentoses, of linear polyols with different chain lengths (1 to 6 carbon atoms) and of the cyclic polyol *myo*-inositol.

**Table 1**
Inhibition of $^{14}$C-sorbitol uptake by various potential competitors or inhibitors in YKY5 cells

| competitor or inhibitor | residual uptake rate for $^{14}$C-sorbitol (%) |
|---|---|
| -------- | 100 |
| sorbitol | 9.5 ± 1.3 |
| mannitol | 65.2 ± 4.8 |
| dulcitol | 49.6 ± 16.5 |
| xylitol | 3.6 ± 0.8 |
| erythritol | 11.3 ± 2.6 |
| glycerol | 37.8 ± 8.2 |
| glycol | 92.5 ± 3.4 |
| methanol | 83.4 ± 21.7 |
| glucose | 52.1 ± 14.6 |
| arabinose | 4.7 ± 0.6 |
| xylose | 6.2 ± 1.9 |
| ribose | 5.7 ± 0.4 |
| *myo*-inositol | 9.4 ± 0.8 |
| sucrose | 88.2 ± 21.7 |
| PCMBS | 90.8 ± 12.5 |
| DNP | 45.5 ± 6.9 |
| CCCP | 10.6 ± 5.3 |

Values represent the mean of at least 3 independent uptake experiments (± standard deviation). Potential competitors (10 mM) or inhibitors (50 µM) were added 30 seconds before $^{14}$C-sorbitol (0.1 mM initial outside concentration).

Table 1 shows that uptake of $^{14}$C-sorbitol was significantly inhibited by many of the tested competitors suggesting that AtPLT5 may represent a transporter with an unusually wide spectrum of substrates. Unlabeled sorbitol (6 carbons), but also linear polyols with 5 (xylitol),

4 (erythritol) or 3 carbons (glycerol) strongly reduced the import of 14C-labeled sorbitol indicating that AtPLT5 accepts a wide range of linear polyols. Inhibition by a 100-fold excess of mannitol was less pronounced (only about 35% and inhibition) and inhibition by a 100-fold excess of dulcitol (= galactitol) was only about 50%. This suggested that despite the negligible rates of 14Cmannitol transport in YKY1 cells (Fig. 2) there may be some mannitol uptake by YKY5 cells. No inhibitory effect was seen for the 2-carbon polyol glycol and for methanol.

Unexpectedly strong inhibition of $^{14}$C-sorbitol uptake was observed also in the presence of a 100-fold excess of *myo*-inositol, of different pentoses, such as xylose and arabinose, and even of ribose, which forms a furanose ring. No significant inhibition was obtained in the presence of the disaccharide sucrose. Table 1 also shows the sensitivities of AtPLT5-dependent transport to uncouplers, such as carbonyl cyanide-*m*-chlorophenylhydrazone (CCCP) and dinitrophenol (DNP), and the effect of the SH-group inhibitor *p*-(chloromercuri)benzene sulfonic acid (PCMBS). Clearly, both uncouplers strongly reduced the transport rates suggesting that AtPLT5 may catalyze the energy-dependent H+-symport of Sorbitol across the yeast plasma membrane. In contrast, PCMBS had no inhibitory effect on AtPLT5-dependent transport (Tab. 1). This agrees with the results published for most of the polyol transporters from polyol translocating plants (Noriaud *et al.,* 2001; Gao *et al.,* 2003; Ramsperger-Gleixner *et al.,* 2004). PCMBS sensitivity was found only for PmPLT1 (Ramsperger-Gleixner *et al.,* 2004) and in this case the sensitivity could be attributed to cystein residue Cys61 in this protein. None of the AtPLT proteins has a cysteine residue at the corresponding position (in AtPLT5 it is Ile51), which explaines the lack of PCMBS sensitivity.

To confirm that the reduced transport rates in the presence of other polyols or sugars (Tab. 1) result indeed from a competition for transport, we analyzed AtPLT5- dependent uptake for selected radiolabeled competitors. In fact, all of the tested monosaccharides (2 hexoses and 2 pentoses) turned out to be transported by AtPLT5 at similar rates (Fig. 3). This was an important observation, because so far significant transport rates for ribose have not been shown for any of the high affinity, STP-like monosaccharide transporters from *Arabidopsis* (Sauer *et al.,* 1990; Büttner and Sauer, 2000).

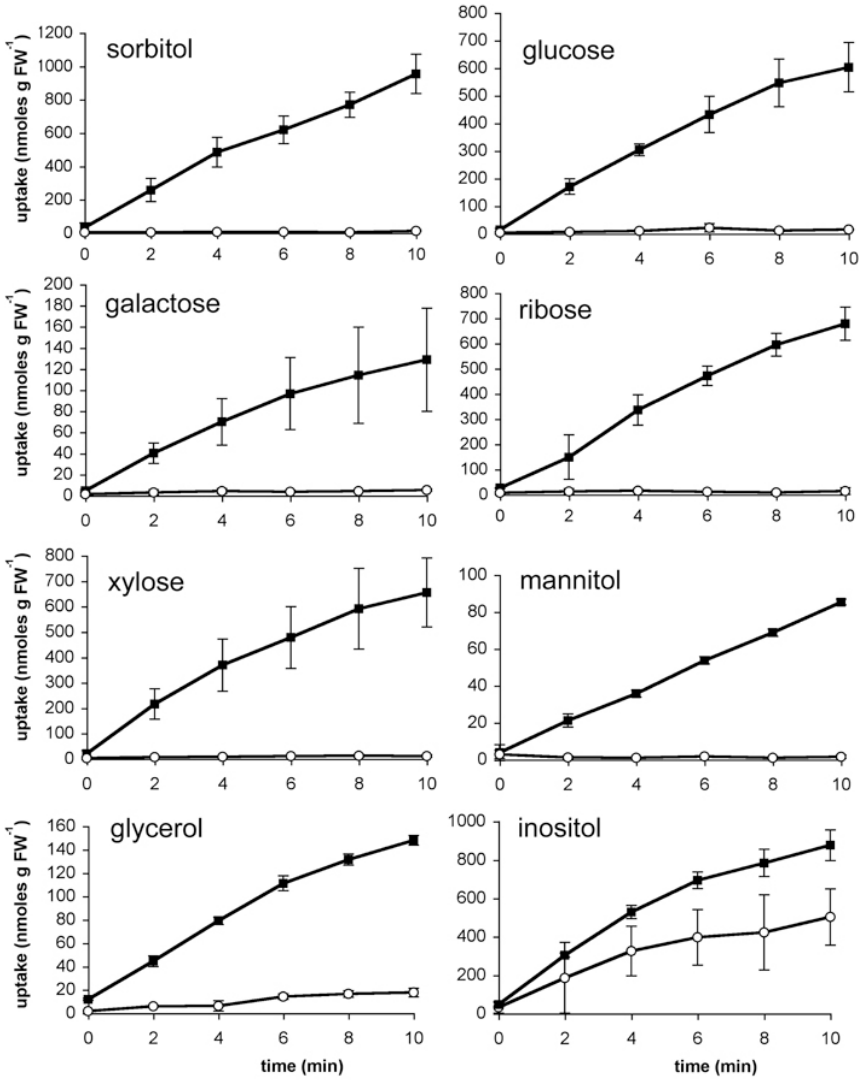


**Figure 3. Transport of several potential substrates in YKY5 and YKY8 cells.**
The transport capacity of AtPLT5 was analyzed in the hexose transport-deficient yeast line EBY.VW-4000 after transformation with ATPLT5 (strain YKY5) sense or antisense (strain YKY8) constructs. Closed squares show the transport rates of the indicated substrates at initial outside concentrations of 0.1 mM in YKY5 (sense).
Open circles show the transport rates of the indicated substrates at initial outside concentrations of 0.1 mM in YKY8 (antisense). Values represent the mean of at least 3 independent transport analyses (± standard deviation).

Figure 3 shows AtPLT5-driven uptake also for glycerol and even for mannitol, when analyzed in YKY5 cells. Together with the competition analyses in table 1 this demonstrates that AtPLT5 can transport linear polyols with chain lengths of 3 to 6 carbons. So far, energy-dependent uptake mechanisms for glycerol have not been described for plant cells. The low rates of mannitol transport correlate with its small inhibitory effect on 14C-sorbitol uptake (Tab. 1), and with the almost undetectalble mannitol transport rates seen in Fig. 2. Obviously, *AtPLT5* is expressed to higher levels in YKY5 cells than in YKY1 cells [see also the

difference in sorbitol uptake in Fig. 2 (YKY1) and Fig. 3 (YKY5)]. This difference is due to the two yeast strains used for these expression analyses (SEY2102 and EBY.VW-4000).

Unexpectedly, even 14C-inositol was transported with higher rates by YKY5 cells than by YKY8 antisense cells (Fig. 3). However, a rather high inherent transport activity for this substrate was also seen in YKY8 control cells. The affinity constants of recombinant AtPLT5 in yeast were determined for Sorbitol (0.5 ± 0.1) and glucose (1.5 ± 0.8) (Fig. 4). These values (mean of 3 analyses) agree with slightly higher sorbitol transport for sorbitol than for glucose (Fig. 3).

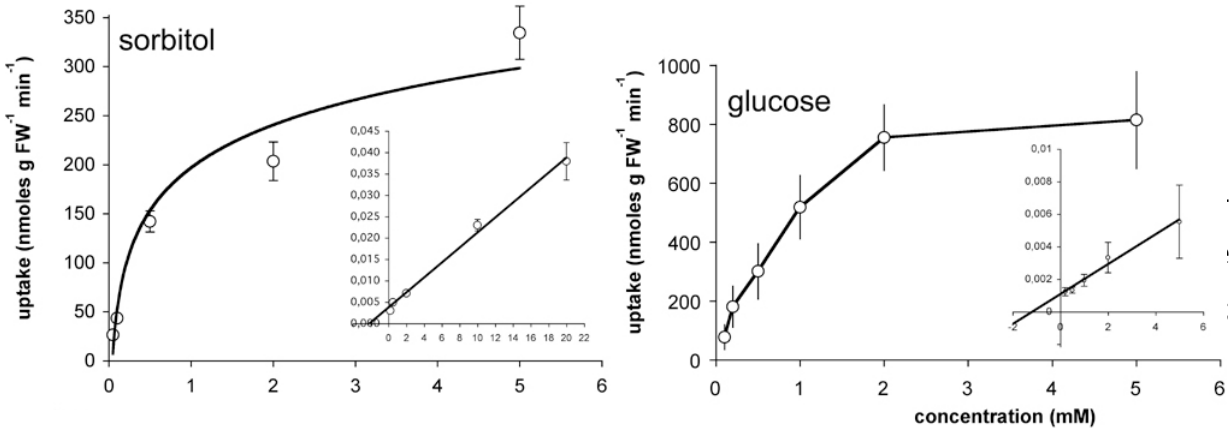


**Figure 4. $K_m$-value of AtPLT5 for sorbitol transport and for glucose transport in transgenic yeast cells.** Michaelis-Menten diagrams and Lineweaver-Burk diagrams (inserts) showing the dependence of the sorbitol or glucose transport rates of the extracellular substrate concentrations. All curvs represent the data of 3 independent experiments, error bars show the standard deviations.

The fact that sorbitol can be accumulated by AtPLT5-expressing yeast cells to intracellular concentrations exceeding the initial outside concentrations (broken line in Fig. 2) as well as the sensitivity of AtPLT5-driven polyol transport to uncouplers (Tab. 1) provide indirect evidence for an energy-dependent uptake mechanism. For a direct analysis of its energy-dependence and for further analyses of its substrate specificity, AtPLT5 was analyzed in *Xenopus* oocytes injected with *AtPLT5* cRNA (Fig. 5).

Figure 5A shows that similar inward currents were obtained upon perfusion with 3 mM solutions of sorbitol, glucose, fructose and *myo*-inositol at an extracellular pH of 5.5. Smaller currents were observed in the presence of 3 mM glycerol and currents almost zero in the presence of mannitol (Fig. 5A). This and the normalized values shown in Fig. 5B confirm the yeast data for sorbitol and glucose transport (Fig. 3) and demonstrate that also fructose and inositol are transported at similar rates. In contrast, glycerol is transported at a clearly lower

rate (about 20%). These data confirm that AtPLT5 is also a transporter for *myo*-inositol and glycerol, two substrates that inhibited the uptake of 14C-sorbitol in yeast (Tab. 1), but yielded only low transport rates (glycerol in Fig. 3) or that were difficult to analyze due to a strong inherent transport activity (*myo*-inositol in Fig. 3). The results also confirm that in contrast to all previously described polyol transporters AtPLT5 does discriminate between sorbitol and mannitol. Finally, the obtained inward currents demonstrate that a positive charge is symported with each of the tested substrates confirming the interpretation that AtPLT5-driven transport is energy-dependent.

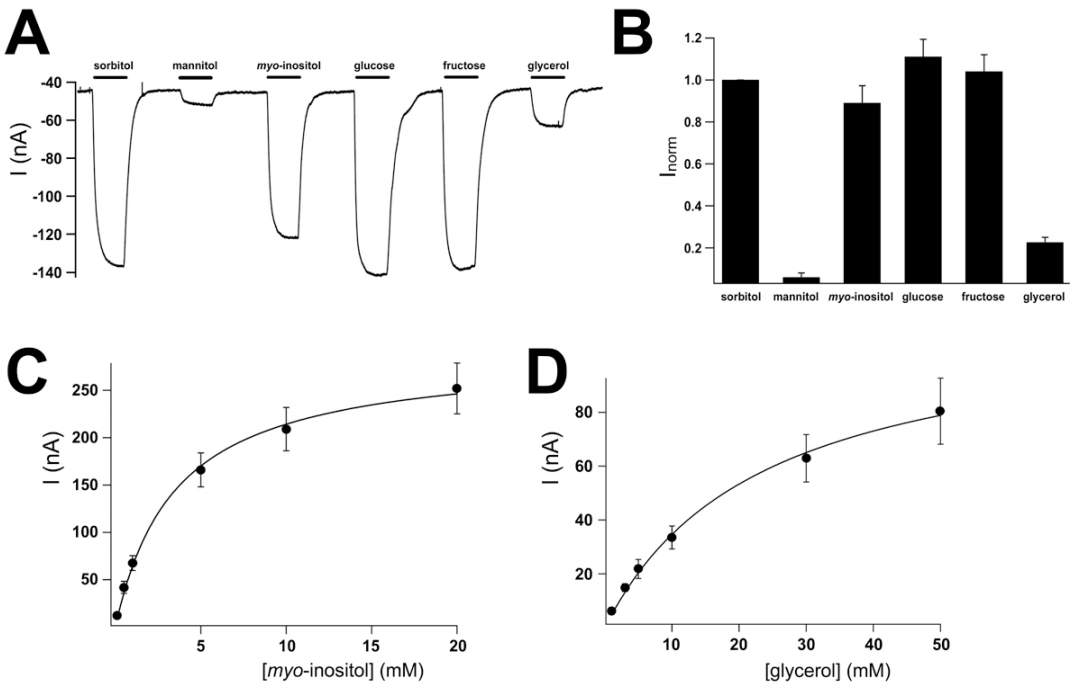


**Figure 5. Substrate specificity and affinities of AtPLT5 in *Xenopus laevis* oocytes.**
(A) AtPLT5-mediated H+ currents in response to various sugars and sugar alcohols (all 3 mM) were recorded at a membrane potential of -60 mV. Substrates were added for 20 s (black bars on top of current transients).
(B) Normalized AtPLT5-mediated H+-currents (Inorm) gained from three independent experiments as shown in (A). Data were normalized to the currents elicited in response to sorbitol.
(C) Saturation curve for *myo*-inositol-induced $H^+$-currents (mean of three experiments ± standard deviation). Data were fitted with Michaelis Menten-type kinetics revealing a Km-value for *myo*-inositol of 3.5 ± 0.3 mM (at -60 mV and pH 5.5).
(D) Saturation curve for glycerol-induced H+-currents (mean of three experiments ± standard deviation). Data were fitted with a Michaelis Menten-type kinetics revealing a Km-value for glycerol of 23.4 ± 2.3 mM (at -60 mV and pH 5.5).

Figures 5C and 5D show the Michaelis-Menten kinetics of AtPLT5 for *myo*-inositol and glycerol in *Xenopus* oocytes. The Km-values were determined at -60 mV and at an extracellular pH of 5.5 and were 3.5 ± 0.3 mM for *myo*-inositol and 23.4 ± 2.3 mM for

glycerol. Additional analyses of the Km-values for *myo*-inositol from 40 to –140 mV revealed that it is voltage (ΔV)-dependent and increases with more negative potentials. At -140 mM the Km of AtPLT5 for *myo*-inositol is about 1 mM (not shown). The nature of the co-transported ion was characterized for glucose (Figs. 6A and 6B) and glycerol (Figs. 6C and 6D). In Na+-free buffer systems inward currents induced by both substrates increased with decreasing extracellular pH-values indicating that protons represent the cotransported ions and characterizing AtPLT5 as $H^+$- symporter. Figs. 6B and 6D show that at extracellular pH-values > 7 the activity of AtPLT5 is almost zero. An identical pH-dependence was obtained for sorbitol uptake in yeast, where transport rates for sorbitol at pH 5.0 and pH 7.0 differed more than 90% (not shown).

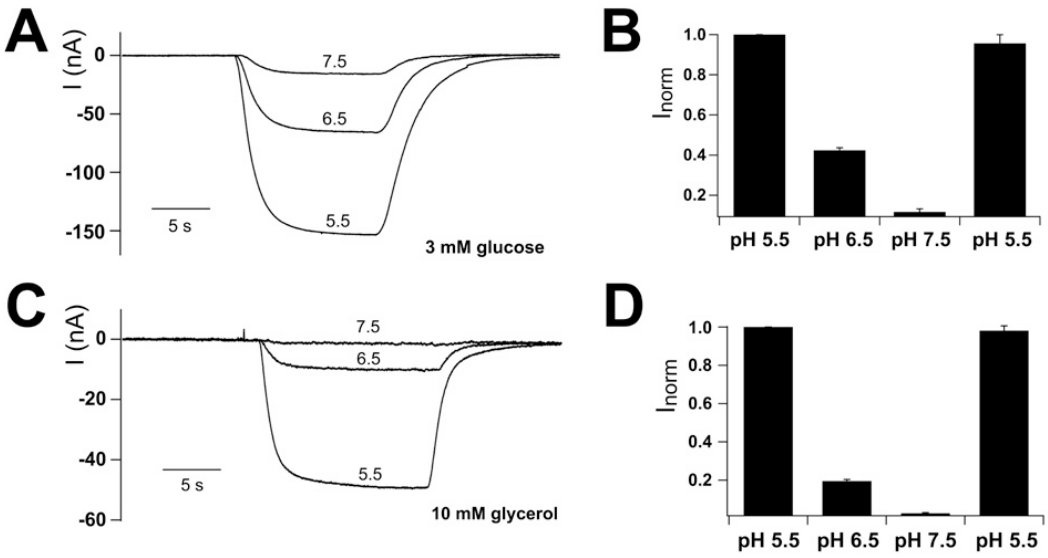


**Figure 6. Glucose- and glycerol-induced AtPLT5 currents depend on the $H^+$-gradient across the plasma membrane.**
(A) *Xenopus* oocytes expressing *AtPLT5* respond to 3-mM glucose in a pHdependent manner. Inward H+-currents were elicited by 15-s glucose pulses at pH 7.5, 6.5 or 5.5 at a membrane potential of -60 mV.
(B) Normalized AtPLT5 currents (Inorm) in response to 3-mM glucose recorded at extracellular pH-values of 5.5, 6.5 or 7.5. Note the lack of AtPLT5-mediated $H^+$ currents at pH 7.5. The complete reversibility of the pH effects was tested by glucose treatments at pH 5.5 before (first column) and after (fourth column) the pH shifts to 6.5 and 7.5 (mean of four experiments ± standard deviation; normalized to currents at pH 5.5).
(C) *Xenopus* oocytes expressing *AtPLT5* were challenged as described in (A), but with 10 mM glycerol.
(D) Normalized, AtPLT5-dependent H+ currents (Inorm) in response to 10 mM glycerol at pH 5.5, 6.5 and 7.5 were gained from four independent experiments as shown in (C) (mean ± SD, n=4). The complete reversibility of the pH effects was shown as described in (B).

**Analysis of *AtPLT5* expression in *AtPLT5* promoter::*GUS* and *AtPLT5* promoter::*GFP* plants**

For analysis of the tissue specificity of *AtPLT5* expression we generated and analyzed *AtPLT5* promoter::*GUS* and *AtPLT5* promoter::*GFP* plants. A 1551-bp promoter fragment was used to drive the expression of *GUS* or *GFP* in plants that had been selected for BASTA-resistance after transformation with the plasmids pYK10 (= *AtPLT5* promoter::*GUS*) or pYK13 (= *AtPLT5* promoter::*GFP*). We obtained numerous GUS or GFP-expressing transformants and analyzed 24 independent *AtPLT5* promoter::*GUS* lines and 24 independent *AtPLT5* promoter::*GFP* lines.

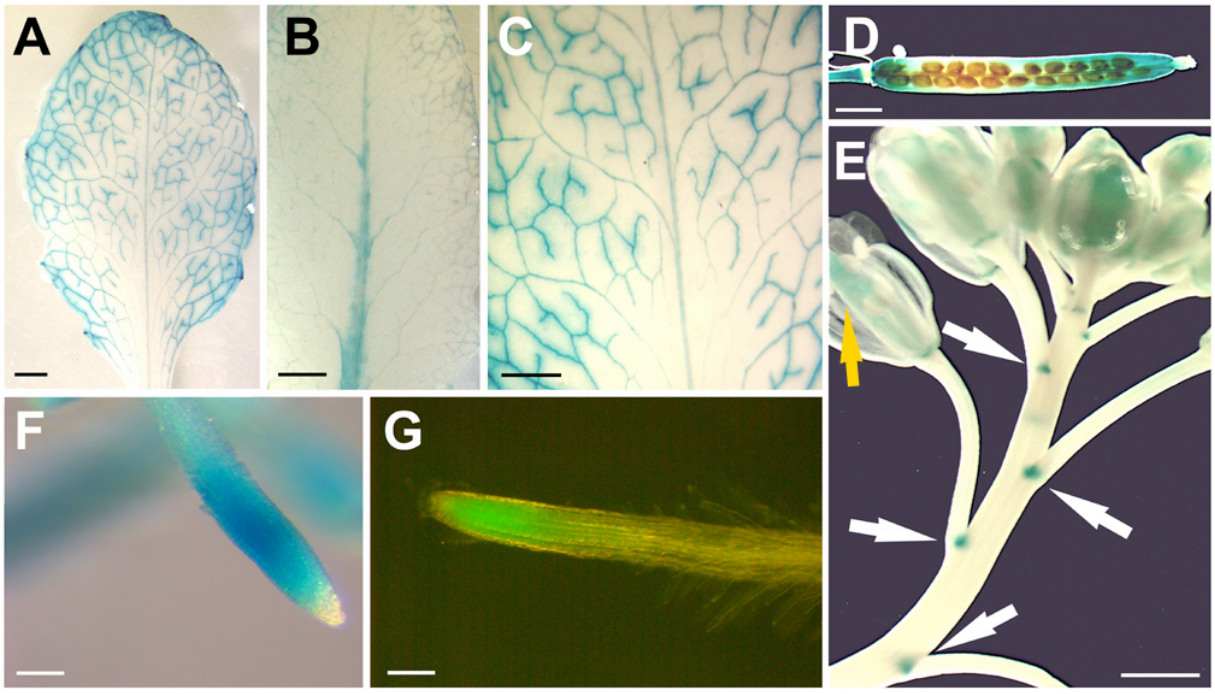


**Figure 7. *GUS* and *GFP* reportergene analyses.**
(A) GUS-histochemical staining of a rosette-leaf from a *AtPLT5*-promoter::*GUS* plant showing patchy GUS-staining in or along the vascular strands.
(B) GUS-histochemical staining of a rosette-leaf from a *AtPLT5*-promoter::*GUS* plant showing significant GUS-staining mainly in the mid-rib.
(C) GUS-histochemical staining of a rosette-leaf of the patchy type as shown in (A).
(D) GUS-histochemical staining of a mature silique showing blue stainig mainly at both ends of the silique.
(E) GUS-histochemical analysis of a fluorescence showing very weak GUS-staining along the vascular strands of the sepals and in the ovary (yellow arrow). GUSstaining is also seen in the axillary regions of each individial flower (white arrows).
(F) GUS-histochemical analysis showing strong GUS-staining in a region of about 300 to 500 µm behind the root tip.
(G) The GFP fluorescence in the tip of an *AtPLT5*-promoter::*GFP* root confirms the GUS activity shown in (F).
Space bars are 1 mm in (A) to (D), 2 mm in (E) and 0.1 mm in (F) and (G).

Figure 7 (A to C) shows the typical GUS-staining found in rosette leaves of *AtPLT5* promoter::*GUS* plants. In all plants analyzed and in most leaves of these plants GUS-staining frequently seen only after a prolonged period of staining, was patchy (Figs. 7A and 7C) and often more or less absent from the mid rib. In other leaves, however, GUS-staining was observed mainly in the mid rib (Fig. 7B) and sometimes the leaves stayed completely white. Weak GUS-staining was also seen along the vascular strands of stems (not shown), of all sepals (Fig. 7E) and of siliques (not shown). Siliques typically showed an additional, more general staining near both ends (Fig. 7D). Distinct *AtPLT5* promoter activity was also seen in the axillary regions of all flowers (white arrows in Fig. 7E). In none of the tested lines GUS-staining was seen in seeds, in pollen or in petals (not shown). In 100% of the plants the strongest GUS-staining was detected over a distance of about 300 to 500 µm behind the root tip (Fig. 7F). Weaker GUS staining was also seen in the upper part of most roots (not shown). Only this strong GUS-activity in the tip regions could was detected in analyses of *AtPLT5* promoter::*GFP* plants (Fg. 7G). Leaf or flower-specific expression has not been found in any of the GFP lines suggesting that expression in these tissues is much weaker than in roots.

**Immunohistochemical analyses of AtPLT5 localization**

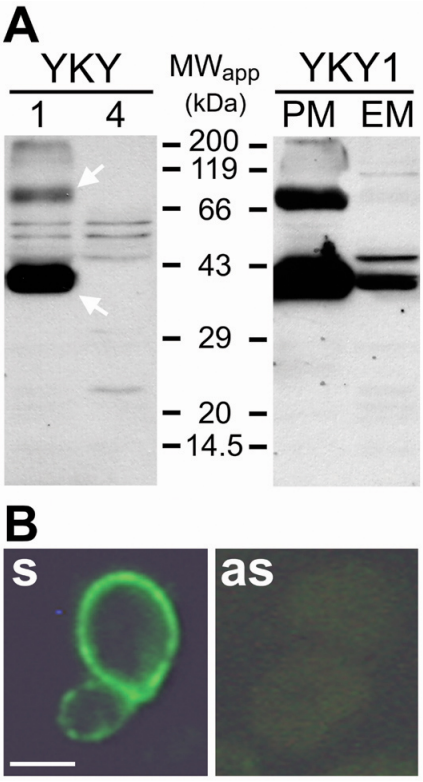


**Figure 8. Identification of the AtPLT5 protein in transgenic yeast cells.**
(A) Protein extracts from total membranes (10 µg per lane) from YKY1 (lane 1 on left Western blot) and YKY4 cells (lane 4 on left Western blot) were separated by gel electrophoresis, transferred to a nitrocellulose filter, and incubated with αAtPLT5-K1 antiserum. AtPLT5 signals at 40 and 80 kDa (arrows) are detected only in total membranes of YKY1 cells.
The right Western blot (10 µg per lane) shows AtPLT5 immunodetection in protein extracts from enriched plasma membranes (PM) and from enriched endomembranes (EM). AtPLT5 signals at 40 and 80 kDa are strongly enriched in the plasma membranes. In both Westerns binding of antiserum was visualized with anti-rabbit IgG antiserum conjugated to peroxidase.
(B) Cross-sections of yeast cells expressing the *AtPLT5* cDNA in sense (s) or antisense orientation (as). Sections were treated with αAtPLT5-K1, decorated with FITC-labeled 2nd antibody and photographed untder FITC-excitation light. AtPLT5-dependent fluoescence is detected only the in the sense strain, where it concentrates at the cell surface, most likely the plasma membrane (see A). The space bar is 2 µm.

Three anti-AtPLT5 antisera (αAtPLT5-K1, αAtPLT5-K2, αAtPLT5-M1) were raised against the peptide NH2-CEIGSNKQWKEGDTQSS-COOH that corresponds to amino acids 524 to 539 from the very C-terminus of AtPLT5. This sequence is unique to AtPLT5 and is lacking in all other AtPLT proteins, which have shorter Cterminal sequences.

The quality of the obtained sera was tested on detergent extracts from total membranes isolated from YKY1 (sense) and YKY4 (antisense) yeast cells. Figure 8A shows a Western-blot of these extracts after gelchromatographic separation and incubation with αAtPLT5-K1. A strong signal at an apparent molecular mass of about 40 kDa and a weaker signal at about 80 kDa were detected only in YKY1 cells and absent in similar extracts from YKY4 controls indicating that these bands represent the monomeric form (40 kDa) and the dimerized form (80 kDa) of the AtPLT5 protein. The difference of about 18 kDa between the apparent molecular mass of the monomeric form and the calculated molecular mass of 58.1 kDa is typical for lipophilic proteins (Beyreuther *et al.,* 1980; Gahrtz *et al.,* 1994; Barth *et al.,* 2003). Similar results were obtained with the other anti-AtPLT5 antisera (data not shown).

Separation of the total membrane fraction into a plasma membrane-enriched fraction and an endomembrane-enriched fraction (Sauer and Stolz, 2000) localized the majority of the label to the plasma membranes. The small amount of AtPLT5 protein detected in the endomembrane fraction is likely to result from contaminating plasma membranes in this fraction (Fig. 8A). This localization was confirmed in immunohistochemical analyses of YKY1 and YKY4 cells, where signals were detected only at the cell surface of the YKY1 sense strain (Fig. 8B). No signals were seen in sections of YKY4 antisense cells (Fig. 8B). The antisera were also used in numerous attempts to immunolocalize AtPLT5 in sections of *Arabidopsis* roots and leaves. Unfortunately, the antisera gave no signals with different embedding and fixation protocols. In view of the specific and strong signals obtained in *AtPLT5*-expressing yeast cells, we speculate that the amount of AtPLT5 protein *in planta* is too low for immunohistochemical detection.

**Analysis of *AtPLT5* expression by RT-PCR**

To confirm the tissue-specific expression shown in Fig. 7 by an independent technique we performed light cycler RT-PCR analyses of *AtPLT5* mRNA levels in different tissues. Parallel reactions were performed with *ACT2* (An *et al.*, 1996) and *UBQ10* (Sun and Callis, 1997) standards to minimize potential tissue specific differences in the expression levels of a single

control. Figure 9 gives the data calculated with the *ACT2* control, results calculated with the *UBG10* are not shown, because they were almost identical. The results show only minor differences in *AtPLT5* mRNA levels of the analyzed tissues, suggesting that there may be low *AtPLT5* expression also in cells and tissues that are not stained in the *AtPLT5* promoter::*GUS* or *AtPLT5* promoter::*GFP* plants. Moreover, these data confirm the higher levels of *AtPLT5* expression in the distal regions of the roots, which were also seen in the *AtPLT5* promoter::reporter gene plants (Fig. 7).

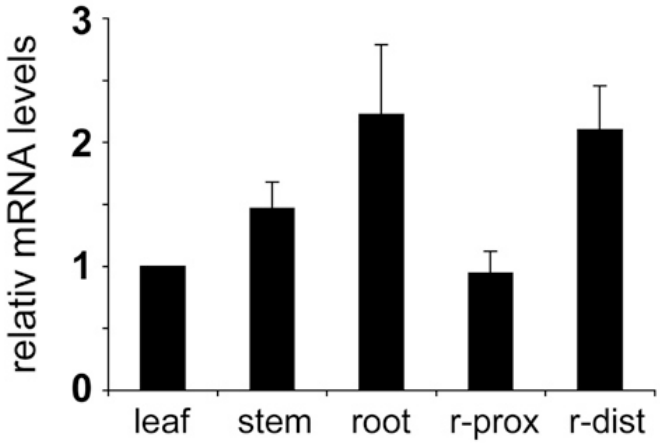


**Figure 9. Real time RT-PCRs with different *Arabidopsis* tissues.**
Relative *AtPLT5* mRNA levels were analyzed in leaves, stems and roots, and in distal (r-dist) and proximal (r-prox) *Arabidopsis* root preparations. Data were calculated on the basis of *AtACT2* control values, normalized for *AtPLT5* mRNA levels in leaves, and represent the mean values of 4 independent analyses (± standard deviations).

**Analysis of mutant plants harboring a T-DNA insertion in the *AtPLT5* gene**

Screening of publically available libraries identified a mutant line (Salk_050162) carrying a T-DNA insertion in the 4th exon of the *AtPLT5* gene, 1966 bp after the start ATG (Fig. 10). An insertion at this position results in a truncated *AtPLT5* mRNA that contains only 1374 bp of the AtPLT5 open reading frame and that codes for a protein of only 458 amino acids. In the wild type AtPLT5 protein the 81 C-terminal amino acids that are lacking in the truncated mutant protein encode transmembrane helix number 12 and a predicted cytoplasmic C-terminus of about 50 amino acids. The corresponding full length mRNA was no longer identified in the mutant line (Fig. 10). When the phenotypes of this mutant line and of the corresponding wild type plants were compared, we observed no differences in the growth phenotype under ambient CO2 concentrations and under the normal growth conditions described in the Methods section.

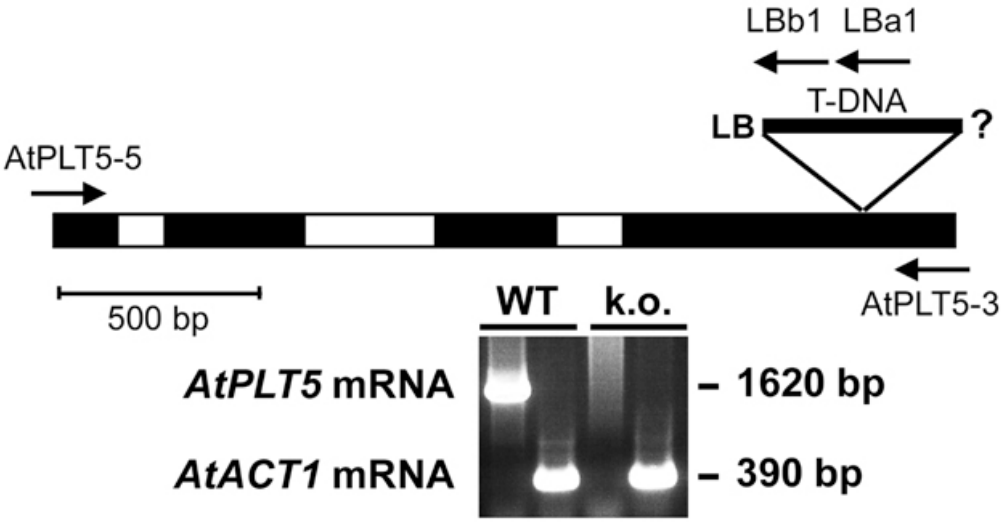


**Figure 10. Identification of a T-DNA insertion in the *AtPLT5* gene.**
The position and orientation of the T-DNA insertion in the *AtPLT5* gene of the mutant line Salk_050162 is presented. The gene has 3 introns (white boxes) and the insertion is located in the 4th exon (black boxes) at a position corresponding to nucleotide 1374 of the *AtPLT5* open reading frame. The orientation of the left border (LB) is indicated, the opposite end of the insertion has not been characterized.
Arrows indicate the position and orientation of primers (AtPLT5-5, AtPLT5-3, LBa1, LBb1) that were used to discriminate between wild type and heterozygous or homozygous mutant plants.
The ethidium bromide-stained agarose gel demonstrates that a 1620-bp full length mRNA, which was present in wild type *Arabidopsis* plants (wt), could no longer be identified in the T-DNA mutant (k.o.) by RT-PCR using the AtPLT5-5 and AtPLT5-3 primers. Under identical conditions a fragment (390 bp) of the *AtACT1* mRNA was amplified in both, wild type and mutant plants.

## DISCUSSION

This paper describes the first member of a new class of plasma membrane localized $H^+$-symporters from *Arabidopsis* exhibiting a new, quite unusual substrate specificity. AtPLT5 represents the first transporter catalyzing the transport of substrates, such as *myo*-inositol, glycerol or ribose across this membrane. AtPLT5 represents one of six transporters that form one (AtPLT1 to AtPLT6) of 7 subfamilies of the *MST*-like superfamily in *Arabidopsis*, which was named after the intensively characterized *AtSTP* gene family that encodes 14 different plasma membranelocalized monosacharide transporters (Sauer *et al.,* 1990; Büttner and Sauer, 2000).

So far, only members of the STP subfamily of the *Arabidopsis MST*-like superfamily were characterized by functional expression, although individual members of several other subfamilies have been studied by several groups [At1g08930 (*AtERD6*), e dehydration

induced gene (Kiyosue *et al.*, 1998); At5g16150 (pGlcT), a putative plastidic transporter (Weber *et al.*, 2000); At5g27350 (AtSFP1), a senescence induced gene (Quirino *et al.*, 2001)]. In all of these cases the functional analysis of the corresponding proteins failed. Here a detailed functional characterization of AtPLT5 (At3g18830) after expression of its cDNA in bakers yeast and in *Xenopus* oocytes is presented. In both expression systems AtPLT5 was characterized as a polyol/cyclitol/monosaccharide-$H^+$-symporter that is able to catalyze the energy-dependent membrane passage of a wide range of linear polyols (3 to 6 carbon backbone), of cyclic polyols (*myo*-inositol) and of numerous monosaccharides, including pyranose ring-forming and furanose ring-forming hexoses and pentoses (Figs. 3 and 5A).

**AtPLT5 is the first plasma membrane-localized plant transporter that mediates transport of inositol, ribose or glycerol**

Although direct proof for a localization of AtPLT5 in plant plasma membranes is missing, our immunolocalization data in yeast cells (Fig. 8B), the accumulation of AtPLT5 protein in yeast plasma membranes (Fig. 8A) and finally the activities in yeast and *Xenopus* plasma membranes (Figs. 2, 3, 5 and 6) support this localization also in plant plasma membranes. For several of the identified substrates so far no transport activity has been described in plant plasma membranes and for others only uptake via facilitated diffusion systems has been published. For example, the only plant inositol transporters cloned so far were identified in the common ice plant (*Mesembryanthemum crystallinum; Mitr1* and *Mitr2*) and the encoded transporters were shown to be located in the tonoplast (Chauhan *et al.*, 2000). Homologs of the Mitr1 and Mitr2 proteins are present in the *Arabidopsis* genome (At1g30220, At2g35740, At2g43330, At4g16480), and like the *AtPLT* genes these four genes form a small subgroup within the *Arabidopsis MST*-like superfamily. To date none of these 4 possible *Arabidopsis* inositol transporters has been functionally characterized, but first localization analyses identified these proteins also in the tonoplast and not in the plasma membrane of *Arabidopsis* (Sauer, N. and Schneider, S., unpublished data).

In animals a $Na^+$/*myo*-inositol symporter gene, *SMIT1*, has been cloned already more than 20 years ago (Kwon *et al.*, 1992). The encoded SMIT1 protein shows significant homology to the animal $Na^+$/glucose symporter SGLT1 (Hediger *et al.*, 1987), but both $Na^+$ symporters do not share significant homology with the plant *MST*-like genes. Energy-dependent inositol transporter genes (*ITR1* and *ITR2*) that are likely to be $H^+$-symporters have also been cloned

from yeast (Nikawa *et al.*, 1991). These proteins have Km-values between 0.1 and 0.2 mM and share homology with the *Arabidopsis* MST-like superfamily.

Glycerol transport activity across plant plasma membranes has so far only been shown for members of the aquaporin family (Weig and Jakob, 2000; Wallace and Roberts, 2004), which perform only facilitated diffusion and are closely related to the *Escherichia coli* GlpF glycerol permease (Sweet *et al.*, 1990; Maurel *et al.*, 1994; Zardoya *et al.*, 2002). To our knowledge, energy-dependent glyerol transporters of plant plasma membranes or internal membranes have not been described so far. In contrast, genes encoding energy-dependent, plasma membrane-localized transporters for glycerol have been cloned from bakers yeast (*GUP1* and *GUP2*, Oliveira and Lucas, 2004), but the corresponding proteins share no significant similarity with AtPLT5.

Finally, the observed capacity of AtPLT5 to transport ribose represents the first report on a plasma membrane localized transporter for this substrate in plants. Although numerous plant monosaccharide transporter genes and cDNAs have been cloned over the last years (Williams *et al.*, 2000) significant amounts of ribose transport have not been shown for any of the analyzed proteins. In contrast, ribose was shown to be excluded from the *Chlorella kessleri* CkHUP1 monosaccharide transporter and used as a non-transported control substrate (Tanner, 1980). This is quite similar for the different *Arabidopsis* monosaccharide transporters of the AtSTP family, which transport ribose either not at all or with extremely low rates (Büttner and Sauer, 2000; Büttner, unpublished data). Even AtSTP6 (Scholz-Starke *et al.*, 2003), the only *Arabidopsis* transporter that transports fructose, a furanose-ring forming hexose, at reasonably high rates (50% of the rate of glucose) exhibits only marginal transport rates for ribose (1% of the rate of glucose). This may be explained with binding sites that are optimized for pyranose rings formed by aldohexoses and by several pentoses, such as arabinose or xylose. In contrast, fructose or ribose, form furanose rings in solution and may, therefore, be poor substrates for STP-type transporters (Büttner and Sauer, 2000; Williams *et al.*, 2000). AtPLT5 does transport ribose, fructose and glucose at similar rates (Figs. 3 and 5A) suggesting little selectivity of the AtPLT5 substrate-binding pocket. A high affinity transporter for ribose has previously been described in *E. coli* (Iida *et al.*, 1984), but RbsC, the membrane component of this transporter, has only 10 transmembrane helices (Steward and Hermodson, 2003) and is not related to the AtPLT transporters of *Arabidopsis*. AtPLT5 and the other 5 members of the AtPLT family share significant homology with known polyol transporters catalyzing the transport of mannitol or sorbitol in polyol translocating plants

(Noriaud *et al.,* 2001; Gao *et al.,* 2003; Ramsperger- Gleixner *et al.,* 2004). These previously characterized transporters exhibited drastic differences with respect to their sensitivities to monosaccharides. Whereas both sorbitol transporters from common plantain showed enhanced transport rates in the presence of glucose, which was interpreted with an additional energy supply for an active transport system (Ramsperger-Gleixner *et al.,* 2004), strong inhibition by glucose and other hexoses was seen for the mannitol transporter AgMAT1 from celery (Noriaud *et al.,* 2001) and for the two sorbitol transporters from sour cherry, PcSOT1 and PcSOT2 (Gao *et al.,* 2003). This inhibition was interpreted as an artefact of the yeast expression system or as repression of transporter gene expression by glucose (Noriaud *et al.,* 2001; Gao *et al.,* 2003). In view of our data it may well be that the observed inhibition of polyol transport by hexoses for AgMAT1, PcSOT1 and PcSOT2 is also due to sugar transport by these proteins.

**AtPLT5 is a $H^+$-symporter**

All plant plasma membrane sugar and polyol transporters of the 12 transmembrane helix-type (STPs, PLTs, and SUCs) were shown to be energy-dependent $H^+$- symporters and to be voltage-dependent (Williams *et al.,* 2000; Ramsperger- Gleixner *et al.,* 2004). Uncoupler sensitivity of AtPLT5 in yeast (Tab. 1) and the intracellular accumulation of sorbitol to concentrations higher than in the external medium (Fig. 2) suggested that this may also be the case for this protein. Figure 6 confirms this interpretation showing that in the absence of $Na^+$ ions inward currents increased with decreasing pH. The voltage-dependence of AtPLT5 was confirmed for *myo*-inositol transport in the range from 40 to –140 mV (not shown).

***AtPLT5* is expressed in most plant tissues**

The presented analyses of *AtPLT5* promoter::*GUS* and of *AtPLT5* promoter::*GFP* plants (Fig. 7) shows *AtPLT5* promoter activity in leaves (preferably along the vascular tissue), in flowers (especially in sepals and siliques), in the root (most strongly in the tip areas) and in the axilary regions of the individual flowers (Fig. 7). No *AtPLT5* expression was seen in anthers and pollen, in petals and in ovules (Fig. 7E and not shown). This distribution of *AtPLT5* promoter activity correlates well with At3g18830 expression patterns determined in numerous analyses. The *Arabidopsis* MPSS database found no specific expression of *AtPLT5* in only one tissue or

organ (http://mpss.udel.edu/at/java.html/) and the result of numerous microarray analyses (http://www.arabidopsis.org/; http://www.cbs.umn.edu/arabidopsis/) was that *AtPLT5* is expressed in almost all tissues and organs analyzed, with the exception of pollen and seeds. Moreover, there was a clear difference between the expression in sepals and petals, with *AtPLT5* mRNAs being almost absent in petals and found in quite high levels in sepals. All of these data agree with our GUS and GFP analyses.

In our light cycler analyses (Fig. 9) we analyzed *AtPLT5* mRNA levels in several *Arabidopsis* tissues and especially the expression in distal and proximal regions of roots. As in the microarray analyses mentioned above, we found only marginal differences between the *AtPLT5* expression levels in roots, leaves and stems. The higher expression levels in the distal parts of the root confirmed the strong GUSactivity in Fig. 7F.

In summary our data suggests that *AtPLT5* is expressed at rather low levels in most tissues. Our GUS and GFP analyses identify those parts of the plant, where expression levels are increased above this basic level. The data are in agreement with microarray analyses.

**What is the physiological substrate of AtPLT5?**

The broad substrate specificity of the protein, on the expression of the gene in multiple tissues and organs, and on the unchanged phenotype of Atplt5-k.o. plants (Fig. 10) make it difficult to speculate on the physiological role of AtPLT5. Open questions are for example, (i) which of the identified substrates of AtPLT5 is the main substrate under physiological conditions, (ii) does AtPLT5 transport only one or several of the characterized substrates *in planta*, and (iii) can AtPLT5 transport even other substrates that have not been tested in the present analyses. For the last part, the answer is probably yes. We have analyzed only a limited set of monosaccharides and linear or cyclic polyols, and most of these substrates were transported with similar rates (Figs. 3 and 5A). It is very likely that other compounds are also accepted as substrates by AtPLT5.

The affinities of AtPLT5 were shown to be 0.5 mM for sorbitol and 1.5 mM for glucose in the yeast system (Fig. 4). The affinities for *myo*-inositol and for glycerol were determined in *Xenopus* oocytes and at a constant $\Delta\psi$ of 60 mV they were shown to be 3.5 mM and 23.4 mM, respectively (Figs. 5C and 5D). However, the affinity for *myo*-inositol increases with more negative potentials and is about 1 mM at -140 mV (not shown), which is in the range of the Km-values for glucose or sorbitol. This explains, why glucose, sorbitol and *myo*-inositol

are transported with similar rates. It is likely that the affinity for glycerol, which is transported at lower rates (Figs. 3 and 5A), shows the same voltage-dependence, and one can calculate a Km-value of 5 to 7 mM for glycerol in fully energized plasma membranes.

A simple explanation for the function of ATPLT5 might be the retrieval of multiple substrates from the apoplast. All identified substrates are major components of the cellular metabolism and may leak out of the cells. However, more specific physiological functions, e.g. in the cell-to-cell distribution of certain compounds, possibly of different substrates in different tissues, can certainly not be excluded.

## METHODS

### Strains and growth conditions

*Arabidopsis thaliana* plants were grown in growth chambers on potting soil under a 16 h light/8 h dark regime at 22°C and 60% relative humidity or in the greenhouse under ambient conditions. For heterologous expression of *AtPLT5* cDNAs in yeast we used strains SEY2102 (Emr *et al.*, 1983) or EBY.VW-4000 (Wieczorke *et al.*, 1999). The *Escherichia coli* strain DH5α (Hanahan, 1983) was used for all cloning steps. Transformation of *Arabidopsis* was performed using *Agrobacterium tumefaciens* strain GV3101 (Holsters *et al.*, 1980).

### cDNA cloning and constructs for expression in yeast

cDNAs of the 6 *Arabidopsis AtPLT* genes were amplified from total RNA isolated from *Arabidopsis thaliana* Col-0 with gene specific primers binding to the very 5´- ends (including the start ATG) or the very 3´-ends (including the stop codon) of the cDNAs. NotI cloning sites were introduced at both ends of *AtPLT1* and *AtPLT2*, EcoRI cloning sites were introduced at both ends of *AtPLT3*, *AtPLT4* and *ATPLT5*. The resulting cDNAs were digested with NotI or EcoRI, cloned into the respective sites of the yeast expression vectosr NEV-E or NEV-N (Sauer and Stolz, 1994), sequenced and the *AtPLT5*-containing plasmid used for transformation of yeast cells (Gietz *et al.*, 1992). If not otherwise indicated, uptake experiments were performed in 50-mM sodium phosphat buffer (pH 5.0) as described (Sauer *et al.*, 1990).

**Heterologous expression in *Xenopus laevis* oocytes**

For functional analysis, *AtPLT5* cRNA was prepared using the T7 mMESSAGE mMACHINE RNA transcription kit (Ambion, Austin, Texas, USA). Oocyte preparation and cRNA injection have been described elsewhere (Becker *et al.*, 1996). In twoelectrode voltage-clamp studies, oocytes were perfused with 100 mM KCl-containing solutions, based on Tris/MES buffers for pH values from 5.5 to 7.5. The standard solution contained 10-mM Tris, pH 5.5, 100-mM KCl, 1-mM CaCl2, and 1-mM MgCl2. Osmolarity was adjusted to 220 mOsmol/kg using sucrose. The content of substrates and the pH values are indicated in the figures and figure legends.

Steady-state currents (ISS) were recorded with single-pulse protocols to 500-ms test voltages from 40 to -140 mV from a holding potential (VH) of -20 mV. Currents in the absence of substrates were subtracted for leak correction.

***AtPLT5* promoter::*GUS* and of *AtPLT5* promoter::*GFP* constructs and plant transformation**

A 1551-bp promoter *AtPLT5* promoter fragment was PCR-amplified from genomic DNA (*Arabidopsis* Col-0) using the primers AtPLT5p-5 (5´-AAA ATT CAT AAG CTT CAT AAC AGC GAT TGC TCT CG-3´) and AtPLT5p-3 (5´-CAT ATC GCC ATG GTG ATA GAG AAT GGG GCG AGA GAG A-3´). The fragment was cloned into pGEM-T Easy (Promega, Madison, Wisconsin, USA) sequenced and the insert was cloned in front of the *GFP* reporter gene in the vector pGA03 or in front of the *GUS* reporter gene in the vector pAF6 [pAF6 and pGA03 are pUC19-based plasmids, harbouring the *GFP* (pGA03) or *GUS* (pAF6) reporter gens]. From the resulting plasmids *AtPLT5* promoter::*GFP* or *AtPLT5* promoter::*GUS* fragments were excised and cloned into pAF16 (Stadler *et al.*, 2004) yielding the plasmids pYK10 (*AtPLT5* promoter::*GUS*) and pYK13 (*AtPLT5* promoter::*GFP*), which were used for transformation of *Arabidopsis* (Clough and Bent, 1998).

**Immunohistochemical techniques and Western blot analyses**

Peptide-specific antisera against the C-terminal peptide NH2- CEIGSNKQWKEGDTQSS-COOH were generated by Pineda-Antikörper-Service (Berlin, Germany). Yeast cells expressing *AtPLT5* in sense or antisense orientation were fixed, embedded, sectioned and treated with antisera as described (Meyer *et al.*, 2004). Binding of anti-AtPLT5 antibodies to yeast sections was visualized by treatment with anti-rabbit IgG-fluorescein isothiocyanate

(FITC)-isomer 1-conjugate (Sigma-Aldrich, Deisenhofen, Germany). Finally, microscopic slides were mounted in anti-fading medium (ProLong Antifade Kit; Molecular Probes, Leiden, Netherlands) and viewed under appropriate excitation light.

Protein extracts of different membrane fractions from bakers yeast were prepared as described (Sauer and Stolz, 2000) separated on sodium dodecylsulphate (SDS) polyacrylamide gels (Laemmli, 1970) and transferred to nitrocellulose filters (Dunn, 1986). AtPLT5 protein bands wer detected by treatment of the filters with anti-rabbit-IgG antiserum-peroxidase conjugate (diluted 1:4000 in blocking buffer) followed by incubation with Lumi-Light Western Blotting Substrate (Roche Diagnostics GmbH, Mannheim, Germany).

**Real time RT-PCR**

Real time RT-PCRs were perfomed on a RotorGene 2000 (Corbett Research, Sydney, Australia) with the following primers: AtACT2g+846f (5´-ATT CAG ATG CCC AGA AGT CTT GTT-3') and AtACT2g+1295r (5´-GAA ACA TTT TCT GTG AAC GAT TCC T-3') for the actin standard (*Arabidopsis ACT2* gene; At3g18780), AtUBQ10g- 315f (5´-ACC GTG ATC AAG ATG CAG ATC TTT GT-3´) and AtUBQ10g+163 (5´-TAC GGC CAT CCT CTA GCT GCT TG-3´) for the ubiquitin standard (*Arabidopsis UBQ10* gene; At4g05320), and AtPLT5cW5 (5´-ATC CTC CTT GGT TAT GAT ATA GGA GTG A-3´) and AtPLT5cW3 (5´-GCG ATC ATG AGA GCA TAT CCG AC-3´) for *AtPLT5*.

**Epifluorescence microscopy and detection of GFP fluorescence**

Images of GFP fluorescence were made with an epifluorescence microscope (Zeiss Axioskop, Carl Zeiss Jena GmbH, Jena, Germany) or stereomicroscopes (Zeiss SV11; Carl Zeiss Jena GmbH, Jena, Germany, or Leica MZFLIII; Leica Microsystems, Bensheim, Germany) with an excitation wavelength of 460- to 500- nm. Emitted fluorescence was monitored at detection wavelengths longer than 510 nm.

**ACKNOWLEDGEMENTS**

We thank Anja Schillinger and Jennifer Tebart for excellent technical assistance and Angelica Wolf for growing the *Arabidopsis* plants. This work was supported by a grant of the Deutsche Forschungsgemeinschaft to NS [*Arabidopsis* Functional Genomics Network (AFGN); Sa 382/13-1].

**REFERENCES**

**An, Y.-Q., McDowell, J.M., Huang, S., McKinney, E.C., Chambliss, S., and Meagher, R.B.** (1996). Strong, constitutive expression of the *Arabidopsis* ACT2/ACT8 actin subclass in vegetative tissues. Plant J. **10,** 107–121.

**Barth, I., Meyer, S., and Sauer, N.** (2003). PmSUC3: Characterization of a SUT2/SUC3-type sucrose transporter from *Plantago major*. Plant Cell **15**, 1375-1385.

**Becker, D., Dreyer, I., Hoth, S., Reid, J.D., Busch, H., Lehnen, M., Palme, K. and Hedrich, R.** (1996). Changes in voltage activation, $Cs^+$ sensitivity, and ion permeability in H5 mutants of the plant $K^+$ channel KAT1. Proc. Natl. Acad. Sci. USA **93**, 8123-8128.

**Beyreuther, K., Bieseler, B., Ehring, R., Griesser, H.-W., Mieschendahl, M., Müller-Hill, B., and Triesch, I.** (1980). Investigation of structure and function of lactose permease of *Escherichia coli*. Biochem. Soc. Trans. **8,** 675-676.

**Büttner, M., and Sauer, N.** (2000). Monosaccharide transporters in plants: structure, function and physiology. Biochim. Biophys. Acta **1465,** 263-274.

**Chauhan, S., Forsthoefel, N., Ran, Y., Quigley, F., Nelson, D.E., and Bohnert, H.J.** (2000). $Na^+$/*myo*-inositol symporters and $Na^+/H^+$-antiport in *Mesembryanthemum crystallinum*. Plant J. **24**, 511-522.

**Clough, S.J., and Bent, A.F.** (1998). Floral dip: a simplified method for *Agrobacterium*-mediated transformation of *Arabidopsis thaliana*. Plant J. **16**, 735-743.

**Dunn, S.D.** (1986). Effects of the modification of transfer buffer composition on the renaturation of proteins in gels on the recognition of proteins on Western blots by monoclonal antibodies. Anal. Biochem. **157**, 144-153.

**Emr, S.D., Scheckman, R., Flessel, M.C., and Thorner, J.** (1983). An MFa1-SUC2 (sfactor-invertase) gene fusion for study of protein localisation and gene expression in yeast. Proc. Natl. Acad. Sci. USA **80,** 7080-7084.

**Gahrtz, M., Stolz, J., and Sauer, N.** (1994). A phloem specific sucrose-$H^+$ Symporter from *Plantago major* L. supports the model of apoplastic phloem loading. Plant J. **6,** 697-706.

**Gao, Z., Maurousset, L., Lemoine, R., Yoo, S.D., Van Nocker, S., and Loescher, W.** (2003). Cloning, expression, and characterization of sorbitol transporters from developing sour cherry fruit and leaf sink tissues. Plant Physiol. **131,**1566-1575.

**Gietz, D., Jean, W.S., Woods, R.A., and Schiestl, R.H.** (1992). Improved method for high efficiency transformation of intact yeast cells. Nucleic Acids Res. **20**, 1425.

**Hanahan, D.** (1983). Studies on transformation of *E. coli* with plasmids. J. Mol. Biol. **166,** 557-580.

**Haritatos, E., Ayre, B.G., and Turgeon, R.** (2000). Identification of phloem involved in assimilate loading in leaves by the activity of the galactinol synthase promoter. Plant Physiol. **123,** 929-937.

**Hediger, M.A., Ikeda, T., Coady, M., Gundersen, C.B., and Wright, E.M.** (1987). Expression of size-selected mRNA encoding the intestinal $Na^+$/glucose cotransporter in *Xenopus laevis* oocytes. Proc. Natl. Acad. Sci. USA **84**, 2634- 2637.

**Holsters, M., Silva, B., Van Vliet, F., Genetello, C., De Block, M., Dhaese, P., Depicker, A., Inze, D., Engler, G., Villarroel, R., Van Montagu, M., and Schell, J.** (1980). The functional organization of the nopaline *Agrobacterium tumefaciens* plasmid pTiC58. Plasmid **3**, 212-230.

**Iida, A., Harayama, S., Iino, T., and Hazelbauer, G.L.** (1984). Molecular cloning and characterization of genes required for ribose transport and utilization in *Escherichia coli* K-12. J. Bacteriol. **158**, 674-682.

**Kiyosue, T., Abe, H., Yamaguchi-Shinozaki, K., and Shinozaki, K.** (1998). ERD6, a cDNA clone for an early dehydration-induced gene of *Arabidopsis*, encodes a putative sugar transporter. Biochim. Biophys. Acta **1370**, 187-191.

**Kwon, H.M., Yamauchi, A., Uchida, S., Preston, A.S., Garcia-Perez, A., Burg, M.B., and Handler, J.S.** (1992). Cloning of the cDNA for a $Na^+$/*myo*-inositol cotransporter, a hypertonicity stress protein. J. Biol. Chem. **267**, 6297-6301.

**Laemmli, U.K.** (1970). Cleavage of structural proteins during the assembly of the head of bacteriophage T4. Nature **227**, 680-685.

**Lohaus, G., and Fischer, K.** (2002). Intracellular and intercellular transport of nitrogen and carbon. In Advances in photosynthesis and respiration, C. Foyer, and G., Noctor, eds. (Kluwer Academic Publishers) Vol. 12, pp.

**Maurel, C., Reizer, J., Schroeder, J.I., Chrispeels, M.J., and Saier, M.H. Jr.** (1994). Functional characterization of the *Escherichia coli* glycerol facilitator, GlpF, in *Xenopus* oocytes. J. Biol. Chem. **269**, 11869-11872.

**Meyer, S., Lauterbach, C., Niedermeier, M., Barth, I., Sjolund, R.D., and Sauer, N.** (2004). Wounding enhances expression of AtSUC3, a sucrose transporter from *Arabidopsis* sieve elements and sink tissues. Plant Physiol. **134**, 684- 693.

**Nikawa, J., Tsukagoshi, Y., and Yamashita, S.** (1991). Isolation and characterization of two distinct *myo*-inositol transporter genes of *Saccharomyces cerevisiae*. J. Biol. Chem. **266**, 11184-11191.

**Noiraud, N., Maurousset, L., and Lemoine, R.** (2001). Identification of a mannitol transporter, AgMaT1, in celery phloem. Plant Cell **13,** 695-705.

**Oliveira, R., and Lucas, C.** (2004). Expression studies of *GUP1* and *GUP2*, genes involved in glycerol active transport in Saccharomyces cerevisiae, using semi-quantitative RT-PCR. Curr Genet., in press.

**Page, R.D.M.** (1996). TREEVIEW: An application to display phylogenetic trees on personal computers. Comp. Appl. Biosci. **12**, 357-358.

**Quirino, B.F., Reiter, W.D., and Amasino, R.D.** (2001). One of two tandem *Arabidopsis* genes homologous to monosaccharide transporters is senescence-associated. Plant Mol Biol. **46**, 447-457.

**Ramsperger-Gleixner, M., Geiger, D., Hedrich, R., and Sauer, N.** (2004). Differential expression of sucrose transporter and polyol transporter genes during maturation of common plantain companion cells. Plant Physiol. **134,** 147-160.

**Sauer, N., Friedländer, K., and Gräml-Wicke, U.** (1990). Primary structure, genomic organization and heterologous expression of a glucose transporter from *Arabidopsis thaliana*. EMBO J. **9,** 3045-3050.

**Sauer, N., and Stolz, J.** (1994). SUC1 and SUC2: two sucrose transporters from Arabidopsis thaliana; expression and characterization in baker's yeast and identification of the histidine tagged protein. Plant J. **6,** 67-77.

**Sauer, N., and Stolz, J.** (2000). Expression of foreign transport proteins in yeast. In: Practical Approach Series (Baldwin, S.A., ed.) Oxford University Press, pp. 79-105.

**Scholz-Starke, J., Büttner, M., and Sauer, N.** (2003). AtSTP6, a new pollen-specific $H^+$-monosaccharide symporter from *Arabidopsis thaliana*. Plant Physiol. **131**, 70-77.

**Stadler, R., Wolf, K., Hilgarth, C., Tanner, W., and Sauer, N.** (1995). Subcellular localization of the inducible *Chlorella* HUP1 monosaccharide-H+ Symporter and cloning of a co-induced galactose-H+ symporter. Plant Physiol. **107**, 33-41.

**Stadler, R., Wright, K.M., Lauterbach, C., Amon, G., Gahrtz, M., Feuerstein, A., Oparka, K.J., and Norbert Sauer, N.** (2004) Expression of *GFP*-fusions in *Arabidopsis* companion cells reveals non-specific protein trafficking into sieve elements and identifies a novel post-phloem domain in roots. Plant J., accepted for publication.

**Stewart, J.B., and Hermodson, M.A.** (2003). Topology of RbsC, the membrane component of the *Escherichia coli* ribose transporter. J. Bacteriol. **185**, 5234-5239.

**Sun, C.-W., and Callis, J.** (1997). Independent modulation of *Arabidopsis thaliana* polyubiquitin mRNAs in different organs and in response to environmental changes. *Plant J.* **11**, 1017-1027.

**Sweet, G., Gandor, C., Voegele, R., Wittekindt, N., Beuerle, J., Truniger, V., Lin, E.C., and Boos, W.** (1990). Glycerol facilitator of *Escherichia coli*: cloning of glpF and identification of the glpF product. J. Bacteriol. **172**, 424-430.

**Tanner, W.** (1980). Proton sugar cotransport in lower and higher plants. Ber. Deutsch. Bot. Ges. **93**, 167-176.

**Thompson, J.D., Gibson, T.J., Plewniak, F., Jeanmougin, F., and Higgins, D.G.** (1997). The ClustalX windows interface: flexible strategies for multiple sequence alignment aided by quality analysis tools. Nucleic Acids Research, **24**, 4876-4882.

**Wallace, I.S., and Roberts, D.M.** (2004). Homology modeling of representative subfamilies of *Arabidopsis* major intrinsic proteins. Classification based on the aromatic/arginine selectivity filter. Plant Physiol. 135, 1059-1068.

**Weber, A., Servaites, J.C., Geiger, D.R., Kofler, H., Hille, D., Groner, F., Hebbeker, U., and Flügge, U.I.** (2000). Identification, purification, and molecular cloning of a putative plastidic glucose translocator. Plant Cell **12**, 787-802.

**Weig, A.R., and Jakob, C.** (2000). Functional identification of the glycerol permease activity of *Arabidopsis thaliana* NLM1 and NLM2 proteins by heterologous expression in *Saccharomyces cerevisiae*. FEBS Lett. **481**, 293-298.

**Wieczorke, R., Krampe, S., Weierstall, T., Freidel, K., Hollenberg, C.P., and Boles, E.** (1999). Concurrent knock-out of at least 20 transporter genes is required to block uptake of hexoses in *Saccharomyces cerevisiae*. FEBS Lett. **464,** 123-128.

**Williams, L.E., Lemoine, R., and Sauer, N.** (2000). Sugar transporters in higher plants – a diversity of roles and complex regulation. Trends Plant Sci. **5**, 283-290.

**Zardoya, R., Ding, X., Kitagawa, Y., and Chrispeels, M.J.** (2002). Origin of plant glycerol transporters by horizontal gene transfer and functional recruitment. Proc. Natl. Acad. Sci. USA **99**, 14893-14896.

**Zimmermann, M.H., and Ziegler, H.** (1975). List of sugars and sugar alcohols in sieve-tube exudates. In Encyclopedia of Plant Physiology, M.H. Zimmermann and J.A. Milburn, eds (Springer Verlag, Berlin), pp. 480-503.

# Kapitel VIII: Phloem-localized, Proton-coupled Sucrose Carrier ZmSUT1 Mediates Sucrose Efflux under Control of Sucrose Gradient and pmf

**Armando Carpaneto, Dietmar Geiger, Ernst Bamberg, Norbert Sauer, Jörg Fromm und Rainer Hedrich**

**Eingereicht bei PNAS, Oktober 2004**

**Eigene Beteiligung an der Arbeit:**

- Biophysikalische Charakterisierung von ZmSUT1 in *Xenopus* Oozyten mit Hilfe der DEVC-Technik in Bezug auf pH- und Saccharose-abhängigen Transportkinetiken. Bestimmung der Spannungsabhängigkeit der Parameter $K_m$ und $I_{max}$.
- $^{14}C$ Saccharose Influx und Efflux Experimente zur direkten Messung des Saccharosetransports.
- Direkte Bestimmung des Protonentransports über die Oozytenmembran mittels pH-sensitiven Mikroelektroden.
- Auswertung der Daten.

# Phloem-localized, proton-coupled sucrose carrier ZmSUT1 mediates sucrose efflux under control of sucrose gradient and pmf

Carpaneto[2]*, A., Geiger[1]*, D., Bamberg[3], E., Sauer[4], N., Fromm[5], J. and Hedrich [1#], R.

1. *Julius-von-Sachs-Institut, Molekulare Pflanzenphysiologie und Biophysik, Universität Würzburg, Julius-von-Sachs Platz 2, D-97082 Würzburg, Germany*
2. *Istituto di Biofisica-CNR, Via De Marini 6, I-16149 Genova, Italy*
3. *Max-Plank-Institut für Biophysik, Kennedyallee 70, D-60596 Frankfurt, Germany*
4. *Universität Erlangen-Nürnberg, Molekulare Pflanzenphysiologie, Staudtstr. 5 D-91058 Erlangen, Germany*
5. *Technische Universität, Holzforschung, Winzererstr. 45, D-80797 München, Germany*

* *These authors contributed equally to this work*

\# *Corresponding author*

**The phloem network is as essential for plants as the vascular system for humans. This network, assembled by nucleus- and vacuole-free interconnected living cells, represents a long-distance transport pathway for nutrients and information. According to the Munch hypothesis osmolytes like sucrose generate the hydrostatic pressure which drives nutrient and water flow between the source and the sink phloem (Münch 1930). Although proton-coupled sucrose carriers have been localized to the sieve tube and companion cell plasma membrane of both, source and sink tissues, the molecular representatives and mechanism of the sucrose phloem efflux is still scant.**

**We expressed ZmSUT1, a maize sucrose/$H^+$ symporter, in *Xenopus* oocytes and studied the transport characteristics of the carrier by electrophysiological methods. Using the patch clamp techniques in the giant inside-out patch mode we altered the chemical and electrochemical gradient across the sucrose carrier and analysed the currents generated by the proton flux. Thereby we could show that ZmSUT1 is capable of mediating both, the sucrose uptake into the phloem in mature leaves (source) as well as the desorption of sugar from the phloem vessels into heterotrophic tissues (sink). As predicted from a perfect molecular machine, the ZmSUT1-mediated sucrose-coupled proton current was reversible, and depended on the direction of the sucrose- and pH-gradient across the transporter.**

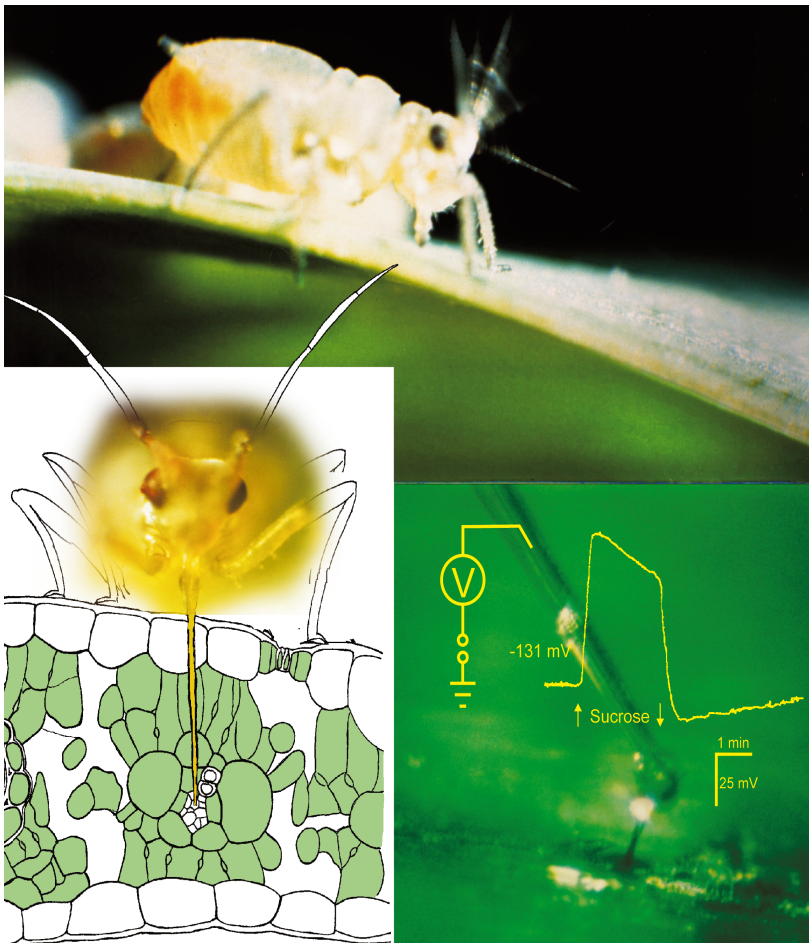


**Supplementary Fig. 1**

**Above:** Side-view of *Rhopalosiphum padi* in feeding position on the upper side of a maize leaf (x 32).

**Below left:** Front-view of *Rhopalosiphum padi* sucking on maize with its stylet inserted into a sieve element of a vascular bundle.

**Below right:** After the aphid separated from its stylet by a laser pulse, the stylet stump exuded sieve tube sap to which the tip of a microelectrode was attached (x 400). Application of sucrose via the apoplast depolarizes phloem potential, pointing to a proton coupled cotransporter. Upon removal of sucrose the membrane potential repolarized.

**Introduction**

In order to ensure adequate partitioning of sucrose throughout the plant body, sucrose has to be translocated from the mesophyll cells to the SE-CC (sieve element-companion cell) complex. Due to energy-dependent $H^+$/sucrose symport in apoplastic loading plant species the transport sugar accumulates at concentrations of several hundred mM to more than one molar. In sink tissues, which are dependent on carbon supply via the phloem, a symplasmic unloading of sucrose along its concentration gradient has been shown for many plant species (Patrick 1997). Interestingly, however, sucrose/$H^+$ symporter transcripts and proteins have also been localized in sink tissues, suggesting a role in sink loading/retrieval or unloading of these transporters (see Lalonde 2003 for review). SUT1 from potato for example has been detected in the sieve elements of mature source leaves as well as in developing sink leaves, in roots (Kühn *et al.,* 1997) and in tubers (Kühn *et al.,* 2003; Viola *et al.,* 2001). Using a sink-specific antisense inhibition for SUT1 under the control of a tuber specific promoter, Kühn *et al.* (2003) could demonstrate the involvement of SUT1 in early tuber development and thus phloem unloading. Further evidence for a sucrose export system was added by the localization of sucrose/$H^+$ symporters expressed in symplasmically isolated tissues, such as developing embryos (Weber *et al.,* 1997; Tegeder *et al.,* 1999) and growing pollen tubes (Lemoine *et al.,* 1999). Although proton-coupled sucrose carriers have been localized to the sieve tube and companion cell plasma membrane of both, source and sink tissues, the molecular representatives and mechanism of the sucrose phloem efflux is still scant. In the present study we tested the biophysical properties and thermodynamics of ZmSUT1, a maize sucrose carrier expressed at a high level in *Xenopus laevis* oocytes. Thereby we could demonstrate that this sugar carrier mediates both sucrose uptake and release. Upon a drop in membrane potential or pH gradient ZmSUT1 would release sucrose from e.g. sink phloem and thus seem to represent the molecular equivalent for the sucrose efflux carrier.

The $H^+$/sucrose cotransporter ZmSUT1 is a member of a large family of membrane proteins mediating the transport of sugars, amino acids, and osmolytes across membranes.

These carriers share the typical 12 transmembrane-spanning α-helices structure (Marger and Saier, 1993; Saier *et al.*, 2000). In most eukaryotic cells these transporters couple the uptake of their substrates to electrochemical ion gradients generated by the $H^+$- or $Na^+/K^+$-ATPase.

**Results**

ZmSUT1 was isolated from maize, expressed in source and sink tissues such as mature leave blades, sheaths as well as pedicels and seeds (Aoki *et al.*, 1999). High sequence homologies to the rice sucrose transporter, OsSUT1 (Hirose *et al.*, 1997) and to known sucrose transporters from dicote species group ZmSUT1 into the SUT2-subfamily of sucrose transporters (for review see Kühn *et al.*, 2003).

Using the aphid stylet technique on maize leaf blades it could be shown that the addition of sucrose reversibly depolarized the phloem potential (Supplementary Information Fig. 1).To elucidate the transport characteristics of the underlying $H^+$/sucrose transporter activity with respect to sucrose affinity gradients and proton-motif-force, we heterologously expressed ZmSUT1 in *Xenopus laevis* oocytes. Functional analysis was performed using both the two-electrode voltage-clamp technique (TEVC) and the patch clamp technique. Oocytes expressing ZmSUT1, efficiently imported radio labeled sucrose with uptake rates of 6 nmol per hour and oocyte, whereas non-injected oocytes did not accumulate sucrose in detectable amounts (Fig. 1A). To monitor the movement of protons accompanying the sucrose transport, we simultaneously recorded sucrose-induced ionic currents and changes in cytoplasmic $pH_i$ by TEVC and proton-selective microelectrodes (Zeuthen *et al.*, 1996). Upon addition of sucrose to the external solution large inward currents were elicited. Inward currents were accompanied by a decrease in $pH_i$, by up to 0.5 units within 10 minutes (lower trace). After removal of sucrose from the bath medium the inward currents returned to the pre-sucrose level again, while the recovery of $pH_i$ was delayed. Control oocytes did neither show sucrose-

induced currents nor sucrose dependent changes in $pH_i$. Stepwise increase in sucrose concentrations resulted in a gradual rise in ZmSUT1-mediated currents (Fig. 1C).

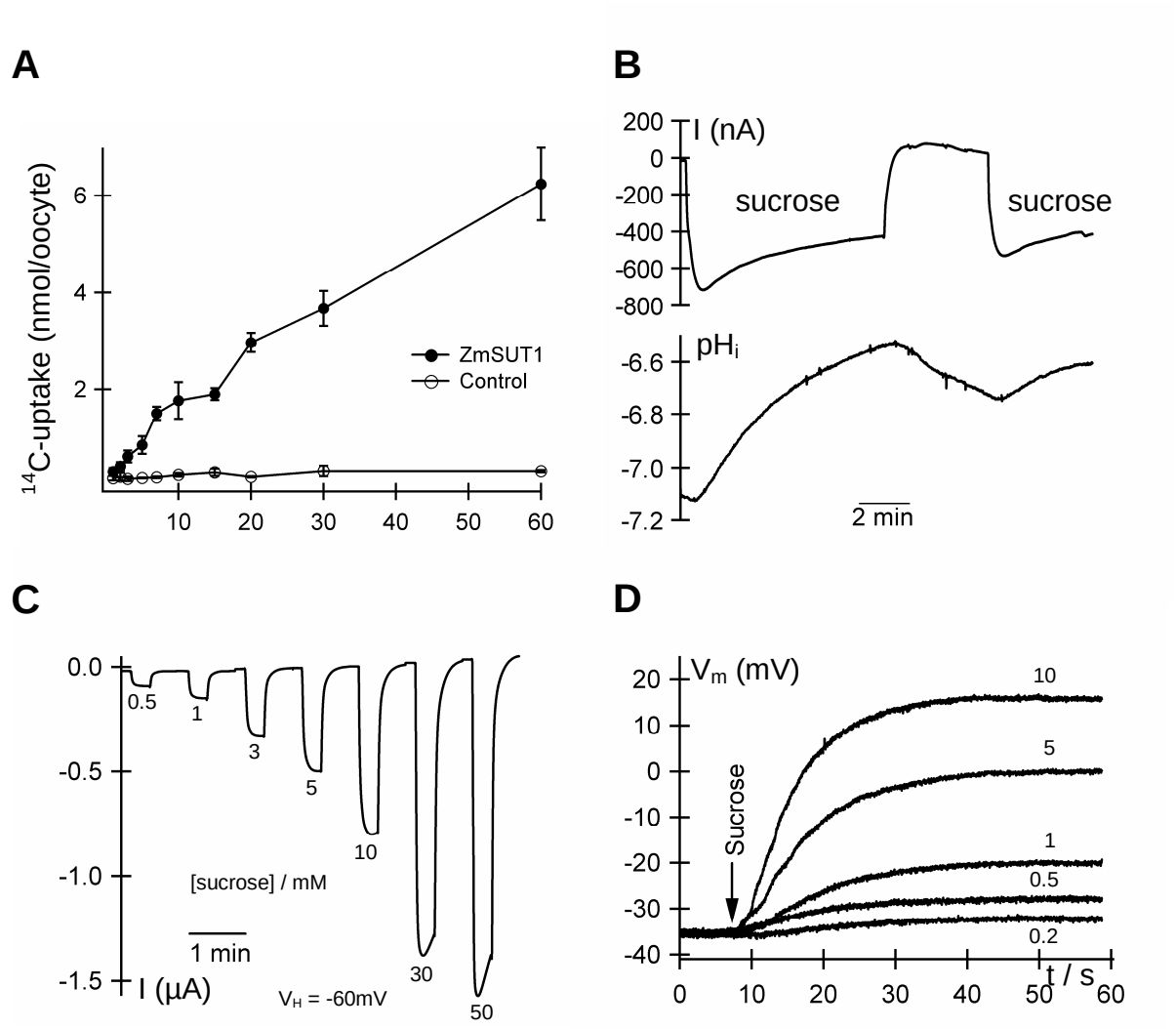


**Fig. 1 ZmSUT1 is a sucrose/$H^+$ Symporter**

(A) Uptake of $^{14}$C sucrose (5 mM final concentration) into ZmSUT1-injected and non-injected Xenopus oocytes over a timescale of 60 minutes at pH 5.6. (B) Parallel measurements of sucrose-dependent inward currents (upper trace) and the cytosolic pH (lower trace) of a ZmSUT1-injected oocyte in response to 5 mM sucrose at an external pH of 5.6 and a holding potential ($V_H$) of -60 mV. Sucrose-induced currents are accompanied by a decrease in cytosolic pH. (C) The sucrose-dependent inward currents were monitored in response to a stepwise increase in sucrose concentrations. $V_H$ = -60 mV. (D) Sucrose concentration-dependent membrane depolarization caused by a series of different sucrose concentrations at pH 5.6.

In the current-clamp mode membrane depolarization in response to different sucrose concentrations could be recorded as well (Fig. 1D). Like the current response in (C), the degree of membrane depolarization depended on the sucrose concentration applied (up to 50 mV with 10 mM sucrose). When the steady-state currents, recorded in presence of extracellular sucrose concentrations between 0.5 and 50 mM, were plotted against the membrane potential, ZmSUT1 currents increased upon hyperpolarization and saturated at 30 mM sucrose (not shown). Plotting the currents as a function of the sucrose concentration a single Michaelis-Menten function could be fitted to the individual, voltage-dependent sucrose saturation curves (Fig. 2A). These current-concentration curves are hyperbolic in shape, suggesting that just one sucrose molecule binds to the transporter. The apparent affinity constant of ZmSUT1, $K_m^S$, exhibited pronounced voltage- and pH-dependence (Fig. 2B; c.f. also Boorer *et al.*, 1996). Hyperpolarizing voltages increased the apparent affinity to sucrose from 16.0 mM at 0 mV to 7.2 mM at -100 mV and pH 5.6. Upon a change to pH 6.5 the sucrose affinity was reduced. Both $K_m^S$-voltage curves could be fitted with a single exponential function, allowing to extrapolate $K_m^S$ to measured phloem potentials of up to –180 mV (Deeken *et al.*, 2002). A $K_m^S$ of 3.7 mM at pH 5.6 and a $K_m^S$ of 12.4 mM at pH 6.5 were calculated. The maximal carrier currents $I_{max}^S$ were found voltage-dependent too (not shown), decreasing linearly with negative-going membrane potentials.

In order to study the proton-coupling of ZmSUT1-mediated sucrose transport, the steady state currents were measured as a function of voltage and pH in the presence of 5 mM sucrose (not shown). As predicted for a proton-coupled transport process, in the pH range between 6.5 and 4.5, ZmSUT1 currents increased with increasing proton concentration and hyperpolarization. At pH values above 7.0 no significant inward currents could be detected. The currents at selected voltages were plotted against the $H^+$ concentration (not shown) and fitted by a single Michaelis-Menten equation to calculate $K_m^H$ and $I_{max}^H$ (not shown). The proton affinity $K_m^H$ of ZmSUT1 exponentially increased with hyperpolarizing membrane potentials (Fig. 2C). This behavior is in line with the results for the sucrose affinities $K_m^S$ (c.f.

Fig. 2B). Thus both, the apparent affinity constants and $I_{max}$ for sucrose as well as for protons decrease upon hyperpolarization.

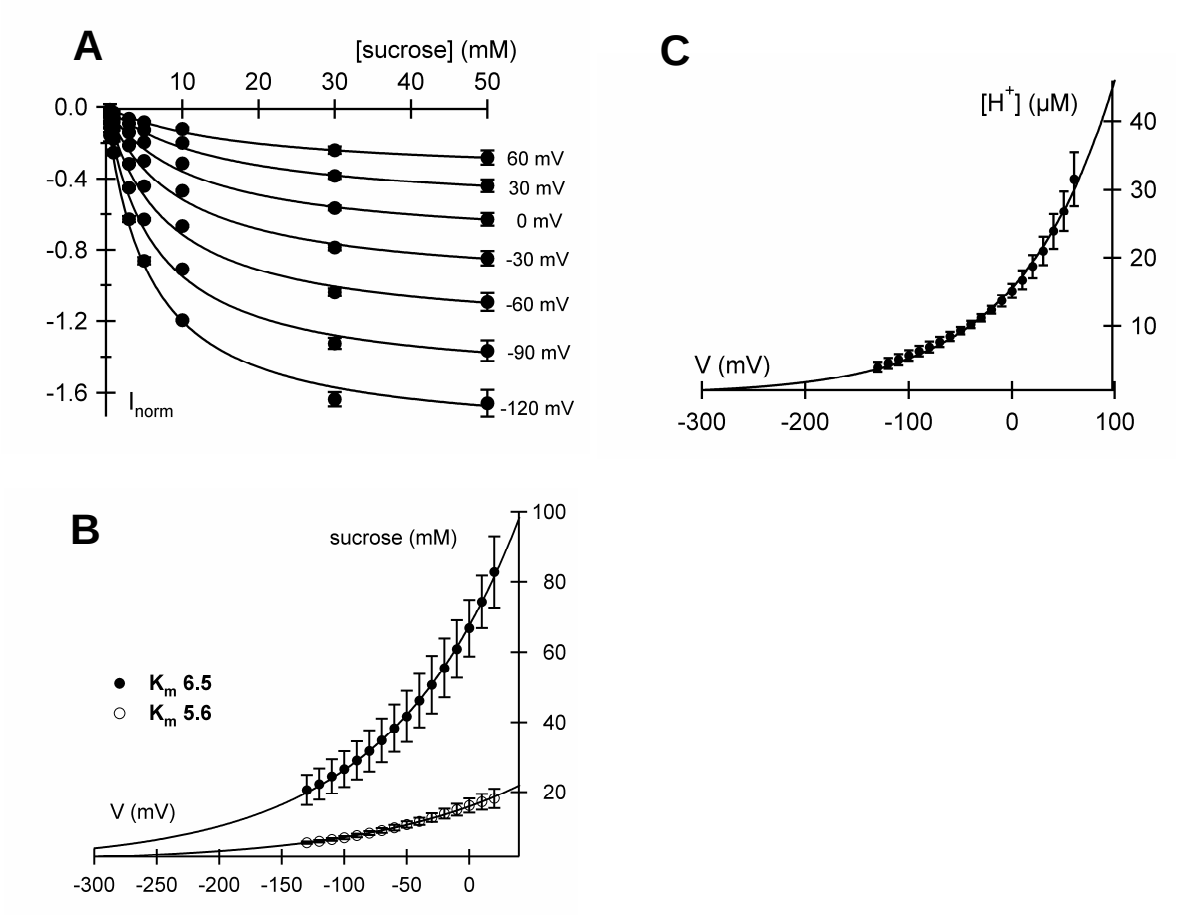


**Fig. 2 Voltage-, sucrose- and pH-dependence of ZmSUT1**

(A) Steady state sugar-dependent inward currents (mean±SD, n=4) at different potentials at pH 5.6 were plotted as a function of the external sucrose concentration. Steady-state currents (currents in the absence of sucrose were subtracted) were normalized to the current induced by 10 mM sucrose and a membrane potential of -100 mV. Curves were fitted with a Michaelis-Menten function. (B) Apparent affinity constants of ZmSUT1 $K_m^S$ (deduced from (A)) as a function of the membrane potential. $K_m^S$ decreases exponentially upon hyperpolarization. Data were fitted with a single exponential function ($[S]=[S_0]$ exp ($V/\tau_0$) with S = substrate) and extrapolated to more positive and more negative voltages. The fitting parameters were at pH 5.6 $S_0$ = 16.1 mM ± 0.7 mM and $\tau_0$ = 122 mV ± 8 mV and $S_0$ = 67 mM ± 3 mM and $\tau_0$ = 108 mV ± 10 mV at 6.5 (C) The half-maximal proton concentration $K_m^H$, was determined from the Michaelis-Menten fit (not shown) and plotted against the membrane potential. Like $K_m^S$, $K_m^H$ was voltage-dependent and could be fitted with a single exponential function as in (B) with $S_0$ =15.4 µM ± 0.3 µM and $\tau_0$ = 98 mV ± 5 mV.

To study the inverse transport mode of ZmSUT1 and affinity towards cytosolic sucrose we applied the giant-patch-clamp technique to ZmSUT1 expressing oocytes. In the inside-out

configuration we varied the "cytosolic" sucrose concentration in the presence of either 0.5, 5 or 50 mM extracellular (pipette) sucrose. Upon a stepwise increase in cytosolic sucrose from 0 to 50, 100, 200 and 500 mM in the presence of 50 mM in the pipette a progressive decrease in inward current was measured (Fig. 3A). This effect was completely reversible - inward currents reached their pre-stimulus levels after the removal of cytosolic sucrose. When plotting the average currents shown in (A) as a function of the cytosolic sucrose concentration, data could be fitted by a Michaelis-Menten equation (continuous line) characterized by an apparent $K_m$ of 160 mM (Fig. 3E). The inset of figure 3E depicts the extrapolation of the sucrose-induced currents from 2 to 3 M, a concentration range in which ZmSUT1 currents would reverse direction (I=0 at 2.38 M sucrose). When the extracellular sucrose concentration was decreased to 5 mM or even 0.5 mM, the ZmSUT1-mediated currents reversed direction at physiological cytosolic sucrose levels (Fig. 3B and C). In the presence of 5 mM external sucrose a $K_m$ of 278 mM was calculated (Fig. 3F). A rise in cytosolic sucrose concentration above 314 mM even inverted the current direction. Upon a further decrease in extracellular sucrose concentration to 0.5 mM and absence of cytosolic sucrose only very small inward currents remained (Fig. 3C). Under these conditions, however, a rise in cytosolic sucrose concentration to just 50 mM inverted the ZmSUT1 current already. From the Michaelis-Menten fit a $K_m$ of 362 mM and a zero current value at 31 mM was obtained (Fig. 3G). When plotting the $K_m$ values versus the external sucrose concentration, a decrease in $K_m$ with the rise in external sucrose concentration became evident (not shown).

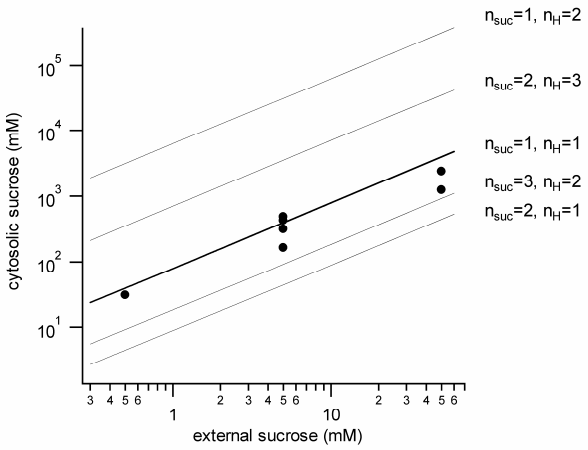


**Supplementary Fig. 2 Stoichiometry between $H^+$ and sucrose of ZmSUT1**

The cytosolic sucrose concentration inducing zero current, obtained by experiments as shown in Fig. 3, plotted against the external sucrose concentration. The continuous lines were obtained by the equilibrium equation (2) with $V_m$ = 0, with $pH_{cyt}$-$pH_{ext}$ = 1.9 and using different values for $n_{suc}$ and $n_H$ (the thicker line correspond to a 1:1 stoichiometry of the ZmSUT1 transporter). The same experimental conditions as in Fig. 3 were used.

Likewise, the cytosolic sucrose concentration causing the ZmSUT1 current to change direction was plotted as a function of external sucrose (supplementary Fig 2). Under equilibrium conditions:

$$n_{suc}\Delta\mu_{suc} + n_H\Delta\mu_{H^+} = 0 \qquad (1)$$

where $n_{suc}$ and $n_H$ are the number of moles of sucrose and protons transported through the membrane, $\Delta\mu_{suc} = \mu_{suc}^{cyt} - \mu_{suc}^{ext}$ is the difference between the cytosolic and external chemical potential (or molar free energy) of sucrose and $\Delta\mu_{H^+} = \mu_{H^+}^{cyt} - \mu_{H^+}^{ext}$ is the difference between the cytosolic and external electro-chemical potential of protons. Equation 1 can be written as:

$$[Suc]_{cyt} = [Suc]_{ext}\ 10^{\frac{n_H}{n_{suc}}\left(pH_{cyt} - pH_{ext} - \frac{FV_m}{2.303RT}\right)} \qquad (2)$$

The continuous lines in supplementary Fig 2 are obtained by equation 2 with V=0 mV and using different values for $n_{suc}$ and $n_H$. This analysis revealed that the ZmSUT1 transporter has a 1 Suc /1 $H^+$ stoichiometry (c.f. Boorer et *al.*, 1996 and Zhou *et al.*, 1997).

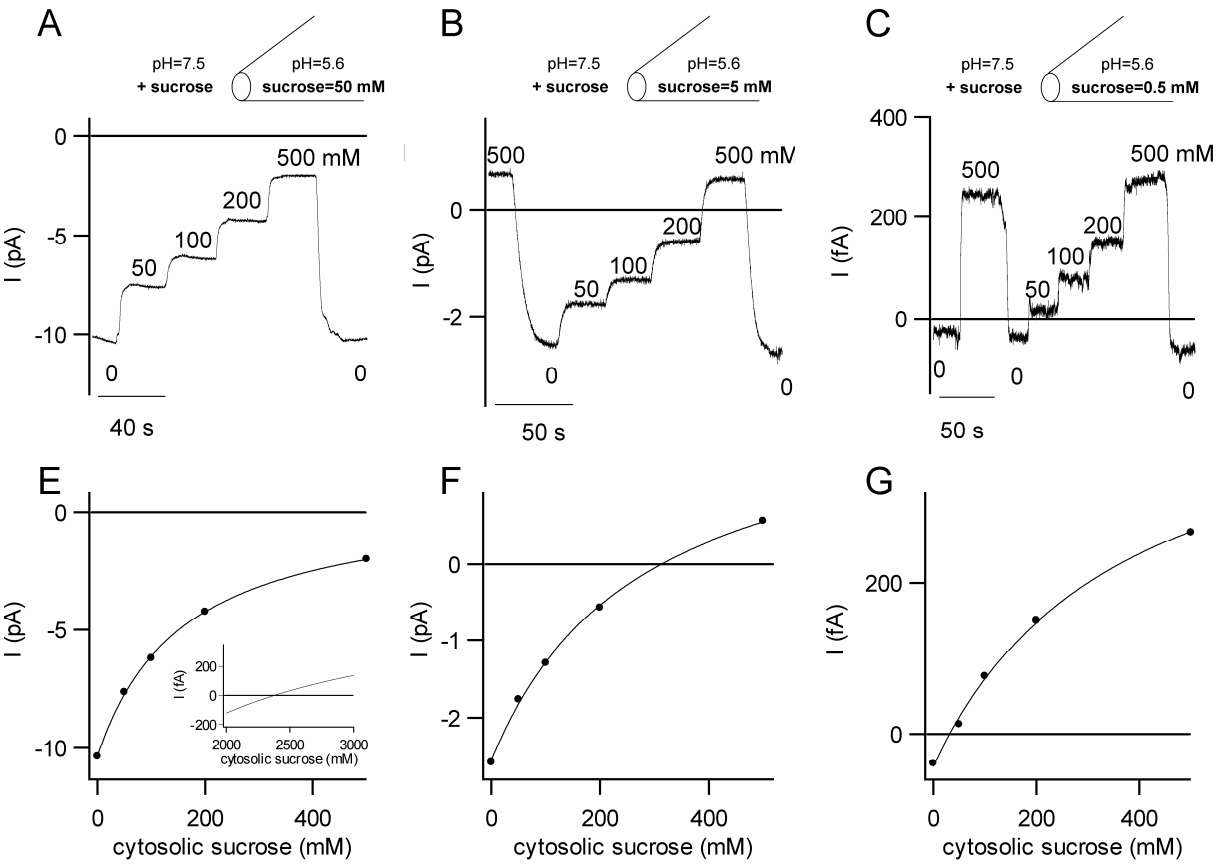

**Fig. 3 Changes in cytosolic sucrose feedback on magnitude and direction of ZmSUT1 currents. (previous page)**

ZmSUT1 currents recorded in inside-out giant-patches in the presence of A) 50 mM B) 5 mM and C) 0.5 mM external sucrose. Schematically representations above each graph depict the proton- and sucrose concentration; cytosolic and external pH were 7.5 and 5.6 respectively, cytosolic sucrose concentrations were elevated from 0 to 50, 100, 200 and 500 mM as indicated. The membrane was clamped to 0 mV. E-F-G) Averaged currents gained from experiments shown in A-B-C were plotted versus the corresponding cytosolic sucrose concentration. Data were fitted by the Michaelis-Menten equation: $I = I_1 \frac{[Suc]_{cyt}}{[Suc]_{cyt} + K_m} - I_0$ with E) $I_1$=11.0 pA, $K_m$=161 mM and $I_0$=10.3 pA, F) $I_1$=4.83 pA, $K_m$=278 mM and $I_0$=2.56 pA, G) $I_1$=536 fA, $K_m$=362 mM and $I_0$=42.7 fA. The inset of panel E shows the current extrapolation for cytosolic sucrose concentrations ranging from 2 to 3 M.

In agreement with a perfect-coupled thermodynamic machine the positive current in Fig. 3 represents the sucrose gradient-driven efflux of protons against the proton gradient. To study the two transport modes of ZmSUT1 in the absence of the pmf, in Fig. 4A we stepped the cytosolic sucrose concentration from 0 to 500 mM (5 mM sucrose in the pipette) in the absence of a pH gradient. With $[Suc]_{cyt}$=0 mM and absence of a membrane potential we recorded an inward current as expected from the steep inward-directed sucrose gradient. Inverting the sucrose gradient by increasing $[Suc]_{cyt}$ to 500 mM, the carrier current reversed direction. In the presence of an inward-directed pH gradient, however the magnitude of outward currents was smaller (c.f. Fig. 3). Inward currents could be re-established again upon removal of the disaccharide. Following a rise in the extracellular sucrose concentration from 5 to 50 mM and the absence of cytosolic sucrose, carrier currents remained inward (Fig. 4B). During bath perfusion to $[Suc]_{cyt}$=500 mM currents changed direction. These experiments indicate that the sucrose gradient can drive the proton flux and vice versa. In the experiment depicted in Fig 4B the ZmSUT1 currents were subject of a fast “run-down” most likely due to the loss of regulatory cytosolic factors. Interestingly, in Fig. 4B the decay of both, inward and outward current could be fitted by single exponential functions (dashed lines) with the same time constant. This indicates that both transport modes of ZmSUT1 are perfectly coupled via the sucrose gradient and pmf.

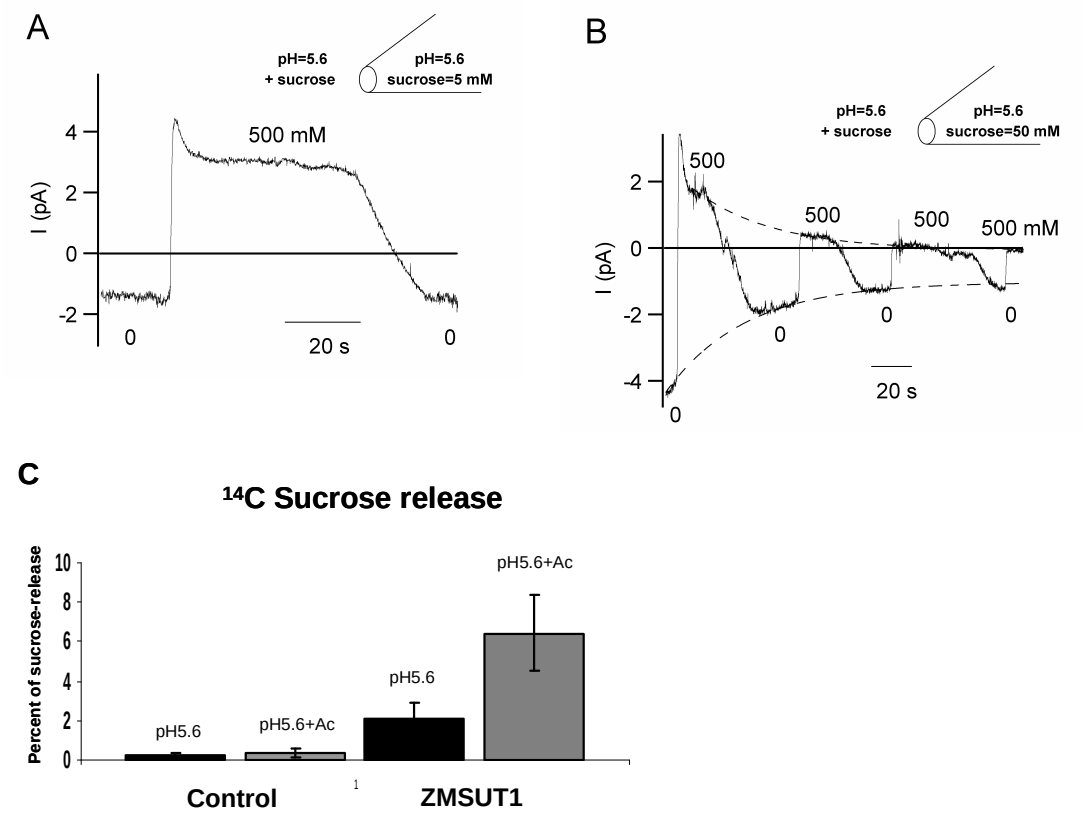


**Fig. 4 Inward and inverse transport mode of ZmSUT1**

A) Change in direction of ZmSUT1 currents upon changes in cytosolic sucrose concentration from 0 to 500 mM recorded in inside-out giant patches. Note that the pH was symmetrical 5.6 on both sides of the membrane. External sucrose was 5 mM and the membrane voltage was 0 mV. B) Similar experiment as in (A) but in the presence of 50 mM external sucrose. This recording was chosen because a fast run-down of the current was apparent. The decay of both positive and negative currents could be fitted by single exponentials with the same time constant (τ = 40 s). C) Percentage of sucrose release from $^{14}C$ sucrose injected, ZmSUT1-expressing and control oocytes. The percentage of sucrose release was measured after two hours of oocyte incubation in a 1 mM sucrose solution at pH 5.6 or pH 5.6 plus 5 mM acetate.

Under the conditions of the sink phloem the sucrose gradient drives the efflux of protons and sucrose. To mimic this situation in the oocyte system in Fig. 4C ZmSUT1-expressing oocytes were injected with $^{14}C$-sucrose (final concentration of 50 mM) and the release of the radioactive-labelled sucrose was measured. In ZmSUT1-oocytes but not in water-injected control-oocytes pronounced sucrose release was measured. As expected from our thermodynamic assumptions, the sucrose-release was enhanced when the cytosol was acidified by acetate treatment.

**Discussion**

Due to the localization of sucrose/$H^+$ transporter in sink tissues it has previously been speculated that phloem unloading may be mediated by the same sucrose-$H^+$ symporters that are responsible for phloem loading (e.g. Truernit and Sauer 1995). The direct demonstration that ZmSUT1, a member of the phloem sucrose carrier family, acts either in the source- or sink mode for the life-maintaining uptake and adsorption of sucrose is underpinned by genetic evidence. *Arabidopsis* mutants, which lack the ZmSUT1 homologue AtSUC2 are strongly impaired in phloem loading and unloading of sucrose which results in stunted growth, retarded development and sterility (Gottwald *et al.*, 2000). Phloem unloading of sucrose is required for starch formation in storage tissues, such as the grains of cereals or potato tubers. When the copy number of StSUT1, a ZmSUT1 orthologue expressed in the phloem of developing tubers, is reduced by antisense repression, reduced fresh weight accumulation during tuber development was observed (Kühn *et al.*, 2003; Viola *et al.*, 2001). Furthermore indirect measurements with the proton-coupled monosaccharide transporter CkHUP1 from the green alga Chlorella suggest that this sugar carrier from single celled organisms can act in the inverse transport mode to release their substrates (Komor and Tanner 1974). In order to study the inverse mode of ZmSUT1 we performed patch-clamp experiments in the giant inside-out configuration. Varying the cytosolic sucrose concentration we were for the first time able to determine the cytosolic affinity constant for sucrose. Upon variation of the sucrose gradient we could reverse the direction of the proton current e.g. by increasing the cytosolic sucrose concentration. The direction of the transport of the ZmSUT1 symporter is therefore dependent on the sum of the free energies of both the sucrose and the proton gradient across the membrane. In agreement with the above considerations we could demonstrate that sucrose could drive the protons through ZmSUT1. Recently the reversibility of the human and rabbit $Na^+$/glucose cotransporters has been documented by measuring the reversion of the glucose-coupled $Na^+$ current (Sauer *et al.*, 2000; Quick *et al.*, 2003). Alike the proton-coupled disaccharide carrier ZmSUT1, the sodium-coupled SGLT1 shows more

than one order of magnitude difference between the sugar affinities of the two transport modes, indicating a functional asymmetry of both carrier types. Under physiological conditions the inverse transport mode of SGLT1 is highly improbable due to the low affinity of the sugar carrier. In the plant phloem, however, both transport modes of ZmSUT1 are probable (Model supplementary Fig. 3): i) in maize source leaves extracellular sucrose concentrations of 2.6 mM were measured (Lohaus *et al.,* 2000). Assuming a pH gradient around 1.5 units and a phloem membrane potential of -150 mV (van Bel 1993) a perfect proton-coupled ZmSUT1 would allow a theoretical phloem sucrose accumulation of up to 26 M (according to the equation (2) with $n_H/n_{suc}=1$). Directly measured sucrose concentrations of maize phloem sap revealed sucrose contents of around 0.85 M (Lohaus *et al.,* 2000). ii) in the sink phloem, however, the external sucrose concentration is reduced to 1 mM or less, due to the activity of cell wall bound invertases (e.g. Roitsch *et al.,* 2003). A symplastic unloading is unlikely, because of the lack of plasmodesmata in the proto- and metaphloem at least in maize leaves (Evert and Russin 1993). Furthermore in the region of the release phloem the proton-motif-force across the phloem membrane is less strong because of the reduced size (or even absence) of the energy-supplying companion cells (van Bel 1993; van Bel and Ehlers 2000). Therefore the phloem membrane potential mainly depends on the potassium conductance mediated by $K^+$-channels (Ache *et al.,* 2001). At an apoplasmic sucrose concentration of 1 mM, a phloem sap sucrose concentration of 0.85 M and a pH gradient of 1 unit sucrose release would occur at membrane potentials positive from -115 mV (according to equation 2 with $n_H/n_{suc}=1$). This regime directs ZmSUT1 into the inverse transport mode and sucrose is released.

The present work revealed the functional asymmetry of the phloem sucrose carrier ZmSUT1. Our data, for the first time, demonstrate the `sink mode´ of this pivotal carrier type, provide for the molecular mechanism of phloem sucrose release and explain the severe phenotype of phloem $H^+$/sucrose carrier loss-of-function mutants and antisense-repression plants**.**

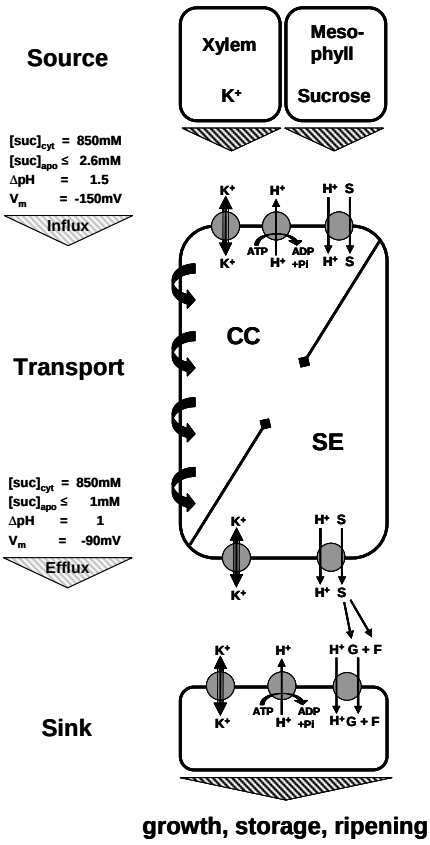


**Supplementary Fig. 3 Model for apoplasmic sucrose loading and unloading by sucrose/$H^+$ Symporter, modified after Ache *et al.,* (2001).**

The source site of the SE/CC complex is characterised by an outward-directed sucrose and inward-directed $H^+$ gradient. The membrane potential is hyperpolarized due to the activity of the $H^+$-ATPases localized in the companion cells. Under these conditions sucrose is accumulated in the phloem cells by $H^+$/sucrose symporters, like ZmSUT1. In the sink phloem the apoplastic concentrations of sucrose is reduced and the membrane potential is depolarized to values around -90 mV. In this region the membrane potential mainly depends on the potassium conductance because of the reduced size (or even absence) of the energy-supplying companion cells. Thus pmf is decreased. This regime directs ZmSUT1 into the inverse transport mode and sucrose is released. Abbreviations: CC =Companion Cell, SE = Sieve Element, F = Fructose, G = Glucose, S =Sucrose.

**References**

**Ache P, Becker D, Deeken R, Dreyer I, Weber H, Fromm J, Hedrich R**. **2001.** VFK1, a *Vicia faba* $K^+$ channel involved in phloem unloading. *Plant Journal* **27:** 571-580.

**Aoki N, Hirose T, Takahashi S, Ono K, Ishimaru K, Ohsugi R**. **1999.** Molecular cloning and expression analysis of a gene for a sucrose transporter in maize (*Zea mays* L.). *Plant Cell Physiol* **40:** 1072-1078.

**Becker D, Dreyer I, Hoth S, Reid JD, Busch H, Lehnen M, Palme K, Hedrich R**. **1996.** Changes in voltage activation, $Cs^+$ sensitivity, and ion permeability in H5 mutants of the plant $K^+$ channel KAT1. *Proc.Natl.Acad.Sci.U.S.A* **93:** 8123-8128.

**Boorer KJ, Loo DDF, Frommer WB, Wright EM**. **1996.** Transport mechanism of the cloned potato $H^+$/sucrose cotransporter StSUT1. *Journal of Biological Chemistry* **271:** 25139-25144.

**Deeken R, Geiger D, Fromm J, Koroleva O, Ache P, Langenfeld-Heyser R, Sauer N, May ST, Hedrich R**. **2002.** Loss of the AKT2/3 potassium channel affects sugar loading into the phloem of *Arabidopsis*. *Planta* **216:** 334-344.

**Evert RF, Russin WA**. **1993.** Structurally, Phloem Unloading in the Maize Leaf Cannot be Symplastic. *American Journal of Botany* **80:** 1310-1317.

**Gottwald JR, Krysan PJ, Young JC, Evert RF, Sussman MR**. **2000.** Genetic evidence for the in planta role of phloem-specific plasma membrane sucrose transporters. *Proc.Natl.Acad.Sci.U.S.A* **97:** 13979-13984.

**Hilgemann D**. **1995.** The Giant Membrane Patch. In: Sakmann B, Neher E, eds. *Single-Channel Recording*. New York; London: Plenum Press, 307-327.

**Hirose T, Imaizumi N, Scofield GN, Furbank RT, Ohsugi R**. **1997.** cDNA cloning and tissue specific expression of a gene for sucrose transporter from rice (*Oryza sativa* L.). *Plant Cell Physiol* **38:** 1389-1396.

**Komor E, Tanner W**. **1974.** Can energy generated by sugar efflux be used for ATP synthesis in Chlorella? *Nature* **248:** 511-512.

**Kühn C**. **2003.** A Comparison of the Sucrose Transporter Systems of Different Plant Species. *Plant Biology* **5:** 215-232.

**Kühn C, Franceschi VR, Schulz A, Lemoine R, Frommer WB**. **1997.** Macromolecular trafficking indicated by localization and turnover of sucrose transporters in enucleate sieve elements. *Science* **275:** 1298-1300.

**Kühn C, Hajirezaei MR, Fernie AR, Roessner-Tunali U, Czechowski T, Hirner B, Frommer WB**. **2003.** The sucrose transporter StSUT1 localizes to sieve elements in potato tuber phloem and influences tuber physiology and development. *Plant Physiol* **131:** 102-113.

**Lalonde S, Tegeder M, Throne-Holst M, Frommer WB, Patrick JW**. **2003.** Phloem loading and unloading of sugars and amino acids. *Plant, Cell and Environment*.

**Lemoine R, Burkle L, Barker L, Sakr S, Kuhn C, Regnacq M, Gaillard C, Delrot S, Frommer WB**. **1999.** Identification of a pollen-specific sucrose transporter-like protein NtSUT3 from tobacco. *FEBS Lett.* **454:** 325-330.

**Lohaus G, Hussmann M, Pennewiss K, Schneider H, Zhu JJ, Sattelmacher B**. **2000.** Solute balance of a maize (*Zea mays* L.) source leaf as affected by salt treatment with special emphasis on phloem retranslocation and ion leaching. *Journal of Experimental Botany* **351:** 1721-1732.

**Marger MD, Saier MH, Jr. 1993.** A major superfamily of transmembrane facilitators that catalyse uniport, symport and antiport. *Trends Biochem.Sci.* **18:** 13-20.

**Münch E**. **1930.** *Die Stoffbewegungen in der Pflanze*. Fischer.

**Patrick J**. **1997.** Phloem unloading: sieve element unloading and post-sieve element transport. *Annual Review of Plant Physiology* **48:** 191-222.

**Quick M, Tomasevic J, Wright EM**. **2003.** Functional asymmetry of the human $Na^+$/glucose transporter (hSGLT1) in bacterial membrane vesicles. *Biochemistry* **42:** 9147-9152.

**Roitsch T, Balibrea ME, Hofmann M, Proels R, Sinha AK**. **2003.** Extracellular invertase: key metabolic enzyme and PR protein. *Journal of Experimental Botany* **54:** 513-524.

**Saier MH, Jr., Beatty JT, Goffeau A, Harley KT, Heijne WH, Huang SC, Jack DL, Jahn PS, Lew K, Liu J, Pao SS, Paulsen IT, Tseng TT, Virk PS**. **2000.** The major facilitator superfamily. *Journal of Biological Chemistry*.

**Sauer GA, Nagel G, Koepsell H, Bamberg E, Hartung K**. **2000.** Voltage and substrate dependence of the inverse transport mode of the rabbit Na(+)/glucose cotransporter (SGLT1). *FEBS Lett.* **469:** 98-100.

**Tegeder M, Wang XD, Frommer WB, Offler CE, Patrick JW**. **1999.** Sucrose transport into developing seeds of *Pisum sativum* L. *Plant Journal* **18:** 151-161.

**Truernit E, Sauer N**. **1995.** The promoter of the *Arabidopsis thaliana* SUC2 sucrose-$H^+$ symporter gene directs expression of beta-glucuronidase to the phloem: evidence for phloem loading and unloading by SUC2. *Planta* **196:** 564-570.

**van Bel A.J.E**. **1993.** The transport phloem. Specifics of its functioning. *Progress in Botany* **54:** 134-150.

**van Bel A.J.E., Ehlers K. 2000.** Symplasmic organization of the transport phloem and implications for photosynthate transfer to the cambium. *Cell and Molecular Biology of Wood Formation* 85-99.

**Viola R, Roberts AG, Haupt S, Gazzani S, Hancock RD, Marmiroli N, Machray GC, Oparka KJ**. **2001.** Tuberization in potato involves a switch from apoplastic to symplastic phloem unloading. *Plant Cell* **13:** 385-398.

**Weber H, Borisjuk L, Heim U, Sauer N, Wobus U**. **1997.** A role for sugar transporters during seed development: Molecular characterization of a hexose and a sucrose carrier in *fava bean* seeds. *Plant Cell* **9:** 895-908.

**Wright J.P., Fisher D.B. 1981.** Measurement of the sieve tube membrane potential. *Plant Physiology* **67:** 845-848.

**Zeuthen T, Hamann S, la Cour M**. **1996.** Cotransport of $H^+$, lactate and $H_2O$ by membrane proteins in retinal pigment epithelium of bullfrog. *J.Physiol.* **497:** 3-17.

**Zhou J-J, Theodoulou F, Sauer N, Sanders D, Miller AJ**. **1997.** A Kinetic Model with Ordered Cytoplasmic Dissociation for SUC1, an *Arabidopsis* $H^+$/Sucrose Cotransporter Expressed in *Xenopus* Oocytes. *J Membr.Biol.* **159:** 113-125.

**Methods**

**Aphid breeding**. *Rhopalosiphum padi* were breeded on barley and maize grown in climate chamber under a 14 h photoperiod.

**Experimental set-up**. To mature leaves of a 4 week-old potted maize plant aphid cages were applied. Aphids feeding on the leaf were dissected from their stylet using a laser as published previously (Wright and Fisher, 1981). The recording electrodes were brought in contact to the phloem exudate appearing at the cut end of the stylet. The leaf was cut 15 cm proximal to the tip and the cut end was incubated with artificial pond water (APW) containing the reference electrode (Ag/AgCl) and 1.0 mM NaCl, 0.1 mM KCl, 0.1 mM $CaCl_2$, 100 mM sorbitol, and 1.0 mM MES, adjusted to pH 6.0 with Tris. Sucrose pulses were applied by perfusion of APW solution. Phloem potential measurements were recorded according to.

**TEVC analysis in *Xenopus* oocytes.** ZmSUT1 cRNA was prepared using the mMESSAGE mMACHINE$^{TM}$ RNA Transcription kit (Ambion Inc., Texas, USA). Oocyte preparation and cRNA injection have been described elsewhere (Becker *et al.,* 1996). In two-electrode voltage-clamp studies oocytes were perfused with a standard-solution containing 30 mM KCl, 1 mM $CaCl_2$, and 1.5 mM $MgCl_2$ based on Tris/Mes buffers for pH values from 5.6 to 8.0 or based on citrate/Tris buffers for the pH values 4.5 and 5.0. The sucrose concentrations and pH values are indicated in the figures and the text. All solutions were adjusted to 220 mosmol $kg^{-1}$ using D-sorbitol. Steady state currents were obtained by stepping the membrane potential from the holding potential ($V_H$) equal 0 mV to a series of 500 ms test pulses from 60 to -130 mV in 10 mV decrements. Difference-currents were calculated by subtracting the currents in the absence of sucrose from the currents in its presence. The sucrose induced steady state currents were measured in respect to ligand concentrations and membrane potential. At each test potential the currents were fitted to the Michaelis-Menten equation,

$$I = I_{max}^{S} [S]/([S] + K_m^{S})$$

where the substrate (S) is either [sucrose] or [$H^+$]. These fits yielded in the maximal currents $I_{max}^S$ for sucrose and $I_{max}^H$ for $H^+$ and the half maximal ligand concentrations $K_m^H$ for $H^+$ and $K_m^S$ for sucrose.

**Intracellular pH measurements.** PH-sensitive microelectrodes were pulled from borosilicate capillary (TW100F-3, WPI, Sarasota, USA) using a laser puller (Sutter Instruments CO., P2000, Novato, USA) and silanized with dimethyl-dichlorsilane (Fulka, Steinheim, Germany) at 200°C for 15 minutes. The tips of the pH microelectrodes were filled with hydrogen ionophore I cocktail B (Fulka, Steinheim, Germany) and then backfilled with a buffer containing 40 mM $KH_2PO_4$, 23 mM NaOH, and 150 mM NaCl (pH 6.8). Only electrodes, with a linear slope of 55 to 60 mV/pH unit over the calibration range before and after the measurement, were used. Signals were recorded with an electrometer (Model FD 223, WPI, Sarasota, USA) in parallel to the currents in the voltage clamp mode of a TEVC amplifier (Turbo TEC 10CD, npi electronic GmbH, Tamm, Germany). On the basis of the calibration curve for the pH microelectrodes, the internal pH ($pH_i$) of the oocytes was calculated in consideration of the membrane potential.

**$^{14}$C sucrose uptake experiments.** In each experiment 10 ZmSUT1 injected oocytes or 10 control oocytes were incubated in 0.05 µCi/ml $^{14}$C sucrose with a final sucrose concentration of 5 mM in the standard solution at pH 5.6. At defined time points the oocytes were rapidly washed three times in ice-cold standard solution and transferred to liquid-scintillation vials containing scintillation cocktail (Emulsifier-Safe™, Packard, Meriden, USA). The $^{14}$C radioactivity was counted in a liquid scintillation analyzer (Model 1900CA, Packard, Meriden, USA) and the sucrose uptake per oocyte was calculated from three independent experiments for each time point.

**$^{14}$C sucrose release experiments.** Control oocytes and ZmSUT1 injected oocytes were loaded with 0.5 µCi radiolabeled sucrose with a final sucrose concentration of about 50 mM by injection (Picospritzer™ II, General Valve™ CO, Fairfield, USA). After a 10 minute washing period in ice cold ND96, each single oocyte was transferred into 200µl of the

standard solution at pH 5.6 or pH 5.6 in the presence of 10 mM acetate. After 2 h the $^{14}C$ radioactivity of the incubation-solution was measured in a scintillation counter. The oocytes were rapidly washed in ice-cold standard solution and transferred to the scintillation cocktail for counting the $^{14}C$ radioactivity in the liquid scintillation analyzer. The percentage of sucrose release was calculated.

**Patch-clamp measurements.** Giant-patch recording (Hilgemann 1995) was performed in inside-out configuration on ZmSUT1 expressing *Xenopus* oocytes. Borosilicate glass pipettes were pulled and fire-polished to have a final tip between diameter between 25 and 30 µm. Oocytes were bathed in the following external solution (in mM): KCl 30, $CaCl_2$ 1, $MgCl_2$ 1.5, $GdCl_3$ 1, sorbitol 145, Mes/Tris 10, pH 5.6. After the seal was obtained, the external solution was changed (in mM: KCl 30, EGTA 1, $MgCl_2$ 2, sorbitol 145 (or 500), Tris/Mes 10, pH 7.5) and the patch was excised. The recording pipette was then placed in front to a polyethylene tube in connection with the desired ionic solutions that were driven by gravity. Standard cytosolic solution contained (in mM): KCl 30, EGTA 1, $MgCl_2$ 2. The cytosolic sucrose concentration ranged from 0 to 500 mM, as indicated in the text; sorbitol was appropriately added to each cytosolic solution to have a total sugar concentration of 500 mM. Cytosolic pH was 7.5 or 5.6 (with 10 mM Tris/Mes or Mes/Tris). The standard pipette solution was (in mM): KCl 30, $CaCl_2$ 1, $MgCl_2$ 1.5, sorbitol 145, Mes/Tris 10, pH 5.6; sucrose was added at concentrations of 0.5, 5 and 50 mM as indicated in the text. Currents, filtered at 10 or 100 Hz and sampled at 200 or 400 Hz, were recorded with an EPC9 amplifier using Pulse 8.3 software (Heka elektronic GmbH, Lembrecht, Germany). Data were analyzed by custom-made programs using Igor (Wavemetrics, Lake Oswego, Ore., USA).

**Acknowledgements.** We would like to thank Dr. N. Aoki for his generous supply of the ZmSUT1 cDNA. This work was funded by Deutsche Forschungsgemeinschaft grants to R.H.. A.C.`s stay was founded by a guest-scientist stipend of the SFB 487, Würzburg.

**Correspondence** and requests for materials should be addressed to R.H. (e-mail: hedrich@botanik.uni-wuerzburg.de).

# 3. Ergebnisse unveröffentlichter Arbeiten

Im Folgenden werden ergänzende unveröffentlichte Ergebnisse dargestellt, die im Zusammenhang mit der Phloemphysiologie stehen.

## Kapitel IX. Elektrophysiologische Charakterisierung von KAT2

KAT2, ein Vertreter der KAT1-Unterfamilie in *Arabidopsis*, ist auf Aminosäureebene zu 72% identisch mit KAT1. Bereits 1997 konnten Bush *et al.* eine Teilsequenz dieses *Shaker*-Kaliumkanals klonieren. Durch 5´Race-Technik und PCR-Walking konnte schließlich die komplette KAT2-cDNA und die Promotorregion isoliert werden (Pilot *et al.*, 2001). Northern-Blot Experimente und Promotor::GUS Analysen haben gezeigt, dass KAT2-Transkripte ausschließlich in den überirdischen Teilen der Pflanze zu finden sind. In sich entwickelnden Blättern war eine GUS-Färbung in allen Zellen zu detektieren, während in ausgewachsenen Blättern vor allem die Stomata und die feinadrigen Gefäße (minor veins) gefärbt waren. In Querschnitten ausgewachsener Blätter war zu erkennen, dass nur die feinadrigen Phloemgefäße aber nicht die Xylemparenchymzellen eingefärbt waren. Des Weiteren konnten GUS-Färbungen in Schließzellen von Stängel, Hypokotyl und Petiole festgestellt werden, jedoch nicht in den Phloemgefäßen dieser Gewebe.

### 1. Funktionelle Charakterisierung in *Xenopus* Oozyten

Für die heterologe Expression von KAT2 in Oozyten des südafrikanischen Krallenfrosches, *Xenopus leavis*, wurde die KAT2-cDNA mit Hilfe des T7 mMessage$^{TM}$ mMachine$^{TM}$ Kits (Ambion Inc., Texas, USA) in die entsprechende cRNA überführt. 24 bis 48 Stunden nach der Injektion von 30-50 ng dieser KAT2-cRNA in unreife *Xenopus* Oozyten konnten die Kanalproteine mit der Zwei-Elektroden-Spannungsklemmen-Technik (DEVC) biophysikalisch charakterisiert werden. Datenerhebung und Auswertung wurden in ähnlicher Weise wie bei der elektrophysiologischen Analyse von KZM1 durchgeführt (Kapitel IV und darin enthaltene Referenzen).

## 2. Spannungsabhängigkeit und Selektivität von KAT2

Ausgehend von einer Haltespannung von -20 mV wurde eine Serie von 2,5 s langen Einzelspannungspulsen appliziert, die in 10 mV Schritten von 20 mV bis -160 mV reichten (Abb.: 3.1A). Die Hyperpolarisation der Oozytenmembran auf Werte negativ von -90 mV führte zu einem makroskopischen Einwärtsstrom mit einer relativ langsamen Aktivierungs- und Deaktivierungskinetik. In nicht-injizierten Kontrolloozyten war diese Stromantwort nicht zu beobachten. Selbst nach einer Hyperpolarisation der Membran für mehr als zehn Sekunden konnte keine Inaktivierung der KAT2-Kanalproteine festgestellt werden (Daten nicht gezeigt). Eine Auftragung der Gleichgewichtsströme ($I_{SS}$) gegen die Membranspannung bei extrazellulären Kaliumkonzentrationen von 10, 30 und 100 mM verdeutlichte die starke Spannungsabhängigkeit sowie die damit verbundene starke Einwärtsgleichrichtung von KAT2 (Abb.: 3.1B). Mit zunehmendem Kaliumangebot im Perfusionsmedium stiegen die Einwärtsströme bei hyperpolarisierenden Potentialen an. In Abbildung 3.1C wurde die relative Offenwahrscheinlichkeit (rel. $P_o$) gegen die Spannung bei den verschiedenen Kaliumkonzentrationen aufgetragen und mit einer Boltzmann-Funktion gefittet. Wie schon für KAT1 gezeigt wurde (Brüggemann *et al.*, 1999), ist auch die spannungsabhängige Aktivierung von KAT2 von der externen Kaliumkonzentration nicht beeinflusst. Bei allen getesteten $K^+$-Konzentrationen war eine Aktivierungsschwelle von ca. -80 bis -90 mV auszumachen. Auch die halbmaximale Aktivierungsspannung ($U_{1/2}$) zeigte keine signifikante Änderung bei den verschiedenen externen Kaliumkonzentrationen. Mit diesem Kalium-unabhängigen Aktivierungsverhalten stehen KAT1 und KAT2 ganz im Gegensatz zu den Depolarisations-aktivierten Auswärtsgleichrichtern SKOR und GORK, deren Aktivierungsschwelle vom Kaliumumkehrpotential ($E_K$) abhängt (Gaymard *et al.*, 1998; Ache *et al.*, 2000).

Um die Kaliumselektivität des KAT2-Kanals zu bestimmen wurden die Umkehrpotentiale ($U_{rev}$) bei unterschiedlichen externen Kaliumkonzentrationen nach Zweifachspannungspulsen ermittelt. Nach einem aktivierenden Vorpuls zu -140 mV wurden die instantanen Ströme ($I_T$) bei t=0 im Folgepuls abgegriffen und das Umkehrpotential ermittelt (siehe auch Inset Abb.: 3.1D). Aus der Auftragung des Umkehrpotentials $U_{rev}$ gegen die $K^+$-Konzentration in halb-logarithmischer Skalierung ist zu erkennen, dass sich bei einer zehnfachen Änderung der externen Kaliumkonzentration das Umkehrpotential um 62,5 ± 4,2 mV verschiebt (Abb.:

3.1D). Dieser Wert liegt in guter Übereinstimmung mit dem theoretischen Nernst Potential für Kalium (59,1 mV) und bestätigt damit die Kaliumselektivität von KAT2.

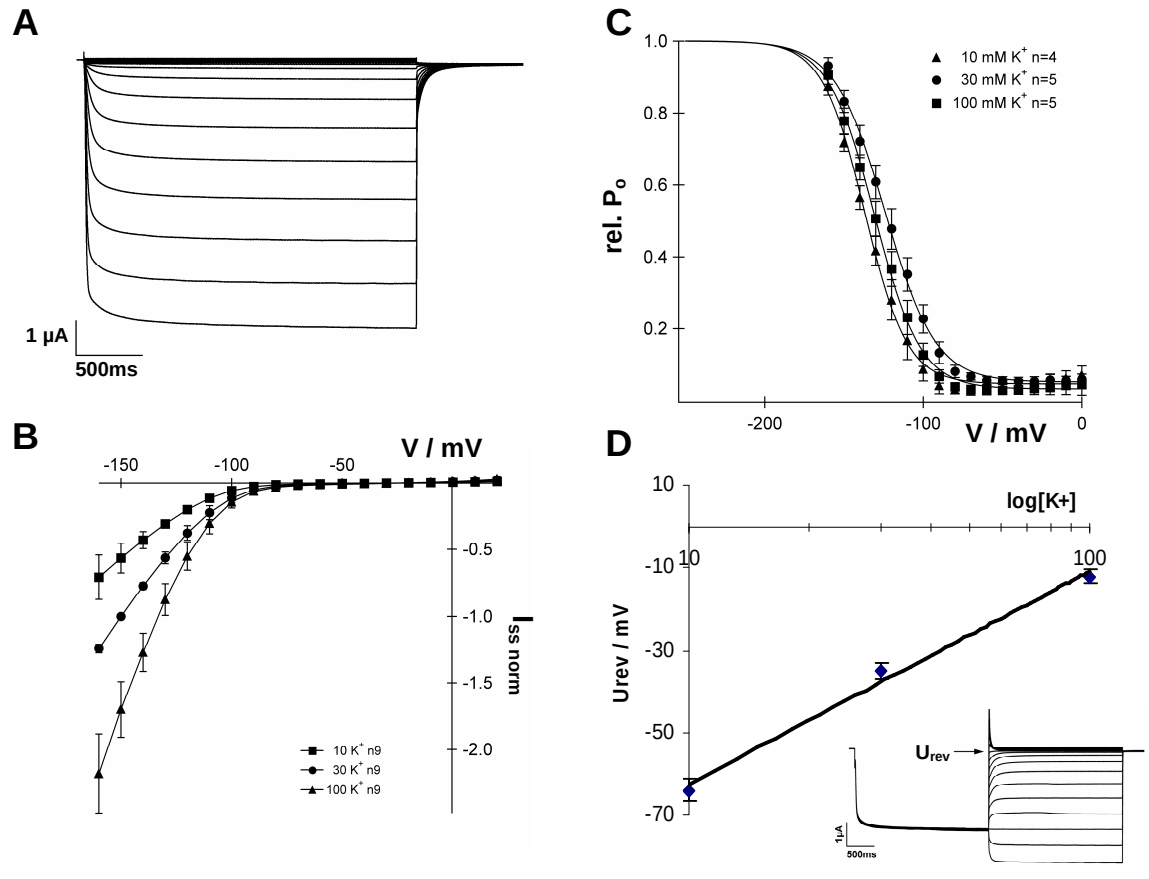


**Abb. 3.1: Spannungsabhängigkeit und Selektivität von KAT2 exprimiert in *Xenopus* Oozyten**

A) Ausgehend von einer Haltespannung von -20 mV wurde eine Serie von 2,5 s langen Einzelspannungspulsen appliziert, die in 10 mV Schritten von 20 mV bis -160 mV reichten. Die Hyperpolarisation der Oozyten Membran auf Werte negativ von -90 mV führten zu einem makroskopischen Einwärtsstrom mit einer zeitabhängigen Aktivierungs- und Deaktivierungskinetik. Die externe Lösung bestand aus 30 mM KCl, 1 mM $CaCl_2$, 1,5 mM $MgCl_2$ und 10 mM Mes/Tris pH 5,6.

B) Trägt man die Gleichgewichtsströme $I_{SS}$ von KAT2 injizierten Oozyten gegen die angelegte Spannung bei 10, 30 und 100 mM KCl in der externen Lösung auf, so ergeben sich mit steigender Kaliumkonzentration stärkere Einwärtsströme. Die Daten von neun Oozyten wurden auf den Strom in 30 mM KCl bei -150 mV normiert und die Standardabweichung berechnet. Die Ionenstärke der Lösungen wurde mit NaCl angeglichen.

C) Aus den Folgepulsen (-60 mV) bei t = 0 wurde die relative Offenwahrscheinlichkeit abgelesen und gegen das Membranpotential der vorher angelegten Testpulse aufgetragen. Eine Änderung der externen Kaliumkonzentration hat keinen Einfluss auf die Offenwahrscheinlichkeit von KAT2. Die Datenpunkte konnten mit einer Boltzmann-Funktion gut beschrieben werden (durchgezogene Linie).

D) Auftragung der Umkehrspannung ($U_{rev}$) gegen die Kaliumkonzentration in logarithmischer Skalierung. Bei einer zehnfachen Veränderung der $K^+$-Konzentration verschiebt sich das Umkehrpotential um 62,5 ± 4,2 mV. (Inset) Zur Bestimmung dieser Umkehrspannung wird ein aktivierender Vorpuls appliziert gefolgt von einem Set an Testspannungen. Aus den instantanen Strömen bei t=0 (nach dem Spannungssprung; Pfeil) wird die Spannung ermittelt, bei der das Vorzeichen des Stroms wechselt (Umkehrspannung).

Zur Ermittlung der relativen Permeabilitäten von KAT2 für andere einwertige Kationen wurde KCl in der Perfusionslösung sukzessive durch NaCl, LiCl, $NH_4Cl$ und RbCl ersetzt. Die Permeabilitäten für die untersuchten Kationen werden relativ zur Permeabilität für $K^+$ (=1) angegeben (Tab.: 3.1). Die ermittelte Reihenfolge entspricht der Eisenman Serie V und ist damit typisch für einen einwärtsgleichrichtenden Kaliumkanal (Schroeder *et al.*, 1994).

| Kation | rel. Permeabilität | n |
|---|---|---|
| $K^+$ | 1 | 7 |
| $Rb^+$ | 0,27 | 7 |
| $NH_4^+$ | 0,13 | 8 |
| $Na^+$ | 0,08 | 3 |
| $Li^+$ | 0,08 | 5 |

**Tabelle 3.1:** Übersicht über die relativen Permeabilitäten von $Rb^+$, $NH_4^+$, $Na^+$ und $Li^+$ gegenüber $K^+$. n = Anzahl Experimente (Oozyten)

Die Inhibierung durch extrazelluläres $Cs^+$ ist ein klassisches Charakteristikum von pflanzlichen und tierischen einwärtsgleichrichtenden $K^+$-Kanälen. Die Spannungsabhängigkeit dieses $Cs^+$-Blocks lässt auf eine Bindung des $Cs^+$ innerhalb der Pore (im elektrischen Feld) schließen. Auch KAT2-injizierte Oozyten zeigten in Anwesenheit von 5 mM CsCl diesen spannungsabhängigen Block der Kaliumeinwärtsströme, wobei bei -150 mV bereits mehr als 72% des Stroms inhibiert wurde (Abb.: 3.2).

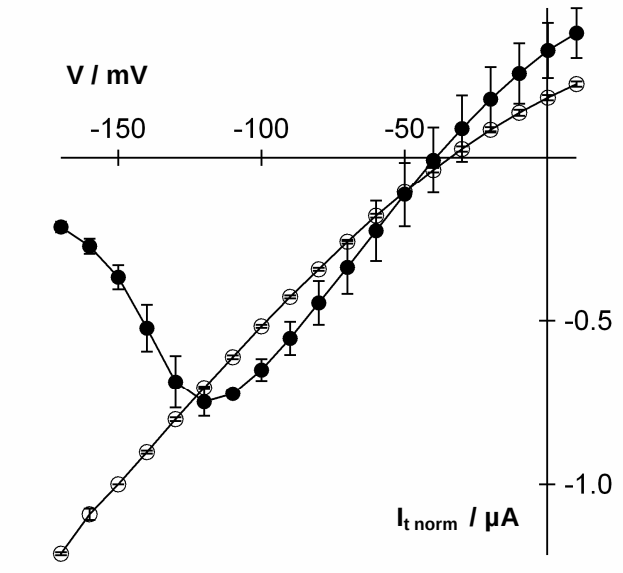


**Abb. 3.2: KAT2 Sensitivität gegenüber dem Kaliumkanal-spezifischen Blocker $Cs^+$.**
Instantane Ströme ($I_t$) gemessen bei Testpulsen von 10 bis -170 mV in 10 mV Schritten nach einem aktivierenden Vorpuls zu -140 mV. In Abwesenheit von $Cs^+$ in der Badlösung verhalten sich die Ströme durch den aktivierten/offenen Kanal nahezu spannungsunabhängig. Bei der Perfusion mit 5 mM CsCl ist eine spannungsabhängige Blockierung der Kaliumeinwärtsströme ab -110 mV zu erkennen. Die Lösung bestand aus 30 mM KCl, 1 mM $CaCl_2$, 1,5 mM $MgCl_2$ und 10 mM Mes/Tris pH 5,6.

Diese Empfindlichkeit gegenüber typischen Kaliumkanalblockern zusammen mit dem Nernstschen Verhalten des Umkehrpotentials bei $K^+$-Konzentrationsänderungen und der typische Permeabilitätsreihe charakterisieren KAT2 als Kalium-selektiven Einwärtskanal.

## 3. Regulation von KAT2 durch den extra- und intrazellulären pH-Wert

Kaliumkanäle können durch Protonen reguliert werden, wobei eine extrazelluläre Ansäuerung aktivierend (KAT1, Very *et al.*, 1995; KST1, Hoth *et al.*, 1997a) oder inhibierend (AKT2/3, Marten *et al.*, 1999) wirken kann. In KAT2-exprimierenden Oozyten konnte durch extrazelluläre Ansäuerung von pH 7,5 zu pH 5,6 eine Zunahme des einwärtsgerichteten Kaliumstroms um etwa 46 % bei einer Membranspannung von -150 mV gezeigt werden. Ein weiterer Anstieg der Protonenkonzentration zu pH 4,5 hatte keine weitere Auswirkung auf die Stromantwort von KAT2 (Abb.: 3.3A).

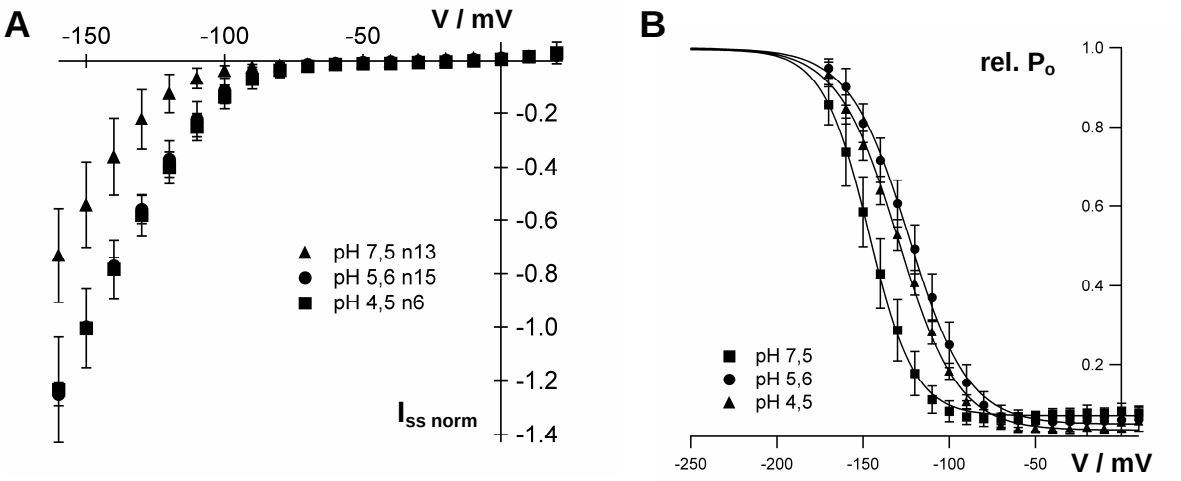


**Abb. 3.3: Externe pH-Abhängigkeit von KAT2**

A) Gleichgewichtsströme $I_{SS}$ in einer 30 mM Kaliumchloridlösung bei pH 7,5, 5,6 und 4,5 aufgetragen gegen das Membranpotential. Bei pH 4,5 und 5,6 sind kaum Unterschiede in der Stromantwort von KAT2 zu erkennen. Bei pH 7,5, jedoch, sind die einwärtsgerichteten Kaliumströme deutlich reduziert. Die Gleichgewichtsströme wurden normiert auf den Wert bei -150 mV in der Lösung mit einem pH-Wert von 5,6.

B) Die relative Offenwahrscheinlichkeit unter den Lösungsbedingungen wie in A aufgetragen gegen die Spannung und mit einer Boltzmann-Funktion gefittet. Die reduzierten Kaliumströme bei einem pH-Wert von 7,5 sind auf die Verschiebung der Offenwahrscheinlichkeit zu negativeren Potentialen zurückzuführen.

Hoth *et al.* (1997a) konnten zeigen, dass diese Säureaktivierung bei KST1 aus einer Verschiebung der halbmaximalen Aktivierungsspannung ($U_{1/2}$) zu positiveren Potentialen mit

zunehmender Protonenkonzentration resultiert. Die Einzelkanalleitfähigkeit bleibt bei einer Ansäuerung oder Alkalisierung des extrazellulären Mediums unverändert. Um zu testen, ob KAT2 ein ähnliches Verhalten zeigt, wurde die relative Offenwahrscheinlichkeit bei pH 7,5, 5,6 und 4,5 gegen die Membranspannung aufgetragen (Abb.: 3.3B). Wie schon bei den Gleichgewichtsströmen in Abbildung 2.3 A zu ersehen war, konnte nur im pH Bereich zwischen 7,5 und 5,6 eine signifikante Verschiebung der halbmaximalen Aktivierungsspannung um ca. 23 mV beobachtet werden. Eine stärkere Ansäuerung brachte keine signifikante weitere Verschiebung von $U_{1/2}$ mit sich. Im Gegensatz zu KAT1 und KST1 ist die Protonensensitivität von KAT2 allerdings zu höheren pH-Werten verschoben.

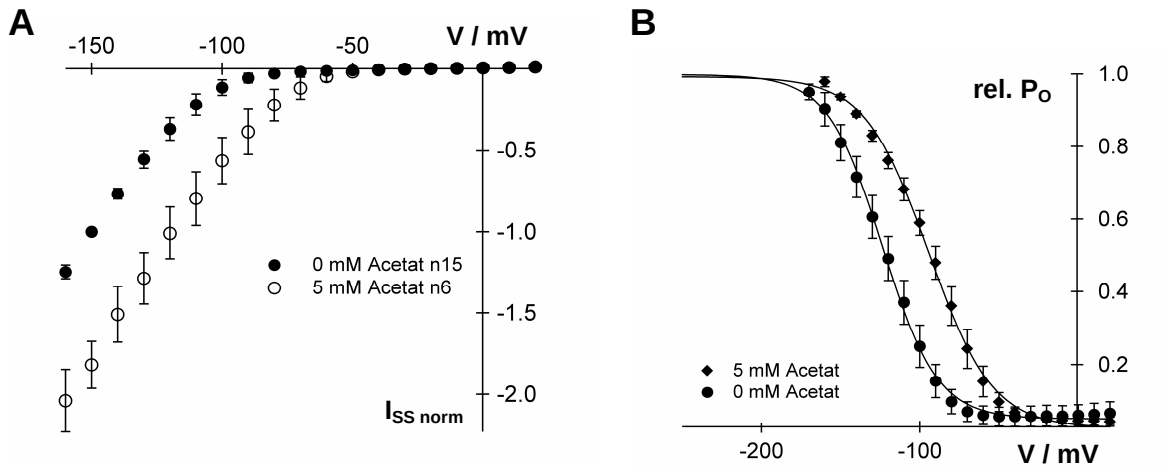


**Abb. 3.4: Interne pH-Abhängigkeit von KAT2**

A) Gleichgewichtsströme $I_{SS}$ gemessen in einer Lösung bestehend aus 30 mM KCl, 1 mM $CaCl_2$, 1,5 mM $MgCl_2$ und 10 mM Mes/Tris pH 5,6 sowie 5 mM NaCl oder 5 mM NaAc. $I_{SS}$ wurden normiert auf den Wert bei -150 mV in der Abwesenheit von Acetat und gegen das Membranpotential aufgetragen. In der Anwesenheit von Acetat aktiviert KAT2 bei positiveren Membranpotentialen, was schließlich auch zu gesteigerten Stromamplituden führt. B) Wie schon in A zu erkennen war, führt die Ansäuerung des Zytosols zu einer Verschiebung der halbmaximalen Aktivierungsspannung $U_{1/2}$ hin zu positiveren Potentialen. Bestätigt wird dies durch die Auftragung der relativen Offenwahrscheinlichkeiten gegen das Membranpotential und die Beschreibung der Daten durch eine Boltzmann-Funktion (durchgezogene Linie).

Obwohl bei der Zwei-Elektroden-Spannungsklemmen-Technik das Zytosol der Oozyte nicht zugänglich ist, kann eine intrazelluläre Ansäuerung durch die Applikation von extrazellulärem Acetat erreicht werden. Die nicht dissoziierte Säure (bei pH 5,6) kann über die Membran permeieren und Protonen in der Oozyte (ca. pH 7,5) freisetzen. Durch direkte Messungen mit Protonen-sensitiven Mikroelektroden konnten Tsai *et al.* (1995) zeigen, dass

sich in Gegenwart von Acetat der intrazelluläre pH-Wert an den extrazellulären pH-Wert anpasst.

Eine Ansäuerung des Zytoplasmas der Oozyten durch eine 15 Minuten dauernde Perfusion mit 5 mM Acetat resultierte bei KAT2-exprimierenden Oozyten in einer Zunahme des Gleichgewichtstroms (Abb.: 3.4A). Eine Analyse der relativen Offenwahrscheinlichkeiten von KAT2 in An- und Abwesenheit von Acetat zeigte, dass die interne pH-Sensitivität nach dem gleichen Mechanismus arbeitet wie es bei der externen Säureaktivierung bereits beobachtet wurde (Abb.: 3.4B). Eine erhöhte zytosolische Protonenkonzentration durch Acetat verändert das spannungsabhängige Aktivierungsverhalten von KAT2. Diese Ansäuerung setzt also die notwendige Aktivierungsenergie zur Öffnung der KAT2-Pore herunter, was in einer Verschiebung der halbmaximalen Aktivierungsspannung zu positiveren Potentialen und somit zu einer erhöhten Offenwahrscheinlichkeit bei einem gegebenen Membranpotential resultiert.

# 4. Diskussion

Das Phloem stellt ein Netzwerk für die Assimilattranslokation sowie für die chemische und elektrische Kommunikation innerhalb der Pflanze dar (van Bel, 2003 und darin enthaltene Referenzen). Die Rückgewinnung von Mineralien und die Entgiftung der Pflanze von Natrium sind weitere wichtige Funktionen dieses Netzwerks (Berthomieu *et al.*, 2003).

In Angiospermen wird dieses Transportsystem aus einer funktionellen Einheit zweier lebender Zelltypen gebildet, den Siebelementen und den Geleitzellen. Über verzweigte Plasmodesmen stehen die Siebzellen in engem Kontakt mit den Geleitzellen, die die Versorgung der partiell autolysierten Siebelemente übernehmen. Trotz dieser Autolyse der Siebelemente bleibt aber ihre Plasmamembran erhalten. Sie ist eine zwingende Voraussetzung für die Generierung und die Kontrolle eines osmotischen Potentials des SE/CC Komplexes, welches für den osmotisch getriebenen Massenstrom durch das Phloem verantwortlich ist (Münch 1930). Zumindest in apoplastisch ladenden Pflanzenarten muss die Phloemmembran mit entsprechenden Membranproteinen ausgestattet sein, die die Gefäße mit Assimilaten beladen und somit das osmotische Potential für den Massenstrom aufbauen. Während der letzten Jahrzehnte intensiver Forschung auf dem Gebiet der Phloemphysiologie wurden Phloem-spezifische Substrattransporter, Ionenpumpen und Ionenkanäle identifiziert, die maßgeblich am Langstreckentransport durch das Phloem beteiligt sind. Molekularbiologische Untersuchungen an Vertretern dieser Transporter- und Kaliumkanalfamilien zeigten die essentielle Bedeutung dieser Membranproteine für die Translokation von Assimilaten durch das Phloem. Das Fehlen einzelner Komponenten in Verlustmutanten, antisense Repressionslinien und Cosuppressionslinien lieferte den direkten genetischen Beweis für die Beteiligung von Kaliumkanälen, Saccharosetransportern und $H^+$-ATPasen an der Beladung des SE/CC Komplexes (Deeken *et al.*, 2002; Riesmeier *et al.*, 1994; Kühn *et al.*, 1996; Lemoine *et al.*, 1996; Bürkle *et al.*, 1998; Gottwald *et al.*, 2000; Zhao *et al.*, 2000). Interessanterweise zeigen all diese transgenen Pflanzenlinien einen gemeinsamen Phänotyp. Sie akkumulieren Saccharose und Stärke in ihren photosynthetisch aktiven Blättern und zeigen ein reduziertes Wachstum, bis hin zum Zwergwuchs. Aufgrund des gemeinsamen Phänotyps ist eine enge Kopplung der einzelnen Komponenten bei der Assimilattranslokation über das Phloem anzunehmen. Während die energetische Kopplung von $H^+$-Pumpen und den sekundär aktiven Saccharosetransportern seit langem bekannt ist, blieb die Rolle von

Kaliumkanälen und die Rolle des Phloemmembranpotentials für den Assimilattransport bisher unerforscht.

In Rahmen dieser Arbeit wurden zwei Komponenten dieser Beladungsmaschinerie im heterologen Expressionssystem der *Xenopus* Oozyten charakterisiert:

- Symporter für die Protonen gekoppelte Aufnahme von Assimilaten (**ZmSUT1**, **AtSUC2, AtPLT5** und **PmPLT1**)
- Kaliumkanäle zur Stabilisierung des Membranpotentials und für die Kaliumhomöostase in der Pflanze (**KAT2**, **KZM1**, **AKT2/3**, **PTK2**)

In abschließenden Coexpressionsstudien von Saccharosetransportern und Kanälen dienten Oozyten als Modellsystem für die Simulation der Verhältnisse an der Phloemmembran.

## 4.1 Charakterisierung von KZM1 aus der KAT1-Unterfamilie der pflanzlichen *Shaker*-Kaliumkanäle

In Kapitel IV (Philippar *et al.*, 2003) wurde der erste Kaliumkanal der KAT1-Unterfamilie aus der $C_4$-Pflanze *Zea maize* vorgestellt. KZM1 gehört zur pflanzlichen *Shaker*-Kaliumkanal-familie. Er zeigt die höchste Homologie zu KAT2 aus *Arabidopsis thaliana* hinsichtlich seiner molekularen Struktur, elektrophysiologischen Eigenschaften und seinem Expressionsmuster. Die höchste Expression von KZM1 im Maisblatt konnte neben den Schließzellen vor allem in den Leitgefäßen beobachtet werden. Im Gegensatz zu ZMK2 aus der AKT2/3-Unterfamilie und ZmSUT1 ($H^+$/Saccharose-Symporter, Kapitel VIII) war das KZM1-Gen während der Blattentwicklung, dem Sink/Source-Übergang und während des Tag/Nacht-Rhythmus konstitutiv exprimiert. Dieses Expressionsmuster lässt auf eine „housekeeping"-Funktion von KZM1 bei der Kaliumhomeostase im Maisblatt schließen.

Bei DEVC-Untersuchungen in *Xenopus* Oozyten zeigte KZM1 die charakteristischen Eigenschaften eines spannungsabhängigen, einwärtsgleichrichtenden *Shaker*-Kaliumkanals der KAT1-Unterfamilie. Unterschiede zu den KAT-Typ Kanälen aus Dikotyledonen (KAT1 und 2, KST1 und SIRK) konnten hinsichtlich der höheren Einzelkanalleitfähigkeit von 20 pS und dem Kalium-abhängigen Schaltverhalten festgestellt werden. Analog zu AKT3 (Kapitel II, Geiger *et al.*, 2002) schaltet KZM1 nur dann in den Offenzustand, wenn in der extrazellulären Lösung Kalium vorhanden ist. KAT1 hingegen trägt in Gegenwart sub-millimolarer Kaliumkonzentrationen signifikante Auswärtsströme, sobald das Umkehr-potential für Kalium ($E_K$) negativer als die Aktivierungsschwelle des $K^+$-Kanals liegt (Brüggemann *et al.*, 1999). Unter diesen Bedingungen ist KZM1 jedoch inaktiviert und verhindert somit das Entlassen von Kalium aus der Zelle. Die Einwärtsgleichrichtung dieses Maiskaliumkanals bleibt durch diese spezifische Eigenschaft unter allen externen Kaliumkonzentrationsbedingungen erhalten und übertrifft in dieser Hinsicht seine orthologen Vertreter aus *Arabidopsis* und der Kartoffel. Aufgrund dieser Tatsache könnte KZM1 eine Funktion als Kaliumsensor übernehmen, der über das Membranpotential und die Kaliumkonzentration im Apoplasten reguliert wird. Übereinstimmend mit seiner konstitutiven Expression könnte die Hauptfunktion des KZM1-Kanals darin bestehen, die Kaliumkonzentration im Apoplasten der Sink- und Source-Gewebe sowie entlang des Transportphloems zu registrieren und die Kaliumaufnahme in wachsende Gewebe zu steuern.

Ein weiterer Unterschied zu den bekannten Vertretern der KAT1-Unterfamilie liegt in der Unempfindlichkeit des Schaltverhaltens von KZM1 gegenüber externer pH-Schwankungen. Während für KST1 und KAT1 eine Säureaktivierung und eine damit verbundene Verschiebung der relativen Offenwahrscheinlichkeit der Kanalproteine zu positiveren Membranpotentialen gezeigt werden konnte, ist die Offenwahrscheinlichkeit des Maiskanals unabhängig von der externen Protonenkonzentration. Diese Insensitivität gegenüber der extrazellulären Protonenkonzentration könnte eine spezifische Anpassung an die Gegebenheiten in $C_4$-Pflanzen sein, die einen auf $C_4$-Säuren basierenden Metabolismus besitzen. Des Weiteren könnte KZM1 auch dann unbeeinflusst arbeiten, wenn es in Folge von Beladungs- oder Entladungsvorgängen am Phloem oder beim Säurewachstum an der Blattbasis zu pH-Veränderungen kommt. In einer solchen Umgebung kann der konstitutiv exprimierte, pH-insensitive Kaliumaufnahme Kanal KZM1 stabil für die $K^+$-Beladung des Phloems und für die Kaliumhomeostase der Pflanze sorgen, unabhängig von Sink/Source-Übergängen, dem Tag/Nacht Rhythmus und dem Entwicklungsstatus der Pflanze.

Um den Einfluss von KZM1 auf die Beladung des Phloems mit Saccharose zu testen, wurde ZmSUT1 mit dem Einwärtsgleichrichter coexprimiert. Bei der Zugabe von Saccharose zur externen Lösung kam es zu einer Depolarisation der Membran, wie sie auch bei Oozyten zu beobachten war, die nur mit dem Zuckertransporter injiziert wurden. Durch den Symport von Saccharose zusammen mit Protonen gelangen positive Ladungen in das Zytosol, was zu dieser Depolarisation führt (siehe auch Kapitel III und VIII). Der Transportprozess von Saccharose scheint von der Präsenz von KZM1 unberührt zu bleiben. KZM1 selbst ist jedoch durch die Saccharose-induzierte Depolarisation stark beeinflusst. Sinkt das Membranpotential unter die Aktivierungsspannung von KZM1, so geht der $K^+$-Kanal, aufgrund seines spannungsabhängigen Öffnungsverhaltens, in seinen deaktivierten Zustand über.

Im Gegensatz zu KZM1 vermittelt ZMK2, ein ebenfalls Phloem-lokalisierter Vertreter der AKT2/3-Unterfamilie aus Mais, sowohl Kaliumeinwärtsströme als auch Kaliumauswärtsströme. Diese Eigenschaft basierend auf der schwachen Spannungsabhängigkeit dieser Kanalunterfamilie führt dazu, dass in Oozyten das Membranpotential auf die Kaliumumkehrspannung ($E_K$) geklemmt wird. Eine Coexpression von ZMK2 und dem $H^+$/Saccharose-Symporter ZmSUT1 (siehe auch Kapitel VIII) verhindert die Saccharose-induzierte Depolarisation der Membran durch kompensatorische Kaliumausströme. Blockiert man die ZMK2-vermittelten Kaliumströme durch den Einsatz von Kaliumkanalinhibitoren

($Ba^{2+}$ und $TEA^{+}$), so kann dieser Kaliumkanal die Depolarisation der Membran durch ZmSUT1 nicht verhindern.

Bezogen auf die Phloemphysiologie spielt KZM1 eine Rolle bei der Beladung des Phloems mit Kalium zur Wahrung der Kaliumhomeostase innerhalb der Pflanze. ZMK2 stabilisiert das Phloemmembranpotential und hat damit einen direkten Einfluss auf die Beladung des SE/CC Komplexes mit Assimilaten. Er verhindert extreme Depolarisationen wie in Kapitel IV gezeigt und hält die Spannung über der Phloemmembran in negativen Spannungsbereichen, wo auch die spannungsabhängigen Transporter optimal arbeiten können (siehe auch Kapitel VI, VII und VIII).

In Bereichen des Phloems, wo sowohl KZM1 als auch ZMK2 exprimiert würden, könnte ZMK2 das Phloempotential weiterhin zu $E_K$ klemmen und Membranpotentialsprünge verhindern. Membranpotentialmessungen in Maisblattscheiben mit der Aphiden-Technik (siehe Kapitel VIII, Supplementary Figure 1) haben allerdings gezeigt, dass das Phloempotential negativer als $E_K$ liegt, so dass eine Kaliumaufnahme sowohl über KZM1 als auch über ZMK2 möglich wäre. Aufgrund der Membranpotential-stabilisierenden Funktion von ZMK2 würde das Phloempotential in Gegenwart von Saccharose nur bis zur Umkehrspannung für Kalium depolarisieren.

## 4.2 Biophysikalische Charakterisierung von KAT2

KAT2 ist ein typischer Vertreter der KAT1-Unterfamilie. Ähnlich wie KZM1 (Kapitel IV) vermittelt KAT2 spannungsabhängige, einwärtsgerichtete Kaliumströme. Er ist je nach *Arabidopsis* Ecotyp in den feinadrigen Gefäßen des Phloems (minor veins) und/oder in den Schließzellen der oberirdischen Teile der Pflanze exprimiert (Pilot *et al.*, 2001; Ivashikina *et al.*, 2003). Eine Hyperpolarisation des Membranpotentials (negativer als -80 mV) führt zu einer zeitabhängigen Aktivierungskinetik von KAT2 in *Xenopus* Oozyten, wobei die Einwärtsströme nach ca. 500 ms in ein Fließgleichgewicht relaxieren. Messungen bei unterschiedlichen Kaliumkonzentrationen zeigten, dass die relative Offenwahrscheinlichkeit von KAT2 unabhängig vom externen Kaliumangebot ist. Im Gegensatz zu KZM1 öffnet KAT2 auch in der Abwesenheit von Kalium in der extrazellulären Lösung, und vermittelt sogar auswärtsgerichtete Kaliumströme, sobald das Umkehrpotential für Kalium ($E_K$) negativer als die Aktivierungsschwelle des $K^+$-Kanals liegt. Ein weiterer Unterschied zu KZM1 zeigt sich in der pH-abhängigen Aktivierung von KAT2. Wie auch für KAT1 und KST1 gezeigt werden konnte (Hedrich 1995, Hoth *et al.*, 1997a, b) reagiert KAT2 auf eine Ansäuerung des extrazellulären Mediums mit einer Verschiebung seiner Aktivierungs-spannung zu positiveren Membranpotentialen. Die Protonensensitivität von KAT2 ist zwischen pH 7,5 und 5,6 am höchsten. KAT1 hingegen ist vor allem unterhalb von pH 5,6 empfindlich auf pH-Änderungen (Hoth und Hedrich 1999). Auf eine Ansäuerung des Zytosols durch die Zugabe von Acetat reagieren alle bisher bekannten KAT-Typ Kanäle gleich. Sie verschieben ihre Aktivierungsspannung deutlich zu positiveren Membran-potentialen. Neben diesen charakteristischen Eigenschaften zeigt KAT2 auch eine Empfindlichkeit gegenüber typischen Kaliumkanalblockern und ein Nernstsches Verhalten des Umkehrpotentials bei $K^+$-Konzentrationsänderungen. All diese biophysikalischen Eigenschaften zusammen mit einer typischen Permeabilitätsreihe für Kationen charakterisieren KAT2 als Kalium-selektiven Einwärtskanal.

In Coexpressionsexperimenten von KAT2 mit dem $H^+$/Saccharose-Symporter AtSUC2 in *Xenopus* Oozyten wurde der Einfluss dieses Einwärtsgleichrichters auf die Saccharosebeladung des Phloems getestet. Wie schon für KZM1 gezeigt wurde, ist auch KAT2 nicht in der Lage die Saccharose-induzierte Depolarisation der Membran durch den AtSUC2-vermittelten Symport von Saccharose zusammen mit Protonen zu verhindern

(Kapitel III). Die Depolarisation der Oozytenmembran erreichte Werte die weit positiv vom Kaliumumkehrpotential ($E_K$) lagen und die aufgrund des spannungsabhängigen Aktivierungsverhaltens von KAT2 zur Deaktivierung des $K^+$-Kanals führten. Die strenge Einwärtsgleichrichtung dieses Kaliumkanals erlaubte unter den gewählten Bedingungen (externe $K^+$-Konzentration = 30 mM) keine Kaliumauswärtsströme zur Kompensation des Einstroms positiver Ladungen ($H^+$) durch die Transportaktivität von AtSUC2. Liegt das Umkehrpotential für Kalium jedoch positiv von der Aktivierungsspannung von KAT2 (externe $K^+$-Konzentrationen im unteren millimolarem Bereich), so sind kompensatorische Auswärtsströme denkbar, die das Membranpotential auf $E_K$ klemmen würden.

Da KAT2 nur in den oberirdischen Teilen der Pflanze exprimiert und dort nur in den Schließzellen und den feinadrigen Gefäßen des Sammelphloems (Pilot *et al.*, 2001), ist eine Funktion bei der Beladung des Phloems mit Kalium anzunehmen. Ache *et al.* (2001) konnten durch Messungen an Petiolen von *Vicia faba* mit der Aphidentechnik zeigen, dass eine Leitfähigkeit von Kaliumkanälen zum Membranpotential des Phloems beiträgt. Ausgehend von einer Kaliumkonzentration von ca. 10 mM im Apoplasten des Sammelphloems (Mühling und Sattelmacher 1997) und einer Phloem-internen Konzentration von etwa 100 mM (Ache *et al.*, 2001) ergibt sich ein Kaliumumkehrpotential ($E_K$) von -60 mV. Somit liegt das gemessene Phloemmembranpotential mit -130 bis -200 mV (Eschrich *et al.*, 1988; Sibaoka 1982; van Bel 1993; van Bel and van Rijen 1994) stets negativer als $E_K$, was einen Kaliumeinstrom zur Folge hat. Derart negative Membranpotentiale weisen außerdem auf einen starken Einfluß von Protonenpumpen bei der Aufrechterhaltung des Membranpotentials hin. Bisher konnten allerdings noch keine Membranpotentialmessungen direkt am Sammelphloem *in planta* durchgeführt werden. Es ist anzunehmen, dass dort durch den Symport von Saccharose und Protonen das Membranpotential weitaus stärker depolarisiert vorliegt als in Bereichen des Transportphloems, wo bisher die meisten Membranpotentialmessungen durchgeführt wurden. In diesem Fall würden das depolarisierte Membranpotential und die damit verbundene Alkalisierung des Apoplasten zu einer Deaktivierung von KAT2 führen. In einer solchen Situation ist KAT2, im Gegensatz zu AKT2/3-ähnlichen Kanälen, nicht in der Lage, die Saccharose-induzierte Depolarisation der Phloemmembran aufzuhalten.

## 4.3 Einfluss von AKT2/3 auf die Phloemphysiologie

### 4.3.1 Struktur-Funktionsanalyse der Porenregion von AKT3 durch den Porenaustausch zwischen AKT3 und KST1

In einer detaillierten Analyse in *Xenopus* Oozyten konnten Marten *et al*. (1999) AKT3 als Phloem-lokalisierten, schwach spannungsabhängigen, $H^+$- und $Ca^{2+}$-geblockten Kaliumkanal beschreiben. Durch diese elektrophysiologische Charakterisierung wurden biophysikalische Eigenschaften identifiziert, die bisher für pflanzliche Kaliumkanäle nicht bekannt waren. Durch seine schwache Spannungsabhängigkeit erscheint er bei allen Membranspannungen als „offener" Kanal und ist damit in der Lage sowohl einen Kaliumausstrom als auch einen Kaliumeinstrom zu vermitteln. Darüber hinaus klemmt AKT2/3 aufgrund dieser Charakteristik das Membranpotential zur Kaliumumkehrspannung ($E_K$). Während die Kaliumkanäle der KAT1- und AKT1-Unterfamilie, über die Verschiebung ihrer spannungsabhängigen Offenwahrscheinlichkeit, durch Protonen aktiviert werden, werden die Ströme durch AKT3 mit steigender Protonenkonzentration über eine Verringerung seiner Einzelkanalleitfähigkeit inhibiert. Des Weiteren wird AKT3 durch extrazelluläre Kalziumionen in millimolaren Konzentrationen geblockt.

Basierend auf diesen einzigartigen elektrophysiologischen Eigenschaften von AKT3 unter den pflanzlichen *Shaker*-Kaliumkanälen wurde eine vergleichende Struktur-Funktionsanalyse zwischen dem Einwärtsgleichrichter KST1 aus der KAT1-Unterfamilie und AKT3 durchgeführt (Kapitel I). Zu diesem Zweck wurden Porenaustausch-Chimären zwischen beiden Kanälen hergestellt. Bei der Chimäre AKT3/(p)KST1 handelt es sich um AKT3 mit der Porenregion von KST1, während es sich bei der Chimäre KST1/(p)AKT3 um KST1 handelt, der mit der Pore von AKT3 ausgestattet wurde. Die elektrophysiologische Analyse dieser Chimären in *Xenopus* Oozyten konnte der Porenregion eine besondere Bedeutung für die spannungsabhängige Gleichrichtung sowie für die Protonen- und Kalziumsensitivität zuordnen. Der spannungsabhängige, einwärtsgleichrichtende Kaliumkanal KST1 wurde durch den Besitz der AKT3 Pore (KST1/(p)AKT3) zu einem schwach spannungsabhängigen und schwach gleichrichtenden $K^+$-Kanal konvertiert. Untersuchungen an der Chimäre AKT3/(p)KST1 ergaben eine Übertragung der Spannungsabhängigkeit und der

Gleichrichtung von KST1 auf AKT3, nur durch die Ausstattung von AKT3 mit der Pore von KST1. Spannungsabhängigkeit und Gleichrichtung werden also maßgeblich von der Porenregion in *Shaker*-Kaliumkanälen mitbestimmt, obwohl der eigentliche Spannungssensor in der Transmembrane S4 lokalisiert zu sein scheint (Dreyer *et al.,* 1997; Hoth *et al.,* 1997a; Marten und Hoshi 1998). Erste Hinweise auf die Bedeutung der Pore hinsichtlich der spannungsabhängigen Aktivierung haben schon Einzelmutationen an den Einwärts-gleichrichtern KAT1 und KST1 ergeben (Becker *et al.,* 1996; Hoth *et al.,* 1997b). Diese Mutationen innerhalb der Porenregion beeinflussten die Spannungsabhängigkeit dieser Kanalproteine. Des Weiteren konnten Marten und Hoshi (1997, 1998) eine Beteiligung des N- und C-Terminus am spannungsabhängigen Öffnungsverhalten von KAT1 zeigen. Es bleibt jedoch weiterhin zu klären, wie diese einzelnen Kanal-intrinsischen Regulations-mechanismen miteinander interagieren. Außerdem ist noch unklar, wie es bei diesen Kanälen, die alle die gleiche Struktur und das stark geladene S4 Segment besitzen, zu derart unterschiedlichen Spannungsabhängigkeiten kommen kann. Die Strukturklasse der *Shaker*-Kanalproteine vereinigt somit sowohl schwach spannungsabhängige Kanäle als auch Einwärtsgleichrichter und Auswärtsgleichrichter.

Weiterführende Untersuchungen der Chimären aus AKT3 und KST1 zeigten, dass durch den Transfer der Porenregion auch die Protonen- und die $Ca^{2+}$-Sensitivität übertragen wurden. So wurde durch die Ausstattung des Säure-aktivierten KST1 Kanals mit der Pore von AKT3 (KST1/(p)AKT3) ein Protonen-geblockter Kaliumkanal, der zusätzlich die ausgeprägte $Ca^{2+}$-Empfindlichkeit von AKT3 erhalten hatte. AKT3 mit der Pore von KST1 (AKT3/(p)KST1) hingegen wurde durch den Porenaustausch zu einem $Ca^{2+}$ unempfindlichen Protonen-aktivierten Kanal. Diese Experimente lokalisieren sowohl den pH-Sensor als auch die $Ca^{2+}$-Bindestelle innerhalb der ausgetauschten Porenregion.

### 4.3.2 Identifikation der molekularen Grundlage der pH- und Kalium-sensitivität von AKT3

Mit Hilfe gerichteter Mutagenese in eben dieser Porenregion wurde in Kapitel II die Identifizierung der molekularen Basis des Protonenblocks in AKT3 gezeigt. Basierend auf Sequenzvergleichen zwischen Mitgliedern der Protonen-geblockten AKT2/3-Unterfamilie

und Kanälen, die eine Säureaktivierung zeigen, wurden die Aminosäuren Histidin228 und Serin271 im äußeren Porenbereich von AKT3 für eine Mutagenese ausgewählt. Beide Mutationen resultierten in einer Verminderung der pH-Sensitivität des AKT3 Kanals. Die deutlichsten Effekte ergaben sich beim Austausch der ursprünglichen Aminosäuren zu negativ geladenen Aminosäuren. Die makroskopischen Ströme der Einzelmutanten H228D und S271E reagierten auf eine Ansäuerung von pH 7,5 zu pH 6,0 nicht mehr, während die AKT3 WT Ströme bis zu 40% blockiert wurden. Ein pH-Sprung zu pH 4,5 führte beim WT-Kanal zu einer völligen Inhibierung des Stroms, während die beiden Mutanten unter diesen Bedingungen noch 30 bis 40% ihres ungeblockten Stroms vermittelten. Die elektrophysiologische Analyse der Doppelmutante H228D/S271E zeigte zudem, dass sich die, bei den beiden Einzelmutanten beobachteten Effekte, in der Doppelmutante gegenseitig verstärkten. Dieses Verhalten der Doppelmutante deutet auf die Beteiligung beider Aminosäuren bei der Ausbildung des Protonensensors hin. Ein Vergleich der Porenregion von AKT3 mit den Strukturdaten des bakteriellen KcsA Kaliumkanals (Doyle *et al.*, 1998) verdeutlicht, dass die Aminosäuren H228 und S271 sehr nahe beieinander sitzen (3-4 Angström), obwohl H228 in der absteigenden und S271 in der aufsteigenden Schleife der Porenregion lokalisiert ist.

Da die Inhibierung von AKT3 durch Protonen auf eine Reduktion der Einzelkanalleitfähigkeit basiert, wurden die Einzelmutanten als auch die Doppelmutante in Patch-Clamp Experimenten auf ihre pH-abhängige Einzelkanalleitfähigkeit hin untersucht. Alle AKT3-Mutanten zeigten in Folge eines pH-Sprungs von pH 7,5 zu pH 5,6 keine Verminderung ihrer Einzelkanalleitfähigkeit, während sich die Leitfähigkeit bei AKT3 WT in diesem pH-Bereich halbierte. Diese Studien der AKT3-Mutanten weisen auf eine Kontrolle der pH-abhängigen Permeation der Kaliumionen durch die Aminosäuren H228 und S271 am äußeren Rand der AKT3 Pore hin.

Im Zuge der Charakterisierung dieser pH-Mutanten des AKT3 Kanals in unterschiedlichen, externen Kaliumkonzentrationen wurde eine weitere bisher unbekannte $K^+$-Sensitivität dieses Kaliumkanals entdeckt. Obwohl mit einer Verringerung der Kaliumkonzentration von 100 mM bis 10 mM in der Badlösung die treibende Kraft für einen $K^+$-Efflux ansteigt, konnte bei AKT3 WT Kanälen keine Erhöhung der Auswärtsströme festgestellt werden. In der Abwesenheit von Kalium im extrazellulären Medium kamen die Auswärtsströme sogar komplett zum Erliegen. Im Gegensatz dazu waren die Mutante S271E und die Doppelmutante

HDSE Kalium-insensitiv und vermittelten auch in Abwesenheit von Kalium signifikante Auswärtsströme. Erst durch die Ansäuerung des externen Mediums zu pH 5,6 konnte die Kaliumsensitivität wieder hergestellt werden. Diese Analysen deuten darauf hin, dass sowohl Protonen als auch Kalium im äußeren Porenbereich von AKT3 um eine gemeinsame regulatorische Bindestelle konkurrieren könnten.

### 4.3.3 Bedeutung von AKT2/3 für die Phloemphysiologie von *Arabidopsis*

Auf der Suche nach Phloem-lokalisierten Kaliumkanälen konnten Ache *et al.* (2001) mit VFK1 einen Kaliumkanal der AKT2/3-Unterfamilie aus *Vicia faba* isolieren. Die Tatsache, dass die Expression dieses Kaliumkanals im Licht und durch Fructose induziert wurde, war ein Hinweis auf eine enge Kopplung von Photosynthese und Kanalaktivität. Mit Hilfe der Aphidentechnik konnte weiterhin gezeigt werden, dass das Membranpotential des SE/CC Komplexes unter Bedingungen, die das VFK1 Gen induzierten, stark von der Kaliumleitfähigkeit dieses Kanals abhängt. Basierend auf diesen Untersuchungen konnte erstmals ein Modell erstellt werden, das die Beteiligung von Kaliumkanälen in der Phloemphysiologie (Assimilatentladung im Sink-Gewebe) schlüssig beschreibt.

Mit der Charakterisierung einer akt2/3 Verlustmutante aus *Arabidopsis* konnten Deeken *et al.* (2002, Kapitel III) weitere wichtige Erkenntnisse über die Rolle von Kaliumkanälen der AKT2/3-Unterfamilie für die Beladung und den Ferntransport von Assimilaten gewinnen.

Die akt2/3 Knockout-Pflanzen sind gekennzeichnet durch die Akkumulierung von Assimilaten in photosynthetisch aktiven Blättern und einer Halbierung der Saccharosekonzentration im Phloemsaft von 163 mM in der Mutante, während in WT-Pflanzen 340 mM Saccharose in den Siebelementen zu finden war. Des Weiteren war die Wiederaufnahme von „herausleckender“ Saccharose im Bereich des Transportphloems gestört. Auch die Kaliumabhängigkeit des Membranpotentials über der Phloemmembran war in den akt2/3 Knockout-Pflanzen im Vergleich zum Wildtyp reduziert. Diese phänotypischen Beobachtungen gaben Anlass zu weiteren Untersuchungen hinsichtlich der Bedeutung von AKT2/3 bei der Saccharosebeladung und dem Ferntransport über das Phloem. Zu diesem Zweck wurden Oozyten und die DEVC-Technik benutzt, um die Interaktion von Kaliumkanälen und Saccharosetransportern in der Phloemmembran zu simulieren. Wie

bereits oben erwähnt, ist der Einwärtsgleichrichter KAT2 nicht in der Lage die Saccharose-induzierte Depolarisation der Membran durch AtSUC2 zu verhindern. Coexprimiert man jedoch AKT3 zusammen mit AtSUC2, so verhindert AKT3 die Depolarisation der Membran in Gegenwart von Saccharose. Durch seine schwache Spannungsabhängigkeit und der damit verbundenen Fähigkeit sowohl Einwärts- als auch Auswärtsströme zu vermitteln, verhält sich AKT3 wie eine Kalium-selektive Elektrode und klemmt das Membranpotential zur Kaliumumkehrspannung. Weicht das Membranpotential z.B. durch die Protonenaufnahme über Zuckertransporter von $E_K$ ab (Depolarisation), so beantwortet der stets geöffnete AKT3 Kanal diese Depolarisation mit kompensatorischen Kaliumauswärtsströmen, die das Membranpotential bei $E_K$ stabilisieren. *In planta* wurden Membranpotentiale gemessen, die weitaus negativer als $E_K$ lagen, was einem Gleichgewicht aus der Leitfähigkeit von Kaliumkanälen und der Pumpaktivität von Protonen-ATPasen entsprechen dürfte. In Messungen mit der Aphiden-Technik (Kapitel VIII, Supplementary Figure 1) konnte allerdings gezeigt werden, dass durch die Zugabe von Saccharose in den Apoplasten das Membranpotential des Phloems nur so weit depolarisiert, bis es das Umkehrpotential für Kalium erreicht (siehe Kapitel III und VIII). Diese Ergebnisse unterstützen die Daten aus den Coexpressionsexperimenten in *Xenopus* Oozyten. Einerseits ist AKT3, durch seine spezifischen elektrophysiologischen Eigenschaften, in der Lage die Saccharose-induzierte Depolarisation der Phloemmembran aufzuhalten und andererseits scheint die Hyperpolarisation der Membran durch $H^+$-ATPasen nicht auszureichen, um eine Depolarisation durch die Aktivität der $H^+$/Saccharose-Symporter zu unterbinden. Um solche immensen Membranpotentialsprünge zu vermeiden, könnte AKT3 zur Stabilisierung des Membranpotentials einen wichtigen Beitrag leisten, zumal auch die spannungsabhängige Aktivität der Zuckertransporter und damit die Effizienz der Saccharoseaufnahme bei einem hyperpolarisierten Membranpotential wesentlich höher ist (Kapitel VIII, Boorer *et al.,* 1996; Zhou *et al.,* 1997). Diese Bedeutung bei der Beladung des Sammelphloems als auch bei der Rückführung von „herausleckenden“ Zuckern im Transportphloem wird durch den Phänotyp der akt2/3-Knockout-Pflanzen unterstrichen.

In wie weit, die in Kapitel I und II beobachteten intrinsischen Eigenschaften von AKT3 wie z.B. seine pH-Abhängigkeit und seine Kaliumsensitivität, einen Einfluss auf die Phloemphysiologie haben, soll in zukünftigen Untersuchungen an akt2/3-Knockout-Pflanzen geschehen, die mit den pH- und $K^+$-insensitiven AKT3 Mutanten H228D, S271E und der Doppelmutante HDSE komplementiert wurden. Auch die Regulation der Stromamplitude und

der Gleichrichtung von AKT2/3 durch die Proteinphosphatase AtPP2CA (Cherel *et al.*, 2002), sowie die Modifikation der elektrophysiologischen Eigenschaften von Phloem-$K^+$-Kanälen durch die Aggregation zu Heterotetrameren unterschiedlicher *Shaker*-Kaliumkanal-Untereinheiten, lässt vermuten, dass weitere posttranslationale Modifikationen des AKT3-Kanals auf seine Aktivität sowie den Transport von Assimilaten rückwirken.

## 4.4 Charakterisierung von PTK2, dem AKT2/3 orthologen Kanal aus dem Kambium der Pappel

Die Jahresringe im Holz werden durch eine periodische (jährliche) Wachstumsaktivität des Kambiums der Bäume verursacht. Im Frühling zu Beginn jeder Wachstumsperiode werden beträchtliche Mengen an Kaliumionen aus den speichernden Holzparenchymzellen und den Holzstrahlzellen zu den meristematisch aktiven Kambiumgeweben des Stamms und der Blattachsen transportiert. Speziell in Bäumen konnte der positive Einfluss von Kalium zusammen mit Kalzium und Magnesium auf die kambiale Zellteilung und Differenzierung der Gewebe gezeigt werden (z. B. Wardrop, 1981; Eklund und Eliasson, 1990). Mit dem Einsetzen der Ruheperiode im Herbst kehrt sich die Richtung des Kaliumflusses um und Kalium wird wieder aus den Blättern in die Speichergewebe des Holzes befördert. Mittels EDXA (für energy dispersive X-ray analysis, energiedispersive Röntgenanalyse) und Perkolationsanalysen konnten Eschrich *et al.* (1988) und Fromm *et al.* (1987) diese saisonalen Kaliumverschiebungen nachweisen. Die hierbei auftretenden Membranübertritte der Kaliumionen können nur von Transportern ermöglicht werden. Unter Kalium-limitierenden Anzuchtbedingungen und nach lokal begrenzter Applikation des Kaliumkanalblockers $TEA^+$ wurden die Gefäßweiten des Holzes sowie die Streckungszone signifikant reduziert (Kapitel V). Diese Beobachtungen lieferten erste Hinweise auf die Beteiligung von Kaliumkanälen an der Holzbildung in mehrjährigen Pflanzen.

Bei der Suche nach den verantwortlichen Kanälen für den Transport von $K^+$ in mehrjährigen Pflanzen (*Populus tremula* L. *x Populus tremuloides* Michx.) wurde unter anderem ein *Shaker*-Kaliumkanal der AKT2/3-Unterfamilie identifiziert (PTK2 für *Populus tremula* $K^+$-Kanal 2) und in den Baststrahlen, Siebröhren und im Phloemparenchym der Pappel lokalisiert. Elektrophysiologische Analysen des PTK2-Kanals in *Xenopus* Oozyten mit der DEVC Technik zeigten, dass auch dieser Vertreter der AKT2/3-Unterfamilie einer holzigen Pflanze die typischen biophysikalischen Charakteristika dieser Unterfamilie aufweist. PTK2 ist ein schwach spannungsabhängiger, $K^+$-selektiver Kanal, der sowohl einen Kaliumeinstrom als auch einen Kaliumefflux vermitteln kann. Er zeigt bei einer Ansäuerung des externen pH-Wertes von pH 7,5 zu pH 5,6 eine Reduktion seiner makroskopischen Ströme und ist zudem spannungsabhängig durch Kalzium- und Cäsiumionen geblockt. Da PTK2 im gesamten Spannungsbereich ausschließlich instantane Kaliumströme vermittelte, ist das spannungs-

abhängige Schaltverhalten dieses Kanals noch schwächer ausgeprägt als beim AKT2/3-Kanal, der zusätzlich zu seiner instantanen Stromkomponente noch eine Zeit-abhängige bei Spannungen negativer als -90 mV aufweist (Marten *et al.*, 1999; Kapitel I, II und III).

Bei Patch-Clamp Analysen an Protoplasten von suspensionskultivierten Pappelzellen, die auch PTK2 schwach exprimierten, konnten die Beobachtungen im Oozytensystem nicht bestätigen. Die $K^+$-selektiven Ströme der Kanäle in der Suspensionskultur waren durch strikte spannungsabhängige Einwärtsgleichrichter charakterisiert. Die ausschließlich zeitabhängigen Stromkomponenten waren typisch für $K^+$-Kanäle der KAT1- und AKT1-Unterfamilie. Im Unterschied zu den bisher bekannten Einwärtsgleichrichtern waren diese Ströme allerdings durch $Ca^{2+}$ blockierbar, eine typische Eigenschaft der AKT2/3-Unterfamilie. Diese Beobachtungen legen die Vermutung nahe, dass Zellen dieser Pappel-Suspensionskultur neben PTK2 noch andere α-Untereinheiten von Kaliumkanälen exprimieren, welche zu Heterotetrameren mit PTK2 assemblieren und damit die elektrophysiologischen Eigenschaften von PTK2 modifizieren (Daram *et al.*, 1997; Dreyer *et al.*, 1997). Ähnlich wie für AKT2 gezeigt, könnte auch eine posttranslationale Modifikation durch eine Proteinphosphatase zu dieser Gleichrichtung der PTK2 Ströme führen (Vranova *et al.*, 2001; Cherel *et al.*, 2002).

Die transiente Expression von PTK2 im März und April und seine Lokalisation in Strahlzellen und Siebröhren sowie die Fähigkeit einen Kaliumeinstrom und –ausstrom zu vermitteln, lassen auf eine wichtige Rolle bei der Versorgung der Sink-Gewebe im Frühjahr schließen. Analog zu VFK1 und AKT2/3 (Ache *et al.*, 2001; Deeken *et al.*, 2002, Kapitel III) könnte PTK2 über die Kontrolle und Stabilisierung des Membranpotentials der $H^+$/Saccharose-Symporter vermittelte Zuckertransport in das Phloem (vertikal) und die Baststrahlen (radial) gesichert werden.

## 4.5 Be- und Entladung von Saccharose durch ZmSUT1

Obwohl bereits seit 2000 das Genom des apoplastischen Laders *Arabidopsis thaliana* sequenziert ist und Saccharosetransporter in der Plasmamembran des SE/CC Komplexes lokalisiert wurden, konnten bisher weder Saccharoseeffluxtransporter identifiziert werden noch der Mechanismus der apoplastischen Phloementladung aufgeklärt werden (siehe auch Einleitung 1.3.3 und 1.3.4). Die Tatsache, dass auch in Bereichen des Entladungsphloems sowohl Transkripte als auch Proteine von $H^+$/Saccharose-Symportern zu finden sind, ließ auf eine duale Funktion dieser Transporter bei der Phloembeladung und der Phloementladung schließen (Riesmeier *et al.*,. 1994; Truernit and Sauer, 1995; Kühn *et al.*,. 1997; Weber *et al.*,. 1997; Bick *et al.*,. 1998; Shakya and Sturm, 1998; Stadler *et al.*,. 1999; Lemoine *et al.*,. 1999). Kühn *et al.* (2003) konnte diese Vermutung durch eine Sink-spezifische antisense-Repression von StSUT1 noch untermauern. In diesen transgenen Pflanzen ist die frühe Knollenentwicklung durch das Fehlen von StSUT1 gestört.

Um zu testen, ob der Saccharoseexport durch einen inversen Transportmode der bereits bekannten $H^+$/Saccharose-Symporter katalysiert werden könnte, haben wir den Mais Saccharosetransporter ZmSUT1 in Oozyten exprimiert und mit Hilfe der DEVC Technik biophysikalisch charakterisiert (Kapitel VIII). In weiterführenden Analysen mittels der Patch-Clamp-Technik im „Giant inside-out“ Mode (Membranflecken mit bis zu 30 µm Durchmesser, wobei die cytosolische Seite der Membran in die Badkammer gerichtet ist) konnten wir die chemischen und elektrischen Gradienten über der Membran so verändern, dass die Transportrichtung von ZmSUT1 umgekehrt werden konnte. Unter diesen Bedingungen vermittelte ZmSUT1 Protonenauswärtsströme und einen damit verbundenen Saccharoseefflux.

### 4.5.1 Transportkinetiken von ZmSUT1 in Abhängigkeit von Saccharose, pH-Wert und der Spannung

Um die kinetischen Eigenschaften des $H^+$/Saccharose-Symporters ZmSUT1 in Hinblick auf die Affinitäten gegenüber Saccharose und dem elektrochemischen Protonengradienten (pmf: proton-motif-force) zu studieren, wurde dieser Transporter im heterologen Expressionssytem

der *Xenopus* Oozyten exprimiert. In $^{14}C$ Saccharose Aufnahmestudien und durch die Bestimmung der zytosolischen pH-Änderung in Gegenwart von Saccharose konnte ZmSUT1 eindeutig als Protonen/Saccharose-Symporter identifiziert werden. Während Kontrolloozyten weder radioaktiv markierte Saccharose in detektierbaren Mengen aufnahmen noch den zytosolischen pH-Wert in Gegenwart von Saccharose änderten, haben ZmSUT1 injizierte Oozyten $^{14}C$ Saccharose zeitabhängig akkumuliert und den pH-Wert der Oozyten innerhalb weniger Minuten bis zu einer pH-Einheit gesenkt.

Schrittweise Perfusion mit zunehmenden Saccharosekonzentrationen im Spannungsklemmenmodus beantworteten ZmSUT1 exprimierende Oozyten mit Saccharose-abhängigen Protoneneinwärtsströmen, die bei einer Konzentration von 30 mM in Sättigung gingen. Ähnliche Versuche im Stromklemmenmodus ergaben Depolarisationen der Oozytenmembran, deren Amplituden ebenfalls Saccharose-abhängig waren. In einer detaillierten Analyse der Gleichgewichtsströme in Abhängigkeit der Saccharosekonzentration wurden mit der Michaelis-Menten Gleichung die kinetischen Parameter ($K_m^S$ und $I_{max}^S$) der Saccharoseaufnahme über ZmSUT1 ermittelt. Dabei zeigte sich, dass die Saccharoseaffinität von ZmSUT1 eine ausgeprägte Spannungsabhängigkeit aufwies. Hyperpolarisierende Spannungen steigerten die Affinität gegenüber Saccharose erheblich. So besitzt ZmSUT1 einen $K_m^S$ von 3,7 mM bei einer typischen Phloemmembranspannung von -180 mV (Deeken *et al.,* 2002), während bei 0 mV der $K_m^S$ auf 16 mM steigt. $K_m^S$-Werte von Vertretern der SUT1-Unterfamilie wurden im Hefe-Expressionssystem auf 1,5 mM und weniger bestimmt (Kühn *et al.,* 2003). Aufgrund der Aktivität der Hefen $H^+$-ATPase, Pma1, liegt das Membranpotential von Hefen bei ca. -200 mV (Adam Bertl, persönliche Kommunikation). ZmSUT1 rangiert mit einem extrapolierten $K_m^S$-Wert von 3.2 mM bei -200 mV und pH 5,5 zwischen der Unterfamilie der hoch-affinen Transporter und der Unterfamilie der niedrig-affinen Transporter. Auch der maximale Transportstrom $I_{max}^S$ zeigte ein spannungsabhängiges Verhalten. Mit negativ werdendem Membranpotential stieg $I_{max}^S$ linear an.

In einem ähnlichen Ansatz, wie bei der Analyse von $K_m^S$ und $I_{max}^S$, wurden die $H^+$-Affinität ($K_m^H$) und die maximalen Transportströme ($I_{max}^H$) von ZmSUT1 in Abhängigkeit des pH-Wertes ermittelt. In Gegenwart von 5 mM Saccharose waren nur im Bereich von pH 6,5 bis pH 4,5 Saccharose induzierte Gleichgewichtsströme zu beobachten. Wie bei einem Protonengekoppelten Transportprozess zu erwarten war, stiegen die Ströme mit steigender Protonenkonzentration und hyperpolarisierenden Spannungen an. Bei pH-Werten über 7,0

konnten keine signifikanten Einwärtsströme beobachtet werden. Analog zum spannungsabhängigen Verhalten von $K_m^S$ stieg auch die Protonenaffinität von ZmSUT1 exponentiell mit hyperpolarisierenden Membranpotentialen. Auch $I_{max}^H$ stieg linear mit hyperpolarisierenden Membranspannungen an, wie es schon bei $I_{max}^S$ beobachtet wurde.

Der Mechanismus für die ausgeprägte Spannungsabhängigkeit der Transportparameter, $K_m$ und $I_{max}$, für das Substrat Saccharose als auch für Protonen könnte mit einer spannungsabhängigen Konformationsänderung in der Bindungstasche des Enzyms zusammenhängen. Analog zu den Untersuchungen an der LacY Permease aus E. coli, von der bereits die Struktur bekannt ist (Abramson *et al.,* 2003), werden wir zukünftig Struktur-Funktionsuntersuchungen an mutierten Saccharosetransportern zur Aufklärung der molekularen Grundlage der Spannungsabhängigkeit des Saccharosetransports durchführen.

### 4.5.2 Reversibilität des Transports von ZmSUT1

Um die Reversibilität des Saccharosetransports und die Affinität von ZmSUT1 gegenüber zytosolischen Saccharosekonzentrationen zu zeigen, verwendeten wir die Giant-Patch Technik. Während in der extrazellulären Lösung 0,5, 5 oder 50 mM (pH 5,6) Saccharose angeboten wurde, wurde die zytosolische Saccharosekonzentration von 0 auf 50, 100, 200 und 500 mM (pH 7,5) schrittweise erhöht. Durch die Erhöhung der zytosolischen Saccharosekonzentration in Gegenwart von 50 mM Saccharose im Außenmedium wurden die Protoneneinwärtsströme graduell erniedrigt. Mit 5 oder 0,5 mM Saccharose in der extrazellulären Lösung und steigender zytosolischer Saccharosekonzentration konnten die Ströme schließlich sogar umgekehrt werden. In Abwesenheit eines elektrischen Gradienten (Haltespannung 0 mV) kann also ZmSUT1 durch den nach außen gerichteten Saccharosegradienten einen Saccharoseefflux vermitteln, obwohl der Protonengradient nach innen gerichtet ist. Dabei ergaben sich $K_m^S$-Werte für die zytosolische Saccharoseaffinität zwischen 160 mM bei einer extrazellulären Saccharosekonzentration von 50 mM und 360 mM bei einer extrazellulären Saccharosekonzentration von 0,5 mM. Thermodynamische Analysen der Daten zur Abhängigkeit des Transports von extrazellulären und zytosolischen Saccharosekonzentrationen über ZmSUT1 ergaben eine Stoichiometrie des Transports von Protonen und Saccharose von 1 zu 1, wie es schon von Boorer *et al.,* (1996) und Zhou *et al.,*

(1997) durch indirekte Messungen für die $H^+$/Saccharose-Transporter StSUT1 und AtSUC1 angenommen wurde. Messungen in Abwesenheit des elektrochemischen Protonengradienten (pH-Wert 5,6 auf beiden Seiten und Haltespannung bei 0 mV) verdeutlichten nochmals die perfekte Kopplung des Protonen- und Saccharosetransports. Wie bereits erwähnt reicht der Saccharosegradient über der Membran aus, um die Richtung der Protonenströme und die damit verbundene Saccharoseaufnahme oder –entladung zu bestimmen. In Übereinstimmung mit einem perfekt gekoppelten thermodynamischen System kann der Saccharosegradient den Protonenstrom antreiben, genauso wie umgekehrt der Protonengradient den Saccharosefluss bestimmen kann.

Neben den genetischen Hinweisen auf die Beteiligung von $H^+$/Saccharose-Transportern an der apoplastischen Phloementladung wurde die Reversibilität des Transports auch für zwei andere Protonen-gekoppelte Transporter durch direkte Messungen gefordert. So konnten Komor und Tanner bereits 1974 für den Monosaccharidtransporter aus der Grünalge *Chlorella* anhand indirekter Befunde einen inversen Transportmode beschreiben. Kürzlich wurde auch die Reversibilität des $Na^+$/Glukose Cotransporters (SGLT1) aus Mensch und Hase berichtet (Sauer *et al.,* 2000; Quick *et al.,* 2003). Hierbei wurde auch die Giant-Patch-Clamp Technik verwandt. Auch bei diesen Transportern, wie bei ZmSUT1, sind die extrazellulären und zytosolischen Substrataffinitäten stark verschieden. Unter physiologischen Bedingungen ist der inverse Transportmode von SGLT1 jedoch aufgrund seiner schwachen zytosolischen Glukoseaffinität sehr unwahrscheinlich. Im pflanzlichen Phloem sind allerdings beide Transportmodi von ZmSUT1 denkbar: i) Im Sammelphloem wurden apoplastische Saccharosekonzentration von ca. 2,6 mM (oder höher, siehe Lalonde *et al.,* 2003 und Kapitel 1.3.2) gemessen (Lohaus *et al.,* 2000). Das Membranpotential liegt zwischen -130 und -180 mV und der externe pH-Wert wurde auf Werte zwischen 5,5 und 6,5 bestimmt, während in den Phloemgefäßen ein pH-Wert von 7,2 bis 7,8 dokumentiert wurde (Mühling und Sattelmacher, 1997; van Bel, 1993). Unter diesen Bedingungen ($V_m$ = -150 mV; $\Delta$pH = 1,5; $[Saccharose]_{ext}$ = 2,6 mM) erlaubt der $H^+$/Saccharose-Transporter ZmSUT1 theoretisch eine Akkumulation von bis zu 26 M Saccharose im SE/CC Komplex (siehe Gleichung 2 in Kapitel VIII mit $n_H/n_{suc}=1$). Direkte Messungen im Phloemsaft von Maispflanzen ergaben jedoch nur Saccharosekonzentrationen von ungefähr 850 mM (Lohaus *et al.,* 2000). Höhere Saccharosekonzentrationen scheinen für das antreiben des Massenstroms im Phloem nicht notwendig zu sein. ii) In den Bereichen des Entladungsphloems liegen die apoplastischen Saccharosekonzentrationen aufgrund der Aktivität von Zellwand-gebundenen Invertasen bei

1mM oder darunter (z.B. Roitsch *et al.,* 2003). Des Weiteren ist im Sink-Phloem die Größe der „energieliefernden“ Geleitzellen im Verhältnis zu den Siebelementen stark reduziert oder zum Teil sind keine Geleitzellen mehr vorhanden (van Bel 1993; van Bel und Ehlers, 2000 und Einleitung 1.1). Evert und Russin (1993) zeigten außerdem, dass eine symplastische Entladung der Saccharose im wachsenden Maisblatt (Sink) aufgrund fehlender Plasmodesmen im Proto- und Metaphloem nicht möglich ist. Diese funktionelle Anatomie könnte zu einer Reduktion des elektrochemischen Potentials für Protonen (pmf) führen, d.h. der extrazelluläre pH-Wert liegt höher und das Membranpotential positiver als im Sammelphloem. Aufgrund dieser Tatsache sollte das Membranpotential im Sink-Phloem hauptsächlich von der Kaliumleitfähigkeit Phloem-lokalisierter Kaliumkanäle des AKT2/3-Typs abhängen, die zudem bei neutralen pH-Werten stärker aktiviert sind und die zum Teil (VfK1) Fruktose-abhängig exprimieren (Ache *et al.,* 2001). Unter der Annahme, dass im Bereich des Sink-Phloems die pH-Differenz zwischen Phloem und Apoplast auf eine pH-Einheit erniedrigt ist und dass die apoplastische Saccharosekonzentration bei 1 mM liegt (im Phloem 850 mM), würde eine Depolarisation des Membranpotentials auf -115 mV ausreichen, um ZmSUT1 in den inversen Transportmode zu zwingen und einen Saccharoseefflux zu erlauben (errechnet nach Gleichung 2 Kapitel VIII mit $n_H/n_{suc}=1$). Ein positiveres Membranpotential im Sink-Phloem senkt zu dem auch die Affinitäten des Transporters für apoplastische Protonen und Saccharose, was ebenfalls eine Entladung des Phloems favorisiert.

Im Modell in Kapitel VIII (Supplementary Figure 3) sind die Verhältnisse an den Membranen des Source- und des Sink-Phloems zusammengefasst, die die beiden Transportmodi von ZmSUT1 ermöglichen könnten. Weitere präzise Messungen des Membranpotentials und der pH-Werte sowie der Kaliumkonzentrationen vor allem im Apoplasten der entsprechenden Gewebe gestalten sich aufgrund der morphologischen Gegebenheiten des Phloems sehr schwierig. Dennoch sprechen die ausgeprägten Defekte von Saccharosetransporter defizienten Mutanten oder von Sink-spezifischen antisense Repressionspflanzen für eine Beteiligung von Saccharosetransportern an der Entladung in den Sink-Geweben apoplastisch entladender Pflanzen.

## 4.6 Biophysikalische Analyse des Phloem-lokalisierten Polyoltransporters PmPLT1

Es ist bis heute noch nicht vollständig verstanden, warum verschiedene Pflanzenarten unterschiedliche Zucker für den Langstreckentransport von Kohlenstoffverbindungen nutzen. Im Fall der Raffinose-transportierenden Arten, die hauptsächlich eine symplastische Phloembeladung betreiben, scheint der Unterschied im Stokes Radius zwischen Saccharose und Raffinose bzw. Stachyiose Ausschlag gebend zu sein. Das Polymer-Treppen-Modell basiert auf der Annahme, dass Saccharose nach dem symplastischen Transport bis in die Geleitzellen (Intermediärzellen) in Raffinose umgewandelt wird und aufgrund des größeren Stokes Radius dieses Trisaccharides dann nicht mehr über die Plasmodesmen zurück diffundieren kann (siehe auch Einleitung 1.3.1; Turgeon, 1996).

Die Translokation von Polyolen wie Sorbitol oder Mannitol anstatt oder in Kombination mit Saccharose kann dagegen mit physiologischen Vorteilen für die Pflanze begründet werden (siehe Einleitung 1.3.5; Ramsperger-Gleixner *et al.*, 2004). Stark reduzierende Zucker bieten Vorteile bei $NADPH^+$ abhängigen Reaktionen, können als Antioxidanzien oder Osmoprotektoren wirken oder spielen eine Rolle bei der Pathogeninteraktion (Hansch *et al.*, 2001; Shen *et al.*, 1997; Jennings *et al.*, 1998; Tarczynski *et al.*, 1993; Everard *et al.*, 1994; Stoop und Pharr, 1994a, 1994b).

Trotz dieser offensichtlichen Vorteile der Translokation von Polyolen konnte bisher noch keiner der bereits klonierten Sorbitol- bzw. Mannitoltransporter eindeutig in der Phloemmembran lokalisiert werden (Gao *et al.*, 2003; Noiraud *et al.*, 2001). In Kapitel VI wurde nun zum ersten Mal mit PmPLT1 und PmPLT2 die Klonierung, Lokalisierung und biophysikalische Analyse zweier Phloem-lokalisierter Polyoltransporter aus *Plantago major* beschrieben.

Erste funktionelle Analysen der beiden Polyoltransporter PmPLT1 und PmPLT2 im Hefeexpressionssystem konnten zeigen, dass diese transgenen Hefen in der Lage waren radioaktiv markiertes Sorbitol bis zu einer 20-fachen Konzentration, verglichen zum Außenmedium, zu akkumulieren. Hefen, die diese Transporter in der antisense Orientierung

exprimierten, konnten Sorbitol nicht aufnehmen. Untersuchungen der Sorbitolaffinität von PmPLT1 mittels einer Michaelis-Menten Analyse ergab einen $K_m$-Wert von 12,3 mM. Dieser Affinität von PmPLT1 unterscheidet sich deutlich von den publizierten $K_m$-Werten für den Mannitoltransporter AgMAT1 aus Sellerie ($K_m$= 0,3 mM) und den Sorbitoltransportern PcSOT1 ($K_m$= 0,6 mM) und PcSOT2 aus der Sauerkirsche ($K_m$= 0,3 mM). Die Substrataffinität von PmPLT2 liegt noch niedriger ($K_m$= 20 mM) als die von PmPLT1. Unter den gewählten Bedingungen wurde der Transporter nicht in Sättigung gebracht. Diese Ergebnisse und die Tatsache, dass auch Mannitol als Substrat aufgenommen wird, charakterisieren die beiden *Plantago* Transporter als schwach affine und wenig-spezifische Sorbitoltransporter. Eine Zugabe von 10 mM Glukose zum Hefe-Inkubationsmedium steigerte die Sorbitolaufnahmerate nochmals erheblich. Diese Steigerung in Anwesenheit von Glukose wurde auch bei der Expression von anderen Zuckertransportern im Hefeexpressionssystem beobachtet (Riesmeier *et al.,* 1992; Gahrtz *et al.,* 1994; Sauer and Stolz, 1994). Es wird vermutet, dass sich durch den Glukosemetabolismus der Energiestatus der Hefezellen erhöht, was zu einer Steigerung der $H^+$-ATPase Aktivität führt und den damit verbundenen sekundär aktiven Transport über Protonen-gekoppelte Transporter positiv beeinflusst. Diese Beobachtung war ein weiterer Hinweis auf eine Energie-gekoppelte Aufnahme von Sorbitol durch PmPLT1 und PmPLT2. Weitere Untersuchungen mit Entkopplern und SH-Gruppen Inhibitoren konnten diese Vermutung bestätigen. Interessanterweise konnte allerdings lediglich die Aktivität von PmPLT1 durch Zugabe des SH-Gruppen Inhibitors PCMBS inhibiert werden, während PmPLT2 keine signifikante Reduktion seiner Transportaktivität in Gegenwart von PCMBS zeigte. Sequenzvergleiche zwischen den beiden Transportern offenbarten, dass PmPLT1 neben fünf Cysteinen, die in beiden Proteinen konserviert vorliegen, noch ein sechstes Cystein in der ersten extrazellulären Schleife zwischen Transmembrane 1 und 2 besitzt. Auch allen bereits untersuchten Polyoltransportern fehlt dieses Cystein in der ersten extrazellulären Schleife und sie zeigen wie PmPLT2 nur eine schwache PCMBS Empfindlichkeit (Noiraud *et al.,* 2001). Die PCMBS Empfindlichkeit von PmPLT1 scheint also in der Zugänglichkeit des SH-Gruppen Inhibitors zu diesem Cystein begründet zu sein. Die Unempfindlichkeit einiger dieser Symporter gegenüber PCMBS stellt überdies die generelle Eingruppierung von Pflanzenarten in symplastische oder apoplastische Lader aufgrund ihrer PCMBS Empfindlichkeit in Frage. Bestätigt wurden diese Zweifel durch die Klonierung von $H^+$/Saccharose-Symportern aus Pflanzenarten, die als typische

symplastische Phloembelader bekannt waren, wie z.B. *Asarina barclaiana Pennell* und *Alonsoa meridionalis* (Knop *et al.*, 2001, 2004).

Gesteigerte Transportraten in Gegenwart von Glukose und die Empfindlichkeit des Transportprozesses gegenüber Entkopplern im Hefeexpressionssystem wiesen bereits indirekt auf einen Protonen-getriebenen Transport der Substrate durch die beiden Polyoltransporter hin. Dass der Transport tatsächlich abhängig ist vom elektrochemischen Protonengradienten (pmf) sollten Untersuchungen in Oozyten zeigen.

Im Spannungsklemmenmodus wurden bei der Zugabe von Sorbitol PmPLT1-vermittelte Einwärtsströme gemessen, die nach der Entfernung des Substrats wieder auf das Ausgangsniveau fielen. Kontrolloozyten reagierten auf die Gabe von Polyolen nicht. Eine Perfusion der PmPLT1 exprimierenden Oozyten mit verschiedenen Polyolen zeigte, dass dieser Transporter schwach substratspezifisch ist. Die Transportraten in Gegenwart von Mannitol waren am höchsten, gefolgt von Sorbitol und *myo*-Inositol (Relative Ströme bei $V_H$ = 60 mV waren $I_{Mannitol}$ = 1, $I_{Sorbitol}$ = 0.66 ± 0.11 und $I_{myo\text{-}Inositol}$ = 0.12 ± 0.05). Weitere Analysen der Affinität und pH-Abhängigkeit wurden deshalb mit Mannitol als Substrat durchgeführt. Wie schon im Hefesystem wurde auch im Oozytensystem der $K_m$-Wert über eine Michaelis-Menten Analyse bestimmt. Analog zur Spannungsabhängigkeit des $K_m$-Wertes vom $H^+$/Saccharose-Transporter ZmSUT1 (Kapitel VIII) sinkt auch der $K_m$-Wert von PmPLT1 bei hyperpolarisierenden Spannungen. Bei einer Membranspannung von 0 mV liegt er beispielsweise bei 18 mM, während er bei -120 mV auf 15 mM sinkt. Diese Affinitäten liegen im gleichen Bereich wie sie auch im Hefesystem für Sorbitol bestimmt wurden und bestätigen damit die Charakterisierung von PmPLT1 als schwach affinen Polyoltransporter.

Um die Abhängigkeit von PmPLT1 von der extrazellulären Protonenkonzentration zu bestimmen wurden Experimente bei unterschiedlichen pH-Werten zwischen 4,5 und 8,5 durchgeführt. In Übereinstimmung mit einem Protonen-gekoppelten Transportprozess stiegen die Einwärtsströme mit zunehmendem Protonengradienten an, die allerdings bei pH-Werten unterhalb von 6,5 wieder abnahmen. Die Tatsache, dass PmPLT1 ein pH-Optimum im Bereich von pH 6,5 besitzt, lässt auf einen intrinsischen Regulationsmechanismus des Proteins über den externen pH-Wert schließen.

In dieser Arbeit konnten zum ersten Mal Polyoltransporter charakterisiert werden, die durch immunohistochemische Lokalisation eindeutig den Phloemgeleitzellen zugeordnet werden

konnten. Sie unterscheiden sich deutlich in ihrer Substrataffinität von den bereits charakterisierten Transportern aus Kirsche und Sellerie (Gao *et al.*, 2003; Noiraud *et al.*, 2001). Die schwache Substrataffinität von PmPLT1 und 2 liegen in der gleichen Größenordnung wie die Affinitäten, die beim Sorbitoltransport im Apfel und bei der Sorbitolbeladung des Phloems im Pfirsich errechnet wurden. *Plantago major* transportiert neben Saccharose (800 mM) vor allem Sorbitol (300 mM) in seinen Siebelementen. Da beide Transporter aber auch Mannitol transportieren, ist eine Bezeichnung als Polyoltransporter (anstatt Sorbitoltransporter) vorzuziehen.

## 4.7 AtPLT5, ein unspezifischer Polyoltransporter aus *Arabidopsis*

In *Arabidopsis* wurden sieben Unterfamilien der MST-ähnlichen Superfamilie identifiziert, die nach der intensiv charakterisierten AtSTP Genfamilie benannt wurden. Die Unterfamilie dieser STPs beherbergt 14 Mitglieder von Plasmamembran-lokalisierten Monosaccharid-transportern (Sauer *et al.*, 1990; Büttner und Sauer 2000). Sie ist die einzige Unterfamilie der MST-ähnlichen Transporter, deren Mitglieder bisher funktionell exprimiert und charakterisiert werden konnten. Mit AtPLT5 konnte nun in Kapitel VII ein Vertreter einer weiteren Unterfamilie beschrieben werden. Diese Familie wurde aufgrund von signifikanten Sequenzhomologien zu bereits bekannten Transportern aus Wegerich, Sauerkirsche und Sellerie als Polyoltransporter eingruppiert. Die physiologische Rolle von Polyoltransportern in *Arabidopsis* war jedoch bisher völlig unklar, da im Phloem dieser Pflanze vor allem Saccharose und kleine Mengen an Raffinose transloziert werden, aber keine Polyole (Haritatos *et al.*, 2000).

Zur Untersuchung der Polyoltransporter-ähnlichen Unterfamilie wurden cDNAs von fünf der sechs in *Arabidopsis* vorhergesagten Gene isoliert und eines der kodierten Proteine (AtPLT5) in heterologen Expressionssystemen funktionell charakterisiert. Mit Hilfe von RT-PCR Analysen wurden verschiedene Gewebe auf die Expression von AtPLT5 mRNA hin untersucht. Es zeigte sich, dass dieser Transporter in allen untersuchten Geweben exprimiert. Die höchsten mRNA-Gehalte wurden vor allem in den distalen Regionen der Wurzel gemessen. AtPLT5 Promoter::GUS und Promoter::GFP Pflanzen bestätigten die hohe Expression dieses Transporters in den distalen Geweben der Wurzel. In Pflanzen, die mit GUS unter der Kontrolle des AtPLT5 Promotors transformiert waren, konnte die Promoteraktivität in weiteren Geweben detektiert werden. So waren GUS-Färbungen vor Allem in oder entlang der Leitgefäße in Blättern zu beobachten sowie etwas schwächer in den Gefäßen des Stängels, der Sepalen und in den Schoten. In Pollen, Samen und Kronblättern konnte keine GUS-Färbung festgestellt werden.

Um die Funktionalität, die Spezifität sowie die Kinetik dieses Transporters zu zeigen, wurde die cDNA von AtPLT5 im heterologen Expressionssystem der Hefe exprimiert. Erste Aufnahmexperimente mit $^{14}$C-markiertem Sorbitol und Mannitol zeigten eine starke Preferenz

von AtPLT5 für Sorbitol. Dies steht im Gegensatz zur Substratspezifität anderer bereits charakterisierter Polyoltransporter, die für Sorbitol und Mannitol gleichwertige Transportraten zeigten (Noriaud *et al.*, 2001; Gao *et al.*, 2003; Ramsperger-Gleixner *et al.*, 2004). Glukose stellt für Hefezellen eine Kohlenstoffquelle dar, die den Energiestatus der Zelle erhöht und somit auch zusätzliche Energie in Form von ATP für die Plasmamembran ATPase liefert. Durch die Erhöhung des elektrochemischen Protonengradienten (pmf) sollte auch der Transport über sekundär aktive $H^+$-Symporter gesteigert sein, wie es bei den Polyoltransportern PmPLT1 und PmPLT2 aus dem Wegerich gezeigt werden konnte. Bei AtPLT5 transformierten Hefen wurde allerdings die Aufnahmerate von $^{14}C$ Sorbitol in Gegenwart von Glukose nicht erhöht, sondern stark inhibiert. Eine Erklärung für diese Tatsache könnte sein, dass es sich bei AtPLT5 um einen Transporter handelt, der unabhängig vom pmf arbeitet und ein anderes Co-Substrat als Protonen nutzt, wie z.B. $Na^+$. Experimente mit radioaktiv markierter Glukose haben jedoch gezeigt, dass Glukose ebenso als Substrat für diesen Transporter dient wie Sorbitol, und dass die Inhibierung der $^{14}C$-Sorbitol Aufnahme in Gegenwart von Glukose in einer kompetitiven Hemmung begründet lag. Diese Transportkapazität von AtPLT5 für Sorbitol und gleichzeitig für Zucker (Glukose) wurde bisher bei keinem anderen pflanzlichen Polyoltransporter gezeigt.

Weitere Kompetitorstudien offenbarten ein sehr breites Substratspektrum von AtPLT5. So war die Aufnahme von $^{14}C$-Sorbitol in der Gegenwart vieler Hexosen, Pentosen sowie linearer Polyole mit Kettenlängen von drei bis sechs C-Atomen und dem zyklischen Polyol *myo*-Inositol signifikant inhibiert (siehe auch Tabelle 1 Kapitel VII). Vor Allem die starke kompetitive Hemmung durch das zyklische Polyol *myo*-Inositol sowie durch die Pentosen Xylose und Arabinose waren unerwartet. Ebenso erstaunlich war der inhibitorische Effekt auf die Sorbitolaufnahme von dem $C_3$-Polyol Glycerin sowie von Ribose, die einen Furanose Ring bildet. Disaccharide wie z.B. Saccharose hingegen behinderten die Aufnahme von $^{14}C$-Sorbitol nicht.

Die Tatsache, dass Sorbitol in AtPLT5-transformierten Hefezellen akkumuliert werden kann, sowie die Sensitivität des AtPLT5-vermittelten Polyoltransports gegenüber Entkopplern (CCCP und DNP), spricht für einen Energie-abhängigen Transportmechanismus. Zur direkten Bestätigung dieser Hypothese und zur weiteren Analyse der Substratspezifität von AtPLT5 wurde das heterologe Expressionssystem der *Xenopus* Oozyten gewählt. Mit Hilfe der Zwei-Elektroden Spannungsklemmen Technik wurden verschiedene Substrate im Wechsel mit

einer Kontrolllösung zur AtPLT5 injizierten Oozyte perfundiert und die resultierenden Ströme aufgezeichnet. Diese Experimente bestätigten das breite Substratspektrum von AtPLT5. Es konnten makroskopische Einwärtsströme in Gegenwart von je 3 mM Sorbitol, Glukose, Fruktose und *myo*-Inositol bei einem pH-Wert von 5,5 und einem Membranpotential von -60 mV aufgezeichnet werden. Unter den gleichen Bedingungen waren auch Einwärtsströme in Gegenwart von Glycerol zu beobachten, die jedoch deutlich kleiner ausfielen. Wie bereits bei Aufnahmestudien mit Hefe zu erkennen war, dient Mannitol nicht oder nur in einem sehr geringem Umfang als Substrat von AtPLT5. Für die Aufnahme von Glycerol und *myo*-Inositol wurden die $K_m$-Werte bei pH 5,5 und einem Membranpotential von -60 mV bestimmt. Dabei ergab sich ein $K_m$-Wert für Glycerol von 23,4 ± 2.3 mM und von 3,5 ± 0,3 mM für *myo*-Inositol. Weiterführende Analysen der Affinität von AtPLT5 gegenüber *myo*-Inositol bei Membranpotentialen im Bereich von 40 bis -140 mV resultierten in einem spannungsabhängigen Verhalten des $K_m$-Wertes, der bei -140 mV schließlich bis auf 1 mM sank. Zusammen mit den Ergebnissen der Aufnahmestudien in Hefe und den elektrophysiologischen Untersuchungen in Oozyten lässt sich AtPLT5 mit $K_m$-Werten im millimolarem Bereich als ein niedrig-affiner und wenig spezifischer Transporter beschreiben. Er transportiert einige Substrate (z.B. *myo*-Inositol, Ribose und Glycerol), für die bisher noch keine sekundär aktive Transportaktivität in pflanzlichen Plasmamembranen publiziert wurde.

Die Substrat-induzierten Einwärtsströme verdeutlichen zudem, dass der AtPLT5-vermittelte Transport an ein geladenes Ion gekoppelt sein muss. Um herrauszufinden, ob auch der Substrattransport von AtPLT5 über den elektrochemischen Protonengradienten angetrieben wird, wurden die Einwärtsströme in Gegenwart von Glukose und Glycerol bei verschiedene extrazellulären pH-Werten in einer Natrium freien Lösung getestet. Je saurer die externe Lösung gewählt wurde, umso höher waren dabei die Substrat-induzierten Einwärtsströme, was auf einen Cotransport von Protonen mit dem jeweiligen Substrat hindeutet. 90% höhere Transportraten von Sorbitol bei pH 5,0 im Vergleich zu pH 7,0 in der Hefe bestätigen diese Vermutung.

Die breite Substratspezifität und das breite Genexpressionsmuster sowie das Fehlen eines Phänotyps in einer Atplt5-Knockout Pflanze gestaltet das Spekulieren über die physiologische Rolle von AtPLT5 schwierig. Es bleiben viele Fragen offen, z.B. bezüglich weiterer nicht getesteter Substrate, dem Hauptsubstrat des Transporters oder ob mehrere Substrate *in planta* transportiert werden. Eine einfache Erklärung für die Funktion von AtPLT5 mag die

Wiederaufnahme von Substraten aus dem Apoplasten sein. Alle untersuchten Substrate sind Hauptkomponenten des zellulären Metabolismus und könnten so nach dem „Herauslecken“ aus den Zellen wieder aufgenommen werden. Auch eine spezifischere Funktion von AtPLT5 z.B. bei der Zell-zu-Zell-Verteilung von bestimmten Substraten kann nicht ausgeschlossen werden.

Diese Fragen müssen jetzt durch die Bestimmung apoplastischer Metabolite in WT und Knockout-Pflanzen beantwortet werden. Dabei muss auch geprüft werden, ob andere Polyoltransporter den Verlust von AtPLT5 kompensieren.

# 5. Zusammenfassung

Das Phloem stellt ein Netzwerk zur Assimilat- und Nährstofftranslokation sowie zur elektrischen Kommunikation innerhalb der Pflanze dar. In apoplastisch beladenden Pflanzen werden die funktionellen Eigenschaften des Phloems im Wesentlichen vom Zusammenspiel eines Transportmoduls, bestehend aus Carriern, Kaliumkanälen und Protonen-ATPasen, bestimmt.

Ausgangspunkt für die biophysikalische Charakterisierung dieses Phloem-Transportmoduls waren Arbeiten zum Saccharosetransport in der *Arabidopsis* akt2/3-1 Mutante. Das *AKT2/3* Gen kodiert für einen Phloem-spezifischen Kaliumkanal vom *Shaker*-Typ. Die Tatsache, dass der Saccharosegehalt im Phloem dieser Mutante um 50% im Vergleich zum Wildtyp reduziert war, ließ eine enge Kopplung von Kalium- und Zuckerflüssen vermuten. Um diesen Phänotyp aufklären zu können und ein Modell für die Beladungsprozesse an der Phloemmembran zu entwickeln, wurde das heterologe Expressionssystem der *Xenopus* Oozyten gewählt. So konnte in Coexpressionsstudien die Interaktion von Phloem-lokalisierten Kaliumkanälen und Transportern sowie die Kopplung des Kalium- und Zuckertransports mit Hilfe biophysikalischer Methoden untersucht werden.

**Charakterisierung von Kaliumkanälen des Phloems**

**Die Einwärtsgleichrichter der KAT1-Unterfamilie:**

Die *Shaker*-ähnlichen Kaliumkanäle KAT2 aus *Arabidopsis* ebenso wie KZM1 aus Mais werden im Phloem exprimiert. Beide Kanalproteine repräsentieren spannungsabhängige, hyperpolarisationsaktivierte Kaliumaufnahmekanäle. Während KAT2 als typischer Vertreter der KAT1-Unterfamilie bei extrazellulärer Ansäuerung sein spannungsabhängiges Schaltverhalten hin zu positiveren Membranpotentialen verschiebt, ist die Aktivität des KZM1 Kanals unabhängig vom extrazellulären pH-Wert. Beide Kanäle reagieren jedoch auf eine Ansäuerung des Zytosols mit einer Verschiebung ihrer halbmaximalen Aktivierungsspannung zu positiveren Spannungen. KZM1 besitzt zusätzlich einen

Kaliumsensor, der bei niedrigen externen Kaliumkonzentrationen für den Schluss der Kanalpore sorgt.

**Die schwach spannungsabhängigen $K^+$ Kanäle AKT2/3-Unterfamilie:**

Die Phloem-lokalisierten Kaliumkanäle der AKT2/3-Unterfamilie (wie z.B. AKT2/3 aus *Arabidopsis*, PTK2 aus der Pappel und ZMK2 aus dem Mais) zeichnen sich durch ihre schwache Spannungsabhängigkeit und ihre Inhibierung durch extrazelluläre Protonen oder Kalziumionen aus. Aufgrund der schwachen Spannungsabhängigkeit dieser Kanäle vermitteln sie in Abhängigkeit des elektrochemischen Gradienten für Kalium sowohl Einwärts- als auch Auswärtsströme. Ebenso wie VFK1 aus *Vicia faba*, ist die transkriptionelle Regulation von AKT2/3 eng an die Photosynthese gekoppelt. Die Analyse einer AKT2/3 Verlustmutante ergab zudem, dass dieser Kanal eine wichtige Rolle bei der Translokation von Assimilaten im Phloem spielt.

In Untersuchungen an Porenchimären zwischen dem schwach spannungsabhängigen AKT2/3 und dem Einwärtsgleichrichter KST1 aus der Kartoffel konnten die Gleichrichtungseigenschaften sowie die Protonen und Kalziumsensitivität des AKT2/3 Kanals der Porenregion zugeschrieben werden . Detaillierte Mutagenesen von Histidin- bzw. Serinresten lokalisierten den pH- und $K^+$-Sensor im äußeren Porenbereich und konvertierten diesen Kanal in einen pH- und Kalium-unabhängigen $K^+$ Kanal.

**<u>Charakterisierung von Phloem-lokalisierten Carriern</u>**

**Der Saccharose/Protonen-Symporter ZmSUT1:**

Elektrophysiologische Untersuchungen des Mais Saccharosetransporters, ZmSUT1, in Oozyten von *Xenopus laevis* charakterisierten diesen Carrier als niedrig-affinen Saccharose/$H^+$-Symporter mit einem $K_m$-Wert für Saccharose von 3 mM. Parallele Messungen der Saccharose-induzierten $H^+$-Ströme und des zytosolischen pH-Wertes der Oozyte identifizierten diesen Transporter eindeutig als einen Saccharose/Protonen-Symporter. Die kinetischen Parameter für Saccharose als auch für Protonen ($K_m$-Wert und $I_{max}$) dieses

Transporters zeigten eine ausgeprägte Spannungsabhängigkeit. In Giant-Patch Experimenten konnte die Reversibilität von ZmSUT1 gezeigt werden. Dabei wurde deutlich, dass sowohl Protonen als auch Saccharose und das Membranpotential Richtung und Geschwindigkeit des Transports bestimmen. Energetisch betrachtet könnte dieser Transporter demnach in Sink-Geweben das Entlassen von Saccharose aus dem Phloem vermitteln.

**Die Polyoltransporter PmPLT1 und AtPLT5**

Ebenso wie für den Saccharosetransporter ZmSUT1 wurde für die beiden Polyoltransporter PmPLT1 und AtPLT5 (aus *Plantago major* bzw. *Arabidopsis*) die Zwei-Elektroden Spannungsklemmen Technik verwendet, um die Spezifität und die Transportkinetiken dieser beiden Transporter zu bestimmen. PmPLT1 wurde als erster Polyoltransporter nachweislich in der Phloemmembran lokalisiert. Die funktionelle Charakterisierung dieses Transporters in Hefe und Oozyten zeigte, dass PmPLT1 spezifisch lineare Polyole transportiert. Dabei nimmt PmPLT1 Mannitol um 40% effektiver auf als beispielsweise Sorbitol. Der ringförmige Zuckeralkohol *myo*-Inositol dient dagegen nicht als Substrat für diesen Transporter. Messungen der Einwärtsströme bei verschiedenen pH-Werten ergaben für den Zuckeralkoholtransport ein pH-Optimum von 6,5 und bestätigen den Cotransport von Polyolen zusammen mit Protonen. Der $K_m$-Wert wurde auf 15 mM bei -120 mV ermittelt und charakterisiert PmPLT1 als einen niedrig-affinen Polyol/$H^+$-Symporter, der die Aufnahme von Sorbitol in das Phloem katalysiert.

Obwohl im Phloem von *Arabidopsis* scheinbar keine Polyole über das Phloem transloziert werden, besitzt diese Pflanze sechs Gene, die für Transporter der MST Familie kodieren. Die Mitglieder dieser Genfamilie, wie auch AtPLT5, weisen eine hohe Sequenzhomologie zu bereits beschriebenen Polyoltransportern aus anderen Pflanzenspezies auf. Die funktionelle Analyse des AtPLT5 Transporters zeigte, dass dieser Carrier ein sehr breites Substratspektrum aufweist und neben Sorbitol und Glukose sogar Glycerol und Ribose transportiert. Ebenso gut wird der ringförmige Zuckeralkohol *myo*-Inositol transportiert, wohingegen Mannitol nicht als Substrat dient. Wie erwartet sind auch bei AtPLT5 Protonen das Cosubstrat zu den Polyolen und Zuckern. Basierend auf dieser ersten Analyse eines Polyoltransporters aus *Arabidopsis* können nun molekulare Analysen an Mutanten von

Mitgliedern der *Arabidopsis* MST Familie zur physiologische Rolle dieser Transporter angeschlossen werden.

**Interaktion von Phloem-lokalisierten Saccharosetransportern und Kaliumkanälen**

Das Expressionssystem der *Xenopus* Oozyten bietet den Vorteil, dass die Interaktion von Proteinen sowie die Kopplung von Transportprozessen unter definierten Bedingungen (Coexpression) studiert werden kann. Zur Untersuchung der Kopplung von Kalium- und Zuckerflüssen an der Phloemmembran wurde der AKT2/3 $K^+$-Kanal gemeinsam mit dem Saccharosetransporter AtSUC2 im Modellsystem der Oozyte coexprimiert. Diese Untersuchungen zeigten, dass nach alleiniger Expression des AtSUC2 Transporters das Membranpotential durch die Saccharose-induzierten Protoneneinströme stark depolarisiert. Bei gleichzeitiger Expression des AKT2/3 Kanals jedoch, wird diese Depolarisation durch den Ausstrom von Kaliumionen kompensiert. Im Vergleich dazu wird bei einer Coexpression des strengen Einwärtsgleichrichters KAT2 mit dem Saccharosetransporter AtSUC2 eine Depolarisation nicht verhindert. Aufgrund der besonderen biophysikalischen Eigenschaften von AKT2/3 wird das Membranpotential des Phloems in Kalium-abhängiger Weise kontrolliert und stabilisiert. Aufgrund der Spannungsabhängigkeit des AtSUC2 Transporters beeinflusst die AKT2/3-abhängige Unterdrückung der Saccharose-induzierten Depolarisationen auch die Saccharoseaufnahme positiv. Die Affinität der Transporter zu Saccharose und Protonen steigt mit der Hyperpolarisation des Membranpotentials stark an und damit auch die Transportraten.

Coexpressionsexperimente mit den orthologen Kanälen und Transportern aus Mais konnten dieses Ergebnis bestätigten: Nur der schwach spannungsabhängige $K^+$ Kanal ZMK2 ist in der Lage, das Membranpotential während der Saccharoseaufnahme durch den Zuckertransporter ZmSUT1 zu stabilisieren. Ebenso wie der KAT2 Kanal, vermag der spannungsabhäbgige Einwärtsgleichrichter KZM1 dies nicht, sondern dient vermutlich zur Erhaltung der Kaliumhomeostase im Phloem.

# 6. Summary

In plants the phloem tissue constitutes a network providing for assimilate and nutrient translocation as well as electrical communication. A transport module, consisting of carriers, channels and pumps plays a pivotal role in apoplasmically loading plant species and determines the specific transport properties of phloem cells.

The AKT2/3 channel represents a phloem-specific *Shaker*-like $K^+$ channel of the model plant *Arabidopsis thaliana*. Based on the observation, that sucrose transport is severely impaired in the corresponding *akt2/3-1* mutant, we hypothesised a tight coupling of potassium and sugar fluxes during phloem loading. In order to allow a biophysical characterisation of the transport processes at the phloem plasma membrane during sugar loading, we decided to employ *Xenopus* oocytes as a model system for the heterologous expression of phloem transport proteins.

**Functional characterisation of phloem-localised potassium channels**

**The voltage-dependent inward rectifiers of the KAT1 subfamily:**

The *Arabidopsis* $K^+$ channel KAT2 and its orthologe KZM1 from Maize are expressed in the phloem. Both represent *Shaker*-like $K^+$ channels of the KAT1 subfamily and were characterised as voltage-dependent, hyperpolarisation activated $K^+$-uptake channels. While extracellular protons shift the voltage dependent gating of KAT2 towards positive potentials, KZM1 gating is insensitive towards changes in extracellular pH. Both channels, however, respond upon an acidification of the cytosol by a shift of the half maximal activation potential ($V_{1/2}$) towards positive voltages and thus increased open probabilities at a given membrane voltage. In addition to these channel intrinsic regulation mechanisms KZM1 is equipped with a potassium sensor, which provides for the closure of the channel pore at low external potassium concentrations.

**The weakly voltage dependent $K^+$ channels of the AKT2/3 subfamily:**

The phloem-localised $K^+$ channels of the AKT2/3-subfamily (e.g. AKT2/3 from *Arabidopsis*, PTK2 from poplar and ZMK2 from Maize) are characterised by weak voltage dependence and inhibition by extracellular protons or calcium ions. As a result of the weak voltage dependence of this channel-type AKT2/3-like channels are capable of mediating both, inward as well as outward currents. Alike the phloem-localised VFK1 channel from *Vicia faba*, the transcriptional regulation of AKT2/3 is tightly coupled to the photosynthetic activity of the plant.

Structure-function analyses of the biophysical properties of AKT2/3 were performed on chimeric channels between AKT2/3 and the inward rectifier KST1 from potato. Thereby, the rectification properties as well as the proton and calcium sensitivity of AKT2/3 were fund to be localised in the pore region. Detailled studies based on site-directed mutagenesis identified histidin and serin residues in the outer pore region as molecular determinants of the pH- and $K^+$-sensor. The corresponding mutations converted AKT2/3 into a pH- and potassium-independent $K^+$ channel.

**<u>Charakterisation of phloem-localised carriers</u>**

**The sucrose/proton symporter ZmSUT1:**

Biophysical studies of the maize sucrose transporter ZmSUT1 following heterologous expression in *Xenopus* oocytes characterised this carrier as a low affinity sucrose transporter exhibiting a $K_m$-value for sucrose in the order of 3 mM. In simultaneous measurements of sucrose-induced proton currents and the accompanied acidification of the cytosol ZmSUT1 was identified as a sucrose/proton symporter. The kinetic parameters for sucrose as well as for protons ($K_m$-value and $I_{max}$) showed a pronounced voltage dependence. Giant-patch experiments revealed that transport through ZmSUT1 is reversible, depending on the electrochemical gradients for sucrose or portons. Thus, it is tempting to speculate whether ZmSUT1 could be involved in sucrose unloading in sink tissues of the phloem network.

**The polyol transporters PmPLT1 and AtPLT5**

In contrast to sugar transporters, polyol transporters are believed to transport sugar alcohols. The substrate specificity and transport kinetics of the polyol transporters PmPLT1 and AtPLT5 (from *Plantago major* and *Arabidopsis*, respectively) were analysed with the two-electrode voltage-clamp technique following heterologous expression in *Xenopus* oocytes. Thereby, PmPLT1 was shown to transport mannitol over sorbitol by about 40%. Mannitol-induced inward currents at different external pH-values exhibited a pH-optimum of 6.5, indicative for a cotransport of polyols together with protons. Kinetic analyses characterised PmPLT1 as a low affinity polyol/proton symporter exhibiting a $K_m$-value for mannitol of 15 mM at -120 mV. Thus, PmPLT1 represents the first functionally expressed, phloem-localised polyol transporter.

Although *Arabidopsis* is supposed not to translocate polyols along the phloem, six genes exhibiting homology to polyol transporter of the MST transporter family are present in the *Arabidopsis* genome. Just as previously characterised MST transporters from other plant species, the *Arabidopsis* AtPLT5, studied here, represents a proton-coupled polyol transporter. AtPLT5 exhibits a broad substrate spectrum and besides sorbitol is able to transport glucose, glycrol and even ribose. The ring-forming sugar alcohol *myo*-inositol is transported just as well as sorbitol, whereas mannitol is not a substrate for AtPLT5. Based on these results molecular studies towards the physiological role of this subfamily of MST transporters in mutant backgrounds of *A. thaliana* may now be conceived.

**Interaction of phloem-localized sucrose transporter and $K^+$ channels**

The oocyte expression system provides the possibility of coexpressing different proteins in the membrane of a single cell under well defined conditions. In order to investigate the energetic coupling of sugar and potassium transport during sucrose loading into the phloem, the *Arabidopsis* phloem channel AKT2/3 was coexpressed with the corresponding sucrose transporter AtSUC2 in the oocyte system. Sole expression of AtSUC2 results in a strong, $H^+$-evoked membrane voltage depolarisation upon application of sucrose. In presence of the weakly voltage-dependent AKT2/3 channel, however, this depolarisation is fully compensated by $K^+$ outward currents. In contrast, the inward rectifier KAT2 coexpressed

together with AtSUC2 is not capable to prevent these membrane voltage changes. Our current model suggests that, as a result of the particular biophysical properties of AKT2/3, this $K^+$ channel is able to control and stabilise the membrane voltage in a $K^+$ dependent manner. Hence, the suppression of sucrose-induced depolarisations in the presence of active AKT2/3 channels positively feeds back on sucrose uptake. The affinity of the sucrose transporter towards sucrose and protons is significantly higher at hyperpolarising compared to depolarised membrane voltages, which results in increased transport rates.

This model was confirmed in coexpression studies of orthologous plant channels and carriers from maize. Only the weakly voltage dependent potassium channel ZMK2 is capable of stabalising the membrane potential during sucrose transport by ZmSUT1, whereas the voltage-dependent inward rectifier KZM1, just as KAT2 is not able to suppress these membrane voltage depolarisations. Thus, the KZM1 $K^+$ channel rather seems to control the potassium homeostasis in the phloem.

# 7. Referenzen

**Abramson J, Smirnova I, Kasho V, Verner G, Kaback HR, Iwata S**. **2003.** Structure and mechanism of the lactose permease of Escherichia coli. *Science* **301:** 610-615.

**Ache P, Becker D, Deeken R, Dreyer I, Weber H, Fromm J, Hedrich R**. **2001.** VFK1, a Vicia faba $K^+$ channel involved in phloem unloading. *Plant Journal* **27:** 571-580.

**Ache P, Becker D, Ivashikina N, Dietrich P, Roelfsema MR, Hedrich R**. **2000.** GORK, a delayed outward rectifier expressed in guard cells of *Arabidopsis thaliana*, is a $K^+$-selective, $K^+$-sensing ion channel. *FEBS Lett.* **486:** 93-98.

**Albers RW**. **1967.** Biochemical Aspects of Active Transport. *Annual Review of Biochemistry* **36:** 727-&.

**Altus DP, Canny MJ**. **1985.** Water Pathways in Wheat Leaves. 1. The Division of Fluxes Between Different Vein Types. *Australian Journal of Plant Physiology* **12:** 173-181.

**Anderson JA, Huprikar SS, Kochian LV, Lucas WJ, Gaber RF**. **1992.** Functional expression of a probable *Arabidopsis thaliana* potassium channel in *Saccharomyces cerevisiae*. *Proc.Natl.Acad.Sci.U.S.A* **89:** 3736-3740.

**Baizabal-Aguirre VM, Clemens S, Uozumi N, Schroeder JI**. **1999.** Suppression of inward-rectifying $K^+$ channels KAT1 and AKT2 by dominant negative point mutations in the KAT1 alpha-subunit. *J.Membr.Biol.* **167:** 119-125.

**Barker SA**. **1955.** Acyclic sugar alcohols. In: *Modern Methods of Plant Analysis.* Berlin: Springer Verlag, 158-192.

**Barth I, Meyer S, Sauer N**. **2003.** PmSUC3: Characterization of a SUT2/SUC3-type sucrose transporter from *Plantago major*. *Plant Cell* **15:** 1375-1385.

**Bauer CS, Hoth S, Haga K, Philippar K, Aoki N, Hedrich R**. **2000.** Differential expression and regulation of $K^+$ channels in the maize coleoptile: molecular and biophysical analysis of cells isolated from cortex and vasculature. *Plant Journal* **24:** 139-145.

**Baunsgaard L, Fuglsang AT, Jahn T, Korthout HAAJ, De Boer AH, Palmgren MG**. **1998.** The 14-3-3 proteins associate with the plant plasma membrane $H^+$-ATPase to generate a fusicoccin binding complex and a fusicoccin responsive system. *Plant Journal* **13:** 661-671.

**Becker D, Dreyer I, Hoth S, Reid JD, Busch H, Lehnen M, Palme K, Hedrich R**. **1996.** Changes in voltage activation, $Cs^+$ sensitivity, and ion permeability in H5 mutants of the plant $K^+$ channel KAT1. *Proc.Natl.Acad.Sci.U.S.A* **93:** 8123-8128.

**Becker D, Zeilinger C, Lohse G, Depta H, Hedrich R. 1993.** Identification and biochemical characterization of the plasma membrane $H^+$-ATPase in guard cells of *Vicia faba* L. *Planta* **190,** 44-50.

**Berthomieu P, Conejero G, Nublat A, Brackenbury WJ, Lambert C, Savio C, Uozumi N, Oiki S, Yamada K, Cellier F, Gosti F, Simonneau T, Essah PA, Tester M, Very AA, Sentenac H, Casse F**. **2003.** Functional analysis of AtHKT1 in *Arabidopsis* shows that $Na^+$ recirculation by the phloem is crucial for salt tolerance. *Embo Journal* **22:** 2004-2014.

**Bertl A, Anderson JA, Slayman CL, Gaber RF**. **1995.** Use of Saccharomyces cerevisiae for patch-clamp analysis of heterologous membrane proteins: characterization of KAT1, an inward- rectifying $K^+$ channel from *Arabidopsis thaliana*, and comparison with endogeneous yeast channels and carriers. *Proc.Natl.Acad.Sci.U.S.A* **92:** 2701-2705.

**Bezanilla F**. **2000.** The voltage sensor in voltage-dependent ion channels. *Physiol Rev.* **80:** 555-592.

**Bick JA, Neelam A, Smith E, Nelson SJ, Hall JL, Williams LE**. **1998.** Expression analysis of a sucrose carrier in the germinating seedling of *Ricinus communis*. *Plant Mol.Biol.* **38:** 425-435.

**Bixby KA, Nanao MH, Shen NV, Kreusch A, Bellamy H, Pfaffinger PJ, Choe S**. **1999.** $Zn^{2+}$-binding and molecular determinants of tetramerization in voltage-gated $K^+$ channels. *Nature Structural Biology* **6:** 38-43.

**Boorer KJ, Loo DDF, Frommer WB, Wright EM**. **1996.** Transport mechanism of the cloned potato $H^+$/sucrose cotransporter StSUT1. *Journal of Biological Chemistry* **271:** 25139-25144.

**Botha CEJ, Cross RHM, van Bel AJE, Peter CI**. **2000.** Phloem loading in the sucrose-export-defective (SXD-1) mutant maize is limited by callose deposition at plasmodesmata in bundle sheath-vascular parenchyma interface. *Protoplasma* **214:** 65-72.

**Bouche-Pillon S, Fleurat-Lessard P, Fromont JC, Serrano R, Bonnemain JL**. **1994.** Immunolocalization of the Plasma Membrane $H^+$-ATPase in Minor Veins of *Vicia faba* in Relation to Phloem Loading. *Plant Physiol* **105:** 691-697.

**Bourquin S, Bonnemain JL, Delrot S**. **1990.** Inhibition of Loading of C-14 Assimilates by Para-Chloromercuribenzenesulfonic Acid - Localization of the Apoplastic Pathway in *Vicia-Faba*. *Plant Physiology* **92:** 97-102.

**Boutry M, Michelet B, Goffeau A**. **1989.** Molecular cloning of a family of plant genes encoding a protein homologous to plasma membrane $H^+$-translocating ATPases. *Biochem.Biophys.Res.Commun.* **162:** 567-574.

**Briskin DP, Basu S, Assmann SM**. **1995.** Characterization of the Red Beet Plasma Membrane $H^+$-ATPase Reconstituted in a Planar Bilayer System. *Plant Physiol* **108:** 393-398.

**Briskin DP, Poole RJ**. **1983.** Evidence for A Beta-Aspartyl Phosphate Residue in the Phosphorylated Intermediate of the Red Beet Plasma-Membrane ATPase. *Plant Physiology* **72:** 1133-1135.

**Briskin DP, Reynoldsniesman I**. **1991.** Determination of $H^+$/ATP Stoichiometry for the Plasma-Membrane H~-ATPase from Red Beet (*Beta-Vulgaris* L) Storage Tissue. *Plant Physiology* **95:** 242-250.

**Brüggemann L, Dietrich P, Becker D, Dreyer I, I, Palme K, Hedrich R**. **1999.** Channel-mediated high-affinity $K^+$ uptake into guard cells from *Arabidopsis*. *Proc.Natl.Acad.Sci. U.S.A* **96:** 3298-3302.

**Buch-Pedersen MJ, Venema K, Serrano R, Palmgren MG**. **2000.** Abolishment of proton pumping and accumulation in the E1P conformational state of a plant plasma membrane $H^+$-ATPase by substitution of a conserved aspartyl residue in transmembrane segment 6. *Journal of Biological Chemistry* **275:** 39167-39173.

**Bürkle L, Hibberd JM, Quick WP, Kühn C, Hirner B, Frommer WB**. **1998.** The $H^+$-sucrose cotransporter NtSUT1 is essential for sugar export from tobacco leaves. *Plant Physiol* **118:** 59-68.

**Büttner M, Sauer N**. **2000.** Monosaccharide transporters in plants: structure, function and physiology. *Biochimica et Biophysica Acta-Biomembranes* **1465:** 263-274.

**Camoni L, Iori V, Marra M, Aducci P**. **2000.** Phosphorylation-dependent interaction between plant plasma membrane $H^+$-ATPase and 14-3-3 proteins. *Journal of Biological Chemistry* **275:** 9919-9923.

**Canny MJP. 1975.** Mass transfer. In: *Encyclopedia of Plant Physiology*, Vol. **1**, M.H. Zimmermann and J.A. Milburn, Springer-Verlag, Berlin.

**Cao Y, Crawford NM, Schroeder JI**. **1995a.** Amino terminus and the first four membrane-spanning segments of the *Arabidopsis* $K^+$ channel KAT1 confer inward-rectification property of plant-animal chimeric channels. *J.Biol.Chem.* **270:** 17697-17701.

**Cao Y, Ward JM, Kelly WB, Ichida AM, Gaber RF, Anderson JA, Uozumi N, Schroeder JI, Crawford NM**. **1995b.** Multiple genes, tissue specificity, and expression-

dependent modulationcontribute to the functional diversity of potassium channels in *Arabidopsis thaliana*. *Plant Physiol* **109:** 1093-1106.

**Chandran D, Reinders A, Ward JM**. **2003.** Substrate specificity of the *Arabidopsis thaliana* sucrose transporter AtSUC2. *J.Biol.Chem.* **278:** 44320-44325.

**Cherel I, Michard E, Platet N, Mouline K, Alcon C, Sentenac H, Thibaud JB**. **2002.** Physical and functional interaction of the *Arabidopsis* $K^+$ channel AKT2 and phosphatase AtPP2CA. *Plant Cell* **14:** 1133-1146.

**Chiou TJ, Bush DR**. **1998.** Sucrose is a signal molecule in assimilate partitioning. *Proc.Natl.Acad.Sci.U.S.A* **95:** 4784-4788.

**Christeller JT, Farley PC, Ramsay RJ, Sullivan PA, Laing WA**. **1998.** Purification, characterization and cloning of an aspartic proteinase inhibitor from squash phloem exudate. *European Journal of Biochemistry* **254:** 160-167.

**Crawford KM, Zambryski PC**. **1999.** Phloem transport: Are you chaperoned? *Current Biology* **9:** R281-R285.

**Czempinski K, Zimmermann S, Ehrhardt T, Müller-Rober B**. **1997.** New structure and function in plant $K^+$ channels: KCO1, an outward rectifier with a steep $Ca^{2+}$ dependency. *EMBO J.* **16:** 2565-2575.

**Dannenhoffer JM, Suhr RC, Thompson GA**. **2001.** Phloem-specific expression of the Pumpkin Fruit Trypsin Inhibitor. *Planta* **212:** 155-162.

**Daram P, Urbach S, Gaymard F, Sentenac H, Cherel I**. **1997.** Tetramerization of the AKT1 plant potassium channel involves its C- terminal cytoplasmic domain. *EMBO J.* **16:** 3455-3463.

**De Boer AH**. **2002.** Plant 14-3-3 proteins assist ion channels and pumps. *Biochem.Soc.Trans.* **30:** 416-421.

**De Boer AH, Volkov V**. **2003.** Logistics of water and salt transport through the plant: structure and functioning of the xylem. *Plant, Cell and Environment* **26:** 87-101.

**Deeken R, Geiger D, Fromm J, Koroleva O, Ache P, Langenfeld-Heyser R, Sauer N, May ST, Hedrich R**. **2002.** Loss of the AKT2/3 potassium channel affects sugar loading into the phloem of *Arabidopsis*. *Planta* **216:** 334-344.

**Deeken R, Sanders C, Ache P, Hedrich R**. **2000.** Developmental and light-dependent regulation of a phloem-localised $K^+$ channel of *Arabidopsis thaliana*. *Plant Journal* **23:** 285-290.

**Delrot S, Atanassova R, Maurousset L**. **2000.** Regulation of sugar, amino acid and peptide plant membrane transporters. *Biochim.Biophys.Acta* **1465:** 281-306.

**Delrot S, Faucher M, Bonnemain JL, Bonmort J**. **1983.** Nycthemeral Changes in Intracellular and Apoplastic Sugars in *Vicia-Faba* Leaves. *Physiologie Vegetale* **21:** 459-467.

**Desbrosses G, Stelling J, Renaudin JP**. **1998.** Dephosphorylation activates the purified plant plasma membrane $H^+$-ATPase - Possible function of phosphothreonine residues in a mechanism not involving the regulatory C-terminal domain of the enzyme. *European Journal of Biochemistry* **251:** 496-503.

**DeWitt ND, Harper JF, Sussman MR**. **1991.** Evidence for a plasma membrane proton pump in phloem cells of higher plants. *Plant J.* **1:** 121-128.

**DeWitt ND, Sussman MR**. **1995.** Immunocytological localization of an epitope-tagged plasma membrane proton pump (H(+)-ATPase) in phloem companion cells. *Plant Cell* **7:** 2053-2067.

**Doyle DA, Morais CJ, Pfuetzner RA, Kuo A, Gulbis JM, Cohen SL, Chait BT, MacKinnon R**. **1998.** The structure of the potassium channel: molecular basis of $K^+$ conduction and selectivity. *Science* **280:** 69-77.

**Dreyer I, Antunes S, Hoshi T, Muller-Rober B, Palme K, Pongs O, Reintanz B, Hedrich R**. **1997.** Plant $K^+$ channel alpha-subunits assemble indiscriminately. *Biophys.J.* **72:** 2143-2150.

**Dreyer I, Becker D, Bregante M, Gambale F, Lehnen M, Palme K, Hedrich R**. **1998.** Single mutations strongly alter the $K^+$-selective pore of the K-in channel KAT1. *Febs Letters* **430:** 370-376.

**Ehrhardt T, Zimmermann S, Muller-Rober B**. **1997.** Association of plant $K^+_{in}$ channels is mediated by conserved C-termini and does not affect subunit assembly. *FEBS Lett.* **409:** 166-170.

**Eklund L, Eliasson L**. **1990.** Effects of Calcium-Ion Concentration on Cell-Wall Synthesis. *Journal of Experimental Botany* **41:** 863-867.

**Eschrich W, Fromm J, Evert RF**. **1988.** Transmission of electric signals in sieve tubes of zucchini plants. *Botanica Acta* **101:** 327-331.

**Everard JD, Gucci R, Kann SC, Flore JA, Loescher WH**. **1994.** Gas-Exchange and Carbon Partitioning in the Leaves of Celery (*Apium-Graveolens* L) at Various Levels of Root-Zone Salinity. *Plant Physiology* **106:** 281-292.

**Evert RF, Russin WA**. **1993.** Structurally, Phloem Unloading in the Maize Leaf Cannot be Symplastic. *American Journal of Botany* **80:** 1310-1317.

**Ewing NN, Bennett AB**. **1994.** Assessment of the number and expression of P-type H(+)-ATPase genes in tomato. *Plant Physiol* **106:** 547-557.

**Flora LL, Madore MA**. **1996.** Significance of minor-vein anatomy to carbohydrate transport. *Planta* **198:** 171-178.

**Fisher DB. 1990.** Measurement of phloem transport rates by an indicator-dilution technique. *Plant Physiol* **94:** 455-462.

**Fondy BR, Geiger DR**. **1977.** Sugar Selectivity and Other Characteristics of Phloem Loading in *Beta-Vulgaris*-l. *Plant Physiology* **59:** 953-960.

**Fromm J, Eschrich W**. **1988.** Transport processes in stimulated and non-stimulated leaves of *Mimosa pudica*. *Trees* **2:** 18-24.

**Fromm J, Essiamah S, Eschrich W**. **1987.** Displacement of frequently occurring heavy metals in autumn leaves of beech (*Fagus sylvatica*). *Trees* **1:** 164-171.

**Fuglsang AT, Visconti S, Drumm K, Jahn T, Stensballe A, Mattei B, Jensen ON, Aducci P, Palmgren MG**. **1999.** Binding of 14-3-3 protein to the plasma membrane H(+)-ATPase AHA2 involves the three C-terminal residues Tyr(946)-Thr-Val and requires phosphorylation of Thr(947). *J Biol.Chem.* **274:** 36774-36780.

**Gahrtz M, Stolz J, Sauer N**. **1994.** A phloem-specific sucrose-$H^+$ symporter from *Plantago major* L. supports the model of apoplastic phloem loading. *Plant J.* **6:** 697-706.

**Gamalei YV**. **1989.** Structure and function of leaf minor veins in trees and herbs. *Trees* **3:** 96-110.

**Gao Z, Maurousset L, Lemoine R, Yoo SD, van Nocker S, Loescher W**. **2003.** Cloning, expression, and characterization of sorbitol transporters from developing *sour cherry* fruit and leaf sink tissues. *Plant Physiol* **131:** 1566-1575.

**Gaymard F, Pilot G, Lacombe B, Bouchez D, Bruneau D, Boucherez J, Michaux-Ferriere N, Thibaud JB, Sentenac H**. **1998.** Identification and disruption of a plant *shaker*-like outward channel involved in $K^+$ release into the xylem sap. *Cell* **94:** 647-655.

**Geiger D, Becker D, Lacombe B, Hedrich R**. **2002.** Outer pore residues control the $H^+$ and $K^+$ sensitivity of the *Arabidopsis* potassium channel AKT3. *Plant Cell* **14:** 1859-1868.

**Giaquinta R**. **1976.** Evidence for Phloem Loading from Apoplast - Chemical Modification of Membrane Sulfhydryl-Groups. *Plant Physiology* **57:** 872-875.

**Goggin FL, Medville R, Turgeon R**. **2001.** Phloem loading in the tulip tree. Mechanisms and evolutionary implications. *Plant Physiology* **125:** 891-899.

**Golecki B, Schulz A, Carstens-Behrens U, Kollmann R**. **1998.** Evidence for graft transmission of structural phloem proteins or their precursors in heterografts of Cucurbitaceae. *Planta* **206:** 630-640.

**Golecki B, Schulz A, Thompson GA**. **1999.** Translocation of structural P proteins in the phloem. *Plant Cell* **11:** 127-140.

**Gottwald JR, Krysan PJ, Young JC, Evert RF, Sussman MR**. **2000.** Genetic evidence for the in planta role of phloem-specific plasma membrane sucrose transporters. *Proc.Natl. Acad.Sci.U.S.A* **97:** 13979-13984.

**Grignon C, Sentenac H**. **1991.** Ph and Ionic Conditions in the Apoplast. *Annual Review of Plant Physiology and Plant Molecular Biology* **42:** 103-128.

**Hansch R, Fessel DG, Witt C, Hesberg C, Hoffmann G, Walch-Liu P, Engels C, Kruse J, Rennenberg H, Kaiser WM, Mendel RR**. **2001.** Tobacco plants that lack expression of functional nitrate reductase in roots show changes in growth rates and metabolite accumulation. *Journal of Experimental Botany* **52:** 1251-1258.

**Haritatos E, Ayre BG, Turgeon R**. **2000.** Identification of phloem involved in assimilate loading in leaves by the activity of the galactinol synthase promoter. *Plant Physiology* **123:** 929-937.

**Harper JF, Manney L, DeWitt ND, Yoo MH, Sussman MR**. **1990.** The *Arabidopsis-Thaliana* Plasma-Membrane $H^+$-ATPase Multigene Family - Genomic Sequence and Expression of A 3Rd Isoform. *Journal of Biological Chemistry* **265:** 13601-13608.

**Harper JF, Manney L, Sussman MR**. **1994.** The Plasma-Membrane $H^+$-Atpase Gene Family in *Arabidopsis* - Genomic Sequence of AHA10 Which Is Expressed Primarily in Developing Seeds. *Molecular and General Genetics* **244:** 572-587.

**Harper JF, Surowy TK, Sussman MR**. **1989.** Molecular-Cloning and Sequence of cDNA-Encoding the Plasma-Membrane Proton Pump ($H^+$-ATPase) of *Arabidopsis-Thaliana*. *Proceedings of the National Academy of Sciences of the United States of America* **86:** 1234-1238.

**Hartmann T**. **1999.** Chemical ecology of pyrrolizidine alkaloids. *Planta* **207:** 483-495.

**Hayashi H, Fukuda A, Suzui N, Fujimaki S**. **2000.** Proteins in the sieve element-companion cell complexes: their detection, localization and possible functions. *Australian Journal of Plant Physiology* **27:** 489-496.

**Hedrich R, Moran O, Conti F, Busch H, Becker D, Gambale F, Dreyer I, Kuch A, Neuwinger K, Palme et a**. **1995.** Inward rectifier potassium channels in plants differ from their animal counterparts in response to voltage and channel modulators. *European Biophysics Journal: EBJ* **24:** 107-115.

**Hoshi T**. **1995.** Regulation of voltage dependence of the KAT1 channel by intracellular factors. *J Gen.Physiol* **105:** 309-328.

**Hoshi T, Zagotta WN, Aldrich RW**. **1990.** Biophysical and molecular mechanisms of *Shaker* potassium channel inactivation. *Science* **250:** 533-538.

**Hoshi T, Zagotta WN, Aldrich RW**. **1991.** Two types of inactivation in *Shaker* $K^+$ channels: effects of alterations in the carboxy-terminal region. *Neuron* **7:** 547-556.

**Hoth S, Dreyer I, Dietrich P, Becker D, Muller-Rober B, Hedrich R**. **1997a.** Molecular basis of plant-specific acid activation of $K^+$ uptake channels. *Proc.Natl.Acad.Sci.U.S.A* **94:** 4806-4810.

**Hoth S, Dreyer I, Hedrich R**. **1997b.** Mutational analysis of functional domains within plant $K^+$ uptake channels. *Journal of Experimental Botany* **48:** 415-420.

**Hoth S, Hedrich R**. **1999.** Distinct molecular bases for pH sensitivity of the guard cell $K^+$ channels KST1 and KAT1. *Journal of Biological Chemistry* **274:** 11599-11603.

**Houlne G, Boutry M**. **1994.** Identification of An *Arabidopsis-Thaliana* Gene Encoding A Plasma-Membrane $H^+$-ATPase Whose Expression Is Restricted to Anther Tissues. *Plant Journal* **5:** 311-317.

**Hu H, Penn SG, Lebrilla CB, Brown PH**. **1997.** Isolation and characterization of soluble boron complexes in higher plants. The mechanism of phloem mobility of boron. *Plant Physiol* **113:** 649-655.

**Ichida AM, Schroeder JI**. **1996.** Increased resistance to extracellular cation block by mutation of the pore domain of the *Arabidopsis* inward-rectifying $K^+$ channel KAT1. *J.Membr.Biol.* **151:** 53-62.

**Imlau A, Truernit E, Sauer N**. **1999.** Cell-to-cell and long-distance trafficking of the green fluorescent protein in the phloem and symplastic unloading of the protein into sink tissues. *Plant Cell* **11:** 309-322.

**Ivashikina N, Deeken R, Ache P, Kranz E, Pommerrenig B, Sauer N, Hedrich R**. **2003.** Isolation of AtSUC2 promoter-GFP-marked companion cells for patch-clamp studies and expression profiling. *Plant Journal* **36:** 931-945.

**Jaspert N, Oecking C**. **2002.** Regulatory 14-3-3 proteins bind the atypical motif within the C terminus of the plant plasma membrane H(+)-ATPase via their typical amphipathic groove. *Planta* **216:** 136-139.

**Jelich-Ottmann C, Weiler EW, Oecking C**. **2001.** Binding of regulatory 14-3-3 proteins to the C terminus of the plant plasma membrane $H^+$-ATPase involves part of its autoinhibitory region. *J Biol.Chem.* **276:** 39852-39857.

**Jennings DB, Ehrenshaft M, Pharr DM, Williamson JD**. **1998.** Roles for mannitol and mannitol dehydrogenase in active oxygen-mediated plant defense. *Proc.Natl.Acad. Sci.U.S.A* **95:** 15129-15133.

**Jorgensen RA, Atkinson RG, Forster RLS, Lucas WJ**. **1998.** Research: Botany - An RNA-based information superhighway in plants. *Science* **279:** 1486-1487.

**Kandler O, Hopf H**. **1982.** Oligosaccharides based on sucrose (sucrosyl oligosaccharides). In:*Encyclopedia of Plant Physiology*. Berlin: Springer-Verlag, 348-383.

**Keller F, Pharr M**. **1996.** Metabolism of carbohydrates in sinks and sources. Galactosyl-Sucrose. In: Zamski E, Schaffer A, eds. New York: Marcel Dekker, Inc, 157-184.

**Ketchum KA, Slayman CW**. **1996.** Isolation of an ion channel gene from *Arabidopsis thaliana* using the H5 signature sequence from voltage-dependent $K^+$ channels. *FEBS Lett.* **378:** 19-26.

**Kinoshita T**. **2003.** Young Investigator Award Blue light signal transduction and regulation of the plasma membrane $H^+$-ATPase in stomatal guard cells. *Plant and Cell Physiology* **44:** S24.

**Kinoshita T, Shimazaki K**. **1999.** Blue light activates the plasma membrane H(+)-ATPase by phosphorylation of the C-terminus in stomatal guard cells. *EMBO J* **18:** 5548-5558.

**Knoblauch M, Noll GA, van Bel AJE, Prufer D, Peters WS**. **2003.** Forisomes consist of a novel class of contractile proteins. *European Journal of Cell Biology* **82:** 70-71.

**Knoblauch M, Peters WS, Ehlers K, van Bel AJE**. **2001.** Reversible calcium-regulated stopcocks in legume sieve tubes. *Plant Cell* **13:** 1221-1230.

**Knoblauch M, van Bel AJE**. **1998.** Sieve tubes in action. *Plant Cell* **10:** 35-50.

**Knop C, Stadler R, Sauer N, Lohaus G**. **2004.** AmSUT1, a sucrose transporter in collection and transport phloem of the putative symplastic phloem loader *Alonsoa meridionalis*. *Plant Physiology* **134:** 204-214.

**Knop C, Voitsekhovskaja O, Lohaus G**. **2001.** Sucrose transporters in two members of the Scrophulariaceae with different types of transport sugar. *Planta* **213:** 80-91.

**Komor E, Rotter M, Tanner W**. **1977.** Proton-Cotransport System in A Higher Plant - Sucrose Transport in *Ricinus-Communis*. *Plant Science Letters* **9:** 153-162.

**Komor E, Tanner W**. **1974.** Can energy generated by sugar efflux be used for ATP synthesis in *Chlorella*? *Nature* **248:** 511-512.

**Kreusch A, Pfaffinger PJ, Stevens CF, Choe S**. **1998.** Crystal structure of the tetramerization domain of the *Shaker* potassium channel. *Nature* **392:** 945-948.

**Kühn C**. **2003.** A Comparison of the Sucrose Transporter Systems of Different Plant Species. *Plant Biology* **5:** 215-232.

**Kühn C, Franceschi VR, Schulz A, Lemoine R, Frommer WB**. **1997.** Macromolecular trafficking indicated by localization and turnover of sucrose transporters in enucleate sieve elements. *Science* **275:** 1298-1300.

**Kühn C, Hajirezaei MR, Fernie AR, Roessner-Tunali U, Czechowski T, Hirner B, Frommer WB**. **2003.** The sucrose transporter StSUT1 localizes to sieve elements in potato tuber phloem and influences tuber physiology and development. *Plant Physiol* **131:** 102-113.

**Kühn C, Quick WP, Schulz A, Riesmeier JW, Sonnewald U, Frommer WB**. **1996.** Companion cell-specific inhibition of the potato sucrose transporter SUT1. *Plant Cell and Environment* **19:** 1115-1123.

**Lacombe B, Pilot G, Michard E, Gaymard F, Sentenac H, Thibaud JB**. **2000.** A *shaker*-like K(+) channel with weak rectification is expressed in both source and sink phloem tissues of *Arabidopsis*. *Plant Cell* **12:** 837-851.

**Lalonde S, Tegeder M, Throne-Holst M, Frommer WB, Patrick JW**. **2003.** Phloem loading and unloading of sugars and amino acids. *Plant, Cell and Environment*.

**Langer K, Ache P, Geiger D, Stinzing A, Arend M, Wind C, Regan S, Fromm J, Hedrich R**. **2002.** Poplar potassium transporters capable of controlling $K^+$ homeostasis and $K^+$-dependent xylogenesis. *Plant Journal* **32:** 997-1009.

**Latorre R, Olcese R, Basso C, Gonzalez C, Munoz F, Cosmellli D, Alvarez O**. **2003.** Molecular coupling between voltage sensor and pore opening in the *Arabidopsis* inward rectifier $K^+$ channel KAT1. *Journal of General Physiology* **122:** 459-469.

**Lemoine R**. **2000.** Sucrose transporters in plants: update on function and structure. *Biochim.Biophys.Acta* **1465:** 246-262.

**Lemoine R, Burkle L, Barker L, Sakr S, Kuhn C, Regnacq M, Gaillard C, Delrot S, Frommer WB**. **1999.** Identification of a pollen-specific sucrose transporter-like protein NtSUT3 from tobacco. *FEBS Lett.* **454:** 325-330.

**Lemoine R, Kuhn C, Thiele N, Delrot S, Frommer WB**. **1996.** Antisense inhibition of the sucrose transporter in potato: Effects on amount and activity. *Plant Cell and Environment* **19:** 1124-1131.

**Lohaus G, Buker M, Hussmann M, Soave C, Heldt HW**. **1998.** Transport of amino acids with special emphasis on the synthesis and transport of asparagine in the Illinois low protein and Illinois high protein strains of maize. *Planta* **205:** 181-188.

**Lohaus G, Burba M, Heldt HW**. **1994.** Comparison of the Contents of Sucrose and Amino-Acids in the Leaves, Phloem Sap and Taproots of High and Low Sugar-Producing Hybrids of Sugar-Beet (*Beta-Vulgaris* L). *Journal of Experimental Botany* **45:** 1097-1101.

**Lohaus G, Fischer K**. **2002.** Intracellular and intercellular transport of nitrogen and carbon. In: Foyer C, Noctor G, eds. *Advances in Photosynthesis*. Kluwer Academic Publishers.

**Lohaus G, Hussmann M, Pennewiss K, Schneider H, Zhu JJ, Sattelmacher B**. **2000.** Solute balance of a maize (*Zea mays* L.) source leaf as affected by salt treatment with special emphasis on phloem retranslocation and ion leaching. *Journal of Experimental Botany* **351:** 1721-1732.

**Lohaus G, Moellers C**. **2000.** Phloem transport of amino acids in two *Brassica napus* L. genotypes and one B-carinata genotype in relation to their seed protein content. *Planta* **211:** 833-840.

**Lohaus G, Pennewiss K, Sattelmacher B, Hussmann M, Muehling KH**. **2001.** Is the infiltration-centrifugation technique appropriate for the isolation of apoplastic fluid? A critical evaluation with different plant species. *Physiologia Plantarum* **111:** 457-465.

**Lohaus G, Winter H, Riens B, Heldt HW**. **1995.** Further-Studies of the Phloem Loading Process in Leaves of Barley and Spinach - the Comparison of Metabolite Concentrations in the Apoplastic Compartment with Those in the Cytosolic Compartment and in the Sieve Tubes. *Botanica Acta* **108:** 270-275.

**Lucas WJ, Ding B, van der Schoot C**. **1993.** Plasmodesmata and the supracellular nature of plants. *New Phytologist* **125:** 435-476.

**Lucas WJ, Lee JY**. **2004.** Plasmodesmata As A Supracellular Control Network In Plants. *Nature Reviews Molecular Cell Biology* **5:** 712-726.

**Ludwig A, Stolz J, Sauer N**. **2000.** Plant sucrose-$H^+$ symporters mediate the transport of vitamin H. *Plant J.* **24:** 503-509.

**Luo H, Morsomme P, Boutry M**. **1999.** The two major types of plant plasma membrane $H^+$-ATPases show different enzymatic properties and confer differential pH sensitivity of yeast growth. *Plant Physiol* **119:** 627-634.

**MacKinnon R, Aldrich RW, Lee AW**. **1993.** Functional Stoichiometry of *Shaker* Potassium Channel Inactivation. *Science* **262:** 757-759.

**Madore MA, Oross JW, Lucas WJ**. **1986.** Symplastic Transport in Ipomea-Tricolor Source Leaves - Demonstration of Functional Symplastic Connections from Mesophyll to Minor Veins by A Novel Dye-Tracer Method. *Plant Physiology* **82:** 432-442.

**Marger MD, Saier MH, Jr. 1993.** A major superfamily of transmembrane facilitators that catalyse uniport, symport and antiport. *Trends Biochem.Sci.* **18:** 13-20.

**Marten I, Hoshi T**. **1997.** Voltage-dependent gating characteristics of the $K^+$ channel KAT1 depend on the N and C termini. *Proc.Natl.Acad.Sci.U.S.A* **94:** 3448-3453.

**Marten I, Hoshi T**. **1998.** The N-terminus of the $K^+$ channel KAT1 controls its voltage-dependent gating by altering the membrane electric field. *Biophys.J.* **74:** 2953-2962.

**Marten I, Hoth S, Deeken R, Ache P, Ketchum KA, Hoshi T, Hedrich R**. **1999.** AKT3, a phloem-localized $K^+$ channel, is blocked by protons. *Proceedings of the National Academy of Sciences of the United States of America* **96:** 7581-7586.

**Mäser P, Thomine S, Schroeder JI, Ward JM, Hirschi K, Sze H, Talke IN, Amtmann A, Maathuis FJ, Sanders D, Harper JF, Tchieu J, Gribskov M, Persans MW, Salt DE, Kim SA, Guerinot ML**. **2001.** Phylogenetic relationships within cation transporter families of *Arabidopsis*. *Plant Physiol* **126:** 1646-1667.

**Maudoux O, Batoko H, Oecking C, Gevaert K, Vandekerckhove J, Boutry M, Morsomme P**. **2000.** A plant plasma membrane $H^+$-ATPase expressed in yeast is activated by phosphorylation at its penultimate residue and binding of 14-3-3 regulatory proteins in the absence of fusicoccin. *J Biol.Chem.* **275:** 17762-17770.

**Meyer S, Melzer M, Truernit E, Hummer C, Besenbeck R, Stadler R, Sauer N**. **2000.** AtSUC3, a gene encoding a new *Arabidopsis* sucrose transporter, is expressed in cells adjacent to the vascular tissue and in a carpel cell layer. *The Plant Journal* **24:** 869-882.

**Michelet B, Boutry M**. **1995.** The Plasma-Membrane $H^+$-ATPase - A Highly Regulated Enzyme with Multiple Physiological Functions. *Plant Physiology* **108:** 1-6.

**Michelet B, Lukaszewicz M, Dupriez V, Boutry M**. **1994.** A plant plasma membrane proton-ATPase gene is regulated by development and environment and shows signs of a translational regulation. *Plant Cell* **6:** 1375-1389.

**Moing A, Langlois N, Svanella L, Zanetto A, Gaudillere JP**. **1997.** Variability in sorbitol: Sucrose ratio in mature leaves of different Prunus species. *Journal of the American Society for Horticultural Science* **122:** 83-90.

**Moriau L, Michelet B, Bogaerts P, Lambert L, Michel A, Oufattole M, Boutry M**. **1999.** Expression analysis of two gene subfamilies encoding the plasma membrane $H^+$-ATPase in

*Nicotiana plumbaginifolia* reveals the major transport functions of this enzyme. *Plant J* **19:** 31-41.

**Mühling KH, Sattelmacher B**. **1997.** Determination of apoplastic $K^+$ in intact leaves by ratio imaging of PBFI fluorescence. *J Exp.Bot.* **48:** 1609-1614.

**Münch E**. **1930.** *Die Stoffbewegungen in der Pflanze*. Fischer.

**Murray C, Christeller JT**. **1995.** Purification of a trypsin inhibitor (PFTI) from pumpkin fruit phloem exudate and isolation of putative trypsin and chymotrypsin inhibitor cDNA clones. *Biol.Chem.Hoppe Seyler* **376:** 281-287.

**Nakamura RL, McKendree WL, Jr., Hirsch RE, Sedbrook JC, Gaber RF, Sussman MR**. **1995.** Expression of an *Arabidopsis* potassium channel gene in guard cells. *Plant Physiol* **109:** 371-374.

**Nelson RS, van Bel A.J.E**. **1998.** The mystery of virus trafficking into, through and out of vascular tissue. *Progress in Botany* **59:** 476-533.

**Noiraud N, Delrot S, Lemoine R**. **2000.** The sucrose transporter of celery. Identification and expression during salt stress. *Plant Physiol* **122:** 1447-1455.

**Noiraud N, Maurousset L, Lemoine R**. **2001.** Identification of a mannitol transporter, AgMaT1, in celery phloem. *Plant Cell* **13:** 695-705.

**Oecking C, Hagemann K**. **1999.** Association of 14-3-3 proteins with the C-terminal antoinhibitory domain of the plant plasma-membrane $H^+$-ATPase generates a fusicoccin-binding complex. *Planta* **207:** 480-482.

**Ohshima T, Hayashi H, Chino M**. **1990.** Collection and Chemical-Composition of Pure Phloem Sap from *Zea-Mays*. *Plant and Cell Physiology* **31:** 735-737.

**Oparka KJ, Cruz SS**. **2000.** The great escape: Phloem transport and unloading of macromolecules. *Annual Review of Plant Physiology and Plant Molecular Biology* **51:** 323-347.

**Oparka KJ, Turgeon R**. **1999.** Sieve elements and companion cells - Traffic control centers of the phloem. *Plant Cell* **11:** 739-750.

**Oufattole M, Arango M, Boutry M**. **2000.** Identification and expression of three new *Nicotiana plumbaginifolia* genes which encode isoforms of a plasma-membrane H(+)-ATPase, and one of which is induced by mechanical stress. *Planta* **210:** 715-722.

**Paganetto A, Bregante M, Downey P, Lo Schiavo F, Hoth S, Hedrich R, Gambale F**. **2001.** A novel $K^+$ channel expressed in carrot roots with a low susceptibility toward metal ions. *Journal of Bioenergetics and Biomembranes* **33:** 63-71.

**Palmgren MG**. **1998.** Proton gradients and plant growth: Role of the plasma membrane $H^+$-ATPase. *Advances in Botanical Research, Vol 28* **28:** 1-70.

**Palmgren MG**. **2001.** Plant plasma membrane $H^+$-ATPases: Powerhouses for nutrient uptake. *Annual Review of Plant Physiology and Plant Molecular Biology* **52:** 817-845.

**Palmgren MG, Christensen G**. **1994.** Functional comparisons between plant plasma membrane H(+)-ATPase isoforms expressed in yeast. *J Biol.Chem.* **269:** 3027-3033.

**Palmgren MG, Larsson C, Sommarin M**. **1990.** Proteolytic activation of the plant plasma membrane H(+)-ATPase by removal of a terminal segment. *J Biol.Chem.* **265:** 13423-13426.

**Palmgren MG, Sommarin M, Serrano R, Larsson C**. **1991.** Identification of an autoinhibitory domain in the C-terminal region of the plant plasma membrane H(+)-ATPase. *J Biol.Chem.* **266:** 20470-20475.

**Papazian DM**. **1999.** Potassium channels: Some assembly required. *Neuron* **23:** 7-10.

**Pardo JM, Serrano R**. **1989.** Structure of a plasma membrane $H^+$-ATPase gene from the plant *Arabidopsis thaliana*. *J Biol.Chem.* **264:** 8557-8562.

**Parets-Soler A, Pardo JM, Serrano R**. **1990.** Immunocytolocalization of plasma membrane $H^+$-ATPase. *Plant Physiology* **93:** 1654-1658.

**Patrick J**. **1994.** Turgor-dependent unloading photosythates from coats of developing seed of *Phaseolus vulgaris* and *Vicia faba*. Turgor homeostasis and set points. *Physiologia Plantarum* **90:** 367-377.

**Patrick J**. **1997.** Phloem unloading: sieve element unloading and post-sieve element transport. *Annual Review of Plant Physiology* **48:** 191-222.

**Patrick J, Offler CR**. **1995.** Post-sieve element transport of sucrose in developing seeds. *Australian Journal of Plant Physiology* **22:** 681-702.

**Penn SG, Hu H, Brown PH, Lebrilla CB**. **1997.** Direct analysis of sugar alcohol borate complexes in plant extracts by matrix-assisted laser desorption/ionization Fourier transform mass spectrometry. *Anal.Chem.* **69:** 2471-2477.

**Philippar K, Buchsenschutz K, Abshagen M, Fuchs I, Geiger D, Lacombe B, Hedrich R**. **2003.** The $K^+$ channel KZM1 mediates potassium uptake into the phloem and guard cells of the C-4 grass *Zea mays*. *Journal of Biological Chemistry* **278:** 16973-16981.

**Philippar K, Fuchs I, Luthen H, Hoth S, Bauer CS, Haga K, Thiel G, Ljung K, Sandberg G, Bottger M, Becker D, Hedrich R**. **1999.** Auxin-induced $K^+$ channel expression represents an essential step in coleoptile growth and gravitropism. *Proceedings of the National Academy of Sciences of the United States of America* **96:** 12186-12191.

**Pilot G, Lacombe B, Gaymard F, Cherel I, Boucherez J, Thibaud JB, Sentenac H**. **2001.** Guard cell inward $K^+$ channel activity in *Arabidopsis* involves expression of the twin channel subunits KAT1 and KAT2. *J.Biol.Chem.* **276:** 3215-3221.

**Piotrowski M, Morsomme P, Boutry M, Oecking C**. **1998.** Complementation of the *Saccharomyces cerevisiae* plasma membrane $H^+$-ATPase by a plant $H^+$-ATPase generates a highly abundant fusicoccin binding site. *J Biol.Chem.* **273:** 30018-30023.

**Plugge B, Gazzarrini S, Nelson M, Cerana R, Van Etten JL, Derst C, DiFrancesco D, Moroni A, Thiel G**. **2000.** A potassium channel protein encoded by chlorella virus PBCV-1. *Science-Washington-D-C.[print] March* **3,@2000;@287:** 1641-1644.

**Post RL, Kume S, Hegyvary C**. **1972.** Activation by Adenosine-Triphosphate in Phosphorylation Kinetics of Sodium and Potassium Ion Transport Adenosine-Triphosphatase. *Journal of Biological Chemistry* **247:** 6530-&.

**Provencher LM, Miao L, Sinha N, Lucas WJ**. **2001.** Sucrose export defective1 encodes a novel protein implicated in chloroplast-to-nucleus signaling. *Plant Cell* **13:** 1127-1141.

**Quick M, Tomasevic J, Wright EM**. **2003.** Functional asymmetry of the human $Na^+$/glucose transporter (hSGLT1) in bacterial membrane vesicles. *Biochemistry* **42:** 9147-9152.

**Ramsperger-Gleixner M, Geiger D, Hedrich R, Sauer N**. **2004.** Differential expression of sucrose transporter and polyol transporter genes during maturation of *common plantain* companion cells. *Plant Physiology* **134:** 147-160.

**Regenberg B, Villalba JM, Lanfermeijer FC, Palmgren MG**. **1995.** C-terminal deletion analysis of plant plasma membrane H(+)-ATPase: yeast as a model system for solute transport across the plant plasma membrane. *Plant Cell* **7:** 1655-1666.

**Reintanz B, Szyroki A, Ivashikina N, Ache P, Godde M, Becker D, Palme K, Hedrich R**. **2002.** AtKC1, a silent *Arabidopsis* potassium channel alpha-subunit modulates root hair $K^+$ influx. *Proceedings of the National Academy of Sciences of the United States of America* **99:** 4079-4084.

**Rhodes JD, Thain JF, Wildon DC**. **1996.** The pathway for systemic electrical signal conduction in the wounded tomato plant. *Planta* **200:** 50-57.

**Riens B, Lohaus G, Heineke D, Heldt HW**. **1991.** Amino-Acid and Sucrose Content Determined in the Cytosolic, Chloroplastic, and Vacuolar Compartments and in the Phloem Sap of Spinach Leaves. *Plant Physiology* **97:** 227-233.

**Riesmeier JW, Hirner B, Frommer WB**. **1993.** Potato Sucrose Transporter Expression in Minor Veins Indicates a Role in Phloem Loading. *Plant Cell* **5:** 1591-1598.

**Riesmeier JW, Willmitzer L, Frommer WB**. **1992.** Isolation and Characterization of A Sucrose Carrier cDNA from Spinach by Functional Expression in Yeast. *Embo Journal* **11:** 4705-4713.

**Riesmeier JW, Willmitzer L, Frommer WB**. **1994.** Evidence for An Essential Role of the Sucrose Transporter in Phloem Loading and Assimilate Partitioning. *Embo Journal* **13:**1-7.

**Robards AW, Lucas WJ**. **1990.** Plasmodesmata. *Annual Review of Plant Physiology and Plant Molecular Biology* **41:** 369-419.

**Roblin G, Sakr S, Bonmort J, Delrot S**. **1998.** Regulation of a plant plasma membrane sucrose transporter by phosphorylation. *FEBS Lett.* **424:** 165-168.

**Roitsch T, Balibrea ME, Hofmann M, Proels R, Sinha AK**. **2003.** Extracellular invertase: key metabolic enzyme and PR protein. *Journal of Experimental Botany* **54:** 513-524.

**Roitsch T, Ehness R, Goetz M, Hause B, Hofmann M, Sinha AK**. **2000.** Regulation and function of extracellular invertase from higher plants in relation to assimilate partitioning, stress responses and sugar signalling. *Australian Journal of Plant Physiology* **27:** 815-825.

**Ruiz-Medrano R, Xoconostle-Cazares B, Lucas WJ**. **1999.** Phloem long-distance transport of CmNACP mRNA: implications for supracellular regulation in plants. *Development* **126:** 4405-4419.

**Ruiz-Medrano R, Xoconostle-Cazares B, Lucas WJ**. **2001.** The phloem as a conduit for inter-organ communication. *Curr.Opin.Plant Biol.* **4:** 202-209.

**Russin WA, Evert RF, Vanderveer PJ, Sharkey TD, Briggs SP**. **1996.** Modification of a specific class of plasmodesmata and loss of sucrose export ability in the sucrose export defective1 maize mutant. *Plant Cell* **8:** 645-658.

**Ryals JA, Neuenschwander UH, Willits MG, Molina A, Steiner HY, Hunt MD**. **1996.** Systemic acquired resistance. *Plant Cell* **8:** 1809-1819.

**Saier MH, Jr., Beatty JT, Goffeau A, Harley KT, Heijne WH, Huang SC, Jack DL, Jahn PS, Lew K, Liu J, Pao SS, Paulsen IT, Tseng TT, Virk PS**. **2000.** The major facilitator superfamily. *Journal of Biological Chemistry*.

**Sauer GA, Nagel G, Koepsell H, Bamberg E, Hartung K**. **2000.** Voltage and substrate dependence of the inverse transport mode of the rabbit Na(+)/glucose cotransporter (SGLT1). *FEBS Lett.* **469:** 98-100.

**Sauer N**. **1997.** Sieve elements and companion cells - extreme division of labour. *Trends in Plant Science* **2:** 285-286.

**Sauer N, Friedlander K, Gramlwicke U**. **1990.** Primary Structure, Genomic Organization and Heterologous Expression of A Glucose Transporter from *Arabidopsis-Thaliana*. *Embo Journal* **9:** 3045-3050.

**Sauer N, Stolz J**. **1994.** SUC1 and SUC2: two sucrose transporters from *Arabidopsis thaliana*; expression and characterization in baker's yeast and identification of the histidine-tagged protein. *Plant J.* **6:** 67-77.

**Savchenko G, Wiese C, Neimanis S, Hedrich R, Heber U**. **2000.** pH regulation in apoplastic and cytoplasmic cell compartments of leaves. *Planta* **211:** 246-255.

**Schachtman DP, Schroeder JI, Lucas WJ, Anderson JA, Gaber RF**. **1992.** Expression of an inward-rectifying potassium channel by the *Arabidopsis* KAT1 cDNA. *Science* **258:** 1654-1658.

**Schobert C, Zhong WJ, Komor E**. **1998.** Inorganic ions modulate the path of phloem loading of sucrose in *ricinus communis* l seedlings. *Plant, Cell and Environment* **21:** 1047-1054.

**Schönknecht G, Spoormaker P, Steinmeyer R, Bruggeman L, Ache P, Dutta R, Reintanz B, Godde M, Hedrich R, Palme K**. **2002.** KCO1 is a component of the slow-vacuolar (SV) ion channel. *FEBS Lett.* **511:** 28-32.

**Schroeder JI, Ward JM, Gassmann W**. **1994.** Perspectives on the physiology and structure of inward-rectifying $K^+$ channels in higher plants: biophysical implications for $K^+$ uptake. *Annu.Rev.Biophys.Biomol.Struct.* **23:** 441-471.

**Schulze W, Weise A, Frommer WB, Ward JM**. **2000.** Function of the cytosolic N-terminus of sucrose transporter AtSUT2 in substrate affinity. *FEBS Lett.* **485:** 189-194.

**Serrano R**. **1989.** Structure and Function of Plasma-Membrane ATPase. *Annual Review of Plant Physiology and Plant Molecular Biology* **40:** 61-94.

**Shakya R, Sturm A**. **1998.** Characterization of source- and sink-specific sucrose/$H^+$ symporters from carrot. *Plant Physiol* **118:** 1473-1480.

**Shen B, Jensen RG, Bohnert HJ**. **1997.** Increased resistance to oxidative stress in transgenic plants by targeting mannitol biosynthesis to chloroplasts. *Plant Physiol* **113:** 1177-1183.

**Sibaoka T**. **1982.** Excitable cells in Mimosa. *Science* **137:** 226.

**Sjölund RD**. **1997.** The phloem sieve element: A river runs through it. *Plant Cell* **9:** 1137-1146.

**Slayman CL, Sanders D**. **1985.** Steady-state kinetic analysis of an electroenzyme. *Biochem.Soc.Symp.* **50:** 11-29.

**Sovonick SA, Geiger DR, Fellows RJ**. **1974.** Evidence for Active Phloem Loading in Minor Veins of *Sugar-Beet*. *Plant Physiology* **54:** 886-891.

**Stadler R, Brandner J, Schulz A, Gahrtz M, Sauer N**. **1995.** Phloem Loading by the PmSUC2 Sucrose Carrier from *Plantago-Major* Occurs Into Companion Cells. *Plant Cell* **7:** 1545-1554.

**Stadler R, Sauer N**. **1996.** The *Arabidopsis thaliana* AtSUC2 gene is specifically expressed in companion cells. *Botanica Acta* **109:** 299-306.

**Stadler R, Truernit E, Gahrtz M, Sauer N**. **1999.** The AtSUC1 sucrose carrier may represent the osmotic driving force for anther dehiscence and pollen tube growth in *Arabidopsis*. *Plant J.* **19:** 269-278.

**Stoop JMH, Pharr DM**. **1994a.** Growth Substrate and Nutrient Salt Environment Alter Mannitol-To-Hexose Partitioning in Celery Petioles. *Journal of the American Society for Horticultural Science* **119:** 237-242.

**Stoop JMH, Pharr DM**. **1994b.** Mannitol Metabolism in Celery Stressed by Excess Macronutrients. *Plant Physiology* **106:** 503-511.

**Sturm A, Tang GQ**. **1999.** The sucrose-cleaving enzymes of plants are crucial for development, growth and carbon partitioning. *Trends in Plant Science* **4:** 401-407.

**Sussman MR**. **1994.** Molecular Analysis of Proteins in the Plant Plasma-Membrane. *Annual Review of Plant Physiology and Plant Molecular Biology* **45:** 211-234.

**Svennelid F, Olsson A, Piotrowski M, Rosenquist M, Ottman C, Larsson C, Oecking C, Sommarin M**. **1999.** Phosphorylation of Thr-948 at the C terminus of the plasma membrane H(+)-ATPase creates a binding site for the regulatory 14-3-3 protein. *Plant Cell* **11:** 2379-2391.

**Sze H, Li XH, Palmgren MG**. **1999.** Energization of plant cell membranes by $H^+$-pumping ATPases: Regulation and biosynthesis. *Plant Cell* **11:** 677-689.

**Taiz L, Zeiger E**. **1998.** Translocation in the phloem. In:*Plant Physiology*. Sunderland: Sinauer Associates, Inc., Publishers, 251-286.

**Tang XD, Xu R, Reynolds MF, Garcia ML, Heinemann SH, Hoshi T**. **2003.** Haem can bind to and inhibit mammalian calcium-dependent Slo1 BK channels. *Nature* **425:** 531-535.

**Tarczynski MC, Jensen RG, Bohnert HJ**. **1993.** Stress Protection of Transgenic Tobacco by Production of the Osmolyte Mannitol. *Science* **259:** 508-510.

**Tegeder M, Wang XD, Frommer WB, Offler CE, Patrick JW**. **1999.** Sucrose transport into developing seeds of *Pisum sativum* L. *Plant Journal* **18:** 151-161.

**Tetlow IJ, Farrar JF**. **1993.** Apoplastic Sugar Concentration and Ph in Barley Leaves Infected with Brown Rust. *Journal of Experimental Botany* **44:** 929-936.

**The Arabidopsis Genome Initiative**. **2000.** Analysis of the genome sequence of the flowering plant *Arabidopsis thaliana*. *Nature* **408:** 796-815.

**Thompson GA, Schulz A**. **1999.** Macromolecular trafficking in the phloem. *Trends in Plant Science* **4:** 354-360.

**Truernit E, Sauer N**. **1995.** The promoter of the Arabidopsis thaliana SUC2 sucrose-$H^+$ symporter gene directs expression of beta-glucuronidase to the phloem: evidence for phloem loading and unloading by SUC2. *Planta* **196:** 564-570.

**Tsai TD, Shuck ME, Thompson DP, Bienkowski MJ, Lee KS**. **1995.** Intracellular H+ inhibits a cloned rat kidney outer medulla $K^+$ channel expressed in *Xenopus* oocytes. *Am.J Physiol* **268:** C1173-C1178.

**Turgeon R**. **1996.** Phloem loading and plasmodesmata. *Trends in Plant Science* **1:** 418-423.

**Turgeon R**. **2000.** Plasmodesmata and solute exchange in the phloem. *Australian Journal of Plant Physiology* **27:** 521-529.

**Turgeon R, Beebe DU**. **1991.** The Evidence for Symplastic Phloem Loading. *Plant Physiology* **96:** 349-354.

**Turgeon R, Beebe DU, Gowan E**. **1993.** The Intermediary Cell - Minor-Vein Anatomy and Raffinose Oligosaccharide Synthesis in the Scrophulariaceae. *Planta* **191:** 446-456.

**Turgeon R, Medville R**. **1998.** The absence of phloem loading in willow leaves. *Proceedings of the National Academy of Sciences of the United States of America* **95:** 12055-12060.

**Turgeon R, Wimmers LE**. **1988.** Different Patterns of Vein Loading of Exogenous [C-14] Sucrose in Leaves of *Pisum-Sativum* and *Coleus-Blumei*. *Plant Physiology* **87:** 179-182.

**Uozumi N, Gassmann W, Cao Y, Schroeder JI**. **1995.** Identification of strong modifications in cation selectivity in an *Arabidopsis* inward rectifying potassium channel by mutant selection in yeast. *J.Biol.Chem.* **270:** 24276-24281.

**Uozumi N, Nakamura T, Schroeder JI, Muto S**. **1998.** Determination of transmembrane topology of an inward-rectifying potassium channel from *Arabidopsis thaliana* based on functional expression in *Escherichia coli*. *Proc.Natl.Acad.Sci.U.S.A* **95:** 9773-9778.

**van Bel A.J.E**. **1993.** The transport phloem. Specifics of its functioning. *Progress in Botany* **54:** 134-150.

**van Bel A.J.E**. **1999.** Evolution, polymorphology and multifunctionality of the phloem system. In:*Perspectives in Plant Ecology, Evolution and Systematics*. 163-184.

**van Bel A.J.E, van Rijen HVM**. **1994.** Microelectrode-recorded development of the symplastic autonomy of the sieve element/companion cell complex in the stem phloem of *Lupinus luteus* L. *Planta* **192:** 165-175.

**van Bel A.J.E., Ehlers K. 2000.** Symplasmic organization of the transport phloem and implications for photosynthate transfer to the cambium. *Cell and Molecular Biology of Wood Formation* 85-99.

**van Bel AJE**. **1995.** The low-profile directors of carbon and nitrogen economy in plants: parenchyma cells associated with translocation channels. In:*Plant Stems*. San Diego: Academic Press, 205-222.

**van Bel AJE**. **2003.** The phloem, a miracle of ingenuity. *Plant Cell and Environment* **26:** 125-149.

**van Bel AJE, Ammerlaan A, van Dijk A.A. 1994.** A three-step screening procedure to identify the mode of phloem loading in intact leaves. Evidence for symplasmic and apoplasmic phloem loading associated with the type of companion cell. *Planta* **192:** 31-39.

**van Bel AJE, Gamalei YV, Ammerlaan A, Bik LPM**. **1992.** Dissimilar phloem loading in leaves with symplastic and apoplastic minor vein configurations. *Planta* **186:** 518-525.

**Vara F, Serrano R**. **1982.** Partial-Purification and Properties of the Proton-Translocating ATPase of Plant Plasma-Membranes. *Journal of Biological Chemistry* **257:** 2826-2830.

**Very AA, Gaymard F, Bosseux C, Sentenac H, Thibaud JB**. **1995.** Expression of a cloned plant $K^+$ channel in *Xenopus* oocytes: analysis of macroscopic currents. *Plant J.* **7:** 321-332.

**Very AA, Sentenac H**. **2002.** Cation channels in the *Arabidopsis* plasma membrane. *Trends Plant Sci.* **7:** 168-175.

**Villalba JM, Lutzelschwab M, Serrano R**. **1991.** Immunocytolocalization of Plasma-Membrane $H^+$-ATPase in Maize Coleoptiles and Enclosed Leaves. *Planta* **185:** 458-461.

**Viola R, Roberts AG, Haupt S, Gazzani S, Hancock RD, Marmiroli N, Machray GC, Oparka KJ**. **2001.** Tuberization in potato involves a switch from apoplastic to symplastic phloem unloading. *Plant Cell* **13:** 385-398.

**Voitsekhovskaja OV, Pakhomova MV, Syutkina AV, Gamalei YV, Heber U**. **2000.** Compartmentation of assimilate fluxes in leaves II. Apoplastic sugar levels in leaves of plants with different companion cell types. *Plant Biology* **2:** 107-112.

**Vranova E, Tahtiharju S, Sriprang R, Willekens H, Heino P, Palva ET, Inze D, Van Camp W**. **2001.** The AKT3 potassium channel protein interacts with the AtPP2CA protein phosphatase 2C. *Journal of Experimental Botany* **52:** 181-182.

**Walker NA, Zhang WH, Harrington G, Holdaway N, Patrick JW**. **2000.** Effluxes of solutes from developing seed coats of *Phaseolus vulgaris* L. and *Vicia faba* l.: locating the effect of turgor in a coupled chemiosmotic system. *Journal of Experimental Botany* **51:** 1047-1055.

**Wang XD, Harrington G, Patrick JW, Offler CE, Fieuw S**. **1995.** Cellular Pathway of Photosynthate Transport in Coats of Developing Seed of *Vicia-Faba* and *Phaseolus-Vulgaris*. Principal Cellular Site(S) of Efflux. *Journal of Experimental Botany* **46:** 49-63.

**Wardrop AB**. **1981.** Lignification and xylogenesis. In:*Xylem and Development*. London: Castle House Publ.Ltd., 115-155.

**Webb KL, Burley JWA**. **1982.** Sorbitol translocation in apple. *Science* **137:** 766.

**Weber H, Borisjuk L, Heim U, Sauer N, Wobus U**. **1997.** A role for sugar transporters during seed development: Molecular characterization of a hexose and a sucrose carrier in *fava bean* seeds. *Plant Cell* **9:** 895-908.

**Weise A, Barker L, Kuhn C, Lalonde S, Buschmann H, Frommer WB, Ward JM**. **2000.** A new subfamily of sucrose transporters, SUT4, with low affinity/high capacity localized in enucleate sieve elements of plants. *Plant Cell* **12:** 1345-1355.

**Wellman CH, Osterloff PL, Mohiuddin U**. **2003.** Fragments of the earliest land plants. *Nature* **425:** 282-285.

**Winter H, Lohaus G, Heldt HW**. **1992.** Phloem Transport of Amino-Acids in Relation to Their Cytosolic Levels in Barley Leaves. *Plant Physiology* **99:** 996-1004.

**Wright J.P., Fisher D.B. 1981.** Measurement of the sieve tube membrane potential. *Plant Physiology* **67:** 845-848.

**Wright KM, Roberts AG, Martens HJ, Sauer N, Oparka KJ**. **2003.** Structural and functional vein maturation in developing tobacco leaves in relation to AtSUC2 promoter activity. *Plant Physiology* **131:** 1555-1565.

**Xoconostle-Cazares B, Yu X, Ruiz-Medrano R, Wang HL, Monzer J, Yoo BC, McFarland KC, Franceschi VR, Lucas WJ**. **1999.** Plant paralog to viral movement protein that potentiates transport of mRNA into the phloem. *Science* **283:** 94-98.

**Zei PC, Aldrich RW**. **1998.** Voltage-dependent gating of single wild-type and S4 mutant KAT1 inward rectifier potassium channels. *J Gen.Physiol* **112:** 679-713.

**Zerangue N, Jan YN, Jan LY**. **2000.** An artificial tetramerization domain restores efficient assembly of functional *Shaker* channels lacking T1. *Proceedings of the National Academy of Sciences of the United States of America* **97:** 3591-3595.

**Zhao RM, Dielen V, Kinet JM, Boutry M**. **2000.** Cosuppression of a plasma membrane $H^+$-ATPase isoform impairs sucrose translocation, stomatal opening, plant growth, and male fertility. *Plant Cell* **12:** 535-546.

**Zhorov BS, Tikhonov DB**. **2004.** Potassium, sodium, calcium and glutamate-gated channels: pore architecture and ligand action. *J Neurochem.* **88:** 782-799.

**Zhou J-J, Theodoulou F, Sauer N, Sanders D, Miller AJ**. **1997.** A Kinetic Model with Ordered Cytoplasmic Dissociation for SUC1, an *Arabidopsis* $H^+$/Sucrose Cotransporter Expressed in *Xenopus* Oocytes. *J Membr.Biol.* **159:** 113-125.

**Ziegler H**. **1975.** Nature of transported substances. In: Zimmermann MH, Milburn JA, eds. *Encyclopedia of plant physiology*. Berlin: Springer-Verlag, 59-100.

**Zimmermann MH, Ziegler H**. **1975.** List of sugars and sugar alcohols in sieve-tube exudates. In: Zimmermann MH, Milburn JA, eds. *Encyclopedia of Plant Physiology*. Berlin: Springer-Verlag, 480-503.

# 8. Anhang

## Veröffentlichungsverzeichnis

Hoth, S., **Geiger, D.**, Becker, D., and Hedrich, R. The pore of plant $K^+$ channels is involved in voltage and pH sensing: domain-swapping between different $K^+$ channel alpha-subunits. *Plant Cell* **13**, 943-952 (2001).

**Geiger, D.**, Becker, D., Lacombe, B. and Hedrich,R. Outer Pore Residues Control the $H^+$ and $K^+$ Sensitivity of the *Arabidopsis* Potassium Channel AKT3. *Plant Cell* **14**, 1859-1868 (2002).

Deeken, R., **Geiger, D.**, Fromm, J., Koroleva, O., Ache, P., Langenfeld-Heyser, R., Sauer, N., May, S. and Hedrich, R. Loss of the AKT2/3 potassium channel affects sugar loading into the phloem of *Arabidopsis*. *Planta* **216**, 334-344 (2002).

Langer, K., Ache, P., **Geiger, D.**, Stinzing, A., Arend, M., Wind, C., Regan, S., Fromm, J. and Hedrich, R. Poplar potassium transporters capable of controlling $K^+$ homeostasis and $K^+$-dependent xylogenesis. *Plant Journal* **32**, 997-1009 (2002).

Philippar, K., Büchsenschütz, K., Abshagen, M., Fuchs, I., **Geiger, D.**, Lacombe, B. and Hedrich, R. The $K^+$ channel KZM1 mediates potassium uptake into the phloem and guard cells of the $C_4$ grass *Zea mays. J. Biol. Chem.* **278**, 16973-16981 (2003).

Langer, K., Levchenko, V., Fromm, J., **Geiger, D.**, Steinmeyer, R., Lautner, S., Ache, P. and Hedrich, R. The poplar $K^+$ channel KPT1 is associated with $K^+$ uptake during stomatal opening and bud development. *Plant Journal* **37**, 828-838 (2004).

Ramsperger-Gleixner, M., **Geiger, D.**, Hedrich, R. and Sauer, N. Differential expression of sucrose transporter and polyol transporter genes during maturation of common plantain companion cells. *Plant Physiology* **134**, 147–160 (2004).

Diatloff, E., **Geiger, D.**, Shang, L., Hedrich, R. and Roberts, S.K. Differential regulation of $K^+$ channels in *Arabidopsis* epidermal and stelar root cells. *Plant & Cell Envir.* **27**, 980-990 (2004).

Becker, D., **Geiger, D.**, Dunkel, M., Roller, A., Bertl, A., Latz, A., Carpaneto, A., Dietrich, P. and Hedrich, R. AtTPK4, a novel *Arabidopsis* pollen $K^+$ channel, poised to control the membrane potential in a pH- and $Ca^{2+}$-dependent manner. *PNAS* in press (September 2004).

Carpaneto, A., **Geiger, D.**, Bamberg, E., Sauer, N., Fromm, J. and Hedrich, R. Phloem-localized, proton-coupled sucrose carrier ZmSUT1 mediates sucrose efflux under control of sucrose gradient and pmf. *PNAS* submitted (Oktober 2004).

Klepek, Y., **Geiger, D.**, Klebl, F., Lemoine, R., Hedrich, R. and Sauer, N. The new *Arabidopsis* transporter AtPLT5 mediates $H^+$-symport of numerous substrates including *myo*-inositol, glycerol and ribose. *Plant Cell* accepted (September 2004).

# Lebenslauf

Dietmar Geiger

Julius-von-Sachs-Institut für Biowissenschaften
Universität Würzburg
Julius-von-Sachs-Platz 2
97082 Würzburg
Tel.: 0931 - 888 6105
Fax: 0931 - 888 6158
E-mail: geiger@botanik.uni-wuerzburg.de

Privat:
Gartenstr. 9
97072 Würzburg
Tel.: 0931/8041241

| | |
|---|---|
| Geboren am: | 24. November 1971 in Coburg |
| Staatsangehörigkeit: | deutsch |
| Familienstand: | ledig |

Ausbildung an Schulen und Universitäten:

| | |
|---|---|
| 1978-1983 | Besuch der Grundschule, Großheirath |
| 1983-1992 | Besuch des Gymnasium Ernestinum, Coburg |
| Juni 1992 | Abitur |
| 1993-1994 | Zivildienst in der Jugendherberge Ketschendorf |
| Oktober 1994 | Beginn des Studiums der Biologie (Diplom) an der Bayerischen Julius-Maximilians-Universität Würzburg mit den Wahlfächern Pflanzenphysiologie, Biotechnologie und Biochemie |
| Februar 1997 | Diplomvorprüfung in den Fächern Botanik, Zoologie, Organische Chemie und Physik |
| September 1999 | Mündliche Diplomhauptprüfung in den Fächern Botanik, Biochemie und Biotechnologie |
| Oktober 1999 bis Oktober 2000 | Anfertigung der Diplomarbeit mit dem Thema "**Struktur- und Funktionsanalyse pflanzlicher Kaliumkanäle**" am Lehrstuhl für Pflanzenphysiologie und Biophysik der Bayerischen Julius-Maximilians-Universität Würzburg, unter der Anleitung von Prof. Dr. R. Hedrich |
| Oktober 2000 | Beginn der experimentellen Arbeiten zur vorliegenden Dissertation |

## Eidesstattliche Erklärung

Hiermit erkläre ich, dass ich die vorliegende Dissertation in allen Teilen selbst angefertigt und keine anderen als die angegebenen Quellen und Hilfsmittel verwendet habe.

Ich habe die Dissertation weder in gleicher noch in ähnlicher Form in anderen Prüfungsverfahren vorgelegt. Außerdem habe ich bislang noch keine weiteren akademischen Grade erworben oder zu erwerben versucht.

Würzburg, Oktober 2004

.....

# Danksagung

An erster Stelle gilt mein Dank Herrn Prof. Dr. Rainer Hedrich für die interessante Themenstellung, für vielfältige Diskussionen und Anregungen sowie für die Förderung meiner wissenschaftlichen Laufbahn.

Bei Prof. Dr. A.J.E. van Bel für das Interesse an meiner Arbeit und die Bereitschaft, die Zweitkorrektur zu übernehmen.

Meinen besonderen Dank möchte ich Herrn PD Dr. Dirk Becker für seine sehr gute und geduldige Betreuung, für seine ständige Hilfsbereitschaft und für den großzügigen Freiraum für mich und meine Arbeit aussprechen.

Ganz herzlich möchte ich mich ausnahmslos bei der gesamten Arbeitsgruppe Hedrich für die angenehme und freundliche Arbeitsatmosphäre, die Hilfsbereitschaft und Kollegialität bedanken. Mit einschließen möchte ich dabei auch alle ehemaligen Mitarbeiter sowie die Werkstatt, den Garten und Marlene.

Des weiteren Danke ich Dr. Armando Carpaneto und Dr. Benoit Lacombe für die lehrreiche und zudem erfolgreiche Zusammenarbeit.

Herrn Prof. Dr. N. Sauer und seiner Arbeitsgruppe danke ich für die nette und erfolgreiche Kooperation.

Herrn Prof. Dr. E. Bamberg und Herrn Prof. Dr. J. Fromm danke ich für die Zusammenarbeit beim Zuckertransporter-Projekt.

Vielen Dank möchte ich auch meinen Kollegen in der Schafkopfrunde für die Zerstreuung nach der Arbeit aussprechen.

Ganz besonders möchte ich mich bei meiner Familie für die Unterstützung und das Verständnis für meine Arbeit bedanken.